Dynamical Mass-to-light Ratios of Populous Star Clusters in the Magellanic Clouds

by

Yingyi Song

A dissertation submitted in partial fulfillment
of the requirements for the degree of
Doctor of Philosophy
(Astronomy and Astrophysics)
in The University of Michigan
2020

Doctoral Committee:

Professor Mario L. Mateo, Chair
Professor Moulinath Banerjee
Professor Eric F. Bell
Professor Edward W. Olszewski, University of Arizona
Research Professor Monica Valluri

Yingyi Song

yysong@umich.edu

ORCID iD: 0000-0002-6270-8851

© Yingyi Song 2020

For my parents,

Guijuan Wang and Liqiang Song.

ACKNOWLEDGEMENTS

I would like to thank many people who have provided me with guidance, support and encouragement over the many years of my pursuit of a doctoral degree. First of all, I would like to thank my PhD advisor, Mario Mateo, who guided me to be a qualified astronomer, observer and researcher. Whether his smart ideas to solve unpredictable observational problems, or his sharp questions on my suspicious scientific results, all push me hard forward and toward a thorough understanding of the theory and facts about star clusters and more. Our discussions have also gone beyond the topics on research, such as touring, cycling, foreign cultures, etc. I am truly grateful to have Mario's guidance and support both scientifically and personally in the past six years.

I would like to thank my dissertation committee members, Edward Olszewski, Eric Bell, Monica Valluri and Moulinath Banerjee, for their advice, insight and feedback. I would like to thank the professors from the Astronomy Department, Eric Bell, Oleg Gnedin, Lee Hartmann, Jon Miller, Nuria Calvet and John Monnier, who have provided comprehensive graduate courses during my first two years. I would also like to thank many other faculty, scientists, postdocs and staff at our department, especially Jiangtao Li, Ke Zhang, Ian Roederer, Brian Cox and Shannon Murphy, who made my life at Michigan smooth, enrich and enjoyable.

I am very grateful to my Master advisor, Shude Mao, who introduced me to the study in astrophysics. Shude's three-year guidance on microlensing, exoplanets and galactic dynamics has been instrumental in shaping my research as a young graduate

student. I appreciate his great recommendation, which provides me an opportunity to pursuit my PhD at Michigan.

Last but not least, I would like to thank my family and friends both at Ann Arbor and back in China. To my parents, Guijuan Wang and Liqiang Song, I feel so lucky to have you both in my life. Without your support and encouragement, I would not be so strong and brave to pursue the career of scientific research I have chosen to do. It has been almost thirteen years since I left you for college, but your care and love make me pretty sure that, wherever I live and study, there is always a sweet home waiting for my return in the city of Jinzhou. To my friends at Ann Arbor and especially Jiangtao Li, Rongxin Lin, Ke Zhang, Shen Li, Fujun Du, Hui Li, Zhijie Qu, Chaoran Wang, Xi Meng, Xiang Li, Yao Zhou and Hang Yang, thank you all for making the past six years so enjoyable. Finally, to my special one, Ruhui Liu, thank you for being my companion binary star and inspiring me on the orbit toward a wonderful life.

This thesis is based on spectroscopic data gathered with the 6.5-meter *Magellan* Telescopes located at Las Campanas Observatory, Chile, using the multi-object spectrograph Michigan/*Magellan* Fiber System (M2FS). I would like to thank Mario Mateo, John I. Bailey, III, Jeff Crane, Steve Shectman and Ian Thompson for invaluable contributions to the design, construction and support of M2FS. I would also like to thank the M2FS Team members and telescope operators for obtaining the spectroscopic data at the *Magellan*/Clay telescope, especially Mario Mateo, John I. Bailey, III, Matthew G. Walker, Ian U. Roederer, Edward W. Olszewski, Megan Reiter, Anthony Kremin and Meghin Spencer.

Chapter II of this thesis is based on work published in *Monthly Notices of the Royal Astronomical Society (MNRAS)*, and is reproduced here with minor modifications. Chapters III, IV and V are based on work to appear in *MNRAS*. Both papers were supported by U.S. National Science Foundation (NSF) grants AST-1312997 and

AST-1815403. I acknowledge the funding support—Rackham One-Term Dissertation Fellowship—from the University of Michigan Rackham Graduate School.

TABLE OF CONTENTS

LIST OF FIGURES

Figure

LIST OF TABLES

Table

LIST OF APPENDICES

Appendix

ABSTRACT

The mass-to-light (M/L) ratio is a fundamental astrophysical parameter that converts the luminosity of a stellar system—which is comparatively easy to measure—to a corresponding baryonic mass. Typically, M/L ratios are estimated using stellar population synthesis models. Testing such models requires independent mass estimates (specifically, only of the baryons) which usually require kinematic data and is considerably more involved than photometric measures. Galaxies are particularly difficult to employ for this task given their typically complex stellar population mixtures and their dark-matter contents. Star clusters, in contrast, are comprised of comparatively simple stellar populations and contain no dark matter, making them ideal laboratories to test M/L predictions.

This thesis aims to estimate in a consistent manner dynamical masses and V-band M/L ratios (M/L_V) of a large sample of star clusters spanning a wide range in age and metallicity. To accomplish this, I have obtained 3137 high-resolution stellar spectra of individual stars in 26 populous star clusters of the Magellanic Clouds using the M2FS multi-object spectrograph on the *Magellan*/Clay Telescope. Combined with 239 published spectroscopic results of comparable quality, I have produced a final sample of 2787 individual stars suitable for kinematic analysis in the target clusters. Line-of-sight (LOS) velocities measured from these spectra and stellar positions within each cluster were used within a customized expectation-maximization (EM) technique to estimate cluster membership probabilities. Using the appropriate cluster structural parameters and corresponding single-mass dynamical models, this technique ultimately provides self-consistent total mass and M/L_V estimates for

each cluster. Mean metallicities for the clusters were also estimated from the spectra and tied to a scale based on calcium IR triplet measurements and high-precision, high-resolution metallicity estimates.

I describe trends of the cluster M/L_V values with cluster age, mass and metallicity, and compare the relations with predictions from simple stellar population (SSP) models. The new observational M/L_V results parallel the systematic behavior of the SSP models as a function of age, but are on average about 40% lower than model predictions. Modified SSP models that account for internal and external dynamical effects greatly improve agreement with our results, as can models that adopt a strongly bottom-light stellar initial mass function (IMF). To the extent that dynamical evolution must occur, a modified IMF is not required to match data and models. In contrast, a bottom-heavy IMF, suggested by other studies, is strongly ruled out for our cluster sample as this would lead to higher predicted M/L_V values, exacerbating the discrepancy with our observations.

CHAPTER I

Introduction

1.1 Converting Luminosity to Mass: The Role of Mass-to-light Ratios in Astrophysics

The baryonic mass-to-light (M/L) ratio is an important parameter in astrophysics as it is frequently used to translate the luminosity of a stellar system to a common baryonic mass scale. Mass-to-light ratios can be applied to either simple stellar systems (e.g. star clusters) that consists of coeval stellar population with the same chemical composition, or composite stellar systems (e.g. galaxies) that have complex mixtures of ages, metallicities and star formation histories. In both applications, parameters such as the form of the stellar initial mass function (IMF), the detailed nature of stellar evolutionary models, and the adopted metallicity scale can have significant effects on the assgined M/L ratio for a given system. As such, M/L ratios offer a convenient method to estimate the baryonic masses of clusters and galaxies from photometric observations, but one that is still subject to many complications, uncertainties and assumptions.

Baryonic masses estimated from the photometry are particularly useful in various astrophysical problems; for instance, to estimate the inventory of baryons in the Universe (e.g. *Fukugita et al.*, 1998; *McGaugh et al.*, 2010); to investigate the stel-

lar/baryonic mass Tully–Fisher relation, which is more physically meaningful than in any specific photometric band (e.g. *Bell and de Jong*, 2001); to study the assembly of galaxies over cosmic times, and thus the formation and evolution of galaxies (e.g. *Bell et al.*, 2003, 2004). These applications are central to much of what we know about the early Universe and about how galaxies evolve with redshift (e.g. *Kauffmann et al.*, 2003; *Bell et al.*, 2003; *Blanton and Roweis*, 2007; *Tojeiro et al.*, 2009; *Chen et al.*, 2012; *Maraston et al.*, 2013).

Th M/L ratio is typically reported using the mass and luminosity of the Sun as a baseline value, and hence is presented in the unit of $M_{\odot}/L_{\odot}$. That convention will be followed throughout this dissertation. Using this scale, it is clear that if all stars in a stellar system are the same as the Sun, the M/L ratio should be unity. Given the steepness of the main-sequence mass-luminosity relation, this implies that stellar systems consisting of older stars have M/L values considerably larger than one, while stellar systems consisting of younger stars have values much smaller than one. Of course, this does not mean that a system with $M/L \sim 1$ is composed only of stars similar to the Sun since M/L values for composite systems arise from the sum of a wide variety of stellar populations. For example, the mean M/L ratio of globular clusters (GCs) in the Milky Way (MW) is about 2 $M_{\odot}/L_{\odot}$ (e.g. *McLaughlin and van der Marel*, 2005; *Kimmig et al.*, 2015; *Baumgardt*, 2017; *Baumgardt and Hilker*, 2018) and yet these systems consist of luminous red giants, dim white dwarfs, and have mean metallicities that can be hundreds of times lower than the Sun. Typical integrated M/L ratios of most galaxies in the local Universe range from 2 to 10 $M_{\odot}/L_{\odot}$ (e.g. *Bell and de Jong*, 2001; *Bell et al.*, 2003; *Kassin et al.*, 2006; *Torres-Flores et al.*, 2011; *Cappellari et al.*, 2013). Nevertheless, strong departures of M/L ratios can provide broad clues regarding the underlying populations in a system. Values ranging from 2–10, typical of the central regions of galaxies in the Local Universe, imply relative more low-luminosity stars, and hence large ages in such systems. M/L ratios considerably

smaller than one imply the presence of relatively large numbers of comparatively young, luminous stars. This behavior provides an illustration of how M/L ratios may vary—in this case—as a function of age, all other parameters held constant.

1.2 Theoretical Mass-to-light Ratios from Simple Stellar Population Models

Over the past several decades, many theoretical models have been developed as tools to predict M/L ratios of simple and composite stellar systems. Such so-called stellar population synthesis (SPS) models rely crucially on stellar evolutionary grids that attempt, often parametrically, to account for the complex star formation and chemical evolutionary histories of galaxies (e.g. *Bruzual and Charlot*, 2003; *Maraston*, 2005; *Vazdekis et al.*, 2010; *Conroy et al.*, 2009; *Conroy and Gunn*, 2010).

All SPS models start with prescriptions for so-called simple stellar populations (SSP) that describe the evolution of a single stellar population formed in the same burst of star formation and with the same chemical composition. Any SSP-predicted M/L ratios require three basic inputs: A form for the stellar initial mass function (IMF), a comprehensive grid of stellar evolutionary models, and an extensive array of stellar spectral libraries(e.g. *Conroy*, 2013). The stellar IMF defines the distribution of stellar masses when a population of stars are born at a given epoch. The IMF is usually considered invariant from one stellar population to another, although some recent studies suggest that IMF variations may exists due to different metallicities and galactic environments (e.g. *Conroy and van Dokkum*, 2012; *Kalirai et al.*, 2013; *Geha et al.*, 2013; *Kroupa et al.*, 2013). Stellar IMFs are often parameterized as single or multiple power laws of initial stellar mass, bounded at both high and low mass by considerations of the physical structures of stars at these limits.

Stellar evolutionary models describe how a star with a certain initial mass and

metallicity changes its physical properties (e.g. size, temperature, surface gravity, mass and luminosity) over the course of time. With the IMF and stellar evolutionary models specified for a stellar population, it is possible to track the numbers of stars over the Luminosity-Temperature plane (the HR diagram) for any SSP.

The final ingredient is stellar spectral libraries which are employed to assign an output spectrum to each of the of different types of stars in a system, suitably weighted by the numbers and luminosities of each type. This places models into various observational planes (e.g., color-magnitude, color-color) and allows one to compute integrated spectral energy distributions for such systems as a function of age and metallicity. Of course, as outlined here, these predictions rely on innumerable assumptions and can be affected by myriad uncertainties in the input parameters or by the exclusion of effects left out of the models. Thus, though termed as 'simple', sophisticated SSP models are not really all that simple even when applied to non-composite stellar systems.

For more complex stellar systems such as galaxies, the so-called composite stellar population (CSP) models are built from well-established SSP models and require even more inputs, e.g. star-formation history (SFH), chemical evolution and interstellar dust component. While the SFH describes the age distribution of stellar populations within a galaxy, the chemical evolution describes how the metallicity distribution of stellar populations vary over time. The role of dust component is twofold: an obscurer of light that both absorbing and scattering starlight, and an emitter of light in the IR. Taking all these inputs into account, the CSP models will predict various physical properties of galaxies, including stellar M/L ratio and photometric colors. These properties are usually used to develop handy tools to place studies of extragalactic systems onto a consistent baryonic-mass scale. For instance, color-M/L relations are popular to estimate stellar masses in external galaxies (e.g. *Bell and de Jong*, 2001; *Bell et al.*, 2003; *Kranz et al.*, 2003; *Kassin et al.*, 2006; *Torres-Flores et al.*, 2011;

McGaugh and Schombert, 2014; *Salim et al.*, 2016).

Direst tests of CSP models are impractical as such tests would require independent knowledge of the SFH, chemical evolution and dust content of a systems. In contrast, SSP models are more amenable to empirical testing as Nature provides reasonably close examples of such systems in the form of star clusters. In this thesis, I aim to test observationally how reliablely SSP models predict M/L ratios of star clusters—in this case, the populous star clusters of the Magellanic Clouds (MCs). I will also explore the extent to which other plausible physical effects or IMF variations are required for these models to account for cluster observations.

1.3 Testing the Models: Observational Constraints on Mass-to-light Ratios

One way to test the reliability of model-dependent M/L ratios is to determine dynamical masses of SSPs. Star clusters are particularly well-suited for such measurements since they are generally regarded as prototypical SSPs (although see e.g. *Gratton et al.*, 2012; *Bastian and Lardo*, 2018, for reviews of population complexities found in some, perhaps most, massive star clusters). In contrast, galaxies are complex mixture of individual SSPs with other non-stellar components, such as interstellar gas, dust and dark matter (e.g. *Conroy*, 2013), and hence are not good for directly testing SSP models. Clusters also span a wide range of metallicity and age, making them useful also as tests of how M/L ratios vary with these fundamental population parameters. Using clusters for M/L ratio determinations also offers simplicity. At the most basic level, measuring the M/L ratio of star clusters involves mass determinations via direct kinematic measurements and straightforward dynamical analyses, and obtaining luminosities from independent photometric observations.

1.3.1 Observational Approaches

There are two broad approaches commonly used to obtain the kinematic data needed to estimate cluster masses, integrated-light spectroscopy and spectroscopy of individual stars within clusters to serve as dynamical tracers. Integrated-light spectroscopy is best suited for star clusters that have very condensed, unresolved cores and/or that are so distant that they cannot be readily resolved into their constituent stars. An influential early example of this approach—though applied to mostly resolved systems—is the study of *Illingworth* (1976) who obtained scanned integrated-light spectra of ten Southern MW GCs. *Mandushev et al.* (1991) employed a similar approach to obtain M/L ratios of 32 MW GCs. Local Group (LG) clusters have also proven to be popular targets for integrated-light kinematic spectroscopy. *Zaritsky et al.* (2012, 2013, 2014) reported M/L ratios obtained using integrated-light spectroscopy of a sample of 29 clusters from four different LG galaxies, including the MW, the Large and Small MCs (LMC and SMC), and the Fornax dwarf spheroidal galaxy. *Larsen et al.* (2002) measured M/L ratios of four suspected intermediate-age M33 GCs, while *Strader et al.* (2009, 2011) produced a large sample of M/L ratios for 163 M31 GCs that comprised new and previously-published results. Some studies have probed beyond the LG to obtain measurements of the internal kinematics of clusters (e.g. *Martini and Ho* 2004 who studied 14 GCs associated with NGC 5128).

The other approach of measuring internal cluster kinematics via observations of individual stars is best suited for comparatively nearby, well-resolved systems. This method has become significantly more practical in recent years with the development of wide-field multi-object spectrographs (MOSs) and comparatively wide-field IFUs. For example, *Lane et al.* (2010b) used the AAOmega spectrograph to derive the M/L ratios in 10 halo GCs. More recently, *Kimmig et al.* (2015) published a new catalog of M/L ratios for 25 MW GCs based solely on MOS measurements of individual stars. Their data, as is the case for most MOS results, are particularly uniform in kinematic

precision. The large number of GCs that have been observed in this manner make it possible to examine trends of M/L as a function of mass and metallicity, but, notably, not in age. Some examples of this approach applied beyond the Galaxy include *Feast and Black* (1980), *Lupton et al.* (1989), *Mateo et al.* (1991), *Fischer et al.* (1992a,b, 1993), *Suntzeff et al.* (1992), *Ferraro et al.* (2006), *Mackey et al.* (2013) and *Kamann et al.* (2018).

The most challenging aspect of cluster kinematic studies, regardless of approach, is the comparatively small velocity dispersions—ranging from 1 to 15 $\mathrm{km\,s^{-1}}$—of these systems. Resolving such dispersions demands moderate to high spectral resolution and excellent instrumental stability. Integrated-light spectroscopy can generally succeed in clusters only when the instrumental resolution is precisely measured—and sufficiently stable—to extract the comparatively small cluster dispersions reliably. In many of the studies cited above, the instrumental resolution ranged from 10 to 50 $\mathrm{km\,s^{-1}}$, meaning that the clusters with dispersions $\sim$5 $\mathrm{km\,s^{-1}}$ or smaller inflated line profiles by at most 10% and often less than 1% compared to the line spread function of the spectrographs. Measuring kinematics using resolved-star spectroscopy also requires moderate to high resolution, though determining line centers—as opposed to line widths—is comparatively much more precise at any given S/N level. The more acute problem here is that moderately large samples are needed to beat down stochastic errors. MOS help in this regard, but they often can target only limited numbers of members in a given cluster, especially for more distant systems.

In contrast to the mass estimates, luminosities of star clusters are determined almost exclusively using calibrated surface brightness/density profiles (e.g. *McLaughlin and van der Marel*, 2005). Together, masses and luminosities measured in these ways can be combined to produce empirical M/L estimates (e.g. *McLaughlin and van der Marel*, 2005; *Strader et al.*, 2009, 2011; *Kimmig et al.*, 2015; *Baumgardt and Hilker*, 2018).

1.3.2 Observations of Globular Clusters

Numerous studies have compared predictions from SSP models with empirical M/L ratios, mostly for old GCs either in the MW (e.g. *Pryor and Meylan*, 1993; *McLaughlin and van der Marel*, 2005; *Kimmig et al.*, 2015; *Baumgardt*, 2017; *Baumgardt and Hilker*, 2018) or associated with local group (LG) galaxies (e.g. *Larsen et al.*, 2002; *Strader et al.*, 2009, 2011).

Some useful compilations of kinematic studies of star clusters include *Pryor and Meylan* (1993) who tabulated central velocity dispersions and M/L ratios of 56 MW GCs with integrated-light and individual-star spectroscopy, the latter often from heroic studies before MOS were available. *McLaughlin and van der Marel* (2005) derived dynamical properties in a consistent manner for 38 MW GCs and 19 LG clusters (16 in the MCs) from published single-star spectroscopic studies. The latter paper also lists photometric structural data for some 46 additional MC clusters that do not have any kinematic measurements.

Many former studies have found significant discrepancies between theoretical V-band M/L_V predictions and observations for old GCs. Given a 'canonical' IMF, the SSP models predict that M/L_V should increase with age and metallicity but be constant with the total mass of the population (e.g. *Bruzual and Charlot*, 2003; *Maraston*, 2005; *Conroy and Gunn*, 2010). From the integrated-light results of 200 GCs in M31, however, *Strader et al.* (2009, 2011) found that M/L_V decreases with [Fe/H] and increases with cluster mass. In the MW, *Kimmig et al.* (2015) found similar trends of M/L_V with cluster mass and metallicity from a uniform sample of 25 GCs. Using extended catalogues of 50 and 59 MW GCs, respectively, both *Baumgardt* (2017) and *Dalgleish et al.* (2020) confirmed that the observed M/L_V-[Fe/H] relation disagree with SSP models, though no clear change of M/L_V with cluster metallicity was found as pronounced as it is for M31.

These discrepancies and trends suggest either dynamical effects or varying stellar

IMF play a significant role in star clusters. The M/L_V trend with cluster mass has been attributed to mass segregation and the preferential escape of low-mass stars over the tidal boundary (e.g. *Kruijssen*, 2008). Hardly to explain by the same dynamical effect, the trend with metallicity may root from a mass segregation bias in the determination of M/L_V from integrated-light properties (e.g. for M31 GCs, *Shanahan and Gieles*, 2015), or reflect variations in the IMF (i.e., top-heavy IMF for metal-rich clusters, *Strader et al.*, 2011; *Zonoozi et al.*, 2016).

In addition to mass and metallicity, cluster age is another important dimension over which to examine M/L_V predictions from SSP models. Young and intermediate-age star clusters are generally not very populous in the MW and hence are ill-suited for high-precision mass estimates. In contrast, the MCs and other LG group dwarf galaxies contain populations of massive clusters that span a mass range similar to that of old GCs, but also span the full range of cluster age from the present-day to over 10^{10} yrs. Using integrated-light spectroscopy, *Zaritsky et al.* (2012, 2013, 2014) obtained M/L_V of a sample of 29 clusters from four different LG galaxies: the MW, the MCs and the Fornax dwarf spheroidal galaxy. Fourteen of these clusters are younger than 3 Gyr allowing the authors to study how M/L_V evolves with age. They found that the observed M/L_V values run first higher and then lower than SSP models with age, interpreted by these studies as possible evidence of the existence of two distinct IMFs within the cluster populations. However, this behavior appears to not be corroborated by M/L_V estimates of intermediate-age MC clusters observed through individual stellar spectroscopy, though, prior to this thesis, only six such MC clusters were available for comparison (*Fischer et al.*, 1992a,b, 1993; *Mackey et al.*, 2013; *Kamann et al.*, 2018; *Patrick et al.*, 2020). These earlier results—discordant among themselves and difficult to reconcile with models—suggest that more M/L_V of young and intermediate-age clusters are needed.

1.4 Expanding the Tests: The Star Clusters of the Magellanic Clouds

Both of the MCs—the LMC and the SMC—are readily visible from the Southern Hemisphere, subtending about $10.8^\circ \times 9.2^\circ$ and $5.2^\circ \times 3.1^\circ$ (on average 20 and 8 times the Moon's diameter) on the sky, respectively (*de Vaucouleurs et al.*, 1991, see Figure 1.1). The LMC is located at a distance of about 50 kpc, and the SMC is about 60 kpc distant (e.g. *Feast and Walker*, 1987). The LMC is dominated by a prominent central bar that geometrically off-center (e.g. *van der Marel and Kallivayalil*, 2014), and hence is classified as a Barred Magellanic spiral or SB(s)m (*de Vaucouleurs and Freeman*, 1972; *de Vaucouleurs et al.*, 1991). The SMC also contains a central bar structure but with a more complex overall structure on the sky and along the line of sight that suggests it has been strongly tidally disturbed, either by the MW, the LMC or both (e.g. *Westerlund*, 1997). The SMC is classified as a Barred irregular dwarf or SB(s)m pec (*de Vaucouleurs and Freeman*, 1972; *de Vaucouleurs et al.*, 1991).

As noted above, one striking feature of the MCs is that they host a large number of populous star clusters (present masses greater than 5000 $M_\odot$) that span a wide range of age and metallicity (e.g. *Baumgardt et al.*, 2013). Figure 1.2 shows the age and metallicity of star clusters in the MW and the MCs. It can be seen that the MW GCs (black dots) are old ($\gtrsim$ 12 Gyr) and relatively metal-poor, while the MW open clusters (OCs, gray dots) are young and metal-rich. The MC star clusters (symbols in red and blue) span the full range of ages exhibited among the MW OCs—though at generally lower mean metallicity—but have masses closer to those of MW GCs, which span a much more limited range of (great) age. For the MC clusters, Figure 1.2 shows distinct age-metallicity relations for the two galaxies in the sense that the clusters in the LMC are relatively more metal-rich at a given age than those in the SMC. Figure 1.2 also shows the well-known age gap for LMC clusters between about 3 to 8

Figure 1.1: Images of the Large and Small Magellanic Clouds as seen from Las Campanas Observatory, Chile in February 2016. In the top image, both MCs are seen as prominent 'clouds' next to the Milky Way. The bottom photo is a zoomed-in view of the MCs. Copyright © Michael Padilla 2016. Reprinted with permission.

Gyr.

Given their moderate distance, the populous star clusters of the MCs are generally compact enough in the sky for both integrated-light spectroscopy and photometry, while still close enough to allow spectroscopy of individual stellar members in sufficient numbers to produce good-quality statistical samples. Further, the fact that both integrated-light and individual-star methods can be applied effectively to many MC clusters makes them particularly useful test cases to understand the relative systematics that may arise from each technique. Indeed, both approaches have been employed in past studies of MC clusters. As described in Section 1.3.2, *Zaritsky et al.* (2012, 2013, 2014) obtained integrated-light spectroscopic observations to measure M/L ratios for a sample of 17 clusters younger than 7 Gyr in the MCs. Prior to this thesis, only six MC clusters were studied through high-precision individual-star spectroscopy (*Fischer et al.*, 1992a,b, 1993; *Mackey et al.*, 2013; *Kamann et al.*, 2018; *Patrick et al.*, 2020).

1.5 This work

My thesis aims to measure in a consistent manner dynamical masses and M/L ratios of resolved massive star clusters in the MCs using individual-star spectroscopy. The ultimate aim of this thesis is to critically compare theoretical M/L estimates with what we glean from this cluster sample.

In Chapter II, I described the basic methodology of our survey and the analysis of the data as applied to the SMC cluster NGC 419 and the LMC cluster NGC 1846. The key motivations behind this work are (a) to obtain data from which reliable masses can be determined for massive clusters that span a large range in metallicity, and most importantly, age, (b) to exploit the availability of an MOS—Michigan/*Magellan* Fiber System (M2FS, *Mateo et al.*, 2012)—that is capable of targeting clustered fields efficiently and obtaining spectra with individual velocity precisions well below the

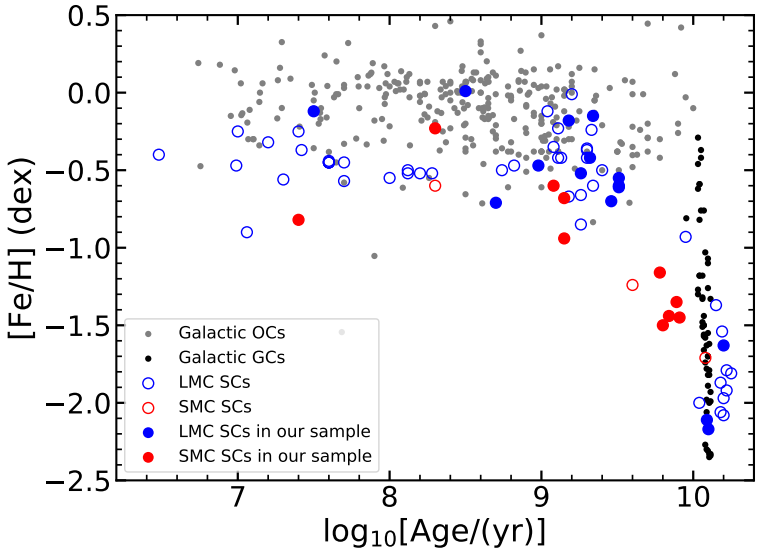

Figure 1.2: A representative plot of metallicity versus log (Age) for star clusters in the Milky Way and the Magellanic Clouds. Filled circles denote the 16 LMC (blue) and 10 SMC (red) clusters studied in this work, respectively. Open circles correspond to other clusters in the LMC (blue) and SMC (red). The metallicities and ages of all these MC clusters are cited from the collected catalog of *Pessev et al.* (2006, 2008). For the Milky Way clusters, we present the Galactic globular clusters listed in *VandenBerg et al.* (2013) (black dots) and the Galactic open clusters listed in *Dias et al.* (2002) (gray dots).

expected internal dispersions of the clusters. The first aim will allow us to critically compare M/L models with SSPs over as broad a range in the metallicity-age plane as feasible, while the second provides us with the unprecedented means of routinely and systematically obtaining precise masses in MC clusters with central dispersions as small as 1 $\mathrm{km\,s^{-1}}$. The more specific aims of Chapter II are to introduce key features of this survey and to assess the quality of our results via comparisons with previous observations of two clusters—NGC 419 in the SMC and NGC 1846 in the LMC—that are in common with our cluster sample (*Kamann et al.* 2018, hereafter K18; *Mackey et al.* 2013, hereafter Ma13).

Chapter III updates the methodology from Chapter II as applied to our full M2FS sample consisting of 26 MC clusters with high-quality kinematic data (10 in the SMC, 16 in the LMC). These clusters were chosen to span the range from ∼100 Myr to ∼13 Gyr in age, and from −2.0 to −0.4 in [Fe/H] (see Figure 1.2) in order to provide the most leverage on our tests of V-band M/L (M/L_V) predictions from populations models. Our study is based on spectroscopic observations obtained using the Michigan/*Magellan* Fiber System (M2FS) from which we measure kinematics and metallicities of samples of individual stars associated the clusters in our sample. From these results, we derive dynamical masses and M/L_V ratios of all 26 clusters, along with the determination of independent spectroscopic estimates of the mean metallicities of the clusters. In Chapter III we describe our target selection, cluster center determination, observational and data reduction procedures adopted for all clusters in our survey.

Chapter IV describes improvements of the Bayesian spectral fitting method we introduced in Chapter II to derive velocity and physical parameters from M2FS spectra. In Section 4.2.1, we obtain the final stellar sample for cluster kinematic analysis and assign a cluster membership probability to each star. Section 4.2 reports our derived dynamical and chemical results for all clusters in our sample, and compares

these results critically with those from previous studies.

In Chapter V, we discuss the trends of our M/L results with respect to various physical parameters, and compare with the predictions by both standard and improved SSP models. Chapter VI summarizes our methods and results, and provide a brief outline of the conclusions. In this final chapter, I also outline some future work inspired by the this dissertation study.

Chapter II of this thesis is based on work, *Song et al.* (2019), published in *Monthly Notices of the Royal Astronomical Society (MNRAS)*, and is reproduced here with minor modifications. Chapters III, IV and V are based on work to appear in a separate paper in *MNRAS* which will be submitted for publication concurrently with submission of this dissertation.

CHAPTER II

How to Measure Mass-to-Light Ratios Using Magellanic Cloud Star Clusters: The Test Cases NGC 419 and NGC 1846

Results in this chapter were published in *Song et al.* (2019) and are presented here with minor, mostly stylistic, revisions.

2.1 Introduction

This chapter represents the first in a series in which we aim to measure in a consistent manner dynamical masses and M/L ratios of resolved massive star clusters in the Magellanic Clouds using individual-star spectroscopy. The key motivations behind this chapter are (a) to obtain data from which reliable masses can be determined for massive clusters that span a large range in metallicity, and most importantly, age, (b) to exploit the availability of an MOS—Michigan/*Magellan* Fiber System (M2FS, *Mateo et al.*, 2012)—that is capable of targeting clustered fields efficiently and obtaining spectra with individual velocity precisions well below the expected internal dispersions of the clusters. The first aim will allow us to critically compare M/L models with SSPs over as broad a range in the metallicity-age plane as feasible, while the second provides us with the unprecedented means of routinely and systematically

obtaining precise masses in MC clusters with central dispersions as small as 1 $\mathrm{km\,s^{-1}}$. As of this writing, we have obtained high-quality data for over 20 MC clusters that span the range from 50 Myr to 13 Gyr in age, and from -2.2 to $+0.0$ in [Fe/H]. The ultimate aim of this thesis is to critically compare theoretical M/L estimates with what we glean from this cluster sample. The more specific aims of this chapter are to introduce key features of this survey and to assess the quality of our results via comparisons with previous observations of two clusters—NGC 419 in the SMC and NGC 1846 in the LMC—that are in common with our cluster sample (*Kamann et al.* 2018, hereafter K18; *Mackey et al.* 2013, hereafter Ma13).

This chapter is organized as follows. In Section 2.2 we describe the target selection, observational and data reduction procedures as they apply to NGC 419 and NGC 1846 and that we will adopt for all clusters in our survey. Section 2.3 starts with a generalized description of the Bayesian method we used to derive velocity and physical parameters from M2FS spectra. We continue to explain our determination of dynamical properties such as systemic velocities and central velocity dispersions, applying the techniques, as feasible, to published and our own new data for NGC 419 and NGC 1846. In Section 2.3 we also discuss the accuracy and limitations of our analyses, and report our derived masses and M/L ratios and their rotation signatures for these two clusters. Section 2.4 compares our results critically with those from previous studies for these two clusters. In Section 2.5 we conclude with a summary of our methods and results, and provide a brief outline of the content and scope of subsequent chapters for this thesis.

2.2 Data Overview

2.2.1 Cluster Candidates

The clusters identified for use in the present chapter and for the following chapters in my thesis were chosen from catalogs of MC clusters with good-quality age and metallicity estimates and for which we could expect to obtain samples of about 50 stellar members. The latter requirement—imposed to ensure that we can obtain statistically reliable mass estimates for the clusters—restricted us in practice to candidates more luminous than an absolute V-band magnitude of -6.

A further selection on our sample was to identify clusters with good integrated-light or star-count analyses. These data are essential for constraining the structural parameters needed to carry out the dynamical analysis of the clusters. Integrated photometry of our candidates was taken from the catalogs of *McLaughlin and van der Marel* (2005) and *Goudfrooij et al.* (2006), while radial profiles based on photometric and/or star-count measurements are taken from *McLaughlin and van der Marel* (2005), *Glatt et al.* (2009) and *Goudfrooij et al.* (2009, 2011, 2014). Good age and metallicity estimates are also required of clusters in our sample. Thus, we identified systems with adequate stellar photometry suitable to provide precise cluster age and (photometric) metallicity estimates from their color-magnitude diagrams (CMDs). We gave preference to clusters with deep *Hubble Space Telescope* (*HST*) photometry, but good-quality ground-based photometry was acceptable. Finally, in the spirit of providing a broad range of SSPs to test modeled M/L ratios, we chose clusters to span as broad a range in age and metallicity as practical within the Magellanic Clouds (see Figure 2.1). Although we include some ancient clusters (age $>$ 10 Gyr) in our sample, we have already noted that there are many dynamical studies and M/L estimates of GCs in the literature (e.g. *Larsen et al.*, 2002; *Lane et al.*, 2010b; *Strader et al.*, 2011; *Kimmig et al.*, 2015). At the other extreme, clusters younger than

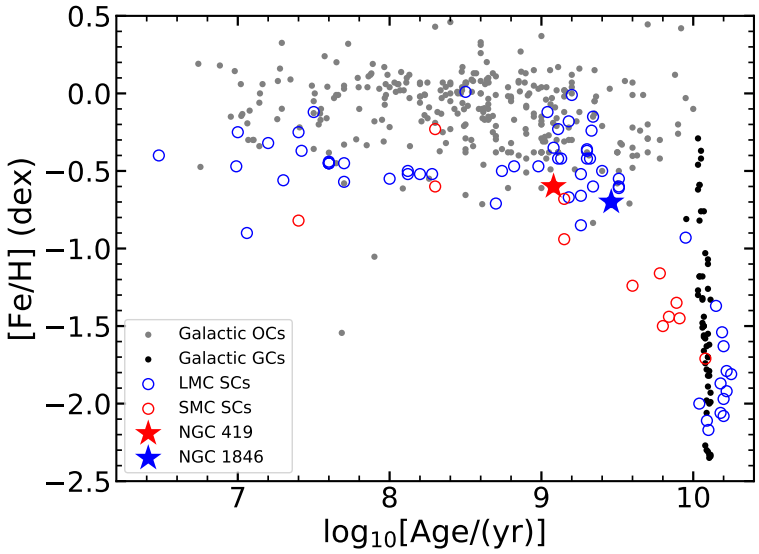

Figure 2.1: A plot of metallicity vs. log (Age) for star clusters (SCs) in the Milky Way and the Magellanic Clouds. Blue circles correspond to the SCs in the LMC (*Pessev et al.*, 2006, 2008), red circles correspond to the SCs in the SMC (*Pessev et al.*, 2006, 2008), black dots correspond to the Galactic GCs (*VandenBerg et al.*, 2013), and gray dots correspond to the Galactic open clusters (*Dias et al.*, 2002). The two clusters studied in this chapter, NGC 419 and NGC 1846, are marked as red and blue star-shaped symbols, respectively.

about 50 Myr were avoided as these may not yet have achieved dynamical equilibrium and hence would yield biased mass estimates. Our resulting sample from which we have drawn clusters to study in detail consists mostly of systems ranging in age from 50 Myr to 13 Gyr, and in [Fe/H] from −2.2 to +0.0 (see Figure 2.1).

The adopted photometric and structural parameters of the two clusters of this introductory study—NGC 419 and NGC 1846—are listed in Table 2.1. The aperture photometry for both clusters come from *Goudfrooij et al.* (2006), while structural profiles are taken from *Goudfrooij et al.* (2009) for NGC 1846, and from a weighted average of previous results (*Glatt et al.*, 2009; *Goudfrooij et al.*, 2014) for NGC 419. As listed in Table 2.2, the centers of NGC 419 and NGC 1846 were taken from *Glatt et al.* (2009) and Ma13, respectively.

For NGC 1846, *Olszewski et al.* (1991) derived a spectroscopic metallicity of

[Fe/H] $= -0.7 \pm 0.2$. The metallicity of NGC 419 was estimated through iron and hydrogen spectral indices calibrated using SSPs by *de Freitas Pacheco et al.* (1998) to be [Fe/H] $= -0.60 \pm 0.21$. Both clusters possess so-called extended main-sequence turnoffs (eMSTOs) confirmed from the photometric analysis of *HST* imaging. If taken as an internal age spread, these eMSTOs imply that the stellar populations of NGC 1846 span an age range of 1.6–1.9 Gyr (e.g., *Mackey and Broby Nielsen*, 2007; *Mackey et al.*, 2008), while for NGC 419 the implied age range is 1.2–1.6 Gyr (*Glatt et al.*, 2008). In the latter case, the specified range in age appears to represent primarily the age uncertainty rather than clear evidence of a composite stellar population (*Martocchia et al.*, 2017).

As noted in Chapter I, the specific selection of NGC 419 and NGC 1846 reflects the fact that both clusters have reasonably recent independent spectroscopic measurements of individual stars within and around the clusters (K18; Ma13). This provides an opportunity for us to critically compare our kinematic results for these clusters with these earlier studies. In the case of NGC 1846, which was observed in a manner similar to the present study but with a smaller sample, we can also compare our analysis by running the earlier data through our machinery to determine how well we recover previous results. For the case of NGC 419, we have an opportunity to compare our analysis and findings with MUSE observations (K18) to determine how the immense multiplexing, but relatively low spectral resolution, of that instrument compares to our smaller sample of target spectra obtained at considerably higher resolution. The focus here on the specific cases of NGC 419 and NGC 1846 also allows us to illustrate in a concrete manner some of the procedures common to all clusters in our M/L-ratio survey.

2.2.2 Selection of Targets Within Cluster Fields

For any given cluster in our study we typically selected a variety of specific types of targets for spectroscopic analysis. The primary science targets are typically drawn from the red giant branch (RGB) of a cluster's CMD. These targets are prioritized also by proximity to their respective cluster center. Additional science targets beyond the formal tidal radii of clusters are also included to allow us to determine the kinematic and chemical distribution of their nearby field populations. These latter targets are typically identified from different photometric studies than candidates close to the cluster centers. In all cases, we identified apparently isolated stars as potential spectroscopic targets. We typically also identify 'sky/background' positions both near the cluster centers and in their surrounding fields. We discuss how we use these to determine backgrounds below in Section 2.2.4.

In the specific cases of the clusters that are the focus of this chapter—NGC 419 and NGC 1846—we used the *HST* images from GO-10396 (NGC 419; PI: Gallagher) and from GO-10595 (NGC 1846; PI: Goudfrooij) to identify stars in the cluster centers. Both programs obtained relatively short exposures with the F555W and F814W filters (i.e., 40 s and 20 s for NGC 419, while 41 s and 9 s for NGC 1846). We photometered all the images using the ACS modules from the `DOLPHOT` package (*Dolphin*, 2000), and the output magnitudes were automatically transformed into the standard Johnson-Cousins VI system. The targets were mainly selected from the RGB in the corresponding $(V-I,\ V)$ CMDs (see the left panels in Figure 2.2). For regions around the clusters, we selected stars to characterize the superimposed field populations on the basis of their position beyond the clusters' tidal radii (the 'r_t' column in Table 2.1), and their location in the same RGB region of the CMD from which candidates cluster members were identified (see the right panels in Figure 2.2). For both clusters, the field stars were drawn from the Magellanic Clouds Photometric Survey (MCPS) $UBVI$ catalog (*Zaritsky et al.*, 2002, 2004). For all targets identified

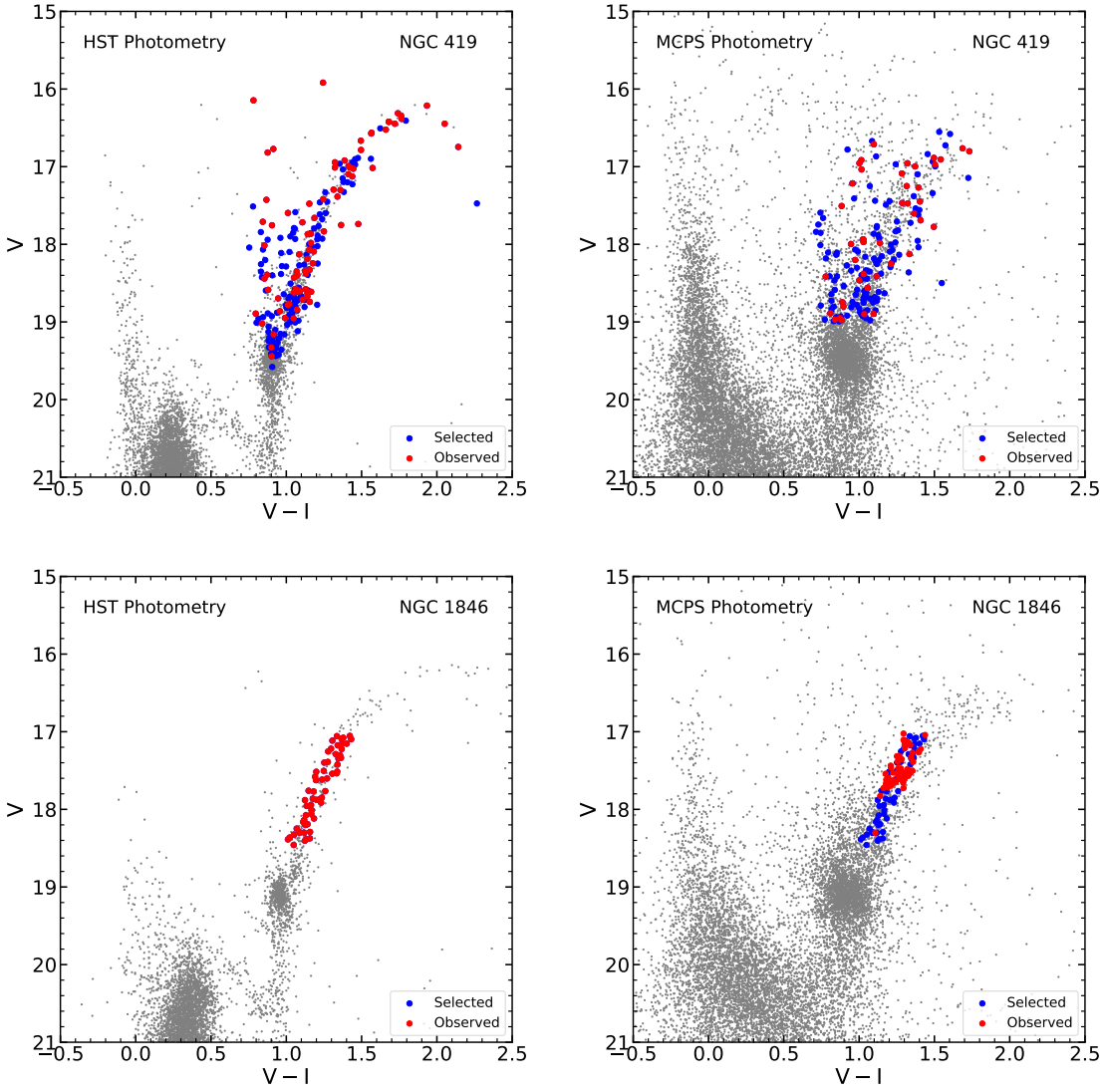

Figure 2.2: Color-magnitude diagrams for NGC 419 and NGC 1846 in the $(V-I,\, V)$ plane. The left panels based on *HST* photometry show the selection of potential targets in the cluster central regions. The right panels from the MCPS catalog (*Zaritsky et al.*, 2002, 2004) show the selection of potential targets in regions outside the tidal radii (see Section 2.2.2). In all panels, gray dots correspond to all the stellar objects from the respective photometric catalog. Colored (blue and red) dots represent targets selected for potential M2FS observation. The red dots denote the objects observed in this study.

Table 2.1: Archival Photometry and Structural Parameters

Cluster	$V_{\rm ap}$ (mag)	Aper. [a] (arcsec)	$(m-M)_0$ (mag)	A_V (mag)	$r_{0,\rm K62}$ (arcsec)	$r_{t,\rm K62}$ (arcsec)	Ref. [b]	$r_{0,\rm K66}$ (arcsec)	$r_{t,\rm K66}$ (arcsec)
NGC 419	10.30 ± 0.16	50	18.85 ± 0.03	0.15 ± 0.02	18.8 ± 6.9	129.7 ± 47.6	1, 2	...	...
	...	...	...	...	15.22 ± 1.78	174.15 ± 18.57	3	...	...
	...	...	...	...	12.98 ± 1.47	207.19 ± 30.11	3	...	...
	...	...	...	...	15.60 ± 1.66	275.91 ± 53.94	3	...	...
	10.30 ± 0.16	50	18.85 ± 0.03	0.15 ± 0.02	14.5 ± 0.9	185.0 ± 14.5	Avg.	14.9 ± 0.9	238.2 ± 18.7
NGC 1846	10.68 ± 0.20	50	18.42 ± 0.03	0.07 ± 0.02	26.0 ± 1.6	161.2 ± 9.9	1, 2, 4	26.9 ± 1.7	212.6 ± 13.0

[a] Radius of aperture used for integrated-light photometry.
[b] References: (1) *Goudfrooij et al.* (2006); (2) *Goudfrooij et al.* (2014); (3) *Glatt et al.* (2009); (4) *Goudfrooij et al.* (2009).

in clusters studied after the *Gaia* DR2 release (*Gaia Collaboration et al.*, 2016, 2018a), we selected only stars identified in that catalog. To minimize the contamination of nearby stars, only apparently isolated stars were accepted into our final candidate sample. We regarded a star to be isolated when the integrated flux of all other stars in the corresponding photometric catalog (*HST* or *Gaia* DR2) located within 1 arcsec of the star adds up to $\leq 20\%$ of the candidate star's flux.

Positions for targets selected and observed before the DR2 release were tied to the NOMAD astrometric system (*Zacharias et al.*, 2004). We cross-matched any stars brighter than 17.5 mag in V-band from *HST* images or MCPS catalog with stars in the NOMAD catalog, and transformed the coordinates onto the NOMAD frame. In some cases for *HST*-selected stars, rather large astrometric corrections of up to 1–2 arcsec were necessary. For reference, the M2FS fiber apertures are 1.2 arcsec in diameter, and systematic precision of 0.25 arcsec is typically required.

Individual background regions within the tidal radii of clusters were identified by eye from the F555W *HST* images when available. For the field regions beyond the clusters' tidal radii, background/sky positions were randomly chosen from the DSS red-band images and at least 2 arcmin from the clusters' centers. As noted below, we often supplemented these sky positions with an observational strategy to better determine the background contributions in the clusters and their surrounding fields.

2.2.3 Observations

The spectral data used in this chapter and throughout our M/L-ratio study have been obtained with the M2FS. This instrument can deploy up to 256 optical fibers in a 29-arcmin diameter field using aluminum plugplates pre-drilled for each target. As noted above, every fiber has a 1.2 arcsec entrance aperture. However, the ferrules in which the fiber are mounted imposes a minimum separation between adjacent fibers of 13 arcsec. The latter feature limits how densely we can pack fibers within the clusters' tidal radii; in practice, this limited the number of observable cluster candidate targets to about 100–140 per field, including sky positions and field stars.

The spectrograph in M2FS (MSpec) consists of twin spectrographs (denoted 'B' and 'R'), each capable of observing 128 targets simultaneously over selected regions within the spectral range 3700–9500 Å. For this project, one arm of MSpec (usually the 'B' arm) was configured to observe 128 targets in the so-called 'HiRes' mode, in which an interference filter is used to isolate a single order of the cross dispersed spectrum spanning 5130 to 5192 Å at an effective resolving power $\mathcal{R} \sim 18,000$ (see the left panel of Figure 2.3). The second spectrograph (the 'R' arm) produced spectra at similar resolution but used a much broader filter that passes 23 orders and covers the range 4058 to 5524 Å (see the right panel of Figure 2.3). In this mode, up to five targets can observed simultaneously, though in practice, one fiber is usually assigned to a background/sky fiber. For this study we only use the same order employed in the single-order spectra (B-arm) from these multi-order data (R-arm). We plan in our future paper to perform detailed chemical analysis of these R-arm spectra (see Section 6.2.2).

Our NGC 419 observations had few suitable background/sky fibers, so we supplemented these by obtaining spectra of fields offset by 5 arcsec from the nominal field position. These spectra were then used to estimate the background contribution in a manner described in detail in Section 2.2.4. This process allowed us to sample the lo-

Table 2.2: Observations

Cluster	α_{2000} (hh:mm:ss)	δ_{2000} (dd:mm:ss)	Obs. Date (UT)	Exp. Type	Exp. Time (s)	$N_{\rm HST}$	$N_{\rm MCPS}$	$N_{\rm sky}$
NGC 419	01:08:17.31	-72:53:02.5	2017 Sep 21	On target	4×2100	77	40	4
				Offset	2×480	0	0	121
NGC 1846	05:07:33.66	-67:27:40.7	2018 Feb 21	On target	4×1200	55	55	14

cal backgrounds for every target throughout the cluster and in the corresponding field. For NGC 1846 we relied on dedicated background/sky fibers (as described earlier in Section 2.2.2) to monitor the background. The full background-subtraction process (including normalization) and a third approach used for other clusters is described in detail below in Section 2.2.4.

Table 2.2 lists the full set of observations—including the offset exposures—used in this study. Though not detailed in the table, ThArNe arc calibration spectra were interleaved between science observations on a cadence of about 1 hour for the purpose of wavelength calibration. Additional calibration data (e.g. flats, aperture reference spectra, twilights, darks and biases) were obtained throughout the relevant M2FS runs when data for this chapter and our overall M/L-ratio study were obtained.

2.2.4 Data Reduction

All data were processed using an M2FS pipeline based on IRAF. The principal end products of this pipeline are the sky-subtracted spectra and their associated variances. Detailed reducing processes were thoroughly described in *Walker et al.* (2015b,a), and a brief description is available in *Song et al.* (2017). To summarize, raw 2-D data obtained on both the 'B' and 'R' arms of MSpec were processed through overscan, bias and dark corrections, the latter using combined bias and dark calibration images obtained throughout M2FS runs. For long science exposures, we then removed cosmic rays using the Laplacian filter algorithm developed by *van Dokkum* (2001). We then subtracted diffuse scattered light by fitting a moderate-order 2D surface to the inter-

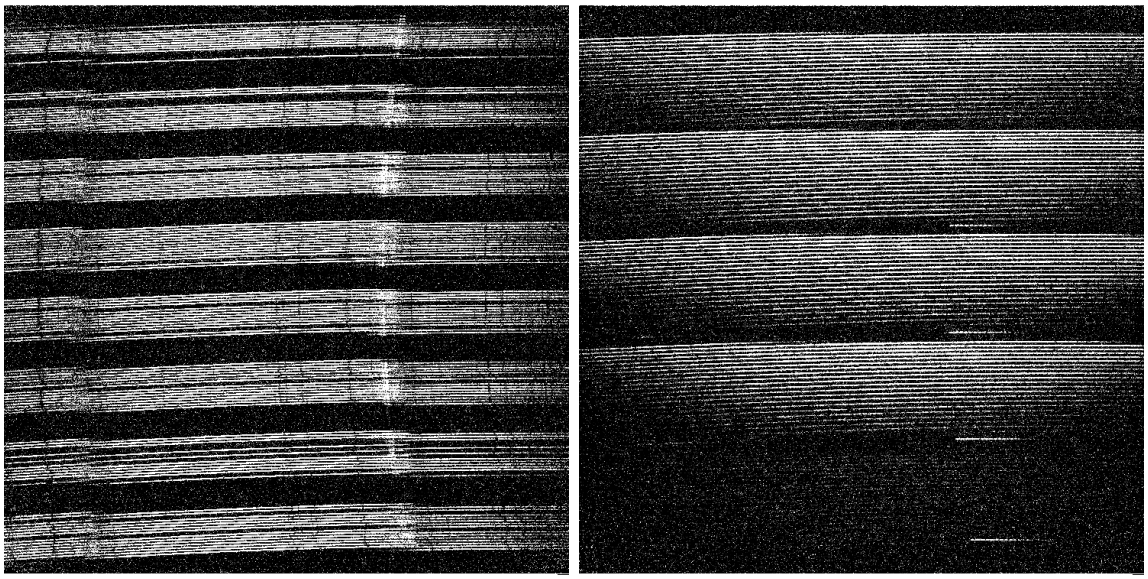

Figure 2.3: Reduced CCD images of 2-D M2FS spectra obtained from the field of the LMC star cluster NGC 1846. The images were reduced using the procedures described in Section 2.2.4. These two images show the differences between the spectra obtained from the B-arm (left panel) and R-arm (right panel) of MSpec. As described in Section 2.2.3, most of the observations for this thesis were obtained with the B-arm of MSpec configured to obtain single-order spectra of up to 128 stars in every exposure, while the R-arm was configured to observe five stars in a multi-order configuration. In the B-arm image (left panel), there are eight groups of 16 individual single-order spectra. The brighter spectra are stars, while the smaller number of faint spectra typically correspond to background/sky positions intentionally targeted to avoid any readily visible stars (see Section 2.2.3). Typically, only the central portions of these spectra (covering the wavelength range 5130–5192 Å) were analyzed. In the R-arm image (right panel), the five groups of spectra each corresponds to a single target for which about 23 usable spectral orders were obtained (covering the approximate range 4058–5524 Å). The four brighter sets of spectra are stellar targets, while the lower group with very faint spectra is of a targeted background/sky position (see Section 2.2.3). For this study, we used only the same order of these spectra as the one in the single-order spectra (5130–5192 Å).

spectral regions in the images. The reduced images of both B and R arms after this step are shown in Figure 2.3 for the case of NGC 1846. Using templates that map the locations and wavelengths along for every fiber/target in an image, the pipeline then extracted and wavelength calibrated the spectra from each fiber. All spectra were normalized to correct for fiber-to-fiber throughput variations using normalization factors obtained from twilight-sky exposures obtained with the fibers in the same spectral configuration used for the target observations. All subsequent reduction steps, including final background subtraction (see below), employed these normalized 1-D spectra.

The last reduction step is background/sky subtraction. At its simplest, this process uses a master sky spectrum produced from all non-contaminated background/sky spectra. This master spectrum typically accounts well for the backgrounds experienced by targets in the outer parts of the clusters and in the surrounding field. A complication is that the internal background light from unresolved/faint cluster stars must also be considered for targets within the clusters' tidal radii. To properly subtract the backgrounds for stars near the cluster centers requires consideration of the variations in the clusters' light backgrounds with distance from the cluster centers.

As noted in Section 2.2.2 and Section 2.2.3, we obtained background spectra for NGC 419 from both dedicated background/sky fibers placed at preselected positions (see Section 2.2.2) as well as from offset exposures. For NGC 1846, we only had background/sky measurements from fibers at pre-selected sky positions within the cluster and field regions. In both cases, we normalized the background/sky measurements with a radial light profile (see below) plus a constant background that was required to pass through the summed counts from the relevant background/sky observations. For NGC 419, the multiple background/sky data were suitable to quasi-independently constrain the background as a function of distance from the cluster center. We refer to this approach as 'Method A' for background removal (see Figure 2.4, left panel).

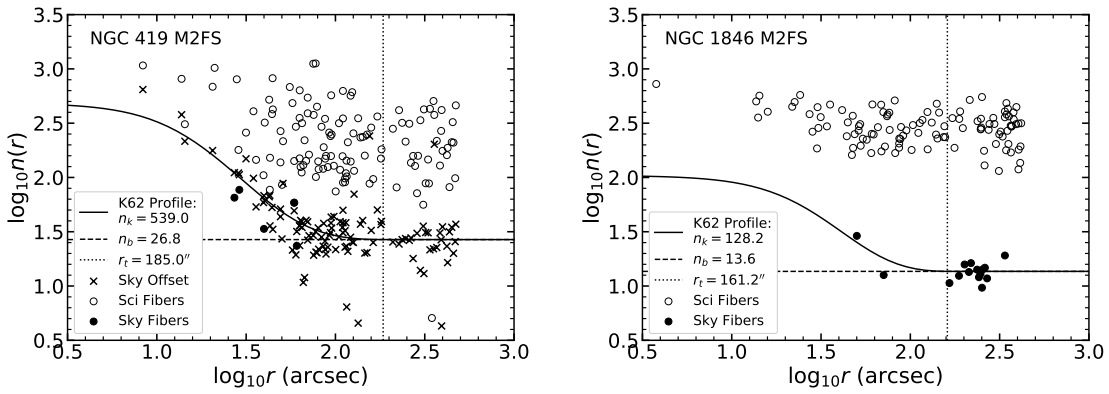

Figure 2.4: Plots of median counts in the spectra of stars in NGC 419 (left panel) and NGC 1846 (right panel) as a function of the stars' projected distances from their respective cluster centers. The adopted cluster centers are listed in Table 2.2. The solid lines correspond to K62 profiles used in the sky subtraction process (see Section 2.2.4). Open circles correspond to the target spectra. Closed circles correspond to dedicate sky spectra observed simultaneously with the targets. Crosses correspond to exposure-time-corrected median counts of sky spectra obtained through all the fibers while offsetting from on-target pointings (see Table 2.2 and Section 2.2.3). The meanings of the symbols in the K62 profile—n_k, n_b and r_t—are described in Section 2.2.4.

For NGC 1846, we adopted the central surface brightness and cluster core radius (Table 2.1) to fit the background/sky spectra ('Method B'; see Figure 2.4, right panel).

In both Method A and B, we start by fitting the median counts of the offset spectra (crosses in Figure 2.4) with a cluster profile assumed to be of the form given by the empirical density law described by *King* (1962, hereafter the K62 profile)

$$n(r) = n_k \left[\frac{1}{\sqrt{1 + (r/r_0)^2}} - \frac{1}{\sqrt{1 + (r_t/r_0)^2}} \right]^2 + n_b, \tag{2.1}$$

where r_0 is the King radius and r_t is the tidal radius. Two constants, n_k and n_b, account for the cluster's internal light (inside r_t) and field light (outside r_t), respectively. In our fitting process, n_k is the only free parameter to be determined. This is because n_b can be pre-determined as the average of the median counts of all offset spectra outside r_t, and we adopted r_0 and r_t listed in Table 2.1. The best-fit K62

profile for NGC 419—which uses Method A to determine n_k—is also plotted in the left panel of Figure 2.4.

For NGC 1846, no associated offset exposures were obtained and so we used Method 'B' for background determination in this case. Specifically, n_b was determined by calculating the median of the 13 sky-fiber outside the cluster's tidal radius, r_t. The value of n_k was determined by scaling from the value of n_k for NGC 419 (see Figure 2.4 for details). The specific scaling factor for n_k considered the ratio of the central surface brightnesses of the two clusters ($\Sigma_{V,0}$, which is constrained from aperture photometry given their K62 profiles using Equation 2.15) and the ratio of exposure times ($t_{\rm exp}$, see Table 2.2). For the general case, this procedure can be described by the equation

$$\frac{n_{k,\,\rm Target}}{n_{k,\,\rm Reference}} = \frac{\Sigma_{V,\,0,\,\rm Target}}{\Sigma_{V,\,0,\,\rm Reference}} \cdot \frac{t_{\rm exp,\,Target}}{t_{\rm exp,\,Reference}}, \tag{2.2}$$

where 'Target' refers to the system in which the background is to be estimated relative to a 'Reference' system; in the present case, NGC 1846 is the 'Target' and NGC 419 serves as the 'Reference'. So long as the data for the Target and Reference were obtained in similar conditions, this procedure will scale the non-cluster background to reasonable precision. If, for example, the photometric conditions for the Target/Reference observations are the same to 20%, since the background typically constitutes no more than 20% of the flux of individual stars, any errors in the background level should be at the ±5% level. The best-fit K62 profile obtained using this approach—Method 'B'—for NGC 1846 is shown in the right panel of Figure 2.4.

The actual background/sky subtraction was preformed as follows. First, all the sky spectra used for the n_b estimation were averaged to serve as the master sky spectrum. Then for every science spectra a scaling factor was determined by the best-fit K62 profile based on the target's projected distance from the cluster center. Finally, we multiplied this factor by the master sky spectrum to determine the background/sky

spectrum for each target and then subtracted this scaled spectrum from the respective target spectrum. Throughout this process, we calculated the variances associated with all spectra to rigorously track the signal-to-noise (S/N) ratio for each pixel. For every spectrum, we take the median over the full spectral range of the per-pixel S/N ratios to estimate the effective S/N ratio of a given spectrum.

Note that for both Methods 'A' and 'B', we presume the background spectra do not depend on position relative to the cluster centers. In reality, any off-target spectrum actually consists of contributions from telluric emission/scattered skylight and moonlight and unresolved/faint-star cluster light. Telluric backgrounds will be mostly constant across a field during an exposure while the cluster background contributions will depend on the light profile of the cluster and is therefore position-dependent. A careful accounting of the compound nature of the background in targets such as LMC clusters is typically beyond the scope of our data, since considerable sampling is required in the cluster centers. The extent to which we can do this in a few cases will be explored in a future paper in which we analyze data from a much larger sample of MC star clusters. For the current analysis of NGC 419 and NGC 1846, we have verified that background subtraction has little effect (< 0.2 km s^{-1} rms) on the kinematic results for individual stellar targets. We therefore restrict ourselves here to background-subtraction Methods 'A' and 'B' for NGC 419 and NGC 1846, respectively.

2.2.5 Previous Spectroscopic Samples for NGC 1846 and NGC 419

As noted in Chapter I and Section 2.2.1, prior to our study of NGC 1846, Ma13 published a spectroscopic results for 105 stars drawn from the RGB region of the cluster's CMD and one planetary nebula Mo-17. These data were obtained using the multi-object spectrograph FLAMES mounted at the ESO Very Large Telescope. With the full dataset of Ma13, we compared our analysis and results with theirs in

Section 2.4.2. As we shall see, these data also allowed us to expand the kinematic sample for NGC 1846 by combining it with our M2FS results. We describe how we combined both datasets in Section 2.3.1.2. For NGC 419, the full data for individual stars observed with MUSE (K18) are not available. As a result, the comparison of the MUSE and our new M2FS results has been confined to higher-level conclusions. A full discussion of those comparisons is also provided in Section 2.4.

2.3 Spectral and Kinematic Analysis

2.3.1 Bayesian Fitting of M2FS Spectra

We have employed the Bayesian method introduced by *Walker et al.* (2015b,a) to analyze the sky-subtracted spectra produced using the procedures described in the previous section. The template spectra for these fits are taken from the SSPP library of stellar model atmospheres (*Lee et al.*, 2008a,b; *Walker et al.*, 2015b). The output of these fits are estimates of the line-of-sight (LOS) velocity ($v_{\rm los}$), surface gravity ($\log g$) and metallicity ([Fe/H]) from individual and combined spectra; a full listing of all parameters provided by the analysis are summarized in Table 2 of *Walker et al.* (2015b). One difference in our present application of this approach is that the effective temperature ($T_{\rm eff}$) was pre-determined by the $V-I$ color and fixed as a constant during the fitting procedure (see *Song et al.* 2017 for details). The present analysis also differs from *Song et al.* (2017) in that we have adopted an extended wavelength range (5130–5192 Å) to reflect a change in the observing parameters that exclude some nuisance spectral ghosts from the red ends of the target spectra. For both NGC 419 and NGC 1846, we have fitted the spectra obtained from individual exposures as well as the spectra extracted from images consisting of the wavelength-calibrated sums of these individual exposures.

We corrected all the LOS velocities to the barycentric frame using the values cal-

Table 2.3: Fits to the Twilight Spectra[a]

Obs. Date (UT)	$T_{\rm eff}$ [b] (K)	$\overline{v_{\rm los,raw}}$ ($\rm km\,s^{-1}$)	$\overline{v_{\rm los,helio}}$ ($\rm km\,s^{-1}$)	$\sigma_{\overline{v_{\rm vlos}}}$ ($\rm km\,s^{-1}$)	$\overline{\log g}$ (dex)	$\sigma_{\overline{\log g}}$ (dex)	$\overline{\rm [Fe/H]}$ (dex)	$\sigma_{\overline{\rm [Fe/H]}}$ (dex)
2017 Sep 21	5778	-1.30	-0.40	0.17	4.45	0.04	-0.22	0.02
2018 Feb 16	5778	+0.29	-0.45	0.13	4.38	0.03	-0.18	0.02

[a] The solar values are $T_{\rm eff,\odot} = 5778$ K, $\log g_\odot = 4.44$ and $\rm [Fe/H]_\odot = 0.0$.
[b] The values of $T_{\rm eff}$ were fixed during our spectral fitting process (see Section 2.3.1).

culated by the 'radial_velocity_correction' function from Astropy. (We have compared the Astropy heliocentric corrections with those from independent algorithms, and we find agreement at the m/s level.) As a check on our zero points, we applied the same Bayesian fitting procedure to twilight spectra obtained during the same observing runs (and often the same nights) as the target spectra. These were used to identify any systematic offsets in $\log g$ and [Fe/H] (as for our target spectra, we fixed the solar effective temperature to its standard value of 5778 K). The twilight results are listed in Table 2.3. We have corrected all science $\log g$ and [Fe/H] values by the small offsets listed in the table. We have not corrected the heliocentric $v_{\rm los}$ offsets listed in Table 2.3 for two reasons. First, the offsets are comparable to the uncertainties in the systemic velocities of the clusters (see Table 2.6). Second, the heliocentric offsets are nearly identical for the two runs in which the data were obtained for NGC 419 and NGC 1846. Consequently, the velocity offsets in Table 2.3 represent a negligible shift in $v_{\rm los}$ that we chose to ignore.

2.3.1.1 Uncertainties in the LOS Velocities

Given the anticipated small internal velocity dispersions of our target clusters, it is crucial to precisely estimate the uncertainties of our radial velocity measurements. To do this, we have compared for every target the LOS velocities obtained from the individual exposures to measure two statistics that we have used to quantify the velocity uncertainties as a function of mean spectral S/N. As noted in Table 2.2, we obtained

four individual exposures of science targets for both NGC 419 and NGC 1846.

The first of these statistics is the standard reduced χ-square. For the full datasets of a given cluster, we define this as

$$\chi^2_\nu = \frac{1}{\nu} \sum_{i=1}^{N} \sum_{j=1}^{4} \frac{(v_{i,j} - \bar{v}_i)^2}{\varepsilon_{i,j}}, \tag{2.3}$$

where $\varepsilon_{i,j}$ is the j-th velocity error of the i-th target, $\bar{v}_i$ is the weighted average velocity of the individual velocities of the i-th target, and $\nu = N(n-1)$ is the total degree of freedom of this sample. For NGC 419, $\chi^2_\nu = 1.54$, while for NGC 1846, $\chi^2_\nu = 1.25$.

The second statistic we employed was taken from *Kamann et al.* (2016) and is defined as

$$\delta v_{12} = \frac{v_2 - v_1}{\sqrt{\varepsilon^2_{v_1} + \varepsilon^2_{v_2}}}, \tag{2.4}$$

where v_1 and v_2 are a pair of repeat velocity measurements with the uncertainty of ε_{v_1} and ε_{v_2}, respectively. The velocity uncertainties (ε_v) can be considered to be well-estimated when δv_{12} is normally distributed with a standard deviation of one. Histograms of δv_{12} are shown in the bottom panels of Figure 2.5, and the standard deviations ($\sigma_{\delta v_{12}}$) of δv_{12} distributions are 1.22 and 1.11 for NGC 419 and NGC 1846, respectively.

Both statistics indicate that the individual velocity uncertainties obtained from our Bayesian fits were underestimated by approximately 23% and 12% for NGC 419 and NGC 1846, respectively. After applying correction factors of 1.23 and 1.12, respectively, we find that $\chi^2_\nu = 1.02$ and $\sigma_{\delta v_{12}} = 1.00$ for NGC 419, and $\chi^2_\nu = 1.00$ and $\sigma_{\delta v_{12}} = 1.00$ for NGC 1846. The median velocity uncertainties for the samples of NGC 419 and NGC 1846 are 0.38 and 0.22 $\mathrm{km\,s^{-1}}$, respectively. The final barycentric LOS velocities of NGC 419 and NGC 1846 are listed in Table 2.4 and Table 2.5, respectively, along with their corrected uncertainties. The table also lists the photo-

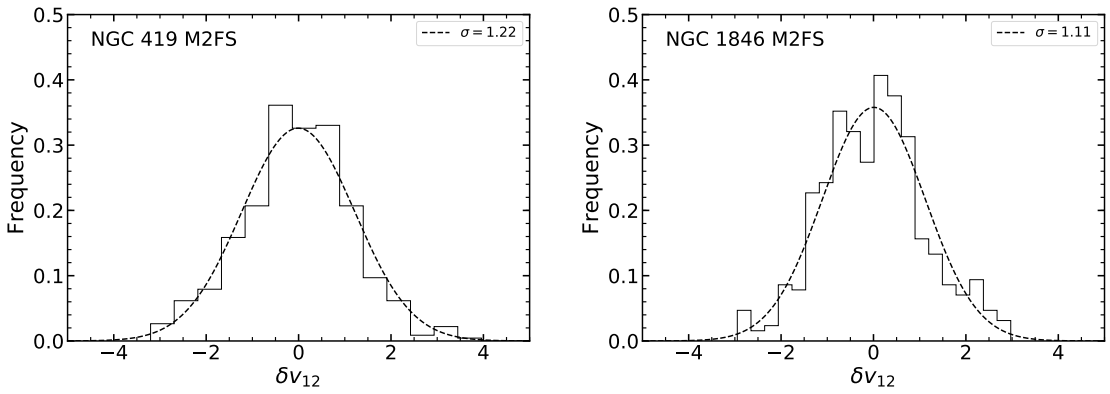

Figure 2.5: Measured line-of-sight (LOS) velocity differences for targets observed in individual M2FS exposures (see Section 2.3.1.1 and Table 2.2). The parameter δv_{12}—defined in Equation 2.4—represents the differences in measured velocities from individual exposures for a given star. The dashed lines are Gaussian fits to the histograms, and the standard deviation of each fitted Gaussian are given in the legend of each panel. In this figure, we have combined results for all stars regardless of the mean S/N of their spectra.

metric data for every target taken from our measurements of *HST* data or the MCPS photometry of *Zaritsky et al.* (2002, 2004) for NGC 419 and NGC 1846. respectively.

The analysis above assumes that all targets are non-variable and that their velocity uncertainties scale with S/N in the same systematic manner. Figure 2.6 is a plot of the corrected velocity uncertainty as a function of the spectral S/N ratio. It is evident that in both clusters a few stars deviate from the clear relationship between velocity uncertainty and S/N. These outliers have been confirmed to be either carbon stars (see Figure 2.7 for representative spectra) or multiple stars too close together to be separated in any of the photometric/astrometric catalogs we used to identify targets, resulting in a composite spectrum. The extracted spectra of these stars are shown in Figure 2.8 and they are noted explicitly in Figure 2.6). At a given S/N, such stars always have larger uncertainties than other targets due to the fact that (a) carbon star spectra are not incorporated in the SSPP stellar library (*Lee et al.*, 2008a,b; *Walker et al.*, 2015b) used in our spectral fitting procedure, and (b) the fitting procedure assumes a single star and will be compromised when the spectrum

Table 2.4: M2FS Sample of NGC 419 (The full table is available in Appendix A)

ID	α_{2000} (h:m:s)	δ_{2000} (d:m:s)	V (mag)	$V-I$ (mag)	$v_{\rm los}$ ($\rm km\,s^{-1}$)	P_{M_i}	Sel. [a]
N419-1-b001	01:08:44.19	-73:00:40.0	16.887 ± 0.047	1.497 ± 0.055	188.41 ± 0.20	0.00	M
N419-1-b002	01:08:46.07	-72:56:35.2	17.942 ± 0.030	1.024 ± 0.056	192.79 ± 0.42	0.00	M
N419-1-b003	01:08:45.46	-72:55:15.4	17.982 ± 0.030	1.138 ± 0.043	153.30 ± 0.39	0.00	M
N419-1-b004	01:08:43.26	-72:53:32.0	18.014 ± 0.008	0.855 ± 0.010	193.60 ± 0.61	0.06	H
N419-1-b005	01:08:42.25	-72:53:12.3	18.769 ± 0.010	1.019 ± 0.013	144.09 ± 1.05	0.00	H
...							

[a] Photometric source that the target were selected from: H stands for *HST* and M stands for MCPS.

Table 2.5: Combined Sample of NGC 1846 (The full table is available in Appendix B)

ID	α_{2000} (h:m:s)	δ_{2000} (d:m:s)	V (mag)	$V-I$ (mag)	$v_{\rm los}$ ($\rm km\,s^{-1}$)	P_{M_i}	Sel. [a]	Spec. [b]
N1846-1-b001	05:07:51.21	-67:33:03.8	17.251 ± 0.307	1.396 ± 0.310	287.97 ± 0.19	0.00	M	M2FS
...								
N1846-1-r049	05:07:32.21	-67:27:51.6	17.154 ± 0.004	1.401 ± 0.006	241.93 ± 0.26	1.00	H	M2FS
N1846-1-r079	05:07:30.12	-67:27:27.7	17.115 ± 0.004	1.306 ± 0.006	238.29 ± 0.17	1.00	H	COMB
...								
ACS-013-R	05:07:33.59	-67:26:41.2	16.99	1.43	238.10 ± 0.46	1.00	H	M13
ACS-019-R	05:07:14.49	-67:28:16.4	...	...	278.73 ± 0.47	0.00	H	M13
...								
MCPS-007	05:05:34.36	-67:26:34.2	16.810 ± 0.063	1.622 ± 0.079	253.77 ± 0.85	0.00	M	M13
...								

[a] Photometric source that the target were selected from: H stands for *HST* and M stands for MCPS.
[b] Spectroscopic source the LOS velocities were measured from: M2FS stands for this work, M13 stands for *Mackey et al.* (2013), and COMB stands for combined.

is actually composite.

We have chosen to ignore the carbon stars because of their larger uncertainties and the likelihood that they are velocity variable. In the case of the blended stars, we have carried out two-star fits with reasonably satisfactory results. However, in all cases, these composite cases appear to be non-members as both velocities are far from the mean velocities of their respective clusters and the velocity differences are too large for them to be plausible red-giant binaries. For these reasons, we have chosen not to include any of these stars (four in each cluster sample) in any of the subsequent analyses described in this chapter. Note that we retroactively removed these stars from the velocity uncertainty estimation described above; that analysis includes only what we consider to be spectra of 'normal,' unblended red giants.

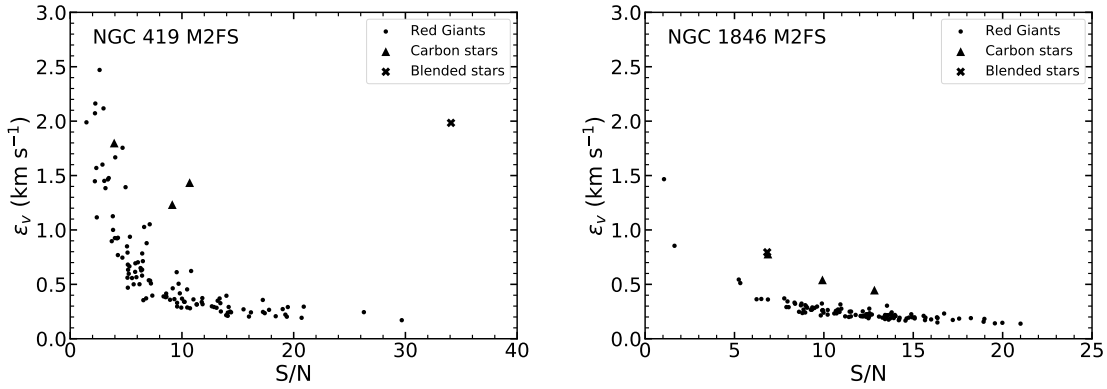

Figure 2.6: Corrected LOS velocity uncertainties vs. median S/Ns per pixel for NGC 419 and NGC 1846. The dots correspond to normal red giants in the samples, while the triangles correspond to carbon stars and the crosses to the blended stars (see Section 2.3.1.1 and Figure 2.8).

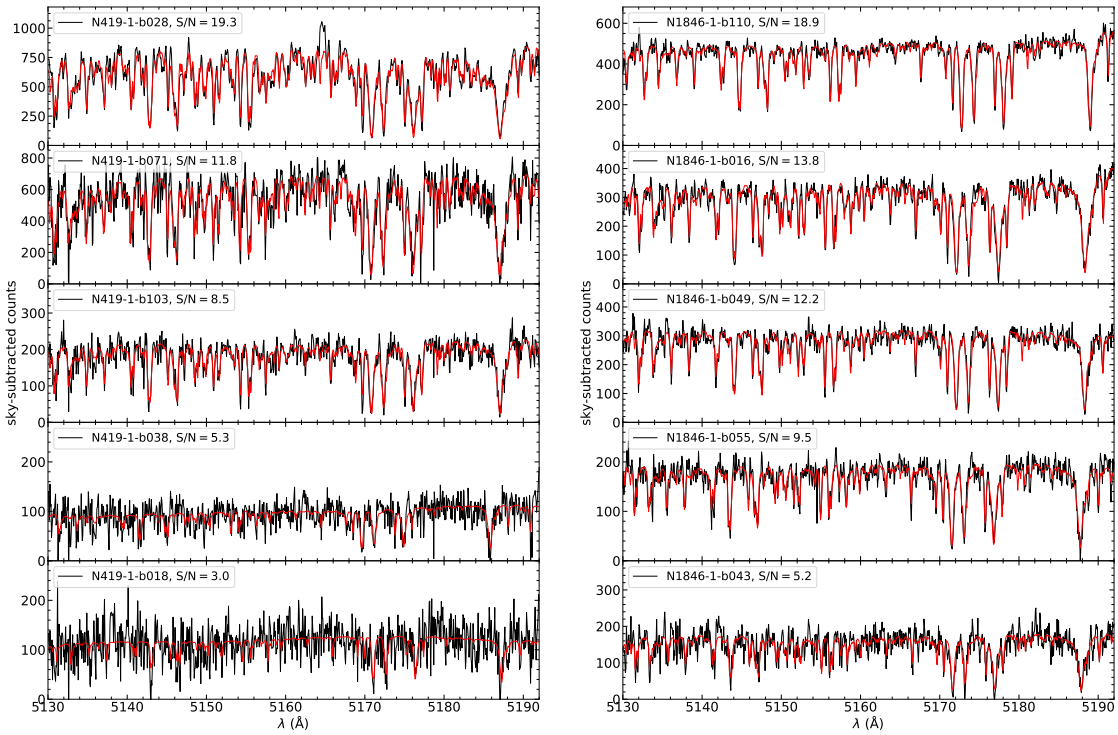

Figure 2.7: Representative M2FS spectra (black) for five stars observed with M2FS in NGC 419 (left panels) and five stars observed with M2FS in NGC 1846 (right panels).The spectra have been corrected for backgrounds as described in Section 2.2.4. The red lines are the best-fitting spectral models described in Section 2.3.1. The legend lists target ID and median S/N per pixel. The spectra shown here span the full range of S/N of M2FS spectra obtained in this study.

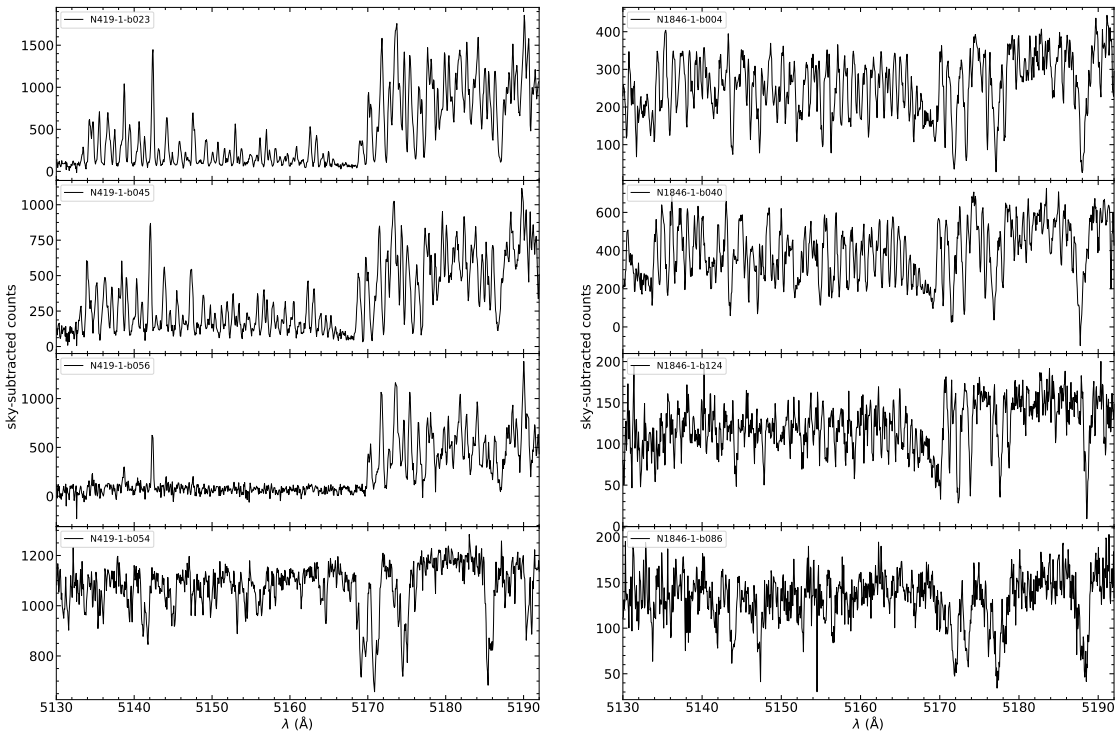

Figure 2.8: M2FS spectra of carbon stars and blended stars in NGC 419 (left panels) and NGC 1846 (right panels) noted in Figure 2.6. The top three panels for each cluster show the spectra of the carbon stars. The bottom panel for each cluster show the spectra of objects with clearly blended spectra from (at least) two unrelated stars (see Section 2.3.1.1). None of the targets corresponding to these spectra were used in our dynamical analyses of either cluster. As noted in Section 2.3.1.1, none of the individual stars (four in total) within the blended spectra are likely members of either cluster.

2.3.1.2 Combined Sample for NGC 1846

Our M2FS sample for NGC 1846 consists of 108 targets with useful spectra. As it happens, 17 of the stars in this group are in common with the dataset from Ma13. As shown in Figure 2.9, apart from one exception among these common stars, the velocity differences from our analysis as Ma13 was found to be small and stable; the exception was a star for which we measure a velocity difference $+5.58$ km s^{-1} between the two datasets. Specifically, Ma13 measured 243.39 ± 0.57 km s^{-1} and we measured 237.81 ± 0.17 km s^{-1} with M2FS for two independent measurements of this star taken 9.23 years apart. The latter star is almost certainly a true binary; its spectrum is not obviously composite and its implied velocity amplitude of a few $km\,s^{-1}$ over a period of about 5 years is consistent with a main-sequence companion slightly less massive than the red giant that dominates the spectrum. For the other 16 stars common to the two samples, we find a small but significant velocity difference of -0.54 ± 0.15 km s^{-1} in the sense Ma13 *minus* M2FS. The scatter in this mean offset is small and entirely consistent with the combined median uncertainties of the Ma13 sample (0.57 km s^{-1}) and the M2FS sample (0.30 km s^{-1}). Consequently, we have defined a 'Combined Sample' consisting of the Ma13 sample corrected by the velocity difference noted above (Figure 2.9). For the stars in common to the two samples, we have calculated their error-weighted mean velocities and velocity uncertainties; these stars are noted and their weighted mean values listed in Table 2.5; all other stars from Ma13 but not in our M2FS sample are also noted in this table. The final Combined Sample for NGC 1846 contains 196 stellar targets, including the binary star.

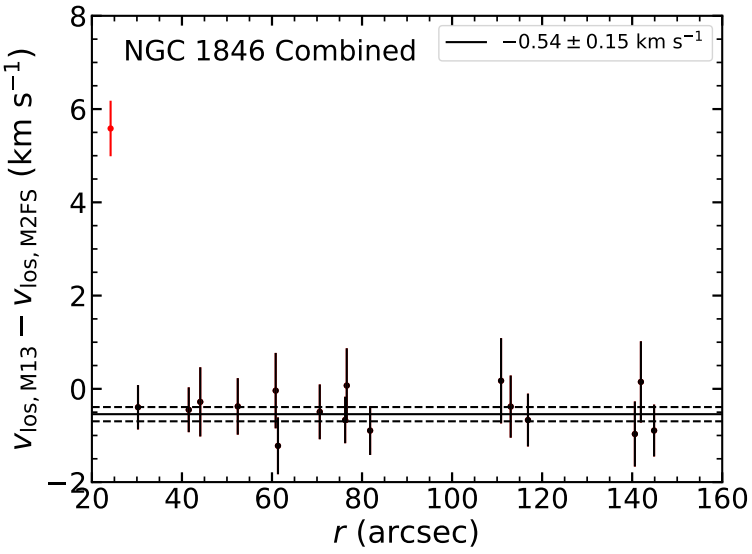

Figure 2.9: Differences of the LOS velocities measured for 17 stars in NGC 1846 in common to the present study and Ma13. The solid line and two dashed lines show the uncertainty-weighted mean and 1σ uncertainty for the 16 stars, respectively. The 17th star—a probable spectroscopic binary—is marked in red and has been excluded in the calculation of the mean and 1σ uncertainty velocity offset (see Section 2.3.1.2).

2.3.2 Systemic Velocity and Velocity Dispersion

2.3.2.1 The EM alogrithm

We used an expectation-maximization (EM) algorithm (*Walker et al.*, 2009; *Kimmig et al.*, 2015) to simultaneously constrain the systemic velocity and the model-dependent central velocity dispersion of each cluster. This method, which can efficiently distinguish cluster members from field stars, iteratively determines the cluster membership probability for each star considering whether its velocity and location is consistent with a selected dynamical model. As this process iterates, membership probabilities and the parameters of the selected model are updated until a convergence criterion is achieved.

In our implementation of this approach, we constrained the systemic velocity and the projected central velocity dispersion of the cluster from its member population, simultaneously with the mean velocity and the velocity dispersion of the field stellar

population (that is, nonmembers). In the present case, the EM analysis of the kinematic and positional data for targets of a given cluster involves the estimation of four parameters

$$\zeta \equiv \{\langle V\rangle_{\rm mem}, \sigma^2_{V_0,{\rm mem}}, \langle V\rangle_{\rm non}, \sigma^2_{V_0,{\rm non}}\}. \tag{2.5}$$

These refer to the mean velocities and velocity dispersions of the cluster (member, 'mem') and field (non-member, 'non') populations assumed to comprise our kinematic samples. The expected log-likelihood used in the EM approach and given our data can be written as

$$\begin{aligned} E(\ln \mathcal{L}(\zeta)|S) &= \sum_{i=1}^{N} P_{M_i} \ln\Big[p_{\rm mem}(V_i)p(r_i)\Big] \\ &+ \sum_{i=1}^{N}(1-P_{M_i})\ln\Big[p_{\rm non}(V_i)[1-p(r_i)]\Big], \end{aligned} \tag{2.6}$$

where $S \equiv \{V_i,\, \varepsilon_{V_i},\, r_i\}_{i=1}^{N}$ represents the full dataset, P_{M_i} is a normalized cluster-membership probability of the i-th star, and $p_{\rm mem}(V_i)$ and $p_{\rm non}(V_i)$ are the cluster membership and non-membership probabilities of the same star. The term $p(r_i)$, referred as the 'unconditional probability function' by *Walker et al.* (2009), represents a non-increasing component of the membership probability that considers the observational selection, the assumed dynamical model, and the uncertainty of the extent of a cluster.

One iteration of the EM algorithm starts with the expectation step (E step) and ends with the maximization step (M step). In the E step, P_{M_i} is estimated from a combination of $p_{\rm mem}(V_i)$, $p_{\rm non}(V_i)$ and $p(r_i)$ through

$$\begin{aligned} P_{M_i} &\equiv P(M_i = 1|V_i, r_i) \\ &= \frac{p_{\rm mem}(V_i)p(r_i)}{p_{\rm mem}(V_i)p(r_i) + p_{\rm non}(V_i)[1-p(r_i)]}, \end{aligned} \tag{2.7}$$

where

$$p_{\rm mem}(V_i) = \frac{\exp\left[-\frac{1}{2}\left(\frac{[V_i-\langle V\rangle_{\rm mem}]^2}{\sigma^2_{V_0,{\rm mem}}+\varepsilon^2_{V_i}}\right)\right]}{\sqrt{2\pi(\sigma^2_{V_0,{\rm mem}}+\varepsilon^2_{V_i})}}, \tag{2.8}$$

and

$$p_{\rm non}(V_i) = \frac{\exp\left[-\frac{1}{2}\left(\frac{[V_i-\langle V\rangle_{\rm non}]^2}{\sigma^2_{V_0,{\rm non}}+\varepsilon^2_{V_i}}\right)\right]}{\sqrt{2\pi(\sigma^2_{V_0,{\rm non}}+\varepsilon^2_{V_i})}}. \tag{2.9}$$

The term $p(r_i)$ in our study has the format of

$$p(r_i) = p_{\rm dyn}(r_i)\cdot \min_{1\le u\le i}\left[\max_{i\le v\le N}\frac{\Sigma_{j=u}^{v}P_{M_j}}{v-u+1}\right], \tag{2.10}$$

where the first part makes sure that a member star must be located within its tidal radius, i.e.

$$p_{\rm dyn}(r_i) = \begin{cases} 1 & \text{if } r_i \le r_t \\ 0 & \text{if } r_i > r_t \end{cases}, \tag{2.11}$$

while the second part reflects the non-increasing feature of $p(r_i)$ that follows the discussion by *Walker et al.* (2009).

In the M step, both $p(r_i)$ and ζ are updated so that they are on track to converge to the best-fit results. To update $p(r_i)$, we simply recalculate Equation 2.10. For the member parts in ζ, we have the following equation pair

$$\langle V\rangle_{\rm mem} = \frac{\sum_{i=1}^{N}\frac{P_{M_i}V_i}{1+\varepsilon^2_{V_i}/\sigma^2_{V_0,{\rm mem}}}}{\sum_{i=1}^{N}\frac{P_{M_i}}{1+\varepsilon^2_{V_i}/\sigma^2_{V_0,{\rm mem}}}}, \tag{2.12}$$

and

$$\sigma^2_{V_0,{\rm mem}} = \frac{\sum_{i=1}^{N}\frac{P_{M_i}[V_i-\langle V\rangle_{\rm mem}]^2}{(1+\varepsilon^2_{V_i}/\sigma^2_{V_0,{\rm mem}})^2}}{\sum_{i=1}^{N}\frac{P_{M_i}}{1+\varepsilon^2_{V_i}/\sigma^2_{V_0,{\rm mem}}}}, \tag{2.13}$$

while $\langle V \rangle_{\rm non}$ and $\sigma^2_{V_0,{\rm non}}$ are in the same forms as in the pair above but with P_{M_i} replaced by $(1 - P_{M_i})$.

When considering the dynamical model of a cluster, $\sigma_{V_0,{\rm mem}}$ should be replaced by $\sigma_{\rm dyn}(r_i)\sigma_{V_0,{\rm mem}}$, where the additional factor $\sigma_{\rm dyn}(r_i)$ represents the projected velocity dispersion profile of a cluster with a central value of 1 $\mathrm{km\,s^{-1}}$. Thus Equation 2.13 becomes

$$\sigma^2_{V_0,{\rm mem}} = \frac{\sum_{i=1}^{N} \frac{P_{M_i}[V_i - \langle V \rangle_{\rm mem}]^2}{\{1 + \varepsilon^2_{V_i}/[\sigma_{\rm dyn}(r_i)\sigma_{V_0,{\rm mem}}]^2\}^2}}{\sum_{i=1}^{N} \frac{P_{M_i}\sigma^2_{\rm dyn}(r_i)}{1 + \varepsilon^2_{V_i}/[\sigma_{\rm dyn}(r_i)\sigma_{V_0,{\rm mem}}]^2}}. \tag{2.14}$$

In the present analysis we have adopted single-mass King models (*King*, 1966, K66) to generate $\sigma_{\rm dyn}(r_i)$. The structural parameters of a K66 model were transformed from those of the best-fit K62 profile, under the assumption that both agreed on three basic parameters of a surface brightness profile: the central value, the core radius where the value is half of the central value, and the total luminosity. The transformed K66 parameters derived from the K62 parameters we adopted in Section 2.2.4 are also listed in Table 2.1. In actual practice, we used the code `LIMEPY` (*Gieles and Zocchi*, 2015) to calculate the appropriate K66 models based on the transformed K62 parameters listed for both NGC 419 and NGC 1846 in Table 1.

At the start of the EM analysis for any dataset, we initialized $p(r_i) = 0.5$ and $P_{M_i} = 0.5$ for all stars and estimated the initial membership parameters in ζ from the stars within its K66 tidal radius and assumed non-membership for the rest. We iterated until a convergence criterion of $\Delta\zeta/\zeta < 1 \times 10^{-5}$ from one iteration to the next. Typically this condition was satisfied within 10-20 iterations. The errors on ζ are estimated via bootstrapping, in which 1000 realizations are randomly sampled from the original dataset.

We illustrate all key aspects of the EM analysis in Figure 2.10. The top panels compare the membership probabilities $P_{\rm M}$ with the $p(r_i)$ profiles, while the bottom

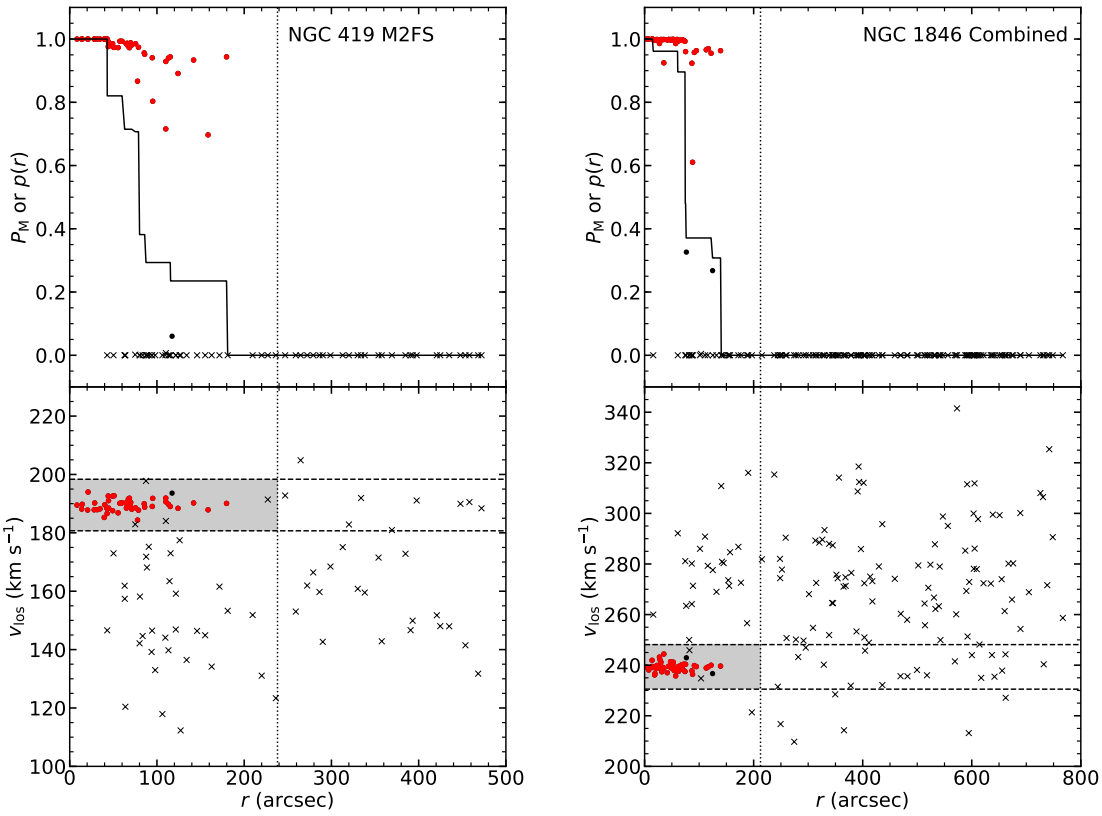

Figure 2.10: Membership probabilities (top) and LOS velocities (bottom) for stars as a function of the projected distance from their respective cluster centers. The adopted cluster centers are listed in Table 2.2. The top panels show the unconditional probability function $p(r)$ (solid line) from the EM algorithm (see Section 2.3.2.1). The shaded regions in the bottom panels denote the 'box' regions we defined in Section 2.3.2.2. Red dots correspond to stars with $P_{\rm M} \geq 0.5$, black dots correspond to stars with $0.05 \leq P_{\rm M} < 0.5$, and crosses correspond to stars with $P_{\rm M} < 0.05$. The vertical lines denote the locations of the tidal radii.

Table 2.6: Velocity and Dispersion Results from the EM method

Cluster	Dataset	Binary?[a]	RC[b]	$V_{\rm sys}$ ($\rm km\,s^{-1}$)	$\sigma_{\rm p,\,0}$ ($\rm km\,s^{-1}$)	$V_{\rm field}$ ($\rm km\,s^{-1}$)	$\sigma_{\rm field}$ ($\rm km\,s^{-1}$)	$N_{\rm total}$	$N_{\rm tidal}$
NGC 419	M2FS	...	N	$189.5^{+0.3}_{-0.3}$	$2.42^{+0.41}_{-0.27}$	$160.3^{+2.8}_{-2.7}$	$21.7^{+1.4}_{-1.6}$	111	83
	M2FS	...	Y	$189.5^{+0.3}_{-0.3}$	$2.20^{+0.33}_{-0.19}$	$160.6^{+2.8}_{-2.7}$	$21.7^{+1.1}_{-1.8}$	111	83
NGC 1846	Combined	N	N	$239.3^{+0.2}_{-0.2}$	$2.05^{+0.32}_{-0.30}$	$269.5^{+2.2}_{-2.0}$	$25.2^{+1.4}_{-1.5}$	195	80
	Combined	N	Y	$239.3^{+0.3}_{-0.2}$	$1.94^{+0.29}_{-0.24}$	$269.5^{+2.2}_{-2.0}$	$25.2^{+1.2}_{-1.5}$	195	80
	Combined	Y	N	$239.3^{+0.2}_{-0.2}$	$2.02^{+0.33}_{-0.31}$	$269.5^{+2.2}_{-2.0}$	$25.2^{+1.4}_{-1.4}$	196	81
	M2FS	Y	N	$239.3^{+0.3}_{-0.3}$	$1.85^{+0.28}_{-0.26}$	$268.4^{+3.1}_{-2.8}$	$24.6^{+1.8}_{-2.4}$	108	69
	M2FS	Y	Y	$239.3^{+0.2}_{-0.2}$	$1.79^{+0.29}_{-0.35}$	$268.3^{+3.3}_{-3.1}$	$24.6^{+1.9}_{-2.4}$	108	69
	Ma13	N	N	$238.6^{+0.5}_{-0.5}$	$2.27^{+0.64}_{-0.83}$	$270.4^{+2.9}_{-2.9}$	$25.5^{+1.5}_{-2.0}$	105	29
	Ma13	N	Y	$239.0^{+0.5}_{-0.5}$	$2.13^{+0.42}_{-0.31}$	$270.4^{+3.0}_{-2.8}$	$25.5^{+1.4}_{-1.9}$	105	29
	Ma13	Y	N	$238.9^{+0.5}_{-0.6}$	$2.59^{+0.47}_{-0.68}$	$270.5^{+2.7}_{-2.9}$	$25.5^{+1.4}_{-2.0}$	106	30
	Ma13	Y	Y	$239.2^{+0.4}_{-0.5}$	$2.15^{+0.33}_{-0.29}$	$270.5^{+2.9}_{-2.6}$	$25.5^{+1.6}_{-1.9}$	106	30

[a] This flag denotes whether the confirmed binary star in NGC 1846 is excluded (N) or included (Y). This star is 'N1846-1-r079' in Table 2.5, and the individual velocities are summarized in Section 2.3.1.2 and Figure 2.9.
[b]This flag indicates whether the rotational correction described in Section 2.3.4 was applied.

panels plot radial velocity versus distance from the center of each cluster. In both panels, all targets are marked differently by their P_{M_i}: red dots correspond to those with $P_{\rm M} \geq 0.5$, black dots correspond to those with $0.05 \leq P_{\rm M} < 0.5$, and black crosses correspond to those with $P_{\rm M} < 0.05$. Table 2.6 lists the best-fit results in the form of $\zeta = \{V_{\rm sys}, \sigma_{\rm p,0}, V_{\rm field}, \sigma_{\rm field}\}$, where now $V_{\rm sys}$ is the systemic cluster velocity, $\sigma_{\rm p,0}$ is the projected cluster central velocity dispersion, $V_{\rm field}$ is the mean velocity of the field population, and $\sigma_{\rm field}$ is the projected velocity dispersion of the field population. The table also lists the total sample size and the number of targets located within the K66 tidal radius. Only the M2FS dataset was considered for NGC 419. For NGC 1846 the situation is more complicated, and we list results for the Ma13, M2FS and Combined Samples. In the Ma13 and Combined cases, we further consider samples that include and exclude the binary star described in Section 2.3.1.2. Note that for the M2FS sample, we obtained precisely the same results with the binary star included or excluded given that in that dataset this star's velocity is very close to the mean cluster velocity derived by the EM algorithm.

2.3.2.2 Assigning Cluster Membership

As a check on the EM algorithm, we have calculated the systemic velocities and projected central cluster dispersions for NGC 419 and NGC 1846 using three methods we refer to as the 'Box', 'PM05' and 'PM50' estimates.

The Box value is simply calculated by using all targets in a rectangular area (the 'Box') in the $v_{\rm los}$-r plane (shaded area in Figure 2.10). The boundaries of this region are a minimum and maximum systemic velocity ($V_{\rm sys,min}$ and $V_{\rm sys,max}$) and the adopted K66 tidal radius (see Table 2.1). The velocity range was determined by assuming (conservatively) that each cluster has a mass of 10^6 $M_\odot$. Using the K66-model realization in LIMEPY (*Gieles and Zocchi*, 2015) and the respective cluster structural parameters (Table 2.1), we estimated the central velocity dispersion, σ_{10^6}. We then set $V_{\rm sys,max}$ and $V_{\rm sys,min}$ as $V_{\rm sys} - n\sigma_{10^6}$ and $V_{\rm sys} + n\sigma_{10^6}$, respectively, where $V_{\rm sys}$ is the straight mean of velocities in an initial estimate of the box boundaries. For both clusters, the term $n\sigma_{10^6}$ came out to be 8.8 $\mathrm{km\,s^{-1}}$ (adopting $n = 1$). The final Box samples converged quickly using this approach with any reasonable first guess for $V_{\rm sys}$.

The PM05 and PM50 samples represent the stars with normalized cluster membership probabilities as determined by the EM algorithm (Section 2.3.2.1) of greater than 5% (i.e., $P_{M_i} \geq 0.05$) and 50% (i.e., $P_{M_i} \geq 0.5$), respectively. What differs here from the EM analysis—where membership probabilities are used to weight individual stars—is that for the PM05 and PM50 samples stars that satisfy these criteria are considered to be certain members and all other are certain non-members which are dropped from the analysis. In practice, for the PM05 and PM50 samples we iterated Equation 2.12 and Equation 2.14 until the velocity dispersions converged to better than 0.0025 $\mathrm{km\,s^{-1}}$ between successive iterations.

The Box, PM05 and PM50 samples are identified in the lower panels of Figure 2.10. We list these results for the Box, PM05 and PM50 samples in Table 2.7. It should be

clear that by regarding all targets in the Box sample as cluster members, the corresponding Box dispersion measurement represents the maximum $\sigma_{\rm p,0}$ we derive from our sample. On the other hand, we calculated the PM50 and PM05 values for avoiding the bias of the EM algorithm, which is caused by the unequal-weight term P_{M_i} and tends to underestimate $\sigma_{\rm p,0}$ for NGC 419 and NGC 1846. Comparing Table 2.6 and Table 2.7, we found that the PM50 values are roughly equal to the results of the EM algorithm, while the PM05 values are slightly larger. For all subsequent analysis in this chapter, we will work exclusively with the PM50 values to explore the dynamical priperties of the clusters. For reference, normalized membership probabilities, P_{M_i}, are listed in Table 2.4 and Table 2.5 for NGC 419 and NGC 1846, respectively.

In Figure 2.11, we show the three-bin velocity dispersion profiles comparing with the best-fit K66 model constrained from both PM05 (top panels) and PM50 (bottom panels) values. The velocity dispersion profiles were constructed by dividing all targets with $P_{M_i} \geq 0.05$ (top panels) and $P_{M_i} \geq 0.5$ (bottom panels) into three bins, respectively. The radius range of each bin is indicated by the horizontal bars of r, and the central dots in radius are chosen as the median r value of the stars in each bin. It is worth stressing that we did not fit any of the kinematic data for NGC 419 or NGC 1846 to their respective K66 velocity dispersion profiles; Figure 2.11 simply indicates that the PM05 and PM50 samples are consistent with the underlying models and, additionally, that the PM50 sample agrees best with those models.

There is one other criterion—metallicity—that we can in principle apply to assess cluster membership. Figure 2.12 shows a plot of the metallicities for all stars in both NGC 419 and NGC 1846 as a function of distance from the centers of the clusters. The metallicities were determined from the spectral fitting of individual spectra as described in Section 2.3.1. We stress that the absolute metallicity values may suffer from systematic offsets that depend on the specific stellar model atmospheres and adopted effective temperatures that we are using here (see Section 2.3.1). However,

Table 2.7: Velocity and Dispersion Results from the PM50, PM05 and Box methods[a]

Cluster	Dataset	Method	Binary?[b]	RC[c]	$N_{\rm mem}$	$V_{\rm sys}$ ($\rm km\,s^{-1}$)	$\sigma_{\rm p,\,0}$ ($\rm km\,s^{-1}$)
NGC 419	M2FS	Box	...	N	51	$189.6^{+0.3}_{-0.4}$	$3.57^{+0.59}_{-0.54}$
	M2FS	PM05	...	N	47	$189.6^{+0.3}_{-0.3}$	$2.53^{+0.39}_{-0.20}$
	M2FS	**PM50**	**...**	**N**	**46**	$\mathbf{189.5^{+0.3}_{-0.3}}$	$\mathbf{2.44^{+0.37}_{-0.21}}$
	M2FS	Box	...	Y	51	$189.5^{+0.3}_{-0.3}$	$3.44^{+0.66}_{-0.56}$
	M2FS	PM05	...	Y	46	$189.5^{+0.3}_{-0.3}$	$2.24^{+0.33}_{-0.14}$
	M2FS	PM50	...	Y	45	$189.5^{+0.3}_{-0.3}$	$2.22^{+0.34}_{-0.14}$
NGC 1846	Combined	Box	N	N	56	$239.3^{+0.3}_{-0.3}$	$2.52^{+0.33}_{-0.32}$
	Combined	PM05	N	N	54	$239.3^{+0.2}_{-0.2}$	$2.17^{+0.25}_{-0.24}$
	Combined	**PM50**	**N**	**N**	**52**	$\mathbf{239.3^{+0.2}_{-0.2}}$	$\mathbf{2.04^{+0.28}_{-0.24}}$
	Combined	Box	N	Y	56	$239.4^{+0.3}_{-0.2}$	$2.43^{+0.32}_{-0.32}$
	Combined	PM05	N	Y	54	$239.3^{+0.2}_{-0.2}$	$2.07^{+0.26}_{-0.23}$
	Combined	PM50	N	Y	52	$239.3^{+0.2}_{-0.2}$	$1.93^{+0.25}_{-0.23}$
	Combined	Box	Y	N	57	$239.3^{+0.3}_{-0.3}$	$2.49^{+0.32}_{-0.32}$
	Combined	PM05	Y	N	55	$239.3^{+0.2}_{-0.2}$	$2.15^{+0.27}_{-0.23}$
	Combined	PM50	Y	N	53	$239.3^{+0.2}_{-0.2}$	$2.02^{+0.28}_{-0.25}$
	M2FS	Box	Y	N	46	$239.3^{+0.3}_{-0.3}$	$2.48^{+0.36}_{-0.39}$
	M2FS	PM05	Y	N	44	$239.3^{+0.2}_{-0.2}$	$2.04^{+0.23}_{-0.25}$
	M2FS	PM50	Y	N	41	$239.4^{+0.2}_{-0.2}$	$1.80^{+0.23}_{-0.24}$
	M2FS	Box	Y	Y	46	$239.3^{+0.3}_{-0.3}$	$2.45^{+0.35}_{-0.39}$
	M2FS	PM05	Y	Y	44	$239.3^{+0.2}_{-0.2}$	$2.00^{+0.23}_{-0.26}$
	M2FS	PM50	Y	Y	41	$239.4^{+0.2}_{-0.2}$	$1.75^{+0.22}_{-0.25}$
	Ma13	Box, PM05	N	N	21	$238.7^{+0.4}_{-0.5}$	$2.39^{+0.53}_{-0.64}$
	Ma13	PM50	N	N	20	$238.5^{+0.4}_{-0.4}$	$2.17^{+0.59}_{-0.68}$
	Ma13	Box, PM05, PM50	N	Y	21	$239.1^{+0.4}_{-0.4}$	$2.21^{+0.40}_{-0.32}$
	Ma13	Box, PM05, PM50	Y	N	22	$239.0^{+0.5}_{-0.5}$	$2.64^{+0.47}_{-0.51}$
	Ma13	Box, PM05, PM50	Y	Y	22	$239.2^{+0.4}_{-0.5}$	$2.16^{+0.33}_{-0.25}$

[a] The rows in bold highlight the best-fit results we adopted in the following sections and tables.
[a] This flag denotes whether the confirmed binary star in NGC 1846 is excluded (N) or included (Y). This star is 'N1846-1-r079' in Table 2.5, and the individual velocities are summarized in Section 2.3.1.2 and Figure 2.9.
[b]This flag indicates whether the rotational correction described in Section 2.3.4 was applied.

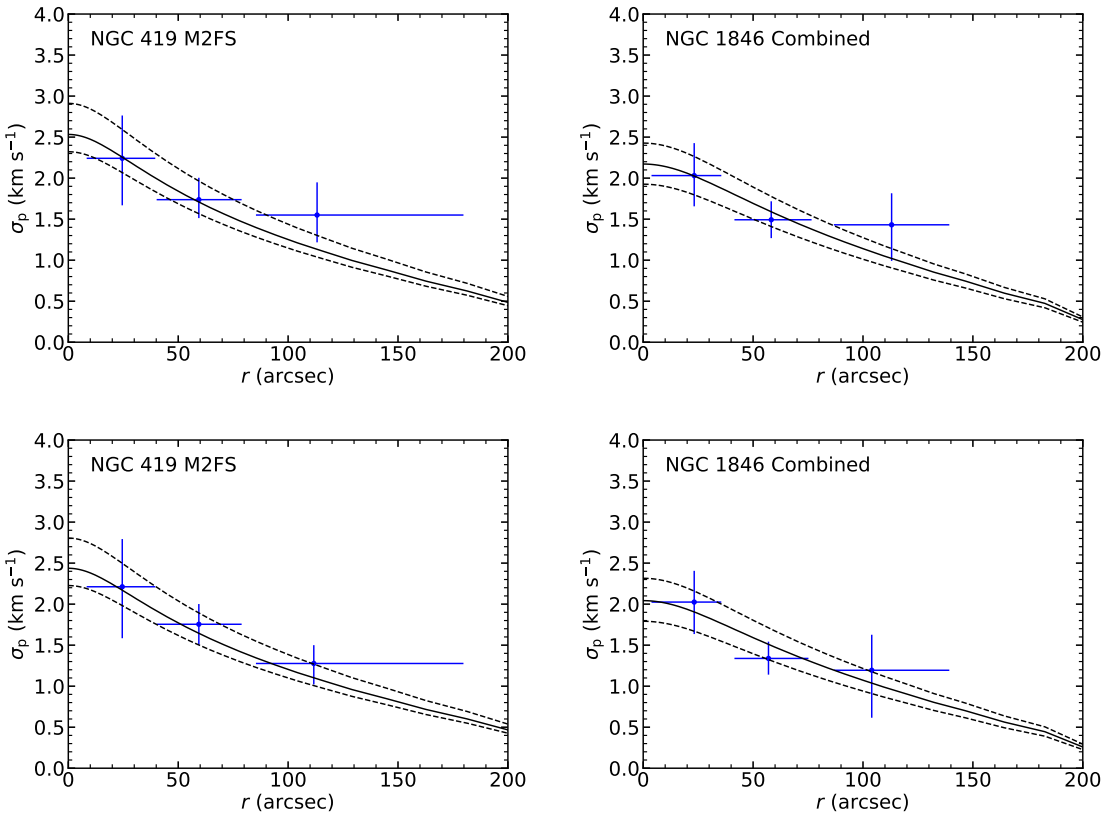

Figure 2.11: Binned velocity dispersion profiles (blue dots) with best-fit K66 models (solid lines) scaled by the PM05 values (top panels) and the PM50 values (bottom panels). The adopted cluster centers are listed in Table 2.2. The two dashed lines in each panel denote the 1σ uncertainties on the central velocity dispersion. The vertical 'error bars' are the 1σ uncertainties of the $\sigma_{\rm p}$ values in each bin. The horizontal 'error bars' represent the radial range of stars in each bin.

the *relative* metallicities should be reliable as all stars are analyzed in the same manner. The color/symbol coding is the same as for Figure 2.10 so that one can easily distinguish the Box, PM05 and PM50 samples. The key features to note are that (a) the metallicity distribution of the field population (located beyond the tidal radius as denoted by the vertical dotted line in Figure 2.12) is skewed to low metallicity as expected from a composite disk+halo population in both Magellanic Clouds (e.g., *Cole et al.*, 2005; *Carrera et al.*, 2011; *Song et al.*, 2017 for the LMC, and *Dobbie et al.*, 2014b for the SMC), (b) the metallicity distributions of the clusters are much more compact, and plausibly more nearly Gaussian in form, and (c) the S/N of the NGC 419 data is typically a bit lower and hence the measured metallicity distribution of that cluster is clearly broader.

In both clusters, one star is plausibly many sigma below the mean cluster metallicity; on this basis, these stars appear to be likely non-members of their clusters despite their both being in the PM50 samples based on their kinematics. Because of this, the removal of either star has negligible effect on the systemic velocity or projected velocity dispersion in either NGC 419 (0.0 and 0.0 $\mathrm{km\,s^{-1}}$, respectively) or NGC 1846 (0.0 and 0.02 $\mathrm{km\,s^{-1}}$). We will return to a comprehensive discussion of the absolute metallicity estimates from our M2FS spectra when we complete the dynamical analyses of all 20+ clusters in our full sample (see Section 2.2.1).

Comparing the results in Table 2.7 reveals that the PM50 sample returns essentially the same kinematic results as the EM algorithm (Section 2.3.2.1). This implies that the EM algorithm is applying weighting that closely mimics what one would do by assigning full membership to stars with membership probabilities $> 50\%$. The PM50 approach also helps to label stars definitively as members or non-members which may be useful for certain types of studies or follow-up observations. Based on this exercise using our NGC 419 and NGC 1846 datasets, we plan in our future papers on MC cluster M/L ratios to base our key dynamical results on the EM estimates

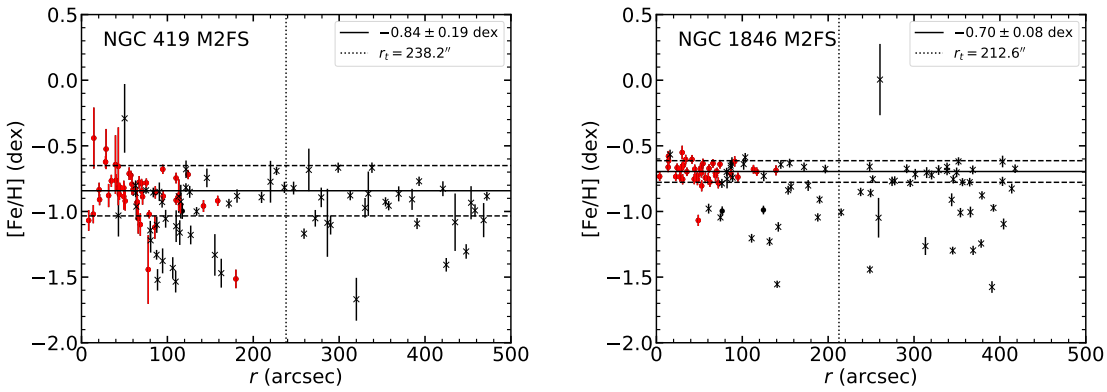

Figure 2.12: Metallicity of stars in NGC 419 (left panel) and NGC 1846 (right panel) as a function of the projected distances from the respective cluster centers. The adopted cluster centers are listed in Table 2.2. As in Figure 2.10, red dots correspond to stars with $P_{\rm M} \geq 0.5$, black dots correspond to stars with $0.05 \leq P_{\rm M} < 0.5$, and black crosses correspond to stars with $P_{\rm M} < 0.05$. In each panel, the vertical dotted line denotes the cluster tidal radius. The solid horizontal line and two dashed horizontal lines denote the mean and standard deviation of the metallicities of all stars with $P_{\rm M} \geq 0.5$. Note that at most two stars in the PM50 samples (one in each cluster) could be argued to be non-members based on their metallicity (see Section 2.3.2.2 for further discussion).

of the kinematic properties of the clusters in our full sample but also to report the PM50 samples in order to identify explicitly the stars we consider to most likely be members of their respective clusters.

2.3.2.3 Recovery of the Central Velocity Dispersion

We now turn to some tests to determine how well we recover the projected central velocity dispersion ($\sigma_{\rm p,0}$) via Equation 2.14 and the reliability of the EM algorithm introduced in Section 2.3.2.1 and under the assumption of a K66 dynamical model. Our procedure is based on simulations of the observed dataset generated by the dynamical-model sampling routine `LIMEPY.SAMPLE`. To mimic NGC 1846, we constructed a mock K66-based cluster with the same structural parameters as listed in Table 2.1, and adopted $V_{\rm sys} = 239$ km s^{-1} and $\sigma_{\rm p,0} = 2$ km s^{-1} which correspond to rounded values for these parameters from Table 2.7. We did not carry out simulations

specifically for NGC 419 since none of the issues we address below are specifically related either of the clusters in our sample and the statistical properties of NGC 419 and NGC 1846 are similar.

We first tested whether the recovery of $\sigma_{\rm p,0}$ exhibits bias due to the distribution of the projected distances of tracers from the cluster center. As an extreme ideal case, we set up iterations in which we selected 30 cluster members at a given radius from the center and assumed that their line-of-sight velocities can be perfectly measured (i.e. $\varepsilon_V = 0$). Both the sample velocity dispersions and their corresponding recovered central values were calculated by Equation 2.12 and Equation 2.14 iteratively until the value converged to better than 0.0025 $\rm km\,s^{-1}$ between successive iterations. In the top left panel of Figure 2.13, we show the median values and the 1σ errors estimated from 1000 different samplings at each of several radii. There is no significant bias along the r-axis apart from a slight tendency to underestimate the central dispersion from samples obtained exclusively at radii approaching the tidal radius of the system.

To explore this further, we ran similar tests but now assuming non-zero velocity uncertainties (ε_V). To show this, we selected as before 30 tracers at a given radius for 1000 times, but for each tracer we replaced its true velocity (V_i) with a random value from a normal distribution of fixed dispersion (ε_{V_i}). We carried out these tests for for ε_{V_i} from 0.5 to 2.0 $\rm km\,s^{-1}$ and the results are summarized in Figure 2.13. As ε_{V_i} is increased beyond 0.5 $\rm km\,s^{-1}$, it is evident that estimates based only on stars in the outer parts of the cluster of the central velocity dispersions become extremely unreliable. For NGC 1846, the median velocity uncertainty is 0.33 $\rm km\,s^{-1}$ for the Combined Sample, close to the case of $\varepsilon_{V_i} = 0.5$ $\rm km\,s^{-1}$ in the top right panel of Figure 2.13. The sample for NGC 419 exhibits a mean $\varepsilon_{V_i} \leq 1.0$ $\rm km\,s^{-1}$ (see Figure 2.6), so the behavior in that case resembles most closely the results in the bottom left panel of Figure 2.13.

Of course, in practice we sample stars over a range of radii for both clusters (these

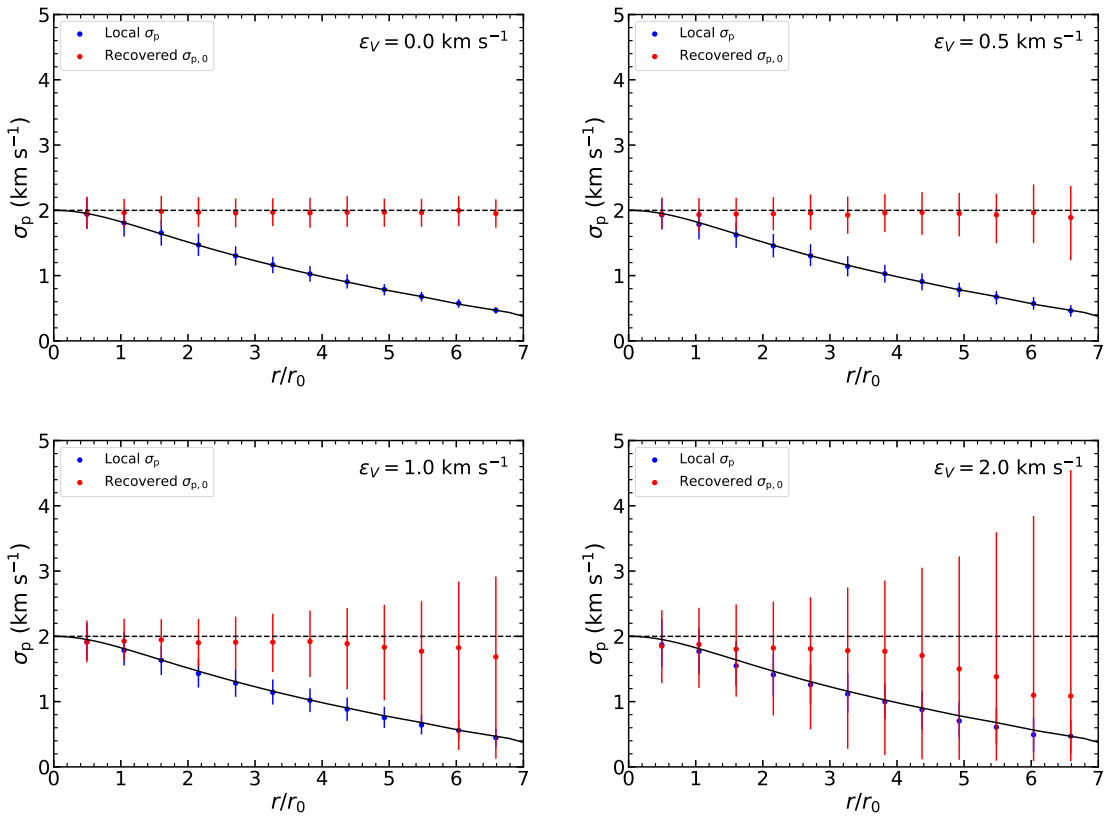

Figure 2.13: Tests of reliability of the EM algorithm to recover $\sigma_{\mathrm{p},0}$ for different radii. Within a given panel, the velocity uncertainties, ε_V, were taken to be constant, varying from 0.0 to 2.0 km s^{-1} as noted. The solid lines show the K66 profiles for NGC 1846. The dashed line shows the assumed 2 km s^{-1} central velocity dispersion. Blue dots correspond to the velocity dispersion measured from 30 members at various radii. Red dots show the recovered $\sigma_{\mathrm{p},0}$ for each sample from a single bin at the same radius. The error bars show the 1σ uncertainties (that is, the 67% confidence ranges) of $\sigma_{\mathrm{p},0}$ based on bootstrapping 30 members from a given bin with their associated ε_V. For $\varepsilon_V \leq 0.5$ km s^{-1}, the EM algorithm returns the correct central dispersion without bias and to reasonable precision. By $\varepsilon_V \sim 1$ km s^{-1}, the method remains reasonably unbiased, but the implied error on $\sigma_{\mathrm{p},0}$ becomes comparable to the inferred dispersion when only 30 tracers are available per bin.

correspond to the shaded areas in Figure 2.10). The previous test implies that our mean bias due to our EM analysis is < 0.2 km s^{-1}. However, we can do better by adopting an 'empirical selection profile' (ESP) that tracks how many members—here defined as stars with with $P_{M_i} \geq 0.50$ (see Section 2.3.2.2)—were observed at given radius from the Combined Sample of NGC 1846, and then using the ESP when selecting members from the mock K66 cluster (left panel of the Figure 2.14). After 1000 samplings, the median value with their corresponding 1σ confidence interval is $1.97^{+0.19}_{-0.20}$ km s^{-1}. Since the model dispersion was taken to be 2.0 km s^{-1}, we find no significant bias caused by our sample selection strategy.

Incorrect or biased identification of field-star contamination can also bias derived kinematic parameters for clusters like NGC 419 and NGC 1846. To test if this is strongly affecting our analyses, we have generated mock kinematic samples based on the Combined Sample for NGC 1846.

These mock samples consisted of clusters members and unassociated field stars, with the total number of cluster members in each set to a Poisson random deviate of 52, the actual number of members in our Combined PM50 sample for NGC 1846 (see Section 2.3.2.2). Kinematics and positions for these members were then drawn at random using LIMEPY assuming (a) the structural parameters from a K66 model adopted for NGC 1846 (see Table 2.1), (b) a systemic velocity and central projected velocity dispersion of 239 km s^{-1} and 2.0 km s^{-1}, respectively, for the mock cluster, and (c) the same spatial sampling profile of mock sample members as for the Combined Sample for NGC 1846 (see left panel of Figure 2.14). All remaining stars—which brought the total in the mock sample to 195—were drawn from a 'background' distribution with a systemic velocity and projected velocity dispersion of 269.5 km s^{-1} and 25.2 km s^{-1}, respectively (see Table 2.6). These field stars were distributed uniformly over the field from which the Combined Sample was drawn. The velocity errors of stars in the mock sample were assigned the uncertainties of stars in the Combined

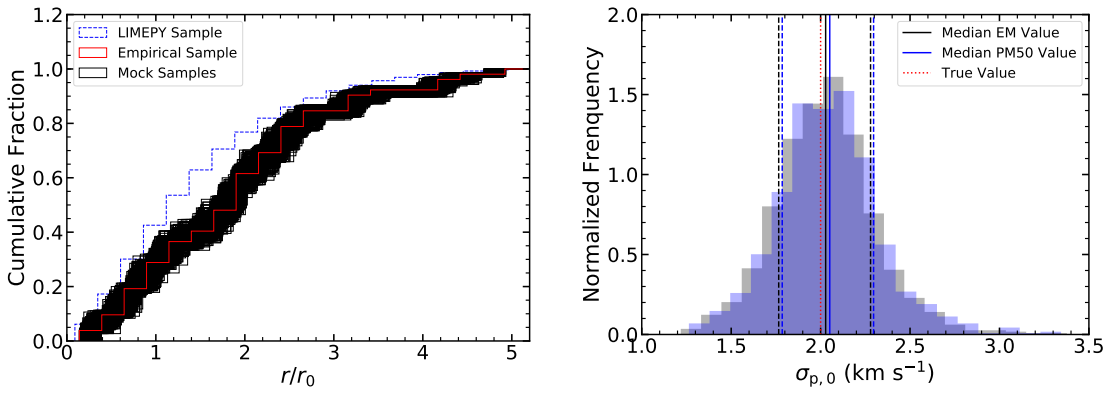

Figure 2.14: Tests of the EM algorithm for recovering $\sigma_{\rm p,0}$ with 1000 mock samples from the empirical selection profile of the M2FS sample for NGC 1846. In the left panel, the blue line corresponds to the normalized cumulative number of stars as a function of distance from the cluster center. The red line corresponds to the cumulative empirical selection profile of NGC 1846 based on the targets observed with M2FS. The black lines correspond to the mock samples we simulated in the tests. The right panel shows a histogram of best-fit $\sigma_{\rm p,0}$ values from our mock samples using the EM algorithm (gray; individual targets are given their weights by the algorithm itself, see Section 2.3.2.1) and the PM50 value (blue; all targets with $P_{\rm M} > 0.5$ are assumed to be certain members, i.e. full weight, while all others are considered to be certain non-members, i.e. zero weight; see Section 2.3.2.2). The vertical lines in the right panel denote the median values (solid lines) and 1σ (68% confidence) limits for the EM (black) and PM50 (blue) cases. The true input value of the simulation (vertical red dotted line) is $\sigma_{\rm p,0} = 2$ km s^{-1}. Section 2.3.2.3 lists the results plotted in this figure.

Sample, and an appropriate Gaussian deviate was added to each mock velocity.

From our analyses of 1000 such samples, we find that both the EM algorithm (see Section 2.3.2.1) and the PM50 sample (see Section 2.3.2.2) return nearly the systemic velocity and central dispersion for the simulated cluster to good precision, of order 0.3 km s^{-1}. The results, summarized in Figure 2.14, from the EM algorithm are $V_{\rm sys} = 239.0^{+0.3}_{-0.2}$ km s^{-1} and $\sigma_{\rm p,0} = 2.03^{+0.26}_{-0.25}$ km s^{-1}. From the PM50 analysis, the results are $V_{\rm sys} = 239.0^{+0.3}_{-0.3}$ km s^{-1} and $\sigma_{\rm p,0} = 2.05^{+0.27}_{-0.25}$ km s^{-1}. The errors are the 1-σ (68.2%) confidence ranges of the various parameters determined from the simulations (Figure 2.14).

The simulation results suggest a possible bias such that the derived dispersion is

about 0.04 ± 0.02 km s^{-1} higher than the true cluster dispersion. Field stars that happen to be close to the cluster will reduce the inferred dispersion only if they have velocities within 1σ of the cluster mean. However, such stars can increase the dispersion over a wider velocity range, about $\pm 3\sigma$. Since the field stars have essentially a flat distribution over the velocity range inhabited by cluster members, they will more often—by about a factor of two—increase the dispersion when mistaken as cluster members. This bias is small compared to the errors inherent in our kinematic results (see Section 2.3.2.1 and Table 2.6), so we will ignore this bias in this chapter. However, the more ambiguous cluster/field separation is—say in a low-density cluster or high-density field—the more likely this bias may lead to statistically significant overestimates in velocity dispersions estimates of star clusters.

2.3.3 Cluster Masses and Mass-to-light Ratios

Our initial estimates for the masses of NGC 419 and NGC 1846 are based on the K66 model using the structural parameters listed in Table 2.1 and scaled by the PM50 $\sigma_{\rm p,0}$ value listed in Table 2.7. The mass uncertainty is estimated following *Illingworth* (1976) by referring to the K66 total-mass estimator, $M_{\rm tot} = 167 r_0 \mu \sigma^2_{\rm p,0}$ (with r_0 in pc, $\sigma_{\rm p,0}$ in km s^{-1} and M in $M_\odot$); the final mass uncertainty is derived from the known errors in the squared velocity dispersion and distance modulus (which propagates to the uncertainty in the scale radius, r_0).

The V-band luminosities of the clusters are obtained by integrated the K62 profile scaled to aperture photometry profiles to a maximal reference radius, x. The resulting relation is

$$L_V(x) = \pi r_0^2 \Sigma_{V,0} \left[\ln(1+x) - 4\frac{(1+x)^{1/2} - 1}{(1+x_t)^{1/2}} + \frac{x}{1+x_t} \right], \qquad (2.15)$$

where $x = (r/r_c)^2$, $x_t = (r_t/r_c)^2$ and $\Sigma_{V,0}$ is the central surface brightness in V-band.

Table 2.8: Mass, Luminosity and M/L_V

Cluster	Dataset	$M_{\rm tot}$ ($\times 10^5$ $M_\odot$)	$L_{V,\rm tot}$ ($\times 10^5$ $L_\odot$)	$M/L_{\rm V}$ ($M_\odot$ $L_\odot^{-1}$)	$\log M_{\rm tot}$ ($M_\odot$)	$\log L_{V,\rm tot}$ ($L_\odot$)	$\log M/L_{\rm V}$ ($M_\odot$ $L_\odot^{-1}$)
NGC 419	M2FS	$0.76^{+0.25}_{-0.13}$	$3.46^{+0.71}_{-0.71}$	$0.22^{+0.08}_{-0.05}$	$4.88^{+0.14}_{-0.08}$	$5.54^{+0.09}_{-0.09}$	$-0.66^{+0.16}_{-0.10}$
NGC 1846	M2FS	$0.42^{+0.11}_{-0.12}$	$1.67^{+0.47}_{-0.47}$	$0.25^{+0.08}_{-0.09}$	$4.62^{+0.11}_{-0.12}$	$5.22^{+0.12}_{-0.12}$	$-0.60^{+0.14}_{-0.15}$
	Combined[a]	$0.54^{+0.15}_{-0.14}$	$1.67^{+0.47}_{-0.47}$	$0.32^{+0.11}_{-0.11}$	$4.73^{+0.12}_{-0.12}$	$5.22^{+0.12}_{-0.12}$	$-0.49^{+0.14}_{-0.14}$

[a] Exclude the confirmed binary star in NGC 1846. This star is 'N1846-1-r079' in Table 2.5, and the individual velocities are summarized in Section 2.3.1.2 and Figure 2.9.

To estimate $\Sigma_{V,0}$, we compared the ground-base aperture photometry $V_{\rm ap}$ listed in Table 2.1 with the results of Equation 2.15 if $x = r_{\rm ap}/r_0$. The total luminosity $L_{V,\rm tot}$ can then be obtained by setting $x = x_t$ in Equation 2.15. When transforming magnitudes to luminosities, we used $M_{V,\odot} = 4.85$ in addition to the distance moduli and extinction values listed in Table 2.1. According to Equation 2.15, the luminosity uncertainty comes from the errors in the central surface brightness, the squared scaled radius in arc and the squared distance.

The empirical M/L_V of a cluster can be derived by comparing the total mass to the total V-band luminosity determined above. The uncertainty in M/L_V is estimated from the errors in the squared velocity dispersion, the central surface brightness, the scaled radius in arc and the distance. Table 2.8 lists the masses, luminosities and M/L ratios.

2.3.4 Rotation

Up to now, our analysis has assumed both NGC 419 and NGC 1846 are exclusively pressure-supported systems. However, in the case of NGC 1846, Ma13 suggested that the cluster may exhibit some coherent rotation. Since rotation can partly dynamically support the clusters, this effect could alter our estimates of their masses. In this subsection we explore the evidence for rotation in both clusters and comment on the magnitude of the effects of rotation on our final mass estimates for both systems.

We examined the observations for evidence of internal rotation in each cluster by

comparing the mean velocity differences on opposite sides of a line passing through the projected cluster centers as the line's orientation is advanced in position angle (PA, east of north; see, e.g., *Cote et al.* 1995; *Lane et al.* 2009, 2010a,b; *Bellazzini et al.* 2012; *Mackey et al.* 2013). For this analysis we used the PM50 sample for NGC 419 and the PM50 subsample derived from the Combined Sample for NGC 1846 (see Section 2.3.2.2 and Table 2.7). If any internal rotation exists that has a significant line-of-sight component, the mean velocity differences between the mean velocities on the two sides of the fiducial line ($\Delta\langle V_{\rm los}\rangle$) should exhibit a sinusoidal pattern (see also, e.g. Eq. 8 from *Kimmig et al.* 2015) with a statistically significant amplitude. We use the following relation to parameterize this behavior:

$$\frac{\Delta\langle V_{\rm los}\rangle}{2} = A_{\rm rot}\sin\left({\rm PA}+\phi\right), \tag{2.16}$$

where $A_{\rm rot}$ is the maximum amplitude of this relation and ϕ is related to the rotation axis $\rm PA_0$. Due to projection, the measured $A_{\rm rot}$ is clearly a lower limit to the true rotation amplitude measured using this parameterization.

The uncertainties in the fitting parameters for the results for NGC 419 and NGC 1846 were estimated in the same manner as described in Ma13 (see their Section 4.1) and using the same projected cylindrical rotation curve used in that paper. In summary, we Monte-Carlo new velocities to each star at their known positions given their velocity measurement errors and the observed cluster dispersion profile consistent with the adopted K66 model for each cluster (Table 2.7), then re-determined the parameters in Equation 2.16 1000 times (see Table 2.9). From this procedure, we estimate rotation amplitudes of $0.5^{+0.3}_{-0.2}$ and $0.6^{+0.2}_{-0.3}$ $\rm km\,s^{-1}$ for NGC 419 and NGC 1846, respectively, with rotation axis PAs of 114^{+43}_{-34} and 58^{+37}_{-25} degrees east of north. We note here that Ma13 used a very similar approach to estimate the rotation position angle of NGC 1846 to be $60^\circ \pm 20^\circ$, in good agreement with our result based on the

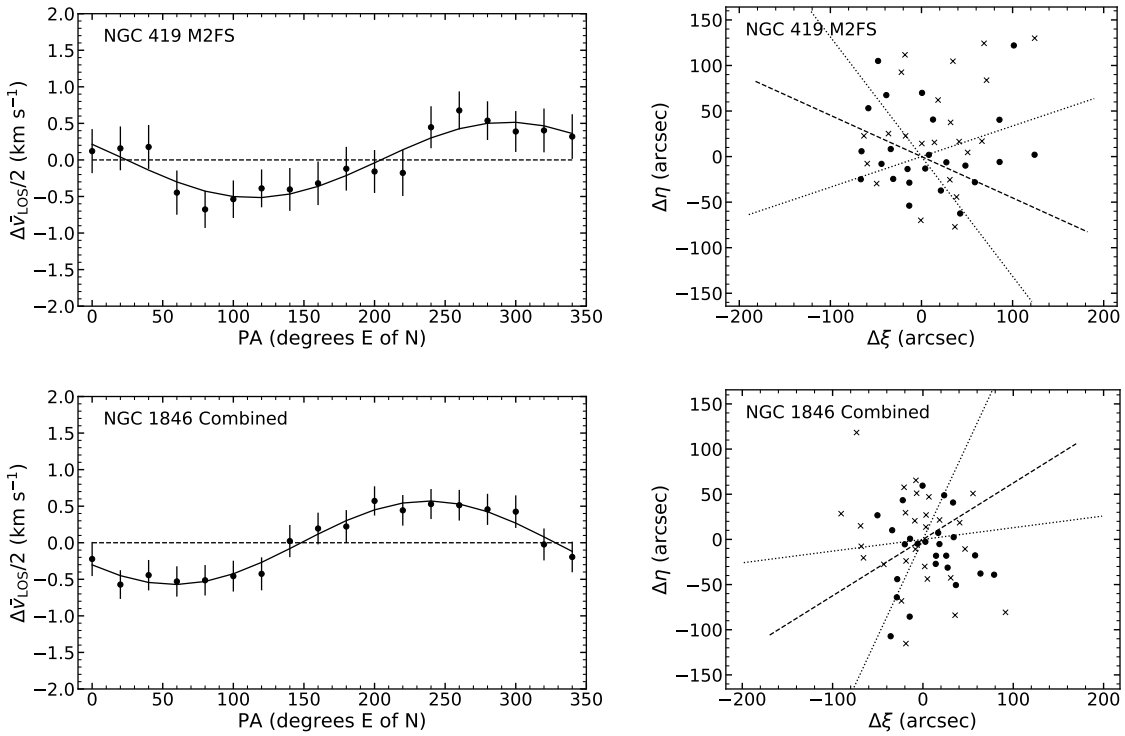

Figure 2.15: Simple rotation analysis for the stars with $P_{\rm M} > 0.5$ in NGC 419 (top) and NGC 1846 (bottom) (see Section 2.3.4 and Table 2.9). The adopted cluster centers are listed in Table 2.2. The left panels show $\Delta\bar{V}_{\rm los}/2$ as a function of the bisector position angle, together with the best-fit sinusoid model. The best-fit parameters are listed in Table 2.9. In the right panels, crosses (dots) indicate stars with velocities greater (less) than the systemic velocity. The best-fit rotation axis from the left panel is marked as a dash line in each panel, and two dotted lines denote the 1σ uncertainties.

PM50 Combined Sample (see Table 2.9).

Based on the results from this section, we can estimate the ratios of the rotational amplitude and observed central dispersion for NGC 419 and NGC 1846 to be $A_{\rm rot}/\sigma_{\rm p,0} \approx 0.2^{+0.1}_{-0.1}$ and $0.3^{+0.1}_{-0.2}$, respectively. Both values are marginally significantly different from zero. However, if we take these ratios at face value, we can estimate the systematic effects on the masses we derive for both clusters as follows. First, we have removed the rotational component of the LOS velocities of every star using the projected rotational velocities our cylindrical rotation model predicts. We then applied our EM estimator to the adjusted samples to obtain a new estimate of the

Table 2.9: Rotation Analysis

Cluster	Dataset	$N_{\rm mem}$	$A_{\rm rot}$ (km s^{-1})	ϕ ($^\circ$)
NGC 419	M2FS	46	$-0.5^{+0.2}_{-0.3}$	-24^{+34}_{-43}
NGC 1846	Combined[a]	52	$-0.6^{+0.3}_{-0.2}$	32^{+25}_{-37}
	Combined	53	$-0.5^{+0.2}_{-0.2}$	31^{+31}_{-37}
	M2FS	41	$-0.4^{+0.3}_{-0.2}$	23^{+35}_{-38}
	Ma13[a]	21	$-1.0^{+0.5}_{-0.3}$	37^{+18}_{-46}
	Ma13	22	$-1.2^{+0.5}_{-0.4}$	38^{+8}_{-39}

[a] Exclude the confirmed binary star in NGC 1846. This star is 'N1846-1-r079' in Table 2.5, and the individual velocities are summarized in Section 2.3.1.2 and Figure 2.9.

projected central velocity dispersion and estimated the masses of the clusters using the techniques in Section 2.3.3; these masses tend to be ∼9% lower than the masses based on the uncorrected central velocity dispersions that are listed in Table 2.7. However, these mass estimates—by design—neglect the mass being supported by the rotational component of the cluster. Without a better rotational model—not to mention one that is more statistically significant—it is difficult to make a more precise rotational correction (see e.g. *Fischer et al.* 1992a).

Another complication has to do with the unknown inclination of any rotation with the plane of the sky. However, even if the rotations of both clusters are fully in the plane of the sky (strictly not possible to the extent that we see a rotation signal), then the observed central dispersion would be about $\sqrt{2}$ smaller than in the no-rotation case, implying an underestimate of order 30% in the true masses of the clusters. We conclude that rotation likely has a negligible impact on the masses we derive for NGC 419 and NGC 1846, and is unlikely to affect our results at a level significantly higher than implied by the error bars on the derived masses (Table 2.8) that are based on the measurement and statistical uncertainties in the kinematic and structural properties of the clusters.

2.4 Comparison with previous studies

As noted in Section 2.2.5, there are previously published kinematic studies of NGC 419 and NGC 1846. For NGC 419, K18 used adaptive optics assisted integral-field spectroscopy using MUSE at the VLT. For NGC 1846, Ma13 obtained individual spectra using VLT/FLAMES. In this section we critically compare the results of the present chapter with the findings of these earlier studies.

2.4.1 NGC 419

Using MUSE, K18 obtained radial velocity measurements of 1049 individual targets within the central 1×1 arcmin^2 field of NGC 419 using the AO system to improve spatial resolution in the core region of the cluster. The spectral resolution of $\mathcal{R} \sim 2,800$ yielded radial velocity uncertainties $\lesssim 10$ km s^{-1} (more on this below). They measured or constrained many of the same dynamical parameters that we have obtained for the cluster. A direct comparison of their results and the results from our PM50 sample is provided in Table 2.7. In the case of the central velocity dispersion of NGC 419, the value in Table 2.10 was obtained by adopting their preferred dynamical model (see below) and extrapolating the corresponding dispersion profile to the cluster center (see their Figure 4). The M/L ratio for NGC 419 was determined by K18 using spherical isotropic Jeans models with different (constant) M/L ratios, and then a maximum likelihood approach was used to sum up the likelihoods for observed radial velocities, given their measurement uncertainties, and the predicted radial velocities for each model at the corresponding positions of each star. This process yields directly the V-band M/L of the cluster from which K18 then estimated a total cluster mass. These values are also listed in Table 2.10 for ease of comparison with our results.

The systemic radial velocities measured by K18 and our study differ by 1.0 ± 0.4 km s^{-1} (see Table 2.10). Given the possible zero-point errors we have identified in

Table 2.10: Comparison of kinematic results with previous studies

Cluster	Dataset	RC[a]	$V_{\rm rot}$ ($\rm km\,s^{-1}$)	$\rm PA_0$ ($^\circ$)	$V_{\rm sys}$ ($\rm km\,s^{-1}$)	$\sigma_{\rm p,0}$ ($\rm km\,s^{-1}$)	$M_{\rm tot}$ ($\times 10^5$ $\rm M_\odot$)	$M/L_{\rm V}$ ($\rm M_\odot$ $\rm L_\odot^{-1}$)
NGC 419	M2FS	N	$0.5^{+0.3}_{-0.2}$	114^{+43}_{-34}	$189.5^{+0.3}_{-0.3}$	$2.44^{+0.37}_{-0.21}$	$0.76^{+0.25}_{-0.13}$	$0.22^{+0.08}_{-0.05}$
	MUSE[b]	N	0.7 ± 0.2	13 ± 17	190.5 ± 0.2	3.3 ± 0.2	1.4 ± 0.2	0.67 ± 0.08
NGC 1846	Combined[c]	N	$0.6^{+0.2}_{-0.3}$	58^{+37}_{-25}	$239.3^{+0.2}_{-0.2}$	$2.04^{+0.28}_{-0.24}$	$0.54^{+0.15}_{-0.14}$	$0.32^{+0.11}_{-0.11}$
	M2FS	N	$0.4^{+0.2}_{-0.3}$	67^{+38}_{-35}	$239.4^{+0.2}_{-0.2}$	$1.80^{+0.23}_{-0.24}$	$0.42^{+0.11}_{-0.12}$	$0.25^{+0.08}_{-0.09}$
	Ma13[d]	N	$1.2^{+0.4}_{-0.5}$	52^{+39}_{-8}	$239.0^{+0.5}_{-0.5}$	$2.64^{+0.47}_{-0.50}$	$0.93^{+0.35}_{-0.37}$	$0.65^{+0.25}_{-0.26}$
	Ma13[d]	Y	$1.2^{+0.4}_{-0.5}$	52^{+39}_{-8}	$239.2^{+0.4}_{-0.5}$	$2.16^{+0.33}_{-0.25}$	$0.63^{+0.20}_{-0.16}$	$0.44^{+0.15}_{-0.12}$
	Ma13[e]	Y	1.1 ± 0.4	60 ± 20	239.1 ± 0.4	$2.52^{+0.26}_{-0.18}$	$0.84^{+0.17}_{-0.12}$	$0.59^{+0.13}_{-0.10}$

[a] Rotation Correction.
[b] The results of K18. $\sigma_{\rm p,0}$ was estimated using the K66 model for NGC 419 listed in Table 3.1 and the measured $M_{\rm tot}$ by K18.
[c] Exclude the confirmed binary star in NGC 1846. This star is 'N1846-1-r079' in Table 2.5, and the individual velocities are summarized in Section 2.3.1.2 and Figure 2.9.
[d] The results of our analysis using the full dataset of Ma13.
[e] The results of Ma13.

our M2FS data (see Table 2.10), these values are in reasonable agreement[1] Of course, the systemic velocity is ultimately immaterial to any of the conclusions regarding the mass or M/L ratio for NGC 419 from either paper. Unlike the case for NGC 1846 (see Section 2.4.2), we could not carry out a star-by-star velocity comparison since K18 did not provide the velocities of individual sources extracted from their IFU observations.

A comparison of the M/L_V values obtained by K18 and this chapter differ by a significant factor: $M/L_{V,\rm K18}/M/L_{V,\rm M2FS} = 3.0^{+1.1}_{-0.8}$. This comparison is complicated by the different paths by which the respective M/L values were obtained. If we compare instead the masses derived by K18 and ourselves, we find a ratio of $M_{\rm K18}/M_{\rm M2FS} = 1.84^{+0.66}_{-0.41}$, a 2-$\sigma$ discrepancy that ultimately arises from the different central velocity dispersions measured by the two studies.

One reason for the differences between the K18 results and our new M2FS results could reflect the very different distributions of the tracers sampled in the cluster by the respective studies. As already noted, the K18 sample consists exclusively of stars within the MUSE field of view, which corresponds almost precisely within the

[1]There could of course be a zero-point shift in the MUSE results, but there is no assessment of this in K18.

region inside the core radius of NGC 419. Our M2FS sample consists of stars spread throughout the cluster from the central core to (and beyond) the tidal radius. If the M/L ratio of NGC 419 varies radially, modeling our sample with an assumed well-mixed population (therefore with constant M/L over all radii) could result in a different value from observations and modeling restricted to the core. K18 noted that the observed velocity dispersion profile was slightly steeper in the cluster core than the Jeans models they adopted. To the extent that this reflects radial variations in M/L in NGC 419, it would imply that neither of the models used in either paper is strictly correct and may result in biased mass and M/L_V ratio estimates. Both studies have to extrapolate to a central dispersion value and the methods by which that was done differ in detail and used different dynamical models.

Another possibility is that the discrepancy in the MUSE and M2FS dynamical results (Table 2.10) reflects some sort of observational issues. Apart from sample size, the key difference in the K18 MUSE and our M2FS results lies in the relative velocity uncertainties. In one case, K18/MUSE, the kinematic errors appear to be comparable and often larger than the intrinsic cluster dispersion (this remains true regardless of which value for the central dispersion is adopted). We can see this in Figure 2.16 where we have plotted, as a function of mean spectral S/N, our estimate of the MUSE errors based on K18's description (red dots) and *Kamann et al.* (2016) (blue squares). The same figure shows our measured M2FS velocity uncertainties (black dots) based on repeat measurements as described in Section 2.3.1.1. The gray shaded horizontal bar in Figure 15 denotes the range of central dispersion values for NGC 419 based on the K18 and M2FS results and shows graphically how each dataset's precision relates to the likely intrinsic cluster dispersion.

We have carried out simulations to determine how the different error distributions may affect inferred central velocity dispersion estimates for NGC 419. In the case of the MUSE data, we adopted a specific ε_V-S/N relation shown as a sequence of solid

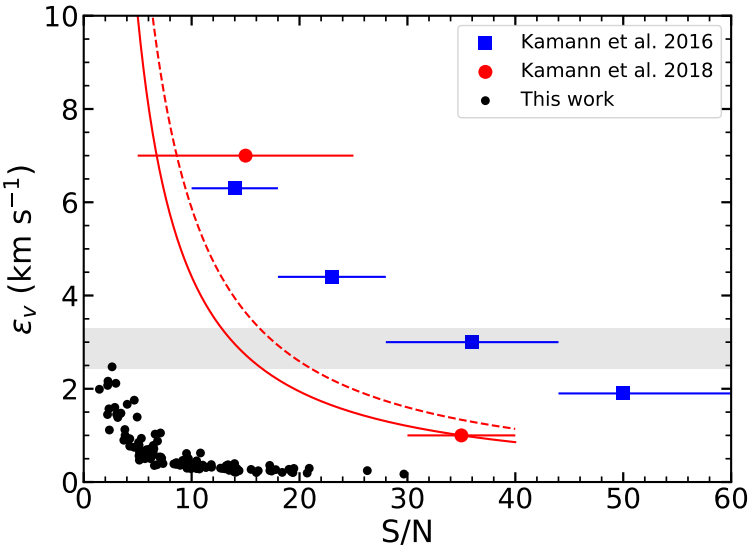

Figure 2.16: Velocity uncertainties for kinematic measurements of NGC 419. The black dots are taken from our sample in Figure 2.6. The red dots show our estimate of ε_V-S/N relation for NGC 419 at fiducial S/N values based on the discussion in K18 (see their Figure 3 and Section 4). The blue squares show the error distribution for stars in NGC 6397 also observed with MUSE but without AO (*Kamann et al.*, 2016, and based on their Figure 3). The gray shaded horizontal bar spans the range of the central velocity dispersion measurements for NGC 419. The lower bound of this region is 2.44 km s^{-1} (the PM50 Combined sample) and the upper bound is 3.3 km s^{-1} (K18). The solid red line denotes the parametric form of the error distribution for NGC 419 that we adopted for the K18 observations (see Section 2.4.1). The dashed red line denotes the same error distribution but multiplied by a factor of $1/0.75 = 1.33$ (see Section 2.4.1). Note that both red curves lie well below the error distribution observed in the NGC 6397 study (*Kamann et al.*, 2016).

red line in Figure 2.16. We then used LIMEPY.SAMPLE to produce a dataset of 1000 targets (roughly comparable to the MUSE sample) from a K66 model with a central dispersion of 2.44 $\mathrm{km\,s^{-1}}$ (the M2FS value; see Table 2.10) and then applied Gaussian deviates to each star according to its expected error as given by the relation in Figure 2.16. The distribution of S/N values adopted for individual targets was chosen based on a luminosity function (translated to S/N) that matches the slope of the LF along the cluster's RGB (e.g., *Paust et al.*, 2007; *Feuillet et al.*, 2014).

If the errors are precisely known, the EM algorithm does an excellent job of returning the correct central dispersion: Out of 1000 samples, the mean dispersion was found to be 2.44 ± 0.2 $\mathrm{km\,s^{-1}}$, in essentially perfect agreement with the input value. Tellingly, this simulation found zero cases out of the 1000 trials where the dispersion was as high as 3.3 $\mathrm{km\,s^{-1}}$, the inferred central dispersion according to K18.

A problem arises, however, if we assume the velocity uncertainties are not precisely known. There are clearly reasons to expect that they may not be. In our M2FS data, we found that the velocity uncertainties returned by the Bayesian spectra fitting underestimate the true errors by about 23% (see Section 2.3.1.1). In the case of the MUSE, the implied errors for the NGC 419 data (red dots in Figure 2.16) are considerably lower, at a given S/N value, to the results presented by *Kamann et al.* (2016) for NGC 6397. The use of AO for the NGC 419 observations would not obviously improve spectral resolution (the effective slit widths are imposed by the MUSE image slicers); this suggests that even after correction (see K18), the velocity uncertainties claimed for NGC 419 (Figure 2.16) may still be significantly underestimated.

To demonstrate how the precision of the velocity uncertainties can affect dynamical results in a system like NGC 419, we carried out the same simulations as above, but this time we adopted a scaling factor F by which we modified the claimed observational errors (solid red line in Figure 2.16) compared to the actual kinematic uncer-

tainties used to assign the simulation velocities (the dashed red line in Figure 2.16). Our results indicate that for $F \sim 0.75$, half of the simulations of the MUSE data drawn from a model with a central dispersion of 2.44 $\mathrm{km\,s^{-1}}$ yield a dispersion of 3.3 $\mathrm{km\,s^{-1}}$ or greater. Thus, a 25% mean underestimate in the velocity uncertainties can alter the inferred dispersion at a level comparable to the differences between the MUSE and M2FS results. The magnitude and direction of this error is comparable to the value we found from our analysis of the kinematic errors in the M2FS data, but the quantitative effect on the central dispersion in this case is very different because the M2FS errors are so much smaller than those in the MUSE data. To quantify this, we ran the same set of simulation on the M2FS dataset including the F factor on the kinematic errors. In this case, when we assume that we have underestimated the true kinematic errors by a factor of two, we find that only 4 out of 1000 trials produce a dispersion as large as 3.3 $\mathrm{km\,s^{-1}}$. Alternatively, if we assume the actual dispersion is 3.3 $\mathrm{km\,s^{-1}}$, only 8 of 1000 trials results in an inferred dispersion as low as 2.44 $\mathrm{km\,s^{-1}}$ for a factor of two underestimate of the velocity uncertainties.

We draw from this the well-known conclusion that when the velocity uncertainties are comparable to the velocity dispersion of a system, the uncertainties must be known to very high precision. In this respect, a sample such as ours for NGC 419 is far more robust to inaccurate estimates of the velocity uncertainties than the far larger but less precise MUSE dataset. A similar conclusion would apply to many integrated-light studies of clusters where the instrumental resolution is often much larger than the intrinsic dispersion of the systems being studied. In such cases one can in principle derive a reliable dispersion, but the instrumental line profile must be shown to have been determined to exceptional precision and be free of any systematics due to, for example, temperature changes, focus drift, optical alignment, *etc.*

2.4.2 NGC 1846

The full dataset for NGC 1846 published by Ma13 consists of radial velocities for 106 targets, 22 of which were deemed to be probable members (including the planetary nebula Mo-17). The measured radial velocities of the remaining 84 stars—considered to be field stars—were not published in Ma13 but are included here in Table 2.5. Ma13 fitted a three-point velocity dispersion profile using the velocities of the 22 likely members using a projected Plummer model scaled by a derived central velocity dispersion of $2.52^{+0.26}_{-0.18}$ km s^{-1} (see Table 2.10). They separately measured a total K62 luminosity of $1.44 \pm 0.14 \times 10^5$ L$_\odot$ in V-band. As a result they obtained $M_{\rm tot} = 8.4^{+1.7}_{-1.2} \times 10^4$ M$_\odot$ and $M/L_V = 0.59^{+0.13}_{-0.10}$ (Table 2.10). Note that before fitting their data with the model dispersion profile, Ma13 corrected the observed velocities by a rotation amplitude 1.1 ± 0.4 km s^{-1} with a position angle of 60 ± 20 degrees east of north (see Table 2.10).

As a check on the dynamical analysis in the present chapter, we have applied our EM analysis (Section 2.3.2.1) using the published kinematic results from Ma13 along with the previously unpublished results for the non-members (Table 2.5). The results we compare here do not include any sort of rotation correction, nor do they exclude the binary identified in Section 2.3.1.2. The results (listed in Table 2.10) indicate that our analysis of the Ma13 data—including the associated but heretofore unpublished field-star data—results in dynamical parameters that agree well (to within 1σ) with Ma13's results obtained using a different analysis technique and different dynamical models. Certainly, at this stage we cannot disentangle any statistically significant systematic offsets that may exist between the Ma13 and M2FS-only due to analysis differences with the expected statistical noise due to the limited samples sizes in the respective studies. We will explore the systematic role of dynamical models in greater detail in later papers as we analysis a larger sample of MC clusters.

2.5 Summary and Conclusions

In this chapter, we present a pair of *Magellan*/M2FS observations of red giants in and around the intermediate-age Magellanic Cloud star clusters NGC 419 and NGC 1846, respectively. We implement a pipeline to these data that extracts stellar spectra from the raw observational data, and apply a Bayesian method to measure the radial velocities and several physical parameters for the individual target stars in our datasets. We estimate the projected central velocity dispersion of each cluster using an Expectation-Maximization (EM) algorithm (*Walker et al.*, 2015b,a) with the assumption that cluster members are spatially and kinematically distributed as expected for a single-mass K66 model and also assuming that superimposed on the cluster is a spatially uniform field population that follows a kinematically much broader Gaussian distribution. We use a number of different approaches to estimate cluster membership probabilities for individual targets in order to properly account for the influence of likely non-members. We find that allowing the EM algorithm to assign probabilities to all targets gives essentially the same results as assigning all stars with membership probabilities $> 50\%$ as certain members and all others as certain non-members.

The primary results of both clusters are as follows:

1. The median velocity uncertainties for the samples of NGC 419 and NGC 1846 are 0.38 and 0.22 $\mathrm{km\,s^{-1}}$, respectively. These are suitably small for recovering velocity dispersion as low as 2 $\mathrm{km\,s^{-1}}$ with high precision even if individual velocity uncertainties are mis-estimated by up to a significant (and unlikely) factor.

2. Our individual velocity measurements of NGC 1846 are in good agreement with those of Ma13 for 17 targets in common (see Figure 2.9). This comparison reveals one target that is a likely binary with a velocity difference of 5.6 $\mathrm{km\,s^{-1}}$ (defined as Ma13 *minus* M2FS). A comparison of the velocities for the remain-

ing in-common stars reveals a systematic velocity offset of -0.54 ± 0.15 km s^{-1} (again, defined as Ma13 *minus* M2FS) and comparable single-star velocity uncertainties from both studies. This small offset has been applied to the Ma13 sample to produce, in combination with our dataset, a larger 'Combined Sample' for this cluster.

3. For NGC 419 we measure a systemic velocity $V_{\rm sys} = 189.5^{+0.3}_{-0.3}$ km s^{-1} and a projected central velocity dispersion $\sigma_{\rm p,0} = 2.44^{+0.37}_{-0.21}$ km s^{-1} based on 46 likely members out of an initial sample of 111 targets. For NGC 1846 we obtain $V_{\rm sys} = 239.3^{+0.2}_{-0.2}$ km s^{-1} and $\sigma_{\rm p,0} = 2.04^{+0.28}_{-0.24}$ km s^{-1} from 52 likely members from our Combined Sample consisting of 195 targets (108 targets from the present study). Details related to these results and the other methodologies used to obtain $V_{\rm sys}$ and $\sigma_{\rm p,0}$ are provided in Table Table 2.7. These results are based on an assumption that both clusters' velocity dispersion profiles are adequately described by the appropriate single-mass King (K66) model that fites their respective surface brightness profiles.

4. The total masses of NGC 419 and NGC 1846 are $7.6^{+2.5}_{-1.3} \times 10^4$ M$_\odot$ and $5.4^{+1.5}_{-1.4} \times 10^4$ M$_\odot$, respectively. We estimate the total masses by scaling the dynamical K66 models with our best-fit $\sigma_{\rm p,0}$ values. The structural parameters of a K66 model are transformed from those of a corresponding empirical surface density profile (K62 profile). These results and variants are listed in Table 2.8.

5. Both clusters show marginal signals of systemic rotation. The amplitudes in the plane of sky are $0.5^{+0.3}_{-0.2}$ (NGC 419) and $0.6^{+0.2}_{-0.3}$ km s^{-1} (NGC 1846), respectively. The rotation signals have negligible impact on the masses we derive for both clusters and do not affect our results at a level significantly higher than implied by the error bars on the derived masses (see above and Table 2.8).

6. The V-band M/L ratios are $0.22^{+0.08}_{-0.05}$ and $0.32^{+0.11}_{-0.11}$ in solar units. In this calcula-

tion, the luminosities of the clusters are obtained by integrating the best-fitting K62 profile scaled to agree with published aperture photometry.

7. The mean metallicities of NGC 419 and NGC 1846 are estimated from out spectra as [Fe/H] $= -0.84 \pm 0.19$ and -0.70 ± 0.08, respectively. These results may suffer from systematic offsets due to uncertainties in background correction (Section 2.2.4) and uncertainties in effective temperatures.

As we have tried to demonstrate in this chapter, our current cluster sample—NGC 419 and NGC 1846—is largely immune to common observational uncertainties. For example, the data on which our analyses are based reside exclusive in the parameter space in which the cluster central dispersions are considerably larger than typical velocity errors for individual targets. This makes the resulting kinematic parameters largely immune to reasonable mis-estimates of velocity uncertainties and cluster structural parameters. By obtaining data on individual stars, we also avoid luminosity biases that arise from, say, integrated-light kinematics measurements or results exclusively from cluster cores where blending and scattered light can present challenges.

In the following chapters, we will apply the techniques described in this chapter to a large sample of homogeneously observed MC clusters. The final aim will be to critically compare our derived M/L ratios for simple stellar systems with those expected from stellar population models. Of course, clusters are not quite so 'simple' as one might like for this comparison, so we will also be exploring ways in which the M/L ratios of clusters can evolve due to internal dynamical processes and not just due to population evolution. Our ultimate aim is to provide a strong empirical test of M/L models that will improve the systematic uncertainties when such models are applied to distant, unresolved systems.

CHAPTER III

Expanding the Sample: Stellar Spectroscopy of 26 Magellanic Cloud Star Clusters

3.1 Introduction

In Chapter II, we described the basic methodology of our survey and the analysis of the data as applied to the SMC cluster NGC 419 and the LMC cluster NGC 1846. Both clusters had been subjects of recent high-quality multi-object spectroscopic studies (*Kamann et al.*, 2018; *Mackey et al.*, 2013) and so represented apt test cases to compare with empirical methodologies dynamical analyses. In general, we found acceptable agreement in Chapter II once the significantly improved kinematic precision of the M2FS data compared to the past studies was taken into account.

In this chapter, I describe how I obtained our full M2FS sample consisting of 26 MC clusters with high-quality kinematic data (10 in the SMC, 16 in the LMC). These clusters were chosen to span the range from ∼100 Myr to ∼13 Gyr in age, and from −2.0 to −0.4 in [Fe/H] (see Figure 3.1 and Table 3.1) in order to provide the most leverage on our tests of V-band M/L (M/L_V) predictions from populations models. Our study is based on spectroscopic observations obtained using the Michigan/*Magellan* Fiber System (M2FS) from which we measure kinematics and metallicities of samples of individual stars associated the clusters in our sample. From these

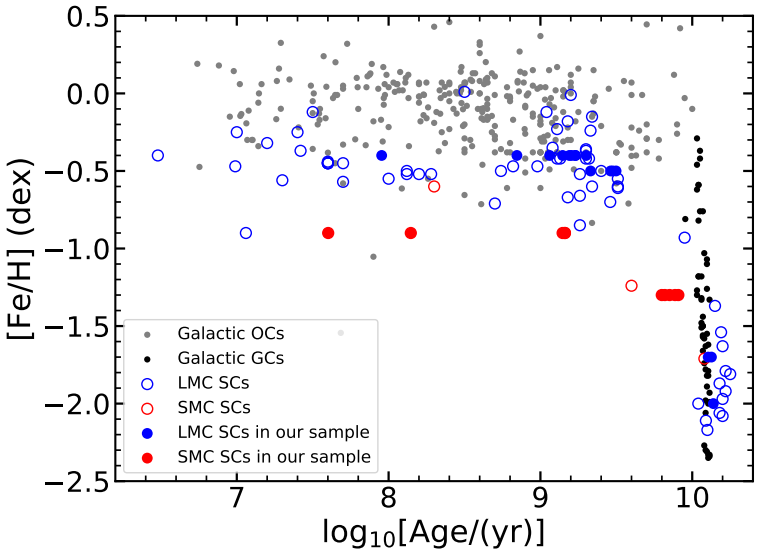

Figure 3.1: A representative plot of metallicity versus log (Age) for star clusters in the Milky Way and the Magellanic Clouds. Filled circles denote the 16 LMC (blue) and 10 SMC (red) clusters studied in this work, respectively. Different from those shown in Figure 1.2, the metallicities and ages of these clusters correspond to the values listed in Table 3.1. The cluster metallicities are adopted differently from before (as those shown in Figure 1.2) for calculating the effective temperatures in a consistent way (see Section 3.2.1 and Section 3.3.2). Open circles correspond to other clusters in the LMC (blue) and SMC (red) from the collected catalog of *Pessev et al.* (2006, 2008). For the Galactic clusters, we present the globular clusters listed in *VandenBerg et al.* (2013) (black dots) and the Galactic open clusters listed in *Dias et al.* (2002) (gray dots).

results, we derive dynamical masses and M/L_V ratios of all 26 clusters, along with the determination of independent spectroscopic estimates of the mean metallicities of the clusters.

3.2 Data Overview

3.2.1 Cluster Candidates

We selected cluster candidates from catalogs of MC clusters with good-quality age and metallicity estimates and for which we could expect to obtain samples of a few dozen stellar members. Table 3.1 lists the general properties of the star clusters in our

Table 3.1: General properties of star clusters in our sample.

Galaxy	Cluster	$V_{\rm ap}$ (mag)	Aper.[a] (arcsec)	Ref.[b]	Age (Gyr)	$(m-M)_0$ (mag)	A_V (mag)	Ref.[b]	[Fe/H][c] (dex)
(1)	(2)	(3)	(4)	(5)	(6)	(7)	(8)	(9)	(10)
SMC	Kron 3	11.41 ± 0.09	50.0	1	7.10 ± 0.70	18.80 ± 0.04	0.08 ± 0.03	7	-1.3
SMC	Lindsay 1	13.32 ± 0.05	31.0	2	7.70 ± 0.70	18.69 ± 0.04	0.15 ± 0.03	7	-1.3
SMC	NGC 152	12.33 ± 0.05	50.0	1	1.40 ± 0.20	18.93 ± 0.04	0.16 ± 0.04	8	-0.9
SMC	NGC 330	9.60 ± 0.01	31.0	2	0.04 ± 0.00	18.80 ± 0.04	0.36 ± 0.04	9	-0.9
SMC	NGC 339	12.12 ± 0.04	50.0	1	6.30 ± 0.50	18.75 ± 0.08	0.19 ± 0.03	7	-1.3
SMC	NGC 361	12.24 ± 0.01	31.0	2	8.10 ± 1.20	18.49 ± 0.04	0.40 ± 0.04	8	-1.3
SMC	NGC 411	11.81 ± 0.07	50.0	1	1.45 ± 0.05	18.82 ± 0.03	0.16 ± 0.02	10	-0.9
SMC	NGC 416	11.42 ± 0.00	31.0	2	6.60 ± 0.80	18.76 ± 0.07	0.25 ± 0.03	7	-1.3
SMC	NGC 419	10.30 ± 0.16	50.0	1	1.45 ± 0.05	18.85 ± 0.03	0.15 ± 0.02	10	-0.9
SMC	NGC 458	11.73 ± 0.03	31.0	2	0.14 ± 0.03	19.11 ± 0.20	0.12 ± 0.06	11	-0.9
LMC	Hodge 4	13.33 ± 0.02	19.0	3	2.14 ± 0.00	18.37 ± 0.03	0.12 ± 0.04	12	-0.5
LMC	NGC 1466	11.59 ± 0.03	30.0	4	13.38 ± 2.00	18.66 ± 0.03	0.16 ± 0.04	13	-1.7
LMC	NGC 1751	11.67 ± 0.13	50.0	1	1.40 ± 0.05	18.50 ± 0.03	0.38 ± 0.02	10	-0.4
LMC	NGC 1783	10.39 ± 0.03	50.0	1	1.70 ± 0.05	18.49 ± 0.03	0.00 ± 0.02	10	-0.4
LMC	NGC 1806	11.00 ± 0.05	50.0	1	1.60 ± 0.05	18.50 ± 0.03	0.05 ± 0.03	10	-0.4
LMC	NGC 1831	11.18 ± 0.02	30.0	4	0.70 ± 0.10	18.23 ± 0.09	0.03 ± 0.06	14	-0.4
LMC	NGC 1841	11.43 ± 0.02	93.5	3	13.77 ± 1.70	18.34 ± 0.04	0.35 ± 0.04	13	-2.0
LMC	NGC 1846	10.68 ± 0.20	50.0	1	1.70 ± 0.05	18.42 ± 0.03	0.07 ± 0.02	10	-0.4
LMC	NGC 1850	9.57 ± 0.20	25.0	3	0.09 ± 0.05	18.45 ± 0.03	0.37 ± 0.02	15	-0.4
LMC	NGC 1978	10.20 ± 0.02	50.0	1	2.00 ± 0.00	18.55 ± 0.04	0.16 ± 0.04	16	-0.4
LMC	NGC 2121	12.37 ± 0.01	31.0	5	2.90 ± 0.50	18.24 ± 0.04	0.22 ± 0.06	14	-0.5
LMC	NGC 2155	12.59 ± 0.48	50.0	1	3.00 ± 0.25	18.32 ± 0.04	0.06 ± 0.03	14	-0.5
LMC	NGC 2203	11.29 ± 0.15	75.0	3	1.55 ± 0.05	18.37 ± 0.03	0.16 ± 0.02	10	-0.4
LMC	NGC 2209	13.15 ± 0.01	34.0	3	1.15 ± 0.05	18.37 ± 0.03	0.23 ± 0.02	17	-0.4
LMC	NGC 2257	12.62 ± 0.02	30.5	3	12.74 ± 2.00	18.25 ± 0.04	0.12 ± 0.04	13	-1.7
LMC	SL 663	22.13 ± 0.24[d]	0.0	6	3.15 ± 0.40	18.32 ± 0.07	0.22 ± 0.06	14	-0.5

[a] Aperture radius used for measuring the $V_{\rm ap}$ magnitude in column 3.

[b] References: (1) *Goudfrooij et al.* (2006); (2) *Alcaino* (1978); (3) *Bica et al.* (1996); (4) *van den Bergh* (1981); (5) *Bernard* (1975); (6) *McLaughlin and van der Marel* (2005); (7) *Glatt et al.* (2008); (8) *Crowl et al.* (2001); (9) *Milone et al.* (2018); (10) *Goudfrooij et al.* (2014); (11) *Alcaino et al.* (2003); (12) *Grocholski et al.* (2007); (13) *Wagner-Kaiser et al.* (2017); (14) *Kerber et al.* (2007); (15) *Correnti et al.* (2017); (16) *Martocchia et al.* (2018); (17) *Correnti et al.* (2014).

[c] The adopted [Fe/H] values were estimated from the age-metallicity relations for the LMC and SMC clusters, respectively. For the LMC clusters, we assumed that [Fe/H] = −0.4 if 0-2 Gyr, [Fe/H] = −0.5 if 2-4 Gyr, [Fe/H] = −1.7 for NGC 1466 and NGC 2257, and [Fe/H] = −2.0 for NGC 1841; while for the SMC clusters, we assumed that [Fe/H] = −0.9 if 0-4 Gyr, and [Fe/H] = −1.3 if 6-9 Gyr. These age-metallicity relations were averaged from multiple papers that fitted cluster CMDs with the Padova isochrones (*Kerber et al.* 2007; *Grocholski et al.* 2007; *Milone et al.* 2009; *Goudfrooij et al.* 2014; *Milone et al.* 2018 for LMC, and *Crowl et al.* 2001; *Glatt et al.* 2008; *Goudfrooij et al.* 2014; *Milone et al.* 2018 for SMC). The final cluster metallicities from this study are listed in Table 4.1.

[d] SL 663 has no V-band aperture photometry in the literature. We have adopted the best-fit V-band extinction-corrected central surface brightness from *McLaughlin and van der Marel* (2005). The value listed here is in unit of mag arcsec^{-2}.

Table 3.2: Positions and structural parameters of star clusters in our sample.

Galaxy	Cluster	$\alpha_{\rm J2000}$ (hh mm ss)	$\delta_{\rm J2000}$ (dd mm ss)	$c_{\rm K62}$[a]	$r_{0,\rm K62}$ (arcsec)	Ref.[b]	$c_{\rm K66}$[a]	$r_{0,\rm K66}$ (arcsec)	Ref.[b]
(1)	(2)	(3)	(4)	(5)	(6)	(7)	(8)	(9)	(10)
SMC	Kron 3	00 24 45.98	−72 47 37.9	$0.79^{+0.01}_{-0.01}$	$29.62^{+0.69}_{-0.69}$	1	$1.14^{+0.05}_{-0.04}$	$23.24^{+1.26}_{-1.31}$	7
SMC	Lindsay 1	00 03 53.50	−73 28 15.0	$0.55^{+0.02}_{-0.02}$	$66.76^{+2.50}_{-2.50}$	1	$0.60^{+0.02}_{-0.02}$	$75.40^{+2.82}_{-2.82}$	...
SMC	NGC 152	00 32 56.76	−73 06 56.4	$0.98^{+0.08}_{-0.09}$	$26.70^{+2.65}_{-1.77}$	...	$1.09^{+0.09}_{-0.10}$	$27.39^{+2.72}_{-1.82}$	7
SMC	NGC 330	00 56 18.55	−72 27 45.1	$1.35^{+0.09}_{-0.08}$	$8.34^{+0.74}_{-0.69}$	...	$1.41^{+0.09}_{-0.08}$	$8.55^{+0.76}_{-0.71}$	7
SMC	NGC 339	00 57 47.62	−74 28 14.6	$0.79^{+0.01}_{-0.01}$	$32.91^{+0.59}_{-0.59}$	1	$0.82^{+0.21}_{-0.17}$	$33.18^{+6.00}_{-4.34}$	7
SMC	NGC 361	01 02 11.11	−71 36 25.3	$0.88^{+0.24}_{-0.18}$	$26.55^{+4.90}_{-3.63}$	...	$0.99^{+0.27}_{-0.20}$	$27.27^{+5.03}_{-3.73}$	7
SMC	NGC 411	01 07 55.64	−71 46 03.1	$0.87^{+0.03}_{-0.03}$	$14.50^{+0.89}_{-0.89}$	2	$1.38^{+0.11}_{-0.11}$	$9.30^{+1.09}_{-0.99}$	7
SMC	NGC 416	01 07 59.03	−72 21 20.5	$0.81^{+0.02}_{-0.02}$	$12.56^{+0.48}_{-0.48}$	1	$0.89^{+0.08}_{-0.07}$	$12.05^{+0.86}_{-0.79}$	7
SMC	NGC 419	01 08 17.26	−72 53 01.8	$1.11^{+0.03}_{-0.03}$	$14.51^{+0.93}_{-0.93}$	1, 2	$1.20^{+0.03}_{-0.03}$	$14.90^{+0.95}_{-0.95}$	...
SMC	NGC 458	01 14 52.94	−71 32 60.0	$0.98^{+0.10}_{-0.11}$	$12.01^{+1.84}_{-1.36}$	...	$1.09^{+0.11}_{-0.12}$	$12.32^{+1.89}_{-1.40}$	7
LMC	Hodge 4	05 32 25.64	−64 44 07.7	$6.54^{+5.10}_{-1.25}$	$14.27^{+1.12}_{-0.61}$	...	$2.45^{+1.91}_{-0.47}$	$14.41^{+1.13}_{-0.62}$	7
LMC	NGC 1466	03 44 32.71	−71 40 18.0	$1.00^{+0.06}_{-0.05}$	$10.81^{+0.68}_{-0.65}$	...	$1.11^{+0.07}_{-0.06}$	$11.06^{+0.70}_{-0.66}$	7
LMC	NGC 1751	04 54 12.91	−69 48 26.8	$0.84^{+0.03}_{-0.03}$	$22.00^{+1.57}_{-1.57}$	2, 3	$0.95^{+0.03}_{-0.03}$	$22.64^{+1.61}_{-1.61}$	...
LMC	NGC 1783	04 59 08.75	−65 59 15.6	$0.96^{+0.02}_{-0.02}$	$37.70^{+1.76}_{-1.76}$	2, 3	$1.08^{+0.02}_{-0.02}$	$38.58^{+1.80}_{-1.80}$	...
LMC	NGC 1806	05 02 11.86	−67 59 08.5	$0.90^{+0.02}_{-0.02}$	$24.50^{+1.12}_{-1.12}$	2, 3	$1.01^{+0.02}_{-0.02}$	$25.15^{+1.15}_{-1.15}$	...
LMC	NGC 1831	05 06 16.12	−64 55 06.9	$1.08^{+0.05}_{-0.05}$	$18.24^{+0.90}_{-1.06}$	...	$1.18^{+0.05}_{-0.05}$	$18.65^{+0.92}_{-1.08}$	7
LMC	NGC 1841	04 45 24.38	−83 59 53.3	$0.53^{+0.26}_{-0.53}$	$42.76^{+77.76}_{-9.61}$	...	$0.57^{+0.28}_{-0.57}$	$49.14^{+89.36}_{-11.04}$	7
LMC	NGC 1846	05 07 34.47	−67 27 37.8	$0.79^{+0.03}_{-0.03}$	$26.00^{+1.59}_{-1.59}$	2, 4	$0.90^{+0.03}_{-0.03}$	$26.92^{+1.64}_{-1.64}$	...
LMC	NGC 1850	05 08 46.32	−68 45 38.7	$0.99^{+0.02}_{-0.02}$	$12.40^{+0.49}_{-0.49}$	5	$0.98^{+0.02}_{-0.02}$	$12.72^{+0.51}_{-0.51}$	...
LMC	NGC 1978	05 28 44.73	−66 14 09.3	$1.16^{+0.05}_{-0.05}$	$17.30^{+0.78}_{-0.78}$	...	$1.26^{+0.05}_{-0.05}$	$17.70^{+0.80}_{-0.80}$	8
LMC	NGC 2121	05 48 12.74	−71 28 45.2	$0.60^{+0.13}_{-0.13}$	$43.21^{+9.28}_{-5.90}$	...	$0.67^{+0.15}_{-0.15}$	$47.30^{+10.16}_{-6.46}$	7
LMC	NGC 2155	05 58 31.98	−65 28 41.0	$0.84^{+0.17}_{-0.14}$	$19.20^{+2.78}_{-1.98}$	...	$0.95^{+0.19}_{-0.16}$	$19.76^{+2.86}_{-2.04}$	7
LMC	NGC 2203	06 04 42.17	−75 26 15.8	$0.69^{+0.02}_{-0.02}$	$32.90^{+1.61}_{-1.61}$	2	$0.79^{+0.02}_{-0.02}$	$34.61^{+1.69}_{-1.69}$	...
LMC	NGC 2209	06 08 36.06	−73 50 07.9	$0.85^{+0.02}_{-0.02}$	$27.30^{+1.40}_{-1.40}$	6	$0.83^{+0.02}_{-0.02}$	$28.09^{+1.44}_{-1.44}$	...
LMC	NGC 2257	06 30 12.62	−64 19 40.0	$0.81^{+0.30}_{-0.21}$	$30.99^{+6.33}_{-3.88}$	...	$0.91^{+0.34}_{-0.24}$	$32.02^{+6.54}_{-4.01}$	7
LMC	SL 663	05 42 28.20	−65 21 50.2	$2.19^{+2.93}_{-1.14}$	$27.85^{+7.10}_{-1.57}$	...	$1.86^{+2.49}_{-0.97}$	$28.58^{+7.29}_{-1.61}$	7

[a] Concentration parameter $c \equiv \log_{10} r_{\rm t}/r_0$, where r_0 and $r_{\rm t}$ are the King radius and truncation radius, respectively.

[b] References: (1) *Glatt et al.* (2009); (2) *Goudfrooij et al.* (2014); (3) *Goudfrooij et al.* (2011); (4) *Goudfrooij et al.* (2009); (5) *Correnti et al.* (2017); (6) *Correnti et al.* (2014); (7) *McLaughlin and van der Marel* (2005); (8) *Fischer et al.* (1992b).

final sample and specifies all the literature sources used to select our spectroscopic targets. Columns 1 and 2 in the table specify the host galaxy and the most common names of each cluster. The V-band aperture magnitude is listed in column 3, with the corresponding aperture radius listed in column 4. Column 5 lists the sources for these photometric results. Columns 6 through 9 list age, metallicity, distance modulus and extinction values taken from the sources listed in column 10; these four parameters were estimated in the cited sources from comparisons of a given cluster's color-magnitude diagram (CMD) with modern synthetic isochrones (see below). We gave preference to clusters with deep *HST* photometry, but if no *HST* data were available good-quality ground-based photometry was also used . Most of the studies listed in Table 3.1 used the isochrones of the Padova group (*Girardi et al.*, 2000, 2002; *Bressan et al.*, 2012). In a few cases, the sources listed in column 10 employed multiple sets of isochrones from different synthetic groups; for consistency, we adopted only their best-fit results using Padova/PARSEC isochrones. Figure 3.1 plots the ages and metallicities from Table 3.1 of our sample, illustrating the wide range of these parameters sampled by the clusters in our study.

Table 3.2 lists the positions and structural parameters of the clusters in our sample. These parameters are essential for the background/sky subtraction processes (see Section 3.2.5.2) and to establish the central velocity dispersions of the clusters (see Section 4.1). The cluster positions listed in Table 3.2 (columns 3 and 4) were derived from the *Gaia* DR2; the details of how we determined these centers will described in Section 3.2.2. For the cluster structural parameters, columns 5 and 6 give the concentration parameter and the King radius of an empirical number density profile by *King* (1962, hereafter the K62 profile). Column 7 lists the references for these structural parameters. Columns 8 and 9 give the same parameters but for a dynamical model developed by *King* (1966, hereafter the K66 model). In cases where only the K62 profile or K66 model is available from the literature, we transformed the

structural parameters from one to the other, as described in Section 2.3.2.1. This approach ensured that the central surface brightness, core radius (defined as the radius at the half of the central surface brightness) and total luminosity agree for both profiles.

3.2.2 Determination of Cluster Centers

As noted above, accurate cluster centers are crucial for both photometric and dynamical analysis. *Carvalho et al.* (2008) showed that errors in the cluster center can cause significant offsets in the resulting structural parameters, especially the central surface brightness, measured from the surface brightness profile. We explore this further at the end of this section to determine specifically how sensitive our final masses are to the centering errors in the cluster centers. As we shall show, the net impact of centering errors described below appears to be generally small, mostly negligible given other sources of errors for the derived dynamical properties of the clusters in our sample.

Many previous studies have determined cluster centers from photometric data as part of their analysis of the surface brightness profiles (e.g. *Carvalho et al.*, 2008; *Glatt et al.*, 2009; *Mackey et al.*, 2013). However, data on cluster centers is not available in the literature for all clusters in our sample. To obtain this information a more convenient approach is to take cluster centers from online astronomical databases (e.g. *Mackey and Gilmore*, 2003a,b), such as SIMBAD (*Wenger et al.*, 2000). A major limitation of this approach, however, is that the methodology, accuracy and uncertainties of the centers cited in this approach are generally not provided nor are they assured of being internally consistent. Some center positions listed for NGC 1850 and NGC 2209, for example, appear to be significantly offset from their locations on DSS images. For this reason, we chose to re-determine the centers of all the clusters in our sample using the *Gaia* DR2, as described next.

For a given cluster, we first selected all stars within 7 arcmin from the center coordinate listed on SIMBAD, brighter than 20.5 mag in G-band and with parallax less than 0.2 mas. This selection radius is considerably larger than the core (and often tidal) radii of our clusters. The selected stars were then used to compute an initial estimate of the position of the cluster center based on the mean positions in RA and Dec. The position was improved over four iterations (in a process similar to the description in *Glatt et al.* 2009) as the selection radius was decreased. For example, a second position estimate was calculated using all stars within a radius of 4 arcmin from the initial guess position. In subsequent iterations, the selection radii were halved from the previous iteration; the last iteration used a selection radius of 0.5 arcmin (for reference, most core radii of the clusters in our sample are smaller than this value; see Table 3.2). The primary reason for simply calculating the mean positions is that the *Gaia* DR2 remains impressively complete near the centers of the target clusters and hence there is a strong positional weighting inherent in the stellar samples used to determine the cluster centers.

The resulting uncertainties of the cluster centers using this procedure are between 0.6–2.0 arcsec in both RA and Dec. We adopted the coordinate of the last iteration as the final result for each cluster. The adopted centers are listed in equatorial coordinates (J2000) in columns 3 and 4 of Table 3.2.

To address any bias or funneling effect in our center determination, we re-derived three extra sets of cluster centers with the different lower magnitude limit of stars—instead of 20.5 mag, we also used 18.6, 19.2 and 19.8 mag. Figure 3.2 provides some examples of the residuals in RA (red dots), and DEC (blue crosses) from the centers determined using 20.5 mag as the lower magnitude limit. For most clusters (e.g. the top two panels of Figure 3.2), the standard deviations of the four best-fit values in either RA or DEC are below 3 arcsec, indicating good stability. For a few clusters, i.e. Kron 3, Lindsay 1, NGC 339, NGC 361, NGC 411 and NGC 1850, at least one of their

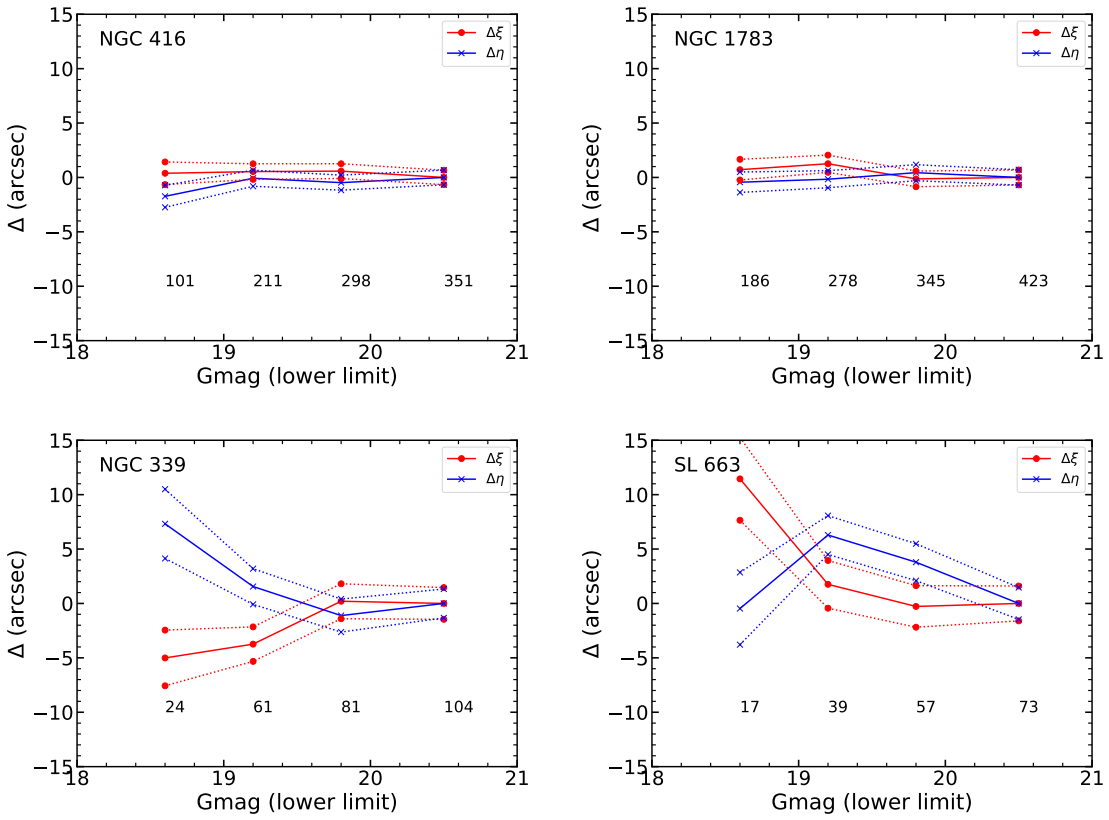

Figure 3.2: Residuals in RA ($\Delta\xi$, red dots) and DEC ($\Delta\eta$, blue dots) as a function of *Gaia* DR2 limiting magnitude for targets in the MC clusters of this study. Four representative clusters—NGC 416, NGC 1783, NGC 339 and SL 663—are presented to illustrate the stability and precision of the cluster centers determined as described in Section 3.2.2. In all panels, the solid red and blue lines represents the best-fit value of RA (ξ) or DEC (η), respectively, while the dotted lines show the corresponding 1-σ error ranges. The numbers below each set of symbols in each panel give the number stars within 30 arcsec in radius from the cluster center to that magnitude limit. The upper two clusters have comparatively large samples of stars in the *Gaia—DR2* and their center positions remain fairly stable as fainter targets are introduced. The lower panels are for sparser clusters for which the center positions vary more strongly with magnitude. These plots suggest that cluster centers determined in this manner become stable when samples of 70 or more stars are used.

standard deviations in RA and Dec falls between 3 and 5 arcsec, which is mostly due to the small number of stars brighter than 18.6 mag (see, e.g. the bottom left panel of Figure 3.2). The worst case is SL 663, for which the values are 6.7 and 4.3 arcsec in RA and DEC, respectively. As shown in the bottom right panel of Figure 3.2, the results can also be attributed to the small number of stars brighter than 18.6 mag.

Figure 3.3 compares the derived cluster centers with those provided by SIMBAD in the ($\Delta\xi$, $\Delta\eta$) plane. The $\Delta\xi$ and $\Delta\eta$ values represent the positional offsets in RA and DEC, respectively, from the SIMBAD centers to the *Gaia* DR2 centers. For NGC 1850 and NGC 2209, the new centers are offset more than 20 arcsec from the old ones (see the left panel of Figure 3.3), but they are consistent with the central locations on the DSS images. Except for these two outliers, the remaining cluster center offsets are all within 8 arcsec (see the right panel of Figure 3.3), which is typically multiple times smaller than the King radii listed in Table 3.2, column 8. To further test the influence of cluster center offsets on the central velocity dispersion, we applied the dynamical analysis described in Section 4.2 to the samples of NGC 419 and NGC 1846 obtained in Section 2.3.1. Using 100 random positions that are 30 arcsec away from the original cluster center, the derived central velocity dispersions are always within the 1-σ range of the original best-fit results. For this study, we will adopt the cluster centers derived from the *Gaia* DR2 data.

3.2.3 Target Selection Within Cluster Fields

For any given cluster, we selected a variety of specific types of targets for spectroscopic analysis. The primary science targets were typically drawn from the red giant branch (RGB) of a cluster's CMD. These targets were prioritized according to their proximity to their respective cluster center. Additional science targets beyond the formal tidal radii of clusters were also included to allow us to determine the kinematic and chemical distribution of the local field populations. For both science target

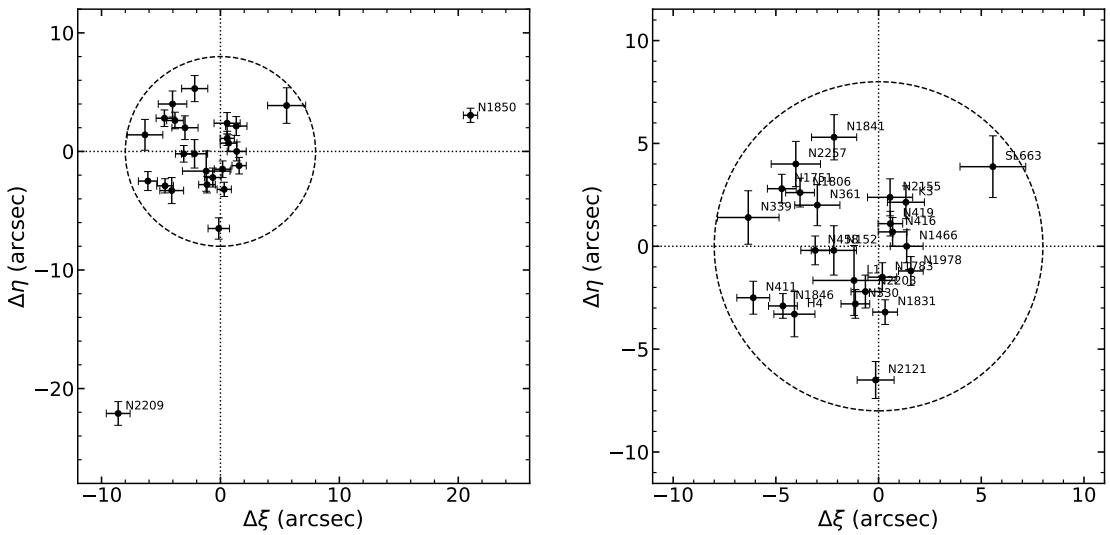

Figure 3.3: A comparison in the $(\Delta\xi, \Delta\eta)$ plane of the cluster centers determined using the *Gaia* DR2 catalog (Section 3.2.2) with centers provided by SIMBAD (*Wenger et al.*, 2000), where Δ is defined as the SIMBAD minus the *Gaia* DR2 center positions. The circles in both panels are 8 arcsec in radius. The left panel shows all the clusters studied in this work, including the two most deviant cases, NGC 1850 and NGC 2209. The right panel highlights the distribution of central position residuals for all other clusters in our sample. Further details are provided in Section 3.2.2.

selections, we identified apparently isolated stars as potential spectroscopic targets. We regarded a star to be isolated when the integrated flux of all other stars in the corresponding photometric catalog within 1 arcsec of the star adds up to $\leq 20\%$ of the candidate star's flux.

The scientific targets were selected in the following manner. Before the *Gaia* DR2 became available on April 2018, our target selection generally relied on archival *Hubble Space Telescope (HST)* images (see below), the Magellanic Clouds Photometric Survey (MCPS) $UBVI$ catalog (*Zaritsky et al.*, 2002, 2004), and the Johnson BV photometry by *Jeon et al.* (2014). Some of these sources exhibited rather large astrometric offsets and/or scale errors, which made the observational data based on these sources less reliable. For all adopted *HST* images[1], short exposures with the F555W

[1]The adopted *HST* images are SNAP-5475 (PI: Shara) for NGC 1850 and NGC 2121, GO-5897 (PI: Bolte) for NGC 1466, GO-9891 (PI: Gilmore) for NGC 1978, GO-10396 (PI: Gallagher) for NGC 339 and NGC 419, and GO-10595 (PI: Goudfrooij) for NGC 1783 and NGC 1846.

and F814W (or F450W when F814W was not available) filters were reduced using the WFPC2 or ACS modules from the `DOLPHOT` package (*Dolphin*, 2000), and the resulting CMDs were mainly used to select science targets within cluster tidal radii. For the selection of science targets beyond the cluster tidal radii, the MCPS catalog, however, was exclusively used. For NGC 1466, NGC 1841 and NGC 2257 (which are not covered by MCPS), we used *Jeon et al.* (2014)'s catalog obtained by the Cerro Tololo Inter-American Observatory (CTIO) 0.9 m SMARTS telescope. Once the *Gaia* DR2 catalog was available, we exclusively selected candidates based on the *Gaia* CMDs and requiring that the parallax of any candidate was ≤ 0.15 mas. The catalogues used for each cluster's target selection are listed in column 7 of Table 3.3.

We adopted the positions of targets from different catalogues in the following way. The coordinates for targets selected and observed before *Gaia* DR2 were tied to the NOMAD astrometric system (*Zacharias et al.*, 2004). We cross-matched all stars brighter than 17.5 mag in V-band from *HST* images or MCPS catalog with stars in the NOMAD catalog, and transformed the coordinates onto the NOMAD frame. For some *HST*-selected stars, rather large astrometric corrections of up to 1–2 arcsec were necessary. For reference, the M2FS fiber apertures are 1.2 arcsec in diameter, and systematic precision of 0.25 arcsec is typically required. After *Gaia* DR2 and to ensure the accuracy of positional-dependent kinematic analysis, we cross-matched all targets with *Gaia* DR2 and adopted their J2000 positions.

Fiber positions to sample the backgrounds in and around the clusters were also identified for many, but not all, of the cluster fields of our sample. Before the release of *Gaia* DR2, background/sky locations were selected by eye within the tidal radii of clusters were identified using F555W *HST* images when available. For regions outside the clusters' tidal radii, background/sky positions were randomly chosen from the DSS red-band images out to at least 2 arcmin from the clusters' centers. After the release of *Gaia* DR2, background/sky positions within the clusters were selected by

Table 3.3: Observations.

Galaxy	Cluster	Obs. Date (UT)	Exp. Time (On Target) (s)	Exp. Time (Offset) (s)	$N_{\rm star}$	Sources[a]	$N_{\rm sky}$	Sky Sub. Method
(1)	(2)	(3)	(4)	(5)	(6)	(7)	(8)	(9)
SMC	Kron 3	2018-08-22	3×1200	2×300	120	1	12	A
SMC	Lindsay 1	2018-08-21	1×1200+1×1500+1×1200	1×600	120	1	12	A
SMC	NGC 152	2018-08-20	3×1200	2×300	120	1	12	A
SMC	NGC 330	2018-08-18	1×1200+2×1500	2×480	39	1	15	A
SMC	NGC 339	2016-09-12	5×2400	2×600	127	2, 3	3	A
SMC	NGC 361	2018-11-26	3×1200	3×600	120	1	12	A*
SMC	NGC 411	2018-08-15	3×1500	2×600	120	1	12	A
SMC	NGC 416	2018-08-21	3×1200	2×300	120	1	12	A
SMC	NGC 419	2017-09-21	4×2100	2×480	123	2, 3	5	A
SMC	NGC 458	2018-08-15	3×1200	2×300	82	1	16	A
LMC	Hodge 4	2018-12-02	2×1080+1×840	2×240	119	1	12	A
LMC	NGC 1466	2016-12-11	3×2400	0	46	4, 5	42	B
LMC	NGC 1751	2019-02-24	3×1730	2×450	118	1	12	A
LMC	NGC 1783	2018-02-16	1×1800+2×2000	0	114	2, 6	9	B
LMC	NGC 1806	2018-11-30	1×1200+2×960	2×240	120	1	12	A
LMC	NGC 1831	2018-12-01	1×1500+1×1200+1×1500	2×300	119	1	12	A
LMC	NGC 1841	2018-02-25	2×1200	0	112	4	12	B
LMC	NGC 1846	2018-02-21	4×1200	0	111	2, 6	13	B
LMC	NGC 1850	2018-02-19	3×1200	0	113	2, 7	13	B
LMC	NGC 1978	2017-03-03	3×1800	0	130	2, 8	1	B
LMC	NGC 1978	2017-11-10	3×2000	0	129	2, 8	0	–
LMC	NGC 2121	2018-02-23	3×1200	0	117	2, 7	8	B
LMC	NGC 2155	2018-12-08	3×1800	2×600	119	1	12	A
LMC	NGC 2203	2018-12-04	1×1200+1×1000+2×1800	4×600	119	1	12	A
LMC	NGC 2203	2019-03-06	1×1600+2×1200	2×600	118	1	12	A
LMC	NGC 2209	2018-12-05	1×1200+1×1800	1×480+1×600	119	1	11	A
LMC	NGC 2209	2019-03-01	3×1850	0	118	1	11	B
LMC	NGC 2257	2018-05-18	3×1800	0	116	4	8	B
LMC	SL 663	2019-02-28	3×1750	0	118	1	12	B

[a] Sources for target selection: (1) GDR2 (*Gaia Collaboration et al.*, 2018a); (2) MCPS (*Zaritsky et al.*, 2002, 2004); (3) *HST* GO-10396 (PI: Gallagher); (4) *Jeon et al.* (2014); (5) *HST* GO-5897 (PI: Bolte); (6) *HST* GO-10595 (PI: Goudfrooij); (7) *HST* SNAP-5475 (PI: Shara); (8) *HST* GO-9891 (PI: Gilmore).

* The adopted n_k applied to all other observations (see Section 3.2.5.2).

identifying random positions that had no stars within a radius of 3 arcsec in *Gaia* DR2.

3.2.4 Observations and Data Reduction

The spectral data used in this study were obtained with the M2FS on the *Magellan*/Clay Telescope over 26 nights during a campaign lasting from September 2016 to March 2019. The detailed spectral configuration parameters are the same as described in Section 2.2.3. In summary, the single-order spectra ranged from 5130 to 5192 Å in wavelength with a mean resolution of 18,000. In parallel to these single-order observations, we usually also obtained data using a broad order-isolating filter that allowed us to obtain spectra covering 23 orders from 4058 to 5524 Å for up to

five targets (typically four stars and one background position). For this study, we use only the same order employed in the single-order spectra from these multi-order data. Table 3.3 lists the full set of observations, including the observing date, the on-target exposures, the offset exposures and the number of background/sky positions ($N_{\rm sky}$) assigned together with scientific targets. Though not detailed in the table, additional calibration data (e.g. flats, aperture reference spectra, ThArNe arc spectra, twilights, darks and biases) were obtained throughout the relevant M2FS runs. These calibration data were required by the standard data reduction steps described in Section 2.2.4.

For most clusters we also obtained exposures while the telescope was deliberately offset from the nominal target positions in order to provide another way to determine background contamination. These offset exposures were taken in order to sample the local background for every target throughout the cluster and in the corresponding field. Such offset exposures are not available for all cluster fields (see Table 3.3). The total exposure times on these offset positions ranged from 10% to 50% of the on-target exposure times (see Table 3.3 for the actual on- and off-target exposure times for all clusters). We obtained offset background measurements of this sort for 18 of the 29 visits for the 26 clusters in our sample (we visited three clusters—NGC 1978, NGC 2203 and NGC 2209—on two separate occasions each; see Table 3.3).

All data were processed using an M2FS pipeline based on IRAF[2]. The principal end products of this pipeline are the sky-subtracted spectra and their associated variances. In the pipeline, the reduction processes were largely the same as those described in Section 2.2.4, except for the last step—an improved background/sky subtraction—as described in the following subsection.

[2]IRAF is a collection of astronomical data reduction software originally written at the National Optical Astronomy Observatory (NOAO).

3.2.5 Background Correction

Background/sky contamination is significant in our dataset and challenging to measure, in part due to the presence of unresolved light from the clusters and also due to telluric components arising from sunlight scattered within the atmosphere and reflected off the moon. Together, these sources cause the backgrounds to vary in intensity and spectral character as a function of location relative to cluster centers. Background uncertainties generally have minor impact on the quality of kinematic measurements in the Mgb spectral region used in this study (see Section 3.2.4). However, good background measurements are required to obtain reliable stellar parameters such as surface gravity and metallicity. Since both of these parameters are used to help determine cluster membership (see Section 4.1), the precision of background subtraction has indirect impact on the derived dynamical properties of many of the clusters in our sample. In this section, we describe how we sampled the backgrounds in our cluster fields and the methods we developed and tested to apply background corrections to our spectral data.

3.2.5.1 Background sampling

For most of the clusters in our sample we assigned from 8 to 16 dedicated sky fibers within the tidal limits of the clusters (see Section 3.2.3 regarding how background locations were identified). There were some exceptions. NGC 1466 had no predetermined background positions (see Section 3.2.3); in this case we plugged 42 unassigned fibers to random open holes in the cluster's plug plate over as much of the full radial extent of the cluster as possible. For NGC 339 and NGC 419, only 3 and 5 sky fibers, respectively, were assigned within their tidal radii. In the case of NGC 1978, our first visit (of two) had only one sky-fiber assigned, while the second visit had none (see Section 3.2.5.2 for more on this system). In all cases, the fairly limited number of sky fibers reflects the relatively large (14 arcsec) minimum spacing

between fibers which made it difficult to pack a large number of background fibers in the central regions of the clusters.

In order to sample the background in more locations, we began to obtain observations at offset positions (see Section 3.2.4). The advantages of this approach are that the local background can be sampled close to each target star (typically about 5 arcsec), and we obtain denser background sampling near the clusters' centers. The disadvantages are that the offset positions were often contaminated by relatively bright stars, the off-target exposure times were typically only 10-50% the total time on the science targets (see Section 3.2.4 and Table 3.3), and the offset exposures were not clearly contemporaneous with target observations which can compromise their utility due to changes in observing conditions (e.g. moonrise/set, airmass changes, onset of twilight).

To better estimate the backgrounds for stars near the cluster centers requires consideration of the variations in unresolved cluster light with distance from the cluster centers. Ideally, this would also take into account spectra variations with distance, but we do not do this here. IFUs or more extensive single-fiber sampling are needed, perhaps in tandem, to properly address this.

3.2.5.2 Background subtraction

In Section 2.2.4 we developed two techniques, dubbed 'Method A' and 'Method B', to estimate background contributions to M2FS data in and around MC star clusters. 'Method A' is suitable for clusters that have dedicated sky fibers *and* offset-sky observations. Method B can be used when offset-sky observations are not available, only sky fibers which may or (usually) may not sample the inner parts of a cluster adequately. This method requires having a set of Method-A clusters available in the sample.

For Method A, we model the background in the vicinity of a cluster as

$$n(r) = n_k \left[\frac{1}{\sqrt{1+(r/r_0)^2}} - \frac{1}{\sqrt{1+(r_t/r_0)^2}} \right]^2 + n_b, \tag{3.1}$$

where $n(r)$ is the median counts obtained from all background sources that contribute to our spectra, n_k is the peak counts that come from a K62 profile with structural parameters equal to those of the cluster being analyzed (see Table 3.2), and n_b is the counts the extended background from non-cluster sources (for instance, unresolved light from LMC/SMC field stars, telluric emission, moonlight). If spectra from dedicated sky fibers and offset observations are both available, we can solve for n_k and n_b given the cluster structural parameters. The key for this method is to have enough sky positions near the cluster center—typically from the offset observations—to effectively constrain n_k.

Strictly speaking, n_k and n_b in Equation 3.1 should be determined for each wavelength to account for spectral variations of the background with distance from a cluster's center. In practice, our background sampling is too sparse in the inner regions of nearly all of our target clusters to attempt this. We therefore took the spectral shape of the background spectrum to be equal to the mean of the spectra from all the dedicated sky fibers (that is, $(n_k/n_b)_\lambda$ = Constant for all wavelengths). Clusters for which Method A was applied are flagged with an 'A' in Table 3.3.

When no offset observations, are available, determining n_k and n_b is less precise due to poor or non-existent sampling of the background near the a cluster's core. For these cases we used 'Method B' (see Section 2.2.4) in which n_k is estimated for a given 'Target' cluster by assuming that the ratio of this parameter for the cluster divided by the value of the parameter in a 'Reference' cluster is the same as the ratio of the photometric central surface brightnesses, $\Sigma_{V,0}$, of the clusters adjusted by exposure

time. That is,

$$\frac{n_{k,\,\mathrm{Target}}}{n_{k,\,\mathrm{Reference}}} = \frac{\Sigma_{V,\,0,\,\mathrm{Target}}}{\Sigma_{V,\,0,\,\mathrm{Reference}}} \cdot \frac{t_{\mathrm{exp,\,Target}}}{t_{\mathrm{exp,\,Reference}}}. \tag{3.2}$$

In practice, a Reference cluster is one for which n_k was determined using Method A; if we have N Reference clusters, we can produce a distribution of estimates for $n_{k,\,\mathrm{Target}}$.

Method B is somewhat crude in that it ignores possible transparency variations between observations of different clusters and it relies on the precision of the central surface brightnesses of the clusters in the sample, typically about 10–50%. But the method has the advantage of being applicable to all the clusters in the sample. A corollary benefit is that we can use any clusters that are suitable for background determination using Equation 3.1 (Method A) and apply Equation 3.2 (Method B) as a check on how well the latter method works.

Figure 3.4 shows the application of Equation 3.1 (Method A) to NGC 419, one of the clusters we analyzed in Chapter II. In this case, n_b and n_k can be determined reliably from dedicated sky fibers and offset observations; the resulting background profile is shown as a black solid curve in the left panel of Figure 3.4. The right panel of this figure illustrates how we apply Method B (Equation 3.2) for the case of NGC 1846, the other cluster in Chapter II. Here, n_b is well-determined from the dedicated sky fibers (filled circles in Figure 3.4) in the field surrounding the cluster, while n_k is poorly constrained due to the lack offset observations to sample the background in the inner parts of the cluster. In this instance, n_k has been estimated by applying Method B (Equation 3.2) in a pairwise manner to all 17 clusters for which Method A could be applied. These background profiles are shown as dashed gray solid lines. These profiles all have the same value of n_b as derived from the NGC 1846 dedicated sky fibers located far from the cluster center, but all have distinct values of n_k values derived by applying Equation 3.2.

As previously noted, we can apply Method B to clusters for which Method A

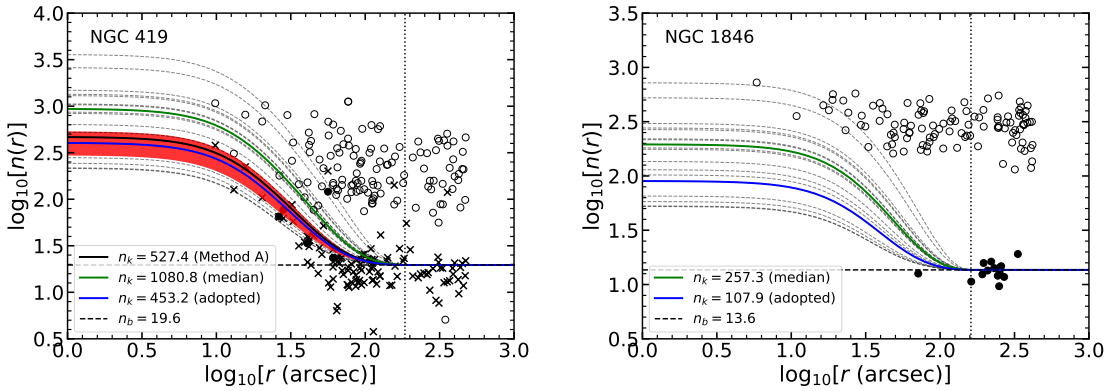

Figure 3.4: Two examples of background subtraction. In both panels, symbols represent the median total counts of target spectra (open circles), dedicated sky fibers (filled circles), and, when available, target fibers when the telescope was offset as described in Section 3.2.5.1. For NGC 419 (*left panel*), the black curve shows the best-fit profile determined using Equation 3.1 (defined as 'Method A' in Section 3.2.5.2) which employs both the dedicated sky fibers and offset-sky observations for that cluster. The y-intercepts of the horizontal dashed line and the solid black curve denote the values of the background and central mean counts (n_b and n_k, respectively; see Equation 3.1) of the fitted profile. The red band shows the central 68-percentile (taken as $\pm 1\sigma$) determined from a bootstrap error estimator that takes into account observational scatter on the estimated value of n_k. The *right panel* illustrates the application of Equation 3.2 (Method B, Section 3.2.5.2) to our data for NGC 1846. Here, the background mean counts, n_b, are determined from the dedicated sky fibers (filled circles) located outside the cluster tidal radius, r_t (denoted as a vertical dotted line for both clusters). The central background profile counts, n_k, are obtained from pairwise applications of Equation 3.2 with the 17 clusters in the sample for which Method A was applicable (see Table 3.3). The dashed gray profiles each represent one application of Equation 3.2 to a specific cluster. The green solid line follows the median (central) curve. The left panel also shows Method B results applied to NGC 419 where we use the outermost offset-sky fibers to estimate n_b and then apply Equation 3.2 as for NGC 1846. Note that the median profile (green line) runs above the black curve obtained using Method A. When this same procedure is applied to all Method-A clusters, we find the best average agreement between Method A and Method B profiles to correspond to the 'minus 1-σ' profile (the fifth-lowest profile of the 17 plotted, shown as a blue curve in both profiles).

is also applicable. In the case of NGC 419 (left panel, Figure 3.4), the median background profile of the set of profiles obtained using Method B (shown as a green solid curve) runs significantly above the one profile obtained using Method A (black line). Applying this test to all the clusters in our sample for which Method A was applicable, we found that the background profile (shown as the blue solid curve in Figure 3.4) was consistently located below the median profile.

For the sake of consistency, the final adopted background profiles for our sample were obtained by applying Method B to all clusters regardless of whether a given cluster had both dedicated sky fibers and offset-sky data. We then adopted the 'median minus 1-σ' profile as the best estimate for a clusters background-light profile. In practice, this profile corresponds to that of NGC 361, the cluster whose background profile is at the 16 percentile (the fifth of 17 profiles; that is, 'median minus 1-σ') of the rank-ordered distribution of the background profiles[3]. The background spectrum for every target star within a given cluster was calculated as the normalized median background spectrum from sky/offset fibers located beyond the tidal radius scaled by the adopted background profile for that cluster.

One cluster in our sample—NGC 1978—has inadequate data for reliable background subtraction. Specifically, our first visit deployed only one sky-fiber position, and no offset observations were obtained. Our second observation of this cluster lacked both a sky-fiber position and offset observations. As a result, neither Method A nor B be applied in this case. This limits our ability to obtain useful surface gravities and metallicities for the stars in NGC 1978. The kinematic data, however, remain useful, though as we shall see, somewhat enigmatic compared to any other cluster in our sample. We will return to this special case in Section 4.2.2.

[3]The use of the 'median minus 1-σ' background profile was found to produce consistently flat metallicity profiles within the clusters (see Section 4.1.2 below). In contrast, the median background profiles produce strong inward-rising radial metallicity gradients in nearly all the clusters of our sample. This is precisely what one would expect if the background is being oversubtracted in the central cluster regions. We take this as corroborating evidence that the 'median minus 1-σ' backgrounds are to be preferred.

3.2.6 Total Working Sample

Based on the reduction steps described in Section 3.2.4 and Section 3.2.5, our full M2FS dataset consists of 3137 background-subtracted target spectra of 2901 distinct targets in the fields of the 26 MC star clusters we observed for this study (see Table 3.1). The final total includes the effect of two clusters, NGC 2203 and NGC 2209, where we have combined background-subtracted spectra results, suitably weighted, from independent visits to each cluster (see Table 3.3). Some representative examples of background-subtracted spectra that span nearly the full range of S/N in our sample are shown in Figure 3.5. A full listing of the results from the 2901 spectra is provided in Table 3.5.

We have expanded this dataset with previously published-kinematic data of comparable quality for targets in and near the clusters of our sample (Table 3.1). We restricted our sources to those with typical velocity precisions of less than about 3 $\mathrm{km\,s^{-1}}$ (*Fischer et al.*, 1992b, 1993; *Ferraro et al.*, 2006; *Mucciarelli et al.*, 2008, 2010, 2014; *Mackey et al.*, 2013; *Patrick et al.*, 2020). Table 3.4 provides some details of the data obtained from these sources, including the total number of targets previously studied and the number of stars in common with our M2FS sample. The table also lists the cluster systemic velocities from the previous studies and the difference relative to the corresponding systemic velocities obtained from the new M2FS data in the sense M2FS results minus previously published results. Details regarding how we combined earlier and M2FS data are described in Section 4.1.3, and final consolidated results are incorporated in Table 3.5. We critically compare repeat measurements of common stars in Section 4.2.3. With the addition of these earlier datasets, our final comprehensive sample consists of 3376 spectroscopic results for 3095 distinct sources in our target clusters.

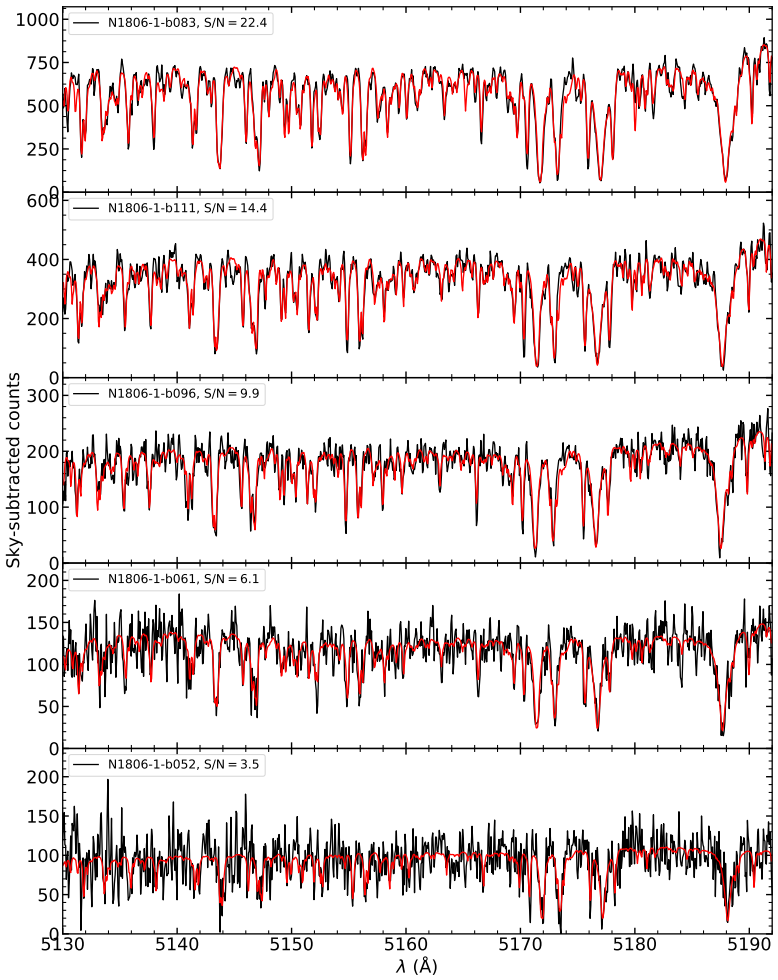

Figure 3.5: Representative spectra (black) for five stars observed with M2FS in NGC 1806 which conveniently span almost the full range of S/N of usable spectra within our full dataset. The spectra shown here have been corrected for backgrounds as described in Section 3.2.5.2. The red lines are the best-fitting spectral models determined with the Bayesian spectral fitting analysis described in Section 3.3.1. The legends within each panel list the target ID (following the naming system of Table 3.5 and the median S/N per pixel of each spectrum.

Table 3.4: Previoius Kinematic Data of Clusters in Our Sample[a]

Galaxy	Cluster	$N_{\rm sample}$	$N_{\rm common}$	$V_{\rm sys,prev}$ ($\rm km\,s^{-1}$)	$\Delta V_{\rm sys}$ ($\rm km\,s^{-1}$)	Source	Code
(1)	(2)	(3)	(4)	(5)	(6)	(7)	(8)
SMC	NGC 330	16	5	153.7 ± 1.0	-0.87 ± 1.27	*Patrick et al.* (2020)	Pa20
LMC	NGC 1783	6	0	277.6 ± 1.0	1.98 ± 1.02	*Mucciarelli et al.* (2008)	Mu08
LMC	NGC 1806	8	2	228.6 ± 0.5	0.93 ± 0.87	*Mucciarelli et al.* (2014)	Mu14
LMC	NGC 1846	105	17	239.1 ± 1.0	0.21 ± 0.46	*Mackey et al.* (2013)	Ma13
LMC	NGC 1850	52	2	251.4 ± 2.0	-2.43 ± 2.16	*Fischer et al.* (1993)	Fi93
LMC	NGC 1978	35	8	293.3 ± 1.0	-0.19 ± 1.11	*Fischer et al.* (1992b)	Fi92
LMC	NGC 1978	11	4	293.1 ± 0.8	0.01 ± 1.03	*Ferraro et al.* (2006)	Fe06
LMC	NGC 2257	6	1	299.4 ± 1.5	2.42 ± 1.53	*Mucciarelli et al.* (2010)	Mu10

[a] Columns 3 and 4 list the number of stars in the studies listed in column 7 with data of sufficient kinematic precision for inclusion in our current sample ($N_{\rm sample}$) and the number of stars in common with our current sample ($N_{\rm common}$), respectively. Columns 5 and 6 list the systemic cluster velocities for each cluster from the cited sources and the difference in the sense $\Delta V_{\rm sys} = V_{\rm sys,M2FS} - V_{\rm sys,prev}$. Column 8 lists for each source cited in Column 7 a short code used in Table 3.5.

Table 3.5: (*1st half*) Sample of all stars. (The full table is available in Appendix C.)

Galaxy	Cluster	ID	RAJ2000 (deg)	DEJ2000 (deg)	G (mag)	$G_{\rm BP} - G_{\rm RP}$ (mag)	$T_{\rm eff}$ (K)	*Gaia* DR2 ID	...
(1)	(2)	(3)	(4)	(5)	(6)	(7)	(8)	(9)	...
SMC	Kron 3	K3-1-b002	6.420511	-72.862261	18.35	1.20	4869	4688782811694646272	...
SMC	Kron 3	K3-1-b004	6.366614	-72.850370	18.29	1.26	4854	4688782983493342336	...
SMC	Kron 3	K3-1-b005	6.307460	-72.842177	17.28	1.45	4577	4688783022152125440	...
				⋮					
LMC	NGC 1978	N1978-3-r049	82.190452	-66.235682	16.14	1.04	3840	4660340443101129856	...
LMC	NGC 1978	N1978-3-b034	82.209310	-66.256802	15.94	1.90	3755	4660340271299657216	...
LMC	NGC 1978	N1978-3-b037	82.211433	-66.245587	15.76	1.95	3755	4660340370035622144	...
				⋮					
LMC	NGC 1978	06	82.193775	-66.236033	–	–	–	–	...
LMC	NGC 1978	07	82.192219	-66.238693	–	–	–	–	...
				⋮					

Table 3.5: (*2nd half*) Sample of all stars. (The full table is available in Appendix C.)

...	S/N[a]	$v_{\rm los}$ ($\rm km\,s^{-1}$)	$\log g$ (dex)	$[\rm Fe/H]_{\rm raw}$ (dex)	P_M	P'_M	Flag[b]	Source[c]
...	(10)	(11)	(12)	(13)	(14)	(15)	(16)	(17)
...	4.1	111.20 ± 0.78	1.63 ± 0.21	-1.03 ± 0.08	0.00	0.00	0000000	M2FS
...	4.3	130.36 ± 0.49	1.35 ± 0.20	-0.88 ± 0.08	0.00	0.00	0000000	M2FS
...	7.3	160.47 ± 0.31	1.21 ± 0.09	-0.75 ± 0.04	0.00	0.00	0000000	M2FS
				⋮				
...	4.4	292.97 ± 0.52	0.51 ± 0.10	-0.89 ± 0.07	1.00	1.00	0000010	M2FS
...	13.5	292.38 ± 0.16	0.84 ± 0.04	-0.65 ± 0.04	0.99	0.99	0000000	M2FS+Fi92+Mu08
...	14.7	295.43 ± 0.26	0.84 ± 0.05	-0.66 ± 0.04	1.00	1.00	0000000	M2FS+Fi92
				⋮				
...	–	291.21 ± 1.30	–	–	1.00	1.00	0000000	Fi92
...	–	288.76 ± 0.20	–	–	1.00	1.00	0000000	Fi92+Mu08
				⋮				

[a] Median S/N per pixel of M2FS spectrum.
[b] These seven-digit flags denote with a '1' the following: Rejection due to poor skew/kurtosis values in the Bayesian spectra fits (Digit 1); Excessive velocity error (Digit 2); Carbon star (Digit 3); Foreground dwarf (Digit 4); Member of a non-cluster/non-MC population (Digit 5); Has a large color offset for $T_{\rm eff}$ determination (Digit 6); Likely metallicity non-member (Digit 7). Details about how these flags are set can be found in Section 3.3.4.1, Section 3.3.4.2, Section 3.3.4.3, Section 4.1.1 and Section 4.1.2.
[c] Sources for the LOS velocities. M2FS denotes this work. Other codes are listed in column 4 of Table 3.4.

3.3 Spectral Analysis

3.3.1 Bayesian Fitting of M2FS Spectra

Our analysis of the background-corrected spectra employed the same Bayesian formalism described in *Walker et al.* (2015b); *Song et al.* (2017) and adopted in Section 2.3.1. The outputs of this analysis include estimates of line-of-sight (LOS) velocity, surface gravity and metallicity for every star along with associated uncertainties. Some examples of the best-fit spectra obtained with this method are shown in Figure 3.5.

For this study we altered one important aspect of the analysis compared to Section 2.3.1. Namely, the effective temperatures of all stars were treated as priors based on the $G_{\rm BP} - G_{\rm RP}$ colors provided in the *Gaia* DR2 rather than from $V - I$ colors from, for example, *HST* images (the method we used for NGC 419 and NGC 1846 in

Section 2.3.1). The resulting temperatures were then force to remain fixed throughout the spectral-fitting process. The details of this procedure are described in the following section.

3.3.2 Effective Temperature Priors

As argued in *Song et al.* (2017), an effective temperature prior ($T_{\rm eff}$) helps to break the temperature-metallicity degeneracy in the posterior probability density functions (PDFs) calculated using our Bayesian analysis (see Section 3.3.1). This degeneracy affects our data strongly due to the limited wavelength range (5130 to 5192 Å) of the single-order spectra we obtained (see Section 3.2.4). To help mitigate this problem, our application of the Bayesian spectral fitting procedure fixes the effective temperature throughout the optimization process for a given star.

One complication with this approach is that if we were to use the *Gaia* DR2 colors to estimate $T_{\rm eff}$ directly, our temperature estimates would likely exhibit significant systematic and random uncertainties. There are two reasons for this. First, many of the stars in our sample are comparatively faint ($G > 17$ mag) for the *Gaia* sample, and so their formal photometric errors are moderate (*Evans et al.*, 2018). Second, given the high source densities in many of our fields, background variations and contamination due to crowding can lead to significant additional uncertainty in the *Gaia* $G_{\rm BP} - G_{\rm RP}$ colors (*Weiler*, 2018; *Maíz Apellániz and Weiler*, 2018). Moreover, in clusters, blending of red giants with typically hotter, fainter cluster members tends to drive colors systematically to the blue.

These issues are particularly problematic for $T_{\rm eff}$ determinations in RGB stars since even a small shift in color can lead to a significant temperature change which, in turn, degrades the precision of the metallicity estimate of a star. To mitigate these problems, we have devised a method to estimate $T_{\rm eff}$ that depends primarily on the observed G magnitude of a star and that relies on the fact that the stars in our sample

were almost exclusively selected to be located on the RGBs of their respective clusters (see Section 3.2.3).

The method starts by identifying an isochrone that matches the adopted age and metallicity of a given cluster (see Table 3.1). For this study we have chosen to use the PARSEC isochrones (version 1.2S, *Bressan et al.*, 2012) converted to the *Gaia* DR2 photometric system following the prescription of *Maíz Apellániz and Weiler* (2018)[4]. We then plotted the synthetic isochrones onto the observational G vs $G_{\rm BP} - G_{\rm RP}$ plane (an example is shown in the top left panel of Figure 3.6). In all cases, we shifted the isochrones to the observational plane with the appropriate reddening values and distance moduli for each cluster (Table 3.1). As suggested by the PARSEC model website, these corrections used the extinction parameters $A_G = 0.86A_V$, $E(G_{\rm BP} - G_{\rm RP}) = 0.42A_V$ and $R_V = 3.1$ within the extinction relations from *Cardelli et al.* (1989) and *O'Donnell* (1994). For computational convenience, we then fit each isochrone in the observational plane to a third-order spline to smooth out round-off noise and some of the non-monotonic evolutionary behavior in the isochrones themselves. An example of such a fit is illustrated in the top left panel of Figure 3.6.

The *Gaia* DR2 photometry for every cluster was corrected to the 'true' G-band system as suggested by *Anders et al.* (2019) before plotting the data in the observational CMD with their respective isochrones. Each star in our spectroscopic sample was then projected at constant G magnitude onto the spline fits to the RGBs on a cluster-by-cluster basis. The corresponding $G_{\rm BP} - G_{\rm RP}$ color at that point in the isochrone was adopted as 'the' color for that star. The top right panel of Figure 3.6 provides a schematic illustration of this process, and was adopted for all clusters older than about 0.5 Gyr since their RGB sequences could be reasonably defined from the models.

For the three clusters in our sample younger than 0.5 Gyr (NGC 330, NGC 458

[4]In practice, we computed tailor-made isochrones for each cluster in the appropriate photometric system using the PARSEC website (`http://stev.oapd.inaf.it/cgi-bin/cmd`).

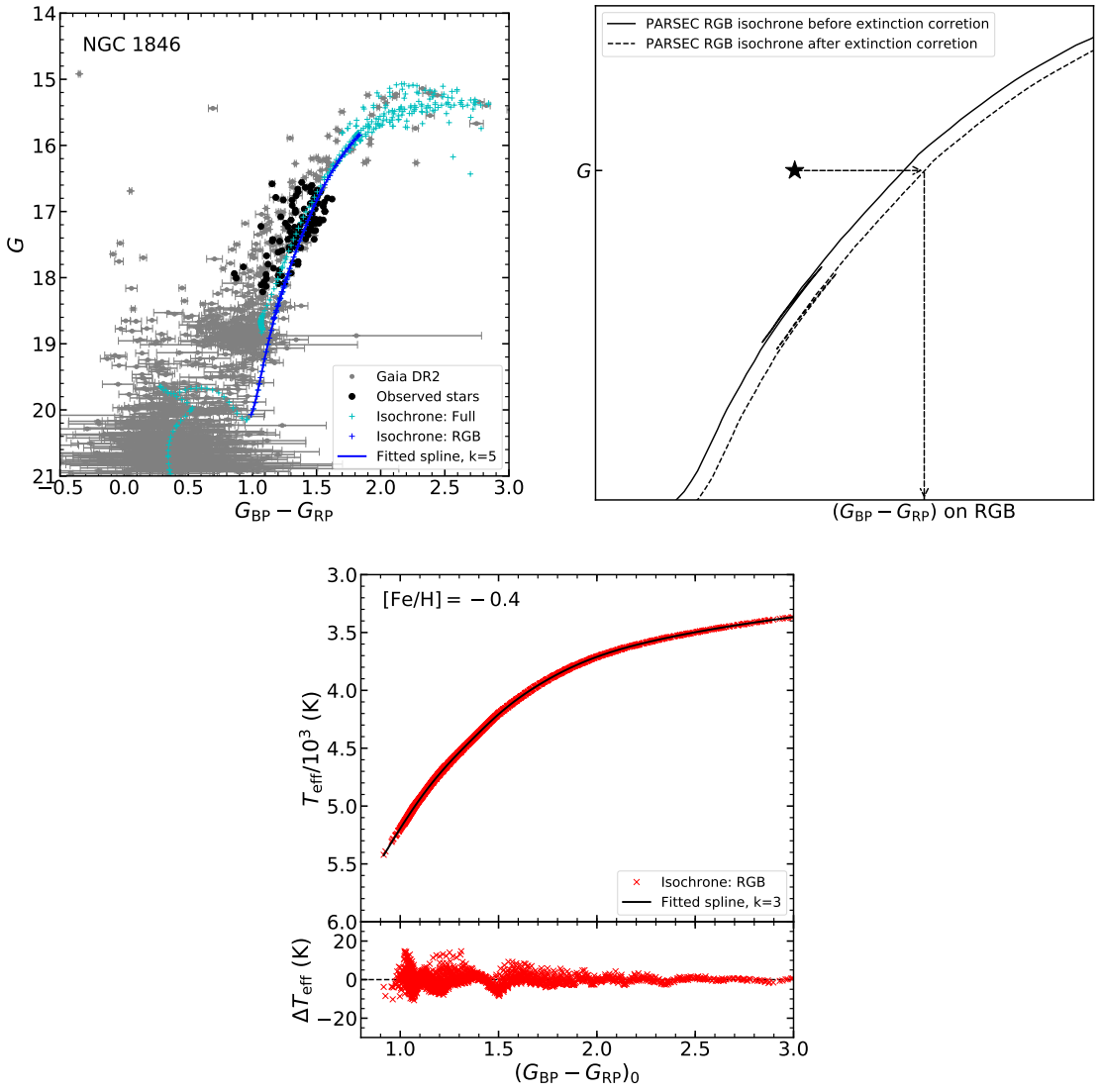

Figure 3.6: (Top left panel) The color-magnitude diagram for NGC 1846 based on *Gaia* DR2 and using the DR2 photometric system. A PARSEC model isochrone (*Bressan et al.*, 2012) using cluster's age and metallicity estimates (see Table 3.1) is overplotted (light blue crosses). Gray dots correspond to all *Gaia* DR2 stars located 2 arcmin from the cluster center, while black dots represent the stars observed in our sample. The blue crosses highlight the RGB sequence of the isochrone, and the blue solid curve is a spline fit to this RGB segment. (Top right panel) Following the discussion in Section 3.3.2, this plot illustrates schematically how a given star in the CMD is projected to the adopted RGB sequence to determine the star's model-based $G_{BP} - G_{RP}$ color. (Bottom panel) The red symbols show the *Gaia* DR2 color/temperature relation for a metallicity of [Fe/H] = −0.4 obtained from the PARSEC models. These individual color-temperature points were fit to a third-order spline (black line; fit residuals are shown in the lower subpanel). We used this spline fit to convert the adjusted colors (see middle panel) to effective temperature for each star. These temperatures were fixed during the Bayesian spectral fitting procedure (see Section 3.3.1).

and NGC 1850), we did not correct the colors in this manner but simply adopted the published *Gaia* DR2 colors corrected as prescribed by *Anders et al.* (2019). For these systems, the red (super)giants tend to brighter than 17 mag in G-band and hence exhibit relatively small color errors, and these stars are less susceptible to crowding/background-related photometric errors. Moreover, these younger stars tend to cluster in a region in the CMD rather than on a distinct giant branch (see, e.g. *Mermilliod*, 1981; *Alcaino et al.*, 2003; *Correnti et al.*, 2017; *Milone et al.*, 2018); hence they are ill-suited for the temperature-determination procedure we used for the rest of our sample which assumes a well-defined red giant locus with little color spread at a given luminosity.

Figure 3.7 shows a histogram of the color shifts in $\Delta(G_{\rm BP} - G_{\rm RP})$ that we determined for every star with a tabulated *Gaia* DR2 color using the method described above. The mode of this distribution is offset from, but close to zero, confirming that most of these objects are consistent with being RGB/AGB stars. This supports the efficacy of our approach. Since the slope of the giant branch is approximately $\delta(G_{\rm BP} - G_{\rm RP})/\delta G \sim 0.2$, the color error is about 20% the G-magnitude error for a given star *if it is on the RGB as assumed*. Consequently, the resulting error distribution of the adopted colors is considerably narrower than the distribution of the 'raw' $\Delta(G_{\rm BP} - G_{\rm RP})$ implied by Figure 3.7. It is also evident in Figure 3.7 that the $\Delta(G_{\rm BP} - G_{\rm RP})$ distribution exhibits a moderate tail to positive values. This implies that some comparatively hot stars fail our assumption that they are on the RGB and hence they have been assigned colors that are systematically too red.

The fact that the mean offset in $\Delta(G_{\rm BP} - G_{\rm RP})$ differs between the LMC and SMC (Figure 3.7) suggests that our color corrections may depend on metallicity (larger effect for larger metallicities in the LMC). We will return to this problem in Section 4.1.2 and Section 4.2.4 where we use Figure 3.7 to help us determine mean cluster metallicities.

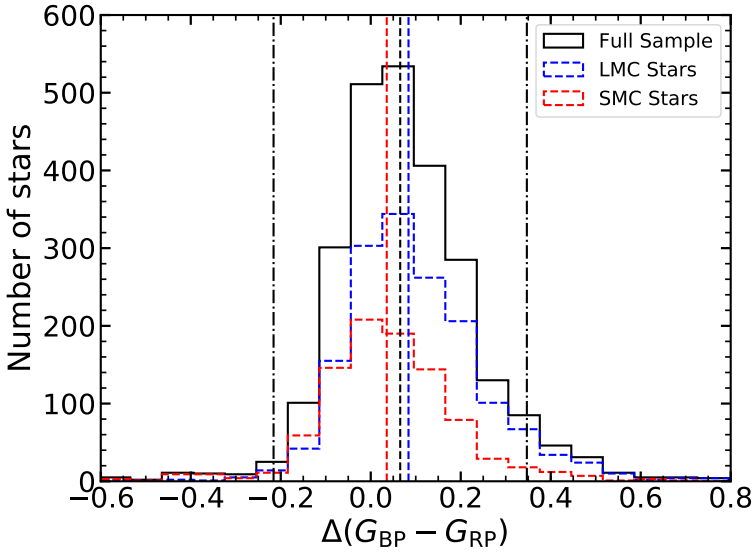

Figure 3.7: A histogram of the color shifts, $\Delta(G_{\rm BP} - G_{\rm RP})$, between the *Gaia* DR2 color of a given star in our dataset and our adjusted color obtained as described in Section 3.3.2 and Figure 3.6. For 2543 stars in the full sample, the biweight mean offset $C_{\rm BI,dcolor}$ in $\Delta(G_{\rm BP} - G_{\rm RP})$ (denoted by the dashed line) is 0.065 with a $2S_{\rm BI,dcolor}$ range of ± 0.281 (denoted by the dot-dash lines). A total of 203 stars are located outside the dashed lines, though the distribution is clearly skewed toward positive values (68 stars on the negative side and 135 on the positive side). This likely represents the fact that some stars located blueward of the adopted RGB sequences in individual clusters (see the middle panel of Figure 3.6) are hotter than red giants. For the purpose of metallicity determination described in Section 4.1.2, we use the stars within two biweight dispersion scales of the biweight mean, i.e. $|\Delta(G_{\rm BP} - G_{\rm RP}) - C_{\rm BI,dcolor}| \leq 2S_{\rm BI,dcolor}$. This ensures that only stars with relatively small color shifts—likely true RGB stars—are used to determine the cluster metallicity. The blue and red dashed histograms show the distributions in $\Delta(G_{\rm BP} - G_{\rm RP})$ for the LMC (1595 stars) and the SMC (948 stars). The mean offsets of these histograms are $C_{\rm BI,dcolor} \pm 2S_{\rm BI,dcolor} = 0.084 \pm 0.283$ for the LMC and 0.036 ± 0.269 for the SMC.

The final step in estimating $T_{\rm eff}$ values for our target stars was to convert their $G_{\rm BP} - G_{\rm RP}$ colors—either the 'raw' values for stars in the three young clusters or the model-based values determined using the procedure above—to temperatures. We again used the PARSEC RGB sequence for each cluster (appropriately reddened and adopting the ages and metallicities in Table 3.1) to define a color-temperature relation for each case (see the bottom panel of Figure 3.6 for an example). The final $T_{\rm eff}$ values were then tabulated for every star and these values are provided in Table 3.5.

3.3.3 Velocity Uncertainty Correction

To reliably measure small internal velocity dispersion of systems such as the star clusters in our sample, high-quality kinematic data and reliable error estimates are essential (see, e.g. *Kamann et al.*, 2016). In Section 2.3.1.1, we analyzed repeat measurements of individual stars to empirically assess the quality of the uncertainties computed by the Bayesian spectral analysis for the cases of NGC 419 and NGC 1846. We found that individual velocity uncertainties returned by the Bayesian analysis underestimated the true uncertainties by approximately 23% and 12%, respectively.

In this study we explore this question again for the two clusters in our sample with the lowest derived central velocity dispersions, NGC 2155 and SL 663 (see Section 4.1). As in Section 2.3.1.1, we compared the velocities from individual exposures, s_i, and then fit a Gaussian to the error distribution expressed in units of the formal error, σ_i, returned by the Bayesian analysis for the i-th spectrum (see *Kamann et al.*, 2016 for analogous analysis). One complication with this test is that there are small systematic velocity shifts in M2FS data that correlates with the temperature of the instrument near the fiber pseudo slit (see *Walker et al.*, 2015a). The spectra from the individual exposures for both clusters were first corrected for these shifts and referenced to a common velocity scale before generating the s/σ distribution. The results of this analysis show that the velocity uncertainties for these clusters were

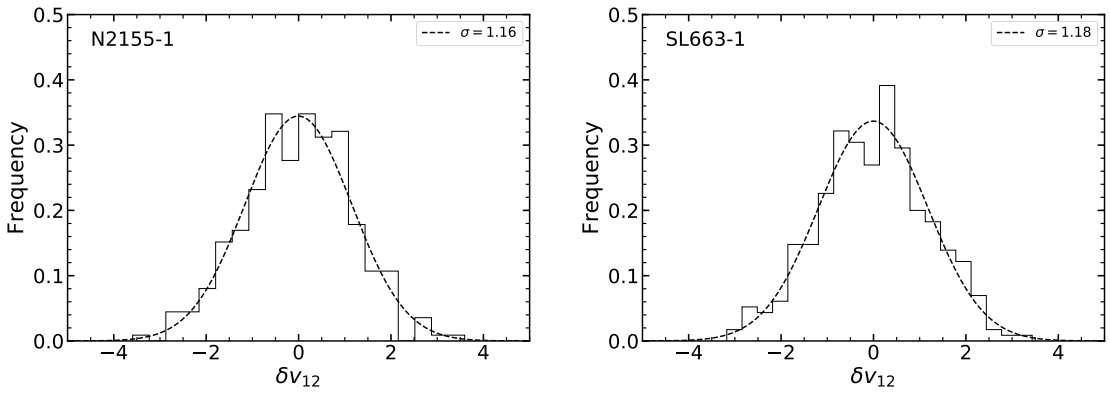

Figure 3.8: Measured LOS velocity differences for targets observed in individual M2FS exposures (see Section 3.3.3 and Table 3.3). The parameter δv_{12}—defined in Equation 2.4 in Section 2.3.1.1—represents the differences in measured velocities from individual exposures for a given star. The dashed lines are Gaussian fits to the histograms, and the standard deviation of each fitted Gaussian are given in the legend of each panel. In this figure, we have combined results for all stars regardless of the mean S/N of their spectra

similarly underestimated as found in Section 2.3.1.1, i.e. approximately 16% and 18% for NGC 2155 and SL 663, respectively (see Figure 3.8).

Together with our earlier results in Section 2.3.1.1, we conclude that our application of the Bayesian spectral analysis underestimates the true velocity errors by $17\% \pm 3\%$. Consequently, we have increased the velocity uncertainties from all Bayesian spectral analysis results by 17% for prior to carrying out any dynamical analyses of these systems (see Section 4.1 and Section 4.2)[5].

[5]The origin of the 17% correction likely lies in the fact that our data-reduction pipeline rebins the data during the extraction and wavelength-calibration steps. This is confirmed by independent reductions of similar data by M. Walker (private communication) who finds that unbinned analyses lead to a much smaller correction consistent with unity. His results also independently confirm the velocity-uncertainty correction factor of 17% that we obtained. We consider the correction to be sufficiently small and sufficiently well-determined to use it to adjust our formal velocity error estimates for the purposes of this study.

3.3.4 Toward a Final M2FS Spectral Sample

3.3.4.1 Rejecting spectra with poorly determined parameters

Our Bayesian analysis as described in Section 3.3.1 generates posterior parameter distribution functions (PDFs) for 14 free parameters (the 15th, $T_{\rm eff}$, is fixed as described in Section 3.3.2) used to characterize the model spectra (see *Song et al.* 2017 for details). The analysis measures the skew, S, and kurtosis, K, of all of these PDFs. We use the S-K values for the PDF of the LOS velocity ($v_{\rm los}$) parameter for every spectrum to carry out an initial quality cut on the data. After inspection of the distribution of the skew/kurtosis values for the LOS velocities, we found that the same cuts in S and K from *Walker et al.* (2015b) were suitable for our data, namely $|S| > 1$, or $|K - 3| > 1$. This 'SK cut' led to the rejection of 71 spectra from our sample. These cases are flagged in column 17 of Table 3.5.

All but three of the stars rejected for skew/kurtosis have low average S/N of 1.2 ± 0.1. Among these 68 stars, three appear to have spectra consistent with those of carbon (C) stars (more on these in Section 3.3.4.2) at low average S/N (~ 1.2 for these three; see Figure 3.9). Apart from these low-S/N cases, the additional three spectra flagged in the SK cut all have fairly high mean S/N (25 ± 8) but contain few identifiable spectral features. The Bayesian analysis was likely unable to settle on well-defined LOS velocity in these cases, resulting in their large skew/kurtosis indices. For reference, the spectra of these three stars are also shown in Figure 3.9. We will not use these stars in any subsequent analyses in this thesis.

3.3.4.2 Stars with anomalous velocity uncertainties

Figure 3.10 shows the distribution of corrected velocity uncertainties, ε_v, as a function of median S/N ratio for every pixel in every target spectrum obtained for this study, in both linear space (left panel) and log-log space (right panel). The well-

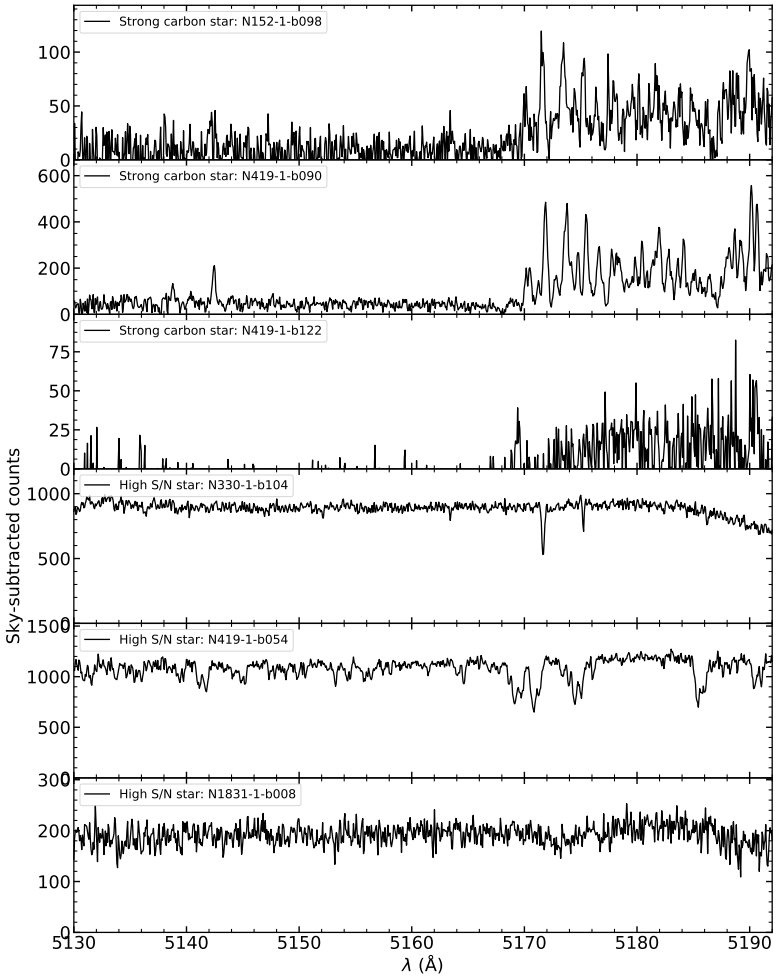

Figure 3.9: Examples of M2FS spectra of stars rejected by the SK cut described in Section 3.3.4.1. The three top panels appear to be strong C stars at low S/N (more on these in Section 3.3.4.2). The bottom three panels show stars that have high mean S/N values, but were still rejected by the SK cut due to having too few or blended lines.

populated ridge lines reveal a robust global trend of velocity error with S/N for our M2FS dataset. The approximately linear trend visible in the log-log plot indicates that a good fit to these data has the form of a power law.

With the aim of using the relation between ε_v and S/N to remove outliers from our kinematic sample, we fit a linear relation in the log-log plane using an unweighted least-squares fit to all points corresponding to spectra with median S/N ≤ 20. Targets removed from the SK-cut described in Section 3.3.4.1 were not used to compute this fit. The fitted relation is shown as a solid straight line in the log-log plot and as a solid line for the corresponding power law in the linear-space plot (the coefficients for the fit equations are provided in Figure 3.10). We then computed logarithmic residuals ($\Delta = \log_{10}\varepsilon_v - \log_{10}\varepsilon_{v,\mathrm{fit}}$) to estimate the Tukey's biweight location ($C_{\mathrm{BI},\Delta}$) and biweight scale ($S_{\mathrm{BI},\Delta}$) of the data about the fitted line in the log-log plot (*Beers et al.*, 1990). The dashed straight line in the log-log plot in Figure 3.10 (right panel) the line offset upward by $C_{\mathrm{BI}} + 3S_{\mathrm{BI}}$ from the fitted relation; the dashed line in the linear plot (left panel) shows the power law relation corresponding to this offset line. We also chose to keep all stars with high-S/N spectra that resulted in $\varepsilon_v \leq 0.5$ km s^{-1}; this condition is shown as a dot-dash line in both panels.

We define the dashed/dot-dashed lines in Figure 3.10 as a 'rejection boundary.' Excluding the 71 stars already rejected as SK outliers (Section 3.3.4.1), 62 additional stars lie above this boundary. We inspected each of these 62 spectra and found that we could classify them into the following distinct categories, each of which are flagged in column 17 of Table 3.5:

Carbon Stars. A total of 21 C stars were identified based on the presence of a clear C_2 Swan band feature at λ5165 Å (*Johnson*, 1927; *King*, 1948). Among these stars, 17 have quite strong absorption features (the first spectrum in Figure 3.12 shows a typical example), while the remaining four C stars have relatively weak Swan-band absorption (the second spectrum in Figure 3.12 shows a typical case). Since the spectral library

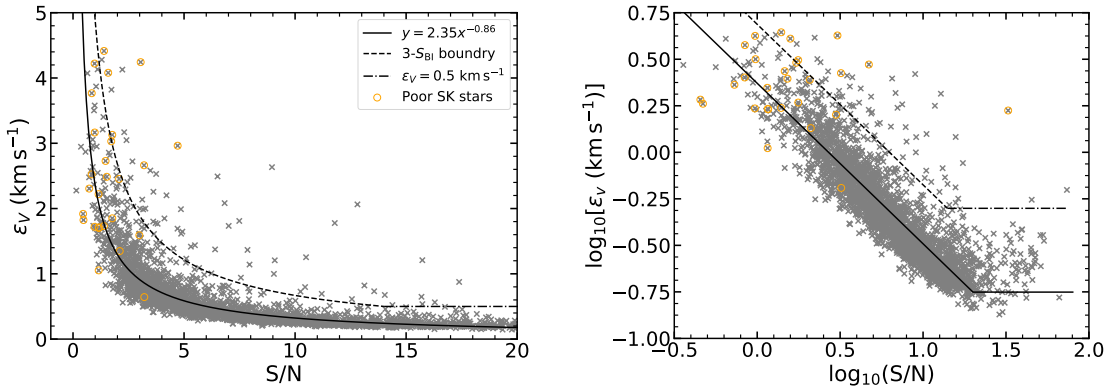

Figure 3.10: Corrected LOS velocity uncertainties versus median S/N per pixel for all stars from the 26 clusters in both linear place (left panel) and log-log space (right panel). The solid lines correspond to a linear relation in the log-log plane (right panel) fit to all points with S/N ≤ 20 (excluding the yellow circles rejected by the SK discussion in Section 3.3.4.1). For S/N > 20, we assume ε_v is constant at 0.18 km s^{-1}. The dashed and dot-dashed lines together denote the upper acceptance limits in these plots as described in Section 3.3.4.2.

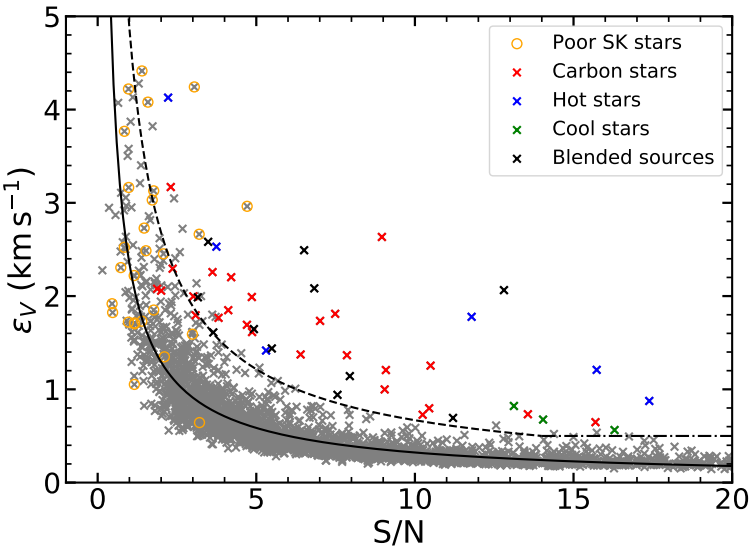

Figure 3.11: The same plot as in the left panel of Figure 3.10 but with some stars highlighted by colored symbols. The meanings of these symbols are given in the legend. Different symbols correspond to different types of anomalous stars identified in Section 3.3.4.2. The cases denoted as 'poor SK stars' are discussed in Section 3.3.4.1.

we are using (*Lee et al.*, 2008a,b) does not model C stars, it is unsurprising that our Bayesian analysis returned LOS velocities with large uncertainties relative to other stars at similar S/N.

Hot Stars. A total of eight stars appear to be hot stars that were forced to an incorrect low temperature using the method to fix $T_{\rm eff}$ described in Section 3.3.2. We chose not to single out these stars and allow their $T_{\rm eff}$ to float as this would be inconsistent with the strategy described in Section 3.3.2. Two examples, one also exhibiting moderate rotation, are shown in Figure 3.12.

Cool Stars. A total of three stars appear to be cool giant stars with the feature of TiO bands above ∼5180 Å (the fifth spectrum in Figure 3.12 shows a typical example). Similar to hot stars, cool stars were forced to an incorrect temperature—in this case too high—as described in Section 3.3.2. Moreover, the spectral library we used does not contain stars sufficiently cool that exhibit TiO bands. For these reasons, it is likely unsurprising that the Bayesian analysis returned poor LOS velocity uncertainties for these cases.

Blended Sources. A total of 12 stars are confirmed as sources with the features of more than one star (see the sixth spectrum in Figure 3.12). The spectra in this category provide poor LOS velocities for a given S/N. We did not carry out dual-star fits as in Section 2.3.1.1 because these stars represent a fairly small sample that may have a different error distribution from the single-star fitted spectra.

Statistical Tail. A total of 18 stars appear to represent the tail of the distribution of the velocity errors relative to the fit line/power law evident in Figure 3.11. These stars represent about 0.6% of the total sample of spectra, roughly consistent with what a 3σ cut would achieve for a normal distribution.

Due to the relatively high frequency of C stars in our sample of rejected spectra, we developed a more objective means of identifying candidate C stars regardless of

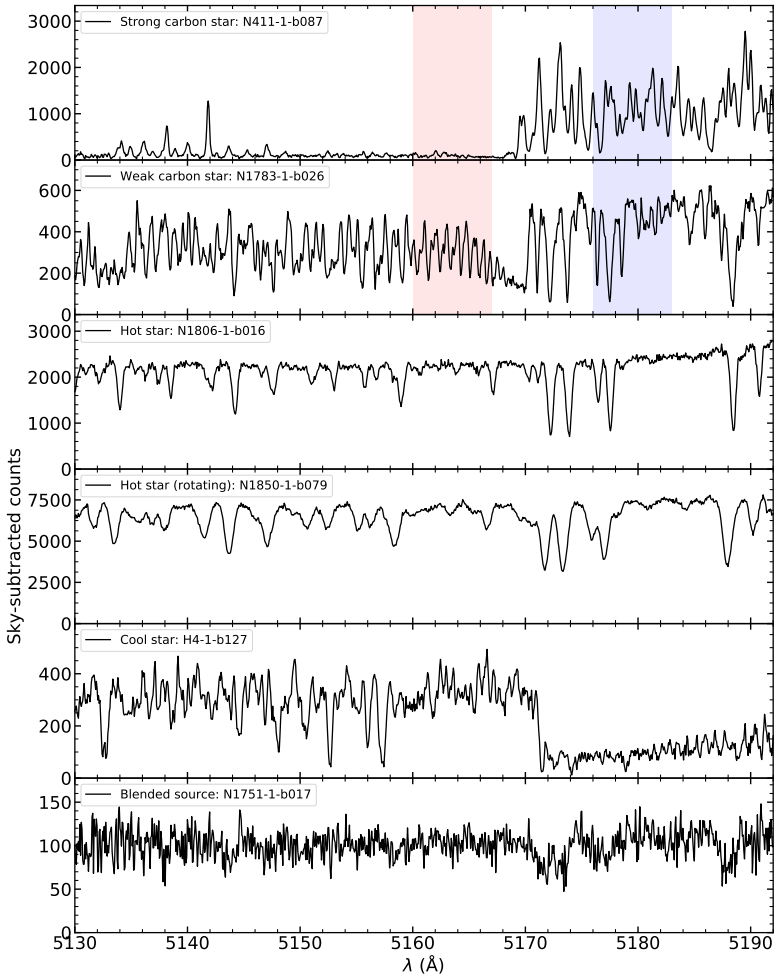

Figure 3.12: Examples of M2FS spectra of stars with anomalous velocity uncertainties as identified in Figure 3.11. From top to bottom, we show the spectra of a strong C star, a weak C star, a star with high surface temperature (hot star), a similarly hot star but with moderate rotation ($v \sin i \sim 30\,\mathrm{km\,s^{-1}}$), an M-type star with low surface temperature (cool star), and a blended source. For the two C stars, we indicate the two bands used to identify such stars as outlined in Section 3.3.4.2. A total of 62 targets with anomalous velocity uncertainties (as described in Section 3.3.4.1 and identified in Figure 3.11) are excluded from our cluster dynamical analysis.

where they lie in Figure 3.11. Specifically, we measured the ratio of the fluxes in all the spectra of our sample on the red and blue sides of the C_2 band head (the first two spectra in Figure 3.12 illustrate where these bands are located). This ratio cleanly identified all C stars in the velocity-error rejection region of Figure 3.11, as well as seven apparent C stars below the rejection boundary. Four of these are are strong C stars similar to the top spectrum in Figure 3.12, and three are weaker C stars with spectra similar to the second panel of this figure. For consistency, we have removed these four strong C-stars from our sample but have retained the three weak C-stars since they show clean atomic features similar to non-C stars of similar color.

This method of identifying C stars found numerous even weaker C stars. We have chosen to accept these in the present sample as they are mildly affected by the C_2 features and in all cases their spectra appear to provide good LOS velocity estimates. We plan to discuss this expanded C-star sample in more detail in a future paper (see Section 6.2.1).

In Section 2.3.1.1 we identified eight stars in NGC 419 and NGC 1846 (four in each) that we rejected using similar criteria as described here but based only on the small samples of these two clusters. The four stars in our NGC 419 sample (three C stars and one blended source) rejected in that section have also been rejected in the present sample. However, the four stars in our NGC 1846 sample that were rejected in Section 2.3.1.1 consist of three weak C stars and one mildly blended source. All four of these stars were *not* rejected in the present analysis using our full spectral sample. This very slightly—and statistically indistinguishably—alters our final dynamical results below (see Section 4.2) for NGC 1846 compared to the results reported in Chapter II.

3.3.4.3 Foreground dwarfs

Surface gravity is one of the parameters returned by the Bayesian analysis (Section 3.3.1) and this can be used to identity foreground dwarf stars in our sample. As seen in Figure 3.13, there is a clear tail in the distribution of $\log g$ extending to larger values. We have adopted $\log g \geq 3.2$ as the dividing value between giants (lower $\log g$) and dwarfs. A total of 84 stars in our sample were removed using this criterion and are flagged in column 17 of Table 3.5. The distinctive spectral signatures of these stars are evident by comparing the dwarf-star spectra in Figure 3.14 with spectra of giants of similar colors and S/N ratios shown in Figure 3.5. As expected, the proper motions of these stars, as provided in *Gaia* DR2, exhibit a large spread that is offset from the mean proper motions of the MCs.

At this stage, our Bayesian spectral-fitting results have allowed us to produce a well-defined M2FS sample consisting of 2680 spectra of (mostly) RGB stars in our 26 target clusters (see Table 3.5). Figure 3.5 presents some representative spectra of normal stars in our sample along with their Bayesian spectral fits.

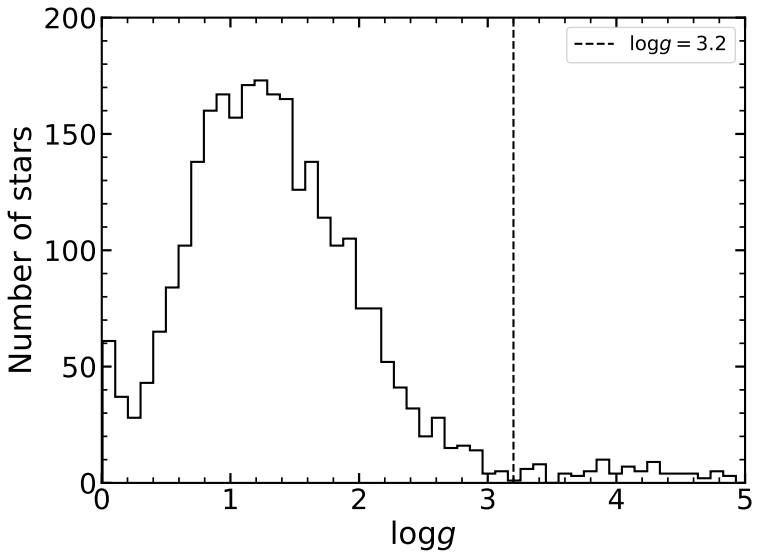

Figure 3.13: A histogram of the surface gravity for 2764 stars in our M2FS sample after removing the stars with either poorly determined parameters (see Section 3.3.4.1) or anomalous velocity uncertainties (see Section 3.3.4.2). The vertical dashed line corresponds to an adopted empirical criterion, $\log\, g = 3.2$, to divide giants and (foreground) dwarfs, as described in Section 3.3.4.3. The 84 stars to the right of dashed line were removed from our sample as likely foreground dwarfs.

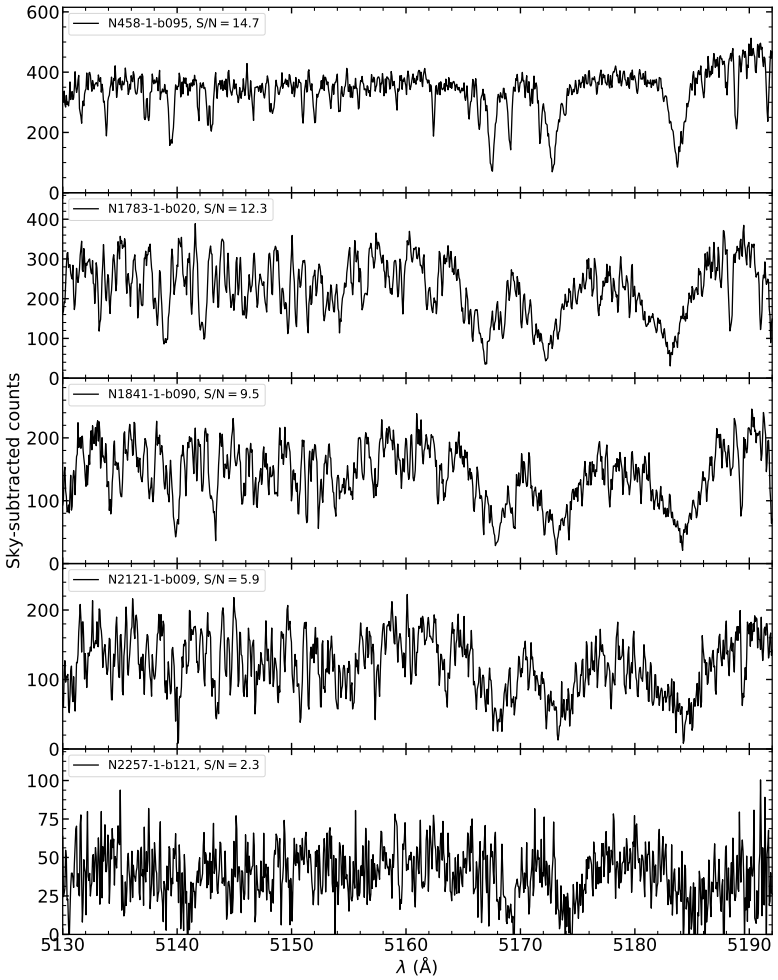

Figure 3.14: Examples of M2FS spectra of dwarf stars confirmed in our sample. From top to bottom, we show dwarf stars span similar S/N range as those giants shown in Figure 3.5; these dwarf stars and giants also have comparable colors. As discussed in Section 3.3.4.3 and Figure 3.13, 84 dwarf stars with spectra similar to these were removed from the sample used to for the dynamical analyses the clusters in this study.

CHAPTER IV

Kinematic Analysis: From Spectral Results to Cluster Mass-to-Light Ratios

4.1 Cluster Membership

We closely follow the expectation-maximization (EM) analysis used in Section 2.3 to determine simultaneously the cluster dynamics and the cluster membership probabilities of all stars in our samples. For most of the clusters, we assume in the EM analysis that there are two stellar populations in each kinematic cluster sample: one corresponding to the cluster, and one corresponding to the LMC/SMC field stars. Following the approach described in Section 2.3.2.1, we still adopt single-mass K66 models[1] (as listed in Table 3.2) to generate the projected velocity dispersion profile of each cluster, while the field population is represented by a Gaussian distribution. In our EM analysis for two old LMC clusters, NGC 1466 and NGC 1841, however, we only assume a single population (also in the form of the K66 model) because both clusters are so distant from their parent galaxy (the LMC) that they lack significant numbers of LMC field stars.

An issue that arises at this stage is that most clusters contain stars that are either associated with a third population not included in our model (see Equation 2.6 in

[1]The K66 models are realized through `LIMEPY` (*Gieles and Zocchi*, 2015) as described in Section 2.3.2.1.

Section 2.3.2.1), or stars that have metallicities that deviate significantly enough from their respective cluster mean metallicity to call in question their membership (keeping in mind that metallicity is not used directly in assigning membership probabilities in our EM analysis; see Section 2.3.2.1). We describe here how we have used preliminary EM analysis results and metallicity estimates from the Bayesian spectral fitting (Section 3.3.1) to develop a final sample for kinematic analysis. We also describe how we have supplemented this final sample with results from previous studies.

4.1.1 Removing Stars From a Third Stellar Population

Stars from a stellar population not explicitly included in our EM model can distort the estimation of the field population and hence the membership probability of other stars in the sample. We flagged such stars on a cluster-by-cluster basis using the following criterion:

$$\frac{\Delta v_{\rm los}}{\sigma} \equiv \frac{|v_{{\rm los},i} - \overline{v_{\rm los}}|}{\sqrt{\varepsilon^2_{v_{{\rm los},i}} + \sigma^2_{v_{\rm los}}}} \geq 3, \tag{4.1}$$

where $v_{{\rm los},i}$ and $\varepsilon_{v_{{\rm los},i}}$ are the LOS velocity and its associated uncertainty of the i-th star in a cluster sample, respectively, while $\overline{v_{\rm los}}$ and $\sigma^2_{v_{\rm los}}$ are weighted average velocity and the corresponding weighted standard deviation of the corresponding cluster sample. Using this process, a total of 35 stars in 17 cluster samples were identified as third-population contaminants (see Figure 4.1); all are flagged in column 17 of Table 3.5. The generally low surface gravities of these rejected stars suggests they are likely Galactic halo giants or giants associated with an extended halo population of the MCs, neither of which were explicitly accounted for in our EM model (see Section 2.3.2.1 and Section 4.1).

Using the remaining sample of 2645 stars, we reran the EM analysis for every cluster to assign a preliminary membership probabilities, $P_{M,i}$, to each star.

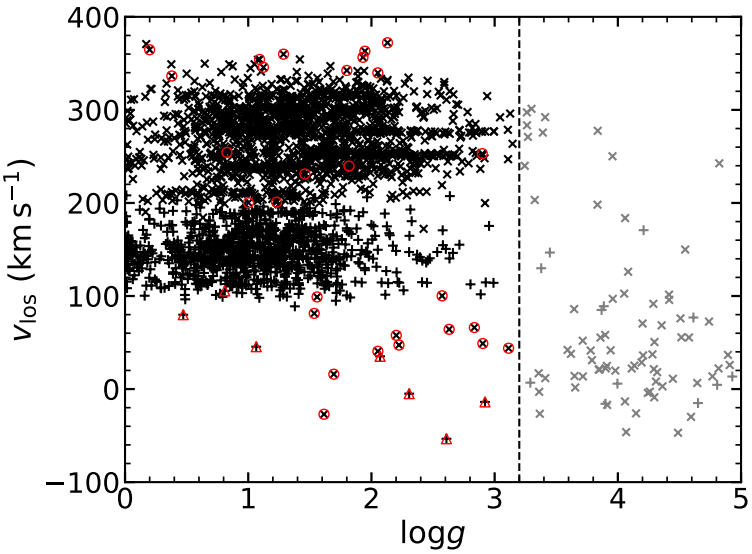

Figure 4.1: A plot on the $v_{\rm los}$-log g plane of 2764 stars in our M2FS sample after removing the stars with either poorly determined parameters (see Section 3.3.4.1) or anomalous velocity uncertainties (see Section 3.3.4.2). Crosses denote stars observed in LMC fields, while plus signs refer to stars observed in SMC fields. The dashed vertical line correspond to the criterion, $\log g = 3.2$, used in Section 3.3.4.3 to separate a total of 84 (foreground) dwarfs (gray crosses and plus signs) from giants (black crosses and plus signs) in our sample. Red circles (LMC) and red triangles (SMC) denote the 35 rejected stars that we concluded are associated with a third population as discussed in Section 4.1.1.

4.1.2 Removing Stars With Anomalous Metallicities

We can also use metallicities obtained from the Bayesian analysis (see Section 3.3.1) to identify stars with chemical abundances that differ significantly from the mean of their respective cluster's [Fe/H] distributions. Such deviant metallicities may indicate non-membership, but they could also result from issues such as poor background subtraction (as is likely, for example, in NGC 339 and Lindsay 1) or poor temperature assignments.

We applied two criteria to identify potential metallicity non-members. First, the preliminary membership probabilities had to satisfy the condition $P_{M,i} \geq 0.5$. Second, the color shifts, $\Delta(G_{\rm BP} - G_{\rm RP})$ to assign effective temperature to each star (see Section 3.3.2) had to satisfy the condition $|\Delta(G_{\rm BP} - G_{\rm RP}) - C_{\rm BI,dcolor}| \leq 2S_{\rm BI,dcolor}$, where $C_{\rm BI,dcolor}$ and $S_{\rm BI,dcolor}$ are the biweight mean offset and dispersion scale determined in Section 3.3.2, respectively. This criterion was designed to avoid metallicity offsets due to systematically invalid temperature estimates (see Section 3.3.2 and Figure 3.7 for details. Stars identified in this manner as likely metallicity outliers are flagged in column 17 of Table 3.5.

Using all stars satisfying these two criteria, we then calculated for each cluster an initial pair of metallicity parameters—the weighted mean metallicity ($\overline{[\rm Fe/H]}_{\rm SC}$) and weighted standard deviation ($\sigma_{\rm [Fe/H],SC}$). Following this process, probable metallicity non-members were identified using the criterion

$$\frac{\Delta[\rm Fe/H]}{\sigma} \equiv \frac{\left|[\rm Fe/H]_i - \overline{[\rm Fe/H]}_{\rm SC}\right|}{\sqrt{\varepsilon^2_{\rm [Fe/H],\it i} + \sigma^2_{\rm [Fe/H],SC}}} \geq 2, \tag{4.2}$$

where $[\rm Fe/H]_i$ and $\varepsilon_{\rm [Fe/H],\it i}$ are the metallicity and its uncertainty of the i-th star in the EM sample, respectively. This procedure resulted in the removal of 51 stars from 22 clusters, and each is flagged in column 17 of Table 3.5. The numbers of stars removed for each cluster using Equation 4.2 are listed in column 6 in Table 4.1. After

applying this metallicity criterion, a total of 2594 stars in 26 clusters remain in our M2FS kinematic sample.

4.1.3 Combining Previous Samples

We have identified all previously published individual stellar velocity measurements with a typical single-star precision better than 3 $\mathrm{km\,s^{-1}}$ (see also Table 3.4) associated with the clusters in our sample. In this section, we identify and compare stars common to our sample and samples from previous studies with the aim of expanding our final kinematic sample.

We first compared published coordinates of individual stars with those of stars associated with our cluster sample. Stars with coordinates agreeing to within 1 *arcsec* in radius were considered to be the same star. There were no ambiguous cases in which more than one star from previous published catalogue satisfied this positional matching tolerance. For NGC 1978, we also cross-matched the *Fischer et al.* (1992b) and *Ferraro et al.* (2006) samples to identify any stars in common. These two samples were found to have nine stars in common, three of which are also found in our M2FS sample.

Before combining results from different samples, we measured the systemic velocity offsets for clusters in common among the various datasets. These offsets were computed by subtracting the published systemic velocities (see column 6 in Table 3.4) from our preliminary EM results (see Section 4.1.1), and the uncertainties in the offsets were estimated by using the sum of errors in quadrature. When combining results from different samples, we then applied the offsets to the previously published velocities while keeping the published velocity uncertainties unchanged. In all cases, we adopted the M2FS velocity zero points for the velocity scale (Table 4.2). For each star with multiple measurements, the weighted mean velocities and their weighted errors were calculated after applying these offsets. This process allowed us to increase the

Table 4.1: Mean Cluster Metallicity on the CG97 Scale.

Galaxy	Cluster	[Fe/H] (dex)	$\sigma_{[Fe/H]}$ (dex)	N_{mem}	N_{non}
(1)	(2)	(3)	(4)	(5)	(6)
SMC	Kron 3	-0.96	0.15	41	1
SMC	Lindsay 1	-0.98	0.13	80	6
SMC	NGC 152	-0.73	0.11	22	2
SMC	NGC 330	-0.65	0.10	4	1
SMC	NGC 339	-1.01	0.17	35	8
SMC	NGC 361	-0.75	0.17	20	0
SMC	NGC 411	-0.66	0.09	19	2
SMC	NGC 416	-0.80	0.17	16	0
SMC	NGC 419	-0.66	0.15	35	2
SMC	NGC 458	-0.70	0.20	14	0
LMC	Hodge 4	-0.49	0.12	30	2
LMC	NGC 1466	-1.40	0.16	22	1
LMC	NGC 1751	-0.46	0.14	20	1
LMC	NGC 1783	-0.54	0.10	52	2
LMC	NGC 1806	-0.53	0.12	27	1
LMC	NGC 1831	-0.41	0.15	49	3
LMC	NGC 1841	-1.96	0.12	64	3
LMC	NGC 1846	-0.49	0.08	36	2
LMC	NGC 1850	-0.31	0.20	26	0
LMC	NGC 1978	-0.49	0.10	37	3
LMC	NGC 2121	-0.54	0.11	38	3
LMC	NGC 2155	-0.59	0.12	36	3
LMC	NGC 2203	-0.45	0.12	64	2
LMC	NGC 2209	-0.52	0.15	50	1
LMC	NGC 2257	-1.64	0.11	57	1
LMC	SL 663	-0.51	0.11	19	1

sample sizes for seven clusters (see Table 3.4).

Most of the stars matched by position as described above agree well in velocity. However, two stars have velocity differences 3 times greater than their combined total velocity errors. The star in NGC 1846, whose detail had been discussed in Section 2.3.1.2, is a likely binary. The other star, in NGC 330, is a well-known binary system identified in earlier studies (see e.g. *Patrick et al.*, 2020, and the references therein). Both stars were removed from our final kinematic sample. For the NGC 1846 binary, there are too few measurements to determine a reliable systemic velocity, while for the NGC 330 binary, its mean velocity and metallicity, though both somewhat poorly determined, make it a likely non-member of the cluster. Indeed, for this reason, this star had already been flagged for removal in Section 4.1.2.

4.1.4 Final Kinematic Sample

After the addition of 193 more stars from the literature, our final working sample consists of 2787 stars in 26 clusters. We will refer to this as the 'Kinematic' sample, and use it exclusively for the final EM analysis following the procedures described in Section 2.3.2.1 and Section 4.1.

A summary of the initial analysis of the full Kinematic sample is provided in Table 4.2: Column 3 lists the total number of stars in our Kinematic sample for each cluster, while column 4 lists the number of stars within each cluster's tidal radius (see Table 3.2); columns 5 and 6 list the estimates of the cluster systemic velocity and projected central velocity dispersion of each cluster; columns 7 and 8 list the mean velocity and velocity dispersion of field population when applicable.

Table 4.2: Results of the EM analysis

Galaxy	Cluster	$N_{\rm total}$	$N_{\rm tidal}$	$V_{\rm sys}$ ($\rm km\,s^{-1}$)	$\sigma_{\rm p,0}$ ($\rm km\,s^{-1}$)	$V_{\rm field}$ ($\rm km\,s^{-1}$)	$\sigma_{\rm field}$ ($\rm km\,s^{-1}$)
(1)	(2)	(3)	(4)	(5)	(6)	(7)	(8)
SMC	Kron 3	116	84	$132.7^{+0.3}_{-0.4}$	$2.1^{+0.2}_{-0.3}$	$143.3^{+3.2}_{-2.4}$	$23.1^{+1.3}_{-1.5}$
SMC	Lindsay 1	99	92	$140.5^{+0.2}_{-0.2}$	$1.8^{+0.2}_{-0.3}$	$137.7^{+3.3}_{-4.4}$	$16.1^{+1.7}_{-2.3}$
SMC	NGC 152	107	86	$172.4^{+0.5}_{-0.9}$	$2.8^{+1.2}_{-1.8}$	$150.7^{+4.0}_{-2.5}$	$25.2^{+1.3}_{-2.4}$
SMC	NGC 330	47	28	$153.0^{+0.7}_{-0.7}$	$2.4^{+0.3}_{-0.7}$	$138.5^{+3.0}_{-3.3}$	$16.0^{+1.7}_{-2.6}$
SMC	NGC 339	94	65	$112.9^{+0.4}_{-0.3}$	$1.8^{+0.2}_{-0.3}$	$161.1^{+2.2}_{-2.5}$	$18.0^{+1.6}_{-2.3}$
SMC	NGC 361	119	70	$170.3^{+0.9}_{-0.9}$	$4.0^{+0.7}_{-1.4}$	$138.6^{+1.3}_{-2.8}$	$20.1^{+1.0}_{-1.2}$
SMC	NGC 411	117	56	$163.8^{+4.5}_{-0.3}$	$1.7^{+16.8}_{-0.6}$	$147.7^{+1.4}_{-3.5}$	$23.3^{+0.8}_{-2.2}$
SMC	NGC 416	114	40	$155.0^{+1.0}_{-0.5}$	$3.4^{+0.6}_{-0.7}$	$149.2^{+2.3}_{-2.9}$	$27.2^{+1.5}_{-1.9}$
SMC	NGC 419	110	81	$189.9^{+0.3}_{-0.2}$	$2.2^{+0.3}_{-0.3}$	$159.8^{+2.7}_{-2.6}$	$21.8^{+1.4}_{-1.7}$
SMC	NGC 458	79	24	$149.0^{+0.8}_{-0.9}$	$3.5^{+0.7}_{-2.2}$	$146.2^{+1.8}_{-1.1}$	$13.3^{+1.5}_{-1.3}$
LMC	Hodge 4	112	112	$312.7^{+0.6}_{-1.3}$	$2.1^{+5.1}_{-0.6}$	$299.8^{+2.0}_{-5.6}$	$21.8^{+3.5}_{-3.9}$
LMC	NGC 1466	27	25	$202.5^{+0.5}_{-0.5}$	$3.6^{+0.4}_{-0.6}$	...	...
LMC	NGC 1751	113	113	$240.4^{+0.7}_{-0.6}$	$2.5^{+0.6}_{-0.7}$	$247.1^{+3.4}_{-2.7}$	$27.4^{+3.0}_{-3.1}$
LMC	NGC 1783	111	111	$279.6^{+0.2}_{-0.2}$	$2.0^{+0.2}_{-0.2}$	$281.9^{+3.9}_{-3.5}$	$24.5^{+2.3}_{-2.4}$
LMC	NGC 1806	120	120	$229.6^{+0.4}_{-0.4}$	$2.4^{+0.4}_{-0.6}$	$265.7^{+3.9}_{-3.0}$	$27.0^{+1.7}_{-2.3}$
LMC	NGC 1831	102	95	$276.8^{+0.2}_{-0.2}$	$1.9^{+0.3}_{-0.3}$	$284.8^{+2.8}_{-2.5}$	$17.5^{+1.9}_{-3.0}$
LMC	NGC 1841	69	64	$210.8^{+0.3}_{-0.3}$	$2.7^{+0.3}_{-0.5}$	...	...
LMC	NGC 1846	196	81	$239.2^{+0.2}_{-0.3}$	$2.1^{+0.3}_{-0.4}$	$269.4^{+1.5}_{-1.8}$	$25.0^{+1.3}_{-1.4}$
LMC	NGC 1850	155	87	$248.9^{+0.4}_{-0.5}$	$2.5^{+1.8}_{-0.4}$	$257.4^{+2.8}_{-2.4}$	$23.6^{+1.7}_{-2.6}$
LMC	NGC 1978	145	86	$293.1^{+0.3}_{-0.3}$	$3.1^{+0.3}_{-0.4}$	$283.7^{+3.0}_{-2.2}$	$25.9^{+2.2}_{-2.1}$
LMC	NGC 2121	109	72	$237.0^{+0.3}_{-0.2}$	$1.8^{+0.1}_{-0.4}$	$262.8^{+2.7}_{-3.1}$	$21.5^{+2.0}_{-2.3}$
LMC	NGC 2155	110	104	$315.0^{+0.1}_{-0.2}$	$0.8^{+0.1}_{-0.3}$	$310.4^{+2.1}_{-1.8}$	$20.7^{+1.3}_{-1.6}$
LMC	NGC 2203	96	77	$252.8^{+0.3}_{-0.2}$	$1.9^{+0.2}_{-0.3}$	$244.2^{+4.3}_{-4.8}$	$23.0^{+4.9}_{-5.2}$
LMC	NGC 2209	113	112	$251.2^{+0.1}_{-0.4}$	$0.8^{+1.2}_{-0.2}$	$251.4^{+2.1}_{-1.6}$	$16.5^{+1.3}_{-1.3}$
LMC	NGC 2257	94	65	$301.8^{+0.3}_{-0.4}$	$2.7^{+0.2}_{-0.4}$	$320.4^{+1.3}_{-2.5}$	$12.8^{+1.6}_{-2.0}$
LMC	SL 663	113	113	$301.1^{+1.4}_{-1.2}$	$3.2^{+6.4}_{-2.2}$	$300.1^{+2.2}_{-2.7}$	$19.5^{+2.5}_{-1.6}$

4.2 Dynamical and Chemical Results

4.2.1 Cluster Systemic Velocity and Velocity Dispersion

The systemic velocity ($V_{\rm sys}$) and projected central velocity dispersion ($\sigma_{\rm p,0}$) listed in Table 4.2 are the two direct kinematic parameters determined by the EM analysis for each cluster. As discussed in Section 2.3.2.2, the 'raw' EM estimates for these parameters rely critically on the membership probabilities, some of which may be skewed due to field contamination that may result from the relatively small samples being used. Here we follow and expand upon our approach in Section 2.3.2.2, by calculating $V_{\rm sys}$ and $\sigma_{\rm p,0}$ using two different sampling methods, 'BOX' and 'PM50'. Both use EM results—systemic velocity in the case of BOX, modified membership probabilities in the case of PM50—to refine the cluster kinematic parameters. The value of these methods lies their utility to better understand the effect that marginal outlier stars may have in the final kinematic results for a given cluster.

In the BOX method, $V_{\rm sys}$ and $\sigma_{\rm p,0}$ are computed from all stars in a rectangular area in the $v_{\rm los}$-r plane (see the shaded area in Figure 2.10). This BOX area is bounded by the cluster center and the adopted K66 tidal radius (see Table 3.2) in x-axis, while in y-axis the minimum and maximum systemic velocities are set by conservatively assuming the target cluster has a (large) total mass of 10^6 $M_\odot$. The value of the BOX method is that it is comparatively easy to specify and compute at the cost of effectively ignoring the EM analysis membership probabilities.

In the PM50 method, $V_{\rm sys}$ and $\sigma_{\rm p,0}$ are computed from probable member stars based on their EM membership probabilities (see Section 4.1.4). A star is assumed to be a cluster member if its initial EM membership probability is greater than or equal to 50% (i.e. $P_M \geq 0.5$). Unlike the full EM analysis in which membership probabilities are used to weight individual stars, the PM50 method implicitly assigns 100% membership probabilities (therefore assumed to be certain members) to any stars

with $P_M \geq 0.5$, and assigns certain non-membership (0% membership probability) to the rest stars in the sample.

Table 4.3 lists the BOX and PM50 results for all clusters in our sample. We list the numbers of members assigned by each method, along with the corresponding values of $V_{\rm sys}$ and $\sigma_{\rm p,0}$ (columns 3–5 for BOX; columns 6–8 for PM50).

Figure 4.2 compares $\sigma_{\rm p,0}$ estimated from the BOX and PM50 methods (top two panels). One obvious and unsurprising conclusion from these figures is that the BOX method systematically overestimates the dispersion compared to PM50. Since the BOX method has no provision for flagging nonmembers, it is more likely to include random outlier stars whose inclusion depends on how the box areas are (arbitrarily) assigned.

To explore how marginal outlier stars may affect the PM50 method, we have defined a third method, PM50′ (PM50-prime), which uses with the PM50 sample pruned of the star exhibiting the most deviant velocity (in absolute value) from the initial systemic velocity of the cluster. These PM50′ results are listed in Table 4.3, columns 9–11. Note that the numbers of stars used in the PM50 and PM50′ samples of a given cluster do not always differ by one. This occurs because when the most probable outlier is removed from the PM50 sample, the EM analysis reassigns membership probabilities that may result in the reassignment of more than one star as members or nonmembers.

We compare the PM50 and PM50′ results in the lower two panels of Figure 4.2. For most clusters, the change in $\sigma_{\rm p,0}$ is within 1-σ to the expectation of removing the most deviant star from a Gaussian distribution (gray bands in the lower panels of Figure 4.2). However, for five clusters—NGC 152, NGC 458, NGC 1751, SL 663 and, marginally, Hodge 4—we found the PM50 results to be overly sensitive to the removal of a single (outlier) star in the EM analysis. These five clusters also exhibited the largest change in the number of likely members in their respective PM50 samples

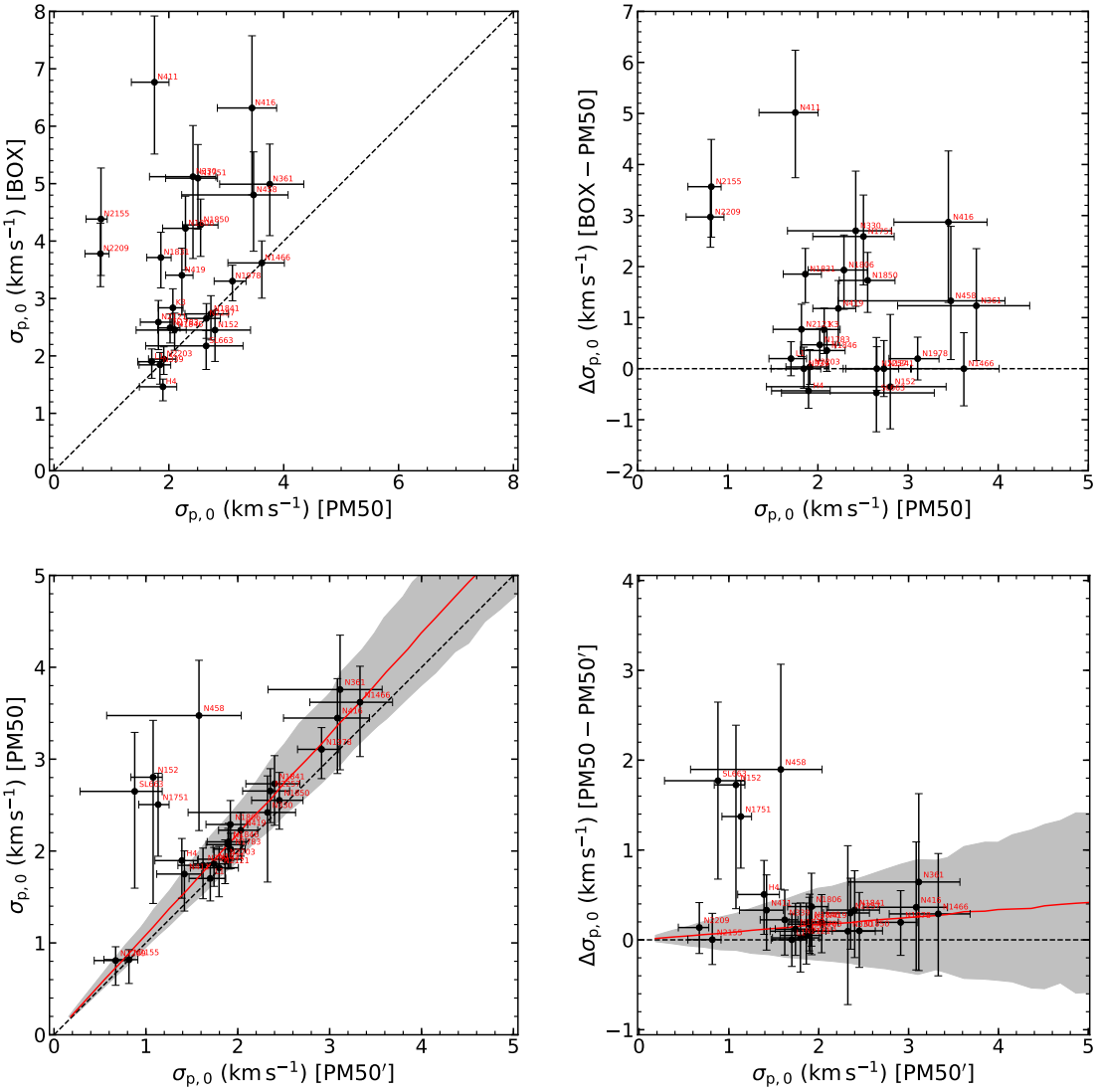

Figure 4.2: Comparisons of estimated $\sigma_{\rm p,0}$ between the BOX and PM50 methods (top panels), and between the PM50 and PM50′ methods (bottom panels). The $\sigma_{\rm p,0}$ values used in the plots are listed in Table 4.3 and described in Section 4.2.1. The gray bands in the lower panels denote the 68% ($\pm1\sigma$) range of 1000 simulated results obtained by removing the most extreme star from the tail of Gaussian distributions consisting of 30 velocities with initial $\sigma_{\rm p,0}$ value ranging between 0.2–8.0 km s^{-1} in 0.2 km s^{-1} intervals. The red lines denote the median results of these simulations. More details are discussed in Section 4.2.1.

Table 4.3: Results of the BOX, PM50 and PM50′ methods

Galaxy	Field	$N_{\rm BOX}$	$V_{\rm sys,BOX}$ ($\rm km\,s^{-1}$)	$\sigma_{\rm p,0,BOX}$ ($\rm km\,s^{-1}$)	$N_{\rm PM50}$	$V_{\rm sys,PM50}$ ($\rm km\,s^{-1}$)	$\sigma_{\rm p,0,PM50}$ ($\rm km\,s^{-1}$)	$N_{\rm PM50'}$	$V_{\rm sys,PM50'}$ ($\rm km\,s^{-1}$)	$\sigma_{\rm p,0,PM50'}$ ($\rm km\,s^{-1}$)
(1)	(2)	(3)	(4)	(5)	(6)	(7)	(8)	(9)	(10)	(11)
SMC	Kron 3	51	$132.5^{+0.3}_{-0.3}$	$2.8^{+0.3}_{-0.4}$	**41**	$\mathbf{132.7^{+0.2}_{-0.3}}$	$\mathbf{2.1^{+0.2}_{-0.3}}$	39	$132.9^{+0.3}_{-0.2}$	$1.9^{+0.2}_{-0.2}$
SMC	Lindsay 1	83	$140.5^{+0.2}_{-0.2}$	$1.9^{+0.2}_{-0.3}$	**80**	$\mathbf{140.5^{+0.2}_{-0.2}}$	$\mathbf{1.7^{+0.2}_{-0.2}}$	79	$140.5^{+0.2}_{-0.2}$	$1.7^{+0.2}_{-0.2}$
SMC	NGC 152	27	$172.8^{+0.4}_{-0.4}$	$2.4^{+0.3}_{-0.5}$	21	$172.6^{+0.5}_{-0.5}$	$2.8^{+0.6}_{-1.4}$	**17**	$\mathbf{172.6^{+0.3}_{-0.3}}$	$\mathbf{1.1^{+0.1}_{-0.2}}$
SMC	NGC 330	18	$152.2^{+0.9}_{-0.9}$	$5.1^{+0.9}_{-1.4}$	**14**	$\mathbf{153.0^{+0.6}_{-0.7}}$	$\mathbf{2.4^{+0.4}_{-0.8}}$	13	$152.8^{+0.6}_{-0.7}$	$2.3^{+0.3}_{-0.9}$
SMC	NGC 339	35	$112.9^{+0.3}_{-0.3}$	$1.8^{+0.2}_{-0.3}$	**35**	$\mathbf{112.9^{+0.3}_{-0.3}}$	$\mathbf{1.8^{+0.2}_{-0.4}}$	34	$113.0^{+0.3}_{-0.3}$	$1.6^{+0.1}_{-0.3}$
SMC	NGC 361	24	$170.4^{+0.7}_{-0.7}$	$5.0^{+0.7}_{-0.9}$	**20**	$\mathbf{170.5^{+0.6}_{-0.6}}$	$\mathbf{3.8^{+0.6}_{-0.9}}$	20	$170.9^{+0.5}_{-0.5}$	$3.1^{+0.5}_{-0.8}$
SMC	NGC 411	35	$162.8^{+0.7}_{-0.7}$	$6.8^{+1.2}_{-1.3}$	**22**	$\mathbf{163.8^{+0.3}_{-0.3}}$	$\mathbf{1.7^{+0.3}_{-0.4}}$	20	$164.0^{+0.2}_{-0.2}$	$1.4^{+0.2}_{-0.3}$
SMC	NGC 416	25	$155.6^{+0.8}_{-0.8}$	$6.3^{+1.3}_{-1.5}$	**19**	$\mathbf{155.0^{+0.6}_{-0.6}}$	$\mathbf{3.4^{+0.4}_{-0.6}}$	18	$154.7^{+0.5}_{-0.6}$	$3.1^{+0.3}_{-0.6}$
SMC	NGC 419	49	$189.9^{+0.3}_{-0.3}$	$3.4^{+0.5}_{-0.7}$	**44**	$\mathbf{189.9^{+0.2}_{-0.2}}$	$\mathbf{2.2^{+0.2}_{-0.3}}$	43	$189.8^{+0.2}_{-0.2}$	$2.0^{+0.2}_{-0.2}$
SMC	NGC 458	19	$148.8^{+0.7}_{-0.7}$	$4.8^{+0.7}_{-1.0}$	14	$149.0^{+0.7}_{-0.8}$	$3.5^{+0.6}_{-1.3}$	**10**	$\mathbf{148.8^{+0.4}_{-0.4}}$	$\mathbf{1.6^{+0.5}_{-1.0}}$
LMC	Hodge 4	33	$313.0^{+0.3}_{-0.3}$	$1.5^{+0.1}_{-0.2}$	33	$312.8^{+0.4}_{-0.3}$	$1.9^{+0.2}_{-0.4}$	**29**	$\mathbf{313.1^{+0.3}_{-0.3}}$	$\mathbf{1.4^{+0.2}_{-0.3}}$
LMC	NGC 1466	25	$202.5^{+0.5}_{-0.5}$	$3.6^{+0.4}_{-0.6}$	**25**	$\mathbf{202.5^{+0.5}_{-0.5}}$	$\mathbf{3.6^{+0.4}_{-0.6}}$	24	$202.7^{+0.5}_{-0.5}$	$3.3^{+0.4}_{-0.5}$
LMC	NGC 1751	46	$240.3^{+0.5}_{-0.6}$	$5.1^{+0.6}_{-0.9}$	28	$240.3^{+0.4}_{-0.4}$	$2.5^{+0.3}_{-0.6}$	**21**	$\mathbf{241.3^{+0.2}_{-0.2}}$	$\mathbf{1.1^{+0.1}_{-0.2}}$
LMC	NGC 1783	75	$279.5^{+0.2}_{-0.2}$	$2.5^{+0.2}_{-0.3}$	**66**	$\mathbf{279.6^{+0.2}_{-0.2}}$	$\mathbf{2.0^{+0.2}_{-0.2}}$	65	$279.5^{+0.2}_{-0.2}$	$1.9^{+0.2}_{-0.2}$
LMC	NGC 1806	43	$230.0^{+0.5}_{-0.5}$	$4.2^{+0.6}_{-0.7}$	**35**	$\mathbf{229.7^{+0.3}_{-0.3}}$	$\mathbf{2.3^{+0.3}_{-0.4}}$	33	$230.0^{+0.3}_{-0.3}$	$1.9^{+0.2}_{-0.3}$
LMC	NGC 1831	77	$276.4^{+0.3}_{-0.3}$	$3.7^{+0.4}_{-0.5}$	**64**	$\mathbf{276.8^{+0.2}_{-0.2}}$	$\mathbf{1.9^{+0.2}_{-0.2}}$	62	$276.9^{+0.2}_{-0.2}$	$1.7^{+0.2}_{-0.2}$
LMC	NGC 1841	64	$210.8^{+0.3}_{-0.3}$	$2.7^{+0.3}_{-0.5}$	**64**	$\mathbf{210.8^{+0.3}_{-0.3}}$	$\mathbf{2.7^{+0.3}_{-0.5}}$	63	$210.6^{+0.3}_{-0.3}$	$2.4^{+0.3}_{-0.3}$
LMC	NGC 1846	55	$239.2^{+0.3}_{-0.3}$	$2.5^{+0.3}_{-0.4}$	**53**	$\mathbf{239.2^{+0.2}_{-0.2}}$	$\mathbf{2.1^{+0.2}_{-0.3}}$	51	$239.1^{+0.2}_{-0.2}$	$1.9^{+0.2}_{-0.2}$
LMC	NGC 1850	74	$249.0^{+0.4}_{-0.4}$	$4.3^{+0.4}_{-0.5}$	**63**	$\mathbf{248.8^{+0.3}_{-0.3}}$	$\mathbf{2.6^{+0.3}_{-0.3}}$	62	$248.9^{+0.3}_{-0.3}$	$2.5^{+0.3}_{-0.3}$
LMC	NGC 1978	76	$293.0^{+0.3}_{-0.3}$	$3.3^{+0.3}_{-0.3}$	**75**	$\mathbf{293.1^{+0.3}_{-0.3}}$	$\mathbf{3.1^{+0.2}_{-0.3}}$	74	$293.2^{+0.3}_{-0.3}$	$2.9^{+0.2}_{-0.3}$
LMC	NGC 2121	49	$236.9^{+0.3}_{-0.3}$	$2.6^{+0.4}_{-0.5}$	**43**	$\mathbf{237.0^{+0.2}_{-0.2}}$	$\mathbf{1.8^{+0.2}_{-0.3}}$	42	$236.9^{+0.3}_{-0.2}$	$1.8^{+0.2}_{-0.3}$
LMC	NGC 2155	57	$314.9^{+0.4}_{-0.4}$	$4.4^{+0.9}_{-1.0}$	**35**	$\mathbf{315.0^{+0.2}_{-0.1}}$	$\mathbf{0.8^{+0.1}_{-0.3}}$	34	$315.0^{+0.2}_{-0.2}$	$0.8^{+0.1}_{-0.3}$
LMC	NGC 2203	73	$252.9^{+0.2}_{-0.2}$	$1.9^{+0.2}_{-0.3}$	**72**	$\mathbf{252.8^{+0.2}_{-0.2}}$	$\mathbf{1.9^{+0.2}_{-0.3}}$	71	$252.9^{+0.2}_{-0.2}$	$1.9^{+0.2}_{-0.3}$
LMC	NGC 2209	74	$250.9^{+0.3}_{-0.3}$	$3.8^{+0.5}_{-0.6}$	**52**	$\mathbf{251.2^{+0.2}_{-0.2}}$	$\mathbf{0.8^{+0.2}_{-0.3}}$	51	$251.3^{+0.1}_{-0.1}$	$0.7^{+0.1}_{-0.2}$
LMC	NGC 2257	63	$301.8^{+0.3}_{-0.3}$	$2.7^{+0.3}_{-0.3}$	**63**	$\mathbf{301.8^{+0.3}_{-0.3}}$	$\mathbf{2.7^{+0.2}_{-0.3}}$	61	$301.6^{+0.3}_{-0.3}$	$2.4^{+0.2}_{-0.3}$
LMC	SL 663	32	$301.0^{+0.4}_{-0.4}$	$2.2^{+0.3}_{-0.4}$	23	$301.2^{+0.5}_{-0.5}$	$2.6^{+0.6}_{-1.1}$	**20**	$\mathbf{301.0^{+0.3}_{-0.2}}$	$\mathbf{0.9^{+0.3}_{-0.6}}$

as a result of removing one extreme star as described above (see Table 4.3). For these five clusters, we will consider their PM50′ velocity dispersions as well as their PM50 dispersions. The preferred velocity dispersion estimates for every cluster in our sample—either the PM50 or PM50′ results—are highlighted with bold font in Table 4.3.

4.2.2 Cluster Mass and Mass-to-light Ratio

A cluster's total luminosity and dynamical mass can be derived by scaling the central surface brightness and the projected central velocity dispersion, respectively, with the dimensionless cluster structural profiles (i.e. the K66 models listed in Table 3.2). The two required scaling parameters, central surface brightness and projected cen-

tral velocity dispersion, were determined, respectively, from aperture photometry (as described in this section) and from the individual stellar velocities (see Section 4.2.1).

To determine the central surface brightness ($\Sigma_{V,0}$), we integrated the dimensionless K66 model to a maximal reference radius within which an aperture luminosity was measured from the ground-base CCD photometry. The dimensionless K66 models were computed using the code `LIMEPY` (*Gieles and Zocchi*, 2015), consistent with how we determine cluster masses (see below). The aperture magnitude and associated reference radius used for each cluster are listed in Table 3.1, columns 3–4, with the sources identified in column 5. When transforming magnitude to luminosity, we adopted $M_{V,\odot} = 4.85$ in addition to the distance modulus and extinction value listed in Table 3.1. We could not find published V-band aperture photometry for SL 663, so instead we adopted the central surface surface brightness reported by *McLaughlin and van der Marel* (2005). This value, and its uncertainty, is given in Table 3.1.

The total luminosity ($L_{V,\,\mathrm{tot}}$) was obtained by integrating the $\Sigma_{V,0}$-scaled K66 model to the K66 tidal radius listed in Table 3.2. Similarly, the total cluster mass (M_{tot}) was derived with the same dimensionless K66 model but scaled to $\sigma_{\mathrm{p},0}$ fitted from the PM50 or PM50′ sample (see Section 4.2.1 and Table 4.3). The dynamical M/L_V ratios of the clusters were then derived from the total masses and total V-band luminosity determined above.

Uncertainties in cluster masses, luminosities and M/L_V ratios were estimated using a bootstrapping technique that accounted for uncertainties in distance modulus and extinction (Table 3.1), the K66 structural parameters (see Table 3.2), the V-band aperture magnitude (for $L_{V,\,\mathrm{tot}}$ and M/L_V; see Table 3.1), and the central velocity dispersion (for M_{tot} and M/L_V; see Table 4.3). All relevant parameters were randomly sampled, assuming that the error distributions are joint-Gaussian to account for the asymmetric uncertainties (e.g. c_{K66} in Table 3.2), or using simple Gaussian distributions for parameters with symmetric uncertainties (e.g. V_{ap} in Table 3.1).

Table 4.4: Mass, Luminosity and M/L_V.

Galaxy	Cluster	Method	$M_{\rm tot}$ ($\times 10^5$ $M_\odot$)	$L_{V,\rm tot}$ ($\times 10^5$ $L_\odot$)	$M/L_{\rm V}$ ($M_\odot$ $L_\odot^{-1}$)	$\log M_{\rm tot}$ ($M_\odot$)	$\log L_{V,\rm tot}$ ($L_\odot$)	$\log M/L_{\rm V}$ ($M_\odot$ $L_\odot^{-1}$)
(1)	(2)	(3)	(4)	(5)	(6)	(7)	(8)	(9)
SMC	Kron 3	PM50	$0.77^{+0.15}_{-0.20}$	$1.41^{+0.18}_{-0.14}$	$0.55^{+0.11}_{-0.14}$	$4.89^{+0.08}_{-0.13}$	$5.15^{+0.05}_{-0.05}$	$-0.26^{+0.08}_{-0.13}$
SMC	Lindsay 1	PM50	$0.76^{+0.16}_{-0.20}$	$0.87^{+0.09}_{-0.08}$	$0.88^{+0.20}_{-0.24}$	$4.88^{+0.08}_{-0.13}$	$4.94^{+0.04}_{-0.04}$	$-0.05^{+0.09}_{-0.14}$
SMC	NGC 152	PM50	$1.67^{+0.83}_{-1.27}$	$0.80^{+0.12}_{-0.10}$	$2.09^{+0.94}_{-1.60}$	$5.22^{+0.18}_{-0.62}$	$4.90^{+0.06}_{-0.06}$	$0.32^{+0.16}_{-0.63}$
		PM50′	$0.25^{+0.07}_{-0.10}$	$0.80^{+0.13}_{-0.09}$	$0.31^{+0.06}_{-0.13}$	$4.39^{+0.10}_{-0.22}$	$4.90^{+0.07}_{-0.06}$	$-0.51^{+0.08}_{-0.23}$
SMC	NGC 330	PM50	$0.54^{+0.22}_{-0.30}$	$8.93^{+1.05}_{-0.86}$	$0.06^{+0.02}_{-0.03}$	$4.74^{+0.15}_{-0.34}$	$5.95^{+0.05}_{-0.04}$	$-1.22^{+0.13}_{-0.33}$
SMC	NGC 339	PM50	$0.57^{+0.23}_{-0.23}$	$0.72^{+0.28}_{-0.16}$	$0.79^{+0.15}_{-0.29}$	$4.76^{+0.15}_{-0.23}$	$4.86^{+0.14}_{-0.10}$	$-0.10^{+0.07}_{-0.20}$
SMC	NGC 361	PM50	$2.15^{+1.36}_{-0.98}$	$1.04^{+0.54}_{-0.31}$	$2.07^{+0.75}_{-0.85}$	$5.33^{+0.21}_{-0.26}$	$5.02^{+0.18}_{-0.15}$	$0.32^{+0.13}_{-0.23}$
SMC	NGC 411	PM50	$0.30^{+0.10}_{-0.13}$	$0.80^{+0.10}_{-0.08}$	$0.38^{+0.11}_{-0.16}$	$4.48^{+0.12}_{-0.24}$	$4.90^{+0.05}_{-0.04}$	$-0.42^{+0.11}_{-0.23}$
SMC	NGC 416	PM50	$0.80^{+0.24}_{-0.30}$	$1.12^{+0.13}_{-0.10}$	$0.72^{+0.17}_{-0.25}$	$4.90^{+0.11}_{-0.20}$	$5.05^{+0.05}_{-0.04}$	$-0.15^{+0.09}_{-0.19}$
SMC	NGC 419	PM50	$0.64^{+0.14}_{-0.15}$	$3.49^{+0.62}_{-0.51}$	$0.18^{+0.05}_{-0.05}$	$4.80^{+0.09}_{-0.12}$	$5.54^{+0.07}_{-0.07}$	$-0.74^{+0.10}_{-0.13}$
SMC	NGC 458	PM50	$1.26^{+0.58}_{-0.73}$	$1.24^{+0.36}_{-0.26}$	$1.02^{+0.44}_{-0.62}$	$5.10^{+0.16}_{-0.37}$	$5.09^{+0.11}_{-0.10}$	$0.01^{+0.16}_{-0.40}$
		PM50′	$0.26^{+0.21}_{-0.22}$	$1.24^{+0.35}_{-0.24}$	$0.21^{+0.15}_{-0.18}$	$4.42^{+0.26}_{-0.80}$	$5.09^{+0.11}_{-0.09}$	$-0.68^{+0.23}_{-0.80}$
LMC	Hodge 4	PM50	$3.39^{+229.01}_{-2.49}$	$2.67^{+202.43}_{-1.82}$	$1.27^{+0.28}_{-0.54}$	$5.53^{+1.84}_{-0.58}$	$5.43^{+1.89}_{-0.50}$	$0.10^{+0.09}_{-0.24}$
		PM50′	$1.82^{+125.83}_{-1.33}$	$2.67^{+228.50}_{-1.81}$	$0.68^{+0.17}_{-0.27}$	$5.26^{+1.84}_{-0.57}$	$5.43^{+1.94}_{-0.49}$	$-0.17^{+0.09}_{-0.22}$
LMC	NGC 1466	PM50	$1.02^{+0.27}_{-0.31}$	$0.94^{+0.09}_{-0.07}$	$1.09^{+0.25}_{-0.33}$	$5.01^{+0.10}_{-0.16}$	$4.97^{+0.04}_{-0.03}$	$0.04^{+0.09}_{-0.15}$
LMC	NGC 1751	PM50	$0.76^{+0.23}_{-0.31}$	$0.90^{+0.14}_{-0.12}$	$0.84^{+0.27}_{-0.34}$	$4.88^{+0.11}_{-0.23}$	$4.96^{+0.06}_{-0.06}$	$-0.08^{+0.12}_{-0.23}$
		PM50′	$0.15^{+0.03}_{-0.05}$	$0.90^{+0.13}_{-0.11}$	$0.17^{+0.04}_{-0.06}$	$4.19^{+0.09}_{-0.19}$	$4.96^{+0.06}_{-0.06}$	$-0.77^{+0.10}_{-0.19}$
LMC	NGC 1783	PM50	$0.98^{+0.17}_{-0.20}$	$3.77^{+0.28}_{-0.27}$	$0.26^{+0.04}_{-0.05}$	$4.99^{+0.07}_{-0.10}$	$5.58^{+0.03}_{-0.03}$	$-0.58^{+0.07}_{-0.09}$
LMC	NGC 1806	PM50	$0.76^{+0.18}_{-0.26}$	$1.42^{+0.10}_{-0.10}$	$0.54^{+0.13}_{-0.18}$	$4.88^{+0.09}_{-0.18}$	$5.15^{+0.03}_{-0.03}$	$-0.27^{+0.09}_{-0.18}$
LMC	NGC 1831	PM50	$0.41^{+0.09}_{-0.11}$	$1.33^{+0.18}_{-0.17}$	$0.31^{+0.07}_{-0.08}$	$4.61^{+0.09}_{-0.14}$	$5.12^{+0.06}_{-0.06}$	$-0.51^{+0.09}_{-0.14}$
LMC	NGC 1841	PM50	$1.04^{+2.53}_{-0.25}$	$0.74^{+1.63}_{-0.02}$	$1.40^{+0.49}_{-0.51}$	$5.02^{+0.54}_{-0.12}$	$4.87^{+0.50}_{-0.01}$	$0.14^{+0.13}_{-0.20}$
LMC	NGC 1846	PM50	$0.57^{+0.13}_{-0.14}$	$1.68^{+0.35}_{-0.30}$	$0.34^{+0.11}_{-0.10}$	$4.75^{+0.09}_{-0.12}$	$5.23^{+0.08}_{-0.09}$	$-0.47^{+0.13}_{-0.15}$
LMC	NGC 1850	PM50	$0.52^{+0.05}_{-0.17}$	$6.56^{+1.30}_{-1.07}$	$0.08^{+0.01}_{-0.03}$	$4.71^{+0.04}_{-0.18}$	$5.82^{+0.08}_{-0.08}$	$-1.10^{+0.06}_{-0.20}$
LMC	NGC 1978	PM50	$1.36^{+0.24}_{-0.29}$	$3.41^{+0.30}_{-0.25}$	$0.40^{+0.06}_{-0.08}$	$5.13^{+0.07}_{-0.11}$	$5.53^{+0.04}_{-0.03}$	$-0.40^{+0.06}_{-0.10}$
LMC	NGC 2121	PM50	$0.50^{+0.22}_{-0.19}$	$0.79^{+0.42}_{-0.26}$	$0.63^{+0.20}_{-0.21}$	$4.69^{+0.16}_{-0.21}$	$4.90^{+0.19}_{-0.17}$	$-0.20^{+0.12}_{-0.18}$
LMC	NGC 2155	PM50	$0.06^{+0.03}_{-0.04}$	$0.22^{+0.14}_{-0.08}$	$0.29^{+0.17}_{-0.18}$	$3.81^{+0.16}_{-0.36}$	$4.35^{+0.22}_{-0.18}$	$-0.54^{+0.20}_{-0.42}$
LMC	NGC 2203	PM50	$0.51^{+0.13}_{-0.13}$	$0.81^{+0.12}_{-0.11}$	$0.63^{+0.19}_{-0.18}$	$4.70^{+0.10}_{-0.13}$	$4.91^{+0.06}_{-0.06}$	$-0.20^{+0.11}_{-0.14}$
LMC	NGC 2209	PM50	$0.09^{+0.02}_{-0.06}$	$0.26^{+0.02}_{-0.02}$	$0.36^{+0.08}_{-0.21}$	$3.97^{+0.09}_{-0.40}$	$4.41^{+0.03}_{-0.03}$	$-0.45^{+0.09}_{-0.39}$
LMC	NGC 2257	PM50	$1.01^{+0.68}_{-0.38}$	$0.51^{+0.39}_{-0.17}$	$2.00^{+0.38}_{-0.53}$	$5.01^{+0.22}_{-0.20}$	$4.71^{+0.25}_{-0.17}$	$0.30^{+0.08}_{-0.13}$
LMC	SL 663	PM50	$3.32^{+778.97}_{-2.65}$	$0.45^{+132.55}_{-0.33}$	$7.31^{+5.34}_{-4.81}$	$5.52^{+2.37}_{-0.70}$	$4.66^{+2.47}_{-0.55}$	$0.86^{+0.24}_{-0.47}$
		PM50′	$0.36^{+69.09}_{-0.33}$	$0.45^{+164.23}_{-0.36}$	$0.80^{+0.71}_{-0.70}$	$4.56^{+2.28}_{-1.03}$	$4.66^{+2.56}_{-0.67}$	$-0.10^{+0.27}_{-0.87}$

For each cluster, we created 1000 samples from the selected parameters to calculate $M_{\rm tot}$, $L_{V,\,\rm tot}$ and M/L_V. We took the 15.9-th and 84.1-th percentiles of the simulated values as the lower and upper 1σ confidence boundaries of the respective parameter. Table 4.4 lists the masses, luminosities and M/L_V ratios for all 26 clusters in our sample.

Our dynamical analysis assumed that all clusters are exclusively pressure-supported systems. However, for two cases—NGC 1978 and NGC 1846—the kinematic data suggest that the clusters may exhibit coherent rotation (see Figure 2.15 and Figure 4.3). For NGC 1846, we roughly addressed the dynamical effect of rotation in Section 2.3.4, concluding that rotation may be causing $\sim$9% overestimation in the cluster's total mass and M/L_V (see Table 2.10). For NGC 1978, *Fischer et al.* (1992b) carried out a more sophisticated analysis in which they fitted single-mass rotating and non-rotating oblate spheroid models to the surface luminosity profiles and their radial velocity data. They found no significant differences in M/L_Vs derived with these models and those derived with single-mass K66 models. However, the mass estimates for the cluster did differ systematically among the rotating and non-rotating models. Our data for NGC 1978, while clearly showing a rotation signature (see right panel of Figure 4.3), are limited by poor background determination as noted in Section 3.2.5.2. For this reason, and because NGC 1978 requires a more involved dynamical modeling approach, we will defer a detailed analysis for this cluster to a later paper (see Section 6.2.4).

4.2.3 Comparison with Previous Work

Previously published studies have reported velocity dispersions and M/L ratios of 13 clusters in common with our work. Seven of these clusters were studied using integrated-light spectroscopy (*Dubath et al.*, 1997; *Zaritsky et al.*, 2012, 2014), and another six clusters were studied from dynamical modelling using radial velocities

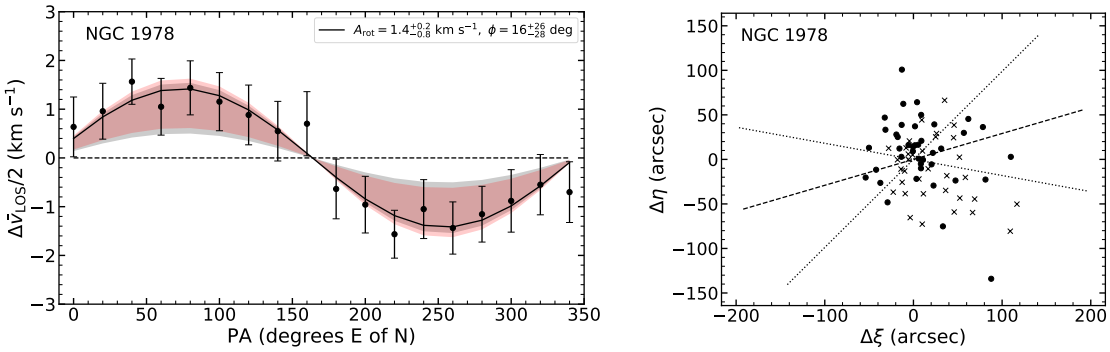

Figure 4.3: Simple rotation analysis for the stars with $P_{\rm M} \geq 0.5$ in NGC 1978 (see Section 4.2.2) using the cluster centers listed in Table 3.2. In the left panel, we show $\Delta\bar{V}_{\rm los}/2$ as a function of the bisector position angle (PA), together with the best-fit sinusoidal model $\Delta\bar{V}_{\rm los}/2 = A_{\rm rot}\sin({\rm PA} + \phi)$ (see Section 2.3.4 for details). The best-fit parameters are listed in the figure legend. In the right panel, crosses (dots) indicate stars with velocities greater (less) than the systemic velocity. The best-fit rotation axis from the left panel is marked as a dash line in the right panel, and two dotted lines denote the 1σ uncertainties. Apart from NGC 1978 shown in this figure, the rotation signature of all other clusters in our sample is negligible ($|A_{\rm rot}|/\sigma_{\rm p,0} \lesssim 0.3$).

of individual cluster member stars similar to this work (*Fischer et al.*, 1992b, 1993; *Suntzeff et al.*, 1992; *Mackey et al.*, 2013; *Kamann et al.*, 2018; *Patrick et al.*, 2020).

The left panel of Figure 4.4 shows the difference in central velocity dispersions between these previous studies and our work (see Table 4.3 and Table 4.4). Our dispersion estimates agree well with studies using individual stellar spectra (red triangles); the average difference (red dashed line) is 0.37 ± 0.19 km s^{-1}. As for the integrated-light studies (blue and green squares), only two clusters with relatively high central values (i.e. NGC 419 and NGC 1466) agree in the dispersions, while we measured lower values for the remaining five clusters. For those studied by *Zaritsky et al.* (2012, 2014) (blue squares), we obtained an average difference of 1.13 ± 0.20 km s^{-1} in dispersion (blue dashed line).

In the right panel of Figure 4.4, we show the difference in M/L_V ratios between these previous studies and our work (see Table 4.3 and Table 4.4). In general, our measured M/L_V ratios agree better with those studied by *Zaritsky et al.* (2012, 2014),

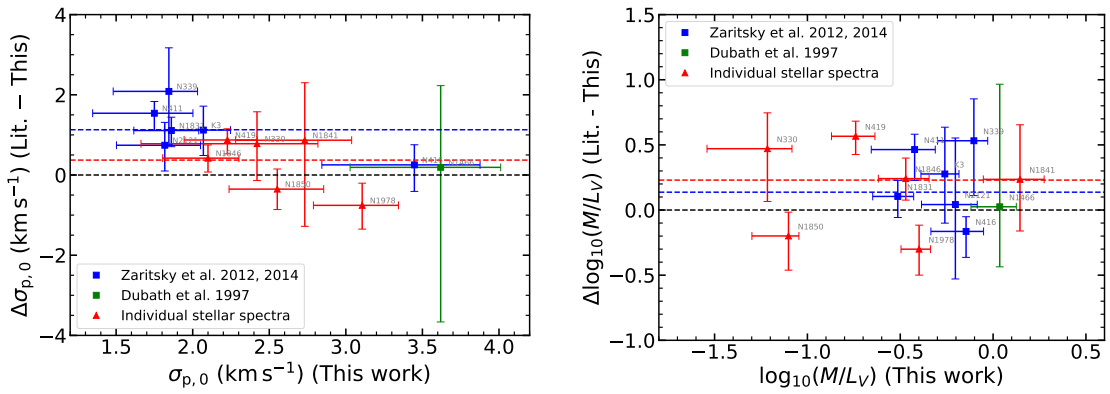

Figure 4.4: Differences between dynamical results—central velocity dispersions (left panel) and M/L_V ratios (right panel)—found in previous studies compared to results of the present work. In both panels, different symbols indicate different spectroscopic measurements used in those studies (see Section 4.2.3). The blue and dashed horizontal lines denote the weighted-average offset values of the corresponding colored data points.

compared to those using individual stellar spectra. For the clusters studied by *Zaritsky et al.* (2012, 2014) (blue squares), we obtain a weighted average of 0.14 ± 0.08 in $\Delta \log_{10}(M/L_V)$ ratio (blue dashed curves); while for the clusters studied using individual stellar spectra (red triangles), the weighted average (red dashed curves) is 0.23 ± 0.08. These differences may be rooted from the various modeling methods used to estimate cluster M/L_V ratio. Indeed, our results are in good agreement with those of the studies adopted the K66 models (i.e., NGC 1466, NGC 1841 and NGC 1850).

Overall, the variations in M/L_V ratios between our work and previous studies seem reasonable given difference in observational technique, data quality, sample size and analysis methods. This conclusion is consistent with the detailed case study for two clusters—NGC 419 and NGC 1846—in Chapter II, where we compared our results with similar studies based on individual stellar velocity measurements (*Kamann et al.*, 2018; *Mackey et al.*, 2013). We explored the effects of both poorly-estimated velocity uncertainties (for NGC 419) and different dynamical modeling (for NGC 1846) on the determination of M/L_V ratios. We presume that similar issues affect the comparisons of results described here, though for the present sample, and in particular for the

integrated-light spectroscopy results (*Dubath et al.*, 1997; *Zaritsky et al.*, 2012, 2014), we are unable to carry out as detailed a comparison as in Section 2.4.

4.2.4 Cluster Metallicity

As described in Section 3.3.2, we estimated effective temperature for each stellar target from their colors in order to break the strong temperature-metallicity degeneracy in our Bayesian fitting analysis (see Section 3.3.1). The stellar metallicities obtained in this analysis were used in Section 4.1.2 to flag chemically discrepant stars as non-members before estimating the 'raw' mean metallicities of the clusters.

An open question remains as to how well these 'raw' metallicities compare to previous chemical analyses. One extensive and consistent source of cluster metallicities come from Ca II triplet (CaT) results that are typically calibrated to two [Fe/H] scales, i.e. *Zinn and West* (1984) (ZW84) and *Carretta and Gratton* (1997) (CG97). For our target clusters, we have collected all the studies using either [Fe/H] scale, and then used the relation in *Carretta et al.* (2001, see their Equation 3) to transfer any ZW84 [Fe/H] values onto the CG97 scale. In the left panel of Figure 4.5, we compared the [Fe/H] values of nine LMC clusters from *Grocholski et al.* (2006) (crosses) and five SMC clusters from *Da Costa and Hatzidimitriou* (1998); *Glatt et al.* (2009); *Parisi et al.* (2015) (open circles). For metal-poor clusters, our raw [Fe/H] values agree well with the CaT results; for metal-rich (and mostly LMC) clusters, our raw [Fe/H] values are systematically lower than those measured by CaT spectroscopy.

The systematic offset in metallicity is found to be related to the color offset between the colors used to calculate $T_{\rm eff}$ (see Section 3.3.2) and those published in the *Gaia* DR2. Figure 4.6 shows the metallicity offsets between the CaT studies and our work as a function of the $G_{\rm BP} - G_{\rm RP}$ color offsets of the target clusters in common. The color offsets were calculated the same as that shown in Figure 3.7 but in a cluster-by-cluster manner, and in the calculation we only considered the cluster

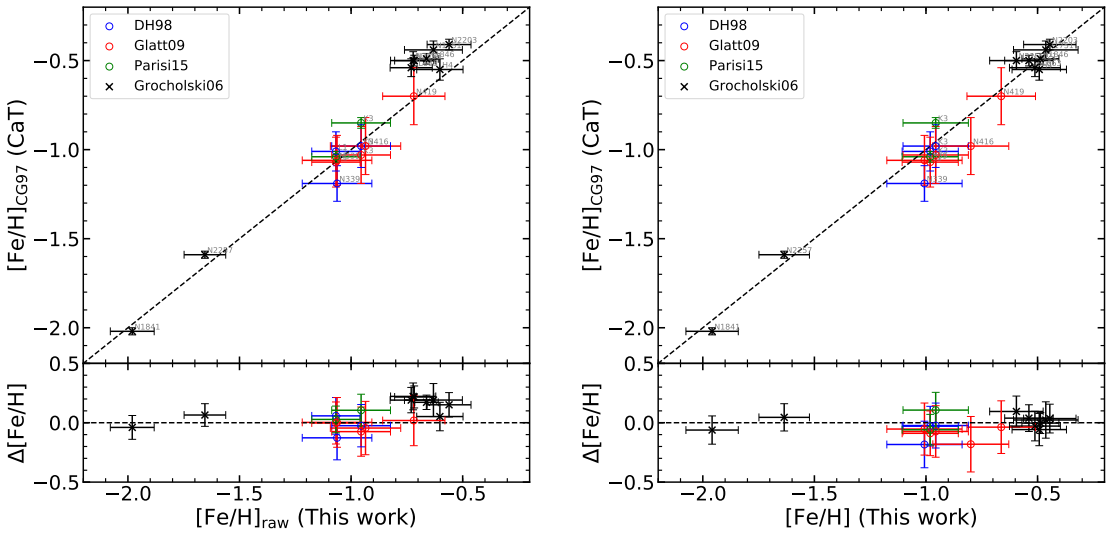

Figure 4.5: Comparisons of metallicities for clusters in common between our work and that of previous CaT studies (*Da Costa and Hatzidimitriou*, 1998; *Glatt et al.*, 2009; *Grocholski et al.*, 2006; *Parisi et al.*, 2015). In both panels, open circles denote the SMC clusters and crosses denote the LMC clusters of our sample (see Table 4.1). The raw cluster metallicities derived in Section 4.1.2 are used in the left panel, while right panel uses the cluster metallicities (as listed in Table 4.1) obtained after the calibration described in Section 4.2.4.

members confirmed in Section 4.1.2. For the three SMC clusters (Kron 3, Lindsay 1 and NGC 339) that have multiple CaT measurements available, we took the weighted average of their [Fe/H] values when calculating the metallicity offsets. We found a clear positive correlation between metallicity offsets and color offsets. We fitted the following linear relation (see the dotted line in Figure 4.5) to calibrate our raw cluster metallicities onto the CaT CG97 scale:

$$[\mathrm{Fe/H}]_{\mathrm{CG97}} = [\mathrm{Fe/H}]_{\mathrm{raw}} + 1.131\Delta(G_{\mathrm{BP}} - G_{\mathrm{RP}}) + 0.021. \tag{4.3}$$

The final $[\mathrm{Fe/H}]_{\mathrm{CG97}}$ values are listed in column 3 of Table 4.1. The weighted standard deviation in $[\mathrm{Fe/H}]_{\mathrm{CG97}}$ about the fitted line is 0.064 dex; we have added this value to the final metallicity errors in quadrature (column 4 of Table 4.1). The comparison between our calibrated cluster metallicities and those in the CG97 scale is shown in

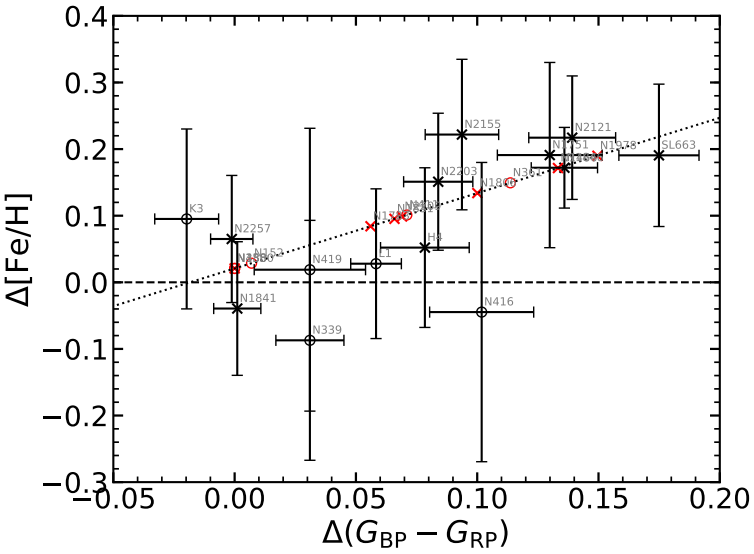

Figure 4.6: Metallicity differences for clusters in common with our work and previous CaT studies as a function of the color offsets raised in the $T_{\rm eff}$ calculation (see Section 3.3.2). Open circles denote the SMC clusters and crosses denote the LMC clusters in our sample (see Table 4.1). The dotted line is the weighted linear fit to these data given by Equation 4.3. This fitted line was used to place our cluster metallicities on the CaT system described in Section 4.2.4 and Figure 4.5. For clusters in our sample lacking published CaT measurements, the adopted Δ[Fe/H] values are denoted as red symbols along the dotted line. The calibrated cluster metallicities are listed in Table 4.1.

the right panel of Figure 4.5. The plot shows that along the full metallicity range, our modified [Fe/H] values now agree well with those in the CG97 scale after the calibration using Equation 4.3.

CHAPTER V

Discussion: How Well to Simple Stellar Population Models Stack Up?

Having produced M/L_V values for 26 clusters spanning a range of ages (Table 3.1), metallicities (Table 4.1) and masses (Table 4.4), we now turn to a discussion regarding the basic trends of M/L_V with respect to these various parameters. Part of that discussion involves a comparison of our results to M/L_V values predicted by canonical Simple Stellar Population (SSP) models. Dynamical effects can also lead to evolution of M/L_V values in clusters, and we consider these effects as well. Given that the SSP+dynamics models appear to explain our results reasonably well, we also explore how cluster M/L_V values may be used to constrain other astrophysical parameters such as the stellar IMF and cluster disruption timescales in the Magellanic Clouds.

5.1 Mass-to-light Ratios Trends versus SSP Models

A fundamental prediction of stellar evolutionary models is that, barring any strong IMF variations or pathological dynamical effects, simple populations should become 'darker' (i.e., higher M/L_V) with increasing age. The top left panel of Figure 5.1 reveals such a trend as a clear positive correlation between M/L_V ratio and age for our cluster sample.

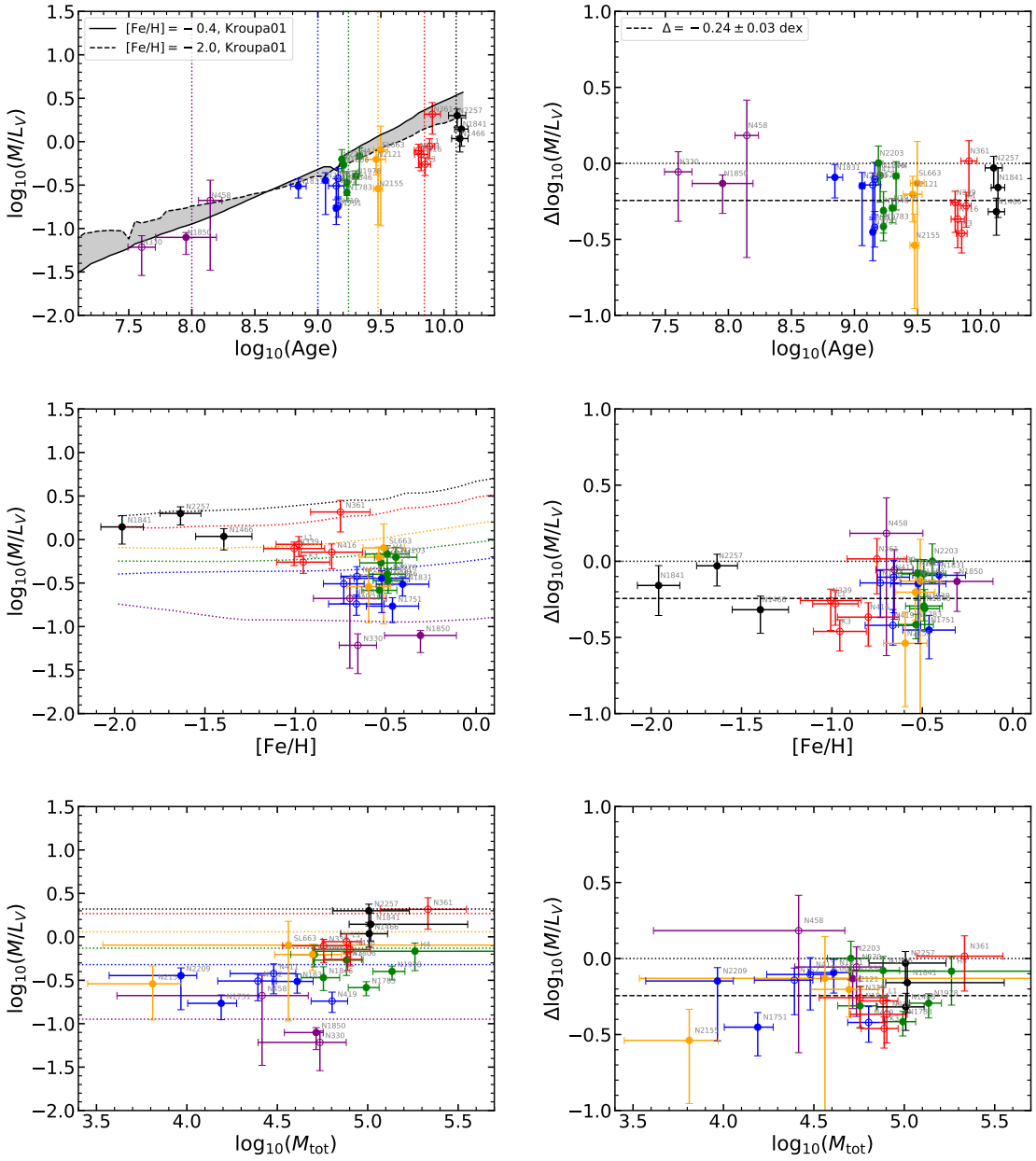

Figure 5.1: Left panels: Dynamical M/L_V ratios of our target clusters in the LMC (filled circles) and SMC (open circles) as a function of age (top), metallicity (middle) and mass (bottom), over-plotted with evolutionary M/L_V ratio isochrones from a set of FSPS SSP models (see Section 5.1 for details). The clusters are binned into distinct age groups denoted by different colors (see Table 5.1 for bin details). In the top left panel, the solid and dashed curves show M/L_V evolutionary tracks for two metallicities (see the legend). In the top and middle left panels, the colored dotted lines denote the ages used to generate the SSP isochrone curves (see column 4 of Table 5.1). In the bottom left panel, the colored dotted lines are calculated for the same ages but in each case we adopted the bin metallicity of the set of clusters denoted by the same color (see column 5 of Table 5.1). Right panels: Differences of M/L_V ratios in log space between our measurements and the SSP predictions. The $\Delta \log_{10}(M/L_V)$ values were calculated in a cluster-by-cluster manner using the age and metallicity of each cluster (we used the ages listed in Table 3.1 and metallicities listed in Table 4.1). In each right-hand panel, the horizontal dashed line shows the weighted mean offset in $\Delta \log_{10}(M/L_V)$ for the entire sample.

In the same panel, we have overplotted evolutionary tracks of a set of SSP models denoted by the solid and dashed black lines and the shaded gray area bounded by these two lines. The tracks were produced using the Flexible Stellar Population Synthesis (FSPS) code (*Conroy et al.*, 2009; *Conroy and Gunn*, 2010) employing Padova isochrones (*Girardi et al.*, 2000; *Marigo et al.*, 2008), a *Kroupa* (2001) IMF, and the BaSeL spectral library (*Lejeune et al.*, 1997, 1998; *Westera et al.*, 2002). We will refer to the tracks produced by this combination of Kroupa/Padova/BaSeL models as 'canonical' SSP models throughout this thesis. The shaded area in the figure is meant to roughly represent the age-metallicity regime appropriate for MC clusters. The colors of the data points denote age bins used to categorize the clusters. The colored dotted lines represent the approximate average ages of these bins (see Table 5.1 and the caption of Figure 5.1 for details regarding these age bins).

We also tested other options in the FSPS code, such as using the MILES spectral library (*Sánchez-Blázquez et al.*, 2006) with both MIST (*Dotter*, 2016; *Choi et al.*, 2016; *Paxton et al.*, 2011, 2013, 2015) and BaSTI theoretical isochrones (*Pietrinferni et al.*, 2004). In all cases, we found good agreement ($\lesssim 10\%$) with the adopted Padova/Kroupa/BaSeL models among predicted M/L_V ratios using alternative isochrones and stellar libraries.

Figure 5.1 reveals that when compared to the adopted canonical SSP models, our dynamical M/L_V ratios tend to run lower than the predictions. This offset leads to an obvious but important conclusion: There is no evidence that the clusters in our sample contain significant amounts of dark matter. This supports our implicit assumption that these clusters are devoid of dark matter and hence 'pure' tests of SSP models.

The offset between the SSP models and our observations is further highlighted in the top right panel of Figure 5.1, where we show the difference between our measured M/L_V ratios and the SSP predictions as a function of cluster age. The $\Delta \log_{10}(M/L_V)$

Table 5.1: Age/Metallcity bins of the cluster sample

Bin	Color[a]	Age Range (Gyr)	Bin Age[b] (Gyr)	Bin [Fe/H][b] (dex)	Clusters
(1)	(2)	(3)	(4)	(5)	(6)
1	Purple	0.04–0.14	0.1	–0.4	NGC 330, 458, 1850
2	Blue	0.7–1.5	1.0	–0.4	NGC 152, 411, 419, 1751, 1831, 2209
3	Green	1.5–2.2	1.8	–0.4	NGC 1783, 1806, 1846, 1978, 2203; Hodge 4
4	Yellow	2.9–3.2	3.0	–0.4	NGC 2121, 2155; SL 663
5	Red	6.3–8.1	7.0	–0.7	NGC 339, 361, 416; Kron 3, Lindsay 1
6	Black	12.7–13.8	12.5	–1.7	NGC 1466, 1841, 2257

[a]These colors are used in Figure 5.1, Figure 5.2 and Figure 5.4 to represent clusters and model results associated with the age/metallicity bins listed here.
[b]These bin age and metallicity values are used to produce the isochrone curves shown in Figure 5.1, Figure 5.2 and Figure 5.4. They are set to equal grid point values in the *Anders et al.* (2009) models.

values were calculated uniquely for each cluster using its own age (see Table 3.1) and metallicity (see Table 4.1). Across the entire sample, our M/L_V ratios are -0.24 ± 0.03 dex lower on average than the theoretical predictions in log space, with an error-weighted standard deviation of 0.16 dex. There is a weak indication that the youngest clusters may more closely follow the SSP predictions. Notably, the overall offset—about 70%—cannot be accounted for by using different input models in the FSPS code.

As shown in the middle left panel of Figure 5.1, we also find a trend of decreasing M/L_V ratio with increasing cluster metallicity. This trend is not unexpected since the more metal-rich clusters in our sample are also younger and hence lower in M/L_V ratio than those of the metal-poor counterparts; this is simply a manifestation of the well-known age-metallicity relation for MC clusters (see Figure 3.1 and, e.g. *Harris and Zaritsky*, 2009; *Parisi et al.*, 2015). In the middle right panel, the $\Delta \log_{10}(M/L_V)$ values are plotted against the metallicities for all clusters in our sample.

The bottom left panel of Figure 5.1 shows a broad trend of increasing M/L_V ratio with increasing cluster mass. This behavior is also seen among old (globular) clusters in both our Galaxy (*Mandushev et al.*, 1991; *Kimmig et al.*, 2015) and M31

(*Strader et al.*, 2011), and were attributed by these authors to be due to dynamical evolutionary effects. The isochrones from canonical SSP models (colored dotted lines) remain constant with cluster mass and so do not to predict a trend of M/L_V with total mass. We will return to this when we consider dynamical evolution effects in the MC clusters. The bottom right panel shows the offsets in $\Delta \log_{10}(M/L_V)$ with the SSP predictions calculated using the appropriate age and metallicity for each cluster.

5.2 Dynamical Effects on Cluster Mass-to-light Ratios

5.2.1 Mass underestimates from single-mass models

Our dynamical analysis employs single-mass models—specifically K66 models—that assume equal-mass particles and a constant cluster M/L_V ratio at all radii. Such models do not account for dynamical effects associated with energy equipartition that lead to observable features such as mass segregation and, hence, spatial evolution of M/L_V over time. In the presence of a tidal field, low-mass stars (with preferentially high M/L_V values) will be lost causing a global decrease of M/L_V as well. Due to these effects, we can expect that any single-mass models, such as the K66 models we used, will tend to underestimate the total mass, especially when the kinematic tracers (such as our observed RGs) are more massive than the mean mass of cluster members and therefore kinematically colder and more concentrated in the inner regions of the cluster.

Sollima et al. (2015) explored this effect quantitatively by comparing different analytic models (including the K66 model) used to simulated observations obtained from a suite of N-body simulations of star clusters in different stages of their evolution. For clusters with high degree of relaxation (i.e., half-mass relaxation time scale $t_{\rm rh} = 0.12$ Gyr), they found that the cluster mass can be underestimated up to 50% of the true value. This accounts for a correction of 0.30 dex in $\log_{10}(M/L_V)$ and could,

in principle, fully explain the offset seen in Section 5.1. However, it is unlikely that most of our clusters are highly relaxed since some are relatively young and most are comparatively low-density systems.

A more applicable estimation using a longer relaxation timescale (i.e., $t_{\rm rh} = 4.97$ Gyr) was also studied by *Sollima et al.* (2015). For this case, they found that K66 models can underestimate the true mass of about 10–20%, depending on the initial cluster mass, the strength of the tidal field and the radial extent of the kinematics tracers (the RGs in our case) used in the dynamical analysis. This is consistent with the work by *Hénault-Brunet et al.* (2019), who used mock data from a star-by-star N-body simulation of M4 to compare mass modelling techniques, including ones using K66 models. They found that the K66 model underestimates the true cluster mass by about 17%. This corresponds to an offset in $\log_{10}(M/L_V)$ of 0.08 dex, insufficient to fully account for the offset between our observed M/L_V and the canonical SSP models (though it can reduce the offset to about half of what is observed. We conclude that our adoption of K66 models tends to underestimate the true cluster mass, but this does not by itself account for the offset we observe between our measured M/L_V ratios and the canonical SSP models (top right panel of Figure 5.1).

5.2.2 External dynamical effects

After a bound star cluster forms from a dense gas cloud and survives the so-called 'infant mortality' stage (the timescale of about 10 Myr for unbound clusters to totally dissolve, e.g, *Lada and Lada*, 2003; *Whitmore*, 2004), its evolution will be driven by both internal and external dynamical effects. The internal effects include those described in Section 5.2.1 as well as changes in the masses of stars due to mass loss or binary mergers (e.g, *Portegies Zwart et al.*, 2010; *Renaud*, 2018). External effects can include tidal perturbations from the host galaxy due to either impulsive effects—e.g. encounters with giant molecular clouds, spiral arms or other clusters—or

secular evolution arising from a changing tidal field as a cluster orbits within a galaxy (see e.g. *Krumholz et al.*, 2019). In the canonical SSP models used here, generally only the internal effects related to stellar evolution are considered. Ignoring cluster dynamical evolution—both the internal dynamics and the external tidal effects—can lead to overestimated M/L_V values over time (we have seen this to be the case for internal dynamical evolution in Section 5.2.1).

To test how dynamical evolution affects cluster M/L_V ratios, we have adapted a suite of evolutionary synthesis models developed by *Anders et al.* (2009). Their models are built from the GALEV code (see, e.g. *Kotulla et al.*, 2009) using the Padova isochrones, a *Kroupa* (2001) IMF and BaSeL spectral library (the same as the SSP models we adopted in Section 5.1). These models account for dynamical evolution of star cluster by introducing a mass-dependent parameter—the total cluster disruption time, $t_{95\%}$, defined as the time when 95% of the initial cluster mass is unbound. This timescale attempts to parameterize the mass-function evolution found in N-body simulations of stars clusters dissolving in tidal fields (*Baumgardt and Makino*, 2003).

In the left panel of Figure 5.2, we compare our empirical M/L_V ratios as a function of age with the *Anders et al.* (2009) models. For purposes of comparison, we assume that the clusters are halfway in time to total disruption (i.e., their disruption times are twice their current ages). Different colored bands in the plot correspond to different disruption times that are two times the ages indicated by the colored dotted lines (see the figure caption for details). The models reveal that external dynamical evolution causes the M/L_V ratio to increase slowly then decrease over time as a cluster ages. This is in contrast to the SSP predictions where cluster M/L_V values steadily increase with time (the light gray band in the left panel of Figure 5.2 and, more clearly, in the top left panel of Figure 5.1).

In the right panel of Figure 5.2, we plot $\Delta \log_{10}(M/L_V)$ as a function of age in a cluster-by-cluster manner, still assuming the disruption time is twice the age of

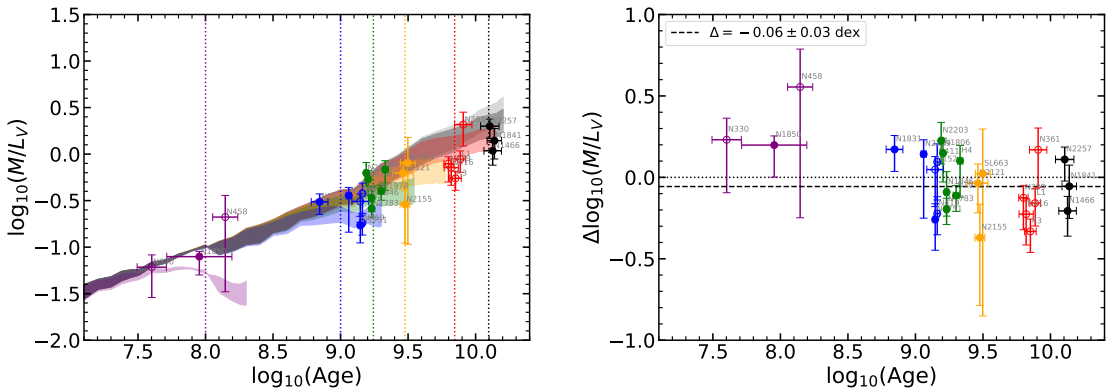

Figure 5.2: The same as the upper panels of Figure 5.1, but now the colored dotted lines denote results from the synthesis models (*Anders et al.*, 2009) that account for cluster dynamical evolution (see Section 5.2.2). For purposes of comparison, we assume the clusters are halfway in time to the total dynamical disruption time, defined when cluster loses 95% of their initial mass. In the left panel, the color bands denote a range of evolutionary tracks over metallicity from -2.0 (lower band boundaries) to -0.7 (upper band boundaries) dex. Different band colors correspond to disruption times of twice the bin ages listed in Table 5.1. In the right panel, the $\Delta \log_{10}(M/L_V)$ values were calculated in a cluster-by-cluster manner using the age and metallicity of each cluster and compared with the *Anders et al.* (2009) models under the assumption that the total disruption time is double the age of the cluster. The horizontal dashed line shows the weighted mean offset in $\Delta \log_{10}(M/L_V)$ for the entire sample.

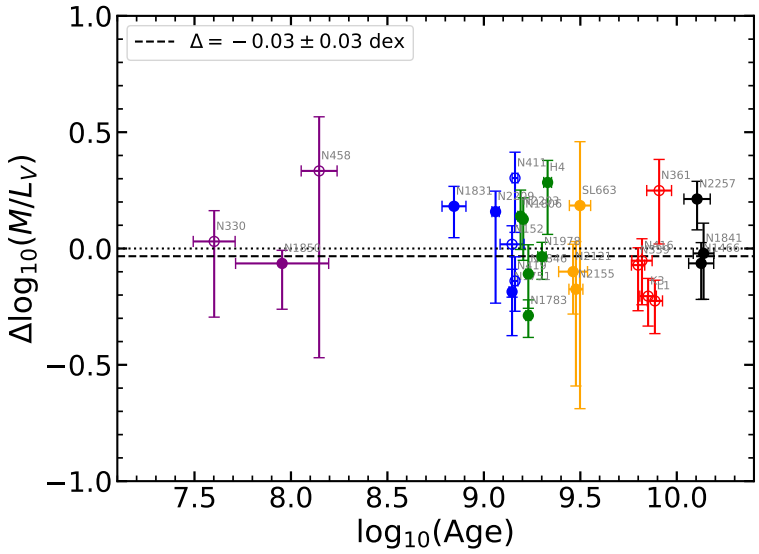

Figure 5.3: The same as the right panel of Figure 5.2, but the corresponding SSP-predicted M/L_V value is predicted under the assumption that the total disruption time is the sum of the age of the cluster and its current core relaxation time (see Equation 5.1).

a given cluster. The error-weighted average in $\Delta \log_{10}(M/L_V)$ is -0.06 ± 0.03 dex (denoted as a dashed black line), with an error-weighted standard deviation of 0.18. This represents better agreement with models accounting for cluster evolution than canonical SSP models (compare with the top right panel in Figure 5.1). Clearly, if we combine mass underestimation discussed in Section 5.2.1, the offset in $\Delta \log_{10}(M/L_V)$ can become negligible, implicitly assuming the two dynamical effects are at least partly independent.

An alternative approach to this analysis is to assume that the clusters will totally dissolve no sooner than their current central relaxation time (see, e.g., *Spitzer*, 1987; *Djorgovski*, 1993; *Mackey et al.*, 2013; *Bianchini et al.*, 2016). This timescale can be defined as

$$t_{\rm rc} = \frac{8.338 \times 10^6 \text{ yr}}{\ln 0.4N} \left(\frac{\bar{m}}{\text{M}_\odot}\right)^{-1} \left(\frac{\rho_0}{\text{M}_\odot \text{ pc}^{-3}}\right)^{1/2} \left(\frac{r_{\rm c}}{\text{pc}}\right)^3, \tag{5.1}$$

where N is the total number of stars in the cluster, $\bar{m}$ is the mean stellar mass, ρ_0 is the central mass density, and $r_{\rm c}$ is the core radius (computed from distance moduli

listed in Table 3.1 and K66 radii listed in Table 3.2). We set $N = M/\bar{m}$ assuming $\bar{m} = 0.5$ $M_\odot$, a reasonable simplification given that the actual range of $\bar{m}$ is 0.46–0.63 $M_\odot$ for the clusters in our sample assuming the canonical SSP models.

In Figure 5.3, we show an analogous plot as the right panel of Figure 5.2 but with under the assumption that $t_{\rm dis} = t_{\rm age} + t_{\rm rc}$. The error-weighted average in $\Delta \log_{10}(M/L_V)$ is -0.03 ± 0.03 dex (denoted as a dashed black line), with an error-weighted standard deviation of 0.18, somewhat better agreement than seen in Figure 5.2. More importantly, however, is the way in which the agreement has systematically improved for the younger clusters, consistent with our findings in the next section of a typical cluster dissolution timescale in the MCs of a few Gyr.

The results shown in Figure 5.2 and Figure 5.3 allow us to conclude that internal/external dynamical effects plausibly account for the offset between our measured M/L_V and the SSP models shown in the upper panels of Figure 5.1.

5.3 Cluster dissolution in the LMC and SMC

For star clusters in a tidal field, the total disruption time depends on the a cluster's initial mass as $t_{95\%} \propto M_i^\gamma$, based on both N-body simulations (*Baumgardt and Makino*, 2003) and observations (e.g. *Boutloukos and Lamers*, 2003; *Lamers et al.*, 2005a). The index γ has been found to be 0.62 and 0.60 ± 0.02, respectively, from N-body simulations (*Baumgardt and Makino*, 2003) and observations of solar-neighborhood open clusters (*Lamers et al.*, 2005b). A scaling factor, t_4, specifies the disruption time of a 10^4 $M_\odot$ star cluster within its host galaxy.

Adopting a model in which both t_4 and the cluster formation rate (CFR) are constant, *Boutloukos and Lamers* (2003) derived $\log t_4 = 9.90 \pm 0.20$ and $\gamma = 0.61 \pm 0.08$ from the analysis of 314 SMC clusters located within 4 kpc from that galaxy's center. For the LMC, *Parmentier and de Grijs* (2008) used the same approach to constrain t_4 but with γ set to a fixed value of 0.62. They concluded only that $t_4 \geq 1$

Gyr, principally due to an apparent steady increase of the CFR in the LMC over the past 5 Gyr, negating one of the assumptions of the analysis.

We show here that we can use our M/L_V results to constrain t_4 in both galaxies. We start with the *Anders et al.* (2009) models as shown in the left panel of Figure 5.2. For a given age and metallicity, we can read off a M/L_V corresponding to a given disruption time. Using Equation 2 from *Anders et al.* (2009), we can write for a given cluster

$$M'_{\rm tot}(t) = f(t) \cdot M_{\rm i} = f(t) \cdot 10^4\, M_\odot \cdot \left(\frac{t_{95\%}}{t_4}\right)^{1/\gamma} \cdot \left[\frac{\mu_{\rm ev}(t_{95\%})}{\mu_{\rm ev}(t_4)}\right]^{-1}, \qquad (5.2)$$

where t is the cluster's age. The parameter $\mu_{\rm ev}$ specifies the mass loss of a cluster due to standard stellar evolutionary effects (e.g. mass loss). The function $f(t)$ specifies the remaining bound mass fraction of a clusters when both stellar evolution and dynamical effects are considered. Given a value for t_4 and γ, we can use this procedure to generate isochrones in the $(M/L_V)'$-$M'_{\rm tot}$ plane.

The left panel of Figure 5.4 shows a set of such isochrones for $t_4 = 8.0$ Gyr (the measured value for the SMC by *Boutloukos and Lamers*, 2003), while the right panel shows results for $t_4 = 0.8$ Gyr (consistent with the lower limit value for the LMC clusters by *Parmentier and de Grijs*, 2008). In both cases, we have adopted $\gamma = 0.62$ (*Boutloukos and Lamers*, 2003). The isochrone colors correspond to the adopted mean ages and metallicities for the bins in which the clusters have been assigned (see the caption). Since the clusters of a given age bin vary in age and metallicity, we have shifted their positions in Figure 5.4 (relative to the lower left panel of Figure 5.1) by using the canonical SSP model (i.e., the model with a disruption time of 200 Gyr in *Anders et al.*, 2009) to determine the small shifts in M and L_V associated with the shift in age and metallicity of each cluster to the corresponding bin values. The 'prime' notation ($M'_{\rm tot}$ and $(M/L_V)'$) is meant to emphasize that the plotted values

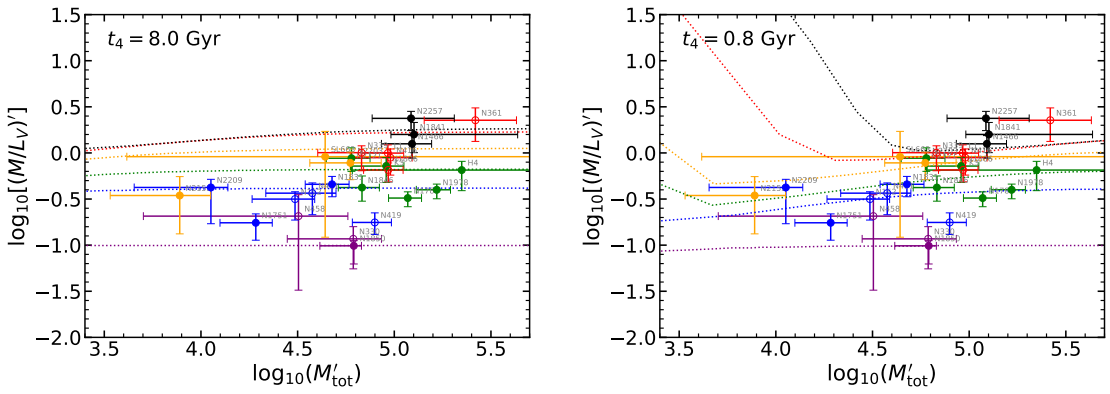

Figure 5.4: Time evolution of M/L_V ratios as a function of (present-day) cluster mass for two fixed local gravitational field strengths (characterized by the characterized disruption time t_4; see Section 5.3). Both panels contain the same data as the bottom left panel in Figure 5.1, but here the colored dotted lines are isochrones calculated from the synthesis models (*Anders et al.*, 2009) accounting for dynamical evolution of star clusters. The bin ages and metallicities used to produce the isochrone curves are listed in Table 5.1.

have been adjusted from the results shown in Figure 5.1.

In both panels of Figure 5.4, we can see that $(M/L_V)'$ is constant for the highest-mass and youngest clusters as these systems have not yet attained internal energy equipartition; thus their $(M/L_V)'$ values are nearly the same as expected for canonical SSP models (see Figure 5.1). For the $t_4 = 0.8$ Gyr models (right panel), it can also be seen that as age increases, $(M/L_V)'$ can increase with decreasing mass. The reflects the fact that, at any given age, low-mass clusters will have lost more low-mass stars due to energy equipartition (*Kruijssen*, 2008). For the lowest mass clusters, (e.g. the black and red dotted lines in the right panel of Figure 5.4) the increasing fraction of bound stellar remnants near the end stages of cluster dissolution (*Anders et al.*, 2009) causes a rapid increase in $(M/L_V)'$. This also implies that clusters found near the minima of the isochrones are very close to complete dissolution.

Note that for the larger value of t_4 (8.0 Gyr; left panel in Figure 5.4), the isochrones tend to run above the data for clusters of corresponding age. For the smaller t_4 value (0.8 Gyr; right panel), the isochrones systematically match the cluster data better in

both the SMC and LMC, with two exceptions. First, the oldest clusters (in black) appear to agree better with the larger t_4 value. These clusters, all associated with the LMC, are located furthest from the galaxy center. This suggests that they may be subjected to a milder tidal field and hence take considerably longer to disrupt. The second exception is NGC 361 that appears to deviate from the lower-t_4 models. This particular cluster has a small kinematic sample that is notably sensitive to contamination by outliers (see Section 4.2.1) and, hence, a potentially large systematic overestimate of its $(M/L_V)'$ value.

Our estimate of t_4 based on Figure 5.4 does not rely on sample completeness, nor any sorts of assumptions regarding the cluster mass functions and cluster formation rates in the MCs. This suggests that we can use our results to test assumptions used in other studies that have used these clusters to estimate t_4. For the LMC, our estimated value of $t_4 \sim 1$ Gyr is similar to the lower limit found by *Parmentier and de Grijs* (2008). That limit resulted from the assumption of a non-constant cluster formation that had a minimum around 5 Gyr ago. For the SMC, our estimated value of t_4 is considerably shorter than the value of 8.0 Gyr found by *Boutloukos and Lamers* (2003) and who assumed a constant CFR. Our results bring this assumption into question but do not allow us to specify an alternate form of the CFR in the SMC.

The LMC cluster NGC 2155 lies closest to the minimum of its corresponding isochrone in the right panel of Figure 5.4, indicating, as noted above, that this cluster may be close to complete dissolution (*Anders et al.*, 2009). This is particularly interesting because NGC 2155 is one of the oldest clusters (at 3.0 Gyr; see Table 3.1) in the LMC found at the young edge of the well-known cluster age gap of that galaxy (*Bertelli et al.*, 1992; *Girardi et al.*, 1995; *Olszewski et al.*, 1996). Given this location in Figure 5.4, the *Anders et al.* (2009) models allow us to estimate that the cluster has lost 80-95% of its initial mass. If we assume for NGC 2155 a factor of 10 mass loss over its lifetime, its initial mass would have been around $10^5 M_\odot$, similar to the

globular-like LMC clusters in our sample (NGC 1466, NGC 1841 and NGC 2157)[1]. This suggests that many present-day intermediate-age LMC clusters may have started out similar in mass to objects we now consider to be globular clusters, but they have succumbed in a comparatively short time to the disruptive tidal field of the LMC disk due to a considerably shorter value of t_4 in that part of the galaxy.

5.4 Variations in the Stellar Initial Mass Function?

Up to this point we have only considered the *Kroupa* (2001) IMF in the canonical SSP models we have employed so far in our analysis. For an IMF of the form $dN/dM \propto M^{-\alpha}$, the *Kroupa* (2001) IMF has three mass ranges: less than 0.5 $M_{\odot}$, between 0.5 and 1.0 $M_{\odot}$, and greater than 1.0 $M_{\odot}$, respectively characterized by α_1, α_2, and α_3 (see also *Strader et al.*, 2011). In the FSPS code (*Conroy et al.*, 2009; *Conroy and Gunn*, 2010) with an initial mass range between 0.08 and 100 $M_{\odot}$, the default values for the *Kroupa* (2001) IMF are $\alpha_1 = 1.3$ and $\alpha_2 = \alpha_3 = 2.3$.

Of course, owing to the immense range in M/L_V among stars of different mass, the integrated M/L_V ratio of a stellar population depends sensitively on the form of the initial mass function (IMF). Broadly speaking, 'bottom heavy' IMFs—ones with relatively more low-mass stars than the Kroupa IMF—will produce larger M/L_V values, while 'bottom light' IMFs will result in lower M/L_V values. We explore here the extent to which IMF variations alone may account for the observed offset of M/L_V relative to canonical SSP models (upper panels of Figure 5.1).

Since the observed M/L_V of the clusters in our sample are smaller than SSP model predictions, the argument above implies that a bottom light IMF is needed to reconcile the data and models in the absence of any other effects—such as dynamical evolution as discussed above—which may alter M/L_V. We follow the discussion of

[1]A similar conclusion may hold for SL 663, the other cluster in our sample of similar age to NGC 2155, but its M/L_V and mass uncertainties (see Figure 5.4) make any estimate of its dynamical state or its total mass loss quite uncertain.

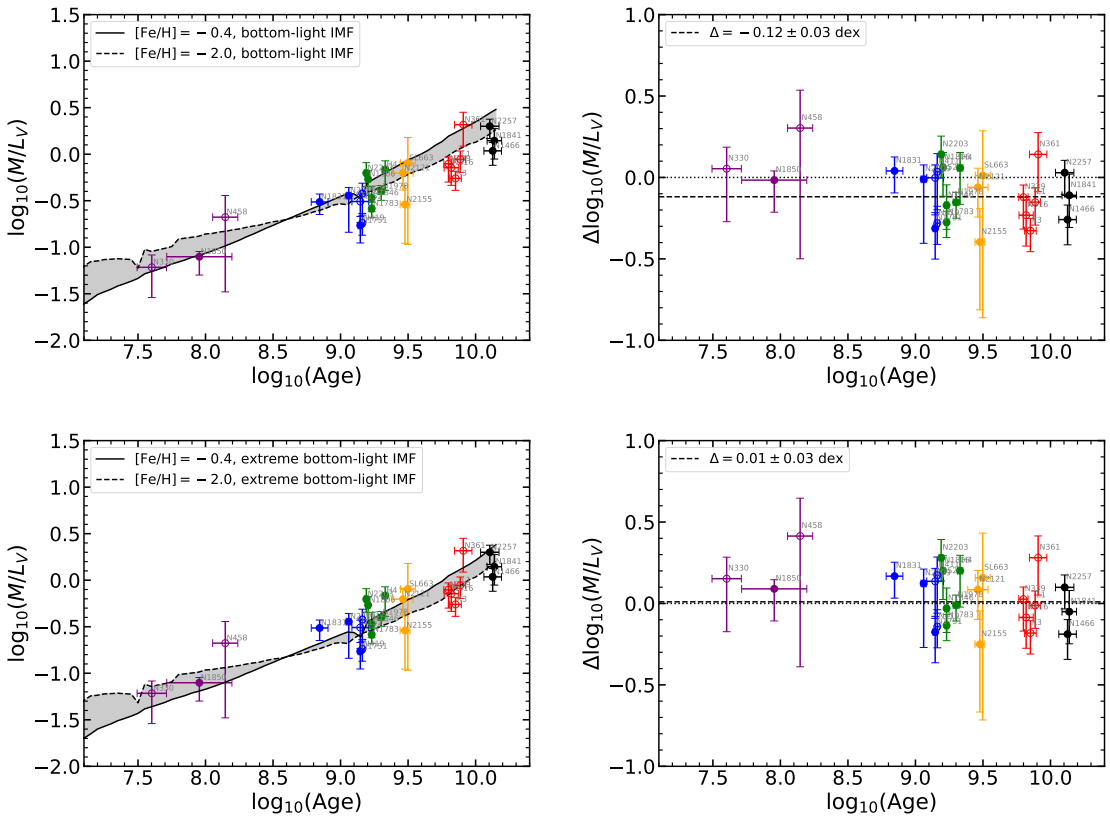

Figure 5.5: The same as the upper panels of Figure 5.1, but now the solid and dashed curves and their enclosed gray band denote the evolutionary tracks of SSP models with a bottom-light (top panels) and an extreme bottom-light IMFs (bottom panels), respectively. These two IMFs are defined in Section 5.4. The $\Delta \log_{10}(M/L_V)$ values in the right panels were again calculated in a cluster-by-cluster manner using the age and metallicity of each cluster similar to those shown in Figure 5.1. The colors of the points correspond to the age bins described in Table 5.1.

Dalgleish et al. (2020) who defined two simple power-law mass functions (MF). In both cases, $\alpha_3 = 2.3$ (the same as the Kroupa IMF), but for lower stellar masses between 0.08 and 1.0 $M_\odot$, $\alpha_1 = \alpha_2 = 1.3$ for their so-called 'bottom-light' MF, and $\alpha_1 = \alpha_2 = 0.3$ for their 'extreme bottom-light' MF. In Figure 5.5 we illustrate how the SSP models are altered by adopting these as IMFs. Both improve the agreement of the models and cluster data; in the case of the 'extreme bottom-light' IMF, the net offset of the data and models is nearly completely accounted for.

This conclusion contrasts with that of *Zaritsky et al.* (2012, 2013, 2014) who used

integrated light spectroscopy to estimate M/L_V ratios for a sample of MC clusters. In the left panel of Figure 5.6 we plot along with our results these integrated light measurements as well as M/L_V estimates MC clusters based on individual-star spectroscopy of intrinsic precision similar to that of our study ((*Fischer et al.*, 1992a,b, 1993; *Suntzeff et al.*, 1992; *McLaughlin and van der Marel*, 2005; *Mackey et al.*, 2013; *Kamann et al.*, 2018; *Patrick et al.*, 2020). This comparison highlights some key points. First, all individual-star results seem to agree systematically over the full range of ages explored by the data. Moreover, these data roughly parallel the model expectations. Second, the integrated-light measurements appear to define a relation that is considerably shallower than the SSP models or the individual-star measurements. Third, modified SSP models based on a bottom-heavy IMF ($\alpha_1 = \alpha_2 = 2.8$ and $\alpha_3 = 2.3$, plotted in the left panel of Figure 5.6) agree well with the *Zaritsky et al.* (2012, 2014) integrated-light results for clusters younger than about 3 Gyr. For older clusters, the integrated-light and individual-star M/L_V results broadly agree.

Integrated-light studies tend to favor high-concentration clusters with moderate to bright central surface brightnesses, while individual-star studies tend to employ more diffuse, larger clusters where obtaining spectra of distinct stars is more feasible. Moreover, the integrated-light spectra tend to only consist of contributions from the innermost regions of the clusters. These may point to a possible physical distinction between the clusters that reveals real IMF variations. However, the systematic tendency of the integrated-light results to run high compared to individual-star results, particularly for clusters younger than about 3 Gyr, suggests a more prosaic explanation. The right panel of Figure 5.6 compares the integrated-light results with the M/L_V results based on the 'Box' samples (see Section 4.2.1). We have already demonstrated (Section 4.2.1) that the Box samples are subject to contamination by non-members, and the broad agreement with the integrated-light values evident in Figure 5.6 suggests that the latter may as well. Unlike individual-star analyses, how-

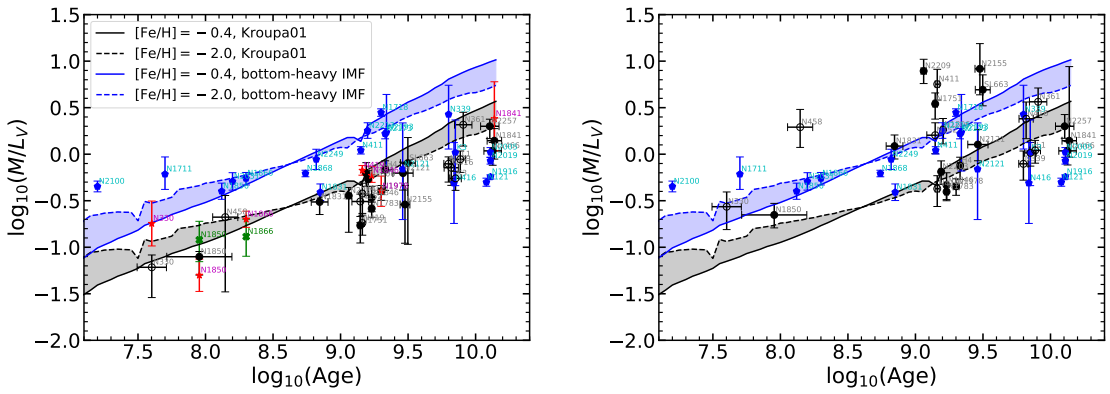

Figure 5.6: Left panel: The same as the top left panel of Figure 5.1, but with all M/L_V values from this work shown in black. Over-plotted are the M/L_V results from previously published studies using either integrated-light spectroscopy (blue) or individual stellar spectra (red and green). The green data points denote the re-calculated results of *McLaughlin and van der Marel* (2005) by fitting K66 models to previously published velocity dispersion results (i.e., NGC 1866 from *Fischer et al.* 1992a and NGC 1850 from *Fischer et al.* 1993), and hence are labelled differently from other individual-star studies shown in red. We also plot the evolutionary tracks of SSP models with a bottom-heavy IMF (blue curves and band) to illustrate the trend of integrated-light results for clusters young than about 3 Gyr (blue pentagons). Right panel: The same as the left panel, but with all our M/L_V values (in black) derived from the BOX samples (see Table 4.3) instead of the PM50/PM50′ as shown in the left panel.

ever, it is not feasible to remove the effects of outliers in an integrated spectrum should such stars be present. Clearly, more studies of clusters observed using both techniques would help explore the nature of this apparent discrepancy.

5.5 Conclusions

In this chapter, I have presented the trends of M/L_V with cluster age, metallicity and mass, and compared these trends with the predictions of canonical SSP models (Section 5.1). Our observed M/L_V values agree well with the age trend as predicted by the canonical SSP models, although the cluster-by-cluster comparison shows that our empirical M/L_V values are about 40% lower than model predictions over the full range of ages exhibited by the clusters in our sample. The offset to lower M/L_V ratios

confirms the underlying assumption of this work that these clusters do not contain any significant amount of dark matter.

I have discussed that both dynamical effects (Section 5.2) and IMF variations (Section 5.4) can account for the offset found between our observations and the SSP models. However, given that dynamical effects must dominate the evolution of star clusters when they survive from their early evolutionary stage, IMF variations—bottom-light IMFs to be specific—are not required to explain the offset. In contrast, bottom-heavy IMFs can increase the model-predicted M/L_V at a given age and exaggerate the offset. Hence these IMFs are ruled out for our cluster sample.

I have also applied simple cluster dissolution model to the observed masses and M/L_V ratios of the clusters in our sample (Section 5.3). Our results suggest that external tidal dynamical effects lead to relatively rapid dissolution in both LMC and SMC ($t_4 \sim 0.8$ Gyr, where t_4 is time to disrupt half of a sample of clusters with initial mass $10^4 M_\odot$). One exception is, perhaps, clusters located well outside the main body of the LMC where a longer t_4 is indicated.

CHAPTER VI

Summary, Conclusions and Future Work

6.1 Summary and Conclusions

In this dissertation, I have presented *Magellan*/M2FS observations of (mostly) red giants in and around 26 Magellanic Cloud star clusters (10 in the SMC and 16 in the LMC) chosen to span the range from ∼100 Myr to ∼13 Gyr in age, and from −2.0 to −0.4 in [Fe/H]. With my collaborators, I have led work on employing an improved version of the data reduction process (described in Section 2.2.4) to extract from the raw data 3137 stellar spectra of 2901 distinct targets. Using stellar effective temperatures estimated with *Gaia* DR2 G-band magnitudes (see Section 3.3.2), we applied a Bayesian methodology to obtain radial velocities, metallcities and surface gravities from these spectra (see Section 3.3.1 and *Song et al.* 2017). These parameters were used to identify peculiar targets, such as C stars, binary/blended stars, extreme M supergiants, etc. (see Section 3.3.4). Combined with previously published velocities of individual stars in the clusters of our sample, we have produced a kinematic dataset of 2787 stars suitable for dynamical and chemical analyses.

Using this sample, we have determined membership probabilities of individual stars in each cluster using an Expectation-Maximization (EM) algorithm (*Walker et al.*, 2015b,a) with the assumption that cluster members are spatially and kinematically distributed as expected for a single-mass K66 model (*King*, 1966). The EM

algorithm we used assumes that superimposed on the cluster is a spatially uniform field population that follows a kinematically much broader Gaussian distribution than the cluster population. In order to properly account for the influence of likely non-members, we followed the approaches described in Section 2.3.2.1 to assign cluster membership probabilities for the stars in each cluster sample (Section 4.1). We found that for five clusters, the so-called PM50 samples (comprised of stars with membership probabilities greater than 50%) still have potential field interlopers. We developed a related approach, PM50′, to identify cases where significant contamination by a single unflagged non-member appears to be present (see Section 4.2.1). Using the cluster members in the resulting PM50 or, for a few clusters, PM50′ samples, we obtained projected central velocity dispersion of each cluster. From these, we have derived total masses, M/L_V ratios and mean metallicities for all 26 clusters in our sample.

Our results exhibit readily understandable trends of M/L_V with cluster age, metallicity and mass (see Section 5.1). When compared with canonical SSP models, we found that our empirical M/L_V values are about 40% (-0.24 dex in $\Delta \log_{10}(M/L_V)$) lower than model predictions over the full range of ages exhibited by the clusters in our sample. We explored the origin of this offset by considering two specific dynamical effects (Section 5.2). First, the single-mass K66 model we adopted do not account for energy equipartition and, hence, mass segregation within clusters. Consequently, these models will tend to underestimate a cluster's total mass compared to more realistic multi-mass models. N-body simulations of star clusters (*Sollima et al.*, 2015; *Hénault-Brunet et al.*, 2019) suggest that this only partially accounts for the offset as we found (about $\sim$0.08 dex). Second, using modified SSP models that account for cluster evolution in a tidal field (*Anders et al.*, 2009), the M/L_V offset can almost be entirely eliminated (to about -0.06 or -0.03 dex) for reasonable cluster disruption timescale assumptions.

The observed masses and M/L_V ratios of the clusters in our sample were used

to try to constrain timescales of cluster dissolution in the MCs using a simple tidal disruption model (see Section 5.3; also *Baumgardt and Makino* 2003; *Boutloukos and Lamers* 2003; *Parmentier and de Grijs* 2008). Our results suggest that external tidal dynamical effects lead to relatively rapid dissolution in both galaxies ($t_4 \sim 0.8$ Gyr, where t_4 is time to disrupt half of a sample of clusters with initial mass $10^4 M_\odot$). One exception is, perhaps, clusters located well outside the main body of the LMC where a longer t_4 is indicated. For the LMC, this model is consistent with the assumption of a non-constant cluster formation rate (CFR) (*Parmentier and de Grijs*, 2008). Our analysis suggests that the LMC cluster NGC 2155—with an age of 3.0 Gyr—may be close to total dissolution, having already lost 65–90% of its initial mass. More detailed kinematic studies of this cluster and other LMC clusters near the temporally more recent edge of the 'age gap' (*Bertelli et al.*, 1992; *Girardi et al.*, 1995; *Olszewski et al.*, 1996) may provide important constraints on the CFR of this galaxy. For the SMC, our analysis suggests a short mean cluster disruption timescale (possibly non-constant CFR in the past), somewhat in contrast to the conclusions of (e.g. *Boutloukos and Lamers*, 2003) who assumed a constant CFR and comparatively long cluster disruption timescale.

In parallel to the discussions about cluster dynamical effects, we also considered the effect of varying stellar IMFs among star clusters to explain the offset between observed and model M/L_V values (Section 5.4). We found that an extreme bottom-light IMF could, by itself, almost fully account for the offset. In contrast, the fact that our observed M/L_V ratios run lower than SSP models with canonical IMF strongly disfavors the presence of a bottom-heavy IMF for these clusters.

A key conclusion of this study is that both dynamical effects and IMF variations can account for the M/L_V values we have measured for our cluster sample (see Figure 5.2, Figure 5.4 and Figure 5.5). It is worth noting, however, that while dynamical effects *must* be affecting the evolution of MC star clusters, it is not as clear that

IMF variations can or must be present. Thus, we favor the dynamical modifications to SSP models as described in Section 5.2.2 and Section 5.3 as the more likely reason to account that our M/L_V results run systematically below the predictions from canonical SSP models. To the extent that IMF variations may be present, our results require these to be in the form of a bottom-light mass function since bottom-heavy IMFs would cause M/L_V values to run higher than canonical models. As long as dynamical or minor IMF variations are allowed, we find that, overall, present-day SSP models such as those used for our analysis do a remarkably good job of explaining the integrated M/L_V values we observe for MC clusters.

6.2 Future Work

This thesis has been mainly focused on deriving consistent masses and M/L_V ratios of populous star clusters in the MCs. To this end, I have employed only a small portion of the M2FS spectral data obtained in Chapter III. Many interesting stellar sources associated with the clusters and in their surrounding field populations remain available for further detailed study. The data also contain information—for example, the chemical abundances of a wide range of elements and stellar rotation—that have not been explored in detail in this study. More importantly, this work also suggests new avenues of research that would benefit from additional new data. In this section I describe five specific areas of future study that directly build upon and extend my thesis research.

6.2.1 Carbon Stars in Magellanic Cloud Clusters and Their Environments

Carbon (C) stars exhibit surface carbon-to-oxygen ratio greater than unity that can produce strong features of carbon-rich molecules (such as CN, CH and C_2) in their spectra (e.g. *Wallerstein and Knapp*, 1998). They are believed to be formed via

two routes: The intrinsic C stars are formed from the evolution of asymptotic giant branch (AGB) stars dredging deep helium burning material up to the surface (e.g. *Iben and Renzini*, 1983); the extrinsic C stars are formed by accreting carbon-rich material from a donor star in a binary system (e.g. *Van Eck et al.*, 1998). Data on C stars in the LMC and SMC have accumulated for many decades; to date, a total of 7760 and 1707 C stars are known in the LMC and SMC, respectively (*Kontizas et al.*, 2001; *Rebeirot et al.*, 1993). These samples of C stars are useful for the studies of stellar evolution, and the structure and chemical evolution of the MCs.

The stellar spectra present in this thesis are mostly obtained from normal RGs in and around the field of each cluster. But, along with these normal stars, I have confirmed the presence of many C stars during the spectral analysis described in Section 3.3.4. As noted in Section 3.3.4.2, I devised a method to identify candidate C stars that produce poor LOS velocity estimates with the aim of removing them from the clusters' kinematic samples. This process identified many strong C stars, but also numerous other stars with considerably weaker C-star features. Here I describe briefly how one can improve that C-star finding approach to identify from the spectra used in this study C stars exhibiting a broad range of characteristic C spectral features. This approach will be used as the basis for developing a subsample of C stars analyze in a future paper.

The most prominent C_2 feature present in the spectra we obtained for this study is a Swan band with a bandhead at a rest-frame wavelength of 5165 Å. To precisely locate this feature, we effectively shifted every spectrum to its rest frame based on its best-fit LOS velocity estimate (i.e. the raw LOS velocity from the Bayesian fitting process described in Section 3.3.1). From this rest-frame spectrum, we computed a spectral index, $R_{\rm cts}$, which measures the flux ratio of the flux at the C_2 bandhead to

the flux in a redward continuum band of similar width, i.e.,

$$R_{\rm cts} = \frac{\text{Mean Counts between 5161.5 and 5165.5 Å}}{\text{Mean Counts between 5174.5 and 5178.5 Å}}, \tag{6.1}$$

(see Figure 6.1 for a visualization of the bands used to calculate $R_{\rm cts}$).[1]

Figure 6.2 plots all measured $R_{\rm cts}$ values against the *Gaia* DR2 colors of all stars in our sample. The bi-weight mean ($C_{\rm BI}$, *Beers et al.* 1990) of the sample is shown as a solid line in Figure 6.2; the dashed lines symmetrically enclose about 95% of the sample and so can be considered roughly 2σ intervals around the mean. All the C stars identified in this approach are located well below the mean value of $R_{\rm cts}$ due to the depressed flux in the C_2 band relative to the continuum band. I have denoted with different colors an arbitrary separation of likely C stars based on their $R_{\rm cts}$ values and additional absorption features (explained below). In the figure, I also highlight all C stars that are possible cluster members (i.e. $P_M \geq 0.5$, see Section 4.2.1) with black circles. Note that stars that extend above the main distribution of points in Figure 6.2 are generally found to exhibit weak to strong TiO absorption from a bandhead coincidentally located in the 'continuum' band of the $R_{\rm cts}$ index.[2]

All formerly identified 25 strong C stars (in red in Figure 6.2) have $R_{\rm cts} < 0.4$, and spread toward extreme red end in $G_{\rm BP} - G_{\rm RP}$ colors. Another six C stars with weaker carbon features (shown in orange) were identified before in Section 3.3.4.1 and Section 4.1.1 also have $R_{\rm cts}$ values below 0.4 but with relatively bluer colors than the strong C stars. Between $R_{\rm cts} = 0.75$ and 0.4, I was able to identify 47 additional stars showing weak absorption feature in the C_2 swan band (in green, blue and purple, respectively).

[1] In reality, we computed the band limits shifted by the observed line-of-sight velocity for each star. For extreme C stars, a good line-of-sight velocity was not measurable (see Section 3.3.4.1), but such stars were easily identified from direct inspection of their spectra (Figure 6.1). For those cases, we simply applied the bands shifted to the mean velocity of the LMC or SMC as applicable.

[2] Which also means that these same bands are a good way to find the coolest M-type giants in samples such as ours.

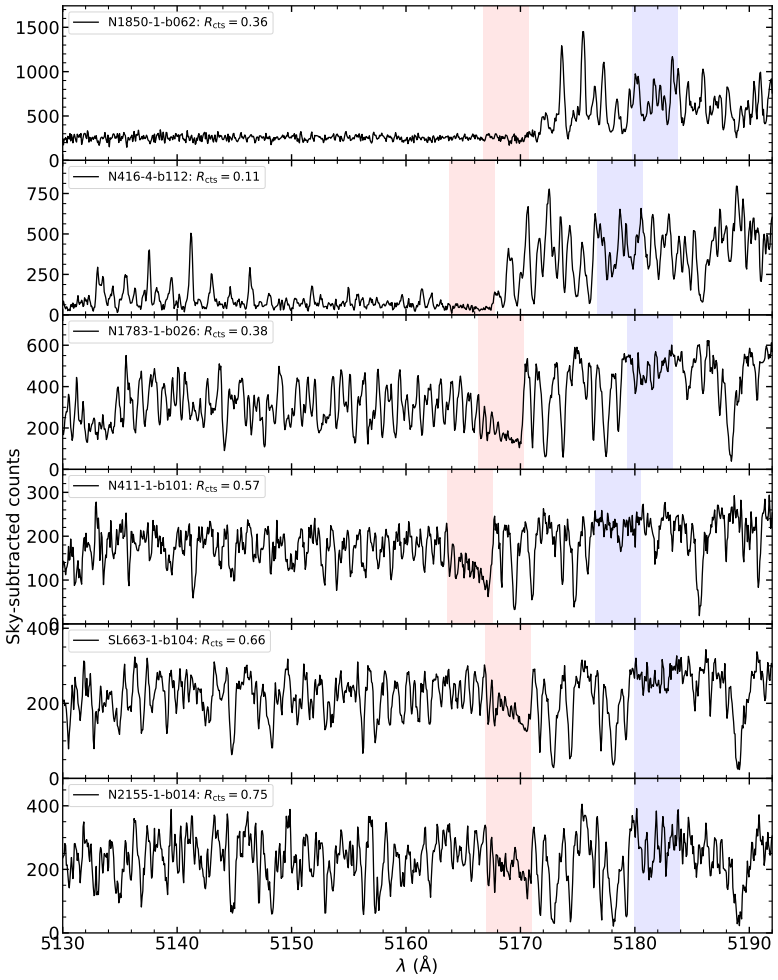

Figure 6.1: Examples of M2FS spectra of C stars identified in Section 6.2.1. From top to bottom, I show the spectra of two strong C stars, a weak C star, and three C-rich stars, indicated by various $R_{\rm cts}$ values in the legend.

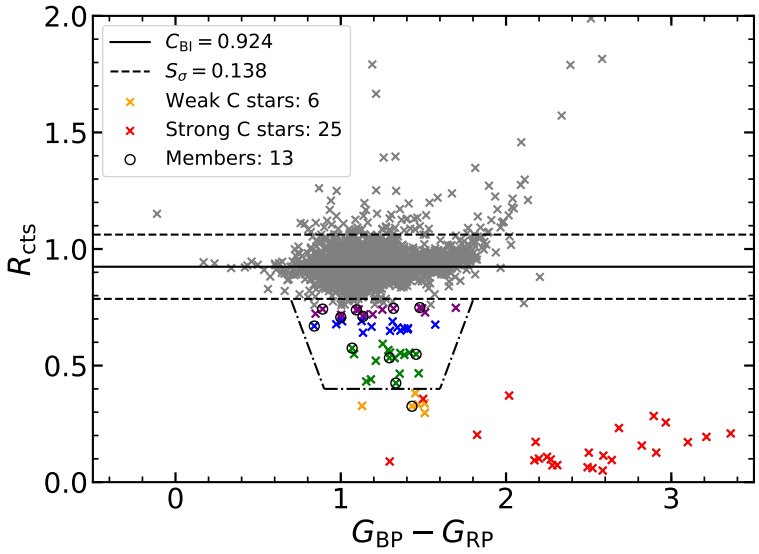

Figure 6.2: Spectral index $R_{\rm cts}$ versus $G_{\rm BP} - G_{\rm RP}$ color of all stars in our sample. Overplotted are the biweight mean ($C_{\rm BI}$, solid line) and 95% range (dashed lines) of all $R_{\rm cts}$ values. The strong C (red) and weak C (orange) stars identified in Section 3.3.4 possess the lower right region on the plot. Other C-rich stars identified in Section 6.2.1 are located within the region enclosed by the dotted-dash curves, and drawn differently for various $R_{\rm cts}$ ranges (green for 0.4–0.6, blue for 0.6–0.7 and purple for 0.7–0.75).

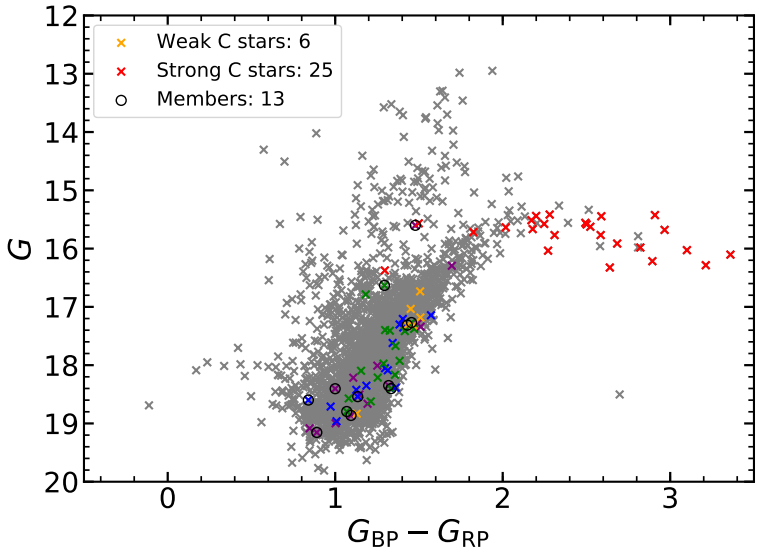

Figure 6.3: Carbon stars on the *Gaia* DR2 CMD. The meanings of the colors are the same as those shown in Figure 6.2.

Six representative C-star spectra with various $R_{\rm cts}$ values are presented in Figure 6.1. The top two panels show two strong C stars with extreme absorption feature below ∼5165 Å in the rest frame. One intermediate and three weak C stars are also shown in the lower panels. Unlike the strong C stars, the absorption features below about 5165 Å at the C_2 bandhead in these weaker C stars are relatively narrower (i.e. extends only over ∼5 Å in wavelength) and hence the C_2 absorption is weaker.

Figure 6.3 presents the locations of all C stars on the *Gaia*-based CMD. The strong C stars (in red) are prominently brighter and redder than all other C stars showing weaker features, which has been well known for decades (see, e.g. *Westerlund et al.*, 1991; *Wallerstein and Knapp*, 1998). What is not so well known is how C stars populate the giant branch along with other normal O-rich RGB stars at similar colors and luminosities. In the future, I will use the sample of 78 C stars from this study to explore the systematic behavior of C stars as a function of age/metallicity and, for the field C stars in my sample, locations in the MCs. It may even be possible to tweak the current bands described in Equation 6.1 to improve the capability of detecting even weaker C stars than we are currently sensitive to.

What makes this sample of C stars particularly interesting is that many are directly associated with clusters of known age and metallicity. In addition, the selection process for targets in the clusters used in this study was not biased in any way to either include or exclude stars as a function of luminosity along the RGB. Consequently, these data may provide for the first time information regarding the relative frequencies of C stars as they form and evolve within stellar populations of known ages and metallicities. This sample may shed light on how and when, in an evolutionary sense, carbon is dredged up along the RGB. For example, in Figure 6.3 there is a hint that C stars may begin to form at surprisingly low luminosities and possibly along the first-ascent giant branch, both contrary to canonical models.

6.2.2 Detailed Chemical Abundances of Red Giants in Magellanic Cloud Clusters

Chemical abundances of MC clusters are fundamental parameters to determine the cluster formation and chemical enrichment histories of these galaxies. Detailed abundances, particularly of a wide range of elements, are also useful to understand the origins and evolution of multiple populations within clusters spanning a range in age (see, e.g. *Gratton et al.*, 2012; *Bastian and Lardo*, 2018, for reviews). Such analyses require high-resolution spectra with good S/N ratios; given the distances to the MCs, it is not surprising that relatively few stars in MC clusters have been so studied. Detailed chemical abundances of stars within 11 LMC clusters have been obtained using high-resolution spectroscopy by various authors (*Hill et al.*, 2000; *Johnson et al.*, 2006; *Mucciarelli et al.*, 2008, 2009, 2010). These results reveal that the abundances of many elements in (old) LMC clusters are quite distinct from their counterpart globular clusters in the MW. For example, lower α-element abundances are observed among LMC clusters at a given mean metallicity. For SMC clusters, NGC 330 is the only SMC cluster studied using high-resolution spectroscopy published to date (*Gonzalez and Wallerstein*, 1999), though there are a few recent studies using low resolution spectra of red supergiants of members in other clusters (*Hollyhead et al.*, 2017, 2018; *Patrick et al.*, 2020).

As described in Section 2.2.3 and Section 3.2.4, in addition to the typical spectra (i.e. those with the wavelength range 5130–5192 Å) obtained from the B-arm of MSpec, the R-arm had simultaneously observed up to four stellar targets at similar resolution but used a much broader filter that covers the range 4058–5524 Å (see the right panel of Figure 2.3). In this thesis, I have analyzed only the same single order—out of 23 recorded in the R-arm spectra—spanning the same wavelength range as the orders isolated in the B-arm spectra.

By analyzing the full wavelength range of all R-arm spectra, I aim to perform detail

chemical abundances of cluster members from different locations of the MCs. These R-arm spectra can be used to measure accurate [Fe/H] values from several Fe I and Fe II lines simultaneously. These results can be used to test the cluster metallicities reported in Section 4.2.4, and compare with those from CaT spectroscopy (*Grocholski et al.*, 2006; *Parisi et al.*, 2015, e.g.). Some α-process elements, such as C (from CH molecular lines), Mg, Ca and Ti, can be detected from this spectral region. These elements are synthesized from both Type Ia and Type II supernovae, and are crucial to trace the chemical evolution within MC clusters. We can also detect the iron-peak elements, such as Cr and Ni, which are mainly produced by Type Ia supernovae that contaminate the material from which the clusters ultimately form. Elements heavier than the Fe group, such as Sr, Y and Ba, are also detectable; and so as more elements, including Sc, Mn, Zn, Zr and Eu, but depending on S/N, $T_{\rm eff}$ and [Fe/H] of the obtained spectra. The processes to survey these and other elements in similar types of stars and at moderate S/N have been discussed in, for example, (*Roederer et al.*, 2016) who studied the detailed chemical abundances of RGs in the LG dwarf galaxy Reticulum 2 at a slightly higher resolution ($\mathcal{R} \sim 30,000$) than this work but over roughly the same wavelength range (4150–5430 Å).

6.2.3 Using Star Clusters and Field Stars to Explore Dynamical Models of the Magellanic Clouds

With the availability of high-precision astrometric measurements from the *Gaia* satellite (*Gaia Collaboration et al.*, 2016), it is now possible to obtain rough tangential velocities of individual stars out to the distances of the MCs and beyond. Since every cluster studied in this thesis contains many stars with their LOS velocities observed, this offers an opportunity to measure the 3-D space motions of the individual clusters to reasonable precision. This type of analysis has already been applied to MW globular clusters: Over the ∼2-yr baseline covered by the *Gaia* DR2, proper

motions (PMs) have been obtained for members in MW CGs. Combined with LOS velocities, these PMs have been used to analyze bulk motions of the clusters to reveal their detailed orbital properties and thereby explore the MW's gravitational potential (e.g. *Gaia Collaboration et al.*, 2018b; *Vasiliev*, 2019; *Watkins et al.*, 2019; *Baumgardt et al.*, 2019) and their internal rotations (e.g. *Bianchini et al.*, 2018; *Sollima et al.*, 2019). This opens up the possibility of using PMs of MC clusters to carry out similar sorts of analyses for those galaxies.

To illustrate the *Gaia* capabilities more concretely, we consider the information from *Gaia Collaboration et al.* (2018a) which states that the uncertainties of PMs published in *Gaia* DR2 are 0.06 mas yr^{-1} (for $G < 15$ mag), 0.2 mas yr^{-1} (for $G = 17$ mag) and 1.2 mas yr^{-1} (for $G = 20$ mag). These should improve by a factor of 3–4 over the full duration of the *Gaia* mission. One can use the fundamental relation $\sigma_v = 4.74\sigma_\mu d$ to convert PM uncertainties to velocity uncertainties, where σ_v (in $\mathrm{km\,s}^{-1}$) and σ_μ (in arcsec yr^{-1}) are the uncertainties in velocity and PM, respectively, and d (in pc) is the distance to the target. At a distance of 50 (60) kpc for the LMC (SMC), the corresponding uncertainties (excluding systematic errors) for *Gaia* DR2 results of transverse velocities range from ∼47 (56) $\mathrm{km\,s}^{-1}$ (for $G =$ 17 mag) to ∼280 (340) $\mathrm{km\,s}^{-1}$ (for $G = 20$ mag). These uncertainties reduce to about ∼13 (16) $\mathrm{km\,s}^{-1}$ (for $G = 17$ mag) and ∼89 (96) $\mathrm{km\,s}^{-1}$ (for $G = 20$ mag) for proper motions from the full-duration *Gaia* data release. Given that most of stars in our sample range from 17–19 mag in G band and assuming sample sizes of 40 stars (the median value of members confirmed in our 26 clusters; see Table 4.3), the mean PMs of clusters could be constrained to 5–10 $\mathrm{km\,s}^{-1}$, comparable, if somewhat worse, than the LOS velocity uncertainties for the clusters (see Table 4.3). This will determine the space motions of individual clusters to very good accuracy relative to the typical expected circular velocities (≈92 and 20–40 $\mathrm{km\,s}^{-1}$ for the LMC and SMC, respectively, *van der Marel and Kallivayalil* 2014; *Dobbie et al.* 2014a) and

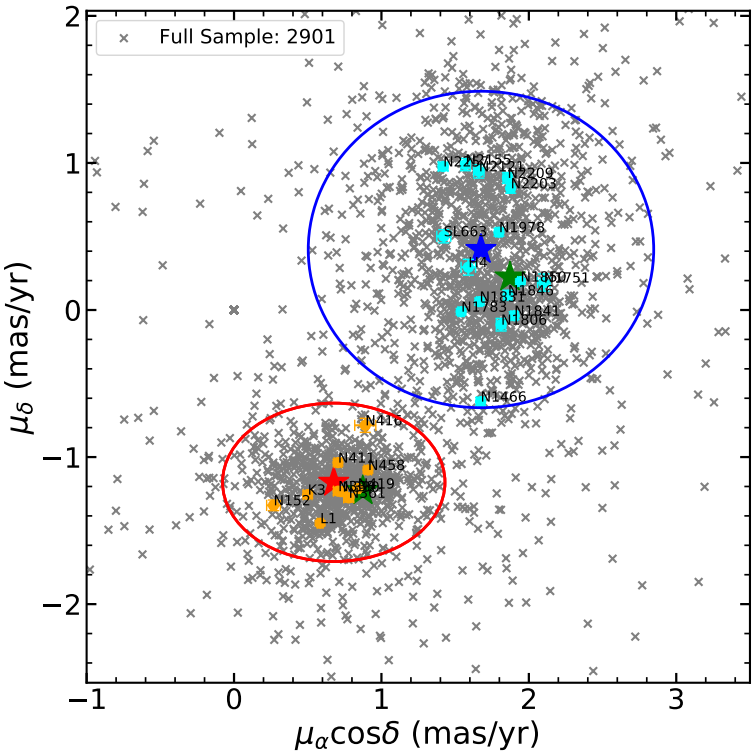

Figure 6.4: *Gaia* DR2 proper motions (PMs) of all stars in our M2FS sample. The weighted mean and weighted standard deviation of PMs for all LMC (blue) and SMC (red) stars are symbolized as the corresponding star and eclipse, respectively, while two green stars are the mean PMs using *Gaia* DR2 (*van der Marel and Sahlmann*, 2016). We also show the mean PMs of our observed clusters in the LMC (cyan) and SMC (orange), respectively. The mean PM of each cluster were calculated from probable cluster members, i.e. the stars in the PM50 (or PM50′) sample (see Table 4.3).

should allow detailed studies of the potentials of both MCs or, as may be likely, evidence of interactions, particularly for the SMC.

Preliminary mean PMs of all clusters in our sample are shown in Figure 6.4. These mean PM of each cluster was measured using all cluster members observed in this work; that is, the stars in the PM50 (or PM50′) sample (see Table 4.3). The clusters spread broadly in the MCs, which suggests we might measure the orbits of these clusters. When longer-baseline *Gaia* PMs are available, our sample can be used to study the mean PMs and orbits of the clusters within their parent galaxies.

6.2.4 Improving Cluster Mass Estimates with More Comprehensive Dynamical Models

In this thesis, I have adopted single-mass K66 models to estimate the total masses of the clusters in our sample (see Section 2.3.2.1 and Section 4.2.1). These models assume a constant M/L ratio within the clusters. However, in Section 5.2.1, I have discussed that the adoption of K66 models tend to underestimate cluster total mass for ignoring dynamical evolution effects, such as energy equipartition and mass segregation. In contrast, many clusters in our sample show dynamical anomalies (e.g. NGC 2155) that require more suitable dynamical models to properly take into account (see Section 5.2.2).

Mass segregation of star cluster can be possible to account for by using multimass King-Michie (KM) models (*Michie*, 1963; *Gunn and Griffin*, 1979) or the `LIMEPY` models (*Gieles and Zocchi*, 2015). These multimass models, together with the K66 models we adopted, are all so-called distribution function (DF)-based models that satisfies the collisionless Boltzmann equation. For example, in a simple three-component DF-based model, the cluster is approximated by three components: (1) (dark) low-mass stars; (2) (visible) stars; and (3) (dark) remnants. As a result, this model can describe the general dynamical behavior of a mass-segregated cluster, although more mass components are required to accurately describe the stellar mass function of clusters. This three-component model provides a simple way to overcome the bias of the K66 model, and is well-suited to cases where data are limited but a more accurate estimate of dynamical mass is required (*Gieles and Zocchi*, 2015). However, for the cases when the effect of mass segregation is not taken into account, *Hénault-Brunet et al.* (2019) found that this model tends to systematically underestimate the mass in the very central region and overestimates the mass at intermediate radii. One direction of possible future work is to apply these sorts of three-component DF models to the stellar samples of each cluster and trace any mass segregation effects in

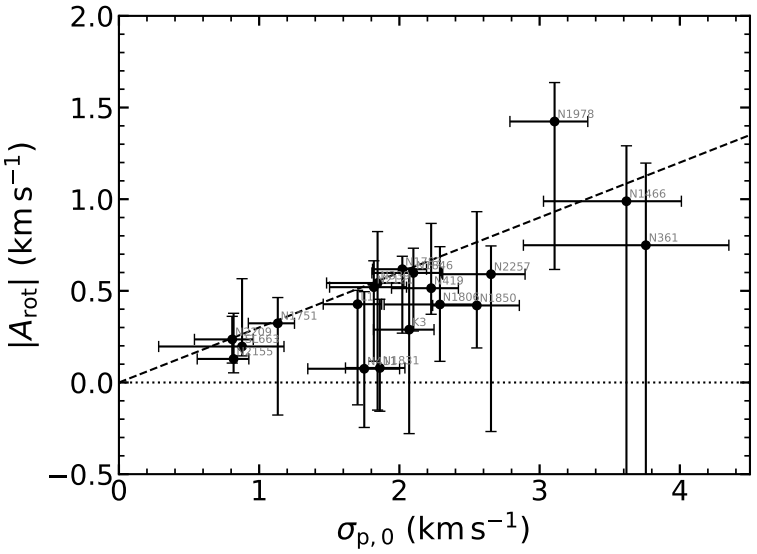

Figure 6.5: A plot of rotation versus velocity dispersions for 19 clusters in our sample. The $|A_{\rm rot}|$ values were calculated through Equation 2.16 using member stars with $P_M \geq 0.5$ in each cluster. The $\sigma_{\rm p,0}$ values are calculated from the PM50 (or PM50′ for some clusters) samples (see Table 4.3). Except for the case of NGC 1978, all clusters have marginal rotation features ($|A_{\rm rot}|/\sigma_{\rm p,0} \lesssim 0.3$, dashed line).

detail. The results from these complex dynamical models may provide key evidence to explain the M/L offsets between our observations and the SSP models discussed in Section 5.1.

Rotation is another dynamical effect of star cluster that can be included in future analyses. Among the clusters in our sample, I have found evidence of strong rotation for NGC 1978 (see Section 4.2.2). Another cluster, NGC 1846, also shows more marginal evidence of rotation that may cause a small ($\sim$9%) overestimate of the cluster's total mass (see Section 2.4.2). I have applied the rotation analysis described in Section 2.3.4 to all clusters in our sample. In Figure 6.5, the measured amplitude values of 19 clusters are plotted against their best-fit central velocity dispersions (see Table 4.3); the remaining seven clusters were not shown because either the cluster has less than 20 members or its rotation amplitude could not be reproduced by the bootstrapping process described in Section 2.3.4. It can be seen that all clusters except

NGC 1978 have ratios of $|A_{\rm rot}|/\sigma_{\rm p,0}$ below $\sim$30% (dashed line), and hence their rotation effects on mass estimation are no greater than the case of NGC 1846. Although these clusters are far from fully rotation supported, it is necessary to estimate precise cluster masses from dynamical models that properly take into account the rotation of star cluster (e.g. *Varri and Bertin*, 2012).

6.2.5 Improved Kinematic Sampling of MC Clusters

The spectral data used in this thesis have been obtained with a multi-object spectrograph, M2FS, that can deploy up to 256 optical fibers in a 29-arcmin diameter field. However, the fibers of M2FS cannot be deployed closer than 13 arcsec from any other fiber in a given pointing. For the purposes of the present study, this limited the number of cluster candidate targets that could be observed in a single M2FS pointing to about 100–140 per cluster field, and typically resulted in only about 10–80 members being observed in each cluster (see Table 4.3). The cluster cores, in particular, were relatively most poorly sampled since only a few fibers could be simultaneously positioned near the central regions of the systems (see Figure 6.6). One way to overcome these limitations is to employ spectrographs fed via an Integral Field Unit (IFU) that provide spectra from small but contiguously-sampled regions of the sky such as the cores of MC clusters (e.g. *Kamann et al.*, 2016, 2018).

In the near future, a new IFU system—IFUM—will be employed with the existing M2FS spectrograph (MSpec). IFUM can deploy three IFUs individually with different field of views (FoVs), and spaxel and spectral resolutions. One of the IFUs of this instrument, denoted as the STD (Standard-seeing) IFU, has field dimensions of 23.9×21.6 in arcsec, with each spaxel having an effective diameter of 1.09 arcsec. IFUM has the unique capability of delivering single-order spectra with resolutions of up to $\sim$20,000, comparable to the spectral resolution of the data used in this study. These capabilities are particularly well suited for observing the crowded and compact

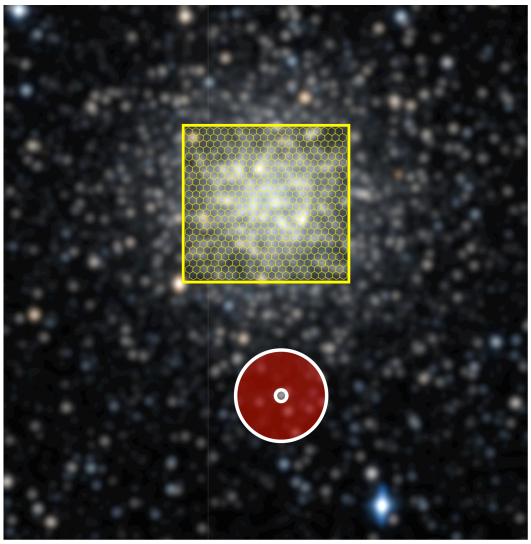

Figure 6.6: Illustration of NGC 416 observation using IFUM. On the image, the core region (∼24 arcsec in diameter, see Table 3.2) of the cluster is properly covered by the FoV of STD IFU mode deployed in the IFUM (on average 22 arcsec on a side, as denoted by the yellow outline). A single M2FS fiber assembly, about 13 arcsec in diameter, is also shown for comparison (red area).

centers of MC clusters.

As an example, Figure 6.6 shows the footprint of the IFUM/STD field superimposed on an image of the SMC cluster NGC 416. This system has a K66 core diameter of ∼24 arcsec (see Table 3.2), comparable to the IFU's FoV denoted by the yellow outline. As a comparison, the size of a single M2FS fiber assembly is also shown in Figure 6.6 in red. Although an M2FS fiber entrance aperture is comparable to a single IFUM/STD spaxel (1.2 arcsec denoted by the small central circle in the red area in Figure 6.6), the comparatively large size of the fiber assembly allows no more than 10—and typically only 5 or 6—fibers to be simultaneously deployed within the core of NGC 416. Given its high spectral resolution (for an IFU), IFUM should readily produce kinematic results of comparable quality to the M2FS data used in this study. Moreover, and especially for more compact clusters, the high concentration of velocities available from IFU measurements near the cluster cores will make

the dynamical analysis less reliant on the extrapolations required to use velocities of outer members to constrain the central dispersion.

Other promising targets for IFU observations are clusters that have been studied both in our sample and in previously works by integrated-light spectroscopy (*Zaritsky et al.*, 2012, 2014) or IFUs (*Kamann et al.*, 2018), such as NGC 1831, NGC 2121, NGC 339, NGC 411, NGC 419 and Kron 3. NGC 2155 is another interesting target to follow-up for it being one of the oldest LMC clusters (at 3.0 Gyr; see Table 3.1) found at the young edge of the well-known cluster age gap of that galaxy (*Bertelli et al.*, 1992; *Girardi et al.*, 1995; *Olszewski et al.*, 1996). As discussed Section 5.3, the anomalously low M/L_V ratio of this cluster may indicate that the cluster has lost most of its initial mass and thus it could be very close to total dissolution. A detailed IFU-based study of the core region of this cluster could help confirm the cluster's actual dynamical state to shed light on its ultimate fate.

APPENDICES

APPENDIX A

Full Sample of Targets in NGC 419

Table A.1: M2FS Sample of NGC 419

ID	α_{2000} (h:m:s)	δ_{2000} (d:m:s)	V (mag)	$V-I$ (mag)	$v_{\rm los}$ ($\rm km\,s^{-1}$)	P_{M_i}	Sel.[a]
N419-1-b001	01:08:44.19	-73:00:40.0	16.887 ± 0.047	1.497 ± 0.055	188.41 ± 0.20	0.00	M
N419-1-b002	01:08:46.07	-72:56:35.2	17.942 ± 0.030	1.024 ± 0.056	192.79 ± 0.42	0.00	M
N419-1-b003	01:08:45.46	-72:55:15.4	17.982 ± 0.030	1.138 ± 0.043	153.30 ± 0.39	0.00	M
N419-1-b004	01:08:43.26	-72:53:32.0	18.014 ± 0.008	0.855 ± 0.010	193.60 ± 0.61	0.06	H
N419-1-b005	01:08:42.25	-72:53:12.3	18.769 ± 0.010	1.019 ± 0.013	144.09 ± 1.05	0.00	H
N419-1-b006	01:08:36.93	-72:53:08.6	18.072 ± 0.007	1.153 ± 0.009	188.79 ± 0.36	0.95	H
N419-1-b007	01:08:45.63	-72:53:00.6	16.447 ± 0.005	1.721 ± 0.005	188.41 ± 0.19	0.89	H
N419-1-b008	01:08:42.71	-72:52:36.2	18.742 ± 0.012	1.156 ± 0.014	163.46 ± 0.75	0.00	H
N419-1-b009	01:08:46.44	-72:59:58.8	18.888 ± 0.090	0.809 ± 0.139	147.99 ± 2.12	0.00	M
N419-1-b010	01:08:53.00	-72:59:08.5	18.126 ± 0.074	1.334 ± 0.113	191.09 ± 0.88	0.00	M
N419-1-b011	01:09:36.98	-72:58:13.9	18.951 ± 0.040	0.873 ± 0.058	131.76 ± 0.77	0.00	M
N419-1-b012	01:09:10.13	-72:57:30.3	16.764 ± 0.108	1.687 ± 0.130	171.52 ± 0.27	0.00	M
N419-1-b013	01:09:25.91	-72:55:17.1	18.384 ± 0.031	1.030 ± 0.054	160.83 ± 0.71	0.00	M
N419-1-b015	01:08:52.25	-72:53:57.3	18.896 ± 0.088	1.096 ± 0.096	134.17 ± 0.93	0.00	M
N419-1-b017	01:09:11.83	-72:48:22.3	17.250 ± 0.029	1.316 ± 0.039	180.94 ± 0.47	0.00	M
N419-1-b018	01:09:03.45	-72:50:13.0	18.416 ± 0.119	0.778 ± 0.126	204.86 ± 1.45	0.00	M
N419-1-b019	01:08:45.59	-72:50:52.7	18.672 ± 0.009	1.140 ± 0.011	190.08 ± 0.53	0.94	H
N419-1-b020	01:08:40.43	-72:51:00.7	17.596 ± 0.007	1.011 ± 0.009	187.88 ± 0.33	0.70	H
N419-1-b021	01:09:49.97	-72:51:21.8	17.449 ± 0.032	1.404 ± 0.043	151.76 ± 0.37	0.00	M
N419-1-b022	01:08:42.54	-72:51:27.5	18.392 ± 0.009	0.871 ± 0.011	146.39 ± 0.58	0.00	H
N419-1-b024	01:08:38.89	-72:52:05.9	18.954 ± 0.012	1.048 ± 0.014	184.06 ± 0.90	0.01	H
N419-1-b025	01:08:33.04	-72:50:58.4	17.834 ± 0.009	1.250 ± 0.010	190.24 ± 0.30	0.93	H
N419-1-b026	01:08:29.54	-72:51:08.5	17.755 ± 0.007	0.905 ± 0.009	177.46 ± 0.36	0.00	H
N419-1-b027	01:08:33.47	-72:51:17.0	18.714 ± 0.009	1.108 ± 0.011	112.31 ± 0.63	0.00	H
N419-1-b028	01:08:33.67	-72:51:38.9	16.385 ± 0.003	1.766 ± 0.004	191.91 ± 0.22	0.72	H
N419-1-b029	01:08:38.81	-72:51:45.7	16.818 ± 0.004	0.876 ± 0.005	146.89 ± 0.27	0.00	H
N419-1-b030	01:08:29.68	-72:51:58.8	17.386 ± 0.005	1.340 ± 0.006	144.66 ± 0.31	0.00	H

Table A.1: (*continued*) M2FS Sample of NGC 419

ID	α_{2000} (h:m:s)	δ_{2000} (d:m:s)	V (mag)	$V-I$ (mag)	$v_{\rm los}$ ($\rm km\,s^{-1}$)	P_{M_i}	Sel.[a]
N419-1-b031	01:08:35.45	-72:52:05.2	18.612 ± 0.008	1.165 ± 0.011	132.97 ± 0.63	0.00	H
N419-1-b032	01:08:36.88	-72:52:22.3	16.422 ± 0.003	1.680 ± 0.004	189.04 ± 0.21	0.94	H
N419-1-b033	01:08:28.67	-72:59:24.5	18.561 ± 0.036	1.056 ± 0.047	172.83 ± 0.56	0.00	M
N419-1-b034	01:08:29.52	-72:57:16.4	17.474 ± 0.063	1.323 ± 0.115	153.03 ± 0.29	0.00	M
N419-1-b035	01:08:27.14	-72:54:05.2	17.010 ± 0.005	1.423 ± 0.006	188.55 ± 0.22	0.99	H
N419-1-b036	01:08:26.24	-72:53:47.1	18.342 ± 0.011	1.124 ± 0.015	190.10 ± 0.61	0.99	H
N419-1-b037	01:08:30.79	-72:53:30.9	17.477 ± 0.005	1.153 ± 0.006	188.48 ± 0.29	0.98	H
N419-1-b038	01:08:31.77	-72:53:13.3	18.697 ± 0.009	0.946 ± 0.012	120.42 ± 0.94	0.00	H
N419-1-b039	01:08:28.43	-72:53:12.6	18.621 ± 0.009	1.051 ± 0.012	187.58 ± 0.79	0.99	H
N419-1-b040	01:08:28.99	-72:52:58.2	17.982 ± 0.008	1.163 ± 0.009	192.70 ± 0.56	0.97	H
N419-1-b041	01:08:33.26	-73:00:25.3	17.997 ± 0.106	0.946 ± 0.301	189.95 ± 0.46	0.00	M
N419-1-b043	01:08:34.41	-72:55:19.0	18.900 ± 0.042	1.034 ± 0.068	144.91 ± 1.60	0.00	M
N419-1-b046	01:08:34.51	-72:52:59.8	15.918 ± 0.002	1.244 ± 0.003	182.92 ± 0.17	0.00	H
N419-1-b047	01:08:32.54	-72:52:45.8	18.615 ± 0.010	1.082 ± 0.012	191.86 ± 0.70	0.97	H
N419-1-b048	01:08:36.71	-72:52:40.4	18.329 ± 0.007	1.155 ± 0.009	171.83 ± 0.40	0.00	H
N419-1-b049	01:08:25.26	-72:48:18.5	18.977 ± 0.044	0.885 ± 0.092	159.73 ± 1.57	0.00	M
N419-1-b050	01:08:22.58	-72:51:11.8	18.949 ± 0.026	0.991 ± 0.032	139.76 ± 1.13	0.00	H
N419-1-b051	01:08:25.32	-72:51:18.1	17.126 ± 0.007	1.438 ± 0.008	190.63 ± 0.35	0.93	H
N419-1-b052	01:08:22.12	-72:51:37.8	17.296 ± 0.005	1.314 ± 0.006	197.80 ± 0.28	0.00	H
N419-1-b053	01:08:28.90	-72:51:42.8	18.442 ± 0.012	0.855 ± 0.016	146.51 ± 1.03	0.00	H
N419-1-b055	01:08:24.75	-72:52:25.3	17.717 ± 0.008	1.107 ± 0.010	192.58 ± 0.45	0.98	H
N419-1-b057	01:08:16.73	-72:51:29.0	17.752 ± 0.008	1.364 ± 0.009	139.19 ± 0.33	0.00	H
N419-1-b058	01:08:17.65	-72:51:52.8	16.563 ± 0.003	1.566 ± 0.004	188.98 ± 0.20	0.99	H
N419-1-b059	01:08:21.63	-72:52:00.7	18.862 ± 0.010	0.958 ± 0.013	190.29 ± 1.00	0.99	H
N419-1-b061	01:08:20.37	-72:52:22.1	16.785 ± 0.004	1.496 ± 0.004	188.40 ± 0.25	1.00	H
N419-1-b063	01:08:13.56	-72:52:40.1	18.429 ± 0.008	1.051 ± 0.010	190.22 ± 1.38	1.00	H
N419-1-b064	01:08:17.60	-72:52:48.4	18.092 ± 0.008	1.183 ± 0.009	189.78 ± 2.07	1.00	H
N419-1-b065	01:08:13.57	-72:54:31.7	18.633 ± 0.010	1.140 ± 0.013	175.23 ± 0.69	0.00	H
N419-1-b066	01:08:10.42	-72:54:16.5	18.245 ± 0.009	1.176 ± 0.011	142.15 ± 0.57	0.00	H
N419-1-b067	01:08:17.34	-72:54:12.7	17.027 ± 0.008	1.445 ± 0.011	190.42 ± 0.35	0.99	H
N419-1-b069	01:08:14.49	-72:53:31.4	17.865 ± 0.006	1.163 ± 0.008	187.93 ± 0.63	1.00	H
N419-1-b070	01:08:10.48	-72:53:27.3	19.161 ± 0.010	0.916 ± 0.014	185.28 ± 1.45	1.00	H
N419-1-b071	01:08:14.04	-72:53:16.4	16.573 ± 0.003	1.564 ± 0.004	187.81 ± 0.37	1.00	H
N419-1-b074	01:08:25.83	-72:54:19.8	18.574 ± 0.013	1.063 ± 0.017	189.96 ± 0.68	0.96	H
N419-1-b075	01:08:21.22	-72:54:03.6	17.017 ± 0.004	1.573 ± 0.005	161.88 ± 0.30	0.00	H
N419-1-b077	01:08:22.33	-72:53:40.0	19.442 ± 0.015	0.903 ± 0.019	186.61 ± 1.99	1.00	H
N419-1-b078	01:08:24.57	-72:53:28.2	17.418 ± 0.005	1.245 ± 0.006	189.61 ± 0.34	1.00	H
N419-1-b079	01:08:18.45	-72:53:15.9	16.921 ± 0.004	1.387 ± 0.005	188.15 ± 0.51	1.00	H
N419-1-b080	01:08:19.35	-72:53:00.9	16.422 ± 0.003	1.682 ± 0.004	189.50 ± 0.62	1.00	H
N419-1-b081	01:08:10.72	-72:49:08.4	16.956 ± 0.033	1.321 ± 0.276	123.35 ± 0.36	0.00	M
N419-1-b082	01:08:13.42	-72:51:11.0	18.842 ± 0.011	1.071 ± 0.014	189.78 ± 0.93	0.94	H
N419-1-b083	01:08:10.12	-72:51:21.7	18.596 ± 0.009	1.093 ± 0.012	117.91 ± 0.85	0.00	H
N419-1-b084	01:08:12.53	-72:51:30.2	17.660 ± 0.006	1.187 ± 0.007	191.81 ± 0.29	0.80	H
N419-1-b086	01:08:12.85	-72:52:25.0	18.587 ± 0.009	0.880 ± 0.012	146.58 ± 1.76	0.00	H
N419-1-b087	01:08:09.31	-72:52:37.5	16.944 ± 0.005	1.323 ± 0.006	192.62 ± 0.34	0.98	H
N419-1-b088	01:08:09.87	-72:52:54.5	16.992 ± 0.005	1.413 ± 0.006	188.23 ± 0.32	1.00	H
N419-1-b089	01:08:06.74	-72:51:17.8	18.399 ± 0.011	1.073 ± 0.014	189.03 ± 0.50	0.94	H
N419-1-b091	01:08:05.25	-72:51:52.7	18.349 ± 0.007	1.069 ± 0.009	168.13 ± 0.78	0.00	H
N419-1-b092	01:08:08.77	-72:51:55.3	19.021 ± 0.012	0.840 ± 0.016	184.36 ± 2.47	0.87	H

Table A.1: (*continued*) M2FS Sample of NGC 419

ID	α_{2000} (h:m:s)	δ_{2000} (d:m:s)	V (mag)	$V-I$ (mag)	$v_{\rm los}$ ($\rm km\,s^{-1}$)	P_{M_i}	Sel.[a]
N419-1-b093	01:08:04.31	-72:52:09.6	17.011 ± 0.005	1.323 ± 0.006	187.75 ± 0.24	0.97	H
N419-1-b094	01:08:05.31	-72:52:30.0	16.772 ± 0.004	0.914 ± 0.005	157.41 ± 0.29	0.00	H
N419-1-b095	01:08:06.26	-72:52:55.3	19.328 ± 0.015	0.901 ± 0.019	172.96 ± 2.16	0.00	H
N419-1-b096	01:08:07.57	-72:53:10.7	17.097 ± 0.006	1.412 ± 0.007	188.48 ± 0.24	0.99	H
N419-1-b097	01:07:34.42	-72:57:42.7	17.215 ± 0.030	0.956 ± 0.055	159.54 ± 0.32	0.00	M
N419-1-b098	01:07:33.01	-72:57:06.7	16.802 ± 0.050	1.732 ± 0.060	175.10 ± 0.27	0.00	M
N419-1-b099	01:07:32.16	-72:56:45.0	16.907 ± 0.037	1.542 ± 0.129	168.45 ± 0.24	0.00	M
N419-1-b100	01:07:46.32	-72:56:03.5	17.036 ± 0.033	1.016 ± 0.102	191.41 ± 0.25	0.00	M
N419-1-b101	01:07:24.42	-72:55:21.7	18.252 ± 0.108	1.212 ± 0.122	161.95 ± 0.54	0.00	M
N419-1-b102	01:06:54.30	-72:55:17.1	17.468 ± 0.029	1.286 ± 0.040	146.65 ± 0.37	0.00	M
N419-1-b103	01:06:38.13	-72:55:16.4	17.603 ± 0.036	1.365 ± 0.271	190.53 ± 0.38	0.00	M
N419-1-b104	01:07:31.81	-72:54:00.3	17.507 ± 0.187	0.884 ± 0.236	151.85 ± 0.37	0.00	M
N419-1-b105	01:08:03.10	-73:00:02.7	17.691 ± 0.030	1.408 ± 0.077	148.05 ± 0.42	0.00	M
N419-1-b106	01:07:51.35	-72:58:01.4	18.800 ± 0.102	0.896 ± 0.111	182.85 ± 1.67	0.00	M
N419-1-b107	01:08:07.38	-72:54:09.8	18.579 ± 0.011	1.129 ± 0.013	158.16 ± 0.67	0.00	H
N419-1-b109	01:08:06.35	-72:53:32.4	16.666 ± 0.004	1.495 ± 0.004	190.11 ± 0.24	0.99	H
N419-1-b110	01:08:02.42	-72:53:27.6	18.188 ± 0.010	1.140 ± 0.013	188.10 ± 0.51	0.98	H
N419-1-b111	01:08:04.02	-72:53:10.5	17.301 ± 0.007	1.359 ± 0.008	190.28 ± 0.34	0.99	H
N419-1-b112	01:08:02.60	-72:52:56.9	18.781 ± 0.010	1.011 ± 0.013	189.47 ± 0.92	0.99	H
N419-1-b114	01:07:51.42	-72:50:55.6	16.972 ± 0.029	1.503 ± 0.151	161.58 ± 0.25	0.00	M
N419-1-b115	01:08:01.76	-72:51:30.5	18.893 ± 0.015	0.797 ± 0.018	172.99 ± 1.39	0.00	H
N419-1-b117	01:07:29.46	-72:52:04.5	18.969 ± 0.036	0.839 ± 0.073	131.08 ± 1.48	0.00	M
N419-1-b118	01:08:03.20	-72:52:40.0	17.869 ± 0.007	1.142 ± 0.009	191.56 ± 0.39	0.98	H
N419-1-b119	01:07:53.96	-72:54:06.2	18.464 ± 0.031	1.001 ± 0.051	159.17 ± 0.50	0.00	M
N419-1-b120	01:07:59.08	-72:54:49.3	17.269 ± 0.040	1.394 ± 0.056	136.46 ± 0.21	0.00	M
N419-1-b121	01:07:30.01	-72:49:42.7	17.971 ± 0.031	1.029 ± 0.042	142.66 ± 0.65	0.00	M
N419-1-b123	01:07:10.06	-72:50:32.3	18.746 ± 0.055	0.889 ± 0.091	191.94 ± 1.46	0.00	M
N419-1-b124	01:07:22.03	-72:50:49.3	18.413 ± 0.036	1.115 ± 0.047	166.43 ± 0.60	0.00	M
N419-1-b126	01:06:48.72	-72:53:33.3	16.916 ± 0.028	1.015 ± 0.040	149.91 ± 0.29	0.00	M
N419-1-b127	01:06:36.00	-72:54:14.6	17.088 ± 0.032	1.284 ± 0.049	141.47 ± 1.12	0.00	M
N419-1-b128	01:06:59.45	-72:54:39.6	16.997 ± 0.030	1.372 ± 0.064	142.84 ± 0.28	0.00	M
N419-1-r049	01:08:14.47	-72:53:56.6	16.214 ± 0.004	1.934 ± 0.004	186.85 ± 0.36	0.97	H
N419-1-r079	01:08:20.73	-72:52:47.2	16.342 ± 0.003	1.762 ± 0.004	193.99 ± 0.29	1.00	H
N419-1-r099	01:08:26.87	-72:52:46.3	16.523 ± 0.004	1.661 ± 0.004	191.02 ± 0.24	0.99	H
N419-1-r127	01:08:23.70	-72:53:09.1	16.312 ± 0.003	1.741 ± 0.004	187.89 ± 0.40	1.00	H

[a] Photometric source that the target were selected from: H stands for *HST* and M stands for MCPS.

APPENDIX B

Full Sample of Targets in NGC 1846

Table B.1: Combined Sample of NGC 1846

ID	α_{2000} (h:m:s)	δ_{2000} (d:m:s)	V (mag)	$V-I$ (mag)	$v_{\rm los}$ (km s^{-1})	P_{M_i}	Sel. [a]	Spec. [b]
N1846-1-b001	05:07:51.21	-67:33:03.8	17.251 ± 0.307	1.396 ± 0.310	287.97 ± 0.19	0.00	M	M2FS
N1846-1-b002	05:07:57.56	-67:32:58.0	17.314 ± 0.049	1.266 ± 0.069	264.51 ± 0.19	0.00	M	M2FS
N1846-1-b003	05:07:49.91	-67:32:21.2	17.559 ± 0.041	1.255 ± 0.058	246.95 ± 0.18	0.00	M	M2FS
N1846-1-b005	05:07:54.32	-67:30:17.6	17.715 ± 0.030	1.192 ± 0.050	221.35 ± 0.23	0.00	M	M2FS
N1846-1-b006	05:07:47.87	-67:29:52.6	17.329 ± 0.028	1.345 ± 0.049	271.34 ± 0.19	0.00	M	M2FS
N1846-1-b007	05:07:56.92	-67:29:28.9	17.387 ± 0.146	1.256 ± 0.151	286.79 ± 0.20	0.00	M	M2FS
N1846-1-b009	05:08:21.28	-67:31:11.1	17.125 ± 0.026	1.301 ± 0.049	287.38 ± 0.17	0.00	M	M2FS
N1846-1-b010	05:08:29.24	-67:31:03.5	17.475 ± 0.050	1.278 ± 0.071	231.89 ± 0.18	0.00	M	M2FS
N1846-1-b011	05:08:24.35	-67:30:58.2	17.212 ± 0.054	1.304 ± 0.067	275.75 ± 0.18	0.00	M	M2FS
N1846-1-b012	05:08:30.22	-67:30:34.4	17.595 ± 0.060	1.194 ± 0.076	274.73 ± 0.19	0.00	M	M2FS
N1846-1-b013	05:08:10.21	-67:29:55.3	17.508 ± 0.038	1.348 ± 0.055	216.72 ± 0.20	0.00	M	M2FS
N1846-1-b015	05:08:34.55	-67:29:23.9	17.601 ± 0.031	1.284 ± 0.051	271.05 ± 0.20	0.00	M	M2FS
N1846-1-b016	05:08:44.83	-67:29:05.7	17.668 ± 0.043	1.178 ± 0.069	273.20 ± 0.21	0.00	M	M2FS
N1846-1-b017	05:08:18.68	-67:24:42.1	17.657 ± 0.031	1.293 ± 0.051	272.52 ± 0.24	0.00	M	M2FS
N1846-1-b019	05:08:39.28	-67:25:53.4	17.271 ± 0.023	1.354 ± 0.046	318.50 ± 0.14	0.00	M	M2FS
N1846-1-b020	05:08:16.63	-67:27:13.4	17.627 ± 0.039	1.228 ± 0.078	274.40 ± 0.15	0.00	M	M2FS
N1846-1-b021	05:08:41.57	-67:27:26.0	17.651 ± 0.053	1.184 ± 0.071	308.68 ± 0.30	0.00	M	M2FS
N1846-1-b022	05:08:39.60	-67:27:39.3	17.530 ± 0.031	1.297 ± 0.054	276.49 ± 0.19	0.00	M	M2FS
N1846-1-b023	05:08:17.46	-67:27:44.8	17.106 ± 0.027	1.295 ± 0.048	277.78 ± 0.15	0.00	M	M2FS
N1846-1-b025	05:08:08.02	-67:22:52.5	17.726 ± 0.242	1.295 ± 0.246	228.47 ± 0.21	0.00	M	M2FS
N1846-1-b027	05:08:10.54	-67:24:20.9	17.619 ± 0.031	1.180 ± 0.051	249.71 ± 0.20	0.00	M	M2FS
N1846-1-b030	05:07:50.87	-67:26:13.7	17.515 ± 0.031	1.283 ± 0.051	268.99 ± 0.19	0.00	M	M2FS
N1846-1-b031	05:08:08.63	-67:26:24.4	17.135 ± 0.031	1.323 ± 0.051	281.85 ± 0.14	0.00	M	M2FS
N1846-1-b032	05:08:06.22	-67:27:24.2	17.569 ± 0.035	1.327 ± 0.055	256.58 ± 0.19	0.00	M	M2FS
N1846-1-b033	05:07:36.65	-67:30:16.5	18.191 ± 0.008	1.141 ± 0.012	284.64 ± 0.32	0.00	H	M2FS
N1846-1-b034	05:07:39.86	-67:29:04.6	17.828 ± 0.031	1.140 ± 0.074	239.85 ± 0.27	0.96	M	M2FS
N1846-1-b035	05:07:40.01	-67:28:31.2	17.944 ± 0.006	1.164 ± 0.010	237.57 ± 0.23	0.99	H	M2FS
N1846-1-b036	05:07:38.41	-67:28:11.9	17.097 ± 0.004	1.431 ± 0.006	237.02 ± 0.18	1.00	H	COMB
N1846-1-b037	05:07:36.12	-67:28:07.8	17.872 ± 0.006	1.223 ± 0.009	238.59 ± 0.21	1.00	H	M2FS
N1846-1-b038	05:07:38.15	-67:27:58.7	17.345 ± 0.005	1.346 ± 0.007	237.39 ± 0.22	1.00	H	M2FS
N1846-1-b039	05:07:39.58	-67:27:38.2	17.223 ± 0.006	1.368 ± 0.008	238.69 ± 0.21	1.00	H	M2FS
N1846-1-b043	05:07:42.35	-67:28:46.1	18.248 ± 0.008	1.069 ± 0.015	245.91 ± 0.54	0.00	H	M2FS
N1846-1-b044	05:07:45.51	-67:28:34.2	18.077 ± 0.008	1.130 ± 0.012	264.15 ± 0.23	0.00	H	M2FS
N1846-1-b045	05:07:47.37	-67:28:19.8	17.580 ± 0.007	1.191 ± 0.011	236.37 ± 0.29	0.61	H	M2FS
N1846-1-b046	05:07:44.74	-67:28:18.5	17.078 ± 0.005	1.378 ± 0.007	237.50 ± 0.17	0.99	H	M2FS

Table B.1: (*continued*) Combined Sample of NGC 1846

ID	α_{2000} (h:m:s)	δ_{2000} (d:m:s)	V (mag)	$V-I$ (mag)	$v_{\rm los}$ (km s^{-1})	P_{M_i}	Sel. [a]	Spec. [b]
N1846-1-b047	05:07:43.71	-67:27:58.4	18.138 ± 0.008	1.119 ± 0.012	238.06 ± 0.29	1.00	H	M2FS
N1846-1-b048	05:07:41.77	-67:27:51.3	18.301 ± 0.008	1.119 ± 0.012	240.36 ± 0.32	1.00	H	M2FS
N1846-1-b049	05:07:42.99	-67:21:35.8	17.481 ± 0.031	1.321 ± 0.040	271.34 ± 0.25	0.00	M	M2FS
N1846-1-b050	05:07:45.88	-67:23:42.5	17.471 ± 0.034	1.260 ± 0.110	282.03 ± 0.21	0.00	M	M2FS
N1846-1-b052	05:07:47.67	-67:26:05.6	17.546 ± 0.033	1.317 ± 0.053	236.68 ± 0.21	0.27	M	M2FS
N1846-1-b053	05:07:41.62	-67:26:27.4	18.302 ± 0.050	1.107 ± 0.068	280.18 ± 0.31	0.00	M	M2FS
N1846-1-b054	05:07:37.75	-67:26:51.9	17.956 ± 0.006	1.135 ± 0.012	237.89 ± 0.27	1.00	H	M2FS
N1846-1-b055	05:07:39.46	-67:26:59.9	18.292 ± 0.006	1.086 ± 0.011	238.90 ± 0.28	1.00	H	M2FS
N1846-1-b056	05:07:40.73	-67:27:22.2	17.760 ± 0.005	1.148 ± 0.009	239.49 ± 0.22	1.00	H	M2FS
N1846-1-b057	05:07:33.97	-67:22:12.1	17.608 ± 0.043	1.266 ± 0.050	240.19 ± 0.25	0.00	M	M2FS
N1846-1-b058	05:07:32.31	-67:26:35.3	17.770 ± 0.007	1.182 ± 0.010	239.90 ± 0.22	1.00	H	M2FS
N1846-1-b059	05:07:32.45	-67:26:49.6	17.398 ± 0.008	1.252 ± 0.010	240.29 ± 0.26	1.00	H	M2FS
N1846-1-b061	05:07:34.81	-67:26:53.6	17.504 ± 0.010	1.249 ± 0.012	241.38 ± 0.21	1.00	H	M2FS
N1846-1-b062	05:07:34.27	-67:27:13.7	17.541 ± 0.005	1.305 ± 0.008	243.18 ± 0.23	0.99	H	M2FS
N1846-1-b063	05:07:36.86	-67:27:19.2	18.201 ± 0.006	1.127 ± 0.011	242.08 ± 0.24	1.00	H	M2FS
N1846-1-b064	05:07:34.23	-67:27:27.0	17.624 ± 0.007	1.197 ± 0.009	239.50 ± 0.31	1.00	H	M2FS
N1846-1-b065	05:07:22.62	-67:33:31.4	17.170 ± 0.048	1.340 ± 0.070	314.15 ± 0.19	0.00	M	M2FS
N1846-1-b066	05:07:28.51	-67:32:40.7	17.527 ± 0.031	1.225 ± 0.061	268.08 ± 0.29	0.00	M	M2FS
N1846-1-b067	05:07:29.05	-67:31:58.0	17.503 ± 0.033	1.354 ± 0.053	290.41 ± 0.85	0.00	M	M2FS
N1846-1-b068	05:07:30.38	-67:29:36.0	17.617 ± 0.006	1.237 ± 0.008	239.36 ± 0.16	0.97	H	COMB
N1846-1-b069	05:07:27.44	-67:29:27.9	17.881 ± 0.006	1.124 ± 0.010	238.88 ± 0.21	0.97	H	COMB
N1846-1-b070	05:07:29.52	-67:28:48.8	18.291 ± 0.008	1.158 ± 0.013	240.42 ± 0.32	1.00	H	M2FS
N1846-1-b071	05:07:28.71	-67:28:24.7	17.516 ± 0.007	1.199 ± 0.010	238.60 ± 0.19	1.00	H	COMB
N1846-1-b072	05:07:26.13	-67:28:08.3	17.878 ± 0.006	1.203 ± 0.009	240.45 ± 0.25	1.00	H	M2FS
N1846-1-b073	05:07:32.70	-67:30:37.3	18.404 ± 0.021	1.123 ± 0.025	272.60 ± 0.25	0.00	H	M2FS
N1846-1-b074	05:07:32.36	-67:29:22.1	18.387 ± 0.010	1.011 ± 0.016	286.00 ± 0.33	0.00	H	M2FS
N1846-1-b075	05:07:31.11	-67:29:06.2	18.162 ± 0.006	1.112 ± 0.011	237.78 ± 0.27	0.92	H	M2FS
N1846-1-b076	05:07:34.98	-67:28:54.9	17.514 ± 0.006	1.338 ± 0.009	281.13 ± 0.21	0.00	H	M2FS
N1846-1-b077	05:07:34.52	-67:28:24.5	17.849 ± 0.008	1.236 ± 0.011	239.55 ± 0.27	1.00	H	COMB
N1846-1-b078	05:07:34.01	-67:28:10.7	18.325 ± 0.006	1.051 ± 0.012	241.18 ± 0.36	1.00	H	M2FS
N1846-1-b079	05:07:30.42	-67:28:04.5	17.090 ± 0.005	1.367 ± 0.007	239.58 ± 0.17	1.00	H	COMB
N1846-1-b080	05:07:34.59	-67:27:55.7	17.289 ± 0.005	1.329 ± 0.007	259.98 ± 0.22	0.00	H	M2FS
N1846-1-b081	05:07:27.72	-67:20:59.1	17.354 ± 0.051	1.283 ± 0.058	272.38 ± 0.21	0.00	M	M2FS
N1846-1-b082	05:07:29.23	-67:25:09.4	17.542 ± 0.033	1.176 ± 0.055	273.57 ± 0.25	0.00	M	M2FS
N1846-1-b083	05:07:29.61	-67:26:27.7	17.914 ± 0.008	1.231 ± 0.011	242.93 ± 0.26	0.33	H	COMB
N1846-1-b084	05:07:30.03	-67:26:43.0	17.175 ± 0.005	1.341 ± 0.007	239.37 ± 0.18	1.00	H	COMB
N1846-1-b085	05:07:29.78	-67:26:57.3	18.303 ± 0.011	1.088 ± 0.015	238.90 ± 0.32	1.00	H	M2FS
N1846-1-b087	05:07:32.10	-67:27:20.1	17.303 ± 0.006	1.357 ± 0.008	239.89 ± 0.22	1.00	H	M2FS
N1846-1-b088	05:07:27.74	-67:27:30.5	17.389 ± 0.006	1.276 ± 0.008	238.90 ± 0.21	1.00	H	M2FS
N1846-1-b089	05:07:27.31	-67:23:08.7	17.222 ± 0.084	1.409 ± 0.142	209.72 ± 0.20	0.00	M	M2FS
N1846-1-b090	05:07:23.74	-67:26:32.8	17.862 ± 0.006	1.176 ± 0.010	271.38 ± 0.24	0.00	H	M2FS
N1846-1-b092	05:07:23.62	-67:26:50.9	17.337 ± 0.007	1.363 ± 0.009	263.45 ± 0.20	0.00	H	COMB
N1846-1-b093	05:07:26.29	-67:26:57.1	18.010 ± 0.006	1.167 ± 0.010	292.12 ± 0.26	0.00	H	COMB
N1846-1-b094	05:07:21.17	-67:27:01.6	17.157 ± 0.004	1.368 ± 0.006	249.96 ± 0.17	0.00	H	COMB
N1846-1-b095	05:07:24.90	-67:27:14.0	18.363 ± 0.008	1.023 ± 0.013	235.76 ± 0.29	0.99	H	M2FS
N1846-1-b096	05:07:21.66	-67:27:25.7	17.603 ± 0.005	1.270 ± 0.008	240.15 ± 0.21	1.00	H	COMB
N1846-1-b097	05:06:41.49	-67:30:29.3	17.523 ± 0.048	1.259 ± 0.069	264.60 ± 0.37	0.00	M	M2FS
N1846-1-b098	05:07:04.08	-67:30:27.1	17.316 ± 0.121	1.251 ± 0.127	315.36 ± 0.22	0.00	M	M2FS
N1846-1-b099	05:06:26.99	-67:29:46.2	17.652 ± 0.055	1.242 ± 0.071	250.96 ± 0.36	0.00	M	M2FS
N1846-1-b100	05:07:06.54	-67:29:29.4	17.172 ± 0.108	1.302 ± 0.116	316.04 ± 0.19	0.00	M	M2FS
N1846-1-b101	05:07:14.70	-67:29:16.2	17.535 ± 0.011	1.335 ± 0.013	280.36 ± 0.19	0.00	H	COMB
N1846-1-b102	05:07:10.60	-67:28:31.4	18.059 ± 0.008	1.166 ± 0.012	280.89 ± 0.25	0.00	H	COMB
N1846-1-b103	05:07:12.27	-67:28:03.4	18.374 ± 0.007	1.157 ± 0.011	277.60 ± 0.27	0.00	H	M2FS
N1846-1-b104	05:07:14.42	-67:27:48.4	18.118 ± 0.010	1.184 ± 0.013	290.83 ± 0.20	0.00	H	COMB
N1846-1-b105	05:07:21.53	-67:34:28.6	17.266 ± 0.036	1.396 ± 0.060	275.00 ± 0.27	0.00	M	M2FS
N1846-1-b106	05:07:17.39	-67:33:22.2	17.688 ± 0.037	1.215 ± 0.055	274.33 ± 0.24	0.00	M	M2FS
N1846-1-b110	05:07:19.98	-67:29:37.3	17.423 ± 0.004	1.340 ± 0.007	310.81 ± 0.15	0.00	H	COMB
N1846-1-b111	05:07:22.21	-67:28:01.1	18.459 ± 0.009	1.049 ± 0.015	240.13 ± 0.37	1.00	H	M2FS
N1846-1-b112	05:07:21.79	-67:27:48.3	17.254 ± 0.004	1.278 ± 0.006	240.07 ± 0.23	1.00	H	M2FS
N1846-1-b114	05:07:14.72	-67:22:39.4	17.653 ± 0.033	1.218 ± 0.054	288.47 ± 0.22	0.00	M	M2FS
N1846-1-b118	05:07:20.90	-67:25:42.3	17.657 ± 0.085	1.197 ± 0.095	239.63 ± 0.26	0.96	M	M2FS
N1846-1-b119	05:07:19.94	-67:26:33.8	17.607 ± 0.049	1.189 ± 0.075	234.77 ± 0.23	0.00	M	M2FS
N1846-1-b120	05:07:17.91	-67:27:12.2	17.388 ± 0.137	1.359 ± 0.143	239.45 ± 0.21	0.96	M	M2FS

Table B.1: (*continued*) Combined Sample of NGC 1846

ID	α_{2000} (h:m:s)	δ_{2000} (d:m:s)	V (mag)	$V-I$ (mag)	$v_{\rm los}$ (km s^{-1})	P_{M_i}	Sel. [a]	Spec. [b]
N1846-1-b121	05:06:59.17	-67:23:06.7	17.024 ± 0.023	1.295 ± 0.080	251.92 ± 0.19	0.00	M	M2FS
N1846-1-b122	05:06:32.56	-67:24:21.3	17.646 ± 0.044	1.188 ± 0.063	245.75 ± 0.30	0.00	M	M2FS
N1846-1-b123	05:06:58.93	-67:24:28.2	17.437 ± 0.085	1.210 ± 0.105	250.13 ± 0.22	0.00	M	M2FS
N1846-1-b126	05:06:31.87	-67:26:14.9	17.533 ± 0.031	1.262 ± 0.052	214.26 ± 0.34	0.00	M	M2FS
N1846-1-b127	05:06:48.68	-67:27:11.0	17.611 ± 0.099	1.301 ± 0.109	250.71 ± 1.47	0.00	M	M2FS
N1846-1-b128	05:06:39.18	-67:27:36.1	17.460 ± 0.031	1.211 ± 0.053	289.27 ± 0.51	0.00	M	M2FS
N1846-1-r049	05:07:32.21	-67:27:51.6	17.154 ± 0.004	1.401 ± 0.006	241.93 ± 0.26	1.00	H	M2FS
N1846-1-r079	05:07:30.12	-67:27:27.7	17.115 ± 0.004	1.306 ± 0.006	238.29 ± 0.17	1.00	H	COMB
N1846-1-r099	05:07:31.18	-67:27:39.9	17.054 ± 0.004	1.422 ± 0.006	239.11 ± 0.19	1.00	H	M2FS
N1846-1-r127	05:07:34.13	-67:27:43.3	17.057 ± 0.004	1.336 ± 0.006	239.22 ± 0.20	1.00	H	M2FS
ACS-001-R	05:07:36.84	-67:27:45.9	16.56	1.70	236.11 ± 0.53	1.00	H	M13
ACS-013-R	05:07:33.59	-67:26:41.2	16.99	1.43	238.10 ± 0.46	1.00	H	M13
ACS-019-R	05:07:14.49	-67:28:16.4	...	...	278.73 ± 0.47	0.00	H	M13
ACS-025-R	05:07:36.19	-67:27:58.8	17.28	1.35	238.28 ± 0.49	1.00	H	M13
ACS-030-R	05:07:39.01	-67:28:23.2	17.43	1.31	240.65 ± 0.60	1.00	H	M13
ACS-046-R	05:07:32.64	-67:27:45.5	17.92	1.24	237.54 ± 0.62	1.00	H	M13
ACS-051-R	05:07:36.60	-67:27:33.5	17.96	1.25	235.60 ± 0.77	1.00	H	M13
ACS-059-R	05:07:28.63	-67:28:44.8	18.04	1.19	237.75 ± 0.77	1.00	H	M13
ACS-066-R	05:07:49.57	-67:29:01.4	18.18	1.18	239.43 ± 0.78	0.96	H	M13
ACS-080-A	05:07:30.30	-67:27:11.2	17.09	1.36	243.87 ± 0.47	0.92	H	M13
ACS-090-A	05:07:30.17	-67:27:46.1	17.53	1.24	238.02 ± 0.62	1.00	H	M13
ACS-112-A	05:07:43.29	-67:26:49.9	18.02	1.12	239.80 ± 0.67	0.96	H	M13
MCPS-007	05:05:34.36	-67:26:34.2	16.810 ± 0.063	1.622 ± 0.079	253.77 ± 0.85	0.00	M	M13
MCPS-010	05:05:40.15	-67:24:55.8	16.820 ± 0.048	1.792 ± 0.063	265.39 ± 0.59	0.00	M	M13
MCPS-016	05:05:48.25	-67:26:42.0	16.622 ± 0.191	1.636 ± 0.195	277.40 ± 0.55	0.00	M	M13
MCPS-017	05:05:48.26	-67:34:31.0	16.868 ± 0.027	1.553 ± 0.047	305.87 ± 0.59	0.00	M	M13
MCPS-018	05:05:49.11	-67:24:18.3	16.586 ± 0.065	2.020 ± 0.076	271.71 ± 1.03	0.00	M	M13
MCPS-021	05:05:55.85	-67:36:24.1	17.015 ± 0.025	1.955 ± 0.052	258.14 ± 0.95	0.00	M	M13
MCPS-022	05:05:56.49	-67:34:03.0	16.537 ± 0.027	1.533 ± 0.047	279.70 ± 0.48	0.00	M	M13
MCPS-023	05:05:56.77	-67:31:03.9	16.619 ± 0.033	1.724 ± 0.053	250.79 ± 0.52	0.00	M	M13
MCPS-026	05:06:01.14	-67:25:34.9	16.452 ± 0.045	1.810 ± 0.060	298.23 ± 0.57	0.00	M	M13
MCPS-027	05:06:03.18	-67:28:46.3	16.855 ± 0.029	1.576 ± 0.049	279.19 ± 0.55	0.00	M	M13
MCPS-029	05:06:04.64	-67:34:09.3	16.687 ± 0.038	1.684 ± 0.064	234.91 ± 0.63	0.00	M	M13
MCPS-031	05:06:06.29	-67:33:19.8	16.406 ± 0.071	1.694 ± 0.087	285.55 ± 0.65	0.00	M	M13
MCPS-033	05:06:07.79	-67:30:26.5	16.857 ± 0.043	1.544 ± 0.059	270.06 ± 0.52	0.00	M	M13
MCPS-035	05:06:12.98	-67:28:56.5	16.732 ± 0.034	1.730 ± 0.055	259.76 ± 0.45	0.00	M	M13
MCPS-038	05:06:16.30	-67:30:11.6	16.652 ± 0.031	1.927 ± 0.049	235.10 ± 0.59	0.00	M	M13
MCPS-040	05:06:17.30	-67:31:45.0	16.762 ± 0.050	1.714 ± 0.066	278.87 ± 0.59	0.00	M	M13
MCPS-042	05:06:21.14	-67:19:38.1	16.737 ± 0.053	1.748 ± 0.058	298.96 ± 0.55	0.00	M	M13
MCPS-043	05:06:22.02	-67:28:51.5	16.834 ± 0.100	1.688 ± 0.107	264.66 ± 0.45	0.00	M	M13
MCPS-044	05:06:26.23	-67:21:24.0	16.601 ± 0.043	1.768 ± 0.051	278.44 ± 0.63	0.00	M	M13
MCPS-045	05:06:26.70	-67:29:36.1	16.463 ± 0.042	1.772 ± 0.057	311.54 ± 0.45	0.00	M	M13
MCPS-047	05:06:29.38	-67:32:50.0	16.731 ± 0.032	1.628 ± 0.050	257.38 ± 0.55	0.00	M	M13
MCPS-048	05:06:29.78	-67:23:06.5	16.635 ± 0.028	1.719 ± 0.050	273.60 ± 0.47	0.00	M	M13
MCPS-049	05:06:30.15	-67:29:54.4	16.547 ± 0.045	1.661 ± 0.065	252.78 ± 0.54	0.00	M	M13
MCPS-050	05:06:32.18	-67:21:02.1	16.887 ± 0.032	1.731 ± 0.051	261.66 ± 0.49	0.00	M	M13
MCPS-051	05:06:34.01	-67:37:13.8	16.689 ± 0.031	1.679 ± 0.051	279.60 ± 0.62	0.00	M	M13
MCPS-052	05:06:34.74	-67:21:09.6	16.317 ± 0.023	1.784 ± 0.033	235.45 ± 0.60	0.00	M	M13
MCPS-058	05:06:40.72	-67:37:16.7	15.643 ± 0.038	1.445 ± 0.055	298.75 ± 0.48	0.00	M	M13
MCPS-059	05:06:40.76	-67:16:24.3	17.147 ± 0.027	1.765 ± 0.036	324.81 ± 0.65	0.00	M	M13
MCPS-060	05:06:42.46	-67:32:28.6	16.804 ± 0.046	1.979 ± 0.060	248.33 ± 1.12	0.00	M	M13
MCPS-064	05:06:45.79	-67:18:23.9	16.706 ± 0.091	1.778 ± 0.104	271.83 ± 0.54	0.00	M	M13
MCPS-066	05:06:50.42	-67:17:35.3	16.561 ± 0.021	1.535 ± 0.032	273.43 ± 0.72	0.00	M	M13
MCPS-067	05:06:51.17	-67:36:00.7	16.463 ± 0.090	1.691 ± 0.104	294.50 ± 0.51	0.00	M	M13
MCPS-070	05:06:53.80	-67:38:02.3	16.586 ± 0.024	1.802 ± 0.047	226.58 ± 0.57	0.00	M	M13
MCPS-071	05:06:57.88	-67:17:13.5	16.403 ± 0.026	1.895 ± 0.036	260.83 ± 0.54	0.00	M	M13
MCPS-074	05:07:01.90	-67:19:20.7	16.718 ± 0.026	1.685 ± 0.036	287.22 ± 0.58	0.00	M	M13
MCPS-075	05:07:03.10	-67:19:53.2	16.650 ± 0.027	1.505 ± 0.037	237.56 ± 0.52	0.00	M	M13
MCPS-076	05:07:07.28	-67:35:51.3	16.745 ± 0.037	1.583 ± 0.054	263.83 ± 0.51	0.00	M	M13
MCPS-078	05:07:10.43	-67:37:17.1	16.799 ± 0.029	1.923 ± 0.050	310.96 ± 0.70	0.00	M	M13
MCPS-079	05:07:10.53	-67:39:57.4	16.680 ± 0.029	1.803 ± 0.049	290.05 ± 0.67	0.00	M	M13
MCPS-082	05:07:14.56	-67:15:30.5	16.693 ± 0.031	1.532 ± 0.056	271.07 ± 0.62	0.00	M	M13
MCPS-084	05:07:16.07	-67:37:32.4	16.806 ± 0.025	1.832 ± 0.049	243.43 ± 0.65	0.00	M	M13

Table B.1: (*continued*) Combined Sample of NGC 1846

ID	α_{2000} (h:m:s)	δ_{2000} (d:m:s)	V (mag)	$V-I$ (mag)	$v_{\rm los}$ (km s^{-1})	P_{M_i}	Sel. [a]	Spec. [b]
MCPS-089	05:07:21.71	-67:36:39.0	16.477 ± 0.116	1.639 ± 0.123	249.40 ± 0.45	0.00	M	M13
MCPS-091	05:07:22.26	-67:39:49.8	16.726 ± 0.026	1.877 ± 0.047	239.79 ± 0.55	0.00	M	M13
MCPS-094	05:07:24.04	-67:17:29.1	16.856 ± 0.026	1.610 ± 0.037	247.63 ± 0.54	0.00	M	M13
MCPS-096	05:07:32.79	-67:17:35.6	16.536 ± 0.046	1.857 ± 0.053	311.32 ± 0.55	0.00	M	M13
MCPS-103	05:07:39.28	-67:35:41.8	17.082 ± 0.027	1.747 ± 0.065	235.06 ± 0.51	0.00	M	M13
MCPS-105	05:07:39.88	-67:17:38.0	16.556 ± 0.022	1.759 ± 0.033	277.58 ± 0.59	0.00	M	M13
MCPS-106	05:07:42.05	-67:17:05.5	16.899 ± 0.027	1.682 ± 0.037	243.45 ± 0.55	0.00	M	M13
MCPS-111	05:07:47.94	-67:23:11.2	16.599 ± 0.031	2.012 ± 0.084	242.68 ± 0.76	0.00	M	M13
MCPS-118	05:07:56.13	-67:17:51.5	16.802 ± 0.029	1.600 ± 0.038	299.40 ± 0.49	0.00	M	M13
MCPS-124	05:08:04.86	-67:36:10.0	16.670 ± 0.063	1.517 ± 0.075	262.77 ± 0.43	0.00	M	M13
MCPS-126	05:08:06.77	-67:37:28.2	16.775 ± 0.023	1.923 ± 0.045	234.44 ± 0.60	0.00	M	M13
MCPS-135	05:08:12.78	-67:31:37.0	16.569 ± 0.024	1.596 ± 0.049	289.09 ± 0.43	0.00	M	M13
MCPS-136	05:08:13.09	-67:36:51.6	16.827 ± 0.025	1.533 ± 0.047	272.33 ± 0.45	0.00	M	M13
MCPS-137	05:08:15.20	-67:26:49.6	16.691 ± 0.031	1.788 ± 0.051	230.93 ± 0.46	0.00	M	M13
MCPS-139	05:08:17.64	-67:18:24.2	16.776 ± 0.070	1.819 ± 0.074	297.20 ± 0.57	0.00	M	M13
MCPS-141	05:08:18.66	-67:36:10.6	16.450 ± 0.023	1.823 ± 0.044	259.56 ± 0.56	0.00	M	M13
MCPS-142	05:08:18.82	-67:24:53.9	16.607 ± 0.028	1.596 ± 0.048	254.21 ± 0.42	0.00	M	M13
MCPS-154	05:08:30.01	-67:32:33.1	16.503 ± 0.040	1.968 ± 0.056	231.60 ± 0.74	0.00	M	M13
MCPS-156	05:08:31.03	-67:27:46.8	16.919 ± 0.036	1.573 ± 0.054	292.88 ± 0.48	0.00	M	M13
MCPS-157	05:08:32.98	-67:35:42.9	16.337 ± 0.040	1.803 ± 0.055	268.78 ± 0.64	0.00	M	M13
MCPS-161	05:08:37.12	-67:18:36.6	16.361 ± 0.024	1.900 ± 0.033	237.30 ± 0.58	0.00	M	M13
MCPS-162	05:08:37.53	-67:31:24.6	16.693 ± 0.028	1.805 ± 0.052	278.47 ± 0.54	0.00	M	M13
MCPS-165	05:08:40.05	-67:26:05.8	16.696 ± 0.023	1.632 ± 0.045	311.85 ± 0.42	0.00	M	M13
MCPS-166	05:08:40.29	-67:33:48.8	16.452 ± 0.028	1.924 ± 0.048	266.18 ± 0.69	0.00	M	M13
MCPS-167	05:08:40.51	-67:29:19.9	16.753 ± 0.027	1.623 ± 0.048	285.36 ± 0.55	0.00	M	M13
MCPS-168	05:08:41.70	-67:20:13.9	16.658 ± 0.023	2.008 ± 0.034	212.62 ± 0.70	0.00	M	M13
MCPS-172	05:08:47.60	-67:26:05.4	16.397 ± 0.032	1.563 ± 0.053	295.20 ± 0.50	0.00	M	M13
MCPS-176	05:08:51.75	-67:37:12.3	16.757 ± 0.179	1.695 ± 0.184	307.53 ± 0.65	0.00	M	M13
MCPS-183	05:09:01.66	-67:35:30.0	16.708 ± 0.028	1.999 ± 0.051	299.60 ± 0.71	0.00	M	M13
MCPS-184	05:09:01.74	-67:26:12.7	16.475 ± 0.026	1.828 ± 0.047	255.23 ± 0.54	0.00	M	M13
MCPS-189	05:09:05.46	-67:32:01.8	16.803 ± 0.045	1.554 ± 0.060	284.73 ± 0.65	0.00	M	M13
MCPS-190	05:09:06.14	-67:31:15.8	16.582 ± 0.027	1.617 ± 0.055	340.95 ± 0.46	0.00	M	M13
MCPS-193	05:09:09.03	-67:35:05.2	16.876 ± 0.034	1.589 ± 0.052	268.29 ± 0.72	0.00	M	M13
MCPS-195	05:09:11.76	-67:26:26.7	16.732 ± 0.090	1.577 ± 0.099	240.95 ± 0.54	0.00	M	M13
MCPS-200	05:09:25.37	-67:30:22.9	16.646 ± 0.036	1.485 ± 0.054	243.73 ± 0.60	0.00	M	M13

[a] Photometric source that the target were selected from: H stands for *HST* and M stands for MCPS.

[b] Spectroscopic source the LOS velocities were measured from: M2FS stands for this work, M13 stands for *Mackey et al.* (2013), and COMB stands for combined.

APPENDIX C

Full Sample of Targets in All 26 Star Clusters

Table C.1: Sample of 3095 Targets from 26 Star Clusters

Galaxy	Cluster	ID	RAJ2000 (deg)	DEJ2000 (deg)	G (mag)	$G_{\rm BP} - G_{\rm RP}$ (mag)	$T_{\rm eff}$ (K)	*Gaia* DR2 ID	S/N[a]	$v_{\rm los}$ ($\rm km\,s^{-1}$)	$\log g$ (dex)	$[{\rm Fe/H}]_{\rm raw}$ (dex)	P_M	P'_M	Flag[b]	Source[c]
(1)	(2)	(3)	(4)	(5)	(6)	(7)	(8)	(9)	(10)	(11)	(12)	(13)	(14)	(15)	(16)	(17)
SMC	Kron 3	K3-1-b002	6.420511	-72.862261	18.35	1.20	4869	4688782811694646272	4.1	111.20 ± 0.78	1.63 ± 0.21	-1.03 ± 0.08	0.00	0.00	0000000	M2FS
SMC	Kron 3	K3-1-b004	6.366614	-72.850370	18.29	1.26	4854	4688782983493342336	4.3	130.36 ± 0.49	1.35 ± 0.20	-0.88 ± 0.08	0.00	0.00	0000000	M2FS
SMC	Kron 3	K3-1-b005	6.307460	-72.842177	17.28	1.45	4577	4688783022152125440	7.3	160.47 ± 0.31	1.21 ± 0.09	-0.75 ± 0.04	0.00	0.00	0000000	M2FS
SMC	Kron 3	K3-1-b006	6.272413	-72.822372	16.86	1.46	4434	4688794841902115200	12.9	136.41 ± 0.25	0.25 ± 0.11	-1.09 ± 0.03	0.02	0.01	0000000	M2FS
SMC	Kron 3	K3-1-b007	6.340753	-72.814660	18.12	1.31	4811	4688794876261838080	5.3	148.97 ± 0.41	1.42 ± 0.16	-0.67 ± 0.06	0.00	0.00	0000000	M2FS
SMC	Kron 3	K3-1-b008	6.306646	-72.798397	18.33	1.19	4864	4688795146841735296	4.7	158.21 ± 0.53	0.93 ± 0.23	-0.79 ± 0.07	0.00	0.00	0000000	M2FS
SMC	Kron 3	K3-1-b009	6.438492	-72.885179	17.85	1.30	4739	4688781991359987840	4.7	172.34 ± 0.52	1.18 ± 0.18	-0.67 ± 0.06	0.00	0.00	0000000	M2FS
SMC	Kron 3	K3-1-b010	6.453838	-72.872464	17.85	1.18	4740	4688782025719719424	4.6	141.59 ± 0.60	1.15 ± 0.18	-0.78 ± 0.06	0.00	0.00	0000000	M2FS
SMC	Kron 3	K3-1-b011	6.508210	-72.859435	17.89	1.32	4752	4688782468097265792	5.3	160.35 ± 0.50	1.24 ± 0.16	-0.94 ± 0.06	0.00	0.00	0000000	M2FS
SMC	Kron 3	K3-1-b012	6.431170	-72.858416	17.27	1.46	4574	4688782811694648064	7.4	171.10 ± 0.32	0.93 ± 0.11	-0.86 ± 0.04	0.00	0.00	0000000	M2FS
SMC	Kron 3	K3-1-b013	6.512062	-72.839362	18.43	1.17	4891	4688783228310538496	4.1	188.72 ± 0.54	1.39 ± 0.22	-0.90 ± 0.09	0.00	0.00	0000000	M2FS
SMC	Kron 3	K3-1-b014	6.433378	-72.838656	18.25	1.25	4843	4688782914773872384	3.8	125.00 ± 0.73	0.83 ± 0.25	-0.89 ± 0.08	0.00	0.00	0000000	M2FS
SMC	Kron 3	K3-1-b015	6.561415	-72.828667	18.18	1.24	4826	4688783258371266688	5.0	182.04 ± 0.48	1.41 ± 0.19	-0.93 ± 0.07	0.00	0.00	0000000	M2FS
SMC	Kron 3	K3-1-b016	6.489697	-72.797894	18.23	1.28	4838	4688795318639447808	5.7	153.18 ± 0.39	1.10 ± 0.15	-0.84 ± 0.06	0.00	0.00	0000000	M2FS
SMC	Kron 3	K3-1-b017	6.502860	-72.722166	17.57	1.18	4662	4688796697327897088	9.8	138.72 ± 0.29	0.88 ± 0.10	-1.11 ± 0.04	0.00	0.00	0000000	M2FS
SMC	Kron 3	K3-1-b018	6.541038	-72.749995	17.42	1.34	4615	4688795696609859200	9.5	123.61 ± 0.31	1.13 ± 0.10	-1.07 ± 0.04	0.00	0.00	0000000	M2FS
SMC	Kron 3	K3-1-b019	6.487608	-72.766718	17.62	1.31	4676	4688795593517081984	9.6	132.85 ± 0.30	0.95 ± 0.10	-1.02 ± 0.04	0.00	0.00	0000000	M2FS
SMC	Kron 3	K3-1-b020	6.447005	-72.777907	15.77	2.11	4047	4688795215559953920	17.5	172.45 ± 0.46	0.65 ± 0.10	-0.73 ± 0.07	0.00	0.00	0000010	M2FS
SMC	Kron 3	K3-1-b021	6.580592	-72.782946	17.79	1.36	4723	4688783606267605376	7.4	117.20 ± 0.35	1.40 ± 0.12	-0.85 ± 0.05	0.00	0.00	0000000	M2FS
SMC	Kron 3	K3-1-b022	6.474870	-72.786151	16.22	1.49	4198	4688795391657872640	18.5	128.26 ± 0.20	0.04 ± 0.03	-1.81 ± 0.03	0.00	0.00	0000000	M2FS
SMC	Kron 3	K3-1-b023	6.518270	-72.786373	16.84	1.52	4429	4688795322938393472	12.0	99.09 ± 0.23	0.79 ± 0.07	-0.92 ± 0.04	0.00	0.00	0000000	M2FS
SMC	Kron 3	K3-1-b024	6.582809	-72.794677	14.61	1.66	4047	4688783537548133760	41.0	126.95 ± 0.20	0.03 ± 0.03	-0.83 ± 0.03	0.00	0.00	0000000	M2FS
SMC	Kron 3	K3-1-b025	6.385661	-72.715063	16.48	1.65	4294	4688799308668015872	14.3	116.13 ± 0.27	0.69 ± 0.06	-0.82 ± 0.03	0.00	0.00	0000000	M2FS
SMC	Kron 3	K3-1-b026	6.375955	-72.746636	17.61	1.26	4674	4688796280711870208	8.8	120.79 ± 0.38	0.86 ± 0.14	-1.41 ± 0.05	0.00	0.00	0000000	M2FS
SMC	Kron 3	K3-1-b027	6.344836	-72.760177	18.42	1.26	4887	4688796074553432960	4.0	132.89 ± 0.60	1.25 ± 0.26	-0.90 ± 0.08	0.87	0.87	0000000	M2FS
SMC	Kron 3	K3-1-b028	6.345517	-72.766321	17.37	1.23	4603	4688795975773421952	10.2	168.07 ± 0.32	0.54 ± 0.20	-2.24 ± 0.05	0.00	0.00	0000000	M2FS
SMC	Kron 3	K3-1-b029	6.420669	-72.766477	18.20	1.19	4831	4688795284280100736	5.2	152.22 ± 0.41	1.06 ± 0.20	-1.02 ± 0.06	0.00	0.00	0000000	M2FS
SMC	Kron 3	K3-1-b030	6.304510	-72.775862	17.64	1.29	4683	4688795975769380480	7.2	131.59 ± 0.56	1.17 ± 0.13	-1.25 ± 0.05	0.77	0.75	0000000	M2FS
SMC	Kron 3	K3-1-b031	6.351443	-72.776955	16.93	1.30	4460	4688796010133164544	14.0	116.10 ± 0.23	0.26 ± 0.12	-1.75 ± 0.03	0.00	0.00	0000000	M2FS
SMC	Kron 3	K3-1-b032	6.429026	-72.788741	17.94	1.35	4765	4688795215559945216	6.0	129.71 ± 0.35	1.12 ± 0.15	-0.64 ± 0.05	0.00	0.00	0000000	M2FS
SMC	Kron 3	K3-1-b033	6.209590	-72.889605	18.53	1.10	4918	4688781235441764608	2.7	124.43 ± 1.35	1.57 ± 0.34	-1.05 ± 0.16	0.00	0.00	0000000	M2FS
SMC	Kron 3	K3-1-b034	6.207440	-72.826240	15.62	1.76	4047	4688793570591800832	17.8	108.41 ± 0.24	0.02 ± 0.02	-1.70 ± 0.03	0.00	0.00	0000000	M2FS
SMC	Kron 3	K3-1-b035	6.151181	-72.821443	17.30	1.46	4583	4688794360865784064	7.3	130.60 ± 0.56	0.10 ± 0.08	-0.70 ± 0.07	0.83	0.74	0000000	M2FS
SMC	Kron 3	K3-1-b036	6.150437	-72.816238	16.40	1.58	4264	4688794360865781504	14.2	136.70 ± 0.22	0.45 ± 0.06	-0.92 ± 0.03	0.18	0.10	0000000	M2FS
SMC	Kron 3	K3-1-b037	6.198748	-72.809907	17.60	1.39	4672	4688794390926587392	6.9	173.18 ± 0.35	1.33 ± 0.11	-0.86 ± 0.05	0.00	0.00	0000000	M2FS
SMC	Kron 3	K3-1-b038	6.187242	-72.807436	18.47	1.07	4901	4688794390941345152	4.3	130.37 ± 0.56	0.96 ± 0.27	-1.01 ± 0.07	1.00	1.00	0000000	M2FS
SMC	Kron 3	K3-1-b039	6.174036	-72.804542	17.72	1.18	4704	4688794429581243392	7.7	132.04 ± 0.30	1.04 ± 0.11	-0.95 ± 0.04	1.00	1.00	0000000	M2FS
SMC	Kron 3	K3-1-b040	6.194509	-72.804049	17.87	1.19	4747	4688794390927498624	4.1	131.99 ± 0.62	1.11 ± 0.25	-0.97 ± 0.08	1.00	1.00	0000000	M2FS
SMC	Kron 3	K3-1-b041	6.227448	-72.882474	17.45	1.21	4624	4688781269805492352	5.9	149.14 ± 0.44	0.70 ± 0.19	-1.21 ± 0.06	0.00	0.00	0000000	M2FS
SMC	Kron 3	K3-1-b043	6.253814	-72.870763	16.69	1.55	4369	4688781475963915776	6.8	176.17 ± 0.41	0.38 ± 0.14	-1.25 ± 0.05	0.00	0.00	0000000	M2FS
SMC	Kron 3	K3-1-b044	6.222192	-72.828159	18.15	1.18	4819	4688793566292766080	5.7	157.28 ± 0.52	1.07 ± 0.16	-1.07 ± 0.06	0.00	0.00	0000000	M2FS
SMC	Kron 3	K3-1-b045	6.252469	-72.823278	18.18	1.18	4826	4688795043761519488	4.4	130.61 ± 0.58	1.42 ± 0.32	-1.75 ± 0.09	-1.00	-1.00	0000001	M2FS
SMC	Kron 3	K3-1-b046	6.228004	-72.813527	17.25	1.38	4570	4688793635012343040	9.3	134.97 ± 0.24	0.69 ± 0.09	-1.01 ± 0.04	0.97	0.97	0000000	M2FS
SMC	Kron 3	K3-1-b047	6.252825	-72.804055	18.07	1.23	4800	4688795116780005376	6.0	132.92 ± 0.44	1.40 ± 0.16	-1.00 ± 0.06	0.99	0.99	0000000	M2FS
SMC	Kron 3	K3-1-b048	6.217366	-72.802925	18.61	1.09	4941	4688794390941479040	3.8	130.09 ± 0.59	1.95 ± 0.22	-0.67 ± 0.08	1.00	1.00	0000000	M2FS
SMC	Kron 3	K3-1-b050	6.277035	-72.728451	18.47	1.17	4903	4688799270009133952	3.8	119.15 ± 0.51	1.49 ± 0.27	-1.20 ± 0.09	0.00	0.00	0000000	M2FS
SMC	Kron 3	K3-1-b051	6.264614	-72.752639	17.45	1.32	4626	4688796211992391040	8.4	121.49 ± 0.26	0.72 ± 0.11	-0.97 ± 0.04	0.00	0.00	0000000	M2FS
SMC	Kron 3	K3-1-b052	6.281402	-72.763268	17.43	1.27	4619	4688796143272902400	5.0	155.83 ± 0.53	1.03 ± 0.20	-1.29 ± 0.07	0.00	0.00	0000000	M2FS
SMC	Kron 3	K3-1-b053	6.266755	-72.780423	18.24	1.25	4842	4688795937114461824	4.2	157.94 ± 0.73	0.62 ± 0.29	-0.90 ± 0.10	0.00	0.00	0000000	M2FS
SMC	Kron 3	K3-1-b054	6.273821	-72.783668	18.07	1.28	4799	4688795941413695872	5.7	129.85 ± 0.32	1.33 ± 0.15	-0.87 ± 0.05	0.65	0.46	0000000	M2FS
SMC	Kron 3	K3-1-b055	6.251029	-72.791741	16.55	1.60	4320	4688795872694228608	14.9	132.87 ± 0.20	0.80 ± 0.05	-0.83 ± 0.03	0.99	0.99	0000000	M2FS
SMC	Kron 3	K3-1-b056	6.270347	-72.793295	17.84	1.31	4739	4688795872694227840	5.4	131.67 ± 0.38	1.32 ± 0.16	-0.90 ± 0.06	0.99	0.99	0000000	M2FS
SMC	Kron 3	K3-1-b057	6.227972	-72.681360	18.08	1.30	4802	4688800541332981632	3.8	109.03 ± 0.61	1.28 ± 0.21	-0.58 ± 0.09	0.00	0.00	0000000	M2FS
SMC	Kron 3	K3-1-b060	6.212075	-72.765439	17.14	1.41	4533	4688794738822846336	9.3	135.24 ± 0.27	0.65 ± 0.10	-1.05 ± 0.04	0.72	0.63	0000000	M2FS

Table C.1: (*continued*) Sample of 3095 Targets from 26 Star Clusters

Galaxy	Cluster	ID	RAJ2000 (deg)	DEJ2000 (deg)	G (mag)	$G_{\rm BP} - G_{\rm RP}$ (mag)	$T_{\rm eff}$ (K)	*Gaia* DR2 ID	S/N	$v_{\rm los}$ ($\rm km\,s^{-1}$)	$\log g$ (dex)	$[{\rm Fe/H}]_{\rm raw}$ (dex)	P_M	P'_M	Flag[a]	Source[b]
(1)	(2)	(3)	(4)	(5)	(6)	(7)	(8)	(9)	(10)	(11)	(12)	(13)	(14)	(15)	(16)	(17)
SMC	Kron 3	K3-1-b061	6.246501	-72.768141	17.58	1.34	4667	4688796147572118912	5.2	116.64 ± 0.46	1.21 ± 0.15	-0.89 ± 0.06	0.00	0.00	0000000	M2FS
SMC	Kron 3	K3-1-b062	6.221267	-72.786049	17.56	1.28	4659	4688794459660953600	7.1	131.75 ± 0.31	1.26 ± 0.11	-0.92 ± 0.05	1.00	1.00	0000000	M2FS
SMC	Kron 3	K3-1-b063	6.231015	-72.788401	17.03	1.38	4495	4688794463944954496	9.6	132.03 ± 0.28	0.94 ± 0.07	-0.86 ± 0.04	1.00	1.00	0000000	M2FS
SMC	Kron 3	K3-1-b064	6.250721	-72.799768	18.41	1.15	4886	4688795868410229376	4.0	134.02 ± 0.64	0.69 ± 0.29	-0.82 ± 0.08	0.98	0.99	0000000	M2FS
SMC	Kron 3	K3-1-b065	6.120829	-72.898523	17.94	1.23	4766	4688781334225897552	3.4	115.55 ± 0.95	1.18 ± 0.29	-0.71 ± 0.09	0.00	0.00	0000000	M2FS
SMC	Kron 3	K3-1-b066	6.061599	-72.881975	15.89	1.28	4074	4688793123915238272	16.7	115.42 ± 0.22	0.01 ± 0.01	-1.34 ± 0.03	0.00	0.00	0000010	M2FS
SMC	Kron 3	K3-1-b068	6.098995	-72.862578	18.35	1.16	4870	4688793222695366016	3.7	147.96 ± 0.60	1.36 ± 0.26	-1.16 ± 0.09	0.00	0.00	0000000	M2FS
SMC	Kron 3	K3-1-b069	6.073462	-72.848987	18.25	1.30	4843	4688793463213537920	3.9	164.86 ± 0.68	0.73 ± 0.23	-0.99 ± 0.08	0.00	0.00	0000000	M2FS
SMC	Kron 3	K3-1-b070	6.121169	-72.803498	16.41	1.66	4270	4688794429585668736	10.9	135.03 ± 0.27	0.79 ± 0.06	-0.87 ± 0.04	0.97	0.96	0000000	M2FS
SMC	Kron 3	K3-1-b071	6.115038	-72.797587	17.67	1.33	4690	4688794528365178112	7.1	131.54 ± 0.29	1.30 ± 0.11	-1.01 ± 0.05	0.99	0.99	0000000	M2FS
SMC	Kron 3	K3-1-b072	6.066770	-72.784948	17.23	1.47	4564	4688797552022165376	8.2	148.31 ± 0.27	1.19 ± 0.09	-0.82 ± 0.04	0.00	0.00	0000000	M2FS
SMC	Kron 3	K3-1-b073	6.145558	-72.876328	17.88	1.29	4750	4688781407244447232	3.8	136.41 ± 0.60	1.89 ± 0.19	-1.29 ± 0.10	0.00	0.00	0000000	M2FS
SMC	Kron 3	K3-1-b074	6.138872	-72.863202	18.47	1.13	4903	4688793153975889536	3.2	76.90 ± 0.78	4.61 ± 0.19	-0.83 ± 0.14	-1.00	-1.00	0001100	M2FS
SMC	Kron 3	K3-1-b075	6.141927	-72.839296	17.77	1.31	4719	4688793536232073344	5.0	125.66 ± 0.47	0.99 ± 0.18	-1.06 ± 0.07	0.00	0.00	0000000	M2FS
SMC	Kron 3	K3-1-b076	6.134333	-72.820768	18.10	1.24	4805	4688794356566750336	4.1	142.39 ± 0.84	1.80 ± 0.23	-1.23 ± 0.10	0.00	0.00	0000000	M2FS
SMC	Kron 3	K3-1-b077	6.146152	-72.804938	18.51	1.13	4912	4688794425286326784	3.9	129.23 ± 0.54	1.39 ± 0.21	-0.84 ± 0.08	0.91	-1.00	0000000	M2FS
SMC	Kron 3	K3-1-b078	6.131022	-72.799909	18.12	1.22	4812	4688794635744098560	4.5	131.24 ± 0.47	1.51 ± 0.19	-0.88 ± 0.07	0.98	0.98	0000000	M2FS
SMC	Kron 3	K3-1-b079	6.141983	-72.794366	19.15	1.01	5070	4688794631459551488	3.6	133.07 ± 0.87	1.77 ± 0.27	-0.83 ± 0.10	1.00	1.00	0000000	M2FS
SMC	Kron 3	K3-1-b080	6.126935	-72.791734	18.89	1.01	5009	4688794635743670272	3.1	133.67 ± 0.89	1.57 ± 0.45	-1.28 ± 0.13	0.99	0.99	0000000	M2FS
SMC	Kron 3	K3-1-b081	6.203106	-72.696373	17.44	1.40	4623	4688800335161055360	4.0	120.68 ± 0.50	1.60 ± 0.16	-0.54 ± 0.07	0.00	0.00	0000000	M2FS
SMC	Kron 3	K3-1-b085	6.209448	-72.769404	15.80	2.31	4047	4688794738822848384	4.9	133.68 ± 1.61	0.59 ± 0.36	-1.89 ± 0.20	-1.00	-1.00	0110010	M2FS
SMC	Kron 3	K3-1-b086	6.195804	-72.778220	17.70	1.36	4699	4688794670103379456	5.3	168.40 ± 0.55	0.71 ± 0.29	-0.80 ± 0.09	0.00	0.00	0000000	M2FS
SMC	Kron 3	K3-1-b087	6.187460	-72.783795	18.43	1.14	4892	4688794665819251968	3.9	135.74 ± 0.67	1.00 ± 0.31	-0.74 ± 0.08	1.00	1.00	0000000	M2FS
SMC	Kron 3	K3-1-b088	6.204460	-72.800446	17.46	1.25	4630	4688794395225501952	6.7	135.41 ± 0.38	0.98 ± 0.13	-0.97 ± 0.05	1.00	1.00	0000000	M2FS
SMC	Kron 3	K3-1-b089	6.171295	-72.712111	17.42	1.36	4615	4688798788972816768	6.1	128.52 ± 0.42	0.85 ± 0.15	-1.16 ± 0.06	0.00	0.00	0000000	M2FS
SMC	Kron 3	K3-1-b090	6.181999	-72.776355	18.20	1.17	4831	4688794738818810496	4.2	130.20 ± 0.46	1.65 ± 0.19	-0.82 ± 0.07	0.97	0.96	0000000	M2FS
SMC	Kron 3	K3-1-b091	6.157664	-72.780162	18.40	1.07	4884	4688794700177431424	2.8	131.24 ± 0.89	1.35 ± 0.37	-1.01 ± 0.11	0.98	0.98	0000000	M2FS
SMC	Kron 3	K3-1-b092	6.157987	-72.786948	17.14	1.39	4534	4688794631459508608	4.9	134.85 ± 0.51	0.86 ± 0.16	-0.93 ± 0.06	1.00	1.00	0000000	M2FS
SMC	Kron 3	K3-1-b093	6.169287	-72.788355	18.08	1.07	4801	4688794631459509632	4.1	133.10 ± 0.57	1.50 ± 0.22	-0.81 ± 0.07	1.00	1.00	0000000	M2FS
SMC	Kron 3	K3-1-b094	6.174351	-72.796473	18.45	1.01	4895	4688794429585239552	2.6	130.54 ± 0.55	1.52 ± 0.35	-0.66 ± 0.10	1.00	1.00	0000000	M2FS
SMC	Kron 3	K3-1-b095	6.158241	-72.799829	18.70	1.05	4963	4688794429581238016	2.2	135.94 ± 0.96	2.44 ± 0.26	-0.63 ± 0.12	1.00	1.00	0000000	M2FS
SMC	Kron 3	K3-1-b096	6.178219	-72.799979	19.17	1.02	5074	4688794425301099264	2.1	134.48 ± 0.82	1.75 ± 0.43	-0.72 ± 0.13	1.00	1.00	0000000	M2FS
SMC	Kron 3	K3-1-b097	5.955288	-72.882257	17.88	1.35	4751	4688792986476290176	3.1	143.83 ± 1.03	0.62 ± 0.32	-0.99 ± 0.11	0.00	0.00	0000000	M2FS
SMC	Kron 3	K3-1-b098	5.875140	-72.855582	17.40	1.26	4611	4688793772451178368	3.9	164.55 ± 0.76	0.85 ± 0.25	-1.29 ± 0.08	0.00	0.00	0000000	M2FS
SMC	Kron 3	K3-1-b099	5.931446	-72.843972	18.01	1.34	4782	4688793875530397696	4.5	117.15 ± 0.78	1.08 ± 0.28	-1.35 ± 0.08	0.00	0.00	0000000	M2FS
SMC	Kron 3	K3-1-b100	5.950494	-72.831742	18.56	1.02	4926	4688794116048664960	3.3	131.88 ± 1.73	0.63 ± 0.44	-1.79 ± 0.14	0.00	0.00	0000000	M2FS
SMC	Kron 3	K3-1-b101	5.930756	-72.820679	17.97	1.30	4772	4688794154703367040	3.7	183.39 ± 0.64	0.87 ± 0.23	-1.03 ± 0.08	0.00	0.00	0000000	M2FS
SMC	Kron 3	K3-1-b102	5.949290	-72.789668	18.47	1.18	4901	4688797212724064640	3.2	182.47 ± 0.62	1.13 ± 0.28	-0.74 ± 0.10	0.00	0.00	0000000	M2FS
SMC	Kron 3	K3-1-b103	5.824815	-72.778369	18.55	1.07	4923	4688798101777987200	2.9	101.42 ± 1.28	2.11 ± 0.34	-1.29 ± 0.16	0.00	0.00	0000000	M2FS
SMC	Kron 3	K3-1-b104	5.957865	-72.774125	17.00	1.54	4487	4688797483302696832	9.7	177.73 ± 0.28	1.18 ± 0.07	-0.69 ± 0.04	0.00	0.00	0000000	M2FS
SMC	Kron 3	K3-1-b105	6.055856	-72.903492	18.48	1.16	4906	4688781368585616256	2.4	140.65 ± 1.54	1.05 ± 0.56	-1.70 ± 0.19	0.00	0.00	0000000	M2FS
SMC	Kron 3	K3-1-b106	6.033365	-72.881687	17.10	1.39	4522	4688793192634715776	7.8	189.48 ± 0.39	0.32 ± 0.16	-1.58 ± 0.05	0.00	0.00	0000000	M2FS
SMC	Kron 3	K3-1-b107	6.003910	-72.875528	17.63	1.30	4679	4688793020836023040	5.3	142.76 ± 0.61	1.30 ± 0.17	-1.09 ± 0.07	0.00	0.00	0000000	M2FS
SMC	Kron 3	K3-1-b108	5.968841	-72.800046	17.83	1.35	4734	4688797139705295232	5.7	166.28 ± 0.39	1.43 ± 0.13	-0.85 ± 0.06	0.00	0.00	0000000	M2FS
SMC	Kron 3	K3-1-b109	5.965813	-72.788501	18.09	1.32	4804	4688797208424780928	4.2	174.49 ± 0.69	1.07 ± 0.27	-0.95 ± 0.08	0.00	0.00	0000000	M2FS
SMC	Kron 3	K3-1-b110	6.010945	-72.786450	18.13	1.30	4815	4688797586381904000	3.8	132.83 ± 0.70	0.85 ± 0.30	-0.92 ± 0.08	0.86	0.86	0000000	M2FS
SMC	Kron 3	K3-1-b111	5.977476	-72.784597	17.27	1.28	4575	4688797208424784128	6.5	153.61 ± 0.41	0.19 ± 0.14	-1.63 ± 0.06	0.00	0.00	0000000	M2FS
SMC	Kron 3	K3-1-b112	5.969775	-72.781958	17.29	1.44	4579	4688797418882487424	6.9	176.96 ± 0.32	1.09 ± 0.11	-0.72 ± 0.05	0.00	0.00	0000000	M2FS
SMC	Kron 3	K3-1-b115	6.091450	-72.734858	15.47	2.20	4047	4688798655833012864	7.9	117.72 ± 1.37	0.27 ± 0.22	-1.69 ± 0.15	-1.00	-1.00	0110010	M2FS
SMC	Kron 3	K3-1-b116	6.112066	-72.765760	17.95	1.29	4768	4688797723820867840	5.1	133.71 ± 0.56	1.36 ± 0.18	-0.98 ± 0.07	0.79	0.80	0000000	M2FS
SMC	Kron 3	K3-1-b117	6.148745	-72.772990	16.54	1.61	4316	4688794704463117696	12.9	131.93 ± 0.19	0.62 ± 0.06	-0.95 ± 0.03	0.99	0.99	0000000	M2FS
SMC	Kron 3	K3-1-b118	6.147129	-72.784224	16.53	1.57	4313	4688794704463574016	10.8	133.03 ± 0.25	0.88 ± 0.06	-0.88 ± 0.04	0.99	0.99	0000000	M2FS
SMC	Kron 3	K3-1-b119	6.152221	-72.790588	17.83	1.18	4734	4688794635739645312	4.1	133.16 ± 0.47	0.89 ± 0.22	-0.81 ± 0.06	1.00	1.00	0000000	M2FS
SMC	Kron 3	K3-1-b120	6.157551	-72.796348	17.60	1.19	4672	4688794425286319104	7.5	135.10 ± 0.35	0.92 ± 0.12	-0.90 ± 0.04	1.00	1.00	0000000	M2FS

Table C.1: (*continued*) Sample of 3095 Targets from 26 Star Clusters

Galaxy	Cluster	ID	RAJ2000 (deg)	DEJ2000 (deg)	G (mag)	$G_{\rm BP} - G_{\rm RP}$ (mag)	$T_{\rm eff}$ (K)	*Gaia* DR2 ID	S/N	$v_{\rm los}$ (km s^{-1})	$\log g$ (dex)	$[{\rm Fe/H}]_{\rm raw}$ (dex)	P_M	P'_M	Flag[a]	Source[b]
(1)	(2)	(3)	(4)	(5)	(6)	(7)	(8)	(9)	(10)	(11)	(12)	(13)	(14)	(15)	(16)	(17)
SMC	Kron 3	K3-1-b121	6.006805	-72.706074	16.89	1.53	4444	4688798960771516416	7.7	143.04 ± 0.31	0.60 ± 0.10	-0.90 ± 0.04	0.00	0.00	0000000	M2FS
SMC	Kron 3	K3-1-b122	6.013955	-72.713688	19.19	1.15	5076	4688798965070652288	4.2	115.39 ± 0.95	1.87 ± 0.26	-1.22 ± 0.10	0.00	0.00	0000000	M2FS
SMC	Kron 3	K3-1-b123	6.041853	-72.714682	18.34	1.24	4866	4688798926411769216	2.6	160.31 ± 0.79	1.89 ± 0.28	-0.72 ± 0.13	0.00	0.00	0000000	M2FS
SMC	Kron 3	K3-1-b124	6.077548	-72.731259	17.64	1.26	4682	4688798651533846400	5.5	123.93 ± 0.45	0.51 ± 0.19	-1.18 ± 0.06	0.00	0.00	0000000	M2FS
SMC	Kron 3	K3-1-b125	5.911522	-72.731925	18.09	1.24	4803	4688798548454634496	1.8	149.43 ± 1.06	0.89 ± 0.41	-0.87 ± 0.14	0.00	0.00	0000000	M2FS
SMC	Kron 3	K3-1-b126	5.968772	-72.733368	18.16	1.16	4820	4688798514094893952	1.9	131.43 ± 1.34	2.04 ± 0.54	-1.71 ± 0.19	0.00	0.00	0000000	M2FS
SMC	Kron 3	K3-1-b127	5.999340	-72.737281	18.05	1.22	4794	4688798690188708224	4.2	127.10 ± 0.51	1.30 ± 0.20	-0.71 ± 0.07	0.00	0.00	0000000	M2FS
SMC	Kron 3	K3-1-b128	5.983062	-72.754936	17.92	1.29	4761	4688798239216959616	3.3	169.12 ± 0.96	0.39 ± 0.25	-1.19 ± 0.09	0.00	0.00	0000000	M2FS
SMC	Kron 3	K3-1-r028	6.189627	-72.796161	17.53	1.07	4653	4688794463940951424	10.6	133.56 ± 0.29	1.12 ± 0.09	-1.06 ± 0.04	1.00	1.00	0000000	M2FS
SMC	Kron 3	K3-1-r049	6.203015	-72.789708	17.29	1.20	4580	4688794463940922112	13.7	132.15 ± 0.21	1.05 ± 0.07	-1.01 ± 0.03	1.00	1.00	0000000	M2FS
SMC	Kron 3	K3-1-r079	6.184323	-72.790320	17.75	1.19	4714	4688794463944966656	8.8	132.95 ± 0.35	1.24 ± 0.12	-1.19 ± 0.05	1.00	1.00	0000000	M2FS
SMC	Kron 3	K3-1-r127	6.209250	-72.793686	17.12	1.14	4527	4688794459661050624	15.7	132.51 ± 0.22	0.77 ± 0.07	-1.22 ± 0.03	1.00	1.00	0000000	M2FS
SMC	Lindsay 1	L1-1-b003	1.016498	-73.518774	18.26	0.92	4847	4689387478665780480	3.2	6.84 ± 1.34	3.29 ± 0.17	-0.63 ± 0.14	-1.00	-1.00	0001100	M2FS
SMC	Lindsay 1	L1-1-b004	1.037900	-73.497180	17.82	1.28	4737	4689387753544914176	4.7	143.50 ± 0.67	1.04 ± 0.21	-1.11 ± 0.07	0.95	0.95	0000000	M2FS
SMC	Lindsay 1	L1-1-b005	1.008265	-73.494031	15.91	1.75	4089	4689399504575436672	13.4	142.70 ± 0.24	0.29 ± 0.07	-1.07 ± 0.03	0.98	0.98	0000000	M2FS
SMC	Lindsay 1	L1-1-b006	1.019903	-73.489884	19.15	0.90	5070	4689399500279784576	2.1	140.61 ± 2.45	1.20 ± 0.71	-2.22 ± 0.29	-1.00	-1.00	1000000	M2FS
SMC	Lindsay 1	L1-1-b007	1.012778	-73.485411	17.48	1.26	4639	4689399504575434240	5.8	139.73 ± 0.50	0.67 ± 0.19	-1.14 ± 0.06	1.00	1.00	0000000	M2FS
SMC	Lindsay 1	L1-1-b008	1.042848	-73.482948	17.34	1.43	4599	4689399504575432320	4.2	138.62 ± 0.83	0.35 ± 0.29	-1.34 ± 0.13	0.99	0.99	0000000	M2FS
SMC	Lindsay 1	L1-1-b009	1.160540	-73.566178	17.01	1.51	4496	4689383492937361664	4.0	159.52 ± 0.59	1.24 ± 0.14	-0.90 ± 0.08	0.00	0.00	0000000	M2FS
SMC	Lindsay 1	L1-1-b010	1.128477	-73.519700	18.08	1.29	4805	4689386787176581888	2.7	149.13 ± 0.92	0.76 ± 0.36	-0.77 ± 0.11	0.00	0.00	0000000	M2FS
SMC	Lindsay 1	L1-1-b011	1.076918	-73.517334	18.71	1.22	4969	4689387440011612160	1.8	136.73 ± 1.77	0.53 ± 0.36	-1.12 ± 0.19	0.77	0.77	0000000	M2FS
SMC	Lindsay 1	L1-1-b012	1.048665	-73.494348	18.39	1.15	4883	4689387749249262080	2.7	136.10 ± 1.24	1.58 ± 0.36	-1.13 ± 0.15	0.86	0.86	0000000	M2FS
SMC	Lindsay 1	L1-1-b013	1.086274	-73.493215	19.00	0.87	5036	4689387719185173120	2.0	142.09 ± 1.48	1.61 ± 0.57	-1.34 ± 0.20	0.99	0.99	0000000	M2FS
SMC	Lindsay 1	L1-1-b014	1.273021	-73.492189	16.52	1.55	4317	4689387203789088384	8.3	126.95 ± 0.28	0.11 ± 0.08	-1.28 ± 0.04	0.00	0.00	0000000	M2FS
SMC	Lindsay 1	L1-1-b015	1.069201	-73.489571	17.81	1.30	4733	4689387783609001216	3.9	138.79 ± 0.56	1.22 ± 0.25	-1.15 ± 0.08	0.99	0.99	0000000	M2FS
SMC	Lindsay 1	L1-1-b016	1.159179	-73.488127	16.23	1.70	4210	4689387822264381952	11.5	131.06 ± 0.25	0.46 ± 0.07	-1.08 ± 0.03	0.00	0.00	0000000	M2FS
SMC	Lindsay 1	L1-1-b017	1.150194	-73.395894	16.65	1.55	4362	4689401016403904640	12.3	144.51 ± 0.20	0.61 ± 0.06	-0.99 ± 0.03	0.00	0.00	0000000	M2FS
SMC	Lindsay 1	L1-1-b018	1.197716	-73.408402	18.08	1.25	4803	4689400771590448128	4.3	143.10 ± 0.68	1.37 ± 0.20	-0.58 ± 0.06	0.00	0.00	0000000	M2FS
SMC	Lindsay 1	L1-1-b019	1.171869	-73.417038	18.50	0.86	4914	4689400737230708608	4.0	166.10 ± 1.29	1.44 ± 0.34	-1.56 ± 0.11	0.00	0.00	0000000	M2FS
SMC	Lindsay 1	L1-1-b020	1.255176	-73.421520	18.01	1.28	4786	4689400324913847040	3.8	159.34 ± 0.48	1.48 ± 0.21	-0.78 ± 0.08	0.00	0.00	0000000	M2FS
SMC	Lindsay 1	L1-1-b021	1.173924	-73.454807	19.18	0.94	5077	4689399637718940160	1.7	139.69 ± 1.63	1.27 ± 0.64	-1.23 ± 0.25	0.86	0.86	0000000	M2FS
SMC	Lindsay 1	L1-1-b022	1.140655	-73.463467	19.36	1.03	5112	4689399642014376576	1.1	138.87 ± 32.06	1.98 ± 1.04	-2.26 ± 0.49	-1.00	-1.00	1000000	M2FS
SMC	Lindsay 1	L1-1-b023	1.210329	-73.477985	18.13	0.75	4818	4689387852328480768	4.7	115.46 ± 0.85	0.62 ± 0.39	-1.86 ± 0.10	0.00	0.00	0000010	M2FS
SMC	Lindsay 1	L1-1-b024	1.299147	-73.481669	15.90	1.72	4086	4689387959703330816	14.0	123.86 ± 0.21	0.39 ± 0.06	-1.22 ± 0.03	0.00	0.00	0000000	M2FS
SMC	Lindsay 1	L1-1-b025	1.117015	-73.405165	18.28	1.08	4852	4689400702870971904	4.5	79.91 ± 0.83	0.47 ± 0.33	-2.22 ± 0.11	-1.00	-1.00	0000100	M2FS
SMC	Lindsay 1	L1-1-b026	1.135182	-73.447684	17.72	1.27	4708	4689399706438222080	5.4	140.75 ± 0.44	0.93 ± 0.17	-0.99 ± 0.06	0.98	0.98	0000000	M2FS
SMC	Lindsay 1	L1-1-b027	1.103073	-73.452145	19.22	1.06	5084	4689399809517633920	1.8	138.57 ± 1.33	1.01 ± 0.48	-0.77 ± 0.16	0.99	0.99	0000000	M2FS
SMC	Lindsay 1	L1-1-b028	1.068025	-73.459161	19.18	0.92	5076	4689399813813068672	1.4	140.54 ± 2.41	1.54 ± 0.71	-1.41 ± 0.28	0.99	0.99	0000000	M2FS
SMC	Lindsay 1	L1-1-b029	1.133132	-73.467376	19.49	0.85	5139	4689399637718931584	1.2	117.71 ± 1.53	0.59 ± 0.49	-1.47 ± 0.30	0.00	0.00	0000000	M2FS
SMC	Lindsay 1	L1-1-b030	1.074314	-73.471776	18.88	0.87	5009	4689399538935164288	1.1	147.25 ± 4.13	2.31 ± 0.88	-1.18 ± 0.48	0.96	-1.00	0000000	M2FS
SMC	Lindsay 1	L1-1-b031	1.099245	-73.473099	18.85	1.00	5003	4689399538933876736	2.2	142.88 ± 1.22	1.44 ± 0.57	-1.52 ± 0.18	0.98	0.98	0000000	M2FS
SMC	Lindsay 1	L1-1-b032	1.135440	-73.483205	17.73	1.25	4710	4689387817968740480	3.9	140.74 ± 0.54	0.77 ± 0.25	-1.15 ± 0.08	0.98	0.98	0000000	M2FS
SMC	Lindsay 1	L1-1-b035	0.951559	-73.508944	19.29	1.11	5099	4689381878028426112	1.0	136.36 ± 2.06	0.50 ± 0.38	-0.16 ± 0.23	-1.00	-1.00	0000001	M2FS
SMC	Lindsay 1	L1-1-b036	0.947136	-73.491747	19.14	0.95	5067	4689393697778418816	1.8	144.70 ± 1.34	1.91 ± 0.49	-1.19 ± 0.20	0.94	0.94	0000000	M2FS
SMC	Lindsay 1	L1-1-b037	0.938176	-73.487612	18.74	0.90	4976	4689393697778416128	2.0	141.26 ± 0.83	1.11 ± 0.46	-1.15 ± 0.16	1.00	1.00	0000000	M2FS
SMC	Lindsay 1	L1-1-b038	0.950298	-73.479920	19.17	0.83	5075	4689393903936834816	1.1	140.16 ± 1.86	2.01 ± 0.76	-1.32 ± 0.32	1.00	1.00	0000000	M2FS
SMC	Lindsay 1	L1-1-b039	0.953742	-73.469851	18.39	1.05	4883	4689393899643567872	2.2	139.97 ± 0.87	1.56 ± 0.35	-0.73 ± 0.14	1.00	1.00	0000000	M2FS
SMC	Lindsay 1	L1-1-b040	0.939919	-73.466932	18.46	0.99	4903	4689393972656292480	1.5	141.15 ± 1.55	1.24 ± 0.53	-1.47 ± 0.19	1.00	1.00	0000000	M2FS
SMC	Lindsay 1	L1-1-b043	0.962906	-73.519591	17.74	1.29	4713	4689381805014518656	1.5	142.24 ± 1.51	0.85 ± 0.45	-0.74 ± 0.18	0.94	0.94	0000000	M2FS
SMC	Lindsay 1	L1-1-b044	0.955792	-73.501526	19.13	1.01	5067	4689393624764691840	1.7	143.96 ± 1.70	0.93 ± 0.65	-1.67 ± 0.26	0.97	0.97	0000000	M2FS
SMC	Lindsay 1	L1-1-b045	0.967558	-73.500664	18.92	1.09	5019	4689393624764692864	1.0	138.30 ± 1.69	2.46 ± 0.60	-0.87 ± 0.28	0.99	0.99	0000000	M2FS
SMC	Lindsay 1	L1-1-b046	0.973162	-73.494985	19.19	0.89	5078	4689393629058941696	1.1	144.46 ± 1.95	2.37 ± 0.77	-1.56 ± 0.36	0.97	0.97	0000000	M2FS
SMC	Lindsay 1	L1-1-b047	0.960364	-73.493442	19.17	0.97	5075	4689393629058941824	1.3	138.92 ± 1.80	0.72 ± 0.52	-1.48 ± 0.30	0.99	0.99	0000000	M2FS
SMC	Lindsay 1	L1-1-b048	0.970149	-73.486308	18.23	1.14	4840	4689393697778410752	4.3	138.50 ± 0.62	1.04 ± 0.24	-1.08 ± 0.08	1.00	1.00	0000000	M2FS

Table C.1: (*continued*) Sample of 3095 Targets from 26 Star Clusters

Galaxy	Cluster	ID	RAJ2000 (deg)	DEJ2000 (deg)	G (mag)	$G_{\rm BP} - G_{\rm RP}$ (mag)	$T_{\rm eff}$ (K)	*Gaia* DR2 ID	S/N	$v_{\rm los}$ ($\rm km\,s^{-1}$)	$\log g$ (dex)	$[{\rm Fe/H}]_{\rm raw}$ (dex)	P_M	P'_M	Flag[a]	Source[b]
(1)	(2)	(3)	(4)	(5)	(6)	(7)	(8)	(9)	(10)	(11)	(12)	(13)	(14)	(15)	(16)	(17)
SMC	Lindsay 1	L1-1-b050	1.051063	-73.401399	17.85	1.18	4743	4689400947684430464	5.9	113.22 ± 0.36	0.85 ± 0.16	-1.19 ± 0.06	0.00	0.00	0000000	M2FS
SMC	Lindsay 1	L1-1-b051	1.060748	-73.456297	18.98	0.92	5033	4689399813811774720	2.0	141.63 ± 1.94	0.95 ± 0.54	-1.61 ± 0.24	0.99	0.99	0000000	M2FS
SMC	Lindsay 1	L1-1-b052	1.052534	-73.462937	16.58	1.52	4335	4689399779453331584	5.9	140.42 ± 0.31	0.53 ± 0.12	-0.91 ± 0.05	0.99	0.99	0000000	M2FS
SMC	Lindsay 1	L1-1-b053	1.049154	-73.466264	16.71	1.49	4386	4689399573294902272	9.8	138.02 ± 0.25	0.48 ± 0.09	-1.08 ± 0.04	0.98	0.98	0000000	M2FS
SMC	Lindsay 1	L1-1-b054	1.061141	-73.468012	18.37	1.04	4878	4689399603359004416	3.5	135.37 ± 0.66	1.02 ± 0.29	-1.15 ± 0.09	0.35	0.35	0000000	M2FS
SMC	Lindsay 1	L1-1-b055	1.059106	-73.471693	19.10	1.06	5059	4689399568999265280	2.1	141.05 ± 1.06	1.74 ± 0.40	-1.10 ± 0.16	0.99	0.99	0000000	M2FS
SMC	Lindsay 1	L1-1-b056	1.043425	-73.477686	17.27	1.10	4579	4689399504575429504	6.2	106.96 ± 0.43	0.59 ± 0.18	-1.27 ± 0.06	0.00	0.00	0000000	M2FS
SMC	Lindsay 1	L1-1-b057	1.035035	-73.435604	19.05	1.05	5048	4689400599791628160	1.6	139.32 ± 1.39	2.37 ± 0.47	-0.84 ± 0.22	0.99	0.99	0000000	M2FS
SMC	Lindsay 1	L1-1-b058	1.035252	-73.447184	18.30	1.18	4860	4689399848172806528	3.4	140.42 ± 0.73	1.40 ± 0.24	-0.95 ± 0.10	0.99	0.99	0000000	M2FS
SMC	Lindsay 1	L1-1-b059	1.027961	-73.450222	19.19	0.82	5078	4689399848171512832	1.8	140.73 ± 1.85	1.92 ± 0.59	-1.43 ± 0.26	-1.00	-1.00	1000000	M2FS
SMC	Lindsay 1	L1-1-b060	1.040624	-73.454443	19.13	0.94	5066	4689399779452036480	1.2	138.24 ± 1.53	0.82 ± 0.52	-1.21 ± 0.34	0.99	0.99	0000000	M2FS
SMC	Lindsay 1	L1-1-b061	1.042606	-73.460055	18.95	1.05	5026	4689399779452039936	1.4	139.91 ± 1.19	1.40 ± 0.39	-0.54 ± 0.26	0.99	0.99	0000000	M2FS
SMC	Lindsay 1	L1-1-b062	1.023024	-73.466323	18.30	1.09	4859	4689399775158829696	2.7	137.93 ± 1.12	0.98 ± 0.39	-1.18 ± 0.12	1.00	1.00	0000000	M2FS
SMC	Lindsay 1	L1-1-b063	1.013408	-73.469895	18.46	0.94	4902	4689399779452056320	3.9	139.69 ± 0.91	1.41 ± 0.37	-1.46 ± 0.11	-1.00	-1.00	0000001	M2FS
SMC	Lindsay 1	L1-1-b064	1.010325	-73.474420	17.26	1.31	4575	4689399573293640832	9.8	140.49 ± 0.31	0.41 ± 0.15	-1.14 ± 0.04	1.00	1.00	0000000	M2FS
SMC	Lindsay 1	L1-1-b065	0.909433	-73.493737	19.13	0.85	5066	4689393659124262272	1.6	141.63 ± 1.52	1.62 ± 0.61	-1.16 ± 0.21	0.99	0.99	0000000	M2FS
SMC	Lindsay 1	L1-1-b066	0.897987	-73.491536	19.03	0.95	5045	4689393865282868096	1.4	142.19 ± 1.73	1.53 ± 0.77	-1.42 ± 0.31	-1.00	-1.00	1000000	M2FS
SMC	Lindsay 1	L1-1-b067	0.881857	-73.480083	19.14	0.93	5068	4689393934002171136	2.0	142.31 ± 2.11	0.94 ± 0.52	-1.62 ± 0.24	0.99	0.99	0000000	M2FS
SMC	Lindsay 1	L1-1-b068	0.901265	-73.480035	18.54	0.95	4925	4689393869577105920	3.1	140.46 ± 0.67	1.44 ± 0.39	-1.41 ± 0.13	0.99	0.99	0000000	M2FS
SMC	Lindsay 1	L1-1-b069	0.906916	-73.475058	16.72	1.51	4390	4689393938297819776	9.4	142.75 ± 0.27	0.47 ± 0.09	-1.03 ± 0.04	1.00	1.00	0000000	M2FS
SMC	Lindsay 1	L1-1-b070	0.891833	-73.472147	19.18	0.82	5075	4689393938296575872	1.0	141.90 ± 3.58	1.29 ± 0.79	-0.94 ± 0.34	0.99	0.99	0000000	M2FS
SMC	Lindsay 1	L1-1-b071	0.905336	-73.470789	16.47	1.56	4299	4689393938297818752	9.5	141.41 ± 0.26	0.41 ± 0.09	-1.10 ± 0.04	1.00	1.00	0000000	M2FS
SMC	Lindsay 1	L1-1-b072	0.909713	-73.460525	19.71	0.74	5179	4689394694210793984	0.4	135.00 ± 60.61	2.34 ± 1.22	0.10 ± 0.89	-1.00	-1.00	1000000	M2FS
SMC	Lindsay 1	L1-1-b075	0.923761	-73.518309	19.38	0.94	5118	4689381839374419328	0.8	-94.14 ± 342.96	2.17 ± 1.21	-2.13 ± 0.81	-1.00	-1.00	1000000	M2FS
SMC	Lindsay 1	L1-1-b076	0.926305	-73.497602	18.83	1.07	4997	4689393659124260480	1.3	140.90 ± 1.89	0.65 ± 0.48	-1.27 ± 0.34	0.99	0.99	0000000	M2FS
SMC	Lindsay 1	L1-1-b077	0.934617	-73.491010	19.12	0.85	5063	4689393663418680960	1.1	139.64 ± 24.97	1.60 ± 0.73	-1.66 ± 0.44	-1.00	-1.00	1000000	M2FS
SMC	Lindsay 1	L1-1-b078	0.922772	-73.482506	17.81	1.18	4734	4689393869578344448	4.3	141.44 ± 0.61	0.53 ± 0.28	-1.23 ± 0.09	1.00	1.00	0000000	M2FS
SMC	Lindsay 1	L1-1-b079	0.932079	-73.477885	18.35	0.85	4872	4689393869578342656	3.3	136.82 ± 0.94	0.88 ± 0.40	-1.57 ± 0.13	-1.00	-1.00	0000001	M2FS
SMC	Lindsay 1	L1-1-b080	0.922089	-73.472902	19.01	0.96	5040	4689393938296570112	2.3	139.82 ± 1.01	1.29 ± 0.46	-0.99 ± 0.16	1.00	1.00	0000000	M2FS
SMC	Lindsay 1	L1-1-b081	1.006559	-73.437004	17.64	0.98	4687	4689400604087050112	5.3	140.14 ± 0.55	0.74 ± 0.33	-1.89 ± 0.08	-1.00	-1.00	0000001	M2FS
SMC	Lindsay 1	L1-1-b082	1.005787	-73.443896	19.11	0.92	5061	4689400599791623040	1.5	141.58 ± 2.73	0.96 ± 0.73	-1.54 ± 0.29	-1.00	-1.00	1000000	M2FS
SMC	Lindsay 1	L1-1-b083	0.998011	-73.448360	15.75	1.82	4036	4689400599791419776	10.2	142.11 ± 0.73	0.16 ± 0.12	-1.36 ± 0.09	-1.00	-1.00	0110000	M2FS
SMC	Lindsay 1	L1-1-b084	1.004899	-73.452612	17.15	1.39	4545	4689399848172807680	6.1	141.57 ± 0.40	0.86 ± 0.15	-1.16 ± 0.06	1.00	1.00	0000000	M2FS
SMC	Lindsay 1	L1-1-b085	0.994484	-73.454953	18.65	1.02	4953	4689393972656257792	2.5	141.14 ± 1.10	1.69 ± 0.41	-0.89 ± 0.13	1.00	1.00	0000000	M2FS
SMC	Lindsay 1	L1-1-b086	1.001562	-73.464725	17.95	1.10	4770	4689399779452051712	4.3	136.90 ± 0.52	0.72 ± 0.23	-1.05 ± 0.07	1.00	1.00	0000000	M2FS
SMC	Lindsay 1	L1-1-b087	1.005230	-73.479188	16.66	1.48	4364	4689399573294909312	8.5	140.74 ± 0.28	0.44 ± 0.10	-1.03 ± 0.04	1.00	1.00	0000000	M2FS
SMC	Lindsay 1	L1-1-b088	0.991295	-73.482369	17.49	1.34	4644	4689393697778401024	6.9	141.35 ± 0.30	1.00 ± 0.12	-0.91 ± 0.05	1.00	1.00	0000000	M2FS
SMC	Lindsay 1	L1-1-b090	0.985102	-73.447414	19.29	0.99	5100	4689394728570497152	1.5	140.58 ± 1.32	0.74 ± 0.48	-1.05 ± 0.21	0.99	0.99	0000000	M2FS
SMC	Lindsay 1	L1-1-b091	0.979899	-73.457049	18.11	1.04	4811	4689393968361952256	3.5	139.40 ± 0.90	1.02 ± 0.37	-1.21 ± 0.10	1.00	1.00	0000000	M2FS
SMC	Lindsay 1	L1-1-b092	0.986285	-73.460983	18.70	0.95	4965	4689393972656264320	1.2	139.82 ± 1.99	1.48 ± 0.79	-1.45 ± 0.26	1.00	1.00	0000000	M2FS
SMC	Lindsay 1	L1-1-b093	0.969891	-73.461998	17.86	1.19	4748	4689393968361951744	4.8	141.54 ± 0.63	1.13 ± 0.20	-1.08 ± 0.08	1.00	1.00	0000000	M2FS
SMC	Lindsay 1	L1-1-b094	0.975901	-73.466584	18.87	0.82	5007	4689393903936800256	2.2	141.40 ± 1.28	1.10 ± 0.50	-1.69 ± 0.19	-1.00	-1.00	0000001	M2FS
SMC	Lindsay 1	L1-1-b095	0.989789	-73.477859	15.87	1.78	4074	4689393697779648768	13.5	144.21 ± 0.19	0.43 ± 0.05	-0.96 ± 0.03	1.00	1.00	0000000	M2FS
SMC	Lindsay 1	L1-1-b096	0.973535	-73.481912	16.25	1.63	4217	4689393697779650432	11.3	140.91 ± 0.22	0.55 ± 0.06	-1.03 ± 0.03	1.00	1.00	0000000	M2FS
SMC	Lindsay 1	L1-1-b097	0.766489	-73.526565	17.91	1.26	4760	4689393521685301248	2.8	138.75 ± 1.24	1.01 ± 0.44	-1.67 ± 0.15	0.01	0.01	0000000	M2FS
SMC	Lindsay 1	L1-1-b098	0.830440	-73.486818	17.54	1.18	4658	4689393835217377280	7.1	-15.82 ± 0.73	3.90 ± 0.25	-2.05 ± 0.10	-1.00	-1.00	0001100	M2FS
SMC	Lindsay 1	L1-1-b099	0.703587	-73.470033	15.85	1.78	4067	4689394453693898880	16.0	142.91 ± 0.23	0.17 ± 0.08	-1.01 ± 0.03	0.00	0.00	0000000	M2FS
SMC	Lindsay 1	L1-1-b100	0.834950	-73.464960	19.20	0.96	5079	4689394655556869760	2.1	139.46 ± 1.48	0.59 ± 0.42	-1.55 ± 0.20	0.99	0.99	0000000	M2FS
SMC	Lindsay 1	L1-1-b101	0.782044	-73.463741	18.02	1.27	4788	4689394831649781248	5.5	139.67 ± 0.51	0.71 ± 0.19	-0.95 ± 0.06	0.97	0.97	0000000	M2FS
SMC	Lindsay 1	L1-1-b102	0.798042	-73.458796	19.20	0.95	5081	4689394827355567104	1.3	143.66 ± 7.64	1.93 ± 0.90	-1.60 ± 0.47	-1.00	-1.00	1000000	M2FS
SMC	Lindsay 1	L1-1-b103	0.834912	-73.451928	17.64	0.76	4687	4689394866009490688	7.0	35.17 ± 0.62	2.07 ± 0.13	-1.68 ± 0.07	-1.00	-1.00	0000110	M2FS
SMC	Lindsay 1	L1-1-b104	0.816718	-73.445182	19.15	0.90	5070	4689394934728958720	2.5	139.21 ± 1.63	1.71 ± 0.50	-1.12 ± 0.19	0.95	0.95	0000000	M2FS
SMC	Lindsay 1	L1-1-b105	0.839322	-73.563240	18.25	1.04	4846	4689381392697649792	1.5	85.00 ± 2.31	3.87 ± 0.40	-0.78 ± 0.31	-1.00	-1.00	0001100	M2FS
SMC	Lindsay 1	L1-1-b106	0.878489	-73.532631	17.56	1.32	4664	4689381770654777856	4.0	138.78 ± 0.61	0.89 ± 0.27	-1.27 ± 0.09	0.00	0.01	0000000	M2FS

Table C.1: (*continued*) Sample of 3095 Targets from 26 Star Clusters

Galaxy	Cluster	ID	RAJ2000 (deg)	DEJ2000 (deg)	G (mag)	$G_{\rm BP} - G_{\rm RP}$ (mag)	$T_{\rm eff}$ (K)	*Gaia* DR2 ID	S/N	$v_{\rm los}$ ($\rm km\,s^{-1}$)	$\log g$ (dex)	$[{\rm Fe/H}]_{\rm raw}$ (dex)	P_M	P'_M	Flag[a]	Source[b]
(1)	(2)	(3)	(4)	(5)	(6)	(7)	(8)	(9)	(10)	(11)	(12)	(13)	(14)	(15)	(16)	(17)
SMC	Lindsay 1	L1-1-b107	0.866615	-73.503080	19.34	0.96	5110	4689393560339473152	1.3	148.62 ± 2.27	1.56 ± 0.90	-1.57 ± 0.34	0.09	0.09	0000000	M2FS
SMC	Lindsay 1	L1-1-b108	0.877886	-73.487629	19.15	0.85	5071	4689393865282871552	1.4	138.63 ± 2.10	0.96 ± 0.66	-1.59 ± 0.31	0.99	0.99	0000000	M2FS
SMC	Lindsay 1	L1-1-b109	0.868919	-73.481326	16.38	1.60	4265	4689393830922955520	11.7	141.42 ± 0.23	0.38 ± 0.08	-1.07 ± 0.03	0.99	0.99	0000000	M2FS
SMC	Lindsay 1	L1-1-b110	0.876119	-73.471037	18.99	1.07	5036	4689394689916603520	1.7	140.34 ± 1.68	2.63 ± 0.52	-1.01 ± 0.31	0.99	0.99	0000000	M2FS
SMC	Lindsay 1	L1-1-b111	0.852506	-73.470421	18.93	1.05	5022	4689394586837389056	1.7	137.92 ± 1.29	2.41 ± 0.37	-0.91 ± 0.26	0.98	0.98	0000000	M2FS
SMC	Lindsay 1	L1-1-b112	0.851782	-73.464270	19.16	1.01	5073	4689394655556871040	1.8	141.70 ± 1.50	1.59 ± 0.59	-1.40 ± 0.24	0.99	0.99	0000000	M2FS
SMC	Lindsay 1	L1-1-b114	0.938756	-73.431209	16.81	1.48	4423	4689395003449696384	11.5	142.41 ± 0.23	0.54 ± 0.08	-1.09 ± 0.03	0.98	0.98	0000000	M2FS
SMC	Lindsay 1	L1-1-b115	0.956758	-73.439363	19.16	1.03	5072	4689394792995842048	2.1	139.61 ± 1.41	0.97 ± 0.59	-1.32 ± 0.19	0.99	0.99	0000000	M2FS
SMC	Lindsay 1	L1-1-b116	0.949569	-73.448414	18.43	1.04	4895	4689394728571791616	3.2	138.85 ± 0.99	1.11 ± 0.32	-1.15 ± 0.11	0.99	0.99	0000000	M2FS
SMC	Lindsay 1	L1-1-b117	0.955725	-73.451413	16.64	1.51	4356	4689394728571792128	10.4	141.32 ± 0.25	0.65 ± 0.07	-1.07 ± 0.04	1.00	1.00	0000000	M2FS
SMC	Lindsay 1	L1-1-b118	0.967827	-73.455842	18.56	1.00	4930	4689393972657548544	3.2	141.13 ± 0.98	1.65 ± 0.35	-1.03 ± 0.14	1.00	1.00	0000000	M2FS
SMC	Lindsay 1	L1-1-b119	0.958340	-73.460434	18.29	1.05	4856	4689393972657550080	3.0	140.61 ± 0.77	1.48 ± 0.31	-1.02 ± 0.11	1.00	1.00	0000000	M2FS
SMC	Lindsay 1	L1-1-b120	0.955323	-73.465110	18.27	0.83	4851	4689393972656284032	3.0	138.55 ± 1.23	0.80 ± 0.42	-1.45 ± 0.13	1.00	1.00	0000000	M2FS
SMC	Lindsay 1	L1-1-b122	0.722113	-73.388012	18.31	1.15	4862	4689398641286341632	4.5	153.20 ± 0.52	0.88 ± 0.32	-1.61 ± 0.09	0.00	0.00	0000000	M2FS
SMC	Lindsay 1	L1-1-b123	0.931635	-73.427329	19.17	1.04	5075	4689395033514017280	2.5	141.67 ± 1.03	1.73 ± 0.43	-1.37 ± 0.18	0.96	0.96	0000000	M2FS
SMC	Lindsay 1	L1-1-b124	0.912304	-73.433259	19.43	0.74	5127	4689394964794537472	1.7	139.87 ± 1.44	1.08 ± 0.52	-1.53 ± 0.22	0.99	0.99	0000000	M2FS
SMC	Lindsay 1	L1-1-b125	0.894319	-73.442815	18.35	1.18	4873	4689394964794328320	4.2	141.23 ± 0.54	1.01 ± 0.24	-1.06 ± 0.08	0.99	0.99	0000000	M2FS
SMC	Lindsay 1	L1-1-b126	0.897378	-73.449529	18.99	0.84	5036	4689394758636096768	2.1	140.55 ± 2.38	2.47 ± 0.61	-1.75 ± 0.25	-1.00	-1.00	0000001	M2FS
SMC	Lindsay 1	L1-1-b127	0.887068	-73.454311	19.18	0.97	5077	4689394758636092416	2.1	139.16 ± 1.36	1.68 ± 0.55	-1.25 ± 0.20	0.99	0.99	0000000	M2FS
SMC	Lindsay 1	L1-1-b128	0.887855	-73.458441	19.15	0.91	5070	4689394758636091264	1.4	138.29 ± 1.51	1.69 ± 0.73	-1.69 ± 0.30	0.99	0.99	0000000	M2FS
SMC	Lindsay 1	L1-1-r028	0.949844	-73.473660	17.51	1.28	4649	4689393903938079488	5.8	138.98 ± 0.37	1.27 ± 0.13	-1.07 ± 0.06	1.00	1.00	0000000	M2FS
SMC	Lindsay 1	L1-1-r049	0.973088	-73.475177	17.93	1.17	4766	4689393899642470144	5.1	139.19 ± 0.55	0.95 ± 0.21	-1.11 ± 0.07	1.00	1.00	0000000	M2FS
SMC	Lindsay 1	L1-1-r079	0.969330	-73.469748	18.11	1.01	4811	4689393899642472960	4.0	141.80 ± 0.59	1.21 ± 0.29	-1.26 ± 0.09	1.00	1.00	0000000	M2FS
SMC	Lindsay 1	L1-1-r127	0.991379	-73.469925	17.57	1.22	4667	4689393899642472320	6.2	140.72 ± 0.50	1.15 ± 0.16	-1.04 ± 0.06	1.00	1.00	0000000	M2FS
SMC	NGC 152	N152-1-b001	8.455949	-73.189326	17.38	1.34	4615	4688900360687023616	5.5	133.68 ± 0.45	1.25 ± 0.13	-0.75 ± 0.06	0.00	0.00	0000000	M2FS
SMC	NGC 152	N152-1-b002	8.428125	-73.141235	18.35	1.13	4883	4688901528904715264	3.8	135.59 ± 0.75	1.23 ± 0.30	-1.05 ± 0.09	0.00	0.00	0000000	M2FS
SMC	NGC 152	N152-1-b003	8.368734	-73.131395	15.59	2.20	4615	4688901700716744960	12.6	187.36 ± 0.61	1.92 ± 0.22	-0.33 ± 0.07	-1.00	-1.00	0100010	M2FS
SMC	NGC 152	N152-1-b004	8.423277	-73.130829	17.49	1.08	4615	4688901528918037760	7.0	165.02 ± 0.40	0.88 ± 0.15	-1.30 ± 0.05	0.00	0.00	0000000	M2FS
SMC	NGC 152	N152-1-b005	8.470469	-73.111890	18.49	1.01	4929	4688901833833691776	3.3	131.03 ± 1.15	1.18 ± 0.47	-1.30 ± 0.11	0.00	0.00	0000000	M2FS
SMC	NGC 152	N152-1-b006	8.374497	-73.110947	17.69	1.35	4671	4688904754411448192	4.9	190.40 ± 0.60	1.27 ± 0.17	-0.81 ± 0.07	0.00	0.00	0000000	M2FS
SMC	NGC 152	N152-1-b007	8.461279	-73.106954	18.24	1.25	4850	4688901902553184000	3.4	117.69 ± 0.91	1.05 ± 0.28	-0.75 ± 0.08	0.00	0.00	0000000	M2FS
SMC	NGC 152	N152-1-b008	8.445545	-73.082959	18.06	1.34	4789	4688904926210207104	2.9	163.67 ± 0.74	1.18 ± 0.31	-0.94 ± 0.10	0.00	0.00	0000000	M2FS
SMC	NGC 152	N152-1-b009	8.481301	-73.185161	18.35	1.11	4884	4688900459443993216	2.4	165.30 ± 0.98	2.15 ± 0.35	-1.08 ± 0.17	0.00	0.00	0000000	M2FS
SMC	NGC 152	N152-1-b010	8.619514	-73.140137	18.41	1.14	4904	4688900944802470016	2.7	125.43 ± 0.68	2.20 ± 0.28	-0.92 ± 0.13	0.00	0.00	0000000	M2FS
SMC	NGC 152	N152-1-b011	8.536726	-73.128588	18.05	1.33	4787	4688901597624090752	3.5	154.53 ± 0.67	0.98 ± 0.29	-1.28 ± 0.10	0.00	0.00	0000000	M2FS
SMC	NGC 152	N152-1-b012	8.619193	-73.123179	16.29	1.81	4615	4688901254040085120	8.6	144.81 ± 0.34	1.37 ± 0.13	-0.55 ± 0.04	0.00	0.00	0000010	M2FS
SMC	NGC 152	N152-1-b013	8.486490	-73.108839	18.49	1.21	4928	4688901833840593792	2.7	161.93 ± 1.09	0.98 ± 0.36	-0.97 ± 0.11	0.00	0.00	0000000	M2FS
SMC	NGC 152	N152-1-b014	8.566285	-73.094130	17.93	1.24	4742	4688902250472457216	3.2	134.09 ± 0.80	0.56 ± 0.29	-1.08 ± 0.09	0.00	0.00	0000000	M2FS
SMC	NGC 152	N152-1-b015	8.599262	-73.089711	18.40	1.20	4899	4688902250472445952	2.9	160.92 ± 0.91	1.63 ± 0.30	-0.86 ± 0.12	0.00	0.00	0000000	M2FS
SMC	NGC 152	N152-1-b016	8.555905	-73.088422	17.21	1.51	4615	4688902314870089344	5.0	162.19 ± 0.76	0.16 ± 0.13	-0.34 ± 0.11	0.00	0.00	0000000	M2FS
SMC	NGC 152	N152-1-b017	8.431695	-73.033834	17.54	1.44	4615	4688906030044107008	3.4	190.30 ± 0.51	1.54 ± 0.18	-0.58 ± 0.07	0.00	0.00	0000000	M2FS
SMC	NGC 152	N152-1-b018	8.469881	-73.034903	17.32	1.23	4615	4688905995683844096	3.8	110.20 ± 0.66	1.16 ± 0.21	-1.20 ± 0.09	0.00	0.00	0000000	M2FS
SMC	NGC 152	N152-1-b019	8.554058	-73.049652	18.22	1.15	4844	4688905544685571456	2.8	125.43 ± 0.72	0.97 ± 0.30	-0.97 ± 0.11	0.00	0.00	0000000	M2FS
SMC	NGC 152	N152-1-b020	8.439396	-73.051283	18.62	1.09	4968	4688905205409903104	2.0	165.25 ± 1.09	0.60 ± 0.40	-1.20 ± 0.16	0.00	0.00	0000000	M2FS
SMC	NGC 152	N152-1-b021	8.420801	-73.053081	18.07	1.31	4793	4688905957002414976	2.3	183.58 ± 0.92	0.80 ± 0.37	-0.78 ± 0.11	0.00	0.00	0000000	M2FS
SMC	NGC 152	N152-1-b022	8.358326	-73.058965	17.68	1.37	4666	4688905858244959360	2.7	157.57 ± 0.84	1.14 ± 0.27	-0.73 ± 0.10	0.00	0.00	0000000	M2FS
SMC	NGC 152	N152-1-b023	8.597759	-73.080454	17.47	1.34	4615	4688902349229844992	5.2	165.98 ± 0.32	1.01 ± 0.13	-0.90 ± 0.06	0.00	0.00	0000000	M2FS
SMC	NGC 152	N152-1-b024	8.363676	-73.103168	17.39	1.22	4615	4688904793093531648	3.6	150.76 ± 0.54	1.21 ± 0.20	-1.15 ± 0.09	0.00	0.00	0000000	M2FS
SMC	NGC 152	N152-1-b025	8.331490	-73.018313	17.35	1.38	4615	4689093870416022912	2.7	173.67 ± 0.69	1.34 ± 0.23	-0.80 ± 0.10	0.00	0.00	0000000	M2FS
SMC	NGC 152	N152-1-b026	8.308195	-73.058623	17.89	1.33	4731	4688905888282917760	2.3	186.04 ± 0.86	1.45 ± 0.33	-0.93 ± 0.12	0.00	0.00	0000000	M2FS
SMC	NGC 152	N152-1-b027	8.303315	-73.076817	17.65	1.40	4651	4688905819563404800	3.7	152.27 ± 0.59	0.90 ± 0.20	-0.76 ± 0.07	0.00	0.00	0000000	M2FS
SMC	NGC 152	N152-1-b028	8.322273	-73.095418	18.23	1.24	4847	4688904994929648768	2.1	150.35 ± 1.11	0.96 ± 0.47	-0.88 ± 0.12	0.00	0.00	0000000	M2FS
SMC	NGC 152	N152-1-b029	8.324572	-73.099373	18.41	1.20	4903	4688904994929641600	1.8	175.02 ± 0.83	2.02 ± 0.33	-0.75 ± 0.14	0.58	0.22	0000000	M2FS
SMC	NGC 152	N152-1-b030	8.320645	-73.104591	18.39	1.23	4896	4688904793093151744	1.9	160.17 ± 1.77	0.80 ± 0.41	-0.94 ± 0.17	0.00	0.00	0000000	M2FS

Table C.1: (*continued*) Sample of 3095 Targets from 26 Star Clusters

Galaxy	Cluster	ID	RAJ2000 (deg)	DEJ2000 (deg)	G (mag)	$G_{\rm BP} - G_{\rm RP}$ (mag)	$T_{\rm eff}$ (K)	*Gaia* DR2 ID	S/N	$v_{\rm los}$ ($\rm km\,s^{-1}$)	$\log g$ (dex)	$[{\rm Fe/H}]_{\rm raw}$ (dex)	P_M	P'_M	Flag[a]	Source[b]
(1)	(2)	(3)	(4)	(5)	(6)	(7)	(8)	(9)	(10)	(11)	(12)	(13)	(14)	(15)	(16)	(17)
SMC	NGC 152	N152-1-b031	8.336998	-73.105211	16.67	1.65	4615	4688904793093150080	7.7	127.76 ± 0.39	1.95 ± 0.11	-0.52 ± 0.05	0.00	0.00	0000010	M2FS
SMC	NGC 152	N152-1-b032	8.300504	-73.109118	18.09	1.20	4801	4688903311302993152	2.7	107.81 ± 0.83	1.62 ± 0.24	-0.76 ± 0.13	0.00	0.00	0000000	M2FS
SMC	NGC 152	N152-1-b036	8.263042	-73.155194	18.42	1.11	4906	4688900184566137088	2.8	168.55 ± 0.63	1.08 ± 0.39	-1.13 ± 0.10	0.01	0.00	0000000	M2FS
SMC	NGC 152	N152-1-b037	8.259351	-73.151091	17.79	1.26	4702	4688900253285620608	4.1	148.91 ± 0.50	1.27 ± 0.18	-0.65 ± 0.07	0.00	0.00	0000000	M2FS
SMC	NGC 152	N152-1-b038	8.272837	-73.149707	18.17	1.13	4825	4688900218925888512	3.8	173.15 ± 0.80	1.39 ± 0.24	-1.09 ± 0.09	-1.00	-1.00	0000001	M2FS
SMC	NGC 152	N152-1-b039	8.266512	-73.124963	17.48	1.29	4615	4688903242609740544	6.3	173.93 ± 0.30	1.09 ± 0.11	-0.89 ± 0.05	0.96	0.97	0000000	M2FS
SMC	NGC 152	N152-1-b040	8.238936	-73.125032	18.81	1.01	5024	4688903276969414656	1.0	171.93 ± 1.72	1.53 ± 0.68	-0.92 ± 0.25	-1.00	-1.00	1000000	M2FS
SMC	NGC 152	N152-1-b042	8.315154	-73.152796	16.46	1.66	4615	4688900012767456256	10.2	132.68 ± 0.26	1.28 ± 0.11	-0.65 ± 0.04	0.00	0.00	0000010	M2FS
SMC	NGC 152	N152-1-b043	8.345216	-73.143144	17.37	1.43	4615	4688901696394660864	3.6	148.96 ± 0.60	1.50 ± 0.20	-0.84 ± 0.08	0.00	0.00	0000000	M2FS
SMC	NGC 152	N152-1-b044	8.316759	-73.142903	17.48	1.36	4615	4688900223248337024	5.8	159.35 ± 0.47	1.36 ± 0.12	-0.87 ± 0.06	0.00	0.00	0000000	M2FS
SMC	NGC 152	N152-1-b045	8.283544	-73.140271	17.19	1.33	4615	4688900291967502720	4.6	179.32 ± 0.45	0.98 ± 0.16	-1.01 ± 0.07	0.00	0.00	0000000	M2FS
SMC	NGC 152	N152-1-b046	8.356772	-73.126940	18.05	1.29	4786	4688901769436212224	4.9	169.45 ± 0.68	1.54 ± 0.17	-0.97 ± 0.07	0.06	0.00	0000000	M2FS
SMC	NGC 152	N152-1-b047	8.321098	-73.124069	17.30	1.20	4615	4688904724373713408	6.4	182.20 ± 0.43	1.01 ± 0.16	-1.38 ± 0.06	0.00	0.00	0000000	M2FS
SMC	NGC 152	N152-1-b048	8.305505	-73.124055	18.61	1.10	4966	4688903246904967040	2.3	173.05 ± 0.91	1.46 ± 0.40	-0.90 ± 0.13	0.88	0.85	0000000	M2FS
SMC	NGC 152	N152-1-b050	8.284726	-73.091063	18.25	1.22	4854	4688903586180381440	2.5	161.04 ± 0.83	0.88 ± 0.36	-0.84 ± 0.11	0.00	0.00	0000000	M2FS
SMC	NGC 152	N152-1-b051	8.272573	-73.099045	17.94	1.08	4748	4688903521769416448	3.6	148.53 ± 1.61	2.79 ± 0.26	-1.87 ± 0.15	-1.00	-1.00	0100000	M2FS
SMC	NGC 152	N152-1-b052	8.271188	-73.103631	18.54	1.14	4943	4688903521782839040	0.7	159.09 ± 83.60	1.41 ± 1.09	-0.99 ± 0.59	-1.00	-1.00	1000000	M2FS
SMC	NGC 152	N152-1-b053	8.290116	-73.105993	16.86	1.51	4615	4688903521782840192	5.7	176.41 ± 0.36	1.20 ± 0.13	-0.62 ± 0.05	0.63	0.00	0000000	M2FS
SMC	NGC 152	N152-1-b054	8.288343	-73.110027	18.39	1.09	4898	4688903311329270144	2.4	159.52 ± 1.16	0.80 ± 0.42	-1.29 ± 0.14	0.00	0.00	0000000	M2FS
SMC	NGC 152	N152-1-b055	8.273986	-73.112006	18.23	1.12	4847	4688903315624422272	2.4	142.28 ± 0.96	1.26 ± 0.39	-1.37 ± 0.13	0.00	0.00	0000000	M2FS
SMC	NGC 152	N152-1-b056	8.294162	-73.118106	17.70	1.28	4674	4688903315624431104	2.8	173.53 ± 0.62	1.47 ± 0.22	-0.71 ± 0.09	0.92	0.95	0000000	M2FS
SMC	NGC 152	N152-1-b057	8.247621	-73.006376	17.98	1.31	4765	4689092637757796992	1.5	146.50 ± 1.90	1.96 ± 0.53	-0.85 ± 0.24	0.00	0.00	0000000	M2FS
SMC	NGC 152	N152-1-b059	8.268274	-73.082685	17.94	1.24	4748	4688904346416523520	3.6	116.51 ± 0.56	1.07 ± 0.26	-1.18 ± 0.08	0.00	0.00	0000000	M2FS
SMC	NGC 152	N152-1-b060	8.250028	-73.087142	17.13	1.40	4615	4688904346416533888	5.0	162.28 ± 0.43	0.86 ± 0.16	-1.07 ± 0.06	0.00	0.00	0000000	M2FS
SMC	NGC 152	N152-1-b061	8.265398	-73.095201	18.24	1.20	4849	4688903586180370048	2.0	175.71 ± 0.98	1.70 ± 0.34	-0.96 ± 0.16	0.74	0.13	0000000	M2FS
SMC	NGC 152	N152-1-b062	8.241868	-73.098846	17.53	1.23	4615	4688903590502311936	5.3	172.97 ± 0.51	1.21 ± 0.18	-1.07 ± 0.07	-1.00	-1.00	0000001	M2FS
SMC	NGC 152	N152-1-b063	8.250509	-73.111799	16.01	2.82	4615	4688903517530542464	1.9	173.91 ± 2.08	0.50 ± 0.44	-1.18 ± 0.20	-1.00	-1.00	0010010	M2FS
SMC	NGC 152	N152-1-b064	8.264566	-73.118961	18.02	1.17	4777	4688903315624440704	2.5	174.90 ± 0.96	1.00 ± 0.34	-0.71 ± 0.10	1.00	1.00	0000000	M2FS
SMC	NGC 152	N152-1-b067	8.187116	-73.200257	17.23	1.39	4615	4688899810931253376	5.6	112.24 ± 0.40	0.46 ± 0.18	-0.98 ± 0.05	0.00	0.00	0000000	M2FS
SMC	NGC 152	N152-1-b068	8.177635	-73.185072	17.29	1.30	4615	4688899879650714624	6.3	101.14 ± 0.44	0.74 ± 0.16	-1.06 ± 0.06	0.00	0.00	0000000	M2FS
SMC	NGC 152	N152-1-b069	8.164091	-73.148671	18.12	1.31	4809	4688903105143901568	3.1	108.36 ± 0.68	0.29 ± 0.22	-0.43 ± 0.08	0.00	0.00	0000000	M2FS
SMC	NGC 152	N152-1-b070	8.155388	-73.136010	18.61	1.14	4965	4688903178172207360	1.1	177.19 ± 1.62	1.33 ± 0.77	-0.99 ± 0.21	0.03	0.01	0000000	M2FS
SMC	NGC 152	N152-1-b071	8.167956	-73.132457	18.27	1.15	4859	4688903173864014464	2.9	145.38 ± 0.88	1.24 ± 0.32	-1.03 ± 0.12	0.00	0.00	0000000	M2FS
SMC	NGC 152	N152-1-b072	8.183023	-73.124365	16.98	1.46	4615	4688903380021923200	6.3	195.10 ± 0.37	0.96 ± 0.14	-0.93 ± 0.05	0.00	0.00	0000000	M2FS
SMC	NGC 152	N152-1-b074	8.210579	-73.217931	18.29	1.24	4866	4688898981975140736	2.0	114.44 ± 1.61	1.10 ± 0.62	-1.09 ± 0.20	0.00	0.00	0000000	M2FS
SMC	NGC 152	N152-1-b075	8.203385	-73.153294	17.61	1.43	4644	4688900154528575104	4.8	133.97 ± 0.43	0.88 ± 0.16	-0.90 ± 0.06	0.00	0.00	0000000	M2FS
SMC	NGC 152	N152-1-b076	8.229065	-73.151119	17.01	1.49	4615	4688900257607783808	5.6	153.09 ± 0.28	1.46 ± 0.12	-0.68 ± 0.05	0.00	0.00	0000000	M2FS
SMC	NGC 152	N152-1-b077	8.215557	-73.143616	17.71	1.29	4676	4688903212545275520	5.0	169.02 ± 0.54	0.34 ± 0.19	-1.18 ± 0.06	0.38	0.00	0000000	M2FS
SMC	NGC 152	N152-1-b078	8.232288	-73.135199	18.17	1.10	4828	4688903212545262592	5.4	148.46 ± 0.97	2.20 ± 0.18	-1.38 ± 0.09	0.00	0.00	0000000	M2FS
SMC	NGC 152	N152-1-b079	8.232401	-73.129774	18.54	1.06	4944	4688903276969402368	2.3	98.01 ± 1.30	1.09 ± 0.47	-1.00 ± 0.16	0.00	0.00	0000000	M2FS
SMC	NGC 152	N152-1-b080	8.204374	-73.126148	17.96	1.26	4757	4688903276949582720	3.1	171.22 ± 0.74	0.91 ± 0.26	-0.62 ± 0.08	0.96	0.96	0000000	M2FS
SMC	NGC 152	N152-1-b081	8.232917	-73.009448	17.28	1.46	4615	4689092633465443712	1.4	124.28 ± 1.78	1.67 ± 0.42	-0.69 ± 0.19	0.00	0.00	0000000	M2FS
SMC	NGC 152	N152-1-b082	8.232249	-73.061221	18.41	1.25	4904	4688904621294401792	1.3	129.84 ± 3.21	3.38 ± 0.59	-1.16 ± 0.30	-1.00	-1.00	0001000	M2FS
SMC	NGC 152	N152-1-b083	8.219213	-73.094124	16.20	1.76	4615	4688904312056812544	9.1	100.66 ± 0.32	1.80 ± 0.11	-0.59 ± 0.05	0.00	0.00	0000010	M2FS
SMC	NGC 152	N152-1-b084	8.217937	-73.101725	18.33	1.09	4879	4688903556142583552	1.9	106.12 ± 1.50	2.26 ± 0.40	-1.25 ± 0.20	0.00	0.00	0000000	M2FS
SMC	NGC 152	N152-1-b085	8.237028	-73.104398	18.13	1.20	4813	4688903556142584960	3.2	173.13 ± 0.52	1.08 ± 0.28	-0.74 ± 0.08	1.00	1.00	0000000	M2FS
SMC	NGC 152	N152-1-b086	8.220942	-73.110171	15.95	2.68	4615	4688903487409738752	2.3	177.36 ± 3.17	2.98 ± 0.66	-2.68 ± 0.29	-1.00	-1.00	0110010	M2FS
SMC	NGC 152	N152-1-b087	8.236222	-73.112291	17.29	1.23	4615	4688903483170752512	4.5	171.60 ± 0.44	1.09 ± 0.15	-0.73 ± 0.06	1.00	1.00	0000000	M2FS
SMC	NGC 152	N152-1-b088	8.218790	-73.120444	17.86	1.17	4728	4688903483170967808	3.1	173.77 ± 0.60	1.50 ± 0.21	-0.71 ± 0.09	1.00	1.00	0000000	M2FS
SMC	NGC 152	N152-1-b089	8.194749	-73.023483	18.16	1.19	4824	4689092599105700608	1.4	146.71 ± 1.58	3.45 ± 0.39	-0.87 ± 0.27	-1.00	-1.00	0001000	M2FS
SMC	NGC 152	N152-1-b090	8.204450	-73.081232	18.60	1.09	4963	4688904376454376704	1.4	160.35 ± 1.09	1.76 ± 0.48	-0.68 ± 0.18	0.00	0.00	0000000	M2FS
SMC	NGC 152	N152-1-b091	8.200312	-73.093844	18.57	1.01	4952	4688904307804475008	1.1	138.12 ± 1.87	0.62 ± 0.50	-0.95 ± 0.25	0.00	0.00	0000000	M2FS
SMC	NGC 152	N152-1-b092	8.184741	-73.096117	18.39	1.33	4898	4688904307734867584	1.1	180.39 ± 1.51	2.33 ± 1.00	-1.06 ± 0.28	0.02	0.00	0000000	M2FS
SMC	NGC 152	N152-1-b093	8.188839	-73.110189	17.80	1.23	4705	4688903551820589568	3.3	173.05 ± 0.58	1.04 ± 0.26	-0.79 ± 0.08	0.96	0.98	0000000	M2FS

Table C.1: (*continued*) Sample of 3095 Targets from 26 Star Clusters

Galaxy	Cluster	ID	RAJ2000 (deg)	DEJ2000 (deg)	G (mag)	$G_{\rm BP} - G_{\rm RP}$ (mag)	$T_{\rm eff}$ (K)	*Gaia* DR2 ID	S/N	$v_{\rm los}$ (km s^{-1})	log g (dex)	[Fe/H]$_{\rm raw}$ (dex)	P_M	P'_M	Flag[a]	Source[b]
(1)	(2)	(3)	(4)	(5)	(6)	(7)	(8)	(9)	(10)	(11)	(12)	(13)	(14)	(15)	(16)	(17)
SMC	NGC 152	N152-1-b094	8.213947	-73.115971	18.14	1.04	4817	4688903487423137664	1.7	171.27 ± 1.31	1.41 ± 0.46	-0.78 ± 0.15	1.00	1.00	0000000	M2FS
SMC	NGC 152	N152-1-b095	8.186609	-73.118407	18.67	1.04	4983	4688903384343935232	1.7	172.58 ± 1.15	1.88 ± 0.54	-1.01 ± 0.16	0.96	0.98	0000000	M2FS
SMC	NGC 152	N152-1-b096	8.207097	-73.121813	17.46	1.30	4615	4688903487423152000	3.9	173.33 ± 0.57	1.19 ± 0.18	-0.76 ± 0.07	1.00	1.00	0000000	M2FS
SMC	NGC 152	N152-1-b097	8.068279	-73.208531	18.38	1.14	4894	4688899463046846208	2.0	141.71 ± 1.51	2.39 ± 0.45	-1.10 ± 0.25	0.00	0.00	0000000	M2FS
SMC	NGC 152	N152-1-b098	7.947713	-73.178978	16.25	2.89	4615	4688902628429800704	1.1	182.03 ± 49.13	2.00 ± 1.08	-2.37 ± 0.54	-1.00	-1.00	1010010	M2FS
SMC	NGC 152	N152-1-b099	8.081954	-73.172897	17.95	1.24	4753	4688902697149257600	4.5	106.24 ± 0.70	1.26 ± 0.22	-1.17 ± 0.08	0.00	0.00	0000000	M2FS
SMC	NGC 152	N152-1-b100	7.903057	-73.172964	17.99	1.15	4770	4688902864625650816	2.7	202.82 ± 1.19	0.42 ± 0.33	-2.02 ± 0.15	0.00	0.00	0000000	M2FS
SMC	NGC 152	N152-1-b101	8.007777	-73.151967	18.43	1.07	4910	4688903006373584128	2.7	157.23 ± 0.91	1.43 ± 0.28	-0.76 ± 0.11	0.00	0.00	0000000	M2FS
SMC	NGC 152	N152-1-b102	7.859894	-73.150094	18.54	1.14	4944	4688903689259422208	1.4	158.94 ± 2.12	0.67 ± 0.48	-1.24 ± 0.24	0.00	0.00	0000000	M2FS
SMC	NGC 152	N152-1-b103	7.883095	-73.137114	18.12	1.07	4810	4688903899740077184	2.8	176.48 ± 1.17	0.67 ± 0.39	-1.41 ± 0.12	0.00	0.00	0000000	M2FS
SMC	NGC 152	N152-1-b104	7.916481	-73.135894	17.11	1.40	4615	4688903727941379072	5.7	195.06 ± 0.38	0.61 ± 0.17	-0.95 ± 0.05	0.00	0.00	0000000	M2FS
SMC	NGC 152	N152-1-b105	8.112437	-73.214434	18.22	1.28	4845	4688899394292000128	2.4	134.88 ± 1.01	1.90 ± 0.30	-0.68 ± 0.12	0.00	0.00	0000000	M2FS
SMC	NGC 152	N152-1-b106	8.102015	-73.198725	18.07	1.28	4794	4688899463011511936	3.3	191.10 ± 0.64	1.77 ± 0.24	-0.57 ± 0.08	0.00	0.00	0000000	M2FS
SMC	NGC 152	N152-1-b107	8.140381	-73.167059	18.37	1.23	4889	4688900115846621824	3.6	152.70 ± 0.85	0.79 ± 0.38	-1.43 ± 0.11	0.00	0.00	0000000	M2FS
SMC	NGC 152	N152-1-b108	8.116245	-73.152588	17.98	1.31	4767	4688903139503630720	3.8	173.16 ± 0.49	1.32 ± 0.20	-0.77 ± 0.08	0.26	0.40	0000000	M2FS
SMC	NGC 152	N152-1-b109	8.119616	-73.146239	18.04	1.19	4784	4688903139503641344	3.9	124.64 ± 0.69	1.40 ± 0.20	-0.76 ± 0.07	0.00	0.00	0000000	M2FS
SMC	NGC 152	N152-1-b110	8.128396	-73.138939	17.69	1.33	4671	4688903349984233472	4.7	165.12 ± 0.39	0.69 ± 0.19	-1.15 ± 0.06	0.00	0.00	0000000	M2FS
SMC	NGC 152	N152-1-b111	8.147488	-73.130183	18.40	1.20	4901	4688903380021848576	3.0	172.75 ± 0.81	1.80 ± 0.25	-0.78 ± 0.11	0.76	0.74	0000000	M2FS
SMC	NGC 152	N152-1-b112	8.127998	-73.127708	17.97	1.30	4759	4688903345662114688	5.0	189.40 ± 0.41	1.35 ± 0.16	-0.64 ± 0.06	0.00	0.00	0000000	M2FS
SMC	NGC 152	N152-1-b116	8.154787	-73.089260	17.44	1.32	4615	4688904273444777088	4.4	132.49 ± 0.59	1.12 ± 0.19	-0.94 ± 0.07	0.00	0.00	0000000	M2FS
SMC	NGC 152	N152-1-b117	8.176802	-73.090352	18.52	1.05	4939	4688904376454358272	2.2	146.11 ± 1.44	0.56 ± 0.38	-0.95 ± 0.15	0.00	0.00	0000000	M2FS
SMC	NGC 152	N152-1-b118	8.119310	-73.107094	18.26	1.17	4858	4688904174617904640	2.3	119.74 ± 1.50	1.59 ± 0.40	-0.96 ± 0.13	0.00	0.00	0000000	M2FS
SMC	NGC 152	N152-1-b119	8.146882	-73.112541	18.05	1.03	4786	4688903448811015424	2.5	123.40 ± 1.38	0.53 ± 0.36	-2.02 ± 0.15	0.00	0.00	0000000	M2FS
SMC	NGC 152	N152-1-b120	8.178515	-73.113580	18.36	1.06	4887	4688903453050039680	1.6	170.63 ± 1.47	2.58 ± 0.37	-0.58 ± 0.19	0.90	0.89	0000000	M2FS
SMC	NGC 152	N152-1-b121	8.109994	-73.022498	18.10	1.23	4803	4689092564745960960	1.2	150.62 ± 2.22	2.22 ± 0.82	-1.23 ± 0.29	-1.00	-1.00	1000000	M2FS
SMC	NGC 152	N152-1-b122	8.094593	-73.041859	17.56	1.41	4617	4689092500318859648	2.6	147.01 ± 1.02	1.68 ± 0.22	-0.72 ± 0.11	0.00	0.00	0000000	M2FS
SMC	NGC 152	N152-1-b123	8.095594	-73.066180	17.57	1.02	4620	4689092186808355200	3.0	142.82 ± 0.90	0.92 ± 0.37	-1.51 ± 0.12	0.00	0.00	0000000	M2FS
SMC	NGC 152	N152-1-b124	8.056862	-73.068404	17.98	1.22	4767	4689092186788829312	1.2	157.96 ± 1.79	0.70 ± 0.45	-0.65 ± 0.22	0.00	0.00	0000000	M2FS
SMC	NGC 152	N152-1-b125	7.866233	-73.086879	18.45	1.21	4917	4689091911910919168	0.8	149.62 ± 3.77	1.73 ± 0.87	-0.65 ± 0.30	-1.00	-1.00	1000000	M2FS
SMC	NGC 152	N152-1-b126	7.934986	-73.092177	18.52	1.14	4938	4689091778764429440	1.2	170.39 ± 2.21	1.80 ± 0.69	-1.08 ± 0.29	0.00	0.00	0000000	M2FS
SMC	NGC 152	N152-1-b127	8.096942	-73.092476	16.21	1.65	4615	4688904449495784576	8.3	176.72 ± 0.34	1.36 ± 0.11	-0.70 ± 0.05	0.00	0.00	0000010	M2FS
SMC	NGC 152	N152-1-b128	8.099780	-73.111786	18.56	1.11	4949	4688904170295868544	1.5	154.14 ± 1.78	2.17 ± 0.64	-0.88 ± 0.20	0.00	0.00	0000000	M2FS
SMC	NGC 152	N152-1-r049	8.243680	-73.120833	17.12	1.29	4615	4688903281264712320	9.3	172.69 ± 0.33	1.39 ± 0.08	-0.82 ± 0.04	1.00	1.00	0000000	M2FS
SMC	NGC 152	N152-1-r079	8.228042	-73.116721	17.26	1.21	4615	4688903487423134976	6.2	170.80 ± 0.38	1.16 ± 0.12	-0.83 ± 0.05	1.00	1.00	0000000	M2FS
SMC	NGC 152	N152-1-r099	8.245365	-73.116650	17.09	1.30	4615	4688903276942707712	8.2	164.18 ± 0.36	1.03 ± 0.11	-0.81 ± 0.04	1.00	-1.00	0000000	M2FS
SMC	NGC 152	N152-1-r127	8.251379	-73.124988	17.11	1.46	4615	4688903276942708352	7.6	171.42 ± 0.35	1.45 ± 0.11	-0.64 ± 0.05	1.00	1.00	0000000	M2FS
SMC	NGC 330	N330-1-b001	14.241090	-72.531883	13.72	1.67	4205	4688995193594265856	20.1	163.70 ± 0.25	0.02 ± 0.02	-0.71 ± 0.03	0.00	0.00	0000000	M2FS
SMC	NGC 330	N330-1-b002	14.157670	-72.484260	14.81	2.02	3841	4688996323122765056	14.3	101.16 ± 0.27	0.49 ± 0.05	-0.74 ± 0.04	0.00	0.00	0000000	M2FS
SMC	NGC 330	N330-1-b004	14.170223	-72.435978	15.06	1.46	4501	4688999591640594432	20.8	135.44 ± 0.18	0.13 ± 0.08	-0.78 ± 0.03	0.00	0.00	0000000	M2FS
SMC	NGC 330	N330-1-b006	14.209092	-72.364483	15.05	1.40	4598	4689000862950649856	25.1	119.56 ± 0.23	0.20 ± 0.11	-0.69 ± 0.03	0.00	0.00	0000000	M2FS
SMC	NGC 330	N330-1-b009	14.282802	-72.520843	14.88	1.49	4453	4688995193594252160	12.7	142.45 ± 0.23	0.10 ± 0.08	-0.81 ± 0.03	0.00	0.00	0000000	M2FS
SMC	NGC 330	N330-1-b010	14.437354	-72.494138	14.77	1.21	4964	4688995502831841920	13.5	159.04 ± 0.33	0.05 ± 0.04	-0.44 ± 0.03	0.00	0.00	0000000	M2FS
SMC	NGC 330	N330-1-b011	14.268847	-72.494510	13.57	1.61	4284	4688996116962618752	30.9	152.35 ± 0.27	0.01 ± 0.01	-0.75 ± 0.03	0.00	0.00	0000000	M2FS
SMC	NGC 330	N330-1-b012	14.342093	-72.481335	14.71	1.54	4388	4688996155666853632	17.2	146.55 ± 0.21	0.04 ± 0.04	-0.80 ± 0.03	0.00	0.00	0000000	M2FS
SMC	NGC 330	N330-1-b013	14.249667	-72.474580	14.94	1.13	5162	4688996396185018368	22.0	158.53 ± 0.25	0.04 ± 0.04	-0.42 ± 0.03	0.00	0.00	0000000	M2FS
SMC	NGC 330	N330-1-b014	14.383778	-72.420067	14.00	1.70	4159	4688999866518403968	25.8	134.34 ± 0.24	0.02 ± 0.02	-0.75 ± 0.03	0.00	0.00	0000000	M2FS
SMC	NGC 330	N330-1-b015	14.249868	-72.401029	14.83	1.39	4616	4688999793486060928	25.0	159.62 ± 0.20	0.58 ± 0.07	-0.76 ± 0.03	0.00	0.00	0000000	M2FS
SMC	NGC 330	N330-1-b016	14.299520	-72.369571	13.74	1.40	4593	4689001000389604608	44.7	149.19 ± 0.29	0.02 ± 0.02	-0.70 ± 0.03	0.00	0.00	0000000	M2FS
SMC	NGC 330	N330-1-b033	14.045783	-72.440569	13.80	1.54	4386	4688994472036827392	37.0	133.30 ± 0.25	0.02 ± 0.02	-0.64 ± 0.03	0.00	0.00	0000000	M2FS
SMC	NGC 330	N330-1-b034	14.049803	-72.418853	13.48	1.76	4095	4688994575116022144	38.1	144.58 ± 0.25	0.01 ± 0.01	-0.74 ± 0.03	0.00	0.00	0000000	M2FS
SMC	NGC 330	N330-1-b035	14.058742	-72.405409	14.44	1.66	4222	4688994781274444160	27.8	136.19 ± 0.24	0.11 ± 0.07	-0.74 ± 0.03	0.00	0.00	0000000	M2FS
SMC	NGC 330	N330-1-b043	14.098930	-72.508791	14.70	1.52	4416	4688990348868473600	11.3	139.48 ± 0.24	0.19 ± 0.11	-0.79 ± 0.03	0.00	0.00	0000000	M2FS
SMC	NGC 330	N330-1-b044	14.102403	-72.479167	15.14	1.32	4730	4688993406885108352	18.7	142.98 ± 0.22	0.16 ± 0.11	-0.61 ± 0.03	0.00	0.00	0000000	M2FS
SMC	NGC 330	N330-1-b045	14.127163	-72.476381	14.88	1.47	4485	4688993406885097600	15.4	119.99 ± 0.26	0.45 ± 0.09	-0.63 ± 0.03	0.00	0.00	0000000	M2FS

Table C.1: (*continued*) Sample of 3095 Targets from 26 Star Clusters

Galaxy	Cluster	ID	RAJ2000 (deg)	DEJ2000 (deg)	G (mag)	$G_{\rm BP} - G_{\rm RP}$ (mag)	$T_{\rm eff}$ (K)	*Gaia* DR2 ID	S/N	$v_{\rm los}$ (km s^{-1})	log g (dex)	[Fe/H]$_{\rm raw}$ (dex)	P_M	P'_M	Flag[a]	Source[b]
(1)	(2)	(3)	(4)	(5)	(6)	(7)	(8)	(9)	(10)	(11)	(12)	(13)	(14)	(15)	(16)	(17)
SMC	NGC 330	N330-1-b067	14.007271	-72.499910	13.55	1.34	4706	4688993269446225152	0.3	-57.49 ± 161.03	3.20 ± 1.24	-1.53 ± 1.35	-1.00	-1.00	1000000	M2FS
SMC	NGC 330	N330-1-b068	14.039260	-72.469297	14.11	1.41	4586	4688993643141502336	34.8	148.28 ± 0.41	1.34 ± 0.06	-1.13 ± 0.03	-1.00	-1.00	0000001	M2FS
SMC	NGC 330	N330-1-b069	14.004046	-72.461011	13.68	1.39	4624	4688993716122719872	47.5	139.13 ± 0.27	0.02 ± 0.02	-0.57 ± 0.03	0.00	0.00	0000000	M2FS
SMC	NGC 330	N330-1-b070	14.024289	-72.405803	15.36	1.22	4944	4688994849993921792	18.0	116.71 ± 0.19	0.65 ± 0.08	-0.82 ± 0.03	0.00	0.00	0000000	M2FS
SMC	NGC 330	N330-1-b097	13.813993	-72.533026	15.45	1.12	5208	4688992788410039808	15.0	100.30 ± 0.35	0.16 ± 0.11	-0.50 ± 0.03	0.00	0.00	0000000	M2FS
SMC	NGC 330	N330-1-b098	13.821494	-72.516326	15.21	1.29	4802	4688993097647625088	17.0	129.75 ± 0.35	0.41 ± 0.12	-0.66 ± 0.03	0.00	0.00	0000000	M2FS
SMC	NGC 330	N330-1-b099	13.789400	-72.515455	13.33	1.63	4260	4688993063287889664	44.8	149.38 ± 0.31	0.01 ± 0.01	-0.71 ± 0.03	0.00	0.00	0000000	M2FS
SMC	NGC 330	N330-1-b100	13.803221	-72.511779	13.31	1.64	4241	4688993063287873664	47.5	153.12 ± 0.29	0.01 ± 0.01	-0.75 ± 0.03	0.00	0.00	0000000	M2FS
SMC	NGC 330	N330-1-b101	13.770097	-72.481635	15.47	1.22	4938	4688994094079933568	19.7	128.94 ± 0.21	0.49 ± 0.08	-0.67 ± 0.03	0.00	0.00	0000000	M2FS
SMC	NGC 330	N330-1-b102	13.875608	-72.480468	13.43	1.66	4222	4688993956640956928	41.1	153.85 ± 0.23	0.01 ± 0.01	-0.72 ± 0.03	0.00	0.00	0000000	M2FS
SMC	NGC 330	N330-1-b103	13.744814	-72.469101	15.24	1.44	4532	4688994162799378688	22.2	111.26 ± 0.21	0.21 ± 0.10	-0.80 ± 0.03	0.00	0.00	0000000	M2FS
SMC	NGC 330	N330-1-b104	13.825936	-72.442789	13.88	1.61	4282	4688994300238250368	32.1	243.07 ± 6.33	0.22 ± 0.19	-4.76 ± 0.05	-1.00	-1.00	1000000	M2FS
SMC	NGC 330	N330-1-b106	13.891704	-72.536923	14.99	1.54	4386	4688989902192014848	17.3	147.87 ± 0.24	0.21 ± 0.10	-0.72 ± 0.03	0.00	0.00	0000000	M2FS
SMC	NGC 330	N330-1-b107	13.966813	-72.517690	14.86	1.40	4607	4688993235086552576	22.7	142.74 ± 0.21	0.13 ± 0.09	-0.68 ± 0.03	0.00	0.00	0000000	M2FS
SMC	NGC 330	N330-1-b108	13.876586	-72.510561	15.13	1.51	4424	4688993132007331456	19.0	151.80 ± 0.23	0.39 ± 0.08	-0.70 ± 0.03	0.00	0.00	0000000	M2FS
SMC	NGC 330	N330-1-b109	13.967765	-72.466541	14.54	1.44	4536	4688993613043525888	30.5	129.70 ± 0.20	0.14 ± 0.09	-0.75 ± 0.03	0.00	0.00	0000000	M2FS
SMC	NGC 330	N330-1-b110	13.935169	-72.461018	13.99	1.62	4271	4688994334598020096	34.4	129.72 ± 0.22	0.03 ± 0.03	-0.72 ± 0.03	0.00	0.00	0000000	M2FS
SMC	NGC 330	N330-1-r028	14.068979	-72.451286	14.35	1.58	4327	4688993750482336640	32.6	149.90 ± 0.17	0.06 ± 0.05	-0.71 ± 0.03	1.00	1.00	0000000	M2FS+Pa20
SMC	NGC 330	N330-1-r049	14.079309	-72.468949	13.00	1.74	4116	4688993471264541056	51.0	156.75 ± 0.35	0.02 ± 0.02	-0.71 ± 0.03	1.00	1.00	0000000	M2FS+Pa20
SMC	NGC 330	N330-1-r099	14.090405	-72.459956	13.60	1.29	4792	4688993681762966400	33.9	151.99 ± 0.27	0.02 ± 0.02	-0.56 ± 0.03	1.00	1.00	0000000	M2FS+Pa20
SMC	NGC 330	N330-1-r127	14.113887	-72.468456	13.77	1.54	4381	4688993471342994048	45.6	151.82 ± 0.19	0.02 ± 0.02	-0.73 ± 0.03	1.00	1.00	0000000	M2FS+Pa20
SMC	NGC 330	A6	14.057897	-72.459001	–	–	–	–	–	154.43 ± 1.10	–	–	1.00	1.00	0000000	Pa20
SMC	NGC 330	A7	14.060674	-72.461792	–	–	–	–	–	151.53 ± 0.90	–	–	1.00	1.00	0000000	Pa20
SMC	NGC 330	A9	14.053589	-72.462953	–	–	–	–	–	153.53 ± 0.90	–	–	1.00	1.00	0000000	Pa20
SMC	NGC 330	A27	14.071179	-72.459725	–	–	–	–	–	148.23 ± 2.40	–	–	1.00	1.00	0000000	Pa20
SMC	NGC 330	A42	14.083926	-72.463082	–	–	–	–	–	153.03 ± 0.60	–	–	1.00	1.00	0000000	Pa20
SMC	NGC 330	A45	14.078450	-72.463194	–	–	–	–	–	151.13 ± 2.20	–	–	1.00	1.00	0000000	Pa20
SMC	NGC 330	A46	14.075067	-72.463848	–	–	–	–	–	156.63 ± 1.40	–	–	1.00	1.00	0000000	Pa20
SMC	NGC 330	A52	14.072379	-72.464592	–	–	–	–	–	161.23 ± 4.00	–	–	1.00	-1.00	0000000	Pa20
SMC	NGC 330	A57	14.081134	-72.464783	–	–	–	–	–	153.73 ± 1.50	–	–	1.00	1.00	0000000	Pa20
SMC	NGC 330	B40	14.105541	-72.471722	–	–	–	–	–	152.23 ± 1.10	–	–	1.00	1.00	0000000	Pa20
SMC	NGC 330	B10	14.151467	-72.446242	–	–	–	–	–	147.13 ± 4.00	–	–	0.00	0.00	0000000	Pa20
SMC	NGC 339	N339-1-b001	14.500860	-74.498237	19.18	1.07	5081	4684816117344798336	1.5	165.11 ± 2.49	0.90 ± 0.60	-0.81 ± 0.23	-1.00	-1.00	1000000	M2FS
SMC	NGC 339	N339-1-b002	14.481652	-74.498207	19.19	1.09	5083	4684816018556124160	1.7	158.14 ± 3.82	1.79 ± 0.73	-0.96 ± 0.28	-1.00	-1.00	0100000	M2FS
SMC	NGC 339	N339-1-b003	14.508306	-74.494279	18.67	0.91	4962	4684816117344838016	1.8	155.32 ± 3.13	1.04 ± 0.67	-1.07 ± 0.21	-1.00	-1.00	1000000	M2FS
SMC	NGC 339	N339-1-b004	14.483106	-74.491978	19.03	0.98	5047	4684816014265653760	1.7	169.13 ± 2.07	1.33 ± 0.82	-1.24 ± 0.26	0.00	0.00	0000000	M2FS
SMC	NGC 339	N339-1-b005	14.502807	-74.490019	18.20	1.24	4835	4684816117344875776	2.8	113.53 ± 1.31	0.68 ± 0.35	-0.88 ± 0.12	0.99	1.00	0000000	M2FS
SMC	NGC 339	N339-1-b006	14.503607	-74.485252	19.31	0.89	5108	4684827872673724160	0.7	115.11 ± 3.11	1.64 ± 0.95	-0.06 ± 0.28	-1.00	-1.00	0000001	M2FS
SMC	NGC 339	N339-1-b007	14.520168	-74.480445	17.91	1.26	4762	4684827868375479552	4.2	111.19 ± 0.65	0.98 ± 0.30	-0.93 ± 0.09	1.00	1.00	0000000	M2FS
SMC	NGC 339	N339-1-b008	14.504019	-74.478013	17.23	1.37	4564	4684827868377967232	7.3	111.00 ± 0.42	0.87 ± 0.14	-0.98 ± 0.06	1.00	1.00	0000000	M2FS
SMC	NGC 339	N339-1-b009	14.800366	-74.557328	17.56	1.38	4662	4684812101553383680	9.7	139.55 ± 0.35	0.88 ± 0.13	-1.03 ± 0.05	0.00	0.00	0000000	M2FS
SMC	NGC 339	N339-1-b010	14.690387	-74.545540	18.11	1.08	4811	4684815086552237952	7.3	171.23 ± 0.72	1.43 ± 0.16	-1.14 ± 0.06	0.00	0.00	0000000	M2FS
SMC	NGC 339	N339-1-b011	14.689154	-74.524106	16.89	1.46	4448	4684815361430344320	16.1	186.02 ± 0.19	0.82 ± 0.06	-0.87 ± 0.03	0.00	0.00	0000000	M2FS
SMC	NGC 339	N339-1-b012	14.787882	-74.502288	17.80	1.13	4729	4684815503167474176	9.3	164.96 ± 0.50	1.27 ± 0.16	-1.28 ± 0.06	0.00	0.00	0000000	M2FS
SMC	NGC 339	N339-1-b013	14.525092	-74.489793	18.99	1.13	5038	4684816117344887680	2.0	115.35 ± 2.51	0.90 ± 0.62	-0.97 ± 0.19	0.98	0.98	0000000	M2FS
SMC	NGC 339	N339-1-b015	14.536889	-74.487491	18.36	1.17	4876	4684816117344898688	2.8	163.08 ± 1.49	1.39 ± 0.63	-0.64 ± 0.12	0.00	0.00	0000000	M2FS
SMC	NGC 339	N339-1-b016	14.540495	-74.480792	17.89	1.35	4755	4684816121642832384	2.9	156.64 ± 0.87	1.97 ± 0.55	-0.40 ± 0.12	0.00	0.00	0000000	M2FS
SMC	NGC 339	N339-1-b017	14.735498	-74.366894	16.88	1.46	4445	4684829620723079296	12.3	152.99 ± 0.25	0.86 ± 0.07	-0.84 ± 0.04	0.00	0.00	0000000	M2FS
SMC	NGC 339	N339-1-b018	14.614899	-74.368194	17.30	1.42	4586	4684829693739461760	6.9	176.14 ± 0.38	0.68 ± 0.14	-0.87 ± 0.05	0.00	0.00	0000000	M2FS
SMC	NGC 339	N339-1-b019	14.578116	-74.375542	17.61	0.88	4677	4684829659379724800	14.4	140.60 ± 0.52	0.37 ± 0.19	-1.60 ± 0.04	-1.00	-1.00	0100010	M2FS
SMC	NGC 339	N339-1-b020	14.771426	-74.387131	17.32	1.54	4591	4684828796089206528	7.6	13.47 ± 0.36	4.93 ± 0.06	-0.45 ± 0.10	-1.00	-1.00	0001100	M2FS
SMC	NGC 339	N339-1-b021	14.786292	-74.396379	18.70	0.98	4967	4684828727369652480	3.7	141.48 ± 0.82	1.47 ± 0.36	-0.87 ± 0.09	0.00	0.00	0000000	M2FS
SMC	NGC 339	N339-1-b022	14.849873	-74.406879	18.37	1.16	4879	4684851920192971904	4.1	180.37 ± 0.67	1.04 ± 0.36	-0.91 ± 0.09	0.00	0.00	0000000	M2FS
SMC	NGC 339	N339-1-b023	14.785577	-74.460290	17.91	1.14	4761	4684816396512389120	8.7	136.13 ± 0.48	1.12 ± 0.14	-0.99 ± 0.05	0.00	0.00	0000000	M2FS

Table C.1: (*continued*) Sample of 3095 Targets from 26 Star Clusters

Galaxy	Cluster	ID	RAJ2000 (deg)	DEJ2000 (deg)	G (mag)	$G_{\rm BP} - G_{\rm RP}$ (mag)	$T_{\rm eff}$ (K)	*Gaia* DR2 ID	S/N	$v_{\rm los}$ ($\rm km\,s^{-1}$)	$\log g$ (dex)	$[{\rm Fe/H}]_{\rm raw}$ (dex)	P_M	P'_M	Flag[a]	Source[b]
(1)	(2)	(3)	(4)	(5)	(6)	(7)	(8)	(9)	(10)	(11)	(12)	(13)	(14)	(15)	(16)	(17)
SMC	NGC 339	N339-1-b024	14.946560	-74.468193	18.53	1.21	4924	4684839035290574336	-0.7	-0.78 ± 23.97	3.72 ± 0.79	-0.13 ± 0.75	-1.00	-1.00	1000000	M2FS
SMC	NGC 339	N339-1-b025	14.568852	-74.362073	18.19	1.07	4831	4684829723802354304	6.0	207.35 ± 0.53	2.64 ± 0.11	-0.73 ± 0.08	0.00	0.00	0000000	M2FS
SMC	NGC 339	N339-1-b026	14.539738	-74.382273	16.68	1.38	4365	4684829659379726080	20.3	175.61 ± 0.27	0.29 ± 0.15	-2.32 ± 0.03	0.00	0.00	0000000	M2FS
SMC	NGC 339	N339-1-b027	14.516717	-74.458377	17.89	1.30	4755	4684827937095138688	4.2	144.20 ± 0.68	1.40 ± 0.26	-0.99 ± 0.10	0.00	0.00	0000000	M2FS
SMC	NGC 339	N339-1-b028	14.503113	-74.458911	17.42	1.32	4618	4684827937097448064	4.4	114.27 ± 0.55	0.66 ± 0.21	-0.91 ± 0.08	1.00	1.00	0000000	M2FS
SMC	NGC 339	N339-1-b029	14.516990	-74.462932	17.52	1.25	4652	4684827937095105792	4.2	166.44 ± 0.68	0.63 ± 0.31	-1.22 ± 0.09	0.00	0.00	0000000	M2FS
SMC	NGC 339	N339-1-b030	14.511417	-74.467994	19.18	1.07	5080	4684827937095075072	0.4	155.12 ± 2.95	2.71 ± 1.40	0.89 ± 0.23	0.00	0.00	0000000	M2FS
SMC	NGC 339	N339-1-b031	14.521357	-74.470773	19.15	0.95	5073	4684827868375557760	0.9	114.16 ± 3.06	2.99 ± 0.85	-0.35 ± 0.50	0.99	1.00	0000000	M2FS
SMC	NGC 339	N339-1-b032	14.546455	-74.472198	18.60	1.16	4943	4684827902735283456	1.7	149.48 ± 0.85	1.92 ± 0.74	-0.34 ± 0.17	0.00	0.00	0000000	M2FS
SMC	NGC 339	N339-1-b033	14.445705	-74.513105	19.31	1.01	5109	4684815915476919424	2.7	128.04 ± 33.13	1.81 ± 0.89	-2.22 ± 0.36	-1.00	-1.00	1000000	M2FS
SMC	NGC 339	N339-1-b034	14.431859	-74.504664	16.36	1.67	4251	4684815979905816064	8.2	152.43 ± 0.26	0.78 ± 0.07	-0.73 ± 0.05	0.00	0.00	0000000	M2FS
SMC	NGC 339	N339-1-b035	14.445461	-74.497797	19.01	0.85	5044	4684816014265583488	2.6	154.61 ± 1.40	2.58 ± 0.40	-0.92 ± 0.26	0.00	0.00	0000000	M2FS
SMC	NGC 339	N339-1-b036	14.439191	-74.489716	16.88	1.48	4442	4684827765298747776	11.4	157.63 ± 0.30	0.66 ± 0.08	-1.20 ± 0.04	0.00	0.00	0000000	M2FS
SMC	NGC 339	N339-1-b037	14.427950	-74.486503	17.77	1.28	4721	4684827838306116608	4.5	110.63 ± 0.60	0.87 ± 0.27	-1.09 ± 0.09	1.00	1.00	0000000	M2FS
SMC	NGC 339	N339-1-b038	14.447633	-74.482867	18.37	1.16	4878	4684827765298765952	3.1	114.06 ± 1.46	1.73 ± 0.44	-1.02 ± 0.13	1.00	1.00	0000000	M2FS
SMC	NGC 339	N339-1-b039	14.427820	-74.482520	18.89	1.05	5014	4684827838306112768	1.8	114.84 ± 2.14	2.41 ± 0.43	-0.52 ± 0.21	1.00	1.00	0000000	M2FS
SMC	NGC 339	N339-1-b040	14.440007	-74.479850	19.14	0.88	5073	4684827838306107136	-0.1	97.10 ± 285.17	2.04 ± 1.50	0.45 ± 0.91	-1.00	-1.00	1000000	M2FS
SMC	NGC 339	N339-1-b041	14.463103	-74.508199	16.66	0.90	4359	4684815949844146944	15.7	14.89 ± 0.54	1.56 ± 0.08	-2.02 ± 0.05	-1.00	-1.00	0100010	M2FS
SMC	NGC 339	N339-1-b042	14.459205	-74.494818	19.16	0.96	5076	4684816014265627520	3.1	-7.19 ± 2.14	2.24 ± 0.60	-1.73 ± 0.22	-1.00	-1.00	0100000	M2FS
SMC	NGC 339	N339-1-b043	14.468580	-74.489886	18.10	1.17	4809	4684827765298747520	3.3	113.21 ± 1.24	0.57 ± 0.32	-1.17 ± 0.11	1.00	1.00	0000000	M2FS
SMC	NGC 339	N339-1-b045	14.476634	-74.486868	19.00	1.01	5040	4684827765296205568	3.0	187.35 ± 4.24	1.11 ± 0.53	-1.83 ± 0.20	-1.00	-1.00	1000000	M2FS
SMC	NGC 339	N339-1-b046	14.461913	-74.483732	17.05	1.32	4507	4684827769594140928	8.9	113.97 ± 0.38	0.62 ± 0.11	-1.12 ± 0.05	1.00	1.00	0000000	M2FS
SMC	NGC 339	N339-1-b047	14.476460	-74.482225	19.24	0.91	5093	4684827765298767232	0.9	115.03 ± 2.64	2.21 ± 0.99	0.12 ± 0.32	-1.00	-1.00	0000001	M2FS
SMC	NGC 339	N339-1-b048	14.469740	-74.477732	18.55	0.97	4929	4684827838306095872	2.2	114.28 ± 1.19	1.13 ± 0.61	-0.80 ± 0.13	1.00	1.00	0000000	M2FS
SMC	NGC 339	N339-1-b049	14.483144	-74.446886	18.44	1.20	4898	4684828216263150208	1.9	174.92 ± 1.18	2.13 ± 0.51	-0.65 ± 0.19	0.00	0.00	0000000	M2FS
SMC	NGC 339	N339-1-b050	14.494051	-74.452330	17.84	1.27	4742	4684828143253614976	3.8	113.18 ± 0.91	0.62 ± 0.31	-0.99 ± 0.09	1.00	1.00	0000000	M2FS
SMC	NGC 339	N339-1-b051	14.477978	-74.453440	19.10	1.00	5063	4684828147543678848	1.0	160.24 ± 4.22	4.45 ± 0.34	0.68 ± 0.35	-1.00	-1.00	1000000	M2FS
SMC	NGC 339	N339-1-b052	14.486698	-74.456395	18.28	1.03	4855	4684828143255878656	2.4	169.18 ± 1.04	0.68 ± 0.45	-0.77 ± 0.13	0.00	0.00	0000000	M2FS
SMC	NGC 339	N339-1-b053	14.475402	-74.468738	16.08	1.70	4145	4684827941392825728	8.9	142.28 ± 0.45	0.70 ± 0.08	-0.77 ± 0.05	0.00	0.00	0000000	M2FS
SMC	NGC 339	N339-1-b054	14.486789	-74.473014	17.45	1.35	4629	4684827941385290624	3.3	112.99 ± 0.74	0.41 ± 0.24	-0.87 ± 0.08	1.00	1.00	0000000	M2FS
SMC	NGC 339	N339-1-b055	14.473096	-74.474179	18.94	0.92	5027	4684827838313613824	2.1	114.94 ± 1.35	2.38 ± 0.42	-0.49 ± 0.16	-1.00	-1.00	1000000	M2FS
SMC	NGC 339	N339-1-b056	14.490424	-74.476725	19.04	1.02	5050	4684827872665828992	0.3	112.77 ± 6.21	2.31 ± 1.12	0.76 ± 0.34	-1.00	-1.00	1000000	M2FS
SMC	NGC 339	N339-1-b057	14.448000	-74.440186	18.83	1.15	5002	4684828967887439232	2.7	116.74 ± 2.72	2.49 ± 0.53	-1.62 ± 0.21	-1.00	-1.00	0100000	M2FS
SMC	NGC 339	N339-1-b058	14.460253	-74.451923	18.65	1.17	4956	4684828211975357184	2.7	112.36 ± 1.38	1.29 ± 0.50	-1.15 ± 0.18	1.00	1.00	0000000	M2FS
SMC	NGC 339	N339-1-b060	14.464394	-74.456367	19.32	0.85	5110	4684828147543682304	0.9	114.62 ± 3.50	2.93 ± 1.33	-0.60 ± 0.37	1.00	1.00	0000000	M2FS
SMC	NGC 339	N339-1-b062	14.455017	-74.463499	18.22	1.14	4838	4684828040176721792	0.8	114.20 ± 2.52	1.86 ± 0.83	-0.44 ± 0.38	-1.00	-1.00	1000000	M2FS
SMC	NGC 339	N339-1-b063	14.452969	-74.467554	18.99	0.88	5038	4684828044464490880	0.9	114.22 ± 2.97	2.45 ± 0.85	0.01 ± 0.30	-1.00	-1.00	0000001	M2FS
SMC	NGC 339	N339-1-b064	14.451546	-74.477287	16.12	1.65	4162	4684827838313616128	11.7	115.22 ± 0.25	0.26 ± 0.09	-1.09 ± 0.04	1.00	1.00	0000000	M2FS
SMC	NGC 339	N339-1-b065	14.370662	-74.495222	19.26	1.07	5097	4684827799655865472	1.4	112.17 ± 3.40	1.71 ± 0.78	-0.85 ± 0.30	0.99	0.99	0000000	M2FS
SMC	NGC 339	N339-1-b066	14.357832	-74.493140	18.37	0.95	4880	4684826322187140608	3.8	176.46 ± 0.99	1.33 ± 0.33	-0.85 ± 0.13	0.00	0.00	0000000	M2FS
SMC	NGC 339	N339-1-b067	14.372874	-74.490889	18.46	1.27	4905	4684827799655903104	2.9	114.54 ± 0.79	1.23 ± 0.55	-1.10 ± 0.12	0.99	0.99	0000000	M2FS
SMC	NGC 339	N339-1-b068	14.354378	-74.484346	19.35	0.85	5117	4684828010104809600	1.2	167.30 ± 1.71	2.06 ± 0.84	-0.92 ± 0.35	-1.00	-1.00	1000000	M2FS
SMC	NGC 339	N339-1-b069	14.380495	-74.481873	19.22	0.93	5089	4684828010104806144	2.3	113.18 ± 1.43	1.07 ± 0.66	-0.73 ± 0.15	1.00	1.00	0000000	M2FS
SMC	NGC 339	N339-1-b070	14.349874	-74.479286	18.31	1.12	4862	4684828005814427648	3.0	112.92 ± 1.08	0.97 ± 0.43	-0.83 ± 0.11	1.00	1.00	0000000	M2FS
SMC	NGC 339	N339-1-b071	14.387669	-74.477184	17.71	1.37	4705	4684828010112308992	4.5	140.35 ± 0.45	0.42 ± 0.23	-0.51 ± 0.06	0.00	0.00	0000000	M2FS
SMC	NGC 339	N339-1-b072	14.346994	-74.474388	18.49	0.93	4911	4684828074533953024	2.4	176.03 ± 1.39	0.54 ± 0.40	-1.33 ± 0.18	0.00	0.00	0000000	M2FS
SMC	NGC 339	N339-1-b073	14.424787	-74.507959	17.32	1.41	4590	4684815979905816192	5.6	154.41 ± 0.48	0.80 ± 0.18	-0.83 ± 0.06	0.00	0.00	0000000	M2FS
SMC	NGC 339	N339-1-b074	14.405005	-74.506889	18.05	1.28	4797	4684815984203885568	3.1	167.51 ± 0.50	2.14 ± 0.30	-0.61 ± 0.10	0.00	0.00	0000000	M2FS
SMC	NGC 339	N339-1-b075	14.415895	-74.500530	18.49	0.96	4913	4684827730936342400	2.3	201.16 ± 1.94	0.62 ± 0.39	-1.28 ± 0.16	0.00	0.00	0000000	M2FS
SMC	NGC 339	N339-1-b076	14.424695	-74.492875	15.56	2.05	4062	4684827735234404992	11.4	181.18 ± 0.35	0.68 ± 0.07	-0.76 ± 0.05	0.00	0.00	0000010	M2FS
SMC	NGC 339	N339-1-b077	14.391476	-74.488656	18.02	1.26	4789	4684827799658486656	3.4	176.50 ± 0.69	0.36 ± 0.25	-1.10 ± 0.11	0.00	0.00	0000000	M2FS
SMC	NGC 339	N339-1-b078	14.393193	-74.480634	19.23	0.89	5092	4684828010104803328	1.0	114.26 ± 3.87	2.23 ± 0.85	-0.74 ± 0.37	0.99	0.99	0000000	M2FS
SMC	NGC 339	N339-1-b079	14.417126	-74.478934	17.49	1.31	4642	4684827838313617280	5.2	113.00 ± 0.62	0.94 ± 0.18	-0.81 ± 0.07	1.00	1.00	0000000	M2FS
SMC	NGC 339	N339-1-b080	14.392228	-74.470353	18.40	0.96	4886	4684828010104774784	2.7	165.65 ± 0.96	1.42 ± 0.55	-0.94 ± 0.14	0.00	0.00	0000000	M2FS

Table C.1: (*continued*) Sample of 3095 Targets from 26 Star Clusters

Galaxy	Cluster	ID	RAJ2000 (deg)	DEJ2000 (deg)	G (mag)	$G_{\rm BP} - G_{\rm RP}$ (mag)	$T_{\rm eff}$ (K)	*Gaia* DR2 ID	S/N	$v_{\rm los}$ (km s^{-1})	$\log g$ (dex)	$[{\rm Fe/H}]_{\rm raw}$ (dex)	P_M	P'_M	Flag[a]	Source[b]
(1)	(2)	(3)	(4)	(5)	(6)	(7)	(8)	(9)	(10)	(11)	(12)	(13)	(14)	(15)	(16)	(17)
SMC	NGC 339	N339-1-b081	14.439761	-74.435505	18.95	0.92	5029	4684828869098172160	0.7	148.09 ± 44.06	3.65 ± 1.44	-0.14 ± 0.78	-1.00	-1.00	1000000	M2FS
SMC	NGC 339	N339-1-b082	14.434598	-74.440784	16.09	1.71	4149	4684828869105755392	10.9	114.96 ± 0.23	0.41 ± 0.07	-0.98 ± 0.04	0.97	0.97	0000000	M2FS
SMC	NGC 339	N339-1-b083	14.437003	-74.444509	17.99	1.21	4780	4684828108893950976	3.3	152.76 ± 0.76	0.81 ± 0.39	-0.86 ± 0.11	0.00	0.00	0000000	M2FS
SMC	NGC 339	N339-1-b084	14.442750	-74.447824	18.83	1.21	5000	4684828108893919232	0.8	170.76 ± 2.92	4.21 ± 0.50	0.45 ± 0.38	-1.00	-1.00	0001000	M2FS
SMC	NGC 339	N339-1-b085	14.436847	-74.455393	16.31	1.59	4235	4684828113191513856	10.1	109.22 ± 0.45	0.29 ± 0.11	-1.13 ± 0.04	0.99	-1.00	0000000	M2FS
SMC	NGC 339	N339-1-b086	14.437044	-74.459054	18.69	1.05	4966	4684828040176670080	1.5	175.31 ± 2.01	2.95 ± 0.79	-0.56 ± 0.28	0.00	0.00	0000000	M2FS
SMC	NGC 339	N339-1-b087	14.433762	-74.470227	17.43	1.23	4620	4684828044464504064	4.4	112.76 ± 0.69	0.58 ± 0.25	-0.97 ± 0.08	1.00	1.00	0000000	M2FS
SMC	NGC 339	N339-1-b088	14.442250	-74.473095	18.12	0.97	4815	4684827838313614080	2.1	111.36 ± 1.42	0.95 ± 0.48	-0.72 ± 0.14	1.00	1.00	0000000	M2FS
SMC	NGC 339	N339-1-b089	14.426355	-74.338398	17.04	1.40	4503	4684832648676957056	11.0	142.49 ± 0.27	0.76 ± 0.09	-0.94 ± 0.04	0.00	0.00	0000000	M2FS
SMC	NGC 339	N339-1-b090	14.398217	-74.366874	16.01	1.84	4121	4684832545597747584	19.2	145.53 ± 0.26	0.90 ± 0.05	-0.66 ± 0.03	0.00	0.00	0000000	M2FS
SMC	NGC 339	N339-1-b091	14.421466	-74.448174	19.25	0.98	5095	4684828113183937792	0.5	111.54 ± 1.92	1.20 ± 0.78	0.93 ± 0.21	-1.00	-1.00	1000000	M2FS
SMC	NGC 339	N339-1-b092	14.400568	-74.450896	19.21	0.95	5086	4684828864808132608	1.5	112.46 ± 2.16	1.37 ± 0.88	-0.99 ± 0.25	0.99	0.99	0000000	M2FS
SMC	NGC 339	N339-1-b093	14.421270	-74.453030	18.67	1.12	4962	4684828108896141568	1.3	115.27 ± 1.37	1.31 ± 0.83	-0.23 ± 0.19	-1.00	-1.00	0000001	M2FS
SMC	NGC 339	N339-1-b094	14.412328	-74.458507	18.71	1.11	4970	4684828113191514496	0.8	114.22 ± 2.58	1.63 ± 1.05	-0.42 ± 0.25	1.00	1.00	0000000	M2FS
SMC	NGC 339	N339-1-b095	14.418209	-74.462942	16.03	1.68	4129	4684828044472428672	9.6	111.16 ± 0.27	0.17 ± 0.09	-0.99 ± 0.04	1.00	1.00	0000000	M2FS
SMC	NGC 339	N339-1-b096	14.406118	-74.465226	18.60	1.03	4941	4684828044464489472	0.9	112.32 ± 2.04	1.65 ± 0.78	-0.18 ± 0.24	-1.00	-1.00	0000001	M2FS
SMC	NGC 339	N339-1-b097	14.163289	-74.556681	18.22	1.22	4838	4684814330637823872	4.3	148.48 ± 1.01	1.19 ± 0.36	-1.18 ± 0.11	0.00	0.00	0000000	M2FS
SMC	NGC 339	N339-1-b098	14.046297	-74.525266	16.63	0.89	4349	4684826012949160576	23.7	45.50 ± 0.35	1.06 ± 0.07	-1.11 ± 0.05	-1.00	-1.00	0000110	M2FS
SMC	NGC 339	N339-1-b099	14.066198	-74.501265	18.33	1.29	4869	4684826871942873216	6.3	150.12 ± 0.53	1.58 ± 0.19	-0.98 ± 0.08	0.00	0.00	0000000	M2FS
SMC	NGC 339	N339-1-b100	13.989957	-74.495856	16.81	1.61	4417	4684827048039716608	16.1	148.22 ± 0.22	0.74 ± 0.07	-0.79 ± 0.03	0.00	0.00	0000000	M2FS
SMC	NGC 339	N339-1-b101	14.029797	-74.485170	17.49	1.44	4642	4684827146820892416	9.4	134.47 ± 0.36	1.16 ± 0.12	-0.80 ± 0.04	0.00	0.00	0000000	M2FS
SMC	NGC 339	N339-1-b102	14.063105	-74.477100	17.64	0.98	4686	4684827146820962304	9.3	157.35 ± 0.54	0.40 ± 0.22	-1.53 ± 0.05	0.00	0.00	0000000	M2FS
SMC	NGC 339	N339-1-b103	14.040452	-74.473358	17.44	1.00	4625	4684827151118921600	13.3	142.79 ± 0.50	1.84 ± 0.09	-1.84 ± 0.05	0.00	0.00	0000000	M2FS
SMC	NGC 339	N339-1-b104	14.112476	-74.457867	17.71	1.18	4705	4684827524778254080	10.0	89.01 ± 0.33	3.89 ± 0.06	-0.60 ± 0.07	-1.00	-1.00	0001000	M2FS
SMC	NGC 339	N339-1-b105	14.220314	-74.570751	18.78	1.01	4988	4684814261918224768	5.3	139.57 ± 0.92	1.18 ± 0.33	-1.33 ± 0.09	0.00	0.00	0000000	M2FS
SMC	NGC 339	N339-1-b106	14.300321	-74.556461	18.00	1.32	4784	4684814193198887936	7.6	169.74 ± 0.43	1.17 ± 0.15	-0.88 ± 0.06	0.00	0.00	0000000	M2FS
SMC	NGC 339	N339-1-b107	14.239991	-74.552972	18.62	1.19	4947	4684814364997601664	4.6	155.98 ± 0.73	1.73 ± 0.31	-1.06 ± 0.11	0.00	0.00	0000000	M2FS
SMC	NGC 339	N339-1-b108	14.165674	-74.549361	17.02	1.40	4495	4684826081668413184	15.1	151.01 ± 0.24	0.64 ± 0.07	-1.05 ± 0.03	0.00	0.00	0000000	M2FS
SMC	NGC 339	N339-1-b109	14.180303	-74.522068	16.71	1.39	4377	4684826360844959616	19.3	182.08 ± 0.21	0.19 ± 0.09	-1.11 ± 0.03	0.00	0.00	0000000	M2FS
SMC	NGC 339	N339-1-b110	14.335887	-74.485252	18.73	0.92	4976	4684826532643561472	2.4	148.19 ± 1.48	1.21 ± 0.73	-1.09 ± 0.19	0.00	0.00	0000000	M2FS
SMC	NGC 339	N339-1-b111	14.322708	-74.480406	16.37	1.61	4254	4684826601363037440	11.8	176.86 ± 0.27	0.50 ± 0.07	-0.93 ± 0.04	0.00	0.00	0000000	M2FS
SMC	NGC 339	N339-1-b112	14.324985	-74.476595	18.40	1.19	4886	4684826601363036288	1.7	178.81 ± 1.55	0.98 ± 0.67	-0.64 ± 0.15	0.00	0.00	0000000	M2FS
SMC	NGC 339	N339-1-b113	14.396703	-74.447084	19.38	0.00	5122	4684828869098181120	1.4	184.61 ± 81.64	1.64 ± 0.97	-2.23 ± 0.56	-1.00	-1.00	1000000	M2FS
SMC	NGC 339	N339-1-b114	14.375665	-74.455327	18.42	1.36	4893	4684828830448369280	1.7	138.08 ± 1.46	0.64 ± 0.42	-0.20 ± 0.15	0.00	0.00	0000000	M2FS
SMC	NGC 339	N339-1-b115	14.362197	-74.456384	18.90	1.20	5017	4684828830448366080	1.8	113.86 ± 2.40	2.14 ± 0.79	-1.50 ± 0.27	0.99	0.99	0000000	M2FS
SMC	NGC 339	N339-1-b116	14.390695	-74.457648	18.18	1.17	4830	4684828074536401408	2.5	114.94 ± 1.14	0.71 ± 0.43	-1.00 ± 0.12	0.99	1.00	0000000	M2FS
SMC	NGC 339	N339-1-b117	14.357352	-74.462450	18.20	1.28	4835	4684828074534046720	2.5	146.31 ± 1.75	2.66 ± 0.32	-0.46 ± 0.14	0.00	0.00	0000000	M2FS
SMC	NGC 339	N339-1-b118	14.393285	-74.463632	17.59	1.26	4672	4684828078831778432	5.0	112.85 ± 0.81	0.82 ± 0.22	-1.00 ± 0.08	1.00	1.00	0000000	M2FS
SMC	NGC 339	N339-1-b119	14.360196	-74.465994	19.20	0.86	5086	4684828074534014592	0.7	112.55 ± 2.48	2.80 ± 0.77	0.02 ± 0.33	-1.00	-1.00	0000001	M2FS
SMC	NGC 339	N339-1-b120	14.379233	-74.468733	18.94	1.11	5028	4684828078824248832	0.9	113.69 ± 1.74	0.88 ± 0.64	-0.24 ± 0.19	-1.00	-1.00	0000001	M2FS
SMC	NGC 339	N339-1-b121	14.134326	-74.367674	18.18	1.05	4829	4684831991544974720	7.9	168.56 ± 0.39	0.99 ± 0.19	-1.22 ± 0.06	0.00	0.00	0000000	M2FS
SMC	NGC 339	N339-1-b122	14.247289	-74.375848	18.40	0.89	4887	4684830995112506880	8.6	166.39 ± 0.71	1.07 ± 0.25	-1.50 ± 0.07	0.00	0.00	0000000	M2FS
SMC	NGC 339	N339-1-b123	14.167256	-74.378767	18.31	1.10	4862	4684831716666982784	7.7	210.12 ± 0.51	1.20 ± 0.20	-1.31 ± 0.06	0.00	0.00	0000000	M2FS
SMC	NGC 339	N339-1-b124	14.292769	-74.383299	17.00	1.50	4487	4684832408158855936	16.7	177.81 ± 0.22	1.15 ± 0.06	-0.78 ± 0.04	0.00	0.00	0000000	M2FS
SMC	NGC 339	N339-1-b126	13.960054	-74.454068	17.21	1.38	4560	4684830342276820608	15.1	124.76 ± 0.27	0.64 ± 0.08	-1.19 ± 0.04	0.00	0.00	0000000	M2FS
SMC	NGC 339	N339-1-b127	14.353902	-74.469435	19.11	1.01	5066	4684828078824253056	1.2	114.96 ± 34.84	1.45 ± 0.92	-1.55 ± 0.50	-1.00	-1.00	1000000	M2FS
SMC	NGC 339	N339-1-b128	14.340510	-74.470185	19.32	1.27	5111	4684826597065235456	2.3	-4.91 ± 1.92	2.31 ± 0.59	-1.09 ± 0.23	-1.00	-1.00	0000100	M2FS
SMC	NGC 339	N339-1-r028	14.401317	-74.474677	16.62	1.51	4346	4684828010112678528	15.5	110.74 ± 0.27	0.36 ± 0.10	-1.24 ± 0.04	1.00	1.00	0000000	M2FS
SMC	NGC 339	N339-1-r049	14.423556	-74.473183	16.52	1.35	4309	4684828044472045056	13.0	111.77 ± 0.43	0.67 ± 0.10	-1.67 ± 0.05	-1.00	-1.00	0000001	M2FS
SMC	NGC 339	N339-1-r079	14.436617	-74.464720	16.84	1.46	4428	4684828044472039552	7.8	151.27 ± 0.38	1.08 ± 0.11	-0.90 ± 0.05	0.00	0.00	0000000	M2FS
SMC	NGC 339	N339-1-r127	14.456814	-74.471403	16.80	1.36	4414	4684827838313612416	13.3	113.50 ± 0.39	0.66 ± 0.09	-1.32 ± 0.04	1.00	1.00	0000000	M2FS
SMC	NGC 361	N361-1-b001	15.690372	-71.698309	18.38	1.16	4868	4690580032175109888	4.9	129.32 ± 0.73	1.72 ± 0.16	-0.89 ± 0.08	0.00	0.00	0000000	M2FS
SMC	NGC 361	N361-1-b002	15.736395	-71.697285	17.84	1.40	4729	4690579997815379072	7.5	171.56 ± 0.44	1.37 ± 0.12	-0.95 ± 0.05	0.00	0.00	0000000	M2FS
SMC	NGC 361	N361-1-b003	15.744214	-71.680295	17.48	1.28	4628	4690580070843976448	8.4	103.79 ± 0.34	0.91 ± 0.10	-0.97 ± 0.04	0.00	0.00	0000000	M2FS

Table C.1: (*continued*) Sample of 3095 Targets from 26 Star Clusters

Galaxy	Cluster	ID	RAJ2000 (deg)	DEJ2000 (deg)	G (mag)	$G_{\rm BP} - G_{\rm RP}$ (mag)	$T_{\rm eff}$ (K)	*Gaia* DR2 ID	S/N	$v_{\rm los}$ (km s^{-1})	$\log g$ (dex)	$[{\rm Fe/H}]_{\rm raw}$ (dex)	P_M	P'_M	Flag[a]	Source[b]
(1)	(2)	(3)	(4)	(5)	(6)	(7)	(8)	(9)	(10)	(11)	(12)	(13)	(14)	(15)	(16)	(17)
SMC	NGC 361	N361-1-b004	15.702523	-71.678462	17.13	1.46	4523	4690580242642669056	11.1	147.51 ± 0.23	0.43 ± 0.11	-1.05 ± 0.03	0.00	0.00	0000000	M2FS
SMC	NGC 361	N361-1-b005	15.762257	-71.674205	18.52	1.25	4908	4690580066535151616	4.4	150.58 ± 0.76	1.23 ± 0.33	-1.06 ± 0.09	0.00	0.00	0000000	M2FS
SMC	NGC 361	N361-1-b006	15.687150	-71.671611	17.81	1.30	4722	4690580307053348608	7.7	158.77 ± 0.33	1.27 ± 0.11	-0.74 ± 0.04	0.00	0.00	0000000	M2FS
SMC	NGC 361	N361-1-b007	15.711423	-71.632587	17.36	1.04	4594	4690583369378788608	11.5	119.80 ± 0.40	0.81 ± 0.12	-1.59 ± 0.04	0.00	0.00	0000010	M2FS
SMC	NGC 361	N361-1-b008	15.748697	-71.625364	17.84	1.18	4731	4690584842540066432	6.8	150.63 ± 0.45	0.72 ± 0.17	-1.00 ± 0.05	0.00	0.00	0000000	M2FS
SMC	NGC 361	N361-1-b009	15.844121	-71.675480	18.17	1.24	4816	4690581513952969984	4.5	154.78 ± 0.69	0.77 ± 0.28	-1.16 ± 0.08	0.00	0.00	0000000	M2FS
SMC	NGC 361	N361-1-b010	15.781172	-71.672629	17.30	1.37	4576	4690581548313301248	8.8	147.42 ± 0.25	0.38 ± 0.14	-1.10 ± 0.04	0.00	0.00	0000000	M2FS
SMC	NGC 361	N361-1-b011	15.781087	-71.660397	18.07	1.08	4790	4690581750162487680	5.6	102.27 ± 0.55	1.41 ± 0.17	-0.99 ± 0.06	0.00	0.00	0000000	M2FS
SMC	NGC 361	N361-1-b012	15.781472	-71.654486	17.33	1.06	4586	4690581754471111680	8.6	121.77 ± 0.38	0.56 ± 0.17	-1.65 ± 0.05	0.00	0.00	0000010	M2FS
SMC	NGC 361	N361-1-b013	15.827072	-71.649334	18.25	1.18	4836	4690581788830839040	4.3	157.93 ± 0.64	0.67 ± 0.29	-1.21 ± 0.08	0.00	0.00	0000000	M2FS
SMC	NGC 361	N361-1-b014	15.827732	-71.625302	18.45	1.15	4889	4690584808203139968	3.1	139.23 ± 0.95	0.84 ± 0.37	-0.85 ± 0.10	0.00	0.00	0000000	M2FS
SMC	NGC 361	N361-1-b015	15.853447	-71.620598	18.17	1.25	4817	4690584915566978176	4.1	129.58 ± 0.68	0.70 ± 0.24	-0.77 ± 0.07	0.00	0.00	0000000	M2FS
SMC	NGC 361	N361-1-b016	15.910317	-71.615894	17.96	1.38	4763	4690581990681839616	5.2	157.92 ± 0.71	0.35 ± 0.25	-0.69 ± 0.10	0.00	0.00	0000000	M2FS
SMC	NGC 361	N361-1-b017	15.722753	-71.507868	17.60	1.32	4666	4690598277198717568	8.5	146.66 ± 0.30	1.29 ± 0.10	-0.75 ± 0.04	0.00	0.00	0000000	M2FS
SMC	NGC 361	N361-1-b018	15.724784	-71.521978	17.31	1.18	4579	4690598075346643584	11.6	163.15 ± 0.22	0.86 ± 0.09	-1.41 ± 0.04	0.00	0.00	0000000	M2FS
SMC	NGC 361	N361-1-b019	15.853954	-71.539679	18.65	1.19	4943	4690586118157703296	4.3	164.64 ± 0.72	2.03 ± 0.21	-0.85 ± 0.09	0.00	0.00	0000000	M2FS
SMC	NGC 361	N361-1-b020	15.707719	-71.546395	17.95	1.30	4761	4690586216930409088	7.5	143.38 ± 0.33	1.14 ± 0.14	-0.82 ± 0.04	0.00	0.00	0000000	M2FS
SMC	NGC 361	N361-1-b021	15.889694	-71.579761	17.94	1.26	4758	4690585224804551552	6.2	101.96 ± 0.42	1.07 ± 0.17	-1.17 ± 0.06	0.00	0.00	0000000	M2FS
SMC	NGC 361	N361-1-b022	15.737251	-71.582977	17.66	1.39	4680	4690585873332451840	7.8	156.05 ± 0.36	1.09 ± 0.11	-0.83 ± 0.04	0.00	0.00	0000000	M2FS
SMC	NGC 361	N361-1-b023	15.737010	-71.602530	18.25	1.11	4835	4690585117418100352	5.4	129.96 ± 0.61	0.58 ± 0.27	-1.21 ± 0.07	0.00	0.00	0000000	M2FS
SMC	NGC 361	N361-1-b024	15.827968	-71.610143	18.13	1.15	4806	4690584876947357952	3.8	149.68 ± 1.06	0.22 ± 0.19	-0.77 ± 0.15	0.00	0.00	0000000	M2FS
SMC	NGC 361	N361-1-b025	15.632450	-71.493761	18.26	1.12	4838	4690599136192222208	5.4	143.26 ± 0.53	0.74 ± 0.23	-1.28 ± 0.06	0.00	0.00	0000000	M2FS
SMC	NGC 361	N361-1-b026	15.624320	-71.522402	18.22	1.14	4829	4690596834089655424	6.0	127.68 ± 0.52	1.05 ± 0.18	-1.04 ± 0.06	0.00	0.00	0000000	M2FS
SMC	NGC 361	N361-1-b028	15.653719	-71.531006	17.42	1.08	4608	4690598247145348480	9.7	96.42 ± 0.28	0.49 ± 0.12	-1.13 ± 0.04	0.00	0.00	0000010	M2FS
SMC	NGC 361	N361-1-b029	15.674383	-71.552261	17.50	1.26	4634	4690597972267462272	9.2	120.44 ± 0.30	0.90 ± 0.09	-0.90 ± 0.04	0.00	0.00	0000000	M2FS
SMC	NGC 361	N361-1-b030	15.661801	-71.567991	18.06	1.22	4788	4690584739461156736	5.2	153.40 ± 0.54	1.29 ± 0.16	-0.84 ± 0.07	0.00	0.00	0000000	M2FS
SMC	NGC 361	N361-1-b031	15.691450	-71.569659	18.67	1.03	4947	4690586152509424896	5.2	145.24 ± 0.74	1.37 ± 0.26	-1.56 ± 0.09	0.00	0.00	0000000	M2FS
SMC	NGC 361	N361-1-b032	15.626111	-71.601587	17.97	1.31	4766	4690584430223333760	5.4	172.73 ± 0.39	1.41 ± 0.14	-0.79 ± 0.06	0.94	0.95	0000000	M2FS
SMC	NGC 361	N361-1-b033	15.590170	-71.713227	18.36	1.13	4863	4690580100918843264	4.6	147.84 ± 0.61	1.45 ± 0.19	-0.87 ± 0.07	0.00	0.00	0000000	M2FS
SMC	NGC 361	N361-1-b037	15.590994	-71.631332	17.95	1.29	4760	4690583502510237696	4.9	127.53 ± 0.70	1.13 ± 0.27	-1.48 ± 0.08	0.00	0.00	0000000	M2FS
SMC	NGC 361	N361-1-b038	15.623477	-71.628472	16.88	1.52	4436	4690583609896958080	11.8	155.40 ± 0.24	0.36 ± 0.12	-0.91 ± 0.04	0.00	0.00	0000000	M2FS
SMC	NGC 361	N361-1-b039	15.609333	-71.610191	17.52	1.08	4639	4690584430223293568	9.6	140.43 ± 0.27	0.72 ± 0.11	-1.19 ± 0.04	0.00	0.00	0000000	M2FS
SMC	NGC 361	N361-1-b040	15.623739	-71.609201	18.18	1.25	4820	4690584361503816576	2.7	169.78 ± 0.95	1.20 ± 0.36	-1.02 ± 0.11	0.94	0.94	0000000	M2FS
SMC	NGC 361	N361-1-b042	15.644866	-71.677701	18.25	1.09	4836	4690580203974055680	6.0	158.90 ± 0.44	0.81 ± 0.16	-0.76 ± 0.05	0.00	0.00	0000000	M2FS
SMC	NGC 361	N361-1-b043	15.661786	-71.642638	17.93	1.08	4754	4690583330710649216	3.6	111.76 ± 0.65	1.41 ± 0.21	-0.91 ± 0.08	0.00	0.00	0000000	M2FS
SMC	NGC 361	N361-1-b044	15.635681	-71.631401	18.21	1.15	4826	4690583609896962176	5.6	123.95 ± 0.51	1.31 ± 0.18	-0.76 ± 0.06	0.00	0.00	0000000	M2FS
SMC	NGC 361	N361-1-b045	15.638763	-71.624807	18.43	1.23	4882	4690583605589483392	3.3	131.44 ± 0.71	1.39 ± 0.32	-0.89 ± 0.09	0.00	0.00	0000000	M2FS
SMC	NGC 361	N361-1-b046	15.678284	-71.618057	17.77	1.32	4711	4690583644256673024	5.8	171.15 ± 0.40	1.22 ± 0.14	-0.77 ± 0.05	0.81	0.86	0000000	M2FS
SMC	NGC 361	N361-1-b047	15.632550	-71.613860	18.43	1.33	4884	4690584361503797632	3.3	175.94 ± 0.99	0.38 ± 0.27	-0.51 ± 0.19	0.72	0.64	0000000	M2FS
SMC	NGC 361	N361-1-b048	15.661681	-71.603220	16.14	3.36	4160	4690584400170882944	2.4	115.05 ± 2.29	2.59 ± 0.87	-2.95 ± 0.38	-1.00	-1.00	0010010	M2FS
SMC	NGC 361	N361-1-b050	15.607019	-71.504602	17.57	1.27	4655	4690597594310294784	7.9	109.95 ± 0.33	0.92 ± 0.11	-0.93 ± 0.04	0.00	0.00	0000000	M2FS
SMC	NGC 361	N361-1-b051	15.594820	-71.525740	18.18	1.29	4819	4690596838396073472	5.0	156.88 ± 0.45	1.33 ± 0.18	-0.72 ± 0.06	0.00	0.00	0000000	M2FS
SMC	NGC 361	N361-1-b052	15.592901	-71.574052	18.50	1.16	4902	4690596456131910272	4.3	107.41 ± 0.69	0.49 ± 0.27	-1.24 ± 0.08	0.00	0.00	0000000	M2FS
SMC	NGC 361	N361-1-b053	15.601048	-71.584706	17.17	1.42	4539	4690584709408501248	11.2	118.18 ± 0.27	0.51 ± 0.10	-1.16 ± 0.04	0.00	0.00	0000000	M2FS
SMC	NGC 361	N361-1-b054	15.593747	-71.589953	17.50	1.01	4633	4690584636381835520	11.2	113.65 ± 0.35	0.60 ± 0.15	-1.56 ± 0.04	0.00	0.00	0000010	M2FS
SMC	NGC 361	N361-1-b055	15.610708	-71.592718	17.74	1.24	4703	4690584636381808256	8.5	171.62 ± 0.26	0.99 ± 0.11	-1.01 ± 0.04	0.95	0.96	0000000	M2FS
SMC	NGC 361	N361-1-b056	15.576996	-71.599861	17.86	1.11	4736	4690584537609838336	7.1	163.49 ± 0.39	1.14 ± 0.14	-1.20 ± 0.05	1.00	-1.00	0000000	M2FS
SMC	NGC 361	N361-1-b057	15.556828	-71.489087	18.56	1.09	4919	4690597834828452096	3.6	132.14 ± 0.86	1.12 ± 0.30	-0.73 ± 0.08	0.00	0.00	0000000	M2FS
SMC	NGC 361	N361-1-b060	15.572285	-71.570176	17.76	1.30	4710	4690596353052711424	7.2	169.50 ± 0.35	1.10 ± 0.11	-0.84 ± 0.04	0.78	0.76	0000000	M2FS
SMC	NGC 361	N361-1-b061	15.575069	-71.574276	17.67	1.18	4684	4690596353052693120	7.6	110.24 ± 0.37	0.61 ± 0.20	-1.72 ± 0.05	0.00	0.00	0000000	M2FS
SMC	NGC 361	N361-1-b062	15.564942	-71.588918	18.05	1.22	4786	4690584602044831360	6.5	163.64 ± 0.34	1.22 ± 0.13	-0.82 ± 0.05	0.49	0.06	0000000	M2FS
SMC	NGC 361	N361-1-b063	15.544254	-71.590283	17.67	1.15	4683	4690584606329299712	8.7	169.47 ± 0.32	0.91 ± 0.10	-0.93 ± 0.04	0.95	0.95	0000000	M2FS
SMC	NGC 361	N361-1-b064	15.561913	-71.595288	17.49	1.34	4630	4690584602022089728	8.1	173.65 ± 0.34	1.19 ± 0.10	-0.79 ± 0.04	1.00	1.00	0000000	M2FS
SMC	NGC 361	N361-1-b066	15.507405	-71.697416	18.24	1.22	4833	4690582716536003840	4.8	125.70 ± 0.70	1.23 ± 0.22	-0.96 ± 0.07	0.00	0.00	0000000	M2FS

Table C.1: (*continued*) Sample of 3095 Targets from 26 Star Clusters

Galaxy	Cluster	ID	RAJ2000 (deg)	DEJ2000 (deg)	G (mag)	$G_{\rm BP} - G_{\rm RP}$ (mag)	$T_{\rm eff}$ (K)	*Gaia* DR2 ID	S/N	$v_{\rm los}$ ($\rm km\,s^{-1}$)	$\log g$ (dex)	$[{\rm Fe/H}]_{\rm raw}$ (dex)	P_M	P'_M	Flag[a]	Source[b]
(1)	(2)	(3)	(4)	(5)	(6)	(7)	(8)	(9)	(10)	(11)	(12)	(13)	(14)	(15)	(16)	(17)
SMC	NGC 361	N361-1-b067	15.481385	-71.682106	17.36	1.36	4593	4690582991421767808	10.5	155.55 ± 0.26	0.74 ± 0.09	-0.99 ± 0.04	0.00	0.00	0000000	M2FS
SMC	NGC 361	N361-1-b068	15.483243	-71.664458	18.86	1.01	4994	4690583094500947968	4.6	136.82 ± 0.86	0.44 ± 0.30	-1.66 ± 0.10	0.00	0.00	0000000	M2FS
SMC	NGC 361	N361-1-b069	15.486391	-71.641946	17.60	1.32	4664	4690583919134632576	8.2	146.34 ± 0.31	0.73 ± 0.13	-0.92 ± 0.05	0.00	0.00	0000000	M2FS
SMC	NGC 361	N361-1-b070	15.521017	-71.637433	18.04	1.25	4783	4690584228372268672	3.4	135.73 ± 0.79	0.18 ± 0.15	-0.69 ± 0.09	0.00	0.00	0000000	M2FS
SMC	NGC 361	N361-1-b071	15.535580	-71.618101	17.80	1.24	4720	4690584292784445056	5.2	169.92 ± 0.51	1.21 ± 0.17	-0.77 ± 0.06	1.00	1.00	0000000	M2FS
SMC	NGC 361	N361-1-b072	15.508149	-71.615937	18.46	1.17	4891	4690584498942728832	4.0	149.83 ± 0.49	1.52 ± 0.20	-0.73 ± 0.07	0.00	0.00	0000000	M2FS
SMC	NGC 361	N361-1-b073	15.565218	-71.714752	17.79	1.41	4717	4690579722937183104	3.7	147.24 ± 0.70	0.75 ± 0.28	-0.97 ± 0.08	0.00	0.00	0000000	M2FS
SMC	NGC 361	N361-1-b075	15.556876	-71.693602	17.83	1.38	4728	4690582746594491904	5.3	112.38 ± 0.52	1.76 ± 0.15	-0.58 ± 0.06	0.00	0.00	0000000	M2FS
SMC	NGC 361	N361-1-b076	15.574704	-71.672747	17.17	1.43	4539	4690583197580169856	9.1	171.72 ± 0.27	1.19 ± 0.08	-0.80 ± 0.04	0.00	0.65	0000000	M2FS
SMC	NGC 361	N361-1-b077	15.581461	-71.634338	16.90	1.61	4442	4690583506817753728	10.3	127.80 ± 0.31	0.74 ± 0.10	-0.67 ± 0.04	0.00	0.00	0000000	M2FS
SMC	NGC 361	N361-1-b078	15.585724	-71.618902	18.86	1.13	4996	4690584258425228416	2.6	134.49 ± 1.28	0.48 ± 0.38	-0.71 ± 0.19	0.00	0.00	0000000	M2FS
SMC	NGC 361	N361-1-b079	15.536973	-71.614461	17.78	1.23	4713	4690584498989359488	5.8	172.11 ± 0.36	1.33 ± 0.14	-0.75 ± 0.05	1.00	1.00	0000000	M2FS
SMC	NGC 361	N361-1-b080	15.581634	-71.612137	19.17	1.01	5066	4690584331451438976	4.4	164.69 ± 0.84	1.30 ± 0.28	-0.87 ± 0.08	1.00	1.00	0000000	M2FS
SMC	NGC 361	N361-1-b081	15.524562	-71.490653	17.63	1.25	4673	4690597899241651456	6.2	131.51 ± 0.49	0.69 ± 0.20	-1.01 ± 0.05	0.00	0.00	0000000	M2FS
SMC	NGC 361	N361-1-b082	15.520576	-71.563925	17.90	1.02	4746	4690596627930642944	7.9	115.90 ± 0.38	0.63 ± 0.21	-1.43 ± 0.05	0.00	0.00	0000000	M2FS
SMC	NGC 361	N361-1-b083	15.515729	-71.570809	18.32	1.28	4852	4690596391719534720	4.8	156.65 ± 0.66	0.92 ± 0.21	-1.04 ± 0.07	0.00	0.00	0000000	M2FS
SMC	NGC 361	N361-1-b084	15.502283	-71.575455	17.33	1.31	4585	4690596391719541760	9.8	116.05 ± 0.28	0.71 ± 0.10	-1.08 ± 0.04	0.00	0.00	0000000	M2FS
SMC	NGC 361	N361-1-b085	15.505161	-71.585998	18.31	1.09	4849	4690596323000079360	5.9	135.29 ± 0.60	0.83 ± 0.22	-1.21 ± 0.06	0.00	0.00	0000000	M2FS
SMC	NGC 361	N361-1-b086	15.521225	-71.595643	16.45	1.36	4276	4690584571969573888	16.6	170.99 ± 0.21	0.15 ± 0.08	-1.19 ± 0.03	1.00	1.00	0000000	M2FS
SMC	NGC 361	N361-1-b087	15.511292	-71.610301	18.74	1.02	4966	4690584503250135680	2.9	170.93 ± 0.88	1.05 ± 0.34	-0.77 ± 0.10	1.00	1.00	0000000	M2FS
SMC	NGC 361	N361-1-b088	15.500472	-71.611727	18.30	1.11	4849	4690584498989358592	4.7	167.96 ± 0.57	0.87 ± 0.22	-0.82 ± 0.06	0.93	0.91	0000000	M2FS
SMC	NGC 361	N361-1-b089	15.477665	-71.511739	17.91	1.24	4749	4690597727487640320	5.3	170.04 ± 0.53	1.31 ± 0.18	-1.00 ± 0.07	0.00	0.00	0000000	M2FS
SMC	NGC 361	N361-1-b090	15.495088	-71.527197	18.34	1.19	4858	4690597525590846208	5.3	149.79 ± 0.52	1.29 ± 0.18	-0.96 ± 0.06	0.00	0.00	0000000	M2FS
SMC	NGC 361	N361-1-b091	15.481580	-71.560633	17.27	1.42	4567	4690596597877954304	8.9	161.27 ± 0.27	1.16 ± 0.08	-0.76 ± 0.04	0.00	0.00	0000000	M2FS
SMC	NGC 361	N361-1-b092	15.478054	-71.583164	16.68	1.12	4359	4690596391711527552	10.4	122.29 ± 0.30	0.08 ± 0.06	-1.49 ± 0.04	0.00	0.00	0000010	M2FS
SMC	NGC 361	N361-1-b093	15.479289	-71.586827	17.03	1.51	4490	4690596391719559680	11.0	167.73 ± 0.29	0.93 ± 0.08	-0.79 ± 0.04	0.84	0.64	0000000	M2FS
SMC	NGC 361	N361-1-b094	15.489303	-71.592409	18.55	1.08	4914	4690596322992075008	4.1	156.44 ± 0.57	1.32 ± 0.22	-0.87 ± 0.08	0.00	0.00	0000000	M2FS
SMC	NGC 361	N361-1-b095	15.465889	-71.595389	18.21	1.16	4826	4690595940735713408	5.0	172.28 ± 0.56	0.91 ± 0.21	-1.01 ± 0.07	0.94	0.95	0000000	M2FS
SMC	NGC 361	N361-1-b096	15.474550	-71.603873	17.21	1.53	4553	4690595945043003264	10.4	122.23 ± 0.28	0.88 ± 0.08	-0.94 ± 0.04	0.00	0.00	0000000	M2FS
SMC	NGC 361	N361-1-b097	15.399424	-71.707373	18.01	1.24	4775	4690582643515041408	6.5	125.53 ± 0.51	1.22 ± 0.14	-0.92 ± 0.05	0.00	0.00	0000000	M2FS
SMC	NGC 361	N361-1-b098	15.402541	-71.690194	18.27	1.11	4841	4690582952752987648	5.2	122.55 ± 0.76	1.60 ± 0.22	-1.47 ± 0.08	0.00	0.00	0000000	M2FS
SMC	NGC 361	N361-1-b099	15.335780	-71.683909	18.51	1.12	4903	4690583678616555648	4.9	114.55 ± 0.51	1.92 ± 0.16	-0.86 ± 0.07	0.00	0.00	0000000	M2FS
SMC	NGC 361	N361-1-b100	15.385572	-71.681304	17.68	1.32	4687	4690583712976283648	7.9	157.74 ± 0.33	0.86 ± 0.12	-1.07 ± 0.04	0.00	0.00	0000000	M2FS
SMC	NGC 361	N361-1-b101	15.327588	-71.678655	18.04	1.33	4784	4690583743027098240	5.7	151.44 ± 0.40	1.00 ± 0.15	-0.69 ± 0.06	0.00	0.00	0000000	M2FS
SMC	NGC 361	N361-1-b102	15.265182	-71.672430	18.55	1.12	4916	4690578073670313856	3.4	152.70 ± 1.10	1.22 ± 0.33	-0.98 ± 0.11	0.00	0.00	0000000	M2FS
SMC	NGC 361	N361-1-b103	15.282957	-71.650100	17.67	1.32	4683	4690589897729139328	7.2	154.11 ± 0.40	0.78 ± 0.13	-0.93 ± 0.05	0.00	0.00	0000000	M2FS
SMC	NGC 361	N361-1-b104	15.366380	-71.638130	17.89	1.26	4743	4690584052265193984	7.6	143.87 ± 0.41	0.48 ± 0.16	-0.96 ± 0.04	0.00	0.00	0000000	M2FS
SMC	NGC 361	N361-1-b105	15.435411	-71.709297	18.30	1.12	4847	4690582677874783488	5.1	101.82 ± 1.17	2.89 ± 0.23	-1.97 ± 0.12	0.00	0.00	0000000	M2FS
SMC	NGC 361	N361-1-b107	15.410685	-71.675244	18.40	1.25	4873	4690583708667432832	4.1	156.98 ± 0.61	0.86 ± 0.24	-0.58 ± 0.07	0.00	0.00	0000000	M2FS
SMC	NGC 361	N361-1-b108	15.477981	-71.670215	18.33	1.20	4857	4690583060141221760	2.1	150.61 ± 1.85	2.60 ± 0.35	-1.31 ± 0.21	0.00	0.00	0000000	M2FS
SMC	NGC 361	N361-1-b109	15.427535	-71.666700	17.69	1.10	4690	4690583712976248832	9.0	118.87 ± 0.35	0.83 ± 0.15	-1.48 ± 0.04	0.00	0.00	0000000	M2FS
SMC	NGC 361	N361-1-b110	15.431690	-71.647139	18.27	1.10	4840	4690583884774905344	5.9	140.31 ± 0.55	1.23 ± 0.20	-0.99 ± 0.06	0.00	0.00	0000000	M2FS
SMC	NGC 361	N361-1-b111	15.478575	-71.620040	18.49	1.23	4900	4690584120985581056	3.3	133.58 ± 0.64	1.48 ± 0.25	-0.84 ± 0.10	0.00	0.00	0000000	M2FS
SMC	NGC 361	N361-1-b112	15.445554	-71.617849	17.16	1.53	4536	4690584194012508032	9.3	125.52 ± 0.42	0.39 ± 0.17	-0.81 ± 0.04	0.00	0.00	0000000	M2FS
SMC	NGC 361	N361-1-b113	15.453258	-71.512477	17.13	1.47	4526	4690597693083159040	8.9	147.67 ± 0.29	0.84 ± 0.09	-0.86 ± 0.04	0.00	0.00	0000000	M2FS
SMC	NGC 361	N361-1-b115	15.462076	-71.548601	17.95	1.34	4761	4690597422511658112	6.8	164.05 ± 0.41	0.97 ± 0.14	-0.97 ± 0.05	0.00	0.00	0000000	M2FS
SMC	NGC 361	N361-1-b116	15.445203	-71.590510	16.57	1.82	4321	4690596013762448640	10.6	177.99 ± 0.27	0.56 ± 0.07	-0.88 ± 0.04	0.00	0.00	0000000	M2FS
SMC	NGC 361	N361-1-b117	15.440317	-71.604836	18.34	1.34	4858	4690595940758485760	4.7	149.71 ± 0.49	1.59 ± 0.19	-0.54 ± 0.06	0.00	0.00	0000000	M2FS
SMC	NGC 361	N361-1-b118	15.411912	-71.630014	18.49	1.14	4899	4690584155345266944	3.8	88.89 ± 0.71	1.38 ± 0.22	-0.72 ± 0.08	0.00	0.00	0000000	M2FS
SMC	NGC 361	N361-1-b119	15.398216	-71.635803	18.47	1.06	4893	4690584056565640832	4.4	147.15 ± 0.68	0.87 ± 0.25	-1.06 ± 0.07	0.00	0.00	0000000	M2FS
SMC	NGC 361	N361-1-b120	15.381794	-71.636696	17.19	1.39	4546	4690584056573586688	9.9	154.17 ± 0.29	0.05 ± 0.05	-1.03 ± 0.04	0.00	0.00	0000000	M2FS
SMC	NGC 361	N361-1-b121	15.358116	-71.558058	18.43	1.13	4881	4690597074607705344	4.5	146.48 ± 0.60	1.26 ± 0.22	-0.84 ± 0.08	0.00	0.00	0000000	M2FS
SMC	NGC 361	N361-1-b122	15.303991	-71.589101	18.43	1.08	4881	4690596868448673792	4.2	131.24 ± 0.66	0.95 ± 0.25	-0.86 ± 0.07	0.00	0.00	0000000	M2FS
SMC	NGC 361	N361-1-b123	15.302820	-71.603811	15.85	1.78	4053	4690596116841711232	17.8	118.04 ± 0.22	0.06 ± 0.05	-1.13 ± 0.03	0.00	0.00	0000000	M2FS

Table C.1: (*continued*) Sample of 3095 Targets from 26 Star Clusters

Galaxy	Cluster	ID	RAJ2000 (deg)	DEJ2000 (deg)	G (mag)	$G_{\rm BP} - G_{\rm RP}$ (mag)	$T_{\rm eff}$ (K)	*Gaia* DR2 ID	S/N	$v_{\rm los}$ (km s^{-1})	$\log g$ (dex)	$[{\rm Fe/H}]_{\rm raw}$ (dex)	P_M	P'_M	Flag[a]	Source[b]
(1)	(2)	(3)	(4)	(5)	(6)	(7)	(8)	(9)	(10)	(11)	(12)	(13)	(14)	(15)	(16)	(17)
SMC	NGC 361	N361-1-b124	15.381892	-71.610815	18.58	1.06	4923	4690595872016152320	4.1	181.21 ± 0.58	1.78 ± 0.21	-0.93 ± 0.09	0.00	0.00	0000000	M2FS
SMC	NGC 361	N361-1-b125	15.356250	-71.626543	18.11	1.24	4801	4690595803296810752	5.5	159.64 ± 0.40	1.49 ± 0.17	-0.62 ± 0.06	0.00	0.00	0000000	M2FS
SMC	NGC 361	N361-1-b126	15.341211	-71.627983	18.19	1.21	4822	4690595807604098560	4.4	103.34 ± 0.73	1.72 ± 0.20	-1.09 ± 0.08	0.00	0.00	0000000	M2FS
SMC	NGC 361	N361-1-b127	15.378973	-71.628783	18.09	1.09	4796	4690584052266046464	6.8	123.07 ± 0.48	1.00 ± 0.15	-0.95 ± 0.05	0.00	0.00	0000000	M2FS
SMC	NGC 361	N361-1-b128	15.260251	-71.643376	17.60	1.32	4665	4690589966448605056	6.2	123.16 ± 0.51	1.30 ± 0.13	-0.80 ± 0.05	0.00	0.00	0000000	M2FS
SMC	NGC 361	N361-1-r049	15.524343	-71.615869	16.72	1.61	4375	4690584503250144128	12.4	170.88 ± 0.23	1.07 ± 0.06	-0.75 ± 0.04	1.00	1.00	0000000	M2FS
SMC	NGC 361	N361-1-r079	15.507652	-71.596180	17.47	1.30	4623	4690584571969576448	9.6	154.21 ± 0.34	0.80 ± 0.10	-1.01 ± 0.04	0.00	0.00	0000000	M2FS
SMC	NGC 361	N361-1-r099	15.600249	-71.596561	16.64	1.56	4343	4690584636381790976	13.3	171.94 ± 0.27	0.63 ± 0.06	-0.86 ± 0.03	0.95	0.95	0000000	M2FS
SMC	NGC 361	N361-1-r127	15.576461	-71.604538	16.43	1.59	4270	4690584537609849856	15.1	174.08 ± 0.21	0.73 ± 0.05	-0.90 ± 0.03	1.00	1.00	0000000	M2FS
SMC	NGC 411	N411-1-b001	17.044860	-71.844401	18.41	1.07	4933	4690536910701214976	6.9	121.93 ± 0.35	1.50 ± 0.16	-1.06 ± 0.05	0.00	0.00	0000000	M2FS
SMC	NGC 411	N411-1-b002	17.094886	-71.793022	18.52	1.09	4966	4690538151952283008	7.2	142.35 ± 0.31	1.98 ± 0.12	-0.60 ± 0.05	0.00	0.00	0000000	M2FS
SMC	NGC 411	N411-1-b003	17.023414	-71.792447	16.89	1.50	4429	4690538388170736512	18.9	164.51 ± 0.19	0.99 ± 0.06	-0.62 ± 0.03	0.85	0.88	0000000	M2FS
SMC	NGC 411	N411-1-b004	17.089728	-71.789687	17.57	1.22	4663	4690538353811020544	10.0	103.10 ± 0.27	0.95 ± 0.09	-0.93 ± 0.04	0.00	0.00	0000000	M2FS
SMC	NGC 411	N411-1-b005	17.030898	-71.776867	17.85	1.35	4745	4690541343108869632	9.2	165.74 ± 0.22	1.38 ± 0.10	-0.57 ± 0.04	-1.00	-1.00	0000001	M2FS
SMC	NGC 411	N411-1-b006	17.080842	-71.775085	16.92	1.40	4429	4690538426839500928	17.5	180.35 ± 0.19	0.56 ± 0.06	-0.99 ± 0.03	0.00	0.00	0000000	M2FS
SMC	NGC 411	N411-1-b007	17.026577	-71.772898	17.83	1.24	4739	4690541347407895808	10.3	164.35 ± 0.22	1.22 ± 0.09	-0.83 ± 0.04	0.98	0.98	0000000	M2FS
SMC	NGC 411	N411-1-b008	17.038980	-71.766829	17.81	1.18	4733	4690541343117139456	9.9	164.34 ± 0.22	1.08 ± 0.09	-0.79 ± 0.04	0.98	0.98	0000000	M2FS
SMC	NGC 411	N411-1-b009	17.166248	-71.864832	17.97	1.22	4790	4687534556761488512	7.1	172.71 ± 0.36	0.94 ± 0.15	-0.99 ± 0.05	0.00	0.00	0000000	M2FS
SMC	NGC 411	N411-1-b010	17.169365	-71.835467	19.09	1.01	5127	4690537155529274880	3.8	134.93 ± 0.76	1.30 ± 0.32	-1.17 ± 0.11	0.00	0.00	0000000	M2FS
SMC	NGC 411	N411-1-b011	17.228327	-71.835108	17.87	1.33	4756	4690537116859798400	7.4	166.88 ± 0.35	0.96 ± 0.16	-1.37 ± 0.05	0.00	0.00	0000000	M2FS
SMC	NGC 411	N411-1-b012	17.128715	-71.833841	17.73	1.20	4713	4690537254353958400	10.9	137.45 ± 0.25	1.22 ± 0.08	-0.74 ± 0.04	0.00	0.00	0000000	M2FS
SMC	NGC 411	N411-1-b013	17.136874	-71.829102	17.98	1.29	4793	4690537258608481920	8.3	141.41 ± 0.30	1.13 ± 0.12	-0.60 ± 0.04	0.00	0.00	0000000	M2FS
SMC	NGC 411	N411-1-b014	17.148950	-71.819393	18.44	1.15	4942	4690537430397834112	5.1	145.71 ± 0.52	1.54 ± 0.18	-0.81 ± 0.07	0.00	0.00	0000000	M2FS
SMC	NGC 411	N411-1-b015	17.223375	-71.816203	17.64	1.40	4683	4690537391737928320	5.2	157.92 ± 0.39	1.36 ± 0.14	-0.61 ± 0.05	0.00	0.00	0000000	M2FS
SMC	NGC 411	N411-1-b016	17.169668	-71.798565	18.13	1.19	4845	4690538186321366272	6.8	127.89 ± 0.36	1.14 ± 0.13	-0.77 ± 0.05	0.00	0.00	0000000	M2FS
SMC	NGC 411	N411-1-b017	17.216576	-71.729978	17.13	1.41	4508	4690547394731069568	14.2	154.57 ± 0.21	0.43 ± 0.09	-1.38 ± 0.03	0.00	0.00	0000000	M2FS
SMC	NGC 411	N411-1-b018	17.224237	-71.780005	17.48	1.30	4639	4690544096196330240	13.0	126.00 ± 0.23	0.97 ± 0.07	-0.83 ± 0.03	0.00	0.00	0000000	M2FS
SMC	NGC 411	N411-1-b019	17.244997	-71.783803	17.12	1.36	4504	4690543340282092032	15.0	123.22 ± 0.20	0.90 ± 0.06	-0.92 ± 0.03	0.00	0.00	0000000	M2FS
SMC	NGC 411	N411-1-b020	17.257609	-71.787187	17.67	1.28	4697	4690543335999201280	10.8	160.42 ± 0.33	0.75 ± 0.16	-1.87 ± 0.04	0.00	0.00	0000000	M2FS
SMC	NGC 411	N411-1-b021	17.274473	-71.793688	18.26	1.23	4886	4690543267253553408	6.3	204.05 ± 0.45	1.34 ± 0.17	-0.84 ± 0.06	0.00	0.00	0000000	M2FS
SMC	NGC 411	N411-1-b022	17.324809	-71.795045	17.72	1.28	4707	4690543099763938816	7.1	156.22 ± 0.39	1.30 ± 0.12	-0.71 ± 0.05	0.00	0.00	0000000	M2FS
SMC	NGC 411	N411-1-b023	17.235851	-71.806463	17.40	1.34	4610	4690537396047394304	9.7	173.87 ± 0.23	1.03 ± 0.08	-0.80 ± 0.04	0.00	0.00	0000000	M2FS
SMC	NGC 411	N411-1-b024	17.327483	-71.807033	17.57	1.03	4664	4690543031044480128	9.6	150.50 ± 0.36	0.37 ± 0.19	-1.28 ± 0.04	0.00	0.00	0000000	M2FS
SMC	NGC 411	N411-1-b025	17.149167	-71.694258	17.95	1.12	4785	4690547734021077888	9.2	178.17 ± 0.31	1.10 ± 0.11	-1.17 ± 0.04	0.00	0.00	0000000	M2FS
SMC	NGC 411	N411-1-b026	17.182500	-71.696188	18.26	1.24	4886	4690547734021072384	6.6	116.78 ± 0.41	0.78 ± 0.21	-0.59 ± 0.06	0.00	0.00	0000000	M2FS
SMC	NGC 411	N411-1-b027	17.144943	-71.712654	18.42	1.02	4935	4690541789786077312	6.3	153.05 ± 0.59	1.45 ± 0.19	-1.37 ± 0.07	0.00	0.00	0000000	M2FS
SMC	NGC 411	N411-1-b028	17.194755	-71.715470	17.80	1.18	4731	4690547463450521728	8.7	125.95 ± 0.33	1.18 ± 0.11	-0.69 ± 0.04	0.00	0.00	0000000	M2FS
SMC	NGC 411	N411-1-b029	17.149532	-71.722908	18.29	1.19	4895	4690541587925850624	6.9	180.38 ± 0.42	0.92 ± 0.19	-1.33 ± 0.06	0.00	0.00	0000000	M2FS
SMC	NGC 411	N411-1-b030	17.199009	-71.733455	18.49	1.19	4958	4690547394731077504	4.5	125.98 ± 0.60	1.46 ± 0.21	-0.86 ± 0.08	0.00	0.00	0000000	M2FS
SMC	NGC 411	N411-1-b031	17.149640	-71.756541	18.43	1.10	4938	4690538564268966016	7.7	158.53 ± 0.28	1.54 ± 0.12	-1.14 ± 0.05	0.00	0.00	0000000	M2FS
SMC	NGC 411	N411-1-b032	17.135534	-71.761918	18.06	1.30	4819	4690538525610140416	8.4	155.76 ± 0.29	1.56 ± 0.11	-0.68 ± 0.04	0.00	0.00	0000000	M2FS
SMC	NGC 411	N411-1-b034	16.978759	-71.811295	17.49	1.35	4641	4690537945803231360	13.1	190.03 ± 0.23	1.18 ± 0.07	-0.82 ± 0.03	0.00	0.00	0000000	M2FS
SMC	NGC 411	N411-1-b035	16.982827	-71.804520	18.19	1.15	4862	4690538014522696832	10.5	136.32 ± 0.30	1.17 ± 0.11	-1.08 ± 0.04	0.00	0.00	0000000	M2FS
SMC	NGC 411	N411-1-b036	16.970478	-71.797425	16.78	1.16	4429	4690538014522687744	26.1	136.30 ± 0.20	0.44 ± 0.07	-1.35 ± 0.03	0.00	0.00	0000000	M2FS
SMC	NGC 411	N411-1-b037	16.981442	-71.790280	15.67	1.85	4429	4690540969460173056	29.5	162.84 ± 0.25	1.58 ± 0.08	-0.44 ± 0.04	0.81	0.72	0000010	M2FS
SMC	NGC 411	N411-1-b038	16.963827	-71.775730	18.54	1.07	4973	4690541038170272896	8.1	160.32 ± 0.30	1.64 ± 0.11	-0.79 ± 0.05	1.00	-1.00	0000000	M2FS
SMC	NGC 411	N411-1-b039	16.974872	-71.771806	18.20	1.08	4865	4690541038179563008	8.2	164.07 ± 0.43	1.55 ± 0.13	-0.76 ± 0.05	1.00	1.00	0000000	M2FS
SMC	NGC 411	N411-1-b040	16.968946	-71.768685	17.56	1.12	4661	4690541038170240384	9.1	164.86 ± 0.29	1.32 ± 0.09	-0.85 ± 0.04	1.00	1.00	0000000	M2FS
SMC	NGC 411	N411-1-b043	17.011562	-71.787303	17.85	1.13	4744	4690538392479789696	7.4	149.27 ± 0.41	0.80 ± 0.16	-1.15 ± 0.05	0.00	0.00	0000000	M2FS
SMC	NGC 411	N411-1-b044	16.985440	-71.785309	15.58	1.98	4429	4690540969460165760	31.3	166.20 ± 0.25	1.69 ± 0.09	-0.43 ± 0.05	0.80	0.64	0000010	M2FS
SMC	NGC 411	N411-1-b045	17.004177	-71.780253	18.34	1.14	4909	4690541343108868736	6.0	165.30 ± 0.49	1.19 ± 0.17	-0.84 ± 0.05	0.96	0.96	0000000	M2FS
SMC	NGC 411	N411-1-b046	16.985331	-71.779106	18.61	1.01	4992	4690540965160016512	6.9	161.88 ± 0.41	1.67 ± 0.14	-0.75 ± 0.05	0.94	0.86	0000000	M2FS
SMC	NGC 411	N411-1-b047	17.000161	-71.776380	18.70	1.04	5019	4690541343153335040	6.6	164.66 ± 0.38	2.31 ± 0.14	-0.56 ± 0.05	-1.00	-1.00	0000001	M2FS
SMC	NGC 411	N411-1-b048	16.988258	-71.771387	17.58	1.07	4669	4690541038170175232	12.7	161.87 ± 0.20	1.16 ± 0.07	-0.81 ± 0.03	1.00	1.00	0000000	M2FS

Table C.1: (*continued*) Sample of 3095 Targets from 26 Star Clusters

Galaxy	Cluster	ID	RAJ2000 (deg)	DEJ2000 (deg)	G (mag)	$G_{\rm BP} - G_{\rm RP}$ (mag)	$T_{\rm eff}$ (K)	*Gaia* DR2 ID	S/N	$v_{\rm los}$ (km s^{-1})	$\log g$ (dex)	$[{\rm Fe/H}]_{\rm raw}$ (dex)	P_M	P'_M	Flag[a]	Source[b]
(1)	(2)	(3)	(4)	(5)	(6)	(7)	(8)	(9)	(10)	(11)	(12)	(13)	(14)	(15)	(16)	(17)
SMC	NGC 411	N411-1-b049	17.062390	-71.664098	17.08	1.40	4491	4690542958069977984	11.5	148.24 ± 0.23	1.16 ± 0.07	-0.76 ± 0.04	0.00	0.00	0000000	M2FS
SMC	NGC 411	N411-1-b053	17.081596	-71.716943	18.46	1.18	4946	4690541828453440512	7.5	125.41 ± 0.37	1.60 ± 0.13	-0.93 ± 0.05	0.00	0.00	0000000	M2FS
SMC	NGC 411	N411-1-b054	17.119418	-71.717092	18.17	1.05	4856	4690541794084266368	10.3	108.02 ± 0.28	1.34 ± 0.10	-0.90 ± 0.04	0.00	0.00	0000000	M2FS
SMC	NGC 411	N411-1-b055	17.073049	-71.735660	17.52	1.42	4646	4690541759733999232	14.4	143.94 ± 0.21	1.17 ± 0.08	-0.58 ± 0.03	0.00	0.00	0000000	M2FS
SMC	NGC 411	N411-1-b056	17.077263	-71.763215	18.17	1.05	4857	4690541377468403200	9.2	151.38 ± 0.30	1.52 ± 0.11	-1.20 ± 0.05	0.00	0.00	0000000	M2FS
SMC	NGC 411	N411-1-b058	16.982585	-71.663783	17.90	1.18	4767	4690554571609396480	11.5	118.97 ± 0.27	0.92 ± 0.10	-1.09 ± 0.04	0.00	0.00	0000000	M2FS
SMC	NGC 411	N411-1-b059	16.982129	-71.710250	18.66	1.08	5007	4690542511360977408	7.7	156.60 ± 0.38	1.63 ± 0.13	-1.05 ± 0.05	0.00	0.00	0000000	M2FS
SMC	NGC 411	N411-1-b060	17.009536	-71.751448	17.52	1.25	4647	4690541622295074688	15.8	163.48 ± 0.22	1.02 ± 0.07	-0.74 ± 0.03	0.98	0.98	0000000	M2FS
SMC	NGC 411	N411-1-b061	17.025323	-71.753648	18.12	1.13	4838	4690541411828305408	8.9	178.53 ± 0.33	1.23 ± 0.12	-1.00 ± 0.04	0.00	0.00	0000000	M2FS
SMC	NGC 411	N411-1-b062	17.004928	-71.756791	17.35	1.07	4590	4690541622295085056	18.4	129.64 ± 0.17	0.73 ± 0.06	-1.23 ± 0.03	0.00	0.00	0000000	M2FS
SMC	NGC 411	N411-1-b063	17.001771	-71.761735	17.92	1.10	4776	4690541416127292800	12.0	163.50 ± 0.22	1.37 ± 0.08	-0.69 ± 0.04	1.00	1.00	0000000	M2FS
SMC	NGC 411	N411-1-b064	16.989298	-71.763960	17.52	1.08	4646	4690541416127336832	13.2	163.11 ± 0.23	1.01 ± 0.08	-0.76 ± 0.03	1.00	1.00	0000000	M2FS
SMC	NGC 411	N411-1-b065	16.912425	-71.880322	18.52	1.19	4965	4690536738902206336	7.8	150.34 ± 0.30	1.57 ± 0.12	-0.89 ± 0.05	0.00	0.00	0000000	M2FS
SMC	NGC 411	N411-1-b066	16.898728	-71.876205	18.07	1.21	4823	4690536743212478464	9.5	144.43 ± 0.32	1.39 ± 0.10	-1.00 ± 0.04	0.00	0.00	0000000	M2FS
SMC	NGC 411	N411-1-b067	16.889742	-71.868120	18.36	1.25	4917	4690537499126713216	10.1	190.74 ± 0.26	1.31 ± 0.10	-0.91 ± 0.04	0.00	0.00	0000000	M2FS
SMC	NGC 411	N411-1-b068	16.906757	-71.865028	18.16	1.15	4853	4690537533477165696	12.9	192.92 ± 0.48	2.32 ± 0.12	-1.31 ± 0.07	0.00	0.00	0000000	M2FS
SMC	NGC 411	N411-1-b070	16.904380	-71.783279	18.37	1.04	4920	4690541003819906432	7.0	154.51 ± 0.37	1.46 ± 0.14	-1.10 ± 0.05	0.00	0.00	0000000	M2FS
SMC	NGC 411	N411-1-b071	16.887842	-71.774509	16.66	1.40	4429	4690541209978322944	22.9	108.78 ± 0.17	0.32 ± 0.08	-1.34 ± 0.03	0.00	0.00	0000000	M2FS
SMC	NGC 411	N411-1-b072	16.901529	-71.770500	17.33	1.38	4586	4690541209978314240	14.4	183.48 ± 0.33	0.99 ± 0.10	-0.58 ± 0.04	0.00	0.00	0000000	M2FS
SMC	NGC 411	N411-1-b073	16.949318	-71.875085	18.03	1.48	4808	4690536708843459712	8.7	149.55 ± 0.31	1.28 ± 0.12	-0.74 ± 0.04	0.00	0.00	0000010	M2FS
SMC	NGC 411	N411-1-b074	16.924526	-71.864585	17.60	1.28	4674	4690536777572201856	13.9	139.01 ± 0.22	1.24 ± 0.06	-0.80 ± 0.03	0.00	0.00	0000000	M2FS
SMC	NGC 411	N411-1-b076	16.948622	-71.851167	18.48	1.16	4952	4690537529176418176	7.7	163.32 ± 0.46	1.44 ± 0.16	-1.27 ± 0.05	0.00	0.00	0000000	M2FS
SMC	NGC 411	N411-1-b077	16.944668	-71.814038	18.30	1.35	4896	4690537975853555200	7.3	155.06 ± 0.42	1.64 ± 0.12	-0.54 ± 0.04	0.00	0.00	0000000	M2FS
SMC	NGC 411	N411-1-b078	16.945592	-71.797178	17.74	1.39	4718	4690540935100450304	11.7	149.95 ± 0.28	1.17 ± 0.09	-0.80 ± 0.04	0.00	0.00	0000000	M2FS
SMC	NGC 411	N411-1-b079	16.928316	-71.794515	15.95	1.13	4429	4690540935100446720	35.8	141.27 ± 0.17	0.02 ± 0.02	-1.37 ± 0.03	0.00	0.00	0000000	M2FS
SMC	NGC 411	N411-1-b080	16.939766	-71.788396	18.28	1.13	4890	4690540935100434432	10.3	160.55 ± 0.34	1.30 ± 0.12	-1.15 ± 0.04	0.01	0.00	0000000	M2FS
SMC	NGC 411	N411-1-b081	16.973398	-71.724998	17.86	1.23	4749	4690542446919335808	10.3	163.10 ± 0.26	1.27 ± 0.09	-0.83 ± 0.04	0.66	0.13	0000000	M2FS
SMC	NGC 411	N411-1-b082	16.952539	-71.738265	17.62	1.30	4677	4690542068971655808	15.2	163.37 ± 0.20	0.95 ± 0.07	-0.80 ± 0.03	0.85	0.82	0000000	M2FS
SMC	NGC 411	N411-1-b083	16.960211	-71.747669	16.46	1.23	4429	4690541313057426816	29.5	155.17 ± 0.16	0.46 ± 0.06	-1.16 ± 0.03	0.00	0.00	0000000	M2FS
SMC	NGC 411	N411-1-b084	16.973740	-71.754067	18.35	1.17	4913	4690541617986735872	8.9	204.83 ± 0.32	1.53 ± 0.10	-0.87 ± 0.04	0.00	0.00	0000000	M2FS
SMC	NGC 411	N411-1-b085	16.953830	-71.755924	16.05	1.81	4429	4690541244337965440	26.6	164.65 ± 0.37	1.03 ± 0.12	-0.48 ± 0.04	0.97	0.98	0000010	M2FS
SMC	NGC 411	N411-1-b086	16.979322	-71.757344	16.89	1.45	4429	4690541622295088256	19.6	163.95 ± 0.21	0.87 ± 0.06	-0.68 ± 0.03	1.00	1.00	0000000	M2FS
SMC	NGC 411	N411-1-b087	16.962311	-71.765290	15.66	2.52	4429	4690541244338036992	7.0	165.29 ± 1.73	1.56 ± 0.55	-1.34 ± 0.24	-1.00	-1.00	0110010	M2FS
SMC	NGC 411	N411-1-b088	16.978934	-71.765869	18.10	1.12	4834	4690541038179559296	6.7	164.93 ± 0.52	1.53 ± 0.14	-0.77 ± 0.05	1.00	1.00	0000000	M2FS
SMC	NGC 411	N411-1-b089	16.941561	-71.656530	18.55	1.09	4975	4690554850794187008	6.0	166.66 ± 0.45	1.84 ± 0.18	-1.30 ± 0.07	0.00	0.00	0000000	M2FS
SMC	NGC 411	N411-1-b090	16.944875	-71.677987	18.12	1.17	4839	4690554537249493376	10.9	156.87 ± 0.33	0.97 ± 0.11	-1.08 ± 0.04	0.00	0.00	0000000	M2FS
SMC	NGC 411	N411-1-b092	16.906460	-71.732397	18.29	1.13	4894	4690542133408434048	9.5	170.17 ± 0.26	1.54 ± 0.10	-0.86 ± 0.04	0.00	0.00	0000000	M2FS
SMC	NGC 411	N411-1-b093	16.932144	-71.746605	16.56	1.77	4429	4690542068971671040	21.1	168.24 ± 0.24	1.18 ± 0.06	-0.68 ± 0.04	0.00	0.00	0000010	M2FS
SMC	NGC 411	N411-1-b094	16.901546	-71.749731	17.41	1.35	4613	4690542034611941248	16.4	155.37 ± 0.19	1.10 ± 0.06	-0.84 ± 0.03	0.00	0.00	0000000	M2FS
SMC	NGC 411	N411-1-b095	16.898379	-71.753222	17.27	1.43	4562	4690542030303773312	16.1	110.46 ± 0.21	1.19 ± 0.06	-0.66 ± 0.03	0.00	0.00	0000000	M2FS
SMC	NGC 411	N411-1-b096	16.924341	-71.759769	17.16	1.37	4522	4690541313057505024	20.0	179.55 ± 0.19	0.55 ± 0.07	-1.10 ± 0.03	0.00	0.00	0000000	M2FS
SMC	NGC 411	N411-1-b097	16.740044	-71.848991	18.09	1.12	4830	4690539281523088000	13.0	107.97 ± 0.23	1.42 ± 0.08	-0.87 ± 0.03	0.00	0.00	0000000	M2FS
SMC	NGC 411	N411-1-b098	16.719779	-71.820937	17.37	1.02	4597	4690539560710965760	19.4	116.57 ± 0.20	0.70 ± 0.07	-1.52 ± 0.03	0.00	0.00	0000000	M2FS
SMC	NGC 411	N411-1-b099	16.757625	-71.815724	18.30	1.08	4898	4690539590806894848	12.4	112.98 ± 0.25	1.31 ± 0.08	-0.69 ± 0.04	0.00	0.00	0000000	M2FS
SMC	NGC 411	N411-1-b100	16.656598	-71.806390	16.47	1.71	4429	4690540282265453440	26.8	142.79 ± 0.21	0.94 ± 0.05	-0.82 ± 0.03	0.00	0.00	0000010	M2FS
SMC	NGC 411	N411-1-b101	16.685794	-71.790944	18.01	1.29	4800	4690540449755055744	9.8	117.79 ± 0.52	0.24 ± 0.18	-0.93 ± 0.07	0.00	0.00	0000000	M2FS
SMC	NGC 411	N411-1-b102	16.712067	-71.790078	17.79	1.27	4730	4690540381061708544	13.5	118.22 ± 0.22	1.15 ± 0.08	-0.94 ± 0.03	0.00	0.00	0000000	M2FS
SMC	NGC 411	N411-1-b103	16.669891	-71.784191	17.52	1.17	4647	4690540660222540032	18.3	139.00 ± 0.21	0.86 ± 0.07	-1.24 ± 0.03	0.00	0.00	0000000	M2FS
SMC	NGC 411	N411-1-b104	16.749760	-71.782531	18.30	1.22	4898	4690540419704361344	11.9	162.34 ± 0.23	1.22 ± 0.10	-0.95 ± 0.04	0.00	0.00	0000000	M2FS
SMC	NGC 411	N411-1-b106	16.802740	-71.863978	18.24	1.34	4878	4690536296535869696	9.7	111.70 ± 0.30	1.61 ± 0.10	-0.69 ± 0.04	0.00	0.00	0000000	M2FS
SMC	NGC 411	N411-1-b107	16.819056	-71.838564	17.99	1.01	4795	4690536360945485184	13.7	154.99 ± 0.24	0.75 ± 0.10	-1.24 ± 0.03	0.00	0.00	0000000	M2FS
SMC	NGC 411	N411-1-b108	16.839901	-71.813818	17.80	1.23	4731	4690540793373880704	13.8	145.82 ± 0.23	0.75 ± 0.10	-1.46 ± 0.03	0.00	0.00	0000000	M2FS
SMC	NGC 411	N411-1-b109	16.883078	-71.805828	18.41	1.07	4931	4690540832021251200	9.4	128.70 ± 0.43	1.31 ± 0.15	-1.51 ± 0.05	0.00	0.00	0000000	M2FS
SMC	NGC 411	N411-1-b110	16.849171	-71.797998	18.06	1.22	4819	4690540900740717952	11.3	172.04 ± 0.29	1.37 ± 0.09	-0.63 ± 0.04	0.00	0.00	0000000	M2FS

Table C.1: (*continued*) Sample of 3095 Targets from 26 Star Clusters

Galaxy	Cluster	ID	RAJ2000 (deg)	DEJ2000 (deg)	G (mag)	$G_{\rm BP} - G_{\rm RP}$ (mag)	$T_{\rm eff}$ (K)	*Gaia* DR2 ID	S/N	$v_{\rm los}$ (km s^{-1})	$\log g$ (dex)	$[{\rm Fe/H}]_{\rm raw}$ (dex)	P_M	P'_M	Flag[a]	Source[b]
(1)	(2)	(3)	(4)	(5)	(6)	(7)	(8)	(9)	(10)	(11)	(12)	(13)	(14)	(15)	(16)	(17)
SMC	NGC 411	N411-1-b111	16.769168	-71.796062	18.56	1.11	4977	4690539659480999424	8.0	127.44 ± 0.37	1.71 ± 0.11	-0.78 ± 0.05	0.00	0.00	0000000	M2FS
SMC	NGC 411	N411-1-b112	16.764809	-71.788152	18.45	1.22	4944	4690540415395386112	9.1	140.35 ± 0.37	1.26 ± 0.14	-0.88 ± 0.04	0.00	0.00	0000000	M2FS
SMC	NGC 411	N411-1-b113	16.862470	-71.668718	18.18	1.23	4861	4690554438477353216	9.8	152.04 ± 0.33	1.69 ± 0.10	-0.57 ± 0.04	0.00	0.00	0000000	M2FS
SMC	NGC 411	N411-1-b114	16.770175	-71.674096	18.00	1.14	4799	4690554365450862592	13.3	121.24 ± 0.20	1.30 ± 0.07	-0.73 ± 0.03	0.00	0.00	0000000	M2FS
SMC	NGC 411	N411-1-b116	16.791050	-71.678198	18.45	1.05	4944	4690554468530021376	10.0	135.81 ± 0.40	1.24 ± 0.15	-1.45 ± 0.05	0.00	0.00	0000000	M2FS
SMC	NGC 411	N411-1-b117	16.841486	-71.697792	18.48	1.16	4954	4690554193651860224	10.1	141.53 ± 0.30	1.61 ± 0.10	-0.77 ± 0.04	0.00	0.00	0000000	M2FS
SMC	NGC 411	N411-1-b118	16.798581	-71.701822	18.54	1.10	4971	4690554094870595200	8.1	133.73 ± 0.37	1.63 ± 0.12	-0.62 ± 0.04	0.00	0.00	0000000	M2FS
SMC	NGC 411	N411-1-b119	16.869502	-71.748471	18.44	1.21	4940	4690542099023168768	9.3	161.20 ± 0.24	1.76 ± 0.09	-0.84 ± 0.04	0.00	0.00	0000000	M2FS
SMC	NGC 411	N411-1-b120	16.794229	-71.750369	17.90	1.24	4768	4690542172050903936	12.6	170.68 ± 0.27	1.32 ± 0.08	-0.86 ± 0.03	0.00	0.00	0000000	M2FS
SMC	NGC 411	N411-1-b121	16.753278	-71.692217	17.35	1.17	4589	4690554365450627968	19.7	131.91 ± 0.20	0.76 ± 0.06	-1.37 ± 0.03	0.00	0.00	0000000	M2FS
SMC	NGC 411	N411-1-b122	16.757991	-71.713489	16.61	1.75	4429	4690554060520317056	22.1	140.13 ± 0.20	1.37 ± 0.05	-0.65 ± 0.03	0.00	0.00	0000010	M2FS
SMC	NGC 411	N411-1-b123	16.695008	-71.733507	18.39	1.05	4925	4690552578751582720	10.2	107.49 ± 0.36	1.06 ± 0.15	-1.35 ± 0.04	0.00	0.00	0000000	M2FS
SMC	NGC 411	N411-1-b124	16.710820	-71.737402	17.50	1.39	4644	4690552514332134656	16.0	173.48 ± 0.23	0.96 ± 0.07	-0.82 ± 0.03	0.00	0.00	0000000	M2FS
SMC	NGC 411	N411-1-b125	16.754118	-71.737461	17.37	1.33	4595	4690542240770359680	19.2	149.54 ± 0.18	0.80 ± 0.06	-0.96 ± 0.03	0.00	0.00	0000000	M2FS
SMC	NGC 411	N411-1-b126	16.619004	-71.743743	17.61	1.27	4676	4690552441304505472	16.3	131.24 ± 0.19	0.94 ± 0.07	-0.78 ± 0.03	0.00	0.00	0000000	M2FS
SMC	NGC 411	N411-1-b127	16.727681	-71.749378	18.46	1.21	4948	4690540758993382144	10.5	164.17 ± 0.24	1.72 ± 0.10	-0.53 ± 0.04	0.00	0.00	0000000	M2FS
SMC	NGC 411	N411-1-b128	16.712396	-71.767280	18.58	1.02	4983	4690540690273602432	8.8	113.86 ± 0.39	1.41 ± 0.13	-0.77 ± 0.04	0.00	0.00	0000000	M2FS
SMC	NGC 411	N411-1-r028	16.950055	-71.764718	16.68	1.65	4429	4690541244338036736	24.0	189.44 ± 0.21	0.97 ± 0.05	-0.81 ± 0.03	0.00	0.00	0000010	M2FS
SMC	NGC 411	N411-1-r049	16.975687	-71.776629	16.70	1.37	4429	4690541038170274432	25.1	164.18 ± 0.18	0.84 ± 0.05	-0.72 ± 0.03	1.00	1.00	0000000	M2FS
SMC	NGC 411	N411-1-r079	16.959234	-71.760977	17.29	1.26	4569	4690541244338027904	18.9	163.10 ± 0.19	1.12 ± 0.06	-0.77 ± 0.03	1.00	1.00	0000000	M2FS
SMC	NGC 411	N411-1-r099	16.975275	-71.761874	17.16	1.25	4523	4690541244338027264	15.6	165.43 ± 0.24	1.09 ± 0.06	-0.78 ± 0.03	1.00	1.00	0000000	M2FS
SMC	NGC 416	N416-4-b001	17.069884	-72.467606	15.78	2.02	4056	4687457148587508736	15.4	138.48 ± 0.33	0.79 ± 0.06	-0.93 ± 0.05	0.00	0.00	0000000	M2FS
SMC	NGC 416	N416-4-b002	17.070409	-72.463133	17.86	1.27	4722	4687457144273719680	7.8	180.91 ± 0.31	1.38 ± 0.10	-0.92 ± 0.05	0.00	0.00	0000000	M2FS
SMC	NGC 416	N416-4-b003	17.078701	-72.445014	18.21	1.13	4816	4687460103525005696	6.2	187.20 ± 0.39	1.31 ± 0.13	-0.63 ± 0.05	0.00	0.00	0000000	M2FS
SMC	NGC 416	N416-4-b004	17.081401	-72.429841	18.35	1.08	4850	4687460167964069504	5.4	99.60 ± 0.63	1.26 ± 0.19	-1.07 ± 0.07	0.00	0.00	0000000	M2FS
SMC	NGC 416	N416-4-b005	17.111990	-72.405960	17.50	1.13	4617	4687460408453202048	8.8	167.48 ± 0.34	1.29 ± 0.09	-0.73 ± 0.04	0.00	0.00	0000000	M2FS
SMC	NGC 416	N416-4-b007	17.119098	-72.401394	17.27	1.26	4553	4687460412762158848	10.7	144.24 ± 0.33	0.44 ± 0.18	-2.10 ± 0.05	0.00	0.00	0000000	M2FS
SMC	NGC 416	N416-4-b008	17.062828	-72.377021	17.05	1.49	4478	4687461301806920064	8.1	149.52 ± 0.28	1.12 ± 0.08	-0.78 ± 0.04	0.00	0.00	0000000	M2FS
SMC	NGC 416	N416-4-b009	17.178234	-72.446541	17.91	1.23	4737	4687457492184492928	5.8	153.18 ± 0.51	0.73 ± 0.17	-1.04 ± 0.05	0.00	0.00	0000000	M2FS
SMC	NGC 416	N416-4-b010	17.168908	-72.440438	17.64	1.04	4661	4687457556594385280	7.9	187.41 ± 0.49	0.89 ± 0.15	-1.26 ± 0.05	0.00	0.00	0000000	M2FS
SMC	NGC 416	N416-4-b011	17.231929	-72.432009	18.52	1.14	4897	4687457522230908800	3.7	125.55 ± 0.79	1.53 ± 0.25	-0.93 ± 0.09	0.00	0.00	0000000	M2FS
SMC	NGC 416	N416-4-b012	17.240518	-72.412738	18.28	1.11	4834	4687457590989475968	5.1	187.61 ± 0.53	1.07 ± 0.22	-0.91 ± 0.07	0.00	0.00	0000000	M2FS
SMC	NGC 416	N416-4-b013	17.137162	-72.390480	17.56	1.19	4636	4687460859438732032	8.4	126.45 ± 0.32	1.06 ± 0.10	-1.06 ± 0.04	0.00	0.00	0000000	M2FS
SMC	NGC 416	N416-4-b014	17.199582	-72.374314	18.61	1.03	4922	4687460893798436096	2.9	206.08 ± 0.98	1.96 ± 0.31	-1.04 ± 0.12	0.00	0.00	0000000	M2FS
SMC	NGC 416	N416-4-b015	17.165962	-72.372512	18.48	1.14	4887	4687461645404401408	3.7	155.42 ± 0.79	1.79 ± 0.23	-0.67 ± 0.08	0.00	0.00	0000000	M2FS
SMC	NGC 416	N416-4-b016	17.152207	-72.370777	16.23	1.82	4174	4687461649712675968	14.9	139.57 ± 0.25	0.28 ± 0.08	-1.10 ± 0.03	0.00	0.00	0000000	M2FS
SMC	NGC 416	N416-4-b017	17.185695	-72.270813	18.60	1.09	4918	4687509341031990400	3.7	174.70 ± 0.64	1.57 ± 0.24	-0.77 ± 0.08	0.00	0.00	0000000	M2FS
SMC	NGC 416	N416-4-b018	17.220649	-72.273200	18.45	1.04	4877	4687509336722930176	4.0	126.84 ± 0.55	2.12 ± 0.21	-0.75 ± 0.08	0.00	0.00	0000000	M2FS
SMC	NGC 416	N416-4-b019	17.178105	-72.308280	18.35	1.07	4852	4687509031794391552	4.9	99.34 ± 0.43	1.31 ± 0.23	-1.57 ± 0.07	0.00	0.00	0000000	M2FS
SMC	NGC 416	N416-4-b020	17.281555	-72.318179	18.00	1.27	4762	4687463333339762688	6.3	121.52 ± 0.38	1.64 ± 0.13	-0.85 ± 0.05	0.00	0.00	0000000	M2FS
SMC	NGC 416	N416-4-b021	17.191240	-72.324242	18.12	1.06	4793	4687462092081892224	5.0	154.22 ± 0.52	1.29 ± 0.20	-1.07 ± 0.07	0.00	0.00	0000000	M2FS
SMC	NGC 416	N416-4-b022	17.328424	-72.375846	18.02	1.09	4768	4687460752051147264	6.2	125.06 ± 0.42	0.90 ± 0.19	-1.34 ± 0.06	0.00	0.00	0000000	M2FS
SMC	NGC 416	N416-4-b023	17.358232	-72.378895	17.12	1.39	4504	4687462165109298176	10.2	166.03 ± 0.24	0.88 ± 0.08	-0.99 ± 0.04	0.00	0.00	0000000	M2FS
SMC	NGC 416	N416-4-b024	17.307112	-72.386578	18.36	1.09	4853	4687460683331582336	3.7	187.22 ± 0.83	1.53 ± 0.55	-2.02 ± 0.13	0.00	0.00	0000000	M2FS
SMC	NGC 416	N416-4-b025	17.089599	-72.263344	17.69	1.32	4676	4687510092637345152	6.4	153.09 ± 0.36	1.00 ± 0.13	-0.77 ± 0.05	0.00	0.00	0000000	M2FS
SMC	NGC 416	N416-4-b027	17.144934	-72.332059	15.48	2.59	4056	4687461993309989504	4.2	191.13 ± 2.20	1.61 ± 0.32	-2.20 ± 0.22	-1.00	-1.00	0110010	M2FS
SMC	NGC 416	N416-4-b028	17.053521	-72.344695	15.66	1.23	4056	4687461580993155712	25.1	178.64 ± 0.27	0.01 ± 0.01	-1.38 ± 0.03	0.00	0.00	0000010	M2FS
SMC	NGC 416	N416-4-b029	17.066520	-72.345442	15.74	1.28	4056	4687461580993155968	24.3	208.16 ± 0.22	0.01 ± 0.01	-1.37 ± 0.03	0.00	0.00	0000010	M2FS
SMC	NGC 416	N416-4-b030	17.082140	-72.347666	15.67	2.02	4056	4687461958950280832	9.0	157.65 ± 1.00	0.22 ± 0.16	-1.08 ± 0.10	-1.00	-1.00	0110000	M2FS
SMC	NGC 416	N416-4-b031	17.077863	-72.352655	18.63	1.18	4927	4687461890216394880	4.0	141.25 ± 0.49	1.63 ± 0.24	-0.72 ± 0.08	0.00	0.00	0000000	M2FS
SMC	NGC 416	N416-4-b032	17.045075	-72.358036	17.88	1.22	4730	4687461580993180800	5.7	152.68 ± 0.40	0.75 ± 0.16	-0.88 ± 0.05	0.76	0.79	0000000	M2FS
SMC	NGC 416	N416-4-b035	16.983899	-72.384255	18.57	1.08	4912	4687461374834805760	3.8	159.57 ± 0.55	1.68 ± 0.24	-0.77 ± 0.08	0.00	0.00	0000000	M2FS
SMC	NGC 416	N416-4-b036	16.969576	-72.381983	16.36	1.74	4223	4687461374834802304	14.6	155.49 ± 0.23	0.81 ± 0.05	-0.85 ± 0.03	0.00	0.00	0000000	M2FS
SMC	NGC 416	N416-4-b037	16.962729	-72.374424	17.40	1.34	4589	4687461443554266752	10.5	135.38 ± 0.27	0.88 ± 0.09	-0.99 ± 0.04	0.00	0.00	0000000	M2FS

Table C.1: (*continued*) Sample of 3095 Targets from 26 Star Clusters

Galaxy	Cluster	ID	RAJ2000 (deg)	DEJ2000 (deg)	G (mag)	$G_{\rm BP} - G_{\rm RP}$ (mag)	$T_{\rm eff}$ (K)	*Gaia* DR2 ID	S/N	$v_{\rm los}$ ($\rm km\,s^{-1}$)	$\log g$ (dex)	$[{\rm Fe/H}]_{\rm raw}$ (dex)	P_M	P'_M	Flag[a]	Source[b]
(1)	(2)	(3)	(4)	(5)	(6)	(7)	(8)	(9)	(10)	(11)	(12)	(13)	(14)	(15)	(16)	(17)
SMC	NGC 416	N416-4-b038	16.989815	-72.371987	18.23	1.14	4821	4687461542320535552	6.0	155.61 ± 0.44	0.95 ± 0.19	-1.25 ± 0.06	0.92	0.91	0000000	M2FS
SMC	NGC 416	N416-4-b039	16.968130	-72.370521	18.60	1.13	4918	4687461443539875328	3.6	155.97 ± 0.60	1.16 ± 0.26	-0.72 ± 0.09	0.90	0.89	0000000	M2FS
SMC	NGC 416	N416-4-b040	16.991376	-72.365424	18.79	1.01	4969	4687461546633461760	2.1	152.42 ± 1.20	0.52 ± 0.34	-0.78 ± 0.13	0.98	0.98	0000000	M2FS
SMC	NGC 416	N416-4-b041	17.022994	-72.444889	18.68	1.12	4941	4687460064911818240	4.0	166.92 ± 0.59	0.89 ± 0.25	-0.91 ± 0.08	0.00	0.00	0000000	M2FS
SMC	NGC 416	N416-4-b042	16.993815	-72.429503	15.59	2.39	4056	4687460344042751872	16.3	175.02 ± 0.56	0.74 ± 0.10	-0.69 ± 0.07	-1.00	-1.00	0100010	M2FS
SMC	NGC 416	N416-4-b043	16.993916	-72.423229	17.62	1.27	4657	4687460344042736000	6.1	120.15 ± 0.38	0.99 ± 0.14	-0.89 ± 0.06	0.00	0.00	0000000	M2FS
SMC	NGC 416	N416-4-b044	17.035982	-72.393776	18.52	1.08	4898	4687461198727415936	5.0	128.06 ± 0.54	1.41 ± 0.20	-1.16 ± 0.07	0.00	0.00	0000000	M2FS
SMC	NGC 416	N416-4-b045	17.038684	-72.379887	17.41	1.47	4593	4687461271755578752	6.2	152.21 ± 0.58	0.09 ± 0.08	-0.73 ± 0.10	0.00	0.00	0000000	M2FS
SMC	NGC 416	N416-4-b046	17.051574	-72.371288	17.07	1.43	4485	4687461507965468288	9.9	139.70 ± 0.25	1.01 ± 0.07	-0.81 ± 0.04	0.00	0.00	0000000	M2FS
SMC	NGC 416	N416-4-b047	17.026199	-72.369921	18.47	1.04	4884	4687461477913992064	4.4	127.33 ± 0.61	1.60 ± 0.20	-0.91 ± 0.07	0.00	0.00	0000000	M2FS
SMC	NGC 416	N416-4-b048	17.040197	-72.368844	17.97	1.20	4755	4687461507960712064	6.9	158.20 ± 0.33	0.97 ± 0.13	-0.74 ± 0.05	0.00	0.00	0000000	M2FS
SMC	NGC 416	N416-4-b049	17.027513	-72.260918	18.47	1.10	4883	4687510268744920576	3.9	114.55 ± 0.59	2.08 ± 0.16	-0.76 ± 0.09	0.00	0.00	0000000	M2FS
SMC	NGC 416	N416-4-b050	17.036676	-72.303745	17.08	1.47	4486	4687509233643280896	9.8	122.80 ± 0.29	0.47 ± 0.11	-1.12 ± 0.04	0.00	0.00	0000000	M2FS
SMC	NGC 416	N416-4-b051	17.014747	-72.337403	16.11	1.27	4129	4687508585117820672	19.1	128.50 ± 0.20	0.02 ± 0.02	-1.29 ± 0.03	0.00	0.00	0000010	M2FS
SMC	NGC 416	N416-4-b052	17.022516	-72.340253	18.57	1.03	4911	4687508516393261184	4.0	164.37 ± 0.56	1.14 ± 0.22	-0.93 ± 0.08	0.00	0.00	0000000	M2FS
SMC	NGC 416	N416-4-b053	17.022182	-72.353921	17.76	1.13	4696	4687461580978761472	7.4	158.81 ± 0.33	1.25 ± 0.12	-0.94 ± 0.05	0.96	0.93	0000000	M2FS
SMC	NGC 416	N416-4-b054	17.024886	-72.359411	17.46	1.36	4606	4687461580993185280	9.2	154.37 ± 0.26	1.04 ± 0.09	-0.82 ± 0.04	0.99	0.99	0000000	M2FS
SMC	NGC 416	N416-4-b055	17.011932	-72.361520	18.30	1.09	4839	4687461542381711232	4.6	152.77 ± 0.52	1.18 ± 0.23	-0.80 ± 0.07	0.98	0.98	0000000	M2FS
SMC	NGC 416	N416-4-b056	17.015027	-72.365776	18.60	1.08	4920	4687461546619069312	3.3	177.64 ± 0.68	0.89 ± 0.35	-0.93 ± 0.16	0.00	0.00	0000000	M2FS
SMC	NGC 416	N416-4-b057	16.999541	-72.243408	18.44	1.06	4874	4687513288093433216	3.9	166.14 ± 0.54	1.59 ± 0.25	-1.27 ± 0.09	0.00	0.00	0000000	M2FS
SMC	NGC 416	N416-4-b058	17.002427	-72.300502	17.12	1.36	4503	4687508859995698560	11.1	116.03 ± 0.23	0.85 ± 0.07	-1.24 ± 0.03	0.00	0.00	0000000	M2FS
SMC	NGC 416	N416-4-b059	17.007633	-72.319204	17.21	1.44	4533	4687508791276238080	10.6	175.38 ± 0.22	0.82 ± 0.08	-0.93 ± 0.04	0.00	0.00	0000000	M2FS
SMC	NGC 416	N416-4-b060	17.011153	-72.340751	16.62	1.15	4316	4687508512124431360	14.9	145.45 ± 0.23	0.16 ± 0.09	-1.33 ± 0.03	0.00	0.00	0000010	M2FS
SMC	NGC 416	N416-4-b061	17.011161	-72.348618	17.84	1.21	4717	4687508477723142528	4.9	150.49 ± 0.58	1.09 ± 0.19	-0.81 ± 0.06	0.92	0.92	0000000	M2FS
SMC	NGC 416	N416-4-b062	16.989516	-72.353639	17.09	1.10	4491	4687508482032212096	10.0	153.80 ± 0.28	0.87 ± 0.08	-1.01 ± 0.04	1.00	1.00	0000010	M2FS
SMC	NGC 416	N416-4-b063	16.992381	-72.357225	17.10	1.02	4496	4687508477764686336	7.1	152.58 ± 0.43	1.00 ± 0.13	-0.84 ± 0.05	1.00	1.00	0000010	M2FS
SMC	NGC 416	N416-4-b064	16.997518	-72.362304	17.80	1.19	4708	4687461542381390208	5.8	153.90 ± 0.44	1.33 ± 0.13	-0.82 ± 0.05	0.98	0.99	0000000	M2FS
SMC	NGC 416	N416-4-b066	16.868863	-72.427304	17.29	1.36	4558	4687437662306012672	9.7	102.55 ± 0.27	0.77 ± 0.09	-0.82 ± 0.04	0.00	0.00	0000000	M2FS
SMC	NGC 416	N416-4-b067	16.881413	-72.414927	18.73	1.02	4953	4687437662306230912	6.0	149.69 ± 0.74	2.05 ± 0.19	-1.44 ± 0.09	0.00	0.00	0000000	M2FS
SMC	NGC 416	N416-4-b070	16.866037	-72.371539	18.13	1.14	4797	4687508413319212672	4.5	172.67 ± 0.66	1.58 ± 0.20	-0.97 ± 0.07	0.00	0.00	0000000	M2FS
SMC	NGC 416	N416-4-b071	16.915483	-72.362780	17.01	1.46	4465	4687508447678947072	10.6	156.85 ± 0.23	0.84 ± 0.07	-0.88 ± 0.04	0.00	0.00	0000000	M2FS
SMC	NGC 416	N416-4-b072	16.895852	-72.354940	17.42	1.49	4595	4687508413319205504	8.8	162.27 ± 0.25	1.17 ± 0.10	-0.61 ± 0.04	0.00	0.00	0000000	M2FS
SMC	NGC 416	N416-4-b075	16.956876	-72.382187	18.20	1.24	4813	4687461374834804096	4.7	158.77 ± 0.46	1.01 ± 0.22	-0.86 ± 0.06	0.00	0.00	0000000	M2FS
SMC	NGC 416	N416-4-b076	16.921567	-72.372812	17.57	1.67	4639	4687508378959474048	5.3	4.54 ± 0.89	4.81 ± 0.17	-1.95 ± 0.10	-1.00	-1.00	0001100	M2FS
SMC	NGC 416	N416-4-b077	16.929002	-72.369903	16.36	2.64	4221	4687508378959473152	4.1	152.89 ± 1.85	1.11 ± 0.39	-1.99 ± 0.21	-1.00	-1.00	0110010	M2FS
SMC	NGC 416	N416-4-b078	16.940427	-72.361760	17.87	1.35	4727	4687508374655195392	6.8	153.28 ± 0.35	1.25 ± 0.12	-0.76 ± 0.05	0.72	0.79	0000000	M2FS
SMC	NGC 416	N416-4-b079	16.935584	-72.357951	15.63	1.12	4056	4687508443363349632	27.8	178.93 ± 0.30	0.02 ± 0.01	-1.63 ± 0.03	0.00	0.00	0000010	M2FS
SMC	NGC 416	N416-4-b080	16.928264	-72.353932	16.96	1.46	4443	4687508443404938368	11.7	175.13 ± 0.25	0.94 ± 0.06	-0.76 ± 0.03	0.00	0.00	0000000	M2FS
SMC	NGC 416	N416-4-b081	16.957847	-72.307106	17.80	1.07	4706	4687509581545113344	4.2	110.35 ± 0.81	0.85 ± 0.24	-1.22 ± 0.08	0.00	0.00	0000000	M2FS
SMC	NGC 416	N416-4-b082	16.982064	-72.330572	18.26	1.23	4828	4687508756916509056	4.3	158.01 ± 0.50	0.93 ± 0.23	-0.92 ± 0.07	0.00	0.00	0000000	M2FS
SMC	NGC 416	N416-4-b083	16.982757	-72.336197	18.31	1.15	4840	4687508546442623232	4.9	94.93 ± 0.40	1.71 ± 0.16	-1.00 ± 0.07	0.00	0.00	0000000	M2FS
SMC	NGC 416	N416-4-b084	16.980250	-72.346291	18.45	1.03	4877	4687508546503483136	4.2	165.54 ± 0.65	1.17 ± 0.20	-0.77 ± 0.07	0.00	0.00	0000000	M2FS
SMC	NGC 416	N416-4-b085	16.978056	-72.349728	18.15	1.02	4800	4687508477784083840	7.0	155.00 ± 0.44	1.32 ± 0.14	-1.13 ± 0.05	0.99	0.99	0000000	M2FS
SMC	NGC 416	N416-4-b086	16.967061	-72.357310	17.26	1.24	4551	4687508477723141888	8.5	156.86 ± 0.20	0.62 ± 0.09	-0.90 ± 0.04	0.98	0.98	0000000	M2FS
SMC	NGC 416	N416-4-b087	16.979282	-72.358054	17.69	1.24	4675	4687508477734410752	4.8	157.89 ± 0.40	1.45 ± 0.15	-0.67 ± 0.06	1.00	1.00	0000000	M2FS
SMC	NGC 416	N416-4-b088	16.968738	-72.363611	17.24	1.37	4543	4687508374644165760	9.2	153.38 ± 0.27	0.41 ± 0.13	-0.88 ± 0.04	0.89	0.91	0000000	M2FS
SMC	NGC 416	N416-4-b089	16.915363	-72.245969	17.85	1.28	4721	4687512948804498816	4.8	105.78 ± 0.45	1.74 ± 0.14	-0.71 ± 0.07	0.00	0.00	0000000	M2FS
SMC	NGC 416	N416-4-b090	16.947914	-72.267869	17.51	1.28	4621	4687509955198431616	7.0	156.85 ± 0.30	0.83 ± 0.12	-0.90 ± 0.04	0.00	0.00	0000000	M2FS
SMC	NGC 416	N416-4-b091	16.945249	-72.272781	17.96	1.23	4752	4687509886512306688	4.1	148.69 ± 0.37	1.14 ± 0.21	-0.59 ± 0.06	0.00	0.00	0000000	M2FS
SMC	NGC 416	N416-4-b093	16.915824	-72.340411	18.30	1.18	4838	4687508653832220800	4.9	131.55 ± 0.39	1.56 ± 0.16	-0.73 ± 0.06	0.00	0.00	0000000	M2FS
SMC	NGC 416	N416-4-b094	16.952570	-72.343941	17.22	1.40	4537	4687508550758089344	8.7	112.17 ± 0.28	1.00 ± 0.08	-0.82 ± 0.04	0.00	0.00	0000000	M2FS
SMC	NGC 416	N416-4-b095	16.939126	-72.347920	17.30	1.34	4561	4687508447678879104	9.6	181.26 ± 0.25	1.14 ± 0.08	-0.94 ± 0.04	0.00	0.00	0000000	M2FS
SMC	NGC 416	N416-4-b096	16.951019	-72.352141	18.29	1.06	4836	4687508443363360000	5.4	113.13 ± 0.39	0.95 ± 0.19	-1.09 ± 0.06	0.00	0.00	0000000	M2FS
SMC	NGC 416	N416-4-b097	16.748551	-72.437350	18.36	1.15	4852	4687437735317749760	6.9	156.64 ± 0.46	1.09 ± 0.14	-1.05 ± 0.05	0.00	0.00	0000000	M2FS

Table C.1: (*continued*) Sample of 3095 Targets from 26 Star Clusters

Galaxy	Cluster	ID	RAJ2000 (deg)	DEJ2000 (deg)	G (mag)	$G_{\rm BP} - G_{\rm RP}$ (mag)	$T_{\rm eff}$ (K)	*Gaia* DR2 ID	S/N	$v_{\rm los}$ ($\rm km\,s^{-1}$)	$\log g$ (dex)	$[{\rm Fe/H}]_{\rm raw}$ (dex)	P_M	P'_M	Flag[a]	Source[b]
(1)	(2)	(3)	(4)	(5)	(6)	(7)	(8)	(9)	(10)	(11)	(12)	(13)	(14)	(15)	(16)	(17)
SMC	NGC 416	N416-4-b098	16.716058	-72.436086	18.37	1.07	4855	4687437769701208320	6.0	98.44 ± 0.42	1.83 ± 0.12	-0.77 ± 0.06	0.00	0.00	0000000	M2FS
SMC	NGC 416	N416-4-b099	16.698126	-72.424196	18.57	1.15	4911	4687484700783972864	6.5	157.96 ± 0.48	1.64 ± 0.15	-1.11 ± 0.06	0.00	0.00	0000000	M2FS
SMC	NGC 416	N416-4-b100	16.653983	-72.405348	18.25	1.19	4827	4687484602009033856	7.0	101.57 ± 0.33	1.28 ± 0.16	-0.57 ± 0.04	0.00	0.00	0000000	M2FS
SMC	NGC 416	N416-4-b101	16.689840	-72.404912	18.07	1.17	4780	4687484769545095808	8.2	113.55 ± 0.36	1.56 ± 0.11	-0.80 ± 0.04	0.00	0.00	0000000	M2FS
SMC	NGC 416	N416-4-b102	16.632638	-72.387315	18.37	1.21	4857	4687485426660816640	4.1	185.83 ± 0.55	1.90 ± 0.19	-0.88 ± 0.09	0.00	0.00	0000000	M2FS
SMC	NGC 416	N416-4-b103	16.712194	-72.369443	18.10	1.18	4787	4687485834716115968	7.2	107.71 ± 0.39	1.03 ± 0.13	-0.90 ± 0.05	0.00	0.00	0000000	M2FS
SMC	NGC 416	N416-4-b104	16.690029	-72.363765	17.18	1.38	4521	4687485838977615744	14.9	171.83 ± 0.21	0.56 ± 0.08	-1.27 ± 0.03	0.00	0.00	0000000	M2FS
SMC	NGC 416	N416-4-b105	16.857377	-72.434284	18.45	1.07	4877	4687437628002444288	5.8	145.11 ± 0.48	1.56 ± 0.16	-0.82 ± 0.06	0.00	0.00	0000000	M2FS
SMC	NGC 416	N416-4-b106	16.811782	-72.410965	18.60	1.05	4919	4687437902824483840	4.3	176.21 ± 0.66	1.61 ± 0.25	-1.17 ± 0.10	0.00	0.00	0000000	M2FS
SMC	NGC 416	N416-4-b107	16.785756	-72.408855	17.46	1.20	4605	4687484838255506304	9.7	188.68 ± 0.30	0.89 ± 0.10	-1.12 ± 0.04	0.00	0.00	0000000	M2FS
SMC	NGC 416	N416-4-b108	16.749025	-72.407217	17.40	1.28	4590	4687484739447979136	9.1	158.53 ± 0.27	0.98 ± 0.09	-0.96 ± 0.04	0.00	0.00	0000000	M2FS
SMC	NGC 416	N416-4-b109	16.773961	-72.385604	18.15	1.06	4800	4687484906947051520	6.8	116.91 ± 0.43	1.13 ± 0.14	-1.15 ± 0.05	0.00	0.00	0000000	M2FS
SMC	NGC 416	N416-4-b110	16.786568	-72.376566	18.44	1.10	4875	4687485113105629696	5.4	119.34 ± 0.51	1.39 ± 0.18	-0.67 ± 0.06	0.00	0.00	0000000	M2FS
SMC	NGC 416	N416-4-b111	16.752069	-72.366831	18.00	1.18	4763	4687485186142587648	6.2	121.77 ± 0.46	0.98 ± 0.16	-0.93 ± 0.05	0.00	0.00	0000000	M2FS
SMC	NGC 416	N416-4-b112	16.765025	-72.356833	15.61	2.25	4056	4687485937739756288	6.4	126.94 ± 1.37	1.26 ± 0.32	-2.04 ± 0.21	-1.00	-1.00	0110010	M2FS
SMC	NGC 416	N416-4-b114	16.891363	-72.282773	18.40	1.17	4865	4687509817753024640	3.7	120.72 ± 0.67	1.30 ± 0.23	-0.74 ± 0.07	0.00	0.00	0000000	M2FS
SMC	NGC 416	N416-4-b115	16.849096	-72.295997	18.36	1.20	4854	4687509749039479296	4.4	151.37 ± 0.80	0.44 ± 0.25	-0.66 ± 0.07	0.00	0.00	0000000	M2FS
SMC	NGC 416	N416-4-b116	16.783145	-72.296514	17.92	1.09	4739	4687486319995611392	5.8	136.36 ± 0.44	1.35 ± 0.16	-1.25 ± 0.06	0.00	0.00	0000000	M2FS
SMC	NGC 416	N416-4-b118	16.878817	-72.314065	17.85	1.35	4720	4687509547190482048	6.4	196.14 ± 0.40	1.12 ± 0.15	-0.68 ± 0.05	0.00	0.00	0000000	M2FS
SMC	NGC 416	N416-4-b119	16.785522	-72.317688	17.52	1.30	4624	4687486251294391168	7.6	174.74 ± 0.37	0.73 ± 0.13	-1.16 ± 0.05	0.00	0.00	0000000	M2FS
SMC	NGC 416	N416-4-b120	16.886397	-72.324830	18.16	1.24	4803	4687509478471013376	5.0	143.35 ± 0.46	1.10 ± 0.19	-0.91 ± 0.07	0.00	0.00	0000000	M2FS
SMC	NGC 416	N416-4-b121	16.749321	-72.267623	17.12	1.43	4503	4687489545507411456	8.7	134.80 ± 0.27	1.08 ± 0.09	-0.76 ± 0.04	0.00	0.00	0000000	M2FS
SMC	NGC 416	N416-4-b122	16.731471	-72.300828	18.57	1.05	4911	4687489236301886720	4.7	159.04 ± 0.69	1.27 ± 0.26	-0.99 ± 0.08	0.00	0.00	0000000	M2FS
SMC	NGC 416	N416-4-b123	16.744901	-72.301005	17.24	1.36	4542	4687489270635321344	10.1	142.61 ± 0.24	1.06 ± 0.08	-0.80 ± 0.04	0.00	0.00	0000000	M2FS
SMC	NGC 416	N416-4-b124	16.760875	-72.311126	18.54	1.20	4902	4687486319995640192	3.1	168.82 ± 0.62	1.82 ± 0.35	-0.40 ± 0.07	0.00	0.00	0000000	M2FS
SMC	NGC 416	N416-4-b125	16.641206	-72.328283	17.75	1.36	4693	4687489103152701696	6.4	162.21 ± 0.34	1.28 ± 0.13	-0.64 ± 0.05	0.00	0.00	0000000	M2FS
SMC	NGC 416	N416-4-b126	16.720204	-72.328359	18.58	1.08	4914	4687486212644879360	3.2	198.78 ± 0.63	1.71 ± 0.21	-0.50 ± 0.08	0.00	0.00	0000000	M2FS
SMC	NGC 416	N416-4-b127	16.732290	-72.329288	18.00	1.18	4764	4687486212618165120	6.8	138.40 ± 0.31	0.99 ± 0.13	-0.79 ± 0.05	0.00	0.00	0000000	M2FS
SMC	NGC 416	N416-4-b128	16.631518	-72.337524	17.14	1.08	4507	4687486148215216000	11.2	164.50 ± 0.26	0.54 ± 0.11	-1.34 ± 0.04	0.00	0.00	0000010	M2FS
SMC	NGC 416	N416-4-r028	16.976627	-72.354239	14.82	1.49	4056	4687508482038680832	41.7	185.67 ± 0.18	0.01 ± 0.01	-0.92 ± 0.03	0.00	0.00	0000000	M2FS
SMC	NGC 416	N416-4-r049	17.006450	-72.356879	16.91	1.23	4426	4687461546619035008	15.3	158.15 ± 0.23	0.69 ± 0.06	-1.14 ± 0.03	1.00	1.00	0000000	M2FS
SMC	NGC 416	N416-4-r079	16.991146	-72.347739	17.34	1.20	4573	4687508482033536128	11.7	159.90 ± 0.28	0.80 ± 0.09	-1.07 ± 0.04	0.91	-1.00	0000000	M2FS
SMC	NGC 416	N416-4-r099	17.008896	-72.353076	17.22	1.04	4536	4687508482038633856	12.7	155.84 ± 0.26	0.83 ± 0.08	-1.11 ± 0.03	1.00	1.00	0000010	M2FS
SMC	NGC 419	N419-1-b001	17.184085	-73.011210	16.38	1.65	4429	4687208658954229632	15.5	188.57 ± 0.20	1.17 ± 0.06	-0.63 ± 0.03	0.00	0.00	0000010	M2FS
SMC	NGC 419	N419-1-b002	17.191760	-72.943245	17.68	1.18	4693	4687221165890779776	9.4	192.75 ± 0.33	1.07 ± 0.11	-0.98 ± 0.04	0.00	0.00	0000000	M2FS
SMC	NGC 419	N419-1-b003	17.189168	-72.921082	17.65	1.34	4678	4687221990534671360	8.0	152.97 ± 0.34	0.94 ± 0.12	-0.83 ± 0.04	0.00	0.00	0000000	M2FS
SMC	NGC 419	N419-1-b004	17.180785	-72.892362	17.85	0.87	4738	4687222261122584064	9.0	193.91 ± 0.53	0.28 ± 0.19	-1.58 ± 0.05	0.02	0.00	0000010	M2FS
SMC	NGC 419	N419-1-b005	17.176625	-72.886889	18.49	0.64	4949	4687222265402188544	6.7	143.84 ± 0.82	1.63 ± 0.20	-1.43 ± 0.07	0.00	0.00	0000010	M2FS
SMC	NGC 419	N419-1-b006	17.154432	-72.885857	17.79	1.26	4727	4687225220350010240	8.4	189.30 ± 0.35	1.27 ± 0.11	-0.72 ± 0.04	0.96	0.96	0000000	M2FS
SMC	NGC 419	N419-1-b007	17.190647	-72.883633	15.81	1.87	4429	4687222299772242816	20.2	188.49 ± 0.22	1.72 ± 0.07	-0.40 ± 0.04	0.78	0.79	0000010	M2FS
SMC	NGC 419	N419-1-b008	17.178501	-72.876846	18.44	1.20	4936	4687225250407416832	4.5	163.85 ± 0.66	1.51 ± 0.29	-0.84 ± 0.08	0.00	0.00	0000000	M2FS
SMC	NGC 419	N419-1-b009	17.193963	-72.999892	19.25	0.96	5166	4687208693313962112	3.0	147.30 ± 1.62	2.53 ± 0.40	-1.31 ± 0.16	0.00	0.00	0000000	M2FS
SMC	NGC 419	N419-1-b010	17.220682	-72.985743	18.37	0.99	4913	4687220444336391296	6.7	191.12 ± 0.78	0.50 ± 0.29	-1.63 ± 0.08	0.00	0.00	0000000	M2FS
SMC	NGC 419	N419-1-b011	17.403961	-72.970651	18.84	1.01	5053	4687209170050568448	4.2	132.51 ± 0.79	1.78 ± 0.29	-1.18 ± 0.11	0.00	0.00	0000000	M2FS
SMC	NGC 419	N419-1-b012	17.292082	-72.958527	16.13	1.81	4429	4687220856663361280	17.1	171.40 ± 0.27	1.41 ± 0.07	-0.61 ± 0.04	0.00	0.00	0000010	M2FS
SMC	NGC 419	N419-1-b013	17.357706	-72.921540	18.07	1.20	4815	4687221268980154496	6.3	161.42 ± 0.57	1.33 ± 0.16	-0.97 ± 0.06	0.00	0.00	0000000	M2FS
SMC	NGC 419	N419-1-b014	17.341739	-72.915912	16.69	1.13	4429	4687221337699623168	15.0	135.18 ± 0.30	0.36 ± 0.10	-1.39 ± 0.03	0.00	0.00	0000000	M2FS
SMC	NGC 419	N419-1-b015	17.217401	-72.899390	18.55	0.99	4967	4687222226762893184	4.2	134.47 ± 0.68	1.19 ± 0.27	-1.18 ± 0.09	0.00	0.00	0000000	M2FS
SMC	NGC 419	N419-1-b016	17.200762	-72.892354	17.55	0.92	4647	4687222295469891968	9.7	-13.81 ± 0.39	2.92 ± 0.07	-0.73 ± 0.07	-1.00	-1.00	0000110	M2FS
SMC	NGC 419	N419-1-b017	17.299401	-72.806289	16.86	1.49	4429	4687249203448832640	5.2	181.10 ± 0.40	0.69 ± 0.13	-0.77 ± 0.06	0.00	0.00	0000000	M2FS
SMC	NGC 419	N419-1-b018	17.264474	-72.837030	18.26	0.95	4877	4687225460867890432	3.1	205.35 ± 1.41	1.54 ± 0.39	-1.47 ± 0.13	0.00	0.00	0000000	M2FS
SMC	NGC 419	N419-1-b019	17.190496	-72.848090	18.22	1.04	4866	4687225525302664448	6.9	190.28 ± 0.43	1.48 ± 0.16	-1.24 ± 0.06	-1.00	-1.00	0000001	M2FS
SMC	NGC 419	N419-1-b020	17.168980	-72.850325	17.36	1.14	4585	4687225529587380736	12.8	188.28 ± 0.26	0.71 ± 0.10	-1.27 ± 0.04	-1.00	-1.00	0000001	M2FS
SMC	NGC 419	N419-1-b021	17.457853	-72.856185	16.95	1.55	4435	4687245763159499776	6.6	151.56 ± 0.32	1.13 ± 0.09	-0.63 ± 0.05	0.00	0.00	0000000	M2FS

Table C.1: (*continued*) Sample of 3095 Targets from 26 Star Clusters

Galaxy	Cluster	ID	RAJ2000 (deg)	DEJ2000 (deg)	G (mag)	$G_{\rm BP} - G_{\rm RP}$ (mag)	$T_{\rm eff}$ (K)	*Gaia* DR2 ID	S/N	$v_{\rm los}$ ($\rm km\,s^{-1}$)	$\log g$ (dex)	$[{\rm Fe/H}]_{\rm raw}$ (dex)	P_M	P'_M	Flag[a]	Source[b]
(1)	(2)	(3)	(4)	(5)	(6)	(7)	(8)	(9)	(10)	(11)	(12)	(13)	(14)	(15)	(16)	(17)
SMC	NGC 419	N419-1-b022	17.177809	-72.857764	18.19	1.03	4857	4687225319126945408	6.3	146.48 ± 0.46	0.75 ± 0.23	-1.21 ± 0.06	0.00	0.00	0000000	M2FS
SMC	NGC 419	N419-1-b023	17.193882	-72.862198	15.54	2.17	4429	4687225323428963072	10.5	190.97 ± 1.25	0.37 ± 0.31	-1.21 ± 0.15	-1.00	-1.00	0110010	M2FS
SMC	NGC 419	N419-1-b024	17.162585	-72.868441	18.72	1.13	5018	4687225289058919168	3.5	184.44 ± 0.82	1.72 ± 0.25	-0.90 ± 0.12	0.00	0.00	0000000	M2FS
SMC	NGC 419	N419-1-b025	17.138205	-72.849692	17.45	1.38	4616	4687225559661943424	9.3	190.52 ± 0.26	1.12 ± 0.09	-0.75 ± 0.04	0.92	0.91	0000000	M2FS
SMC	NGC 419	N419-1-b026	17.123631	-72.852497	17.57	1.15	4653	4687225563936793216	10.5	177.64 ± 0.32	0.24 ± 0.15	-1.40 ± 0.04	0.00	0.00	0000000	M2FS
SMC	NGC 419	N419-1-b027	17.140011	-72.854841	18.46	1.19	4940	4687225490942494592	5.0	112.01 ± 0.71	1.27 ± 0.26	-0.91 ± 0.07	0.00	0.00	0000000	M2FS
SMC	NGC 419	N419-1-b028	17.140823	-72.860931	15.74	1.85	4429	4687225495227656704	18.8	191.82 ± 0.30	1.83 ± 0.08	-0.40 ± 0.05	0.88	0.81	0000010	M2FS
SMC	NGC 419	N419-1-b029	17.162238	-72.862832	16.65	1.01	4429	4687225323428966656	18.5	147.31 ± 0.25	0.15 ± 0.10	-1.70 ± 0.03	0.00	0.00	0000010	M2FS
SMC	NGC 419	N419-1-b030	17.124222	-72.866455	17.00	1.52	4451	4687225495227665152	10.6	144.59 ± 0.27	0.73 ± 0.08	-0.73 ± 0.04	0.00	0.00	0000000	M2FS
SMC	NGC 419	N419-1-b031	17.148253	-72.868223	18.32	1.26	4897	4687225284779511552	5.8	133.16 ± 0.49	0.96 ± 0.18	-0.68 ± 0.06	0.00	0.00	0000000	M2FS
SMC	NGC 419	N419-1-b032	17.154217	-72.872989	15.84	1.81	4429	4687225289069242624	17.7	189.12 ± 0.27	1.60 ± 0.07	-0.39 ± 0.04	0.95	0.96	0000010	M2FS
SMC	NGC 419	N419-1-b033	17.119386	-72.990252	18.31	1.21	4895	4687220474403074688	5.3	172.72 ± 0.50	1.54 ± 0.16	-0.74 ± 0.07	0.00	0.00	0000000	M2FS
SMC	NGC 419	N419-1-b034	17.122829	-72.954697	17.05	1.44	4473	4687221509498394752	10.3	152.75 ± 0.26	0.65 ± 0.08	-1.02 ± 0.04	0.00	0.00	0000000	M2FS
SMC	NGC 419	N419-1-b035	17.113610	-72.901571	16.58	1.56	4429	4687221887455427456	13.1	188.76 ± 0.21	1.20 ± 0.06	-0.58 ± 0.03	0.96	0.96	0000000	M2FS
SMC	NGC 419	N419-1-b036	17.109863	-72.896543	18.08	1.20	4817	4687224842392915200	5.2	190.54 ± 0.47	1.43 ± 0.17	-0.64 ± 0.07	0.99	0.99	0000000	M2FS
SMC	NGC 419	N419-1-b037	17.128835	-72.892043	17.17	1.28	4517	4687225220350024576	11.7	188.83 ± 0.28	0.85 ± 0.08	-1.01 ± 0.04	0.99	0.99	0000000	M2FS
SMC	NGC 419	N419-1-b038	17.132923	-72.887159	18.52	1.00	4959	4687225216064587264	4.8	120.96 ± 0.67	1.72 ± 0.20	-1.09 ± 0.08	0.00	0.00	0000000	M2FS
SMC	NGC 419	N419-1-b039	17.119016	-72.886975	18.39	1.00	4919	4687224842392891776	4.4	188.53 ± 0.58	1.18 ± 0.24	-0.81 ± 0.08	0.99	0.99	0000000	M2FS
SMC	NGC 419	N419-1-b040	17.121348	-72.882954	17.68	1.24	4695	4687225289069484416	4.9	192.64 ± 0.45	1.06 ± 0.16	-0.78 ± 0.06	0.98	0.98	0000000	M2FS
SMC	NGC 419	N419-1-b041	17.138530	-73.007149	17.79	0.98	4727	4687220409986842496	8.8	190.26 ± 0.41	0.77 ± 0.17	-1.63 ± 0.05	0.00	0.00	0000000	M2FS
SMC	NGC 419	N419-1-b043	17.143084	-72.922087	18.61	1.12	4986	4687221612567322624	3.0	145.50 ± 1.26	1.51 ± 0.47	-1.27 ± 0.14	0.00	0.00	0000000	M2FS
SMC	NGC 419	N419-1-b044	17.151071	-72.902227	17.22	1.01	4533	4687222261110084480	13.4	-53.41 ± 0.34	2.61 ± 0.06	-0.57 ± 0.05	-1.00	-1.00	0000100	M2FS
SMC	NGC 419	N419-1-b045	17.153540	-72.894370	15.70	2.18	4429	4687222265412528128	9.1	171.73 ± 1.21	0.72 ± 0.50	-1.30 ± 0.21	-1.00	-1.00	0110010	M2FS
SMC	NGC 419	N419-1-b046	17.144349	-72.883418	15.59	1.43	4429	4687225220350006400	28.4	182.82 ± 0.16	0.20 ± 0.08	-0.84 ± 0.03	0.00	0.00	0000000	M2FS
SMC	NGC 419	N419-1-b047	17.136117	-72.879530	18.36	0.96	4911	4687225284784064256	5.5	192.25 ± 0.59	1.44 ± 0.19	-0.87 ± 0.07	0.97	0.96	0000000	M2FS
SMC	NGC 419	N419-1-b048	17.153482	-72.878022	18.06	1.25	4810	4687225216048476032	6.6	172.12 ± 0.41	1.21 ± 0.15	-0.86 ± 0.05	0.00	0.00	0000000	M2FS
SMC	NGC 419	N419-1-b049	17.105356	-72.805213	18.71	0.97	5015	4687226624785729152	2.4	160.67 ± 1.39	2.01 ± 0.45	-1.49 ± 0.21	0.00	0.00	0000000	M2FS
SMC	NGC 419	N419-1-b050	17.094605	-72.853413	18.83	1.08	5049	4687225563947125376	3.7	139.21 ± 0.80	1.74 ± 0.25	-0.71 ± 0.11	0.00	0.00	0000000	M2FS
SMC	NGC 419	N419-1-b051	17.106024	-72.855160	16.68	1.57	4429	4687225559660430336	12.7	190.80 ± 0.34	1.00 ± 0.07	-0.69 ± 0.03	0.96	0.95	0000000	M2FS
SMC	NGC 419	N419-1-b052	17.092720	-72.860617	16.91	1.46	4429	4687225185990013952	10.4	197.78 ± 0.23	0.58 ± 0.08	-1.22 ± 0.04	0.00	0.00	0000000	M2FS
SMC	NGC 419	N419-1-b053	17.120963	-72.862030	18.27	0.82	4880	4687225490942493568	6.3	146.45 ± 0.81	1.21 ± 0.31	-1.80 ± 0.08	0.00	0.00	0000000	M2FS
SMC	NGC 419	N419-1-b054	17.106111	-72.864975	16.19	0.94	4429	4687225495227663616	32.6	100.49 ± 1.68	1.99 ± 0.27	-3.27 ± 0.06	-1.00	-1.00	1000010	M2FS
SMC	NGC 419	N419-1-b055	17.103655	-72.873809	17.44	1.21	4615	4687225117270775424	8.8	192.70 ± 0.37	0.12 ± 0.09	-0.89 ± 0.05	0.98	0.98	0000000	M2FS
SMC	NGC 419	N419-1-b056	17.092940	-72.876053	15.62	2.50	4429	4687225112985517568	3.1	188.05 ± 1.79	0.77 ± 0.53	-1.34 ± 0.21	-1.00	-1.00	0010010	M2FS
SMC	NGC 419	N419-1-b057	17.070261	-72.858178	17.35	1.50	4583	4687225185990009728	8.9	138.96 ± 0.28	1.20 ± 0.10	-0.65 ± 0.04	0.00	0.00	0000000	M2FS
SMC	NGC 419	N419-1-b058	17.074076	-72.864808	16.05	1.71	4429	4687225185990020096	17.9	189.24 ± 0.27	1.37 ± 0.06	-0.51 ± 0.04	0.99	0.99	0000010	M2FS
SMC	NGC 419	N419-1-b059	17.090684	-72.866992	18.63	0.98	4993	4687225112980728576	3.5	190.54 ± 0.87	0.97 ± 0.33	-0.99 ± 0.10	0.99	0.99	0000000	M2FS
SMC	NGC 419	N419-1-b061	17.085438	-72.872942	16.28	1.55	4429	4687225117260411136	11.9	188.67 ± 0.25	1.10 ± 0.07	-0.59 ± 0.04	0.99	0.99	0000000	M2FS
SMC	NGC 419	N419-1-b063	17.057000	-72.877922	18.15	0.93	4844	4687225117270596096	2.0	190.61 ± 0.79	1.36 ± 0.42	-0.48 ± 0.12	1.00	1.00	0000000	M2FS
SMC	NGC 419	N419-1-b064	17.073863	-72.880240	17.68	0.80	4693	4687225117270719488	1.1	190.29 ± 1.29	1.09 ± 0.58	-0.27 ± 0.18	1.00	1.00	0000010	M2FS
SMC	NGC 419	N419-1-b065	17.057064	-72.908935	18.26	1.27	4880	4687224808033203072	5.4	175.76 ± 0.59	1.44 ± 0.18	-0.63 ± 0.06	0.00	0.00	0000000	M2FS
SMC	NGC 419	N419-1-b066	17.043966	-72.904704	17.91	1.19	4763	4687224808033198720	5.5	141.74 ± 0.52	1.62 ± 0.14	-0.90 ± 0.07	0.00	0.00	0000000	M2FS
SMC	NGC 419	N419-1-b067	17.072816	-72.903658	16.55	1.59	4429	4687224808033195776	6.6	190.53 ± 0.32	1.27 ± 0.10	-0.64 ± 0.05	0.99	0.99	0000000	M2FS
SMC	NGC 419	N419-1-b069	17.060942	-72.892175	17.52	1.06	4642	4687224872451198592	5.0	188.83 ± 0.51	1.20 ± 0.15	-0.83 ± 0.07	1.00	1.00	0000000	M2FS
SMC	NGC 419	N419-1-b070	17.044214	-72.891042	18.97	0.84	5087	4687224872467225600	1.9	186.37 ± 1.34	1.52 ± 0.57	-0.70 ± 0.19	1.00	1.00	0000000	M2FS
SMC	NGC 419	N419-1-b071	17.059059	-72.888018	15.96	1.41	4429	4687224876752490880	7.8	188.22 ± 0.27	1.41 ± 0.09	-0.56 ± 0.05	1.00	1.00	0000000	M2FS
SMC	NGC 419	N419-1-b073	17.094436	-72.970154	16.32	3.21	4429	4687220753584175872	2.0	137.91 ± 2.06	1.11 ± 0.56	-2.06 ± 0.28	-1.00	-1.00	0010010	M2FS
SMC	NGC 419	N419-1-b074	17.108183	-72.905638	18.29	1.19	4888	4687221883153836160	4.8	190.24 ± 0.54	1.30 ± 0.22	-1.01 ± 0.08	0.96	0.96	0000000	M2FS
SMC	NGC 419	N419-1-b075	17.088966	-72.901121	16.47	1.67	4429	4687224842392926208	11.7	161.92 ± 0.32	1.43 ± 0.07	-0.55 ± 0.04	0.00	0.00	0000010	M2FS
SMC	NGC 419	N419-1-b077	17.093625	-72.894575	19.27	0.85	5171	4687224842392910336	1.5	187.71 ± 1.30	0.96 ± 0.54	-0.77 ± 0.20	0.99	0.99	0000000	M2FS
SMC	NGC 419	N419-1-b078	17.102905	-72.891286	17.07	1.35	4479	4687224838107744384	8.7	190.08 ± 0.28	0.79 ± 0.09	-0.74 ± 0.04	0.99	0.99	0000000	M2FS
SMC	NGC 419	N419-1-b079	17.077408	-72.887890	16.37	1.03	4429	4687224911112188160	6.6	188.88 ± 0.41	0.96 ± 0.11	-0.87 ± 0.05	1.00	1.00	0000010	M2FS
SMC	NGC 419	N419-1-b080	17.081155	-72.883682	15.63	1.48	4429	4687224911101874432	6.2	190.16 ± 0.47	1.36 ± 0.12	-0.67 ± 0.07	1.00	1.00	0000000	M2FS
SMC	NGC 419	N419-1-b081	17.044774	-72.819074	16.43	1.66	4429	4687226216782126976	8.8	123.48 ± 0.31	1.13 ± 0.08	-0.70 ± 0.04	0.00	0.00	0000010	M2FS

Table C.1: (*continued*) Sample of 3095 Targets from 26 Star Clusters

Galaxy	Cluster	ID	RAJ2000 (deg)	DEJ2000 (deg)	G (mag)	$G_{\rm BP} - G_{\rm RP}$ (mag)	$T_{\rm eff}$ (K)	*Gaia* DR2 ID	S/N	$v_{\rm los}$ ($\rm km\,s^{-1}$)	$\log g$ (dex)	$[{\rm Fe/H}]_{\rm raw}$ (dex)	P_M	P'_M	Flag[a]	Source[b]
(1)	(2)	(3)	(4)	(5)	(6)	(7)	(8)	(9)	(10)	(11)	(12)	(13)	(14)	(15)	(16)	(17)
SMC	NGC 419	N419-1-b082	17.056441	-72.853198	18.57	1.13	4974	4687225941904248576	3.9	190.06 ± 0.75	0.98 ± 0.27	-0.57 ± 0.11	0.96	0.96	0000000	M2FS
SMC	NGC 419	N419-1-b083	17.042702	-72.856145	18.31	1.16	4894	4687225941893928704	4.8	118.63 ± 0.68	0.56 ± 0.29	-1.28 ± 0.07	0.00	0.00	0000000	M2FS
SMC	NGC 419	N419-1-b084	17.052745	-72.858512	17.35	1.32	4583	4687225181688006912	9.5	191.77 ± 0.26	1.06 ± 0.08	-0.81 ± 0.04	0.90	0.86	0000000	M2FS
SMC	NGC 419	N419-1-b085	17.039920	-72.869775	17.26	1.52	4548	4687225147329057536	5.4	-15.03 ± 0.35	4.65 ± 0.17	-0.38 ± 0.13	-1.00	-1.00	0001100	M2FS
SMC	NGC 419	N419-1-b086	17.054093	-72.873742	18.39	0.76	4918	4687225112980675328	3.7	145.87 ± 1.23	1.40 ± 0.32	-1.35 ± 0.12	0.00	0.00	0000010	M2FS
SMC	NGC 419	N419-1-b087	17.039326	-72.877223	16.56	1.43	4429	4687225078624089600	9.9	192.68 ± 0.28	0.74 ± 0.08	-0.77 ± 0.04	0.98	0.98	0000000	M2FS
SMC	NGC 419	N419-1-b088	17.041658	-72.881934	16.54	1.45	4429	4687225082911018240	8.4	188.77 ± 0.28	1.05 ± 0.08	-0.58 ± 0.04	1.00	1.00	0000000	M2FS
SMC	NGC 419	N419-1-b089	17.028608	-72.855069	18.12	1.23	4831	4687225903242514560	5.4	189.29 ± 0.48	1.25 ± 0.16	-0.85 ± 0.06	0.96	0.96	0000000	M2FS
SMC	NGC 419	N419-1-b090	17.024251	-72.860444	16.06	3.10	4429	4687225907544522496	3.0	193.53 ± 12.44	1.53 ± 0.68	-2.19 ± 0.33	-1.00	-1.00	1010010	M2FS
SMC	NGC 419	N419-1-b091	17.022421	-72.864773	18.08	1.06	4820	4687225151630284416	6.0	168.12 ± 0.62	1.49 ± 0.21	-1.48 ± 0.07	0.00	0.00	0000000	M2FS
SMC	NGC 419	N419-1-b092	17.037114	-72.865483	18.85	0.76	5056	4687225147340387712	2.6	185.72 ± 2.47	2.28 ± 0.52	-1.81 ± 0.22	-1.00	-1.00	0100000	M2FS
SMC	NGC 419	N419-1-b093	17.018515	-72.869473	16.60	1.41	4429	4687225151630292224	15.1	187.86 ± 0.21	0.58 ± 0.07	-0.91 ± 0.03	0.97	0.97	0000000	M2FS
SMC	NGC 419	N419-1-b094	17.022632	-72.875122	16.56	1.02	4429	4687225147345125632	19.3	157.52 ± 0.29	0.75 ± 0.08	-1.68 ± 0.03	0.00	0.00	0000010	M2FS
SMC	NGC 419	N419-1-b095	17.026653	-72.882150	19.16	0.75	5141	4687225078625649792	2.0	176.49 ± 2.62	2.00 ± 0.43	-0.42 ± 0.26	0.00	0.00	0000000	M2FS
SMC	NGC 419	N419-1-b096	17.032080	-72.886439	16.65	1.41	4429	4687225078625745024	11.7	188.81 ± 0.23	1.09 ± 0.07	-0.63 ± 0.04	0.99	0.99	0000000	M2FS
SMC	NGC 419	N419-1-b097	16.893427	-72.961952	16.96	1.16	4438	4687220203828360576	11.7	159.61 ± 0.26	0.43 ± 0.11	-1.29 ± 0.04	0.00	0.00	0000000	M2FS
SMC	NGC 419	N419-1-b098	16.887563	-72.951944	16.15	1.88	4429	4687223193125584640	14.9	175.14 ± 0.31	1.63 ± 0.07	-0.53 ± 0.04	0.00	0.00	0000010	M2FS
SMC	NGC 419	N419-1-b099	16.884058	-72.945941	16.38	1.79	4429	4687223193125575296	13.6	168.39 ± 0.29	1.50 ± 0.07	-0.46 ± 0.04	0.00	0.00	0000010	M2FS
SMC	NGC 419	N419-1-b100	16.942969	-72.934393	16.79	1.19	4429	4687224666291592576	16.6	191.51 ± 0.22	0.39 ± 0.08	-1.14 ± 0.03	0.00	0.00	0000000	M2FS
SMC	NGC 419	N419-1-b101	16.851753	-72.922802	17.92	1.35	4767	4687223429341081984	6.7	162.08 ± 0.45	1.23 ± 0.16	-0.78 ± 0.05	0.00	0.00	0000000	M2FS
SMC	NGC 419	N419-1-b102	16.726181	-72.921525	17.10	1.47	4491	4687224120838482176	9.8	146.69 ± 0.31	0.89 ± 0.08	-0.96 ± 0.04	0.00	0.00	0000000	M2FS
SMC	NGC 419	N419-1-b103	16.658803	-72.921338	17.18	1.51	4522	4687224017759271296	8.2	190.87 ± 0.33	1.16 ± 0.09	-0.75 ± 0.04	0.00	0.00	0000000	M2FS
SMC	NGC 419	N419-1-b104	16.882489	-72.900186	17.33	0.98	4577	4687223532420419712	12.6	151.56 ± 0.33	0.68 ± 0.12	-1.60 ± 0.04	0.00	0.00	0000000	M2FS
SMC	NGC 419	N419-1-b105	17.012953	-73.000857	17.29	1.46	4563	4687220547425793920	8.3	147.89 ± 0.33	0.91 ± 0.11	-1.03 ± 0.04	0.00	0.00	0000000	M2FS
SMC	NGC 419	N419-1-b106	16.963812	-72.967191	18.66	0.90	5002	4687221440768779008	3.9	183.69 ± 1.48	1.41 ± 0.48	-1.76 ± 0.13	0.00	0.00	0000000	M2FS
SMC	NGC 419	N419-1-b107	17.031299	-72.902832	18.25	1.11	4875	4687224872451145984	4.9	158.84 ± 0.65	1.61 ± 0.17	-0.91 ± 0.09	0.00	0.00	0000000	M2FS
SMC	NGC 419	N419-1-b108	17.015566	-72.899777	17.99	1.31	4788	4687224872451146240	1.5	188.58 ± 1.52	2.11 ± 0.44	-0.43 ± 0.21	0.92	0.93	0000000	M2FS
SMC	NGC 419	N419-1-b109	17.027021	-72.892457	16.18	1.55	4429	4687224876752650496	15.5	190.37 ± 0.25	1.38 ± 0.06	-0.49 ± 0.04	0.99	1.00	0000000	M2FS
SMC	NGC 419	N419-1-b110	17.010612	-72.891132	17.88	1.20	4751	4687225078609578624	6.4	188.77 ± 0.44	1.50 ± 0.13	-0.74 ± 0.06	0.99	0.99	0000000	M2FS
SMC	NGC 419	N419-1-b111	17.017301	-72.886371	16.87	1.46	4429	4687225082911067776	9.3	190.60 ± 0.30	1.03 ± 0.08	-0.70 ± 0.04	0.99	0.99	0000000	M2FS
SMC	NGC 419	N419-1-b112	17.011378	-72.882599	18.54	0.96	4965	4687225082900740992	3.9	190.03 ± 0.72	1.93 ± 0.24	-0.99 ± 0.11	0.99	0.99	0000000	M2FS
SMC	NGC 419	N419-1-b114	16.964358	-72.848890	16.48	1.67	4429	4687226075058008320	13.8	161.61 ± 0.25	1.28 ± 0.06	-0.70 ± 0.04	0.00	0.00	0000010	M2FS
SMC	NGC 419	N419-1-b115	17.007875	-72.858589	18.75	0.84	5026	4687225903242507392	4.6	173.62 ± 1.18	0.66 ± 0.36	-1.43 ± 0.10	0.00	0.00	0000000	M2FS
SMC	NGC 419	N419-1-b117	16.872631	-72.868032	18.78	0.94	5035	4687226044973365760	3.4	131.40 ± 1.34	1.36 ± 0.45	-1.10 ± 0.13	0.00	0.00	0000000	M2FS
SMC	NGC 419	N419-1-b118	17.013903	-72.877896	17.57	1.26	4656	4687225151630528256	7.8	191.70 ± 0.35	0.96 ± 0.12	-0.72 ± 0.05	0.98	0.98	0000000	M2FS
SMC	NGC 419	N419-1-b119	16.974793	-72.901819	18.22	1.17	4865	4687224979831889664	5.9	159.63 ± 0.49	1.41 ± 0.17	-0.72 ± 0.06	0.00	0.00	0000000	M2FS
SMC	NGC 419	N419-1-b120	16.996173	-72.913816	16.85	1.53	4429	4687224704954002176	13.3	136.35 ± 0.20	0.96 ± 0.06	-0.81 ± 0.03	0.00	0.00	0000000	M2FS
SMC	NGC 419	N419-1-b121	16.875163	-72.828674	17.76	1.19	4716	4687413786576448768	6.2	142.72 ± 0.54	1.01 ± 0.18	-1.27 ± 0.06	0.00	0.00	0000000	M2FS
SMC	NGC 419	N419-1-b122	16.788267	-72.836917	16.41	1.30	4429	4687412377852816512	-0.6	38.99 ± 99.92	2.93 ± 1.29	-2.78 ± 0.77	-1.00	-1.00	1010000	M2FS
SMC	NGC 419	N419-1-b123	16.791948	-72.842404	18.53	1.04	4962	4687412373543777280	3.4	192.24 ± 1.04	1.78 ± 0.32	-1.15 ± 0.13	0.00	0.00	0000000	M2FS
SMC	NGC 419	N419-1-b124	16.841868	-72.847105	18.09	1.28	4823	4687412304824263040	5.1	165.59 ± 0.52	1.34 ± 0.19	-0.77 ± 0.07	0.00	0.00	0000000	M2FS
SMC	NGC 419	N419-1-b126	16.702868	-72.892710	16.68	1.20	4429	4687224464435816064	13.8	150.04 ± 0.23	0.57 ± 0.08	-1.26 ± 0.03	0.00	0.00	0000000	M2FS
SMC	NGC 419	N419-1-b127	16.649894	-72.904185	16.77	1.45	4429	4687224086478716032	2.4	141.37 ± 1.10	1.17 ± 0.26	-0.85 ± 0.12	0.00	0.00	0000000	M2FS
SMC	NGC 419	N419-1-b128	16.747669	-72.911111	16.63	1.51	4429	4687224223917677056	12.8	142.62 ± 0.26	0.96 ± 0.06	-0.80 ± 0.03	0.00	0.00	0000000	M2FS
SMC	NGC 419	N419-1-r049	17.060823	-72.899191	15.46	2.03	4429	4687224808033187712	15.4	187.01 ± 0.37	1.67 ± 0.10	-0.31 ± 0.05	0.97	0.97	0000010	M2FS
SMC	NGC 419	N419-1-r079	17.086892	-72.879910	15.61	1.59	4429	4687224911101977472	13.1	194.24 ± 0.32	1.50 ± 0.07	-0.58 ± 0.04	1.00	-1.00	0000000	M2FS
SMC	NGC 419	N419-1-r099	17.112497	-72.879659	15.89	1.68	4429	4687224911102016256	21.9	191.32 ± 0.30	1.45 ± 0.06	-0.48 ± 0.04	0.99	0.99	0000010	M2FS
SMC	NGC 419	N419-1-r127	17.099284	-72.885975	15.69	1.81	4429	4687224911101881216	12.5	188.05 ± 0.30	1.72 ± 0.09	-0.40 ± 0.05	1.00	1.00	0000010	M2FS
SMC	NGC 458	N458-1-b001	18.788492	-71.646031	16.46	1.53	4250	4687634650976213632	9.7	154.11 ± 0.28	0.08 ± 0.06	-1.33 ± 0.04	0.00	0.00	0000000	M2FS
SMC	NGC 458	N458-1-b003	18.808539	-71.586265	16.32	1.14	4904	4687635578689082752	16.5	146.84 ± 0.22	0.52 ± 0.08	-0.83 ± 0.03	0.00	0.00	0000000	M2FS
SMC	NGC 458	N458-1-b004	18.784392	-71.558110	16.01	1.32	4573	4687638808504461952	22.5	150.50 ± 0.19	0.63 ± 0.06	-0.88 ± 0.03	0.78	0.09	0000000	M2FS
SMC	NGC 458	N458-1-b005	18.815428	-71.546180	16.58	1.58	4184	4687644684019651456	12.2	165.87 ± 0.20	0.17 ± 0.09	-1.23 ± 0.03	0.00	0.00	0000000	M2FS
SMC	NGC 458	N458-1-b009	18.826835	-71.647534	16.32	0.95	5395	4687634444818447872	13.1	144.90 ± 0.31	1.78 ± 0.10	-0.71 ± 0.04	0.00	0.00	0000000	M2FS
SMC	NGC 458	N458-1-b011	18.888104	-71.599604	17.16	0.70	5482	4687640629570637056	11.6	124.88 ± 0.51	0.41 ± 0.23	-1.36 ± 0.05	0.00	0.00	0000000	M2FS

Table C.1: (*continued*) Sample of 3095 Targets from 26 Star Clusters

Galaxy	Cluster	ID	RAJ2000 (deg)	DEJ2000 (deg)	G (mag)	$G_{\rm BP} - G_{\rm RP}$ (mag)	$T_{\rm eff}$ (K)	*Gaia* DR2 ID	S/N	$v_{\rm los}$ ($\rm km\,s^{-1}$)	$\log g$ (dex)	$[{\rm Fe/H}]_{\rm raw}$ (dex)	P_M	P'_M	Flag[a]	Source[b]
(1)	(2)	(3)	(4)	(5)	(6)	(7)	(8)	(9)	(10)	(11)	(12)	(13)	(14)	(15)	(16)	(17)
SMC	NGC 458	N458-1-b012	18.925413	-71.598320	17.04	1.15	4869	4687640595210897024	8.5	144.14 ± 0.27	0.88 ± 0.12	-0.91 ± 0.04	0.00	0.00	0000000	M2FS
SMC	NGC 458	N458-1-b013	18.848935	-71.596078	16.67	1.20	4778	4687641385484879232	12.6	151.66 ± 0.21	0.80 ± 0.09	-0.85 ± 0.03	0.00	0.00	0000000	M2FS
SMC	NGC 458	N458-1-b014	18.946260	-71.532010	16.46	0.99	5302	4687641866521087744	13.2	136.30 ± 0.25	1.68 ± 0.09	-0.59 ± 0.04	0.00	0.00	0000000	M2FS
SMC	NGC 458	N458-1-b015	18.846234	-71.510630	16.30	1.49	4303	4687644993257260672	17.2	121.63 ± 0.17	0.59 ± 0.05	-0.87 ± 0.03	0.00	0.00	0000000	M2FS
SMC	NGC 458	N458-1-b033	18.725396	-71.664188	16.79	1.18	4815	4687634307378849920	9.6	142.64 ± 0.25	0.70 ± 0.11	-0.99 ± 0.04	0.00	0.00	0000000	M2FS
SMC	NGC 458	N458-1-b034	18.727951	-71.644448	16.93	1.12	4940	4687634582256737024	8.7	147.70 ± 0.35	0.92 ± 0.13	-0.89 ± 0.04	0.00	0.00	0000000	M2FS
SMC	NGC 458	N458-1-b036	18.724500	-71.613144	16.60	1.10	4998	4687635441250162432	14.6	132.22 ± 0.26	0.90 ± 0.09	-0.83 ± 0.03	0.00	0.00	0000000	M2FS
SMC	NGC 458	N458-1-b037	18.724676	-71.581596	16.86	1.32	4562	4687635819207248384	13.3	162.78 ± 0.21	0.87 ± 0.07	-0.86 ± 0.03	0.00	0.00	0000000	M2FS
SMC	NGC 458	N458-1-b038	18.726256	-71.559577	16.36	0.96	5361	4687638842864203264	21.7	148.20 ± 0.25	1.56 ± 0.07	-0.64 ± 0.03	1.00	0.97	0000000	M2FS
SMC	NGC 458	N458-1-b039	18.723452	-71.527243	16.65	1.21	4750	4687639147808392576	20.6	147.45 ± 0.18	0.69 ± 0.07	-0.90 ± 0.03	0.77	0.17	0000000	M2FS
SMC	NGC 458	N458-1-b040	18.721119	-71.515672	15.27	1.26	4674	4687639908015990400	25.6	143.63 ± 0.20	0.05 ± 0.05	-0.81 ± 0.03	0.00	0.00	0000000	M2FS
SMC	NGC 458	N458-1-b041	18.768646	-71.630261	16.03	0.79	5482	4687634616617133952	17.6	157.41 ± 0.36	0.52 ± 0.13	-0.78 ± 0.03	0.00	0.00	0000000	M2FS
SMC	NGC 458	N458-1-b042	18.778899	-71.623561	15.12	1.53	4250	4687634719696346624	31.1	158.46 ± 0.16	0.06 ± 0.05	-0.88 ± 0.03	0.00	0.00	0000000	M2FS
SMC	NGC 458	N458-1-b043	18.749891	-71.575719	16.50	1.53	4251	4687635819207243392	15.3	145.85 ± 0.42	0.22 ± 0.13	-1.75 ± 0.05	0.00	0.00	0000000	M2FS
SMC	NGC 458	N458-1-b044	18.737907	-71.558432	16.44	1.22	4731	4687638774144725120	21.6	147.74 ± 0.17	0.86 ± 0.06	-0.82 ± 0.03	1.00	0.96	0000000	M2FS
SMC	NGC 458	N458-1-b045	18.729686	-71.555256	16.75	1.04	5150	4687638842860547584	12.3	149.06 ± 0.25	1.39 ± 0.11	-0.51 ± 0.03	1.00	1.00	0000000	M2FS
SMC	NGC 458	N458-1-b046	18.782008	-71.553876	15.68	1.97	3805	4687638808504454912	18.6	130.20 ± 0.33	0.56 ± 0.05	-1.21 ± 0.04	0.00	0.00	0000000	M2FS
SMC	NGC 458	N458-1-b047	18.735852	-71.534155	16.24	0.86	5482	4687639083383097856	25.1	127.41 ± 0.31	0.57 ± 0.10	-0.66 ± 0.03	0.00	0.00	0000000	M2FS
SMC	NGC 458	N458-1-b049	18.724540	-71.434832	16.59	1.03	5178	4690648618505832064	17.6	137.49 ± 0.24	0.62 ± 0.10	-0.81 ± 0.03	0.00	0.00	0000000	M2FS
SMC	NGC 458	N458-1-b050	18.821330	-71.442457	17.26	0.99	5281	4687646264564679936	8.9	168.36 ± 0.41	0.97 ± 0.20	-0.89 ± 0.05	0.00	0.00	0000000	M2FS
SMC	NGC 458	N458-1-b051	18.710026	-71.449540	16.79	1.44	4376	4690648549786356480	14.1	141.91 ± 0.22	0.65 ± 0.06	-0.90 ± 0.03	0.00	0.00	0000000	M2FS
SMC	NGC 458	N458-1-b052	18.740620	-71.449683	16.87	1.49	4315	4690648545489496320	11.9	128.72 ± 0.24	0.21 ± 0.10	-1.25 ± 0.03	0.00	0.00	0000000	M2FS
SMC	NGC 458	N458-1-b053	18.961352	-71.474758	16.42	1.16	4865	4687645508653306880	13.8	139.03 ± 0.23	1.26 ± 0.08	-0.85 ± 0.03	0.00	0.00	0000000	M2FS
SMC	NGC 458	N458-1-b054	18.975080	-71.475584	16.42	1.18	4800	4687645508653307264	14.8	139.84 ± 0.23	0.74 ± 0.08	-0.86 ± 0.03	0.00	0.00	0000000	M2FS
SMC	NGC 458	N458-1-b055	18.963839	-71.488548	15.39	1.48	4319	4687645302494886528	24.2	154.22 ± 0.21	0.12 ± 0.07	-0.82 ± 0.03	0.00	0.00	0000000	M2FS
SMC	NGC 458	N458-1-b056	18.952627	-71.496126	15.46	1.24	4702	4687644924537770752	22.1	137.06 ± 0.18	0.06 ± 0.05	-0.84 ± 0.03	0.00	0.00	0000000	M2FS
SMC	NGC 458	N458-1-b057	18.623375	-71.469395	16.96	1.32	4565	4690642708630836352	14.2	105.51 ± 0.21	0.81 ± 0.07	-1.08 ± 0.03	-1.00	-1.00	0000100	M2FS
SMC	NGC 458	N458-1-b058	18.701885	-71.487385	16.60	1.30	4592	4687640182893874176	18.1	159.24 ± 0.17	0.73 ± 0.06	-1.30 ± 0.03	0.00	0.00	0000000	M2FS
SMC	NGC 458	N458-1-b061	18.701298	-71.498183	16.57	0.60	5482	4687639972442261248	21.7	138.08 ± 0.37	0.14 ± 0.11	-1.47 ± 0.03	0.00	0.00	0000000	M2FS
SMC	NGC 458	N458-1-b062	18.655058	-71.500167	16.43	0.81	5482	4687640144240939264	20.8	162.26 ± 0.32	0.52 ± 0.10	-0.66 ± 0.03	0.00	0.00	0000000	M2FS
SMC	NGC 458	N458-1-b063	18.682941	-71.521928	16.99	0.97	5351	4687639873652603904	12.2	110.52 ± 0.31	1.66 ± 0.12	-0.77 ± 0.04	0.00	0.00	0000000	M2FS
SMC	NGC 458	N458-1-b064	18.634736	-71.528488	17.05	1.13	4915	4687639770577050624	14.4	154.15 ± 0.23	1.10 ± 0.08	-0.83 ± 0.03	0.00	0.00	0000000	M2FS
SMC	NGC 458	N458-1-b065	18.647868	-71.627439	16.72	1.17	4835	4687635028933322112	15.6	152.92 ± 0.23	0.92 ± 0.07	-0.89 ± 0.03	0.00	0.00	0000000	M2FS
SMC	NGC 458	N458-1-b070	18.598290	-71.611901	16.86	0.99	5285	4687635299517208960	12.8	121.46 ± 0.30	1.57 ± 0.10	-0.80 ± 0.04	0.00	0.00	0000000	M2FS
SMC	NGC 458	N458-1-b071	18.614232	-71.600384	16.54	1.59	4170	4687638258748698880	12.4	138.82 ± 0.24	0.56 ± 0.05	-0.96 ± 0.03	0.00	0.00	0000000	M2FS
SMC	NGC 458	N458-1-b072	18.653995	-71.589843	16.42	1.25	4691	4687638636705808512	18.6	153.60 ± 0.19	0.70 ± 0.07	-0.88 ± 0.03	0.00	0.00	0000000	M2FS
SMC	NGC 458	N458-1-b074	18.690761	-71.602008	16.59	1.21	4739	4687635643128914944	16.5	147.67 ± 0.19	0.78 ± 0.07	-0.87 ± 0.03	0.00	0.00	0000000	M2FS
SMC	NGC 458	N458-1-b075	18.708898	-71.599069	16.77	1.20	4777	4687635647408578944	13.5	144.39 ± 0.20	0.99 ± 0.08	-0.87 ± 0.03	0.00	0.00	0000000	M2FS
SMC	NGC 458	N458-1-b076	18.683542	-71.560236	16.09	0.85	5482	4687638739785718528	22.6	148.11 ± 0.25	0.44 ± 0.12	-0.64 ± 0.03	1.00	0.97	0000000	M2FS
SMC	NGC 458	N458-1-b077	18.710738	-71.560039	16.53	0.91	5482	4687638838570393216	20.4	147.26 ± 0.39	1.97 ± 0.08	-0.87 ± 0.03	1.00	0.94	0000000	M2FS
SMC	NGC 458	N458-1-b078	18.709749	-71.552507	16.21	0.61	5482	4687638842864136576	23.2	155.96 ± 0.25	0.33 ± 0.14	-1.07 ± 0.03	1.00	-1.00	0000000	M2FS
SMC	NGC 458	N458-1-b079	18.698560	-71.551071	16.28	0.86	5482	4687639049022622464	19.9	152.32 ± 0.28	0.60 ± 0.11	-0.64 ± 0.03	1.00	1.00	0000000	M2FS
SMC	NGC 458	N458-1-b080	18.708926	-71.542657	16.81	1.01	5223	4687639049022557440	17.8	143.52 ± 0.21	1.34 ± 0.08	-0.59 ± 0.03	1.00	0.01	0000000	M2FS
SMC	NGC 458	N458-1-b081	18.567050	-71.450529	16.53	0.83	5482	4690642876132659200	16.7	171.50 ± 0.49	1.11 ± 0.24	-0.97 ± 0.05	0.00	0.00	0000000	M2FS
SMC	NGC 458	N458-1-b082	18.518331	-71.464910	16.61	1.24	4692	4690642846069789568	20.1	150.10 ± 0.19	0.83 ± 0.06	-0.89 ± 0.03	0.00	0.00	0000000	M2FS
SMC	NGC 458	N458-1-b084	18.584739	-71.493458	16.70	1.19	4787	4690642536832146816	17.1	148.36 ± 0.20	0.90 ± 0.07	-0.88 ± 0.03	0.00	0.00	0000000	M2FS
SMC	NGC 458	N458-1-b085	18.567157	-71.514656	15.54	0.89	5482	4687640079814685184	40.5	144.29 ± 0.26	0.09 ± 0.08	-0.64 ± 0.03	0.00	0.00	0000000	M2FS
SMC	NGC 458	N458-1-b086	18.562626	-71.541398	17.06	1.28	4642	4687639426979686016	13.1	179.63 ± 0.24	0.49 ± 0.13	-1.58 ± 0.03	0.00	0.00	0000000	M2FS
SMC	NGC 458	N458-1-b087	18.617818	-71.545321	16.27	1.19	4796	4687639736217383680	20.6	153.58 ± 0.19	0.66 ± 0.07	-0.84 ± 0.03	0.00	0.00	0000000	M2FS
SMC	NGC 458	N458-1-b088	18.598983	-71.547296	16.68	1.14	4889	4687639736217388288	17.2	144.45 ± 0.22	0.96 ± 0.08	-0.80 ± 0.03	0.00	0.00	0000000	M2FS
SMC	NGC 458	N458-1-b089	18.484905	-71.468060	16.53	1.25	4676	4690642468112774016	18.6	146.58 ± 0.22	0.77 ± 0.07	-0.91 ± 0.03	0.00	0.00	0000000	M2FS
SMC	NGC 458	N458-1-b090	18.473519	-71.513232	16.80	1.02	5198	4690642090155659648	19.9	151.98 ± 0.24	1.30 ± 0.07	-0.94 ± 0.03	0.00	0.00	0000000	M2FS
SMC	NGC 458	N458-1-b091	18.503216	-71.524029	16.07	2.27	3710	4687639701857573376	4.7	147.82 ± 1.69	0.68 ± 0.34	-2.34 ± 0.21	-1.00	-1.00	0110000	M2FS
SMC	NGC 458	N458-1-b092	18.375633	-71.528504	16.42	1.61	4154	4690642017137614848	16.3	121.65 ± 0.19	0.56 ± 0.05	-0.97 ± 0.03	0.00	0.00	0000000	M2FS

Table C.1: (*continued*) Sample of 3095 Targets from 26 Star Clusters

Galaxy	Cluster	ID	RAJ2000 (deg)	DEJ2000 (deg)	G (mag)	$G_{\rm BP} - G_{\rm RP}$ (mag)	$T_{\rm eff}$ (K)	*Gaia* DR2 ID	S/N	$v_{\rm los}$ (km s^{-1})	log g (dex)	[Fe/H]$_{\rm raw}$ (dex)	P_M	P'_M	Flag[a]	Source[b]
(1)	(2)	(3)	(4)	(5)	(6)	(7)	(8)	(9)	(10)	(11)	(12)	(13)	(14)	(15)	(16)	(17)
SMC	NGC 458	N458-1-b093	18.390298	-71.529187	16.82	1.50	4294	4690642055795925760	15.7	165.86 ± 0.19	0.84 ± 0.05	-0.98 ± 0.03	0.00	0.00	0000000	M2FS
SMC	NGC 458	N458-1-b094	18.462097	-71.534044	15.92	0.86	5482	4687639667498651008	39.3	134.71 ± 0.38	0.08 ± 0.07	-1.31 ± 0.03	0.00	0.00	0000000	M2FS
SMC	NGC 458	N458-1-b095	18.429365	-71.559313	17.17	0.92	5473	4687639495696233344	14.7	5.81 ± 0.32	4.00 ± 0.05	-0.52 ± 0.04	-1.00	-1.00	0001100	M2FS
SMC	NGC 458	N458-1-b096	18.419630	-71.561702	15.96	1.68	4075	4687639461340226560	20.7	132.76 ± 0.18	0.48 ± 0.04	-0.92 ± 0.03	0.00	0.00	0000000	M2FS
SMC	NGC 458	N458-1-b097	18.477826	-71.621840	15.49	0.79	5482	4687638155670185600	37.2	147.87 ± 0.37	1.96 ± 0.09	-0.87 ± 0.03	0.00	0.00	0000000	M2FS
SMC	NGC 458	N458-1-b098	18.421171	-71.614538	15.79	1.29	4618	4687638361828614144	28.1	152.97 ± 0.18	0.45 ± 0.07	-0.86 ± 0.03	0.00	0.00	0000000	M2FS
SMC	NGC 458	N458-1-b099	18.447555	-71.613234	15.20	1.31	4578	4687638361828613248	42.0	147.31 ± 0.17	0.08 ± 0.06	-0.82 ± 0.02	0.00	0.00	0000000	M2FS
SMC	NGC 458	N458-1-b100	18.439272	-71.601650	15.66	1.23	4716	4687638430548084992	33.9	146.31 ± 0.17	0.70 ± 0.05	-0.93 ± 0.03	0.00	0.00	0000000	M2FS
SMC	NGC 458	N458-1-b101	18.461271	-71.595606	16.40	1.19	4799	4687638464907820928	23.3	135.78 ± 0.22	0.65 ± 0.07	-0.90 ± 0.03	0.00	0.00	0000000	M2FS
SMC	NGC 458	N458-1-b102	18.483941	-71.594863	16.20	1.23	4723	4687638464907820544	21.3	137.05 ± 0.18	0.63 ± 0.07	-0.96 ± 0.03	0.00	0.00	0000000	M2FS
SMC	NGC 458	N458-1-b105	18.574142	-71.655186	16.59	1.44	4387	4687634990276682368	15.1	177.64 ± 0.19	0.61 ± 0.06	-0.97 ± 0.03	0.00	0.00	0000000	M2FS
SMC	NGC 458	N458-1-b106	18.542220	-71.642658	16.53	1.43	4400	4687635093355930880	17.7	144.21 ± 0.19	0.52 ± 0.06	-0.79 ± 0.03	0.00	0.00	0000000	M2FS
SMC	NGC 458	N458-1-b107	18.585929	-71.618571	16.80	1.18	4800	4687635269451483136	17.6	147.67 ± 0.20	0.97 ± 0.07	-0.91 ± 0.03	0.00	0.00	0000000	M2FS
SMC	NGC 458	N458-1-b108	18.519722	-71.599786	16.65	1.53	4253	4687638499266869888	15.3	146.26 ± 0.19	0.53 ± 0.06	-1.09 ± 0.03	0.00	0.00	0000000	M2FS
SMC	NGC 458	N458-1-b109	18.583431	-71.594560	16.72	1.58	4194	4687638327468170496	16.0	165.08 ± 0.22	0.03 ± 0.02	-1.50 ± 0.03	0.00	0.00	0000000	M2FS
SMC	NGC 458	N458-1-b110	18.544987	-71.583813	16.71	1.17	4844	4687638499266850816	18.5	149.81 ± 0.17	0.75 ± 0.07	-0.84 ± 0.03	0.00	0.00	0000000	M2FS
SMC	NGC 458	N458-1-b111	18.591331	-71.562566	16.82	0.79	5482	4687638980303164544	18.7	149.74 ± 0.34	0.45 ± 0.15	-0.89 ± 0.04	0.00	0.00	0000000	M2FS
SMC	NGC 458	N458-1-b112	18.581098	-71.559549	16.49	1.20	4775	4687638602346039296	23.1	138.12 ± 0.17	0.71 ± 0.06	-0.89 ± 0.03	0.00	0.00	0000000	M2FS
SMC	NGC 458	N458-1-r028	18.722306	-71.542408	16.52	1.17	4827	4687639044741547008	20.2	148.52 ± 0.15	0.90 ± 0.07	-0.77 ± 0.03	1.00	1.00	0000000	M2FS
SMC	NGC 458	N458-1-r049	18.727122	-71.551800	15.72	1.05	5121	4687638842864175104	32.2	148.62 ± 0.19	1.01 ± 0.08	-0.45 ± 0.03	1.00	1.00	0000000	M2FS
SMC	NGC 458	N458-1-r099	18.740720	-71.546908	15.93	1.29	4611	4687638838584792960	19.0	148.73 ± 0.20	0.74 ± 0.06	-0.81 ± 0.03	1.00	1.00	0000000	M2FS
SMC	NGC 458	N458-1-r127	18.728298	-71.548217	16.66	0.85	5482	4687638842860511872	19.4	149.41 ± 0.25	1.84 ± 0.09	-0.37 ± 0.03	1.00	1.00	0000000	M2FS
LMC	Hodge 4	H4-1-b002	83.152025	-64.779552	17.05	1.57	4331	4660911055243877632	10.9	283.36 ± 0.22	1.11 ± 0.06	-0.59 ± 0.03	0.00	0.00	0000000	M2FS
LMC	Hodge 4	H4-1-b003	83.158425	-64.774342	17.47	1.46	4479	4660912528394256768	8.8	273.42 ± 0.28	1.39 ± 0.07	-0.45 ± 0.04	0.00	0.00	0000000	M2FS
LMC	Hodge 4	H4-1-b004	83.152905	-64.767209	18.79	1.07	4892	4660912528395175552	3.6	296.90 ± 0.55	1.32 ± 0.24	-0.52 ± 0.07	0.00	0.00	0000000	M2FS
LMC	Hodge 4	H4-1-b005	83.171386	-64.763298	18.80	1.07	4894	4660912567072360064	3.4	332.64 ± 0.68	1.26 ± 0.34	-0.83 ± 0.08	0.00	0.00	0000000	M2FS
LMC	Hodge 4	H4-1-b006	83.157994	-64.757056	18.86	1.18	4909	4660912562754657664	3.9	290.16 ± 0.74	1.41 ± 0.31	-1.35 ± 0.10	0.00	0.00	0000000	M2FS
LMC	Hodge 4	H4-1-b007	83.172405	-64.752078	18.56	1.02	4822	4660912670145561216	4.6	288.18 ± 0.53	1.36 ± 0.22	-1.07 ± 0.07	0.00	0.00	0000000	M2FS
LMC	Hodge 4	H4-1-b008	83.163039	-64.738394	18.45	1.09	4791	4660912700192982400	4.6	331.79 ± 0.56	1.32 ± 0.16	-0.80 ± 0.07	0.00	0.00	0000000	M2FS
LMC	Hodge 4	H4-1-b011	83.185964	-64.765685	18.63	1.21	4844	4660912356595571456	3.5	298.01 ± 2.58	3.18 ± 0.21	-1.32 ± 0.13	-1.00	-1.00	0100000	M2FS
LMC	Hodge 4	H4-1-b012	83.194168	-64.757817	16.24	1.42	4030	4660912463993144576	18.8	298.97 ± 0.20	0.02 ± 0.02	-0.77 ± 0.03	0.00	0.00	0000000	M2FS
LMC	Hodge 4	H4-1-b013	83.178829	-64.756085	16.34	1.65	4068	4660912670151572224	14.2	306.08 ± 0.22	0.75 ± 0.04	-0.67 ± 0.03	0.00	0.00	0000000	M2FS
LMC	Hodge 4	H4-1-b014	83.188561	-64.751090	18.95	1.03	4934	4660912463987143936	2.6	304.07 ± 1.11	1.63 ± 0.43	-1.00 ± 0.13	0.00	0.00	0000000	M2FS
LMC	Hodge 4	H4-1-b015	83.193625	-64.747947	18.38	1.04	4768	4660912494046669440	4.7	306.45 ± 0.52	1.34 ± 0.19	-0.83 ± 0.07	0.01	0.00	0000000	M2FS
LMC	Hodge 4	H4-1-b016	83.188257	-64.742840	18.31	1.01	4748	4660912700205065472	5.5	48.95 ± 0.49	2.90 ± 0.08	-0.43 ± 0.07	-1.00	-1.00	0000100	M2FS
LMC	Hodge 4	H4-1-b017	83.204613	-64.713688	17.19	0.95	4382	4660913009430652544	14.2	98.99 ± 0.40	1.56 ± 0.07	-1.44 ± 0.05	-1.00	-1.00	0000110	M2FS
LMC	Hodge 4	H4-1-b018	83.205852	-64.721125	18.31	1.32	4748	4660912906351430528	5.5	260.20 ± 0.36	2.05 ± 0.11	-0.59 ± 0.06	0.00	0.00	0000000	M2FS
LMC	Hodge 4	H4-1-b019	83.184703	-64.727333	17.73	1.16	4564	4660913082468416640	9.8	311.10 ± 0.28	0.70 ± 0.13	-1.56 ± 0.04	0.62	0.47	0000000	M2FS
LMC	Hodge 4	H4-1-b020	83.200471	-64.731423	18.97	1.05	4940	4660912876303930880	3.8	316.14 ± 0.56	1.87 ± 0.23	-0.66 ± 0.08	0.17	0.02	0000000	M2FS
LMC	Hodge 4	H4-1-b021	83.187944	-64.732837	18.78	1.08	4887	4660913078162185856	3.5	298.63 ± 0.69	2.20 ± 0.24	-0.63 ± 0.09	0.00	0.00	0000000	M2FS
LMC	Hodge 4	H4-1-b022	83.198265	-64.735938	18.79	1.04	4890	4660912876309994496	3.7	288.77 ± 0.58	0.66 ± 0.33	-1.01 ± 0.09	0.00	0.00	0000000	M2FS
LMC	Hodge 4	H4-1-b023	83.187739	-64.737334	18.04	1.20	4661	4660912700192982272	6.2	300.29 ± 0.35	1.38 ± 0.11	-0.92 ± 0.05	0.00	0.00	0000000	M2FS
LMC	Hodge 4	H4-1-b024	83.210170	-64.739291	18.85	1.09	4906	4660912876303975296	3.2	286.85 ± 0.56	1.39 ± 0.28	-0.55 ± 0.09	0.00	0.00	0000000	M2FS
LMC	Hodge 4	H4-1-b025	83.171262	-64.704140	18.78	1.07	4889	4660913215589725696	4.0	319.46 ± 0.60	1.47 ± 0.24	-0.84 ± 0.08	0.00	0.00	0000000	M2FS
LMC	Hodge 4	H4-1-b026	83.167612	-64.707659	18.85	1.14	4908	4660913112521791744	3.7	301.84 ± 0.86	1.43 ± 0.31	-0.53 ± 0.08	0.00	0.00	0000000	M2FS
LMC	Hodge 4	H4-1-b027	83.165845	-64.713275	18.77	0.96	4886	4660913116821889280	4.2	318.39 ± 0.70	1.59 ± 0.20	-0.80 ± 0.09	0.07	0.00	0000000	M2FS
LMC	Hodge 4	H4-1-b028	83.156260	-64.719387	17.36	1.08	4441	4660913082468397568	10.5	314.43 ± 0.26	1.02 ± 0.07	-1.12 ± 0.04	-1.00	-1.00	0000001	M2FS
LMC	Hodge 4	H4-1-b029	83.164602	-64.720064	17.42	1.43	4462	4660913082468401280	8.5	308.47 ± 0.26	1.34 ± 0.07	-0.64 ± 0.04	0.20	0.01	0000000	M2FS
LMC	Hodge 4	H4-1-b030	83.158499	-64.723467	17.54	1.25	4503	4660913082468405248	6.9	292.69 ± 0.37	0.68 ± 0.12	-1.08 ± 0.05	0.00	0.00	0000000	M2FS
LMC	Hodge 4	H4-1-b031	83.165502	-64.726011	18.01	1.29	4653	4660913082468410368	6.8	315.11 ± 0.32	1.68 ± 0.11	-0.52 ± 0.05	0.56	0.45	0000000	M2FS
LMC	Hodge 4	H4-1-b032	83.152737	-64.726970	18.85	1.05	4906	4660912704511286400	3.1	294.59 ± 0.83	1.26 ± 0.32	-0.81 ± 0.10	0.00	0.00	0000000	M2FS
LMC	Hodge 4	H4-1-b034	83.107418	-64.752896	18.85	1.12	4908	4660912601426025216	3.1	310.85 ± 0.72	2.08 ± 0.22	-0.59 ± 0.09	0.92	0.87	0000000	M2FS
LMC	Hodge 4	H4-1-b035	83.112297	-64.749909	18.63	0.95	4842	4660912635785750016	4.4	272.10 ± 0.68	1.21 ± 0.22	-0.69 ± 0.07	0.00	0.00	0000000	M2FS
LMC	Hodge 4	H4-1-b036	83.102811	-64.749057	18.84	1.15	4904	4660915552051258496	3.5	312.51 ± 0.66	1.40 ± 0.24	-0.64 ± 0.08	0.94	0.94	0000000	M2FS

Table C.1: (*continued*) Sample of 3095 Targets from 26 Star Clusters

Galaxy	Cluster	ID	RAJ2000 (deg)	DEJ2000 (deg)	G (mag)	$G_{\rm BP} - G_{\rm RP}$ (mag)	$T_{\rm eff}$ (K)	*Gaia* DR2 ID	S/N	$v_{\rm los}$ ($\rm km\,s^{-1}$)	$\log g$ (dex)	$[{\rm Fe/H}]_{\rm raw}$ (dex)	P_M	P'_M	Flag[a]	Source[b]
(1)	(2)	(3)	(4)	(5)	(6)	(7)	(8)	(9)	(10)	(11)	(12)	(13)	(14)	(15)	(16)	(17)
LMC	Hodge 4	H4-1-b037	83.114251	-64.741865	18.81	0.97	4895	4660912635785710592	3.8	315.10 ± 0.62	2.20 ± 0.20	-0.78 ± 0.09	0.99	0.98	0000000	M2FS
LMC	Hodge 4	H4-1-b038	83.105851	-64.740278	18.84	0.90	4904	4660915590723188608	3.5	310.95 ± 0.55	2.61 ± 0.16	-0.51 ± 0.09	1.00	1.00	0000000	M2FS
LMC	Hodge 4	H4-1-b039	83.115869	-64.738478	18.24	1.13	4725	4660912738864906496	4.9	314.33 ± 0.36	1.81 ± 0.13	-0.50 ± 0.06	1.00	1.00	0000000	M2FS
LMC	Hodge 4	H4-1-b040	83.105698	-64.736297	17.77	0.98	4577	4660915693802363776	4.3	312.88 ± 0.58	1.03 ± 0.19	-1.14 ± 0.07	-1.00	-1.00	0000001	M2FS
LMC	Hodge 4	H4-1-b041	83.129116	-64.777267	18.78	1.05	4888	4660911123963350656	3.5	288.22 ± 0.89	1.86 ± 0.33	-0.61 ± 0.09	0.00	0.00	0000000	M2FS
LMC	Hodge 4	H4-1-b042	83.131623	-64.771113	18.75	1.14	4879	4660911119645635584	4.0	308.48 ± 0.49	1.74 ± 0.21	-0.61 ± 0.07	0.07	0.00	0000000	M2FS
LMC	Hodge 4	H4-1-b043	83.144120	-64.758134	18.82	1.13	4899	4660912567072353920	2.8	311.91 ± 0.73	1.51 ± 0.29	-0.64 ± 0.09	0.67	0.63	0000000	M2FS
LMC	Hodge 4	H4-1-b044	83.130487	-64.747426	18.23	1.27	4723	4660912631473497728	5.8	275.92 ± 0.38	1.91 ± 0.11	-0.54 ± 0.05	0.00	0.00	0000000	M2FS
LMC	Hodge 4	H4-1-b045	83.122966	-64.745177	18.85	1.04	4908	4660912635785741312	1.4	312.84 ± 1.46	2.26 ± 0.50	-0.85 ± 0.22	0.99	0.99	0000000	M2FS
LMC	Hodge 4	H4-1-b046	83.137024	-64.741236	18.68	1.00	4860	4660912738864953088	3.6	312.12 ± 0.74	1.39 ± 0.27	-0.97 ± 0.10	0.94	0.94	0000000	M2FS
LMC	Hodge 4	H4-1-b047	83.123940	-64.740082	17.61	1.28	4525	4660912738864929152	7.2	314.59 ± 0.24	1.34 ± 0.08	-0.53 ± 0.04	0.99	0.99	0000000	M2FS
LMC	Hodge 4	H4-1-b048	83.136919	-64.737124	18.00	1.25	4649	4660912734552722944	7.2	306.78 ± 0.32	1.32 ± 0.10	-0.65 ± 0.04	0.29	0.00	0000000	M2FS
LMC	Hodge 4	H4-1-b050	83.143793	-64.689646	18.65	1.23	4849	4660913284308580224	3.9	318.30 ± 0.56	1.82 ± 0.19	-0.65 ± 0.08	0.00	0.00	0000000	M2FS
LMC	Hodge 4	H4-1-b051	83.144526	-64.701258	18.77	1.31	4885	4660913181241119616	3.0	291.70 ± 0.89	2.42 ± 0.22	-0.78 ± 0.12	0.00	0.00	0000000	M2FS
LMC	Hodge 4	H4-1-b053	83.129800	-64.712899	18.72	1.11	4869	4660913146881285248	4.2	309.01 ± 0.54	1.63 ± 0.20	-0.73 ± 0.08	0.32	0.05	0000000	M2FS
LMC	Hodge 4	H4-1-b054	83.148934	-64.714159	17.64	1.32	4536	4660913151187868672	9.4	276.67 ± 0.29	1.03 ± 0.08	-0.65 ± 0.04	0.00	0.00	0000000	M2FS
LMC	Hodge 4	H4-1-b055	83.129657	-64.721680	18.26	1.14	4730	4660912768924159616	6.5	311.85 ± 0.37	1.06 ± 0.13	-0.75 ± 0.05	0.94	0.93	0000000	M2FS
LMC	Hodge 4	H4-1-b056	83.137688	-64.731331	18.29	1.03	4741	4660912768912467328	5.5	308.73 ± 1.07	2.00 ± 0.15	-1.25 ± 0.08	0.78	0.45	0000000	M2FS
LMC	Hodge 4	H4-1-b060	83.126108	-64.694244	18.57	1.13	4826	4660913181229993088	4.2	303.91 ± 0.64	1.13 ± 0.21	-0.39 ± 0.08	0.00	0.00	0000000	M2FS
LMC	Hodge 4	H4-1-b061	83.128071	-64.707211	18.60	1.07	4836	4660913146881272576	3.8	302.73 ± 0.88	1.91 ± 0.24	-1.25 ± 0.11	0.00	0.00	0000000	M2FS
LMC	Hodge 4	H4-1-b062	83.122666	-64.716210	18.80	1.11	4892	4660913151181586816	3.9	312.55 ± 0.46	1.97 ± 0.17	-0.55 ± 0.07	0.91	0.94	0000000	M2FS
LMC	Hodge 4	H4-1-b063	83.129143	-64.726997	18.10	1.17	4683	4660912773224559872	6.3	303.96 ± 0.31	1.32 ± 0.13	-0.59 ± 0.05	0.01	0.00	0000000	M2FS
LMC	Hodge 4	H4-1-b064	83.120925	-64.728822	18.85	1.05	4907	4660912738864820864	3.3	314.42 ± 0.55	1.40 ± 0.27	-0.63 ± 0.08	0.99	0.99	0000000	M2FS
LMC	Hodge 4	H4-1-b065	83.072076	-64.774695	18.57	1.08	4826	4660914040222747904	4.6	295.89 ± 0.53	1.41 ± 0.21	-0.83 ± 0.07	0.00	0.00	0000000	M2FS
LMC	Hodge 4	H4-1-b066	83.064586	-64.771385	16.28	1.72	4044	4660914040234056448	13.1	305.84 ± 0.22	0.71 ± 0.05	-0.63 ± 0.04	0.00	0.00	0000000	M2FS
LMC	Hodge 4	H4-1-b067	83.057685	-64.768870	18.76	1.10	4882	4660914108942230272	4.1	316.59 ± 0.62	1.94 ± 0.18	-0.64 ± 0.08	0.12	0.01	0000000	M2FS
LMC	Hodge 4	H4-1-b068	83.080047	-64.763639	15.37	2.51	3777	4660914078900838016	17.3	282.81 ± 0.40	0.93 ± 0.08	-0.72 ± 0.07	0.00	0.00	0000010	M2FS
LMC	Hodge 4	H4-1-b069	83.073733	-64.756954	17.70	1.33	4555	4660914078900831360	7.5	287.49 ± 0.31	1.29 ± 0.09	-0.52 ± 0.04	0.00	0.00	0000000	M2FS
LMC	Hodge 4	H4-1-b070	83.078025	-64.753362	18.73	1.05	4873	4660915556363492096	2.3	316.50 ± 1.58	1.89 ± 0.41	-1.09 ± 0.18	0.62	0.58	0000000	M2FS
LMC	Hodge 4	H4-1-b071	83.071000	-64.751507	18.78	1.14	4888	4660914078894720384	3.3	275.78 ± 0.60	1.64 ± 0.23	-0.57 ± 0.08	0.00	0.00	0000000	M2FS
LMC	Hodge 4	H4-1-b072	83.060649	-64.747100	18.75	1.14	4878	4660915620792003968	3.3	301.19 ± 0.75	1.27 ± 0.31	-0.76 ± 0.09	0.00	0.00	0000000	M2FS
LMC	Hodge 4	H4-1-b074	83.093816	-64.776097	18.56	0.93	4822	4660914040222745856	3.8	317.98 ± 0.77	1.69 ± 0.20	-0.87 ± 0.09	0.04	0.00	0000000	M2FS
LMC	Hodge 4	H4-1-b075	83.097369	-64.755517	18.98	1.05	4944	4660915556363526400	2.8	299.13 ± 1.13	2.03 ± 0.33	-0.78 ± 0.13	0.00	0.00	0000000	M2FS
LMC	Hodge 4	H4-1-b076	83.079974	-64.744043	18.85	0.98	4907	4660915552051265408	3.1	314.25 ± 0.87	1.57 ± 0.28	-0.62 ± 0.08	0.93	0.93	0000000	M2FS
LMC	Hodge 4	H4-1-b077	83.095370	-64.743613	18.87	0.95	4912	4660915590723194752	3.1	312.47 ± 0.68	2.08 ± 0.23	-0.52 ± 0.09	0.99	0.99	0000000	M2FS
LMC	Hodge 4	H4-1-b078	83.089202	-64.740804	18.85	0.94	4908	4660915590723161216	3.2	312.57 ± 0.58	1.78 ± 0.25	-0.66 ± 0.09	0.99	0.99	0000000	M2FS
LMC	Hodge 4	H4-1-b079	83.100204	-64.733227	18.63	0.84	4844	4660915693802317440	3.5	312.32 ± 0.86	0.50 ± 0.32	-0.49 ± 0.08	1.00	1.00	0000000	M2FS
LMC	Hodge 4	H4-1-b080	83.091672	-64.732892	18.65	0.75	4848	4660915590723074048	4.2	323.02 ± 0.87	2.02 ± 0.19	-0.89 ± 0.09	0.02	0.00	0000010	M2FS
LMC	Hodge 4	H4-1-b081	83.102326	-64.693466	18.82	0.97	4900	4660916136166863744	2.9	341.86 ± 0.88	1.94 ± 0.32	-1.23 ± 0.13	0.00	0.00	0000000	M2FS
LMC	Hodge 4	H4-1-b082	83.116004	-64.703200	18.83	1.13	4902	4660916101807750016	3.7	312.72 ± 0.74	2.01 ± 0.19	-0.51 ± 0.08	0.69	0.69	0000000	M2FS
LMC	Hodge 4	H4-1-b083	83.102863	-64.707027	18.34	1.03	4757	4660916101807115008	5.5	304.45 ± 0.48	1.45 ± 0.15	-0.73 ± 0.06	0.00	0.00	0000000	M2FS
LMC	Hodge 4	H4-1-b084	83.113346	-64.714814	18.81	1.13	4895	4660915723861558528	3.5	313.84 ± 0.67	1.44 ± 0.24	-0.59 ± 0.08	0.81	0.86	0000000	M2FS
LMC	Hodge 4	H4-1-b085	83.100500	-64.718672	18.74	1.08	4875	4660915728161950720	4.1	303.70 ± 0.67	1.90 ± 0.19	-0.65 ± 0.08	0.01	0.00	0000000	M2FS
LMC	Hodge 4	H4-1-b086	83.118093	-64.721408	18.87	1.06	4913	4660912773224492928	3.3	313.20 ± 0.84	1.92 ± 0.24	-0.62 ± 0.08	0.94	0.94	0000000	M2FS
LMC	Hodge 4	H4-1-b087	83.109439	-64.725241	18.50	1.25	4804	4660915693808508672	3.6	312.92 ± 0.51	2.13 ± 0.19	-0.64 ± 0.08	0.99	0.99	0000000	M2FS
LMC	Hodge 4	H4-1-b088	83.117299	-64.733142	18.69	0.91	4862	4660912738871021824	3.7	312.11 ± 0.65	1.71 ± 0.23	-0.57 ± 0.08	1.00	1.00	0000000	M2FS
LMC	Hodge 4	H4-1-b090	83.078552	-64.689645	18.74	1.14	4876	4660916209204555648	3.8	241.73 ± 0.61	1.69 ± 0.19	-0.78 ± 0.09	0.00	0.00	0000000	M2FS
LMC	Hodge 4	H4-1-b091	83.076144	-64.702417	18.92	1.16	4927	4660915792570105856	3.3	266.15 ± 0.76	2.16 ± 0.22	-0.61 ± 0.11	0.00	0.00	0000000	M2FS
LMC	Hodge 4	H4-1-b092	83.091709	-64.702632	18.56	1.20	4824	4660916106118979328	3.2	314.22 ± 0.71	2.15 ± 0.21	-0.36 ± 0.09	0.65	0.63	0000000	M2FS
LMC	Hodge 4	H4-1-b093	83.085500	-64.705551	18.90	1.14	4922	4660915723850627328	3.3	330.19 ± 0.67	1.89 ± 0.23	-0.65 ± 0.11	0.00	0.00	0000000	M2FS
LMC	Hodge 4	H4-1-b094	83.089991	-64.716311	17.66	1.16	4542	4660915728168238208	8.0	302.01 ± 0.28	0.94 ± 0.09	-0.74 ± 0.04	0.00	0.00	0000000	M2FS
LMC	Hodge 4	H4-1-b095	83.098339	-64.729734	17.65	1.36	4539	4660915689490236288	7.2	313.10 ± 0.31	1.65 ± 0.08	-0.54 ± 0.04	1.00	1.00	0000000	M2FS
LMC	Hodge 4	H4-1-b096	83.086861	-64.729842	18.40	1.13	4775	4660915693802260224	5.1	307.18 ± 0.39	2.01 ± 0.13	-0.52 ± 0.06	0.84	-1.00	0000000	M2FS
LMC	Hodge 4	H4-1-b097	82.958599	-64.759433	18.80	1.10	4892	4660914250699496960	3.4	305.21 ± 0.70	1.45 ± 0.31	-0.75 ± 0.09	0.00	0.00	0000000	M2FS

Table C.1: (*continued*) Sample of 3095 Targets from 26 Star Clusters

Galaxy	Cluster	ID	RAJ2000 (deg)	DEJ2000 (deg)	G (mag)	$G_{\rm BP} - G_{\rm RP}$ (mag)	$T_{\rm eff}$ (K)	*Gaia* DR2 ID	S/N	$v_{\rm los}$ ($\rm km\,s^{-1}$)	$\log g$ (dex)	$[{\rm Fe/H}]_{\rm raw}$ (dex)	P_M	P'_M	Flag[a]	Source[b]
(1)	(2)	(3)	(4)	(5)	(6)	(7)	(8)	(9)	(10)	(11)	(12)	(13)	(14)	(15)	(16)	(17)
LMC	Hodge 4	H4-1-b098	83.027273	-64.753650	18.69	0.91	4861	4660914108942890752	3.9	299.71 ± 0.96	1.87 ± 0.24	-1.12 ± 0.10	0.00	0.00	0000000	M2FS
LMC	Hodge 4	H4-1-b099	82.999964	-64.753425	18.41	1.01	4776	4660914319414623232	5.3	277.28 ± 0.57	1.15 ± 0.18	-0.71 ± 0.06	0.00	0.00	0000000	M2FS
LMC	Hodge 4	H4-1-b100	82.996310	-64.748126	18.90	1.14	4922	4660914319412712960	3.4	300.68 ± 0.77	1.16 ± 0.33	-0.92 ± 0.09	0.00	0.00	0000000	M2FS
LMC	Hodge 4	H4-1-b101	83.012216	-64.747345	17.82	1.35	4595	4660914315100683904	6.3	312.82 ± 0.38	1.28 ± 0.11	-0.73 ± 0.05	0.43	0.21	0000000	M2FS
LMC	Hodge 4	H4-1-b102	83.002436	-64.741428	17.77	1.28	4577	4660914349481685632	6.2	281.10 ± 0.38	1.08 ± 0.12	-0.92 ± 0.06	0.00	0.00	0000000	M2FS
LMC	Hodge 4	H4-1-b103	83.010581	-64.740240	18.78	1.07	4887	4660914353772421632	3.4	294.90 ± 1.05	1.44 ± 0.29	-0.70 ± 0.09	0.00	0.00	0000000	M2FS
LMC	Hodge 4	H4-1-b104	83.019941	-64.739793	17.92	1.19	4624	4660914349460429056	8.6	271.57 ± 0.41	0.77 ± 0.14	-1.37 ± 0.05	0.00	0.00	0000000	M2FS
LMC	Hodge 4	H4-1-b105	83.052277	-64.779732	18.86	1.10	4910	4660914005863654272	3.5	290.53 ± 1.03	2.06 ± 0.23	-0.74 ± 0.11	0.00	0.00	0000000	M2FS
LMC	Hodge 4	H4-1-b106	83.028020	-64.773528	18.35	1.15	4758	4660914010181359104	3.9	277.68 ± 0.88	1.66 ± 0.32	-1.65 ± 0.11	0.00	0.00	0000000	M2FS
LMC	Hodge 4	H4-1-b107	83.043959	-64.764499	18.66	1.16	4853	4660914108953407488	3.5	259.02 ± 0.69	2.30 ± 0.17	-0.43 ± 0.09	0.00	0.00	0000000	M2FS
LMC	Hodge 4	H4-1-b108	83.046771	-64.761235	18.04	0.82	4664	4660914108942238464	3.7	340.69 ± 1.47	1.39 ± 0.43	-1.90 ± 0.13	0.00	0.00	0000010	M2FS
LMC	Hodge 4	H4-1-b109	83.052501	-64.757981	18.88	1.08	4915	4660914143302879872	3.4	291.52 ± 0.56	2.09 ± 0.21	-0.52 ± 0.08	0.00	0.00	0000000	M2FS
LMC	Hodge 4	H4-1-b110	83.036574	-64.755566	18.83	0.88	4902	4660914108942888448	3.8	305.11 ± 0.89	1.92 ± 0.26	-1.09 ± 0.11	0.00	0.00	0000000	M2FS
LMC	Hodge 4	H4-1-b111	83.050051	-64.754510	16.57	1.65	4154	4660914147620303104	11.6	324.49 ± 0.24	0.95 ± 0.05	-0.61 ± 0.04	0.00	0.00	0000000	M2FS
LMC	Hodge 4	H4-1-b112	83.052962	-64.743868	18.68	1.04	4860	4660915620771386112	3.9	340.70 ± 0.88	0.78 ± 0.35	-1.31 ± 0.10	0.00	0.00	0000000	M2FS
LMC	Hodge 4	H4-1-b113	83.051374	-64.698622	17.10	1.37	4351	4660915796887697536	12.7	307.56 ± 0.18	0.59 ± 0.06	-0.86 ± 0.03	0.00	0.00	0000000	M2FS
LMC	Hodge 4	H4-1-b114	83.059477	-64.701870	18.86	1.03	4911	4660915792570106752	4.2	315.08 ± 0.69	1.69 ± 0.20	-0.67 ± 0.09	0.29	0.09	0000000	M2FS
LMC	Hodge 4	H4-1-b115	83.044229	-64.710115	18.95	1.25	4935	4660915758209730688	3.6	232.99 ± 0.92	1.84 ± 0.23	-0.63 ± 0.09	0.00	0.00	0000000	M2FS
LMC	Hodge 4	H4-1-b116	83.075545	-64.717271	18.90	1.07	4922	4660915689501568000	3.4	301.20 ± 0.69	1.78 ± 0.27	-0.70 ± 0.09	0.00	0.00	0000000	M2FS
LMC	Hodge 4	H4-1-b117	83.065654	-64.722197	18.00	1.05	4650	4660915762527976960	7.9	330.51 ± 0.73	2.13 ± 0.11	-1.42 ± 0.06	0.00	0.00	0000000	M2FS
LMC	Hodge 4	H4-1-b118	83.075167	-64.724931	18.71	1.01	4868	4660915693808502784	4.0	314.85 ± 0.58	1.99 ± 0.21	-0.76 ± 0.08	0.92	0.90	0000000	M2FS
LMC	Hodge 4	H4-1-b119	83.070547	-64.730588	18.52	1.14	4812	4660915590723027840	4.5	312.76 ± 0.50	1.92 ± 0.16	-0.56 ± 0.07	0.94	0.95	0000000	M2FS
LMC	Hodge 4	H4-1-b120	83.064789	-64.733680	17.42	1.22	4462	4660915659448769792	10.2	290.43 ± 0.28	0.78 ± 0.08	-0.80 ± 0.04	0.00	0.00	0000000	M2FS
LMC	Hodge 4	H4-1-b121	83.035927	-64.633053	18.92	1.21	4928	4660922423999648000	3.4	285.51 ± 1.05	2.01 ± 0.24	-0.61 ± 0.10	0.00	0.00	0000000	M2FS
LMC	Hodge 4	H4-1-b124	83.019175	-64.702923	18.71	1.21	4868	4660915968679947520	4.2	292.87 ± 0.85	0.68 ± 0.38	-1.22 ± 0.11	0.00	0.00	0000000	M2FS
LMC	Hodge 4	H4-1-b125	83.026505	-64.705252	15.45	2.28	3777	4660915968686389888	7.5	308.16 ± 1.81	0.89 ± 0.36	-1.84 ± 0.23	-1.00	-1.00	0110010	M2FS
LMC	Hodge 4	H4-1-b126	83.018763	-64.712772	18.34	1.22	4756	4660915861299897728	5.2	304.32 ± 0.45	1.98 ± 0.14	-0.67 ± 0.06	0.00	0.00	0000000	M2FS
LMC	Hodge 4	H4-1-b127	83.040331	-64.715931	15.82	2.81	3853	4660915762527968512	13.1	301.24 ± 0.82	0.61 ± 0.11	-1.01 ± 0.07	-1.00	-1.00	0100010	M2FS
LMC	Hodge 4	H4-1-b128	83.009282	-64.733300	18.80	1.11	4893	4660914349461075200	3.3	310.72 ± 0.85	1.34 ± 0.30	-0.57 ± 0.09	0.30	0.07	0000000	M2FS
LMC	Hodge 4	H4-1-r028	83.076631	-64.738993	16.39	1.65	4088	4660915590729300608	17.0	370.71 ± 0.24	0.17 ± 0.09	-0.82 ± 0.04	0.00	0.00	0000000	M2FS
LMC	Hodge 4	H4-1-r049	83.087047	-64.737178	16.80	1.56	4239	4660915590729301376	13.4	314.73 ± 0.20	1.31 ± 0.05	-0.56 ± 0.04	0.99	0.99	0000000	M2FS
LMC	Hodge 4	H4-1-r079	83.107621	-64.729839	16.76	1.51	4226	4660915689490235520	14.5	309.50 ± 0.22	1.16 ± 0.05	-0.61 ± 0.03	1.00	1.00	0000000	M2FS
LMC	Hodge 4	H4-1-r099	83.132159	-64.734192	17.09	1.48	4347	4660912738871027328	12.0	314.67 ± 0.20	1.14 ± 0.05	-0.73 ± 0.04	0.99	0.99	0000000	M2FS
LMC	NGC 1466	N1466-1-b049	56.462567	-71.582803	15.55	2.09	4100	4642001654245668480	5.4	24.87 ± 0.36	3.91 ± 0.33	-1.83 ± 0.07	-1.00	-1.00	0001100	M2FS
LMC	NGC 1466	N1466-1-b050	56.409858	-71.597210	19.62	0.80	5157	4642001512511263232	2.4	-4.67 ± 2.41	2.75 ± 0.52	-1.58 ± 0.23	-1.00	-1.00	0100000	M2FS
LMC	NGC 1466	N1466-1-b051	56.458078	-71.719175	18.81	1.27	5004	4641998145256823808	3.2	51.78 ± 2.66	4.92 ± 0.09	-1.27 ± 0.11	-1.00	-1.00	1000000	M2FS
LMC	NGC 1466	N1466-1-b052	56.358812	-71.732845	19.05	0.91	5054	4641998286991426176	3.6	25.24 ± 1.36	4.13 ± 0.24	-1.16 ± 0.16	-1.00	-1.00	0001100	M2FS
LMC	NGC 1466	N1466-1-b057	56.313289	-71.585642	18.81	0.87	5003	4642004501808331520	4.1	85.95 ± 1.06	3.65 ± 0.18	-0.94 ± 0.13	-1.00	-1.00	0001100	M2FS
LMC	NGC 1466	N1466-1-b058	56.247226	-71.613363	18.23	1.06	4863	4642004055131729024	10.2	199.45 ± 0.40	0.97 ± 0.19	-1.83 ± 0.05	0.00	0.00	0000000	M2FS
LMC	NGC 1466	N1466-1-b059	56.196209	-71.654143	15.95	1.65	4172	4642002444519754240	30.1	202.07 ± 0.14	0.18 ± 0.06	-1.37 ± 0.03	1.00	1.00	0000000	M2FS
LMC	NGC 1466	N1466-1-b060	56.188727	-71.664374	17.01	1.36	4546	4642002341440543488	19.8	202.47 ± 0.15	0.65 ± 0.06	-1.54 ± 0.03	1.00	1.00	0000000	M2FS
LMC	NGC 1466	N1466-1-b061	56.250457	-71.668730	19.19	0.94	5080	4641999485288669056	5.4	199.33 ± 0.74	0.59 ± 0.37	-1.82 ± 0.09	1.00	1.00	0000000	M2FS
LMC	NGC 1466	N1466-1-b062	56.207270	-71.673815	18.16	1.13	4846	4641999382207578496	4.1	203.85 ± 0.77	1.12 ± 0.33	-1.83 ± 0.11	1.00	1.00	0000000	M2FS
LMC	NGC 1466	N1466-1-b063	56.187614	-71.678009	18.26	1.11	4871	4642002337144776320	10.4	202.19 ± 0.32	1.08 ± 0.15	-1.62 ± 0.04	1.00	1.00	0000000	M2FS
LMC	NGC 1466	N1466-1-b064	56.237014	-71.684094	17.42	1.20	4654	4641999386503049728	17.3	202.51 ± 0.22	0.38 ± 0.13	-1.84 ± 0.03	1.00	1.00	0000000	M2FS
LMC	NGC 1466	N1466-1-b081	56.179274	-71.662348	18.40	1.14	4905	4642002337144792960	3.2	120.20 ± 0.64	4.84 ± 0.11	-0.49 ± 0.11	-1.00	-1.00	1000000	M2FS
LMC	NGC 1466	N1466-1-b082	56.162505	-71.665320	18.11	1.14	4835	4642002341439224448	5.7	199.10 ± 0.51	0.81 ± 0.29	-1.67 ± 0.07	1.00	1.00	0000000	M2FS
LMC	NGC 1466	N1466-1-b083	56.176535	-71.670942	18.32	1.08	4886	4642002337146893568	9.2	204.21 ± 0.39	1.20 ± 0.18	-1.60 ± 0.05	1.00	1.00	0000000	M2FS
LMC	NGC 1466	N1466-1-b084	56.165514	-71.671351	16.53	1.32	4380	4642002341439238656	17.7	206.62 ± 0.20	0.62 ± 0.07	-1.73 ± 0.03	1.00	1.00	0000000	M2FS
LMC	NGC 1466	N1466-1-b085	56.181707	-71.674104	18.80	0.89	5001	4642002341440546432	6.7	198.50 ± 0.47	1.25 ± 0.25	-1.60 ± 0.06	1.00	1.00	0000000	M2FS
LMC	NGC 1466	N1466-1-b086	56.166245	-71.674689	17.07	1.26	4562	4642002341440545664	20.2	201.57 ± 0.19	0.52 ± 0.08	-1.77 ± 0.03	1.00	1.00	0000000	M2FS
LMC	NGC 1466	N1466-1-b087	56.167627	-71.686098	18.90	0.88	5023	4642002307079511552	5.5	202.10 ± 0.80	1.37 ± 0.32	-1.56 ± 0.09	1.00	1.00	0000000	M2FS
LMC	NGC 1466	N1466-1-b088	56.160856	-71.701797	16.28	1.55	4291	4641998974186188928	28.8	204.26 ± 0.13	0.14 ± 0.07	-1.44 ± 0.02	1.00	1.00	0000000	M2FS
LMC	NGC 1466	N1466-1-b089	56.143476	-71.665089	17.15	1.12	4584	4642002405864755584	16.0	201.00 ± 0.19	0.77 ± 0.08	-1.59 ± 0.03	1.00	1.00	0000000	M2FS

Table C.1: (*continued*) Sample of 3095 Targets from 26 Star Clusters

Galaxy	Cluster	ID	RAJ2000 (deg)	DEJ2000 (deg)	G (mag)	$G_{\rm BP} - G_{\rm RP}$ (mag)	$T_{\rm eff}$ (K)	*Gaia* DR2 ID	S/N	$v_{\rm los}$ ($\rm km\,s^{-1}$)	$\log g$ (dex)	$[{\rm Fe/H}]_{\rm raw}$ (dex)	P_M	P'_M	Flag[a]	Source[b]
(1)	(2)	(3)	(4)	(5)	(6)	(7)	(8)	(9)	(10)	(11)	(12)	(13)	(14)	(15)	(16)	(17)
LMC	NGC 1466	N1466-1-b090	56.128189	-71.666160	17.97	0.95	4800	4642002375800229760	5.5	199.79 ± 0.65	1.58 ± 0.20	-1.41 ± 0.08	1.00	1.00	0000000	M2FS
LMC	NGC 1466	N1466-1-b091	56.134423	-71.668796	18.90	0.00	5022	4642002375800268160	17.4	-5.71 ± 0.88	2.61 ± 0.13	-2.09 ± 0.07	-1.00	-1.00	0100000	M2FS
LMC	NGC 1466	N1466-1-b092	56.155371	-71.669172	18.67	0.89	4972	4642002341440540928	4.1	202.75 ± 0.76	1.23 ± 0.36	-1.52 ± 0.10	1.00	1.00	0000000	M2FS
LMC	NGC 1466	N1466-1-b093	56.137129	-71.678290	18.75	0.00	4991	4642002375798976000	2.8	199.86 ± 1.47	2.92 ± 0.36	-1.83 ± 0.18	1.00	1.00	0000000	M2FS
LMC	NGC 1466	N1466-1-b094	56.122927	-71.682986	18.90	0.94	5022	4642001993549469568	5.2	197.48 ± 0.56	1.46 ± 0.24	-1.36 ± 0.08	1.00	-1.00	0000000	M2FS
LMC	NGC 1466	N1466-1-b095	56.147395	-71.683379	17.21	1.31	4600	4642002307080808192	17.0	205.77 ± 0.19	0.89 ± 0.07	-1.48 ± 0.03	1.00	1.00	0000000	M2FS
LMC	NGC 1466	N1466-1-b096	56.139178	-71.685894	19.56	0.88	5147	4642001924830004608	1.3	190.63 ± 87.70	4.01 ± 0.91	-2.50 ± 0.58	-1.00	-1.00	1000000	M2FS
LMC	NGC 1466	N1466-1-b097	55.970577	-71.783319	19.22	1.14	5086	4641977739867961088	3.7	244.55 ± 1.78	2.10 ± 0.49	-1.84 ± 0.21	-1.00	-1.00	0100000	M2FS
LMC	NGC 1466	N1466-1-b098	55.809345	-71.780528	17.18	1.57	4591	4641977946026387584	-0.3	119.86 ± 11.59	4.44 ± 0.44	0.49 ± 0.65	-1.00	-1.00	1000000	M2FS
LMC	NGC 1466	N1466-1-b099	56.457080	-71.760451	19.80	0.90	5185	4641997939098236416	2.4	183.74 ± 2.11	4.06 ± 0.44	-0.91 ± 0.31	-1.00	-1.00	0001100	M2FS
LMC	NGC 1466	N1466-1-b100	55.917293	-71.753226	17.15	1.44	4584	4641978392702986240	7.1	22.14 ± 0.38	4.82 ± 0.11	-0.60 ± 0.08	-1.00	-1.00	0001100	M2FS
LMC	NGC 1466	N1466-1-b117	56.099329	-71.669900	16.56	1.47	4388	4642002375800228608	25.1	203.20 ± 0.15	0.31 ± 0.07	-1.47 ± 0.03	1.00	1.00	0000000	M2FS
LMC	NGC 1466	N1466-1-b118	56.117720	-71.672073	17.73	0.99	4740	4642002375798946304	11.4	205.20 ± 0.34	0.67 ± 0.17	-1.55 ± 0.04	1.00	1.00	0000000	M2FS
LMC	NGC 1466	N1466-1-b119	56.086014	-71.677452	17.38	1.25	4644	4642001997843107840	3.5	201.20 ± 0.94	1.45 ± 0.36	-1.96 ± 0.12	-1.00	-1.00	0000001	M2FS
LMC	NGC 1466	N1466-1-b120	56.108702	-71.680758	19.02	1.04	5049	4642001993547411072	1.4	201.82 ± 6.76	2.79 ± 1.06	-2.04 ± 0.40	-1.00	-1.00	1000000	M2FS
LMC	NGC 1466	N1466-1-b122	55.909753	-71.571048	17.70	1.26	4733	4642050818734850304	0.1	6.54 ± 2.28	4.64 ± 0.31	0.90 ± 0.23	-1.00	-1.00	0001100	M2FS
LMC	NGC 1466	N1466-1-b123	55.970137	-71.618897	19.40	1.02	5119	4642003475311851648	1.1	149.93 ± 2.55	4.55 ± 0.30	-0.71 ± 0.26	-1.00	-1.00	0001100	M2FS
LMC	NGC 1466	N1466-1-b124	55.980848	-71.619306	19.84	0.93	5192	4642003471018155392	0.9	252.98 ± 2.37	2.90 ± 1.59	0.00 ± 0.39	-1.00	-1.00	0000100	M2FS
LMC	NGC 1466	N1466-1-b126	56.073159	-71.686588	18.98	1.11	5039	4642001963483417344	0.9	198.13 ± 13.00	1.88 ± 0.75	-0.73 ± 0.45	-1.00	-1.00	1000000	M2FS
LMC	NGC 1466	N1466-1-b127	55.956464	-71.694893	18.26	1.09	4872	4642002096626589824	3.4	203.27 ± 1.26	1.61 ± 0.35	-1.51 ± 0.13	0.00	0.00	0000000	M2FS
LMC	NGC 1466	N1466-1-b128	56.036376	-71.749338	18.36	1.22	4896	4641978255264134528	3.0	242.56 ± 1.13	4.82 ± 0.12	-0.07 ± 0.14	-1.00	-1.00	0001100	M2FS
LMC	NGC 1466	N1466-1-r028	56.134399	-71.681580	18.09	1.04	4830	4642002302785053824	14.7	207.27 ± 0.23	1.39 ± 0.09	-1.56 ± 0.03	1.00	1.00	0000000	M2FS
LMC	NGC 1466	N1466-1-r049	56.153237	-71.676346	18.20	0.94	4857	4642002307079504384	8.1	200.93 ± 0.50	1.51 ± 0.17	-1.62 ± 0.06	1.00	1.00	0000000	M2FS
LMC	NGC 1466	N1466-1-r079	56.125484	-71.675119	17.96	0.75	4798	4642002375798962176	12.4	202.91 ± 0.34	1.30 ± 0.15	-1.80 ± 0.05	1.00	1.00	0000010	M2FS
LMC	NGC 1466	N1466-1-r099	56.142196	-71.673507	18.68	0.00	4975	4642002375800242560	10.0	204.74 ± 0.59	2.16 ± 0.14	-1.64 ± 0.06	1.00	1.00	0000000	M2FS
LMC	NGC 1751	N1751-1-b001	73.613398	-69.842060	17.35	1.47	4346	4655138511826202112	10.5	236.97 ± 0.80	0.12 ± 0.11	-1.03 ± 0.11	-1.00	-1.00	0110000	M2FS
LMC	NGC 1751	N1751-1-b002	73.601740	-69.840719	18.62	1.15	4780	4655138516136851072	6.9	220.82 ± 0.48	1.41 ± 0.13	-0.85 ± 0.05	0.00	0.00	0000000	M2FS
LMC	NGC 1751	N1751-1-b003	73.612475	-69.838382	17.88	1.22	4525	4655138516109302272	11.4	237.84 ± 0.26	1.02 ± 0.07	-0.78 ± 0.04	0.01	0.00	0000000	M2FS
LMC	NGC 1751	N1751-1-b004	73.642872	-69.830935	16.67	1.54	4129	4655138550496593152	19.1	262.75 ± 0.18	0.45 ± 0.05	-0.90 ± 0.03	0.00	0.00	0000000	M2FS
LMC	NGC 1751	N1751-1-b005	73.605489	-69.830938	18.74	0.99	4817	4655326188987052544	6.5	231.81 ± 0.54	2.38 ± 0.11	-0.81 ± 0.07	0.00	0.00	0000000	M2FS
LMC	NGC 1751	N1751-1-b006	73.604573	-69.827226	16.20	1.48	4129	4655326223365983616	30.0	242.90 ± 0.18	0.05 ± 0.04	-0.78 ± 0.03	0.32	0.06	0000000	M2FS
LMC	NGC 1751	N1751-1-b007	73.619563	-69.824306	18.45	1.11	4720	4655138546159278976	8.0	239.96 ± 0.34	1.61 ± 0.11	-0.83 ± 0.05	0.74	0.24	0000000	M2FS
LMC	NGC 1751	N1751-1-b008	73.632667	-69.812903	16.21	1.91	4129	4655138649350208000	18.6	247.77 ± 0.25	1.35 ± 0.06	-0.41 ± 0.04	0.00	0.00	0000000	M2FS
LMC	NGC 1751	N1751-1-b010	73.643106	-69.825404	18.45	1.12	4720	4655138546159281408	6.6	273.03 ± 0.37	1.48 ± 0.12	-0.93 ± 0.06	0.00	0.00	0000000	M2FS
LMC	NGC 1751	N1751-1-b011	73.655693	-69.824440	16.94	1.62	4190	4655138653575808512	14.3	263.12 ± 0.18	0.88 ± 0.04	-0.62 ± 0.03	0.00	0.00	0000000	M2FS
LMC	NGC 1751	N1751-1-b012	73.647923	-69.819009	18.38	1.08	4697	4655138649238503296	7.7	311.18 ± 0.53	0.44 ± 0.23	-1.88 ± 0.06	0.00	0.00	0000000	M2FS
LMC	NGC 1751	N1751-1-b013	73.660570	-69.812778	18.69	1.19	4801	4655138687935543936	6.0	231.19 ± 0.45	1.74 ± 0.13	-0.66 ± 0.06	0.00	0.00	0000000	M2FS
LMC	NGC 1751	N1751-1-b014	73.647412	-69.810278	18.73	1.15	4816	4655138683598257408	4.9	215.28 ± 0.77	1.91 ± 0.28	-1.98 ± 0.09	0.00	0.00	0000000	M2FS
LMC	NGC 1751	N1751-1-b015	73.657563	-69.804888	17.59	1.46	4430	4655138683598508928	11.3	281.39 ± 0.21	1.13 ± 0.06	-0.60 ± 0.03	0.00	0.00	0000000	M2FS
LMC	NGC 1751	N1751-1-b016	73.670967	-69.804536	18.62	1.29	4778	4655138683598268672	5.6	245.49 ± 0.40	2.00 ± 0.13	-0.50 ± 0.05	0.00	0.00	0000000	M2FS
LMC	NGC 1751	N1751-1-b017	73.618231	-69.771297	18.92	0.84	4875	4655349858595644928	6.5	259.79 ± 2.49	2.54 ± 0.43	-2.61 ± 0.13	-1.00	-1.00	0100010	M2FS
LMC	NGC 1751	N1751-1-b018	73.649613	-69.786854	16.90	1.70	4174	4655162155640719872	14.4	290.13 ± 0.20	1.19 ± 0.05	-0.46 ± 0.04	0.00	0.00	0000000	M2FS
LMC	NGC 1751	N1751-1-b019	73.642927	-69.795114	17.02	1.50	4225	4655162151299583232	18.9	190.28 ± 0.17	0.17 ± 0.08	-1.69 ± 0.03	0.00	0.00	0000000	M2FS
LMC	NGC 1751	N1751-1-b020	73.664549	-69.796081	18.87	1.23	4860	4655162155619192832	6.0	258.66 ± 0.42	1.56 ± 0.17	-0.81 ± 0.06	0.00	0.00	0000000	M2FS
LMC	NGC 1751	N1751-1-b021	73.606360	-69.796641	18.53	2.70	4749	4655326356534551936	1.7	10.04 ± 3.03	4.86 ± 0.11	-0.89 ± 0.17	-1.00	-1.00	1000000	M2FS
LMC	NGC 1751	N1751-1-b022	73.628279	-69.800427	17.48	1.37	4391	4655326356509758336	12.7	184.30 ± 0.23	0.63 ± 0.07	-1.46 ± 0.04	0.00	0.00	0000000	M2FS
LMC	NGC 1751	N1751-1-b023	73.620530	-69.808090	18.45	1.02	4721	4655326322129403136	7.4	253.99 ± 0.41	1.61 ± 0.11	-0.85 ± 0.06	0.00	0.00	0000000	M2FS
LMC	NGC 1751	N1751-1-b024	73.602472	-69.809193	18.46	1.15	4724	4655326322149956736	6.9	261.19 ± 0.35	1.39 ± 0.13	-0.64 ± 0.05	0.00	0.00	0000000	M2FS
LMC	NGC 1751	N1751-1-b025	73.589581	-69.767991	17.20	1.12	4293	4655349892910066688	19.1	269.78 ± 0.28	0.30 ± 0.09	-1.49 ± 0.03	0.00	0.00	0000010	M2FS
LMC	NGC 1751	N1751-1-b026	73.596374	-69.771693	17.96	0.94	4551	4655349897228205568	12.4	275.20 ± 0.40	1.12 ± 0.09	-1.48 ± 0.04	0.00	0.00	0000010	M2FS
LMC	NGC 1751	N1751-1-b027	73.592630	-69.777381	18.98	1.10	4893	4655349897228207360	5.1	241.24 ± 0.46	2.01 ± 0.13	-0.69 ± 0.07	0.65	0.65	0000000	M2FS
LMC	NGC 1751	N1751-1-b028	73.580511	-69.783750	18.03	1.41	4578	4655326425229107712	8.4	298.00 ± 0.30	0.63 ± 0.16	-1.57 ± 0.05	0.00	0.00	0000000	M2FS
LMC	NGC 1751	N1751-1-b029	73.592075	-69.786071	18.17	1.26	4623	4655326356489245952	8.2	295.33 ± 0.30	0.74 ± 0.13	-1.23 ± 0.05	0.00	0.00	0000000	M2FS
LMC	NGC 1751	N1751-1-b030	73.584239	-69.799200	18.97	1.13	4891	4655326322174854272	3.6	241.02 ± 0.59	1.74 ± 0.24	-0.57 ± 0.08	0.96	0.98	0000000	M2FS

Table C.1: (*continued*) Sample of 3095 Targets from 26 Star Clusters

Galaxy	Cluster	ID	RAJ2000 (deg)	DEJ2000 (deg)	G (mag)	$G_{\rm BP} - G_{\rm RP}$ (mag)	$T_{\rm eff}$ (K)	*Gaia* DR2 ID	S/N	$v_{\rm los}$ ($\rm km\,s^{-1}$)	$\log g$ (dex)	$[{\rm Fe/H}]_{\rm raw}$ (dex)	P_M	P'_M	Flag[a]	Source[b]
(1)	(2)	(3)	(4)	(5)	(6)	(7)	(8)	(9)	(10)	(11)	(12)	(13)	(14)	(15)	(16)	(17)
LMC	NGC 1751	N1751-1-b031	73.599321	-69.800233	17.59	1.09	4430	4655326326425955968	14.1	236.92 ± 0.46	0.99 ± 0.08	-1.40 ± 0.04	0.56	0.00	0000010	M2FS
LMC	NGC 1751	N1751-1-b032	73.586377	-69.806635	18.26	1.10	4653	4655326322174909056	7.0	256.53 ± 0.34	1.46 ± 0.11	-0.65 ± 0.05	0.00	0.00	0000000	M2FS
LMC	NGC 1751	N1751-1-b034	73.571316	-69.847466	18.02	1.42	4573	4655325776689385600	7.2	222.57 ± 0.29	1.38 ± 0.09	-0.66 ± 0.04	0.00	0.00	0000000	M2FS
LMC	NGC 1751	N1751-1-b035	73.571291	-69.842295	18.34	1.17	4683	4655325806763864832	4.8	224.60 ± 0.64	0.75 ± 0.32	-1.70 ± 0.08	0.00	0.00	0000000	M2FS
LMC	NGC 1751	N1751-1-b036	73.562887	-69.838424	17.95	1.34	4547	4655325806733235456	9.7	257.44 ± 0.30	1.58 ± 0.07	-0.60 ± 0.04	0.00	0.00	0000000	M2FS
LMC	NGC 1751	N1751-1-b037	73.554625	-69.833978	18.71	1.28	4807	4655325806763865600	5.7	240.83 ± 0.35	2.08 ± 0.14	-0.57 ± 0.05	0.73	0.63	0000000	M2FS
LMC	NGC 1751	N1751-1-b038	73.549858	-69.828495	17.63	1.41	4444	4655325879749357696	11.8	242.33 ± 0.23	1.13 ± 0.07	-0.72 ± 0.04	0.82	0.80	0000000	M2FS
LMC	NGC 1751	N1751-1-b039	73.556648	-69.822989	18.34	1.02	4681	4655326253455340544	9.4	269.31 ± 0.44	1.30 ± 0.10	-1.11 ± 0.05	0.00	0.00	0000010	M2FS
LMC	NGC 1751	N1751-1-b040	73.545988	-69.817673	18.54	1.09	4749	4655326253455338368	3.9	239.17 ± 0.57	1.91 ± 0.16	-0.66 ± 0.08	0.97	0.89	0000000	M2FS
LMC	NGC 1751	N1751-1-b044	73.574848	-69.834122	18.31	1.14	4672	4655325806778743680	9.2	240.02 ± 0.27	1.61 ± 0.08	-0.71 ± 0.04	0.74	0.25	0000000	M2FS
LMC	NGC 1751	N1751-1-b045	73.589952	-69.826064	18.65	1.06	4788	4655326184735866624	4.5	266.23 ± 0.48	2.05 ± 0.14	-0.60 ± 0.07	0.00	0.00	0000000	M2FS
LMC	NGC 1751	N1751-1-b046	73.571591	-69.819402	17.97	1.13	4555	4655326184692282496	10.0	241.75 ± 0.34	0.96 ± 0.09	-1.08 ± 0.04	-1.00	-1.00	0000001	M2FS
LMC	NGC 1751	N1751-1-b047	73.579668	-69.816089	18.90	1.27	4869	4655326219070677632	4.2	211.29 ± 0.46	1.99 ± 0.20	-0.50 ± 0.07	0.00	0.00	0000000	M2FS
LMC	NGC 1751	N1751-1-b048	73.592930	-69.812527	18.72	0.94	4812	4655326223365966720	6.9	240.52 ± 0.37	2.01 ± 0.11	-0.68 ± 0.05	0.96	0.97	0000010	M2FS
LMC	NGC 1751	N1751-1-b050	73.574832	-69.777296	18.29	1.37	4666	4655326425208731904	7.7	226.73 ± 0.34	1.48 ± 0.09	-0.52 ± 0.04	0.00	0.00	0000000	M2FS
LMC	NGC 1751	N1751-1-b051	73.563771	-69.794061	17.49	1.52	4396	4655326395164617600	8.5	240.17 ± 0.22	1.33 ± 0.07	-0.53 ± 0.04	0.96	0.96	0000000	M2FS
LMC	NGC 1751	N1751-1-b053	73.560195	-69.801350	18.60	1.11	4770	4655326287790098176	5.3	236.08 ± 0.53	2.06 ± 0.12	-0.61 ± 0.06	1.00	0.00	0000000	M2FS
LMC	NGC 1751	N1751-1-b054	73.577634	-69.804319	17.53	1.37	4408	4655326326445161472	12.6	239.39 ± 0.31	1.49 ± 0.06	-0.69 ± 0.04	0.97	0.91	0000000	M2FS
LMC	NGC 1751	N1751-1-b055	73.562361	-69.806483	18.44	0.92	4717	4655326287815079808	4.3	242.03 ± 0.51	2.15 ± 0.16	-0.37 ± 0.07	1.00	1.00	0000010	M2FS
LMC	NGC 1751	N1751-1-b056	73.574844	-69.809870	17.53	1.29	4410	4655326219053169920	10.0	207.00 ± 0.37	0.87 ± 0.09	-1.02 ± 0.04	0.00	0.00	0000000	M2FS
LMC	NGC 1751	N1751-1-b057	73.538804	-69.765073	18.93	1.17	4879	4655350099068525440	4.9	235.17 ± 0.48	2.36 ± 0.13	-0.58 ± 0.07	0.00	0.00	0000000	M2FS
LMC	NGC 1751	N1751-1-b058	73.538372	-69.773495	17.09	1.40	4251	4655326631367183104	14.6	215.33 ± 0.24	1.02 ± 0.05	-0.69 ± 0.03	0.00	0.00	0000000	M2FS
LMC	NGC 1751	N1751-1-b059	73.536098	-69.783613	18.04	1.20	4580	4655326601322961152	11.3	259.08 ± 0.36	0.82 ± 0.09	-1.09 ± 0.03	0.00	0.00	0000000	M2FS
LMC	NGC 1751	N1751-1-b060	73.552374	-69.785133	18.85	1.24	4855	4655326395164540928	4.9	220.49 ± 0.48	1.67 ± 0.17	-0.48 ± 0.06	0.00	0.00	0000000	M2FS
LMC	NGC 1751	N1751-1-b061	73.534547	-69.787623	18.49	1.24	4733	4655326601322963968	4.6	272.84 ± 0.46	1.68 ± 0.13	-0.57 ± 0.06	0.00	0.00	0000000	M2FS
LMC	NGC 1751	N1751-1-b062	73.547590	-69.801498	17.73	1.14	4476	4655326287815142144	10.2	242.69 ± 0.28	1.06 ± 0.07	-0.96 ± 0.04	1.00	1.00	0000010	M2FS
LMC	NGC 1751	N1751-1-b063	73.533467	-69.807578	17.43	1.48	4376	4655326292085364480	10.6	242.37 ± 0.24	1.24 ± 0.06	-0.53 ± 0.04	1.00	0.96	0000000	M2FS
LMC	NGC 1751	N1751-1-b064	73.557560	-69.812607	18.00	0.90	4567	4655326287815245440	10.9	241.19 ± 0.43	1.86 ± 0.08	-1.47 ± 0.05	1.00	1.00	0000010	M2FS
LMC	NGC 1751	N1751-1-b066	73.527621	-69.846754	16.48	1.16	4129	4655325845389750528	25.1	262.66 ± 0.29	0.02 ± 0.02	-1.35 ± 0.03	0.00	0.00	0000010	M2FS
LMC	NGC 1751	N1751-1-b067	73.512133	-69.841894	18.64	1.09	4784	4655325845389747968	7.2	289.90 ± 0.35	1.83 ± 0.10	-0.72 ± 0.05	0.00	0.00	0000000	M2FS
LMC	NGC 1751	N1751-1-b068	73.524443	-69.841589	18.97	1.11	4891	4655325845408835328	5.6	252.81 ± 0.49	1.49 ± 0.17	-0.78 ± 0.06	0.00	0.00	0000000	M2FS
LMC	NGC 1751	N1751-1-b069	73.519839	-69.837699	17.05	1.18	4236	4655325841123612800	19.3	236.36 ± 0.26	0.02 ± 0.02	-1.23 ± 0.03	0.00	0.00	0000010	M2FS
LMC	NGC 1751	N1751-1-b070	73.515346	-69.834089	16.12	1.77	4129	4655325845389588096	13.2	226.92 ± 0.23	1.35 ± 0.05	-0.43 ± 0.04	0.00	0.00	0000000	M2FS
LMC	NGC 1751	N1751-1-b071	73.512755	-69.827489	18.28	1.11	4660	4655325875454635392	8.7	269.53 ± 0.39	1.08 ± 0.11	-0.96 ± 0.04	0.00	0.00	0000000	M2FS
LMC	NGC 1751	N1751-1-b072	73.519747	-69.811825	18.58	1.27	4765	4655326253454158464	5.6	241.95 ± 0.34	2.22 ± 0.10	-0.41 ± 0.05	0.95	0.97	0000000	M2FS
LMC	NGC 1751	N1751-1-b074	73.536810	-69.839677	18.89	1.11	4866	4655325845389626880	7.2	238.62 ± 0.45	1.86 ± 0.11	-0.73 ± 0.05	0.42	0.00	0000000	M2FS
LMC	NGC 1751	N1751-1-b075	73.543085	-69.836582	17.79	1.44	4495	4655325879768578432	9.6	255.39 ± 0.25	1.22 ± 0.07	-0.59 ± 0.04	0.00	0.00	0000000	M2FS
LMC	NGC 1751	N1751-1-b076	73.536084	-69.830634	17.93	1.18	4541	4655325879768569216	9.9	233.76 ± 0.33	0.77 ± 0.09	-0.97 ± 0.04	0.00	0.00	0000000	M2FS
LMC	NGC 1751	N1751-1-b077	73.534296	-69.826660	18.86	1.26	4858	4655325875497038848	2.1	236.67 ± 1.21	2.88 ± 0.26	-0.29 ± 0.15	0.57	0.03	0000000	M2FS
LMC	NGC 1751	N1751-1-b078	73.544924	-69.824945	17.53	1.16	4408	4655326253422817536	14.4	241.68 ± 0.27	0.31 ± 0.10	-1.19 ± 0.03	0.87	0.91	0000010	M2FS
LMC	NGC 1751	N1751-1-b079	73.532317	-69.819651	18.09	1.40	4595	4655326253454142976	7.5	241.37 ± 0.35	1.67 ± 0.09	-0.60 ± 0.05	0.96	0.98	0000000	M2FS
LMC	NGC 1751	N1751-1-b080	73.542659	-69.812284	17.79	1.14	4497	4655326257725609344	10.7	234.88 ± 0.31	1.12 ± 0.07	-0.72 ± 0.04	1.00	-1.00	0000000	M2FS
LMC	NGC 1751	N1751-1-b082	73.531433	-69.769342	18.64	1.26	4784	4655326635663425536	6.2	265.17 ± 0.43	2.00 ± 0.12	-0.53 ± 0.06	0.00	0.00	0000000	M2FS
LMC	NGC 1751	N1751-1-b083	73.522798	-69.776478	17.81	1.40	4502	4655326631367186304	10.7	256.35 ± 0.27	0.85 ± 0.07	-0.75 ± 0.04	0.00	0.00	0000000	M2FS
LMC	NGC 1751	N1751-1-b084	73.525934	-69.781096	18.64	1.24	4786	4655326597007417344	5.6	236.11 ± 0.51	2.02 ± 0.13	-0.52 ± 0.06	0.01	0.00	0000000	M2FS
LMC	NGC 1751	N1751-1-b085	73.528302	-69.793292	18.24	1.33	4648	4655326493972328704	8.0	258.85 ± 0.30	1.80 ± 0.08	-0.49 ± 0.04	0.00	0.00	0000000	M2FS
LMC	NGC 1751	N1751-1-b086	73.520284	-69.798431	18.22	1.36	4640	4655326498243751552	7.3	262.15 ± 0.38	1.90 ± 0.09	-0.58 ± 0.05	0.00	0.00	0000000	M2FS
LMC	NGC 1751	N1751-1-b087	73.533092	-69.803596	17.83	1.31	4508	4655326287772625408	8.1	240.37 ± 0.32	1.24 ± 0.09	-0.56 ± 0.04	0.97	0.97	0000000	M2FS
LMC	NGC 1751	N1751-1-b088	73.519987	-69.807024	18.42	1.27	4710	4655326459612588928	6.0	241.02 ± 0.37	1.92 ± 0.11	-0.57 ± 0.05	0.96	0.98	0000000	M2FS
LMC	NGC 1751	N1751-1-b089	73.512869	-69.768136	18.97	1.12	4892	4655326635682674432	4.2	246.87 ± 0.69	2.38 ± 0.15	-0.61 ± 0.08	0.00	0.00	0000000	M2FS
LMC	NGC 1751	N1751-1-b090	73.510861	-69.771911	17.48	1.17	4391	4655326635682677632	15.9	228.69 ± 0.30	0.48 ± 0.10	-1.37 ± 0.03	0.00	0.00	0000010	M2FS
LMC	NGC 1751	N1751-1-b091	73.506952	-69.776212	19.00	0.96	4899	4655326597052310784	4.8	228.25 ± 0.56	0.75 ± 0.24	-0.89 ± 0.07	0.00	0.00	0000000	M2FS
LMC	NGC 1751	N1751-1-b092	73.514250	-69.784793	18.44	1.08	4716	4655326597007403520	5.7	184.93 ± 0.63	1.05 ± 0.20	-1.32 ± 0.07	0.00	0.00	0000000	M2FS
LMC	NGC 1751	N1751-1-b093	73.505698	-69.786953	18.69	1.27	4802	4655326493928183680	6.1	266.64 ± 0.48	2.26 ± 0.12	-0.44 ± 0.06	0.00	0.00	0000000	M2FS

Table C.1: (*continued*) Sample of 3095 Targets from 26 Star Clusters

Galaxy	Cluster	ID	RAJ2000 (deg)	DEJ2000 (deg)	G (mag)	$G_{\rm BP} - G_{\rm RP}$ (mag)	$T_{\rm eff}$ (K)	*Gaia* DR2 ID	S/N	$v_{\rm los}$ ($\rm km\,s^{-1}$)	$\log g$ (dex)	$[{\rm Fe/H}]_{\rm raw}$ (dex)	P_M	P'_M	Flag[a]	Source[b]
(1)	(2)	(3)	(4)	(5)	(6)	(7)	(8)	(9)	(10)	(11)	(12)	(13)	(14)	(15)	(16)	(17)
LMC	NGC 1751	N1751-1-b094	73.510392	-69.790566	17.59	1.39	4429	4655326493928170240	11.1	281.90 ± 0.28	1.42 ± 0.06	-0.64 ± 0.04	0.00	0.00	0000000	M2FS
LMC	NGC 1751	N1751-1-b095	73.516263	-69.794187	17.74	1.12	4480	4655326493972311168	11.8	250.55 ± 0.35	0.79 ± 0.08	-1.20 ± 0.04	0.00	0.00	0000010	M2FS
LMC	NGC 1751	N1751-1-b096	73.509788	-69.801490	18.41	1.37	4705	4655326463884010624	6.8	241.84 ± 0.35	1.99 ± 0.10	-0.52 ± 0.05	0.86	0.89	0000000	M2FS
LMC	NGC 1751	N1751-1-b097	73.465335	-69.832742	18.55	1.12	4756	4655325944172233984	7.2	240.63 ± 0.47	0.97 ± 0.15	-0.84 ± 0.05	0.40	0.15	0000000	M2FS
LMC	NGC 1751	N1751-1-b098	73.456548	-69.829948	17.84	1.31	4512	4655325948488124800	10.4	183.28 ± 0.27	0.92 ± 0.08	-0.80 ± 0.04	0.00	0.00	0000000	M2FS
LMC	NGC 1751	N1751-1-b099	73.445878	-69.826022	18.86	0.92	4856	4655326116015201536	7.0	238.03 ± 0.57	1.77 ± 0.14	-1.05 ± 0.06	0.00	0.00	0000010	M2FS
LMC	NGC 1751	N1751-1-b100	73.442803	-69.818611	17.37	1.51	4355	4655326120286609920	14.6	225.63 ± 0.30	0.06 ± 0.05	-0.88 ± 0.04	0.00	0.00	0000000	M2FS
LMC	NGC 1751	N1751-1-b101	73.472331	-69.817128	18.72	1.16	4810	4655326081631381888	6.2	230.81 ± 0.38	1.90 ± 0.13	-0.56 ± 0.05	0.00	0.00	0000000	M2FS
LMC	NGC 1751	N1751-1-b102	73.452683	-69.813272	18.28	1.16	4662	4655326154646348544	7.6	238.55 ± 0.42	1.41 ± 0.11	-0.95 ± 0.05	0.11	0.00	0000000	M2FS
LMC	NGC 1751	N1751-1-b103	73.461106	-69.810971	18.19	1.09	4632	4655326154646350464	9.9	224.78 ± 0.38	0.70 ± 0.13	-1.26 ± 0.04	0.00	0.00	0000000	M2FS
LMC	NGC 1751	N1751-1-b104	73.474580	-69.809732	17.88	1.46	4525	4655326081611261312	11.7	250.85 ± 0.24	1.25 ± 0.07	-0.57 ± 0.03	0.00	0.00	0000000	M2FS
LMC	NGC 1751	N1751-1-b106	73.496456	-69.839930	18.91	1.11	4871	4655326047251408000	5.6	288.86 ± 0.50	2.03 ± 0.14	-0.62 ± 0.07	0.00	0.00	0000000	M2FS
LMC	NGC 1751	N1751-1-b107	73.498017	-69.831783	18.48	0.96	4730	4655326047251439744	8.1	255.75 ± 0.48	1.47 ± 0.11	-0.94 ± 0.05	0.00	0.00	0000010	M2FS
LMC	NGC 1751	N1751-1-b109	73.508673	-69.822703	18.14	1.36	4613	4655326081611205248	8.3	248.62 ± 0.40	2.08 ± 0.09	-0.38 ± 0.04	0.00	0.00	0000000	M2FS
LMC	NGC 1751	N1751-1-b110	73.487418	-69.817958	18.73	1.07	4816	4655326081611225216	6.2	246.27 ± 0.50	1.49 ± 0.14	-0.83 ± 0.06	0.00	0.00	0000000	M2FS
LMC	NGC 1751	N1751-1-b111	73.499528	-69.817876	18.30	1.20	4667	4655326081614213376	7.4	237.94 ± 0.38	0.93 ± 0.12	-0.97 ± 0.05	0.74	0.00	0000000	M2FS
LMC	NGC 1751	N1751-1-b112	73.502875	-69.811824	17.92	1.43	4540	4655326459588610048	11.9	296.27 ± 0.23	1.35 ± 0.06	-0.63 ± 0.04	0.00	0.00	0000000	M2FS
LMC	NGC 1751	N1751-1-b114	73.489143	-69.773595	18.88	1.21	4863	4655326665726929792	5.9	267.79 ± 0.58	1.97 ± 0.14	-0.79 ± 0.07	0.00	0.00	0000000	M2FS
LMC	NGC 1751	N1751-1-b115	73.492843	-69.779016	18.85	1.23	4853	4655326665729092736	5.7	261.90 ± 0.40	1.78 ± 0.15	-0.55 ± 0.06	0.00	0.00	0000000	M2FS
LMC	NGC 1751	N1751-1-b116	73.488947	-69.786350	18.42	1.18	4708	4655326562647668864	5.3	166.90 ± 0.56	0.72 ± 0.25	-1.52 ± 0.07	0.00	0.00	0000000	M2FS
LMC	NGC 1751	N1751-1-b117	73.481105	-69.791660	18.94	1.19	4881	4655326562647653632	5.9	238.28 ± 0.46	1.39 ± 0.15	-0.73 ± 0.06	0.42	0.00	0000000	M2FS
LMC	NGC 1751	N1751-1-b118	73.482466	-69.796788	18.11	1.60	4603	4655326459568414976	7.3	243.15 ± 0.39	1.74 ± 0.10	-0.50 ± 0.05	0.25	0.04	0000000	M2FS
LMC	NGC 1751	N1751-1-b119	73.493734	-69.796967	18.87	0.89	4859	4655326463864741760	5.2	250.26 ± 0.67	1.52 ± 0.16	-0.76 ± 0.06	0.00	0.00	0000010	M2FS
LMC	NGC 1751	N1751-1-b120	73.493285	-69.807011	18.67	1.27	4794	4655326459568391552	5.8	241.34 ± 0.52	1.93 ± 0.12	-0.48 ± 0.05	0.89	0.91	0000000	M2FS
LMC	NGC 1751	N1751-1-b122	73.474655	-69.773857	18.68	1.38	4798	4655326665726941056	5.6	229.21 ± 0.51	1.85 ± 0.15	-0.42 ± 0.06	0.00	0.00	0000000	M2FS
LMC	NGC 1751	N1751-1-b123	73.462688	-69.777421	18.84	1.14	4850	4655326566963181056	6.0	263.56 ± 0.38	1.91 ± 0.12	-0.61 ± 0.06	0.00	0.00	0000000	M2FS
LMC	NGC 1751	N1751-1-b124	73.460706	-69.783728	18.41	1.24	4707	4655326562647696896	7.1	224.43 ± 0.36	1.57 ± 0.11	-0.78 ± 0.05	0.00	0.00	0000000	M2FS
LMC	NGC 1751	N1751-1-b125	73.442976	-69.799032	17.95	1.34	4549	4655326150330777088	10.0	276.69 ± 0.31	1.11 ± 0.08	-0.83 ± 0.04	0.00	0.00	0000000	M2FS
LMC	NGC 1751	N1751-1-b126	73.470393	-69.799078	17.62	1.45	4440	4655326528287902080	12.0	336.44 ± 0.26	0.38 ± 0.10	-1.35 ± 0.03	-1.00	-1.00	0000100	M2FS
LMC	NGC 1751	N1751-1-b127	73.472454	-69.804308	18.47	1.00	4727	4655326532584213632	8.5	283.34 ± 0.39	1.44 ± 0.11	-1.13 ± 0.05	0.00	0.00	0000010	M2FS
LMC	NGC 1751	N1751-1-b128	73.443681	-69.808074	18.92	0.86	4874	4655326154646338688	5.0	228.33 ± 0.64	1.43 ± 0.20	-1.05 ± 0.08	0.00	0.00	0000010	M2FS
LMC	NGC 1751	N1751-1-r028	73.516440	-69.816365	17.15	1.57	4275	4655326257725600128	15.7	222.43 ± 0.21	0.99 ± 0.05	-0.67 ± 0.03	0.00	0.00	0000000	M2FS
LMC	NGC 1751	N1751-1-r049	73.543076	-69.808679	17.47	1.16	4388	4655326292085367936	13.2	240.61 ± 0.22	1.30 ± 0.05	-0.78 ± 0.04	1.00	1.00	0000010	M2FS
LMC	NGC 1751	N1751-1-r079	73.529133	-69.814575	17.25	1.59	4312	4655326253422816512	14.5	272.28 ± 0.21	1.12 ± 0.05	-0.66 ± 0.03	0.00	0.00	0000000	M2FS
LMC	NGC 1751	N1751-1-r099	73.550426	-69.804978	17.61	1.09	4437	4655326287815096576	9.7	242.71 ± 0.31	1.17 ± 0.07	-0.67 ± 0.04	1.00	1.00	0000010	M2FS
LMC	NGC 1783	N1783-1-b001	74.887411	-66.094858	17.61	1.28	4506	4662233870821273472	11.7	286.81 ± 0.26	1.11 ± 0.07	-0.75 ± 0.04	0.00	0.00	0000000	M2FS
LMC	NGC 1783	N1783-1-b002	74.856351	-66.081198	16.69	1.45	4180	4662233973900524928	22.4	322.42 ± 0.16	0.21 ± 0.07	-1.47 ± 0.03	0.00	0.00	0000000	M2FS
LMC	NGC 1783	N1783-1-b003	74.886281	-66.067016	16.77	1.51	4208	4662234076979740544	20.3	328.33 ± 0.15	0.34 ± 0.05	-0.95 ± 0.03	0.00	0.00	0000000	M2FS
LMC	NGC 1783	N1783-1-b006	74.854788	-65.993750	17.19	1.41	4363	4662234935973340160	17.0	281.72 ± 0.21	0.99 ± 0.05	-0.63 ± 0.03	0.97	0.97	0000000	M2FS
LMC	NGC 1783	N1783-1-b007	74.848407	-65.990691	17.20	1.32	4368	4662234935973308416	15.0	282.84 ± 0.20	1.12 ± 0.05	-0.61 ± 0.03	0.90	0.89	0000000	M2FS
LMC	NGC 1783	N1783-1-b008	74.840069	-65.981800	18.17	0.92	4690	4662234935965395456	8.2	294.36 ± 0.40	1.03 ± 0.12	-0.95 ± 0.05	0.00	0.00	0000000	M2FS
LMC	NGC 1783	N1783-1-b009	74.921499	-66.080807	16.72	1.54	4192	4662234008260265856	12.7	260.66 ± 0.20	0.81 ± 0.05	-0.65 ± 0.03	0.00	0.00	0000000	M2FS
LMC	NGC 1783	N1783-1-b010	74.953719	-66.061750	17.37	1.39	4427	4662233660336217088	11.8	306.04 ± 0.21	1.08 ± 0.06	-0.72 ± 0.03	0.00	0.00	0000000	M2FS
LMC	NGC 1783	N1783-1-b011	74.916150	-66.047944	17.09	1.38	4328	4662234416250465920	15.7	248.01 ± 0.21	0.62 ± 0.05	-1.15 ± 0.03	0.00	0.00	0000000	M2FS
LMC	NGC 1783	N1783-1-b012	74.941593	-66.036765	17.43	1.31	4446	4662234558016120192	13.7	273.28 ± 0.19	0.76 ± 0.05	-0.91 ± 0.03	0.00	0.00	0000000	M2FS
LMC	NGC 1783	N1783-1-b013	74.967539	-66.034669	16.74	1.50	4198	4662233836461650816	18.2	282.17 ± 0.20	0.58 ± 0.05	-0.68 ± 0.03	0.00	0.00	0000000	M2FS
LMC	NGC 1783	N1783-1-b014	75.023466	-66.028435	17.60	1.24	4505	4662235245210926464	10.3	302.20 ± 0.35	0.52 ± 0.11	-1.05 ± 0.04	0.00	0.00	0000000	M2FS
LMC	NGC 1783	N1783-1-b015	75.043352	-66.003278	16.62	1.57	4151	4662235417009654656	-0.1	448.65 ± 111.42	1.72 ± 1.40	0.69 ± 0.52	-1.00	-1.00	1000000	M2FS
LMC	NGC 1783	N1783-1-b017	74.980847	-65.916801	17.57	1.12	4493	4662236855792129280	9.2	301.40 ± 0.27	1.12 ± 0.08	-0.79 ± 0.04	0.00	0.00	0000000	M2FS
LMC	NGC 1783	N1783-1-b018	74.982279	-65.928713	17.43	1.40	4448	4662236855791980672	6.8	309.00 ± 0.31	1.27 ± 0.09	-0.58 ± 0.05	0.00	0.00	0000000	M2FS
LMC	NGC 1783	N1783-1-b019	74.984567	-65.952221	17.24	1.40	4381	4662236653960286336	15.8	247.32 ± 0.37	0.09 ± 0.07	-0.65 ± 0.05	0.00	0.00	0000000	M2FS
LMC	NGC 1783	N1783-1-b020	75.022285	-65.957081	17.11	1.25	4335	4662235898046044672	12.3	-26.53 ± 0.22	3.37 ± 0.06	-0.45 ± 0.07	-1.00	-1.00	0001100	M2FS
LMC	NGC 1783	N1783-1-b021	74.964598	-65.962467	17.52	1.25	4478	4662236688320002432	11.3	270.53 ± 0.24	0.36 ± 0.11	-1.22 ± 0.03	0.00	0.00	0000000	M2FS
LMC	NGC 1783	N1783-1-b023	75.008647	-65.977752	17.00	1.42	4296	4662235863686284288	16.8	277.24 ± 0.20	0.09 ± 0.07	-1.99 ± 0.03	0.00	0.00	0000000	M2FS

Table C.1: (*continued*) Sample of 3095 Targets from 26 Star Clusters

Galaxy	Cluster	ID	RAJ2000 (deg)	DEJ2000 (deg)	G (mag)	$G_{\rm BP} - G_{\rm RP}$ (mag)	$T_{\rm eff}$ (K)	*Gaia* DR2 ID	S/N	$v_{\rm los}$ ($\rm km\,s^{-1}$)	$\log g$ (dex)	$[{\rm Fe/H}]_{\rm raw}$ (dex)	P_M	P'_M	Flag[a]	Source[b]
(1)	(2)	(3)	(4)	(5)	(6)	(7)	(8)	(9)	(10)	(11)	(12)	(13)	(14)	(15)	(16)	(17)
LMC	NGC 1783	N1783-1-b024	75.064483	-65.999425	17.15	1.41	4349	4662235417009655936	11.5	283.68 ± 0.21	0.80 ± 0.06	-0.77 ± 0.03	0.00	0.00	0000000	M2FS
LMC	NGC 1783	N1783-1-b025	74.927550	-65.893016	17.22	1.40	4374	4662242937465690112	14.6	272.45 ± 0.21	0.85 ± 0.05	-0.86 ± 0.03	0.00	0.00	0000000	M2FS
LMC	NGC 1783	N1783-1-b026	74.929336	-65.901390	17.07	1.45	4319	4662237061950425472	15.7	275.91 ± 0.65	0.12 ± 0.10	-1.12 ± 0.08	-1.00	-1.00	0110000	M2FS
LMC	NGC 1783	N1783-1-b028	74.925523	-65.926432	17.03	1.51	4306	4662236928838204288	12.8	264.64 ± 0.23	0.93 ± 0.06	-0.73 ± 0.04	0.00	0.00	0000000	M2FS
LMC	NGC 1783	N1783-1-b030	74.842317	-65.961785	17.45	1.15	4452	4662236447794058240	12.4	278.61 ± 0.23	0.93 ± 0.06	-0.74 ± 0.04	0.99	0.99	0000000	M2FS
LMC	NGC 1783	N1783-1-b032	74.866632	-65.979930	16.71	1.47	4187	4662236413442060288	15.2	280.55 ± 0.17	0.90 ± 0.04	-0.64 ± 0.03	0.99	0.99	0000000	M2FS
LMC	NGC 1783	N1783-1-b033	74.800021	-66.025887	17.87	1.26	4592	4662234386217454720	9.3	278.89 ± 0.30	1.28 ± 0.08	-0.67 ± 0.04	0.99	0.99	0000000	M2FS
LMC	NGC 1783	N1783-1-b034	74.795501	-66.017961	17.41	1.32	4441	4662281695250474752	10.9	304.02 ± 0.23	0.98 ± 0.07	-0.72 ± 0.04	0.00	0.00	0000000	M2FS
LMC	NGC 1783	N1783-1-b035	74.794647	-66.014365	17.15	1.41	4350	4662281699573288704	13.6	279.55 ± 0.21	1.03 ± 0.05	-0.62 ± 0.03	0.99	0.99	0000000	M2FS
LMC	NGC 1783	N1783-1-b036	74.803229	-66.012510	17.27	1.28	4391	4662281695250479872	13.8	309.91 ± 0.22	0.84 ± 0.06	-0.69 ± 0.03	0.00	0.00	0000000	M2FS
LMC	NGC 1783	N1783-1-b037	74.801232	-66.001944	17.92	1.24	4609	4662281733909932032	7.9	345.77 ± 0.31	1.12 ± 0.10	-0.63 ± 0.04	-1.00	-1.00	0000100	M2FS
LMC	NGC 1783	N1783-1-b038	74.813474	-65.999556	17.84	1.15	4581	4662234901613561472	9.6	279.90 ± 0.33	1.46 ± 0.09	-0.62 ± 0.04	0.99	0.99	0000000	M2FS
LMC	NGC 1783	N1783-1-b039	74.799013	-65.997330	17.96	1.05	4621	4662281733910458496	8.1	280.71 ± 0.33	1.38 ± 0.11	-0.54 ± 0.04	1.00	1.00	0000000	M2FS
LMC	NGC 1783	N1783-1-b040	74.797244	-65.992492	17.37	1.02	4426	4662281837012382464	6.7	276.65 ± 0.36	1.12 ± 0.09	-0.53 ± 0.05	1.00	1.00	0000010	M2FS
LMC	NGC 1783	N1783-1-b041	74.815941	-66.066784	17.16	1.37	4353	4662234180058952832	13.2	258.23 ± 0.20	1.17 ± 0.05	-0.73 ± 0.03	0.00	0.00	0000000	M2FS
LMC	NGC 1783	N1783-1-b042	74.822655	-66.025010	17.51	1.18	4473	4662234759847858944	13.4	279.59 ± 0.25	1.04 ± 0.06	-0.69 ± 0.03	0.99	0.99	0000000	M2FS
LMC	NGC 1783	N1783-1-b043	74.829986	-66.012745	16.95	1.43	4275	4662234798534317568	11.4	279.94 ± 0.24	0.95 ± 0.05	-0.67 ± 0.04	0.99	0.99	0000000	M2FS
LMC	NGC 1783	N1783-1-b044	74.820913	-66.008816	16.81	1.40	4223	4662234794207610880	18.5	284.02 ± 0.20	0.74 ± 0.04	-0.76 ± 0.03	0.58	-1.00	0000000	M2FS
LMC	NGC 1783	N1783-1-b045	74.825435	-66.004354	17.63	1.24	4512	4662234794207791488	8.9	279.37 ± 0.32	1.01 ± 0.09	-0.65 ± 0.04	0.99	0.99	0000000	M2FS
LMC	NGC 1783	N1783-1-b046	74.828959	-65.992217	17.34	1.20	4415	4662234901613565440	12.9	287.48 ± 0.27	0.88 ± 0.06	-0.83 ± 0.03	0.00	0.00	0000000	M2FS
LMC	NGC 1783	N1783-1-b047	74.823425	-65.989090	18.75	0.94	4872	4662234935965371264	5.9	280.40 ± 0.58	2.12 ± 0.14	-0.53 ± 0.06	0.99	0.99	0000000	M2FS
LMC	NGC 1783	N1783-1-b048	74.816684	-65.986078	17.52	1.12	4479	4662281871349452032	11.6	278.46 ± 0.23	1.35 ± 0.07	-0.58 ± 0.04	1.00	1.00	0000000	M2FS
LMC	NGC 1783	N1783-1-b049	74.809330	-65.910962	17.09	1.48	4328	4662283967316360832	12.6	228.19 ± 0.27	0.78 ± 0.06	-0.89 ± 0.03	0.00	0.00	0000000	M2FS
LMC	NGC 1783	N1783-1-b050	74.840067	-65.933725	16.88	1.46	4251	4662283520639739776	17.6	277.23 ± 0.20	0.73 ± 0.05	-0.77 ± 0.03	0.00	0.00	0000000	M2FS
LMC	NGC 1783	N1783-1-b051	74.821979	-65.940118	17.10	1.38	4333	4662283486280000768	13.7	276.43 ± 0.26	0.86 ± 0.05	-0.71 ± 0.03	0.00	0.00	0000000	M2FS
LMC	NGC 1783	N1783-1-b052	74.792264	-65.952265	17.19	1.43	4365	4662283417560489344	9.9	280.73 ± 0.26	1.17 ± 0.06	-0.62 ± 0.04	0.99	0.99	0000000	M2FS
LMC	NGC 1783	N1783-1-b053	74.791075	-65.975197	16.94	1.23	4272	4662281871372095744	15.2	247.69 ± 0.25	0.24 ± 0.12	-1.98 ± 0.04	0.00	0.00	0000000	M2FS
LMC	NGC 1783	N1783-1-b054	74.810589	-65.977241	17.54	1.17	4485	4662281867049384832	10.7	276.68 ± 0.28	1.14 ± 0.07	-0.56 ± 0.04	0.97	0.97	0000000	M2FS
LMC	NGC 1783	N1783-1-b055	74.814677	-65.981545	17.51	1.21	4475	4662281871349433216	10.9	283.60 ± 0.33	1.27 ± 0.07	-0.56 ± 0.04	0.91	0.89	0000000	M2FS
LMC	NGC 1783	N1783-1-b056	74.804331	-65.989665	17.83	1.06	4578	4662281836989681024	6.9	277.96 ± 0.43	1.20 ± 0.13	-0.52 ± 0.05	1.00	1.00	0000000	M2FS
LMC	NGC 1783	N1783-1-b057	74.786115	-65.883018	17.31	1.40	4407	4662284207834550272	10.9	51.98 ± 0.31	3.71 ± 0.07	-0.35 ± 0.07	-1.00	-1.00	0001100	M2FS
LMC	NGC 1783	N1783-1-b058	74.771281	-65.883418	17.41	1.37	4441	4662284207834549376	15.2	293.00 ± 0.26	1.28 ± 0.06	-0.55 ± 0.03	0.00	0.00	0000000	M2FS
LMC	NGC 1783	N1783-1-b061	74.778570	-65.969451	18.04	1.19	4647	4662281940069042560	6.5	280.53 ± 0.44	1.72 ± 0.11	-0.45 ± 0.05	0.99	0.99	0000000	M2FS
LMC	NGC 1783	N1783-1-b062	74.783689	-65.972746	16.66	1.29	4169	4662281940069048064	15.0	282.96 ± 0.49	0.07 ± 0.06	-0.55 ± 0.06	0.95	0.94	0000000	M2FS
LMC	NGC 1783	N1783-1-b063	74.766785	-65.974387	17.23	1.34	4379	4662281901408941696	12.5	278.35 ± 0.23	1.23 ± 0.06	-0.56 ± 0.03	0.99	0.99	0000000	M2FS
LMC	NGC 1783	N1783-1-b064	74.778936	-65.977326	16.75	1.31	4203	4662281905709100672	15.6	281.50 ± 0.26	0.71 ± 0.05	-0.63 ± 0.03	1.00	1.00	0000000	M2FS
LMC	NGC 1783	N1783-1-b065	74.762629	-66.082919	16.91	1.52	4261	4662140343616797184	16.4	259.38 ± 0.26	0.56 ± 0.05	-0.84 ± 0.03	0.00	0.00	0000000	M2FS
LMC	NGC 1783	N1783-1-b066	74.755512	-66.016959	17.35	1.39	4419	4662281390335639296	12.2	281.70 ± 0.25	1.35 ± 0.05	-0.58 ± 0.03	0.97	0.97	0000000	M2FS
LMC	NGC 1783	N1783-1-b067	74.745793	-66.009404	17.81	1.22	4572	4662281390335636736	3.0	279.16 ± 0.99	1.51 ± 0.23	-0.74 ± 0.10	0.99	0.99	0000000	M2FS
LMC	NGC 1783	N1783-1-b068	74.762762	-66.008579	17.47	1.30	4462	4662281768292762112	10.6	276.60 ± 0.30	1.10 ± 0.07	-0.63 ± 0.04	0.94	0.94	0000000	M2FS
LMC	NGC 1783	N1783-1-b069	74.756408	-66.006161	17.99	1.10	4632	4662281768292760320	9.1	279.70 ± 0.32	1.40 ± 0.08	-0.66 ± 0.04	0.99	0.99	0000000	M2FS
LMC	NGC 1783	N1783-1-b070	74.735949	-66.005000	18.16	1.22	4685	4662281390312488064	7.5	277.42 ± 0.28	1.80 ± 0.09	-0.55 ± 0.04	0.97	0.97	0000000	M2FS
LMC	NGC 1783	N1783-1-b071	74.722372	-66.004608	17.08	1.43	4323	4662281596494063872	15.0	279.09 ± 0.20	1.05 ± 0.05	-0.58 ± 0.03	0.99	0.99	0000000	M2FS
LMC	NGC 1783	N1783-1-b072	74.740371	-65.999166	18.33	1.09	4742	4662281768269611136	6.3	279.74 ± 0.54	1.77 ± 0.13	-0.47 ± 0.05	0.99	0.99	0000000	M2FS
LMC	NGC 1783	N1783-1-b073	74.768684	-66.018222	17.19	1.36	4362	4662281321616164480	14.7	279.86 ± 0.22	0.81 ± 0.05	-0.70 ± 0.03	0.99	0.99	0000000	M2FS
LMC	NGC 1783	N1783-1-b074	74.782148	-66.015878	16.83	1.50	4232	4662281699573287808	16.2	276.86 ± 0.23	1.05 ± 0.04	-0.61 ± 0.03	0.95	0.95	0000000	M2FS
LMC	NGC 1783	N1783-1-b075	74.772767	-66.007505	16.77	1.45	4210	4662281699550173952	-0.4	-13.84 ± 18.60	2.65 ± 0.90	0.09 ± 0.76	-1.00	-1.00	1000000	M2FS
LMC	NGC 1783	N1783-1-b076	74.792583	-66.005613	16.81	1.44	4225	4662281733933026816	14.5	280.21 ± 0.20	0.99 ± 0.05	-0.59 ± 0.03	0.99	0.99	0000000	M2FS
LMC	NGC 1783	N1783-1-b077	74.764378	-66.000180	17.10	1.26	4330	4662281768292761856	12.9	279.24 ± 0.24	0.75 ± 0.06	-0.75 ± 0.03	0.99	0.99	0000000	M2FS
LMC	NGC 1783	N1783-1-b078	74.781432	-65.998183	16.99	1.41	4290	4662281733933279104	11.7	281.52 ± 0.30	0.93 ± 0.06	-0.63 ± 0.04	1.00	1.00	0000000	M2FS
LMC	NGC 1783	N1783-1-b079	74.770188	-65.997477	18.22	0.00	4708	4662281798329894400	5.9	281.06 ± 0.52	2.08 ± 0.13	-0.40 ± 0.05	1.00	1.00	0000000	M2FS
LMC	NGC 1783	N1783-1-b080	74.764919	-65.991184	17.03	1.28	4307	4662281802652746112	10.8	278.85 ± 0.27	1.05 ± 0.06	-0.57 ± 0.04	1.00	1.00	0000000	M2FS
LMC	NGC 1783	N1783-1-b081	74.765018	-65.953985	17.16	1.38	4354	4662283417560485760	11.1	266.00 ± 0.27	0.35 ± 0.10	-1.15 ± 0.04	0.00	0.00	0000000	M2FS
LMC	NGC 1783	N1783-1-b082	74.759305	-65.957882	16.95	1.38	4276	4662281940091735680	14.1	278.92 ± 0.22	0.77 ± 0.05	-0.69 ± 0.03	0.99	0.99	0000000	M2FS

Table C.1: (*continued*) Sample of 3095 Targets from 26 Star Clusters

Galaxy	Cluster	ID	RAJ2000 (deg)	DEJ2000 (deg)	G (mag)	$G_{\rm BP} - G_{\rm RP}$ (mag)	$T_{\rm eff}$ (K)	*Gaia* DR2 ID	S/N	$v_{\rm los}$ ($\rm km\,s^{-1}$)	$\log g$ (dex)	$[{\rm Fe/H}]_{\rm raw}$ (dex)	P_M	P'_M	Flag[a]	Source[b]
(1)	(2)	(3)	(4)	(5)	(6)	(7)	(8)	(9)	(10)	(11)	(12)	(13)	(14)	(15)	(16)	(17)
LMC	NGC 1783	N1783-1-b083	74.758426	-65.970230	18.02	1.18	4642	4662281901408942720	7.4	279.17 ± 0.36	1.52 ± 0.11	-0.62 ± 0.05	0.99	0.99	0000000	M2FS
LMC	NGC 1783	N1783-1-b084	74.752193	-65.975627	18.34	1.16	4745	4662281905708726272	5.0	278.87 ± 0.64	1.86 ± 0.15	-0.47 ± 0.06	0.99	0.99	0000000	M2FS
LMC	NGC 1783	N1783-1-b085	74.758076	-65.979042	16.83	1.47	4231	4662281905731744000	13.3	279.82 ± 0.27	1.00 ± 0.05	-0.51 ± 0.04	0.99	0.99	0000000	M2FS
LMC	NGC 1783	N1783-1-b086	74.764039	-65.983372	16.83	1.38	4231	4662281901409107840	11.8	279.27 ± 0.22	0.98 ± 0.06	-0.53 ± 0.04	1.00	1.00	0000000	M2FS
LMC	NGC 1783	N1783-1-b087	74.756897	-65.986055	17.99	1.14	4631	4662281802652529408	6.1	278.96 ± 0.48	1.42 ± 0.13	-0.46 ± 0.05	1.00	1.00	0000000	M2FS
LMC	NGC 1783	N1783-1-b088	74.758564	-65.995966	18.04	1.14	4648	4662281798329891328	5.4	279.90 ± 0.51	1.72 ± 0.16	-0.38 ± 0.06	-1.00	-1.00	0000001	M2FS
LMC	NGC 1783	N1783-1-b089	74.733941	-65.952316	16.98	1.52	4289	4662282146250163712	12.4	233.94 ± 0.23	0.68 ± 0.05	-0.87 ± 0.03	0.00	0.00	0000000	M2FS
LMC	NGC 1783	N1783-1-b090	74.734116	-65.972543	17.71	1.27	4539	4662282111890166912	10.2	278.99 ± 0.30	1.26 ± 0.08	-0.61 ± 0.04	0.99	0.99	0000000	M2FS
LMC	NGC 1783	N1783-1-b092	74.747733	-65.979629	18.00	1.18	4634	4662281802652525056	7.2	281.41 ± 0.50	1.54 ± 0.11	-0.47 ± 0.05	0.99	0.98	0000000	M2FS
LMC	NGC 1783	N1783-1-b093	74.738224	-65.980834	17.93	1.09	4611	4662282008810952832	8.9	275.95 ± 0.38	1.36 ± 0.09	-0.61 ± 0.04	0.89	0.89	0000000	M2FS
LMC	NGC 1783	N1783-1-b094	74.743859	-65.985460	17.41	1.34	4439	4662281802652524544	11.6	277.83 ± 0.34	1.10 ± 0.07	-0.62 ± 0.04	0.99	0.99	0000000	M2FS
LMC	NGC 1783	N1783-1-b095	74.747498	-65.992495	17.41	0.89	4439	4662281802629509376	12.7	281.71 ± 0.26	1.00 ± 0.06	-0.83 ± 0.03	0.98	0.98	0000010	M2FS
LMC	NGC 1783	N1783-1-b096	74.731888	-65.995396	17.96	0.98	4622	4662281768292783872	10.8	279.08 ± 0.34	1.54 ± 0.07	-0.83 ± 0.04	-1.00	-1.00	0000001	M2FS
LMC	NGC 1783	N1783-1-b097	74.600992	-66.064899	16.94	1.50	4273	4662187485172237184	12.6	251.56 ± 0.24	0.45 ± 0.07	-1.14 ± 0.03	0.00	0.00	0000000	M2FS
LMC	NGC 1783	N1783-1-b098	74.606998	-66.053976	17.43	1.41	4445	4662187519531975808	11.3	282.35 ± 0.24	1.30 ± 0.06	-0.61 ± 0.03	0.00	0.00	0000000	M2FS
LMC	NGC 1783	N1783-1-b099	74.684447	-66.037305	17.19	1.35	4363	4662281424695360896	18.2	317.67 ± 0.20	0.77 ± 0.05	-0.80 ± 0.03	0.00	0.00	0000000	M2FS
LMC	NGC 1783	N1783-1-b100	74.565506	-66.031177	17.59	1.42	4499	4662188447244937472	12.5	322.37 ± 0.32	1.23 ± 0.07	-0.64 ± 0.04	0.00	0.00	0000000	M2FS
LMC	NGC 1783	N1783-1-b101	74.655252	-66.027149	17.11	1.45	4336	4662281493414836352	14.8	251.16 ± 0.21	1.02 ± 0.05	-0.67 ± 0.03	0.00	0.00	0000000	M2FS
LMC	NGC 1783	N1783-1-b102	74.574402	-66.024347	17.61	1.30	4506	4662188442921748224	9.8	275.28 ± 0.27	1.29 ± 0.07	-0.60 ± 0.04	0.00	0.00	0000000	M2FS
LMC	NGC 1783	N1783-1-b104	74.689545	-65.997499	16.97	1.42	4283	4662281596494061184	17.2	280.66 ± 0.22	0.97 ± 0.04	-0.65 ± 0.03	0.99	0.99	0000000	M2FS
LMC	NGC 1783	N1783-1-b105	74.691200	-66.095053	17.11	1.45	4334	4662187210294307456	15.2	300.30 ± 0.22	0.75 ± 0.05	-0.82 ± 0.03	0.00	0.00	0000000	M2FS
LMC	NGC 1783	N1783-1-b106	74.692557	-66.048471	17.44	1.37	4451	4662187588251456128	10.0	237.48 ± 0.31	1.07 ± 0.07	-0.73 ± 0.04	0.00	0.00	0000000	M2FS
LMC	NGC 1783	N1783-1-b109	74.717432	-66.016012	17.70	1.16	4535	4662281351653092224	11.5	279.22 ± 0.27	1.32 ± 0.07	-0.72 ± 0.04	0.99	0.99	0000000	M2FS
LMC	NGC 1783	N1783-1-b110	74.701603	-66.003114	17.49	1.32	4468	4662281596494061696	12.1	279.31 ± 0.30	0.95 ± 0.07	-0.65 ± 0.04	0.99	0.99	0000000	M2FS
LMC	NGC 1783	N1783-1-b111	74.719926	-65.999680	17.62	0.00	4510	4662281596470908288	10.7	279.87 ± 0.31	1.24 ± 0.07	-0.61 ± 0.04	0.99	0.99	0000000	M2FS
LMC	NGC 1783	N1783-1-b112	74.714874	-65.996586	18.05	1.27	4652	4662281596494062464	6.8	279.00 ± 0.44	1.47 ± 0.11	-0.49 ± 0.05	0.99	0.99	0000000	M2FS
LMC	NGC 1783	N1783-1-b114	74.720488	-65.922299	16.76	1.58	4206	4662283726798162560	16.5	294.43 ± 0.22	0.93 ± 0.04	-0.60 ± 0.03	0.00	0.00	0000000	M2FS
LMC	NGC 1783	N1783-1-b115	74.711487	-65.933779	17.41	1.32	4439	4662283692438423808	14.6	289.37 ± 0.22	0.98 ± 0.06	-0.84 ± 0.03	0.00	0.00	0000000	M2FS
LMC	NGC 1783	N1783-1-b118	74.707872	-65.966165	17.01	1.50	4298	4662282008811209088	0.4	80.43 ± 177.07	3.75 ± 1.07	-0.47 ± 1.31	-1.00	-1.00	1000000	M2FS
LMC	NGC 1783	N1783-1-b119	74.731092	-65.984766	17.22	1.35	4374	4662282004488317568	13.3	278.44 ± 0.26	1.01 ± 0.06	-0.68 ± 0.04	0.98	0.99	0000000	M2FS
LMC	NGC 1783	N1783-1-b120	74.714062	-65.988022	17.04	1.42	4310	4662281974451211136	14.6	279.68 ± 0.26	0.79 ± 0.05	-0.68 ± 0.03	0.99	0.99	0000000	M2FS
LMC	NGC 1783	N1783-1-b121	74.690903	-65.897817	17.08	1.48	4325	4662284585791645056	15.6	282.71 ± 0.23	1.12 ± 0.05	-0.57 ± 0.03	0.00	0.00	0000000	M2FS
LMC	NGC 1783	N1783-1-b122	74.603789	-65.917481	17.08	1.35	4323	4662283241438465152	12.4	308.60 ± 0.25	0.32 ± 0.09	-1.09 ± 0.03	0.00	0.00	0000000	M2FS
LMC	NGC 1783	N1783-1-b124	74.543571	-65.943629	16.82	1.52	4229	4662282764725446144	10.6	313.18 ± 0.30	0.76 ± 0.06	-0.65 ± 0.04	0.00	0.00	0000000	M2FS
LMC	NGC 1783	N1783-1-b125	74.550461	-65.969718	17.59	1.34	4500	4662282661645968768	9.8	295.12 ± 0.26	1.48 ± 0.07	-0.58 ± 0.04	0.00	0.00	0000000	M2FS
LMC	NGC 1783	N1783-1-b127	74.635073	-65.981437	17.31	1.39	4405	4662282416805007744	2.3	292.69 ± 1.11	0.34 ± 0.22	-0.75 ± 0.09	0.00	0.00	0000000	M2FS
LMC	NGC 1783	N1783-1-b128	74.698173	-65.992454	18.15	1.21	4684	4662281596494087296	8.4	278.32 ± 0.32	1.67 ± 0.09	-0.59 ± 0.04	0.98	0.99	0000000	M2FS
LMC	NGC 1783	N1783-1-r028	74.772480	-65.988886	17.02	0.98	4301	4662281802652680704	17.0	278.68 ± 0.19	0.75 ± 0.05	-0.78 ± 0.03	1.00	1.00	0000010	M2FS
LMC	NGC 1783	N1783-1-r049	74.785840	-65.989964	16.90	0.74	4258	4662281837012315648	11.5	281.04 ± 0.31	0.84 ± 0.07	-0.95 ± 0.04	1.00	1.00	0000010	M2FS
LMC	NGC 1783	N1783-1-r079	74.773035	-65.984227	16.57	1.23	4135	4662281905709041920	17.2	277.68 ± 0.22	0.77 ± 0.04	-0.77 ± 0.03	1.00	1.00	0000000	M2FS
LMC	NGC 1783	N1783-1-r127	74.798398	-65.984393	16.67	1.17	4172	4662281837012409344	12.8	279.66 ± 0.23	0.61 ± 0.05	-0.77 ± 0.03	1.00	1.00	0000010	M2FS
LMC	NGC 1783	1783-22	74.726489	-65.972356	–	–	–	–	–	279.38 ± 0.20	–	–	0.99	0.99	0000000	Mu08
LMC	NGC 1783	1783-23	74.779313	-65.986232	–	–	–	–	–	277.08 ± 0.20	–	–	1.00	1.00	0000000	Mu08
LMC	NGC 1783	1783-29	74.783072	-65.995770	–	–	–	–	–	277.18 ± 0.20	–	–	1.00	1.00	0000000	Mu08
LMC	NGC 1783	1783-30	74.801063	-65.962930	–	–	–	–	–	283.18 ± 0.20	–	–	0.85	0.83	0000000	Mu08
LMC	NGC 1783	1783-32	74.770787	-65.979964	–	–	–	–	–	279.88 ± 0.20	–	–	1.00	1.00	0000000	Mu08
LMC	NGC 1783	1783-33	74.801166	-65.990670	–	–	–	–	–	280.78 ± 0.20	–	–	1.00	1.00	0000000	Mu08
LMC	NGC 1806	N1806-1-b001	75.606271	-68.034032	18.60	1.23	4828	4661454965697882496	4.9	295.89 ± 0.48	1.81 ± 0.18	-0.60 ± 0.06	0.00	0.00	0000000	M2FS
LMC	NGC 1806	N1806-1-b002	75.600243	-68.025823	18.98	1.03	4940	4661455068663943552	4.6	230.50 ± 0.60	2.15 ± 0.17	-0.60 ± 0.07	0.86	0.89	0000000	M2FS
LMC	NGC 1806	N1806-1-b003	75.599236	-68.019010	18.39	0.83	4761	4661455279161199232	8.5	330.05 ± 0.68	1.58 ± 0.15	-1.61 ± 0.06	0.00	0.00	0000010	M2FS
LMC	NGC 1806	N1806-1-b004	75.592913	-68.016049	17.19	1.40	4357	4661455279161193088	14.4	235.35 ± 0.19	1.11 ± 0.05	-0.71 ± 0.03	0.00	0.00	0000000	M2FS
LMC	NGC 1806	N1806-1-b005	75.619431	-68.004803	18.98	0.98	4940	4661456580492473728	4.2	271.16 ± 0.73	1.52 ± 0.22	-0.61 ± 0.07	0.00	0.00	0000000	M2FS
LMC	NGC 1806	N1806-1-b006	75.602482	-67.999934	18.49	1.30	4792	4661456790989674240	6.0	230.47 ± 0.37	2.11 ± 0.11	-0.48 ± 0.05	0.93	0.94	0000000	M2FS
LMC	NGC 1806	N1806-1-b007	75.605936	-67.994894	18.00	1.13	4630	4661456790989672832	8.9	259.98 ± 0.35	0.97 ± 0.10	-0.84 ± 0.04	0.00	0.00	0000000	M2FS

Table C.1: (*continued*) Sample of 3095 Targets from 26 Star Clusters

Galaxy	Cluster	ID	RAJ2000 (deg)	DEJ2000 (deg)	G (mag)	$G_{\rm BP} - G_{\rm RP}$ (mag)	$T_{\rm eff}$ (K)	*Gaia* DR2 ID	S/N	$v_{\rm los}$ (km s^{-1})	log g (dex)	[Fe/H]$_{\rm raw}$ (dex)	P_M	P'_M	Flag[a]	Source[b]
(1)	(2)	(3)	(4)	(5)	(6)	(7)	(8)	(9)	(10)	(11)	(12)	(13)	(14)	(15)	(16)	(17)
LMC	NGC 1806	N1806-1-b008	75.598779	-67.990473	18.96	1.01	4934	4661456786668660352	4.5	231.54 ± 0.76	1.64 ± 0.22	-0.73 ± 0.08	0.96	0.96	0000000	M2FS
LMC	NGC 1806	N1806-1-b010	75.623318	-68.022088	18.90	1.08	4917	4661455068663951616	4.4	216.93 ± 0.53	1.77 ± 0.19	-0.66 ± 0.07	0.00	0.00	0000000	M2FS
LMC	NGC 1806	N1806-1-b011	75.623414	-68.017564	15.80	2.58	3910	4661455107362518912	4.9	230.49 ± 1.99	1.75 ± 0.32	-1.88 ± 0.28	-1.00	-1.00	0110010	M2FS
LMC	NGC 1806	N1806-1-b012	75.673374	-68.012056	18.11	1.04	4669	4661456511770642176	7.6	282.33 ± 0.27	1.79 ± 0.09	-0.57 ± 0.04	0.00	0.00	0000000	M2FS
LMC	NGC 1806	N1806-1-b013	75.686496	-68.004418	17.69	1.30	4527	4661456550471620096	9.7	278.30 ± 0.24	0.98 ± 0.08	-0.78 ± 0.04	0.00	0.00	0000000	M2FS
LMC	NGC 1806	N1806-1-b014	75.632247	-67.995548	18.88	1.11	4910	4661456614880734080	4.4	282.35 ± 0.53	1.35 ± 0.24	-0.82 ± 0.07	0.00	0.00	0000000	M2FS
LMC	NGC 1806	N1806-1-b015	75.662646	-67.995270	18.32	1.15	4738	4661456614965314432	6.4	267.49 ± 0.55	1.62 ± 0.15	-1.35 ± 0.06	0.00	0.00	0000000	M2FS
LMC	NGC 1806	N1806-1-b016	75.646111	-67.990024	15.61	0.67	3910	4661456619190997504	45.2	279.53 ± 0.56	0.35 ± 0.11	-2.51 ± 0.04	-1.00	-1.00	0100010	M2FS
LMC	NGC 1806	N1806-1-b017	75.659274	-67.960339	18.94	0.98	4928	4661457134565866496	5.4	248.29 ± 0.39	1.89 ± 0.14	-0.64 ± 0.06	0.00	0.00	0000000	M2FS
LMC	NGC 1806	N1806-1-b018	75.679395	-67.961133	16.11	1.98	3946	4661457134587067136	18.9	290.03 ± 0.22	0.85 ± 0.05	-0.65 ± 0.04	0.00	0.00	0000010	M2FS
LMC	NGC 1806	N1806-1-b019	75.670025	-67.965844	18.86	1.11	4904	4661457130266271616	5.9	248.75 ± 0.46	1.20 ± 0.22	-1.27 ± 0.06	0.00	0.00	0000000	M2FS
LMC	NGC 1806	N1806-1-b020	75.659087	-67.971912	18.88	1.07	4910	4661456752291242752	6.0	255.22 ± 0.45	1.93 ± 0.14	-0.68 ± 0.06	0.00	0.00	0000000	M2FS
LMC	NGC 1806	N1806-1-b021	75.686347	-67.976293	18.91	1.04	4920	4661456683571754112	4.9	265.00 ± 0.50	1.84 ± 0.16	-0.72 ± 0.07	0.00	0.00	0000000	M2FS
LMC	NGC 1806	N1806-1-b022	75.694057	-67.979820	18.25	1.32	4713	4661456683569508480	7.0	220.55 ± 0.36	1.58 ± 0.11	-0.60 ± 0.04	0.00	0.00	0000000	M2FS
LMC	NGC 1806	N1806-1-b023	75.678844	-67.982000	17.85	1.24	4583	4661456683569498752	9.8	230.04 ± 0.29	1.14 ± 0.08	-0.79 ± 0.04	0.79	0.84	0000000	M2FS
LMC	NGC 1806	N1806-1-b024	75.670359	-67.984568	17.87	1.32	4589	4661456722270220928	8.6	258.00 ± 0.28	1.64 ± 0.08	-0.51 ± 0.04	0.00	0.00	0000000	M2FS
LMC	NGC 1806	N1806-1-b026	75.633560	-67.957669	18.72	0.73	4863	4661456958564072832	9.8	262.51 ± 0.59	1.67 ± 0.13	-1.61 ± 0.06	0.00	0.00	0000010	M2FS
LMC	NGC 1806	N1806-1-b027	75.624564	-67.959586	18.61	1.06	4829	4661456962788342400	7.0	227.38 ± 0.41	1.71 ± 0.11	-0.69 ± 0.05	0.66	0.31	0000000	M2FS
LMC	NGC 1806	N1806-1-b028	75.625694	-67.965986	18.76	1.22	4876	4661456962788349440	4.9	236.94 ± 0.48	2.32 ± 0.15	-0.48 ± 0.07	0.00	0.00	0000000	M2FS
LMC	NGC 1806	N1806-1-b029	75.607204	-67.966195	18.13	1.06	4674	4661456924087758848	8.8	272.84 ± 0.39	0.91 ± 0.11	-0.91 ± 0.04	0.00	0.00	0000000	M2FS
LMC	NGC 1806	N1806-1-b030	75.642123	-67.981520	16.35	1.76	4042	4661456722270203264	14.3	258.00 ± 0.20	0.55 ± 0.04	-0.80 ± 0.03	0.00	0.00	0000000	M2FS
LMC	NGC 1806	N1806-1-b031	75.631788	-67.988329	18.79	0.84	4885	4661456614965392512	5.6	286.98 ± 0.61	1.70 ± 0.17	-1.03 ± 0.06	0.00	0.00	0000000	M2FS
LMC	NGC 1806	N1806-1-b032	75.622565	-67.989147	18.69	1.02	4855	4661456614880738304	5.2	229.11 ± 0.54	1.89 ± 0.13	-0.69 ± 0.06	0.94	0.94	0000000	M2FS
LMC	NGC 1806	N1806-1-b033	75.551248	-68.025978	18.82	1.09	4893	4661455171771750912	4.2	267.23 ± 0.68	1.69 ± 0.18	-0.67 ± 0.07	0.00	0.00	0000000	M2FS
LMC	NGC 1806	N1806-1-b034	75.532933	-68.019314	18.98	1.13	4940	4661455240480212608	4.0	231.29 ± 0.70	1.39 ± 0.25	-0.77 ± 0.09	0.82	0.83	0000000	M2FS
LMC	NGC 1806	N1806-1-b035	75.525445	-68.015328	18.53	1.16	4806	4661455240491233152	6.0	251.63 ± 0.39	1.80 ± 0.12	-0.67 ± 0.06	0.00	0.00	0000000	M2FS
LMC	NGC 1806	N1806-1-b036	75.533827	-68.012429	18.22	1.31	4703	4661455240480214656	7.7	287.01 ± 0.24	1.44 ± 0.09	-0.66 ± 0.04	0.00	0.00	0000000	M2FS
LMC	NGC 1806	N1806-1-b037	75.542016	-68.007197	18.88	1.03	4912	4661455347859406592	4.8	242.81 ± 0.40	2.37 ± 0.14	-0.63 ± 0.07	0.00	0.00	0000000	M2FS
LMC	NGC 1806	N1806-1-b038	75.511240	-68.006857	18.91	1.12	4919	4661455996376916480	5.0	271.62 ± 0.45	1.84 ± 0.18	-0.55 ± 0.06	0.00	0.00	0000000	M2FS
LMC	NGC 1806	N1806-1-b039	75.536381	-68.003785	18.24	1.04	4711	4661455347859382016	7.7	230.53 ± 0.38	1.25 ± 0.11	-0.86 ± 0.04	0.98	0.98	0000000	M2FS
LMC	NGC 1806	N1806-1-b040	75.513415	-67.998869	17.04	1.45	4303	4661456099454005632	7.7	230.32 ± 0.22	1.01 ± 0.06	-0.62 ± 0.04	0.98	0.98	0000000	M2FS
LMC	NGC 1806	N1806-1-b042	75.592796	-68.030232	18.83	1.01	4896	4661455176081990272	6.2	270.56 ± 0.38	1.53 ± 0.16	-0.99 ± 0.06	0.00	0.00	0000000	M2FS
LMC	NGC 1806	N1806-1-b043	75.579131	-68.020810	18.52	1.08	4802	4661455279161189504	4.4	290.31 ± 0.58	1.13 ± 0.23	-0.76 ± 0.07	0.00	0.00	0000000	M2FS
LMC	NGC 1806	N1806-1-b044	75.572526	-68.009925	18.85	1.00	4902	4661455279161176960	5.9	319.67 ± 0.46	1.71 ± 0.15	-0.58 ± 0.06	0.00	0.00	0000000	M2FS
LMC	NGC 1806	N1806-1-b045	75.559115	-68.003993	18.43	1.06	4774	4661455377899499136	3.2	227.74 ± 0.50	2.16 ± 0.19	-0.50 ± 0.08	0.97	0.95	0000000	M2FS
LMC	NGC 1806	N1806-1-b046	75.591979	-68.003529	18.88	1.12	4912	4661455309179839616	3.8	260.11 ± 0.66	2.29 ± 0.19	-0.52 ± 0.08	0.00	0.00	0000000	M2FS
LMC	NGC 1806	N1806-1-b047	75.575320	-67.997030	17.29	1.38	4392	4661455309179874560	11.8	232.52 ± 0.23	1.23 ± 0.06	-0.58 ± 0.04	0.93	0.91	0000000	M2FS
LMC	NGC 1806	N1806-1-b048	75.582775	-67.992463	16.57	1.62	4128	4661456790989655680	17.3	256.41 ± 0.22	1.04 ± 0.05	-0.50 ± 0.04	0.00	0.00	0000000	M2FS
LMC	NGC 1806	N1806-1-b050	75.590667	-67.942509	17.52	1.36	4471	4661457405154784896	12.7	277.81 ± 0.23	1.31 ± 0.06	-0.59 ± 0.03	0.00	0.00	0000000	M2FS
LMC	NGC 1806	N1806-1-b051	75.593593	-67.967512	18.58	1.17	4820	4661456924087751680	5.5	229.51 ± 1.44	2.89 ± 0.14	-1.22 ± 0.10	-1.00	-1.00	0100000	M2FS
LMC	NGC 1806	N1806-1-b052	75.578616	-67.972356	18.87	0.94	4908	4661456894068841600	3.5	258.69 ± 0.65	1.69 ± 0.24	-0.77 ± 0.09	0.00	0.00	0000000	M2FS
LMC	NGC 1806	N1806-1-b053	75.580164	-67.976996	16.48	1.35	4094	4661456894068847616	22.8	310.90 ± 0.17	0.05 ± 0.04	-0.82 ± 0.03	0.00	0.00	0000000	M2FS
LMC	NGC 1806	N1806-1-b054	75.574613	-67.980862	18.83	1.07	4895	4661456855484853376	4.4	236.67 ± 0.55	2.21 ± 0.20	-0.40 ± 0.07	-1.00	-1.00	0000001	M2FS
LMC	NGC 1806	N1806-1-b055	75.589331	-67.988704	18.65	1.02	4841	4661456786764014208	6.2	230.97 ± 0.41	2.14 ± 0.12	-0.51 ± 0.05	0.97	0.97	0000000	M2FS
LMC	NGC 1806	N1806-1-b056	75.575615	-67.989124	18.38	0.76	4756	4661456786668589056	8.0	228.71 ± 0.49	1.93 ± 0.11	-1.40 ± 0.06	0.99	0.99	0000010	M2FS
LMC	NGC 1806	N1806-1-b058	75.565405	-67.934909	18.65	0.92	4843	4661457409464750208	7.0	290.79 ± 0.43	1.42 ± 0.13	-0.83 ± 0.05	0.00	0.00	0000000	M2FS
LMC	NGC 1806	N1806-1-b059	75.565435	-67.940996	16.88	1.42	4244	4661457027167128832	18.9	289.91 ± 0.19	0.54 ± 0.05	-0.72 ± 0.03	0.00	0.00	0000000	M2FS
LMC	NGC 1806	N1806-1-b060	75.547279	-67.941496	16.96	0.71	4275	4661457783081373056	18.2	284.21 ± 0.38	0.87 ± 0.08	-2.24 ± 0.04	0.00	0.00	0000010	M2FS
LMC	NGC 1806	N1806-1-b061	75.563862	-67.967081	18.47	1.15	4786	4661456894068824320	6.1	231.51 ± 0.41	1.90 ± 0.13	-0.63 ± 0.06	0.96	0.96	0000000	M2FS
LMC	NGC 1806	N1806-1-b062	75.547305	-67.975239	18.81	0.84	4890	4661456855484485632	5.6	229.17 ± 0.47	2.05 ± 0.15	-0.88 ± 0.07	0.99	0.99	0000000	M2FS
LMC	NGC 1806	N1806-1-b063	75.563468	-67.981054	17.64	1.00	4512	4661456859687852672	10.9	227.63 ± 0.20	1.41 ± 0.06	-0.62 ± 0.04	1.00	1.00	0000000	M2FS
LMC	NGC 1806	N1806-1-b064	75.563742	-67.988874	18.73	0.72	4868	4661456859687881856	4.8	224.47 ± 0.57	1.84 ± 0.16	-0.54 ± 0.06	1.00	-1.00	0000010	M2FS
LMC	NGC 1806	N1806-1-b067	75.479607	-68.030330	18.07	1.35	4654	4661455584057608704	9.3	285.90 ± 0.27	1.44 ± 0.09	-0.68 ± 0.04	0.00	0.00	0000000	M2FS
LMC	NGC 1806	N1806-1-b068	75.475319	-68.003557	17.58	1.20	4492	4661455996374604160	12.2	265.42 ± 0.20	0.90 ± 0.06	-0.95 ± 0.03	0.00	0.00	0000000	M2FS

Table C.1: (*continued*) Sample of 3095 Targets from 26 Star Clusters

Galaxy	Cluster	ID	RAJ2000 (deg)	DEJ2000 (deg)	G (mag)	$G_{\rm BP} - G_{\rm RP}$ (mag)	$T_{\rm eff}$ (K)	*Gaia* DR2 ID	S/N	$v_{\rm los}$ ($\rm km\,s^{-1}$)	$\log g$ (dex)	$[{\rm Fe/H}]_{\rm raw}$ (dex)	P_M	P'_M	Flag[a]	Source[b]
(1)	(2)	(3)	(4)	(5)	(6)	(7)	(8)	(9)	(10)	(11)	(12)	(13)	(14)	(15)	(16)	(17)
LMC	NGC 1806	N1806-1-b069	75.490560	-68.000640	18.99	0.92	4941	4661455996376927616	4.9	297.27 ± 0.60	1.03 ± 0.24	-0.86 ± 0.07	0.00	0.00	0000000	M2FS
LMC	NGC 1806	N1806-1-b070	75.473258	-67.996185	18.78	0.85	4881	4661456065094118784	3.6	255.99 ± 0.65	1.77 ± 0.22	-0.88 ± 0.09	0.00	0.00	0000000	M2FS
LMC	NGC 1806	N1806-1-b071	75.490391	-67.995832	18.00	1.24	4632	4661456103794703104	8.5	229.75 ± 0.28	1.18 ± 0.09	-0.67 ± 0.04	0.94	0.95	0000000	M2FS
LMC	NGC 1806	N1806-1-b072	75.472315	-67.990924	18.28	1.27	4725	4661456168173361536	7.2	258.36 ± 0.31	1.51 ± 0.11	-0.60 ± 0.05	0.00	0.00	0000000	M2FS
LMC	NGC 1806	N1806-1-b074	75.492407	-68.032908	18.92	1.07	4923	4661455584090300672	4.4	316.97 ± 1.21	2.45 ± 0.16	-0.77 ± 0.10	0.00	0.00	0000000	M2FS
LMC	NGC 1806	N1806-1-b075	75.495532	-68.026796	18.91	0.97	4918	4661455584077467008	4.4	295.64 ± 0.51	2.19 ± 0.16	-0.51 ± 0.07	0.00	0.00	0000000	M2FS
LMC	NGC 1806	N1806-1-b076	75.492859	-68.013259	18.69	1.12	4855	4661455966355885696	5.0	285.35 ± 0.43	1.73 ± 0.18	-0.74 ± 0.06	0.00	0.00	0000000	M2FS
LMC	NGC 1806	N1806-1-b077	75.510024	-68.003141	18.70	0.99	4859	4661455996394378624	5.3	251.99 ± 0.41	1.71 ± 0.15	-0.67 ± 0.06	0.00	0.00	0000000	M2FS
LMC	NGC 1806	N1806-1-b078	75.499644	-67.998407	18.90	0.93	4917	4661456103773455616	5.2	246.99 ± 0.61	1.90 ± 0.16	-0.72 ± 0.07	0.00	0.00	0000000	M2FS
LMC	NGC 1806	N1806-1-b079	75.508155	-67.995271	18.85	1.04	4902	4661456103773459072	4.5	227.04 ± 0.42	2.30 ± 0.16	-0.62 ± 0.07	0.95	0.91	0000000	M2FS
LMC	NGC 1806	N1806-1-b080	75.497781	-67.990764	18.80	1.01	4887	4661456103773434752	5.5	276.25 ± 0.55	1.33 ± 0.17	-0.65 ± 0.06	0.00	0.00	0000000	M2FS
LMC	NGC 1806	N1806-1-b081	75.545112	-67.936883	17.92	1.32	4606	4661457783081395328	7.4	281.44 ± 0.28	1.60 ± 0.09	-0.72 ± 0.05	0.00	0.00	0000000	M2FS
LMC	NGC 1806	N1806-1-b082	75.545857	-67.957314	17.44	1.33	4444	4661457753062142976	12.3	240.25 ± 0.43	0.13 ± 0.10	-0.48 ± 0.06	0.00	0.00	0000000	M2FS
LMC	NGC 1806	N1806-1-b083	75.536719	-67.960736	16.38	1.48	4055	4661457649982925568	22.4	247.38 ± 0.17	0.13 ± 0.06	-0.77 ± 0.03	0.00	0.00	0000000	M2FS
LMC	NGC 1806	N1806-1-b084	75.545946	-67.962706	18.92	1.02	4921	4661456894068691328	4.8	232.38 ± 0.54	1.72 ± 0.21	-0.61 ± 0.06	0.76	0.73	0000000	M2FS
LMC	NGC 1806	N1806-1-b085	75.528371	-67.964803	18.97	1.07	4935	4661457645661885056	4.4	254.94 ± 0.60	1.76 ± 0.20	-0.71 ± 0.08	0.00	0.00	0000000	M2FS
LMC	NGC 1806	N1806-1-b086	75.539742	-67.966833	17.37	1.39	4420	4661457649982935296	11.7	232.63 ± 0.20	1.20 ± 0.06	-0.61 ± 0.03	0.91	0.88	0000000	M2FS
LMC	NGC 1806	N1806-1-b087	75.523897	-67.970343	18.94	1.15	4926	4661457611398721152	3.9	218.32 ± 0.79	1.34 ± 0.28	-1.18 ± 0.09	0.00	0.00	0000000	M2FS
LMC	NGC 1806	N1806-1-b088	75.530381	-67.973622	16.81	1.53	4217	4661457611288102912	16.0	298.23 ± 0.18	0.83 ± 0.04	-0.68 ± 0.03	0.00	0.00	0000000	M2FS
LMC	NGC 1806	N1806-1-b090	75.511478	-67.935500	18.52	1.31	4801	4661457821781573376	7.2	225.29 ± 0.37	1.46 ± 0.12	-0.93 ± 0.05	0.00	0.00	0000000	M2FS
LMC	NGC 1806	N1806-1-b091	75.523314	-67.938208	18.76	0.94	4876	4661457753062108032	5.4	205.59 ± 0.59	1.38 ± 0.30	-1.71 ± 0.08	0.00	0.00	0000000	M2FS
LMC	NGC 1806	N1806-1-b092	75.515282	-67.946702	18.83	1.00	4895	4661457753062111360	3.2	230.04 ± 0.77	2.24 ± 0.25	-0.67 ± 0.11	0.91	0.92	0000000	M2FS
LMC	NGC 1806	N1806-1-b093	75.507268	-67.948639	18.61	1.31	4828	4661457649982892288	4.9	286.84 ± 1.65	3.00 ± 0.16	-1.17 ± 0.10	-1.00	-1.00	0100000	M2FS
LMC	NGC 1806	N1806-1-b094	75.502220	-67.969417	18.21	1.05	4701	4661457611282499968	8.3	292.66 ± 0.31	1.26 ± 0.10	-0.89 ± 0.04	0.00	0.00	0000000	M2FS
LMC	NGC 1806	N1806-1-b095	75.510280	-67.971016	18.78	0.96	4882	4661457611284699520	5.2	229.05 ± 0.54	1.95 ± 0.15	-0.85 ± 0.07	0.97	0.97	0000000	M2FS
LMC	NGC 1806	N1806-1-b096	75.517648	-67.995429	17.95	1.19	4616	4661456103794837248	9.9	223.69 ± 0.24	1.20 ± 0.08	-0.65 ± 0.04	0.30	0.01	0000000	M2FS
LMC	NGC 1806	N1806-1-b097	75.439718	-68.019905	18.87	1.31	4909	4661455657096819840	5.1	222.24 ± 0.42	2.25 ± 0.14	-0.53 ± 0.06	0.00	0.00	0000000	M2FS
LMC	NGC 1806	N1806-1-b098	75.437260	-68.008697	18.23	1.27	4707	4661456030765232000	7.6	257.31 ± 0.38	1.74 ± 0.10	-0.61 ± 0.05	0.00	0.00	0000000	M2FS
LMC	NGC 1806	N1806-1-b099	75.424853	-68.008436	18.97	0.90	4937	4661455652796690432	5.5	208.88 ± 0.58	1.70 ± 0.16	-0.76 ± 0.07	0.00	0.00	0000000	M2FS
LMC	NGC 1806	N1806-1-b100	75.421409	-68.004491	18.64	1.20	4838	4661455863276495744	6.8	280.67 ± 0.39	2.04 ± 0.11	-0.59 ± 0.05	0.00	0.00	0000000	M2FS
LMC	NGC 1806	N1806-1-b101	75.429171	-67.996638	18.85	1.02	4903	4661456030765928064	5.9	283.56 ± 0.45	1.36 ± 0.17	-0.74 ± 0.06	0.00	0.00	0000000	M2FS
LMC	NGC 1806	N1806-1-b102	75.426648	-67.987385	18.56	0.97	4814	4661456275593341440	5.8	259.77 ± 0.43	1.67 ± 0.14	-0.78 ± 0.06	0.00	0.00	0000000	M2FS
LMC	NGC 1806	N1806-1-b103	75.413736	-67.980842	16.65	1.64	4159	4661456275593326720	16.7	274.03 ± 0.18	1.20 ± 0.04	-0.49 ± 0.04	0.00	0.00	0000000	M2FS
LMC	NGC 1806	N1806-1-b104	75.423756	-67.980590	16.18	1.74	3974	4661456275593331712	23.8	310.32 ± 0.20	0.85 ± 0.04	-0.60 ± 0.03	0.00	0.00	0000000	M2FS
LMC	NGC 1806	N1806-1-b106	75.457992	-68.011164	18.92	1.07	4922	4661456035075219584	5.2	289.09 ± 0.55	1.16 ± 0.21	-0.69 ± 0.07	0.00	0.00	0000000	M2FS
LMC	NGC 1806	N1806-1-b107	75.457405	-68.006178	18.94	1.11	4927	4661456030765230976	5.0	235.78 ± 0.60	1.45 ± 0.22	-0.96 ± 0.08	0.00	0.00	0000000	M2FS
LMC	NGC 1806	N1806-1-b108	75.455755	-67.999593	17.95	1.16	4615	4661456065094099456	5.9	241.93 ± 0.43	0.59 ± 0.20	-1.30 ± 0.06	0.00	0.00	0000000	M2FS
LMC	NGC 1806	N1806-1-b109	75.445337	-67.999129	18.72	1.11	4865	4661456030765232896	6.3	265.73 ± 0.36	1.45 ± 0.14	-0.84 ± 0.06	0.00	0.00	0000000	M2FS
LMC	NGC 1806	N1806-1-b110	75.455328	-67.989262	17.44	1.37	4443	4661456065094158208	12.4	234.56 ± 0.23	1.28 ± 0.06	-0.58 ± 0.03	0.00	0.00	0000000	M2FS
LMC	NGC 1806	N1806-1-b111	75.449860	-67.985711	16.97	1.60	4277	4661456065094176256	14.4	231.25 ± 0.18	0.90 ± 0.05	-0.79 ± 0.03	0.81	0.81	0000000	M2FS
LMC	NGC 1806	N1806-1-b112	75.466243	-67.985360	18.99	1.11	4942	4661456168175650432	5.0	273.53 ± 0.46	2.20 ± 0.17	-0.51 ± 0.07	0.00	0.00	0000000	M2FS
LMC	NGC 1806	N1806-1-b114	75.499817	-67.935887	18.96	1.07	4932	4661457817460474112	5.5	235.59 ± 0.43	2.10 ± 0.14	-0.58 ± 0.06	0.00	0.00	0000000	M2FS
LMC	NGC 1806	N1806-1-b115	75.502452	-67.940282	16.33	1.81	4037	4661457821781572736	19.7	255.78 ± 0.17	1.03 ± 0.04	-0.53 ± 0.04	0.00	0.00	0000000	M2FS
LMC	NGC 1806	N1806-1-b116	75.472456	-67.943686	18.71	0.96	4860	4661457714381167744	6.2	291.51 ± 0.36	1.57 ± 0.13	-0.56 ± 0.05	0.00	0.00	0000000	M2FS
LMC	NGC 1806	N1806-1-b117	75.471936	-67.948077	18.31	1.13	4733	4661457714381163392	8.6	250.09 ± 0.29	1.55 ± 0.09	-0.66 ± 0.04	0.00	0.00	0000000	M2FS
LMC	NGC 1806	N1806-1-b118	75.501352	-67.956243	18.86	1.07	4905	4661457714381264896	4.9	276.16 ± 0.41	1.80 ± 0.20	-0.59 ± 0.06	0.00	0.00	0000000	M2FS
LMC	NGC 1806	N1806-1-b119	75.475574	-67.979735	18.96	0.98	4934	4661456168173425280	4.8	229.68 ± 0.59	1.81 ± 0.19	-0.52 ± 0.07	0.94	0.95	0000000	M2FS
LMC	NGC 1806	N1806-1-b120	75.498852	-67.985622	16.70	1.48	4178	4661456103794698496	18.3	298.96 ± 0.18	0.57 ± 0.04	-0.76 ± 0.03	0.00	0.00	0000000	M2FS
LMC	NGC 1806	N1806-1-b122	75.452554	-67.960595	18.53	1.13	4806	4661456202564652032	7.6	270.23 ± 0.94	3.54 ± 0.21	-2.09 ± 0.10	-1.00	-1.00	0100000	M2FS
LMC	NGC 1806	N1806-1-b123	75.422155	-67.965880	17.71	0.99	4536	4661456378672533504	12.0	298.67 ± 0.38	1.21 ± 0.08	-1.30 ± 0.04	0.00	0.00	0000000	M2FS
LMC	NGC 1806	N1806-1-b124	75.415255	-67.969637	16.30	1.75	4025	4661456378672532736	18.6	208.13 ± 0.20	0.59 ± 0.04	-0.75 ± 0.03	0.00	0.00	0000000	M2FS
LMC	NGC 1806	N1806-1-b125	75.430141	-67.971604	18.07	1.19	4654	4661456378672543104	9.3	282.36 ± 0.35	1.29 ± 0.09	-0.57 ± 0.04	0.00	0.00	0000000	M2FS
LMC	NGC 1806	N1806-1-b126	75.417788	-67.975650	18.13	1.23	4675	4661456275571997696	7.4	273.60 ± 0.32	1.05 ± 0.14	-1.11 ± 0.05	0.00	0.00	0000000	M2FS
LMC	NGC 1806	N1806-1-b127	75.459566	-67.977078	18.74	1.06	4870	4661456168175672960	7.1	230.78 ± 0.36	1.64 ± 0.12	-0.71 ± 0.05	0.88	0.89	0000000	M2FS

Table C.1: (*continued*) Sample of 3095 Targets from 26 Star Clusters

Galaxy	Cluster	ID	RAJ2000 (deg)	DEJ2000 (deg)	G (mag)	$G_{\rm BP} - G_{\rm RP}$ (mag)	$T_{\rm eff}$ (K)	*Gaia* DR2 ID	S/N	$v_{\rm los}$ ($\rm km\,s^{-1}$)	$\log g$ (dex)	$[\rm Fe/H]_{\rm raw}$ (dex)	P_M	P'_M	Flag[a]	Source[b]
(1)	(2)	(3)	(4)	(5)	(6)	(7)	(8)	(9)	(10)	(11)	(12)	(13)	(14)	(15)	(16)	(17)
LMC	NGC 1806	N1806-1-b128	75.459385	-67.980567	18.38	1.22	4757	4661456168173420032	6.5	303.04 ± 0.32	1.60 ± 0.12	-0.57 ± 0.05	0.00	0.00	0000000	M2FS
LMC	NGC 1806	N1806-1-r049	75.567671	-67.992558	14.79	2.09	3910	4661455382240368256	39.6	229.15 ± 0.39	0.87 ± 0.06	-0.68 ± 0.05	1.00	1.00	0000010	M2FS
LMC	NGC 1806	N1806-1-r127	75.576955	-67.984664	15.27	1.93	3910	4661456855368246400	35.2	269.55 ± 0.29	0.98 ± 0.05	-0.59 ± 0.04	0.00	0.00	0000000	M2FS
LMC	NGC 1806	N1806-1-r028	75.516278	-67.986723	15.99	1.70	3910	4661456138133193088	26.3	227.43 ± 0.12	0.89 ± 0.04	-0.65 ± 0.03	0.99	0.98	0000000	M2FS+Mu14
LMC	NGC 1806	N1806-1-r079	75.515356	-67.979272	15.97	1.76	3910	4661456138154441728	25.3	229.81 ± 0.14	0.87 ± 0.04	-0.61 ± 0.03	0.98	0.98	0000000	M2FS+Mu14
LMC	NGC 1806	1806-25	75.568519	-67.980821	–	–	–	–	–	231.53 ± 0.20	–	–	1.00	1.00	0000000	Mu14
LMC	NGC 1806	1806-27	75.563940	-67.983553	–	–	–	–	–	230.03 ± 0.20	–	–	1.00	1.00	0000000	Mu14
LMC	NGC 1806	1806-30	75.547372	-67.991805	–	–	–	–	–	227.93 ± 0.20	–	–	1.00	1.00	0000000	Mu14
LMC	NGC 1806	1806-40	75.532303	-67.986833	–	–	–	–	–	229.93 ± 0.20	–	–	1.00	1.00	0000000	Mu14
LMC	NGC 1806	1806-33	75.563853	-67.994906	–	–	–	–	–	228.83 ± 0.20	–	–	0.99	0.99	0000000	Mu14
LMC	NGC 1806	1806-39	75.590867	-67.958843	–	–	–	–	–	230.23 ± 0.20	–	–	0.91	0.92	0000000	Mu14
LMC	NGC 1831	N1831-1-b002	76.621821	-64.954339	16.89	1.22	4562	4663805961962183552	13.7	295.27 ± 0.22	1.08 ± 0.07	-0.62 ± 0.03	0.00	0.00	0000000	M2FS
LMC	NGC 1831	N1831-1-b003	76.607780	-64.950372	18.88	0.98	5307	4663805961962185856	3.8	283.44 ± 0.58	3.26 ± 0.18	-0.41 ± 0.09	-1.00	-1.00	0001000	M2FS
LMC	NGC 1831	N1831-1-b004	76.607217	-64.939994	18.70	0.93	5307	4663805966262529920	5.0	274.34 ± 0.57	2.64 ± 0.15	-0.35 ± 0.07	0.62	0.53	0000000	M2FS
LMC	NGC 1831	N1831-1-b005	76.617047	-64.939756	17.54	1.06	4788	4663806000632305536	11.2	262.97 ± 0.69	2.25 ± 0.10	-1.49 ± 0.05	-1.00	-1.00	0100000	M2FS
LMC	NGC 1831	N1831-1-b006	76.595117	-64.937474	16.46	1.51	4523	4663806722177277184	18.4	226.68 ± 0.15	0.96 ± 0.06	-1.01 ± 0.03	0.00	0.00	0000000	M2FS
LMC	NGC 1831	N1831-1-b007	76.615649	-64.933172	18.02	1.03	4964	4663806000632304768	8.1	294.41 ± 0.33	1.64 ± 0.13	-0.59 ± 0.05	0.00	0.00	0000000	M2FS
LMC	NGC 1831	N1831-1-b008	76.608767	-64.925986	18.12	0.17	5001	4663806756537018880	9.6	264.88 ± 37.61	1.15 ± 1.23	-4.53 ± 0.18	-1.00	-1.00	1000010	M2FS
LMC	NGC 1831	N1831-1-b009	76.694638	-65.007850	18.02	1.12	4964	4663805102968671104	2.6	283.72 ± 0.86	1.36 ± 0.44	-0.72 ± 0.11	0.00	0.00	0000000	M2FS
LMC	NGC 1831	N1831-1-b011	76.636042	-64.947886	17.79	1.15	4882	4663805961962188416	7.0	292.76 ± 0.43	1.74 ± 0.14	-0.79 ± 0.05	0.00	0.00	0000000	M2FS
LMC	NGC 1831	N1831-1-b012	76.622811	-64.947330	18.77	1.10	5307	4663805961962189312	2.7	282.63 ± 1.13	2.19 ± 0.57	-0.33 ± 0.11	0.00	0.00	0000000	M2FS
LMC	NGC 1831	N1831-1-b013	76.646819	-64.946884	18.82	1.12	5307	4663805927602451328	4.3	314.85 ± 0.59	2.94 ± 0.18	-0.29 ± 0.08	0.00	0.00	0000000	M2FS
LMC	NGC 1831	N1831-1-b014	76.645316	-64.942902	18.35	0.99	5092	4663805927602456448	3.6	276.64 ± 0.93	2.60 ± 0.20	-0.54 ± 0.10	0.75	0.75	0000000	M2FS
LMC	NGC 1831	N1831-1-b015	76.649862	-64.935284	17.52	1.38	4779	4663806034992044800	10.8	282.52 ± 0.29	1.53 ± 0.12	-0.49 ± 0.04	0.00	0.00	0000000	M2FS
LMC	NGC 1831	N1831-1-b016	76.637150	-64.934247	18.69	0.97	5307	4663805996321944704	4.0	277.00 ± 0.92	2.99 ± 0.17	-0.45 ± 0.10	0.92	0.92	0000000	M2FS
LMC	NGC 1831	N1831-1-b019	76.671929	-64.850950	18.48	1.03	5161	4663900519961240576	6.0	299.15 ± 0.42	2.44 ± 0.14	-0.44 ± 0.06	0.00	0.00	0000000	M2FS
LMC	NGC 1831	N1831-1-b020	76.659222	-64.852219	17.86	1.40	4907	4663900519961239808	8.7	300.19 ± 0.26	2.51 ± 0.08	-0.39 ± 0.04	0.00	0.00	0000010	M2FS
LMC	NGC 1831	N1831-1-b021	76.669107	-64.886495	17.59	1.25	4806	4663900111946466816	9.4	276.89 ± 0.32	2.15 ± 0.09	-0.44 ± 0.04	0.85	0.86	0000000	M2FS
LMC	NGC 1831	N1831-1-b022	76.658627	-64.919149	18.97	1.00	5307	4663806069351803392	2.8	275.61 ± 0.60	3.39 ± 0.21	-0.43 ± 0.11	-1.00	-1.00	0001000	M2FS
LMC	NGC 1831	N1831-1-b023	76.738833	-64.920485	18.91	1.07	5307	4663899660967965312	1.8	301.71 ± 1.48	2.53 ± 0.53	-0.39 ± 0.17	0.00	0.00	0000000	M2FS
LMC	NGC 1831	N1831-1-b024	76.768654	-64.926889	18.99	1.05	5307	4663899660974648192	3.3	284.82 ± 0.64	2.84 ± 0.21	-0.30 ± 0.09	0.00	0.00	0000000	M2FS
LMC	NGC 1831	N1831-1-b025	76.626120	-64.887881	18.88	0.99	5307	4663900764781495168	2.8	276.17 ± 1.19	2.18 ± 0.32	-0.42 ± 0.12	0.70	0.70	0000000	M2FS
LMC	NGC 1831	N1831-1-b026	76.630287	-64.891757	18.78	1.09	5307	4663899974499596288	0.7	252.99 ± 37.49	2.51 ± 1.06	-0.49 ± 0.54	-1.00	-1.00	1000000	M2FS
LMC	NGC 1831	N1831-1-b027	76.626577	-64.898652	17.71	1.20	4851	4663899970205414912	7.1	277.35 ± 0.39	2.07 ± 0.12	-0.35 ± 0.05	0.93	0.93	0000000	M2FS
LMC	NGC 1831	N1831-1-b028	76.637443	-64.904890	18.78	0.94	5307	4663899970212089728	3.1	280.41 ± 1.05	2.82 ± 0.24	-0.41 ± 0.12	0.29	0.28	0000000	M2FS
LMC	NGC 1831	N1831-1-b029	76.643022	-64.908456	18.33	1.01	5082	4663806138061909632	3.5	278.00 ± 0.62	2.22 ± 0.26	-0.47 ± 0.08	0.89	0.89	0000000	M2FS
LMC	NGC 1831	N1831-1-b030	76.624834	-64.911316	18.90	1.03	5307	4663806138071279488	1.5	270.37 ± 0.82	2.32 ± 0.49	0.07 ± 0.14	0.00	0.00	0000000	M2FS
LMC	NGC 1831	N1831-1-b031	76.636901	-64.912393	18.33	1.07	5083	4663806133760916864	3.6	268.43 ± 0.55	1.82 ± 0.29	-0.40 ± 0.08	0.00	0.00	0000000	M2FS
LMC	NGC 1831	N1831-1-b032	76.622741	-64.925007	16.81	1.59	4530	4663806103711520256	8.8	251.32 ± 0.31	1.69 ± 0.09	-0.43 ± 0.04	0.00	0.00	0000010	M2FS
LMC	NGC 1831	N1831-1-b034	76.567945	-64.958101	18.16	1.16	5014	4663806305559562496	3.8	293.05 ± 0.51	2.43 ± 0.18	-0.41 ± 0.07	0.00	0.00	0000000	M2FS
LMC	NGC 1831	N1831-1-b035	76.567798	-64.952615	18.47	1.03	5155	4663806305559568128	4.9	274.46 ± 0.61	2.53 ± 0.18	-0.39 ± 0.08	0.60	0.49	0000000	M2FS
LMC	NGC 1831	N1831-1-b036	76.576131	-64.947404	16.88	1.45	4555	4663806344229494016	14.9	269.87 ± 0.23	1.45 ± 0.06	-0.52 ± 0.03	0.00	0.00	0000000	M2FS
LMC	NGC 1831	N1831-1-b037	76.573456	-64.941030	16.86	1.16	4551	4663806344229493376	15.6	277.51 ± 0.20	0.90 ± 0.07	-0.70 ± 0.03	0.95	0.95	0000000	M2FS
LMC	NGC 1831	N1831-1-b038	76.573205	-64.937540	18.24	1.10	5045	4663806722176760448	6.7	273.74 ± 0.31	2.59 ± 0.09	-0.35 ± 0.05	1.00	1.00	0000000	M2FS
LMC	NGC 1831	N1831-1-b039	76.578564	-64.929157	18.21	0.68	5035	4663806722177234944	8.5	276.59 ± 0.31	1.99 ± 0.12	-0.46 ± 0.04	1.00	1.00	0000010	M2FS
LMC	NGC 1831	N1831-1-b040	76.573620	-64.925505	18.20	0.66	5032	4663806722177213440	2.6	277.27 ± 1.02	2.13 ± 0.34	-0.45 ± 0.10	1.00	1.00	0000010	M2FS
LMC	NGC 1831	N1831-1-b042	76.584447	-64.947504	18.87	0.89	5307	4663806344229494528	5.1	275.76 ± 0.53	2.79 ± 0.14	-0.33 ± 0.06	0.90	0.89	0000000	M2FS
LMC	NGC 1831	N1831-1-b043	76.581941	-64.943529	18.68	0.88	5307	4663806344229494400	3.0	276.59 ± 0.92	2.90 ± 0.26	-0.20 ± 0.10	0.92	0.91	0000000	M2FS
LMC	NGC 1831	N1831-1-b044	76.591688	-64.942334	18.80	1.03	5307	4663806717876439680	4.8	270.34 ± 0.66	2.72 ± 0.16	-0.67 ± 0.08	0.00	0.00	0000000	M2FS
LMC	NGC 1831	N1831-1-b045	76.580714	-64.935688	17.91	0.92	4924	4663806722186615552	6.4	280.03 ± 0.51	2.01 ± 0.14	-1.01 ± 0.07	-1.00	-1.00	0000001	M2FS
LMC	NGC 1831	N1831-1-b046	76.587823	-64.932460	18.17	1.04	5020	4663806722177267072	7.9	274.78 ± 0.30	1.62 ± 0.14	-0.55 ± 0.04	1.00	1.00	0000000	M2FS
LMC	NGC 1831	N1831-1-b047	76.586583	-64.927228	18.27	0.70	5057	4663806752236222464	8.7	279.24 ± 0.38	2.02 ± 0.12	-0.68 ± 0.05	1.00	1.00	0000010	M2FS
LMC	NGC 1831	N1831-1-b048	76.588847	-64.923682	18.55	0.79	5205	4663806756536994688	5.1	278.58 ± 0.63	3.11 ± 0.14	-0.49 ± 0.08	1.00	1.00	0000000	M2FS
LMC	NGC 1831	N1831-1-b049	76.609235	-64.894395	18.04	0.71	4974	4663900726119660032	5.6	278.11 ± 0.92	2.32 ± 0.21	-1.54 ± 0.10	0.88	0.88	0000010	M2FS

Table C.1: (*continued*) Sample of 3095 Targets from 26 Star Clusters

Galaxy	Cluster	ID	RAJ2000 (deg)	DEJ2000 (deg)	G (mag)	$G_{\rm BP} - G_{\rm RP}$ (mag)	$T_{\rm eff}$ (K)	*Gaia* DR2 ID	S/N	$v_{\rm los}$ ($\rm km\,s^{-1}$)	$\log g$ (dex)	$[{\rm Fe/H}]_{\rm raw}$ (dex)	P_M	P'_M	Flag[a]	Source[b]
(1)	(2)	(3)	(4)	(5)	(6)	(7)	(8)	(9)	(10)	(11)	(12)	(13)	(14)	(15)	(16)	(17)
LMC	NGC 1831	N1831-1-b050	76.618222	-64.894717	18.95	1.16	5307	4663900730421750016	3.2	282.76 ± 0.98	1.99 ± 0.43	-0.64 ± 0.13	0.00	0.00	0000000	M2FS
LMC	NGC 1831	N1831-1-b051	76.608093	-64.900257	18.04	0.82	4973	4663806893985521792	6.6	296.67 ± 0.49	1.82 ± 0.14	-0.69 ± 0.06	0.00	0.00	0000000	M2FS
LMC	NGC 1831	N1831-1-b053	76.609677	-64.910807	18.44	1.00	5136	4663806855315424384	1.7	274.97 ± 1.47	1.41 ± 0.52	-0.15 ± 0.14	1.00	1.00	0000000	M2FS
LMC	NGC 1831	N1831-1-b054	76.602846	-64.915391	17.69	1.19	4842	4663806859625760768	5.1	276.03 ± 0.46	2.36 ± 0.14	-0.29 ± 0.06	1.00	1.00	0000000	M2FS
LMC	NGC 1831	N1831-1-b055	76.610541	-64.917723	18.69	0.96	5307	4663806855315418496	4.0	276.72 ± 0.63	2.99 ± 0.18	-0.25 ± 0.08	1.00	1.00	0000000	M2FS
LMC	NGC 1831	N1831-1-b056	76.619366	-64.918206	15.05	2.04	4523	4663806103711519616	16.2	278.54 ± 0.35	2.71 ± 0.09	-0.09 ± 0.06	0.90	0.89	0000010	M2FS
LMC	NGC 1831	N1831-1-b058	76.592525	-64.884539	18.11	1.32	4998	4663900726119662464	5.6	305.46 ± 0.38	2.70 ± 0.12	-0.36 ± 0.06	0.00	0.00	0000010	M2FS
LMC	NGC 1831	N1831-1-b059	76.584688	-64.889235	18.89	1.02	5307	4663806962695597952	4.2	277.34 ± 0.63	1.93 ± 0.25	-0.56 ± 0.08	0.92	0.92	0000000	M2FS
LMC	NGC 1831	N1831-1-b060	76.600155	-64.893389	18.87	0.83	5307	4663900730421746432	3.7	272.06 ± 0.79	2.73 ± 0.21	-0.31 ± 0.10	0.02	0.01	0000000	M2FS
LMC	NGC 1831	N1831-1-b061	76.584208	-64.898863	16.77	1.16	4523	4663806893985519616	8.5	277.25 ± 0.26	0.64 ± 0.10	-0.80 ± 0.04	1.00	1.00	0000000	M2FS
LMC	NGC 1831	N1831-1-b062	76.598765	-64.904317	18.47	0.69	5152	4663806889675167872	4.1	276.51 ± 0.85	2.15 ± 0.27	-0.54 ± 0.09	1.00	1.00	0000000	M2FS
LMC	NGC 1831	N1831-1-b063	76.594497	-64.908523	18.21	0.88	5035	4663806859616400128	4.9	276.60 ± 0.37	1.89 ± 0.22	-0.53 ± 0.06	1.00	1.00	0000000	M2FS
LMC	NGC 1831	N1831-1-b064	76.592499	-64.917605	17.74	0.82	4862	4663806859616196864	10.7	278.99 ± 0.32	1.94 ± 0.08	-0.62 ± 0.04	1.00	1.00	0000000	M2FS
LMC	NGC 1831	N1831-1-b066	76.541856	-64.939135	18.45	1.05	5142	4663806408638798976	6.0	278.52 ± 0.44	2.13 ± 0.20	-0.40 ± 0.05	0.90	0.90	0000000	M2FS
LMC	NGC 1831	N1831-1-b067	76.542837	-64.934756	18.77	0.80	5307	4663806412939099904	4.6	276.92 ± 0.64	2.89 ± 0.16	-0.35 ± 0.07	1.00	1.00	0000000	M2FS
LMC	NGC 1831	N1831-1-b068	76.544953	-64.924157	18.13	0.83	5006	4663806790906265344	7.0	277.39 ± 0.37	2.14 ± 0.14	-0.52 ± 0.05	1.00	1.00	0000000	M2FS
LMC	NGC 1831	N1831-1-b069	76.553892	-64.923899	18.22	0.46	5037	4663806790906267904	15.7	278.87 ± 1.21	2.46 ± 0.17	-2.62 ± 0.07	-1.00	-1.00	0100010	M2FS
LMC	NGC 1831	N1831-1-b070	76.548899	-64.921101	18.03	0.93	4970	4663806790906233600	4.5	275.65 ± 0.66	1.67 ± 0.23	-0.52 ± 0.06	1.00	1.00	0000000	M2FS
LMC	NGC 1831	N1831-1-b071	76.553688	-64.918198	18.02	0.43	4964	4663806825265919616	6.0	279.85 ± 0.67	2.10 ± 0.18	-0.63 ± 0.07	1.00	1.00	0000010	M2FS
LMC	NGC 1831	N1831-1-b072	76.535661	-64.918087	18.29	0.88	5068	4663806790896382976	8.5	277.26 ± 0.35	2.34 ± 0.11	-0.50 ± 0.05	1.00	1.00	0000000	M2FS
LMC	NGC 1831	N1831-1-b073	76.558388	-64.949656	18.88	0.99	5307	4663806309859897856	2.6	275.48 ± 0.76	2.81 ± 0.29	-0.22 ± 0.10	0.88	0.86	0000000	M2FS
LMC	NGC 1831	N1831-1-b074	76.562331	-64.944725	18.37	0.91	5101	4663806339919314176	6.8	292.17 ± 0.38	2.18 ± 0.14	-0.48 ± 0.05	0.00	0.00	0000000	M2FS
LMC	NGC 1831	N1831-1-b075	76.561150	-64.940130	18.12	0.97	5001	4663806412948968320	6.5	268.38 ± 0.47	1.68 ± 0.15	-0.62 ± 0.06	0.00	0.00	0000000	M2FS
LMC	NGC 1831	N1831-1-b076	76.557198	-64.936038	18.70	0.74	5307	4663806412948967680	3.6	307.72 ± 18.01	4.05 ± 0.90	-3.02 ± 0.38	-1.00	-1.00	1000000	M2FS
LMC	NGC 1831	N1831-1-b077	76.564933	-64.932752	18.25	1.10	5048	4663806790906271488	6.9	275.58 ± 0.38	2.62 ± 0.10	-0.40 ± 0.05	1.00	1.00	0000000	M2FS
LMC	NGC 1831	N1831-1-b078	76.564799	-64.929114	17.90	0.97	4923	4663806790896678912	7.4	280.71 ± 0.41	2.08 ± 0.14	-0.47 ± 0.05	1.00	1.00	0000000	M2FS
LMC	NGC 1831	N1831-1-b079	76.554539	-64.928415	18.53	0.94	5194	4663806790896661760	4.3	275.27 ± 0.69	2.85 ± 0.17	-0.38 ± 0.08	1.00	1.00	0000000	M2FS
LMC	NGC 1831	N1831-1-b080	76.564250	-64.922161	18.05	0.34	4974	4663806825265888640	5.9	275.69 ± 0.99	2.21 ± 0.18	-0.99 ± 0.09	1.00	1.00	0000010	M2FS
LMC	NGC 1831	N1831-1-b081	76.578596	-64.879862	18.61	1.12	5253	4663900794839140352	1.8	297.34 ± 1.51	3.26 ± 0.38	-0.73 ± 0.22	-1.00	-1.00	0001000	M2FS
LMC	NGC 1831	N1831-1-b082	76.575917	-64.897956	18.44	0.99	5139	4663806962695596800	3.3	277.86 ± 0.95	2.71 ± 0.23	-0.49 ± 0.11	1.00	1.00	0000000	M2FS
LMC	NGC 1831	N1831-1-b083	76.575339	-64.905266	15.42	1.73	4523	4663806924034910976	20.2	275.16 ± 0.27	2.58 ± 0.06	-0.13 ± 0.05	1.00	1.00	0000010	M2FS
LMC	NGC 1831	N1831-1-b084	76.582393	-64.907192	18.61	0.74	5259	4663806859616393088	2.0	277.57 ± 1.54	3.84 ± 0.32	-0.39 ± 0.18	-1.00	-1.00	0001000	M2FS
LMC	NGC 1831	N1831-1-b085	76.583128	-64.911688	18.50	0.68	5176	4663806859616161024	3.9	272.32 ± 0.99	2.82 ± 0.20	-0.25 ± 0.09	1.00	-1.00	0000000	M2FS
LMC	NGC 1831	N1831-1-b086	76.579846	-64.915918	15.07	1.83	4523	4663806756546384000	17.2	277.29 ± 0.31	2.84 ± 0.08	-0.02 ± 0.05	1.00	1.00	0000010	M2FS
LMC	NGC 1831	N1831-1-b087	76.569481	-64.917445	16.30	0.82	4523	4663806825256314624	14.4	277.37 ± 0.28	1.52 ± 0.07	-0.58 ± 0.04	1.00	1.00	0000010	M2FS
LMC	NGC 1831	N1831-1-b088	76.572443	-64.921517	17.26	0.76	4687	4663806756536737536	4.0	276.67 ± 0.56	2.44 ± 0.15	-0.15 ± 0.08	1.00	1.00	0000010	M2FS
LMC	NGC 1831	N1831-1-b089	76.565032	-64.884826	18.84	0.95	5307	4663806958394665472	2.9	276.68 ± 0.67	2.92 ± 0.26	-0.35 ± 0.10	0.93	0.93	0000000	M2FS
LMC	NGC 1831	N1831-1-b090	76.559666	-64.893289	18.36	0.99	5098	4663806958394659584	5.3	277.00 ± 0.44	2.17 ± 0.15	-0.40 ± 0.06	0.93	0.93	0000000	M2FS
LMC	NGC 1831	N1831-1-b091	76.563742	-64.903605	18.44	0.89	5140	4663806928335849216	2.3	277.12 ± 1.25	2.32 ± 0.70	-0.60 ± 0.16	1.00	1.00	0000000	M2FS
LMC	NGC 1831	N1831-1-b092	76.567571	-64.907738	18.47	0.75	5155	4663806928335858176	2.6	276.71 ± 0.93	2.52 ± 0.34	-0.54 ± 0.15	1.00	1.00	0000000	M2FS
LMC	NGC 1831	N1831-1-b093	76.559113	-64.908524	18.49	0.73	5164	4663806825256380672	4.0	270.97 ± 0.68	3.27 ± 0.15	-0.14 ± 0.08	-1.00	-1.00	0001000	M2FS
LMC	NGC 1831	N1831-1-b094	76.555335	-64.911781	17.62	0.89	4818	4663806820956157696	8.2	279.23 ± 0.41	1.75 ± 0.11	-0.67 ± 0.05	1.00	1.00	0000000	M2FS
LMC	NGC 1831	N1831-1-b095	76.566853	-64.911916	17.74	0.42	4860	4663806825265873536	3.5	276.66 ± 1.04	2.48 ± 0.24	-0.77 ± 0.13	1.00	1.00	0000010	M2FS
LMC	NGC 1831	N1831-1-b096	76.561989	-64.915078	17.98	0.24	4951	4663806825265858944	5.3	278.20 ± 1.42	2.42 ± 0.33	-1.98 ± 0.15	-1.00	-1.00	0100010	M2FS
LMC	NGC 1831	N1831-1-b098	76.496399	-65.002981	18.56	0.50	5219	4663804621932338560	4.7	200.18 ± 2.96	1.71 ± 0.87	-3.22 ± 0.26	-1.00	-1.00	1000010	M2FS
LMC	NGC 1831	N1831-1-b100	76.331079	-64.950206	16.03	1.58	4523	4663808130935862912	15.3	274.22 ± 0.24	1.84 ± 0.07	-0.37 ± 0.04	0.00	0.00	0000010	M2FS
LMC	NGC 1831	N1831-1-b101	76.321092	-64.941232	18.86	0.97	5307	4663808130925854336	3.0	296.04 ± 0.70	3.13 ± 0.21	-0.51 ± 0.11	0.00	0.00	0000000	M2FS
LMC	NGC 1831	N1831-1-b102	76.496404	-64.936461	17.07	1.27	4623	4663806584747656320	14.1	278.91 ± 0.26	1.30 ± 0.07	-0.59 ± 0.03	0.23	0.23	0000000	M2FS
LMC	NGC 1831	N1831-1-b103	76.483479	-64.935845	17.91	1.01	4925	4663806584747655936	11.5	291.30 ± 0.27	1.70 ± 0.09	-0.53 ± 0.04	0.00	0.00	0000000	M2FS
LMC	NGC 1831	N1831-1-b104	76.478828	-64.931069	16.85	1.09	4545	4663806653467132416	18.4	321.03 ± 0.21	0.43 ± 0.08	-1.05 ± 0.03	0.00	0.00	0000000	M2FS
LMC	NGC 1831	N1831-1-b105	76.519515	-65.032320	18.94	1.02	5307	4663804140907782912	1.6	292.01 ± 2.86	3.04 ± 0.44	-0.65 ± 0.24	0.00	0.00	0000000	M2FS
LMC	NGC 1831	N1831-1-b106	76.527880	-64.953783	17.64	1.38	4826	4663806271199827840	11.5	295.02 ± 0.24	1.80 ± 0.09	-0.52 ± 0.03	0.00	0.00	0000010	M2FS
LMC	NGC 1831	N1831-1-b107	76.509153	-64.942210	17.47	1.20	4762	4663806580437485824	14.3	303.73 ± 0.22	1.38 ± 0.07	-0.71 ± 0.03	0.00	0.00	0000000	M2FS
LMC	NGC 1831	N1831-1-b108	76.512203	-64.937490	18.26	0.99	5055	4663806584747656704	2.9	269.88 ± 1.02	1.77 ± 0.33	-0.53 ± 0.10	0.00	0.00	0000000	M2FS

Table C.1: (*continued*) Sample of 3095 Targets from 26 Star Clusters

Galaxy	Cluster	ID	RAJ2000 (deg)	DEJ2000 (deg)	G (mag)	$G_{\rm BP} - G_{\rm RP}$ (mag)	$T_{\rm eff}$ (K)	*Gaia* DR2 ID	S/N	$v_{\rm los}$ ($\rm km\,s^{-1}$)	$\log g$ (dex)	$[{\rm Fe/H}]_{\rm raw}$ (dex)	P_M	P'_M	Flag[a]	Source[b]
(1)	(2)	(3)	(4)	(5)	(6)	(7)	(8)	(9)	(10)	(11)	(12)	(13)	(14)	(15)	(16)	(17)
LMC	NGC 1831	N1831-1-b109	76.526644	-64.935326	18.21	1.04	5033	4663806408638803072	7.6	276.10 ± 0.45	2.05 ± 0.12	-0.45 ± 0.05	0.95	0.95	0000000	M2FS
LMC	NGC 1831	N1831-1-b110	76.522692	-64.923265	17.46	1.23	4760	4663806619107417856	11.2	276.01 ± 0.24	1.80 ± 0.08	-0.42 ± 0.04	1.00	1.00	0000000	M2FS
LMC	NGC 1831	N1831-1-b111	76.513925	-64.922175	18.12	1.07	5000	4663806614797246464	8.5	272.77 ± 0.28	1.74 ± 0.12	-0.49 ± 0.04	0.09	0.03	0000000	M2FS
LMC	NGC 1831	N1831-1-b112	76.524064	-64.913122	18.03	0.54	4970	4663806997064538496	11.8	380.95 ± 1.78	2.56 ± 0.26	-2.92 ± 0.09	-1.00	-1.00	0100010	M2FS
LMC	NGC 1831	N1831-1-b113	76.540867	-64.884497	16.32	1.43	4523	4663807168863422080	20.6	315.45 ± 0.18	0.82 ± 0.05	-0.83 ± 0.03	0.00	0.00	0000000	M2FS
LMC	NGC 1831	N1831-1-b114	76.541283	-64.892784	18.26	0.73	5054	4663807130193352064	5.1	118.08 ± 1.23	3.07 ± 0.18	-1.33 ± 0.11	-1.00	-1.00	0100000	M2FS
LMC	NGC 1831	N1831-1-b115	76.541348	-64.897678	18.07	0.97	4981	4663807130193347840	5.4	276.72 ± 0.64	2.09 ± 0.19	-0.61 ± 0.06	0.96	0.95	0000000	M2FS
LMC	NGC 1831	N1831-1-b116	76.554920	-64.901292	18.29	0.92	5067	4663806928335843712	3.7	277.08 ± 1.00	1.98 ± 0.27	-0.48 ± 0.09	1.00	1.00	0000000	M2FS
LMC	NGC 1831	N1831-1-b117	76.550791	-64.905040	18.86	0.82	5307	4663806825266040064	3.9	276.42 ± 1.01	2.84 ± 0.21	-0.16 ± 0.09	-1.00	-1.00	0000001	M2FS
LMC	NGC 1831	N1831-1-b118	76.540479	-64.906930	18.16	0.95	5016	4663806820955701760	5.9	276.51 ± 0.53	1.96 ± 0.17	-0.55 ± 0.06	1.00	1.00	0000000	M2FS
LMC	NGC 1831	N1831-1-b119	76.546742	-64.911485	18.07	0.65	4982	4663806825256134016	7.9	276.73 ± 0.78	1.96 ± 0.16	-1.27 ± 0.07	1.00	1.00	0000010	M2FS
LMC	NGC 1831	N1831-1-b120	76.545219	-64.917295	18.20	0.66	5030	4663806790906113536	5.5	276.60 ± 0.60	2.23 ± 0.18	-0.44 ± 0.06	1.00	1.00	0000010	M2FS
LMC	NGC 1831	N1831-1-b123	76.525278	-64.890294	17.98	1.09	4949	4663807130193353728	6.4	276.85 ± 0.52	2.37 ± 0.12	-0.37 ± 0.05	0.94	0.94	0000000	M2FS
LMC	NGC 1831	N1831-1-b124	76.523888	-64.896178	18.35	0.81	5092	4663807027114133632	3.9	267.19 ± 0.69	2.43 ± 0.24	-0.92 ± 0.12	0.00	0.00	0000000	M2FS
LMC	NGC 1831	N1831-1-b125	76.361389	-64.904181	18.06	1.31	4978	4663809775893190144	2.5	288.16 ± 0.65	2.66 ± 0.21	-0.35 ± 0.10	0.00	0.00	0000000	M2FS
LMC	NGC 1831	N1831-1-b126	76.521330	-64.907466	18.19	1.00	5026	4663807031414532096	5.5	273.97 ± 0.47	1.97 ± 0.20	-0.48 ± 0.06	0.67	0.55	0000000	M2FS
LMC	NGC 1831	N1831-1-b127	76.529064	-64.909238	18.20	1.10	5030	4663807027114664704	6.2	275.43 ± 0.56	2.25 ± 0.15	-0.61 ± 0.06	1.00	1.00	0000000	M2FS
LMC	NGC 1831	N1831-1-b128	76.536577	-64.911365	17.80	0.90	4885	4663806820956235136	7.3	275.15 ± 0.52	1.38 ± 0.14	-0.93 ± 0.06	-1.00	-1.00	0000001	M2FS
LMC	NGC 1831	N1831-1-r028	76.535272	-64.925112	17.51	1.08	4776	4663806786596496512	14.1	277.54 ± 0.21	1.43 ± 0.08	-0.57 ± 0.03	1.00	1.00	0000000	M2FS
LMC	NGC 1831	N1831-1-r049	76.597573	-64.929841	18.14	1.13	5006	4663806756537013632	9.2	276.64 ± 0.38	1.88 ± 0.10	-0.62 ± 0.05	1.00	1.00	0000000	M2FS
LMC	NGC 1831	N1831-1-r079	76.581185	-64.921483	17.88	0.66	4915	4663806756546387328	7.6	278.98 ± 0.48	1.98 ± 0.14	-0.68 ± 0.06	1.00	1.00	0000010	M2FS
LMC	NGC 1831	N1831-1-r127	76.597240	-64.920757	16.85	1.27	4547	4663806756537005696	18.0	275.77 ± 0.20	1.21 ± 0.06	-0.55 ± 0.03	1.00	1.00	0000000	M2FS
LMC	NGC 1841	N1841-1-b002	71.809265	-84.032196	18.98	1.29	5069	4614892263053582464	2.7	213.02 ± 1.24	1.36 ± 0.61	-2.23 ± 0.19	0.00	0.00	0000000	M2FS
LMC	NGC 1841	N1841-1-b004	71.592041	-84.021049	18.12	1.33	4870	4614892537931499264	3.9	209.45 ± 0.77	1.34 ± 0.47	-2.11 ± 0.12	1.00	1.00	0000000	M2FS
LMC	NGC 1841	N1841-1-b005	71.615318	-84.018039	16.90	1.50	4557	4614892473508916352	9.8	210.99 ± 0.48	0.55 ± 0.20	-2.10 ± 0.05	1.00	1.00	0000000	M2FS
LMC	NGC 1841	N1841-1-b006	71.576327	-84.012500	18.17	1.30	4883	4614892537931508992	6.3	214.57 ± 0.66	0.80 ± 0.35	-2.02 ± 0.08	1.00	1.00	0000000	M2FS
LMC	NGC 1841	N1841-1-b007	71.622296	-84.011835	17.73	1.38	4779	4614892572291248512	5.3	210.88 ± 0.85	0.59 ± 0.35	-1.82 ± 0.09	1.00	1.00	0000000	M2FS
LMC	NGC 1841	N1841-1-b008	71.687597	-84.007885	18.21	1.33	4892	4614892503571776384	3.8	213.57 ± 1.21	1.28 ± 0.44	-2.20 ± 0.16	1.00	1.00	0000000	M2FS
LMC	NGC 1841	N1841-1-b009	72.592375	-84.141672	18.06	1.33	4855	4614864534745755008	2.6	21.41 ± 0.97	4.29 ± 0.18	-0.60 ± 0.17	-1.00	-1.00	0001100	M2FS
LMC	NGC 1841	N1841-1-b010	72.394064	-84.135297	18.56	1.24	4982	4614865256300267008	2.7	95.84 ± 0.74	4.42 ± 0.17	-0.48 ± 0.16	-1.00	-1.00	0001100	M2FS
LMC	NGC 1841	N1841-1-b011	72.394887	-84.120486	18.73	1.22	5019	4614865294955873408	3.1	55.42 ± 0.82	4.58 ± 0.15	-0.14 ± 0.15	-1.00	-1.00	0001100	M2FS
LMC	NGC 1841	N1841-1-b012	72.060859	-84.081395	18.62	1.14	4995	4614865737336645248	3.6	22.10 ± 0.59	4.11 ± 0.11	-0.16 ± 0.10	-1.00	-1.00	0001100	M2FS
LMC	NGC 1841	N1841-1-b013	72.498286	-84.059092	17.82	1.17	4800	4614889101957633280	7.2	-2.98 ± 0.48	3.36 ± 0.07	-0.28 ± 0.06	-1.00	-1.00	0001100	M2FS
LMC	NGC 1841	N1841-1-b015	72.246064	-84.050635	18.38	1.28	4938	4614889205036854144	4.2	-46.25 ± 0.58	4.07 ± 0.11	-0.22 ± 0.10	-1.00	-1.00	0001100	M2FS
LMC	NGC 1841	N1841-1-b016	71.895722	-84.011589	18.47	1.19	4960	4614892400492555264	4.8	14.05 ± 0.59	3.65 ± 0.09	-0.30 ± 0.08	-1.00	-1.00	0001100	M2FS
LMC	NGC 1841	N1841-1-b017	72.285563	-83.909328	17.92	1.29	4823	4614894947409857024	2.7	13.64 ± 0.58	4.77 ± 0.14	-0.34 ± 0.15	-1.00	-1.00	0001100	M2FS
LMC	NGC 1841	N1841-1-b018	72.602437	-83.936512	18.85	1.14	5045	4614891919456294784	0.6	91.59 ± 2.87	4.29 ± 0.50	0.47 ± 0.40	-1.00	-1.00	0001100	M2FS
LMC	NGC 1841	N1841-1-b019	72.255129	-83.963775	19.02	1.14	5077	4614894393357433600	3.2	200.82 ± 0.91	1.23 ± 0.37	-1.05 ± 0.13	-1.00	-1.00	0000100	M2FS
LMC	NGC 1841	N1841-1-b020	72.163045	-83.971158	18.36	1.27	4931	4614892920185294848	5.4	37.28 ± 0.45	4.28 ± 0.09	-0.67 ± 0.09	-1.00	-1.00	0001100	M2FS
LMC	NGC 1841	N1841-1-b021	72.166867	-83.985275	16.99	1.47	4581	4614892885825556736	9.3	210.66 ± 0.37	0.25 ± 0.17	-2.02 ± 0.05	0.00	0.00	0000000	M2FS
LMC	NGC 1841	N1841-1-b022	72.219402	-83.989262	19.03	1.28	5078	4614889926591416320	2.6	11.06 ± 0.89	4.45 ± 0.25	-0.91 ± 0.18	-1.00	-1.00	0001100	M2FS
LMC	NGC 1841	N1841-1-b023	72.316572	-83.990466	17.74	1.34	4782	4614889926591413248	7.2	13.56 ± 0.39	3.72 ± 0.07	-0.18 ± 0.06	-1.00	-1.00	0001100	M2FS
LMC	NGC 1841	N1841-1-b024	72.569946	-84.028002	18.00	1.40	4841	4614889552930937600	5.3	25.87 ± 0.33	4.91 ± 0.07	-0.50 ± 0.08	-1.00	-1.00	0001100	M2FS
LMC	NGC 1841	N1841-1-b025	71.809185	-83.890668	17.13	1.35	4616	4614895634604621312	8.1	1.70 ± 0.30	3.65 ± 0.06	-0.32 ± 0.06	-1.00	-1.00	0001100	M2FS
LMC	NGC 1841	N1841-1-b026	71.773101	-83.911900	17.75	1.32	4783	4614894736954867840	6.7	8.06 ± 0.40	4.31 ± 0.07	-0.27 ± 0.07	-1.00	-1.00	0001100	M2FS
LMC	NGC 1841	N1841-1-b029	71.705462	-83.972473	17.31	1.37	4662	4614893087687366528	7.2	210.58 ± 0.43	0.89 ± 0.22	-2.07 ± 0.06	1.00	1.00	0000000	M2FS
LMC	NGC 1841	N1841-1-b030	71.714462	-83.983368	17.40	1.44	4686	4614892641010753792	9.3	214.31 ± 0.36	0.29 ± 0.18	-1.95 ± 0.05	1.00	1.00	0000000	M2FS
LMC	NGC 1841	N1841-1-b031	71.769030	-83.992116	17.84	1.28	4804	4614892641010743936	7.6	21.10 ± 0.44	3.85 ± 0.06	-0.23 ± 0.06	-1.00	-1.00	0001100	M2FS
LMC	NGC 1841	N1841-1-b033	71.425153	-84.066126	18.45	1.16	4953	4614868898432583424	3.2	31.02 ± 1.69	3.79 ± 0.17	-0.36 ± 0.13	-1.00	-1.00	0001100	M2FS
LMC	NGC 1841	N1841-1-b034	71.342605	-84.025563	19.03	1.00	5079	4614869791784695424	1.4	207.15 ± 4.41	2.46 ± 0.89	-2.38 ± 0.39	-1.00	-1.00	1000000	M2FS
LMC	NGC 1841	N1841-1-b035	71.361541	-84.015529	17.93	1.27	4826	4614869830441330432	5.2	212.50 ± 0.83	1.19 ± 0.39	-1.97 ± 0.10	1.00	1.00	0000000	M2FS
LMC	NGC 1841	N1841-1-b036	71.408945	-84.014259	18.48	1.22	4962	4614869830440096256	2.5	210.75 ± 1.71	1.03 ± 0.56	-1.85 ± 0.19	1.00	1.00	0000000	M2FS
LMC	NGC 1841	N1841-1-b037	71.377785	-84.012496	17.01	1.35	4585	4614869830441329536	11.1	210.17 ± 0.29	0.72 ± 0.15	-1.95 ± 0.04	1.00	1.00	0000000	M2FS
LMC	NGC 1841	N1841-1-b038	71.410788	-84.004434	18.30	1.08	4916	4614893298142632576	3.7	212.34 ± 1.17	1.62 ± 0.47	-1.98 ± 0.13	1.00	1.00	0000000	M2FS

Table C.1: (*continued*) Sample of 3095 Targets from 26 Star Clusters

Galaxy	Cluster	ID	RAJ2000 (deg)	DEJ2000 (deg)	G (mag)	$G_{\rm BP} - G_{\rm RP}$ (mag)	$T_{\rm eff}$ (K)	*Gaia* DR2 ID	S/N	$v_{\rm los}$ ($\rm km\,s^{-1}$)	$\log g$ (dex)	$[{\rm Fe/H}]_{\rm raw}$ (dex)	P_M	P'_M	Flag[a]	Source[b]
(1)	(2)	(3)	(4)	(5)	(6)	(7)	(8)	(9)	(10)	(11)	(12)	(13)	(14)	(15)	(16)	(17)
LMC	NGC 1841	N1841-1-b039	71.324374	-84.004017	17.69	1.24	4770	4614869826145862400	3.1	209.58 ± 1.05	1.36 ± 0.43	-1.77 ± 0.13	1.00	1.00	0000000	M2FS
LMC	NGC 1841	N1841-1-b040	71.366263	-83.995257	18.56	0.96	4980	4614893293846225280	2.3	211.90 ± 1.82	2.39 ± 0.62	-1.69 ± 0.23	1.00	1.00	0000000	M2FS
LMC	NGC 1841	N1841-1-b042	71.422413	-84.037759	17.03	1.44	4590	4614869040166120448	9.5	209.77 ± 0.36	0.35 ± 0.19	-1.83 ± 0.05	1.00	1.00	0000000	M2FS
LMC	NGC 1841	N1841-1-b043	71.508129	-84.017402	18.28	1.18	4911	4614869074527086976	3.0	212.59 ± 1.61	1.01 ± 0.51	-1.94 ± 0.16	1.00	1.00	0000000	M2FS
LMC	NGC 1841	N1841-1-b044	71.456249	-84.016026	17.75	1.32	4783	4614869074527086848	4.6	211.55 ± 0.60	0.98 ± 0.36	-2.01 ± 0.10	1.00	1.00	0000000	M2FS
LMC	NGC 1841	N1841-1-b045	71.421203	-84.010034	16.93	1.45	4564	4614893298142634624	6.3	217.25 ± 0.47	0.63 ± 0.27	-2.04 ± 0.07	1.00	-1.00	0000000	M2FS
LMC	NGC 1841	N1841-1-b046	71.528758	-84.009418	19.17	1.10	5103	4614892537931975296	0.9	211.52 ± 14.34	2.61 ± 1.09	-1.55 ± 0.51	-1.00	-1.00	1000000	M2FS
LMC	NGC 1841	N1841-1-b047	71.561909	-84.004812	17.59	1.32	4744	4614892572291714816	2.3	210.60 ± 0.96	1.50 ± 0.45	-1.64 ± 0.15	1.00	1.00	0000000	M2FS
LMC	NGC 1841	N1841-1-b048	71.466242	-84.004253	17.08	1.38	4606	4614893298142633472	7.3	213.37 ± 0.51	0.41 ± 0.23	-1.97 ± 0.06	1.00	1.00	0000000	M2FS
LMC	NGC 1841	N1841-1-b049	71.580808	-83.871647	17.27	1.48	4653	4614895703324096384	7.2	50.54 ± 0.24	4.30 ± 0.07	-0.26 ± 0.07	-1.00	-1.00	0001100	M2FS
LMC	NGC 1841	N1841-1-b050	71.669914	-83.898711	19.02	1.18	5077	4614895527228860544	2.6	200.20 ± 0.91	1.00 ± 0.40	-1.09 ± 0.14	-1.00	-1.00	0000100	M2FS
LMC	NGC 1841	N1841-1-b051	71.576107	-83.914904	18.53	1.19	4973	4614894084119835648	2.5	-2.84 ± 1.08	4.26 ± 0.16	-0.33 ± 0.14	-1.00	-1.00	0001100	M2FS
LMC	NGC 1841	N1841-1-b052	71.590919	-83.975291	18.09	1.33	4864	4614892709730240384	4.5	211.62 ± 0.72	0.54 ± 0.32	-1.97 ± 0.10	1.00	1.00	0000000	M2FS
LMC	NGC 1841	N1841-1-b053	71.548052	-83.989383	18.68	1.33	5009	4614892675374340096	4.0	209.85 ± 0.96	1.32 ± 0.49	-2.04 ± 0.12	1.00	1.00	0000000	M2FS
LMC	NGC 1841	N1841-1-b054	71.580573	-83.991949	17.90	1.37	4818	4614892675370484480	7.7	213.54 ± 0.50	1.47 ± 0.23	-2.05 ± 0.07	1.00	1.00	0000000	M2FS
LMC	NGC 1841	N1841-1-b055	71.684389	-83.993617	17.93	1.35	4824	4614892606651004544	3.6	210.16 ± 1.80	0.71 ± 0.42	-2.56 ± 0.17	-1.00	-1.00	0100000	M2FS
LMC	NGC 1841	N1841-1-b056	71.628348	-84.000912	18.72	1.23	5018	4614892572291261056	6.1	210.21 ± 0.77	1.60 ± 0.28	-1.78 ± 0.08	1.00	1.00	0000000	M2FS
LMC	NGC 1841	N1841-1-b057	71.443688	-83.919965	17.67	1.38	4765	4614894054056655616	8.7	211.44 ± 0.41	0.68 ± 0.22	-2.05 ± 0.06	0.00	0.00	0000000	M2FS
LMC	NGC 1841	N1841-1-b061	71.521563	-83.973150	18.66	1.27	5003	4614893465644487168	3.4	210.36 ± 1.27	0.97 ± 0.41	-1.47 ± 0.13	-1.00	-1.00	0000001	M2FS
LMC	NGC 1841	N1841-1-b062	71.457541	-83.991669	17.89	1.33	4815	4614893328205960704	6.0	212.60 ± 0.61	0.98 ± 0.36	-1.94 ± 0.08	1.00	1.00	0000000	M2FS
LMC	NGC 1841	N1841-1-b063	71.492571	-83.994655	18.09	1.23	4863	4614893328206911232	6.1	206.25 ± 0.78	1.21 ± 0.30	-1.94 ± 0.08	1.00	1.00	0000000	M2FS
LMC	NGC 1841	N1841-1-b064	71.511202	-84.003075	18.98	1.04	5070	4614892537934742656	2.9	68.50 ± 1.22	4.36 ± 0.16	-0.20 ± 0.15	-1.00	-1.00	0001100	M2FS
LMC	NGC 1841	N1841-1-b065	71.217554	-84.021290	17.29	1.39	4658	4614869864801068928	8.9	209.87 ± 0.42	0.49 ± 0.21	-1.94 ± 0.05	1.00	1.00	0000000	M2FS
LMC	NGC 1841	N1841-1-b066	71.252303	-84.016258	19.13	1.03	5096	4614869864801068032	1.1	191.01 ± 91.69	1.58 ± 1.14	-2.22 ± 0.65	-1.00	-1.00	1000000	M2FS
LMC	NGC 1841	N1841-1-b068	71.229829	-84.011572	17.89	1.26	4817	4614869860504652160	5.5	211.91 ± 0.76	0.80 ± 0.30	-1.98 ± 0.09	1.00	1.00	0000000	M2FS
LMC	NGC 1841	N1841-1-b069	71.258746	-84.009823	18.30	1.26	4915	4614869894864391424	3.8	210.36 ± 0.89	1.21 ± 0.42	-1.81 ± 0.12	1.00	1.00	0000000	M2FS
LMC	NGC 1841	N1841-1-b070	71.206167	-84.000429	16.82	1.46	4534	4614869899160797312	9.3	211.17 ± 0.36	0.78 ± 0.17	-2.05 ± 0.05	1.00	1.00	0000000	M2FS
LMC	NGC 1841	N1841-1-b071	71.221089	-83.995862	17.46	1.28	4704	4614869899160795264	6.3	212.39 ± 0.54	0.73 ± 0.26	-2.13 ± 0.07	1.00	1.00	0000000	M2FS
LMC	NGC 1841	N1841-1-b072	71.255435	-83.992827	18.21	1.22	4893	4614893362565705216	2.9	205.11 ± 1.46	1.08 ± 0.54	-2.11 ± 0.18	1.00	1.00	0000000	M2FS
LMC	NGC 1841	N1841-1-b073	71.345823	-84.101509	18.60	1.22	4991	4614868318612702208	1.8	55.35 ± 0.77	3.86 ± 0.24	-0.48 ± 0.22	-1.00	-1.00	0001100	M2FS
LMC	NGC 1841	N1841-1-b074	71.264669	-84.020143	18.62	1.15	4995	4614869791785173504	2.5	209.82 ± 1.60	0.95 ± 0.55	-1.75 ± 0.19	1.00	1.00	0000000	M2FS
LMC	NGC 1841	N1841-1-b075	71.326635	-84.018730	19.18	0.98	5105	4614869791785173632	1.4	207.61 ± 10.04	0.77 ± 0.52	-1.16 ± 0.36	-1.00	-1.00	1000000	M2FS
LMC	NGC 1841	N1841-1-b076	71.286864	-84.013266	19.17	1.06	5103	4614869796080353536	1.8	207.00 ± 1.80	0.91 ± 0.62	-1.83 ± 0.22	1.00	1.00	0000000	M2FS
LMC	NGC 1841	N1841-1-b077	71.292287	-84.007657	18.88	1.06	5050	4614869899159559680	1.7	214.06 ± 1.56	1.95 ± 0.83	-1.91 ± 0.27	1.00	1.00	0000000	M2FS
LMC	NGC 1841	N1841-1-b078	71.287610	-84.001749	18.59	1.07	4988	4614869899159538048	2.6	209.07 ± 1.45	1.62 ± 0.66	-1.77 ± 0.17	1.00	1.00	0000000	M2FS
LMC	NGC 1841	N1841-1-b079	71.257020	-83.999204	18.39	1.11	4939	4614869894864400000	2.8	208.53 ± 1.40	2.17 ± 0.45	-1.96 ± 0.17	1.00	1.00	0000000	M2FS
LMC	NGC 1841	N1841-1-b080	71.291288	-83.995265	17.54	1.19	4731	4614893366862101120	5.8	210.07 ± 0.89	1.24 ± 0.32	-2.05 ± 0.09	1.00	1.00	0000000	M2FS
LMC	NGC 1841	N1841-1-b081	71.377441	-83.964194	17.37	1.39	4677	4614893500004237312	6.6	211.85 ± 0.56	0.75 ± 0.28	-2.03 ± 0.07	1.00	1.00	0000000	M2FS
LMC	NGC 1841	N1841-1-b082	71.405413	-83.973026	18.60	1.20	4990	4614893431284748928	3.1	210.91 ± 1.30	1.20 ± 0.56	-1.87 ± 0.16	1.00	1.00	0000000	M2FS
LMC	NGC 1841	N1841-1-b083	71.407438	-83.978532	18.78	1.27	5030	4614893431284743680	2.1	211.07 ± 1.62	1.25 ± 0.65	-2.05 ± 0.24	1.00	1.00	0000000	M2FS
LMC	NGC 1841	N1841-1-b084	71.420744	-83.983207	19.12	0.98	5094	4614893332501053568	2.6	212.76 ± 1.58	2.34 ± 0.65	-2.03 ± 0.17	1.00	1.00	0000000	M2FS
LMC	NGC 1841	N1841-1-b085	71.384562	-83.987245	18.98	1.18	5069	4614893332501059840	2.9	205.63 ± 1.05	1.07 ± 0.49	-1.58 ± 0.14	-1.00	-1.00	0000001	M2FS
LMC	NGC 1841	N1841-1-b086	71.417732	-83.987737	17.97	1.30	4834	4614893328206910848	5.4	208.97 ± 0.89	1.39 ± 0.28	-1.95 ± 0.09	1.00	1.00	0000000	M2FS
LMC	NGC 1841	N1841-1-b087	71.371041	-83.991388	17.70	1.21	4773	4614893293847171968	6.0	211.35 ± 0.53	1.15 ± 0.27	-1.88 ± 0.08	1.00	1.00	0000000	M2FS
LMC	NGC 1841	N1841-1-b088	71.418953	-83.993408	17.51	1.33	4723	4614893328205965184	7.4	207.77 ± 0.49	0.33 ± 0.21	-2.08 ± 0.06	1.00	1.00	0000000	M2FS
LMC	NGC 1841	N1841-1-b089	71.337492	-83.937608	17.42	1.37	4693	4614894122776336640	4.0	210.95 ± 0.83	0.96 ± 0.36	-1.98 ± 0.11	0.00	0.00	0000000	M2FS
LMC	NGC 1841	N1841-1-b090	71.342271	-83.963240	16.66	1.38	4477	4614893504301047296	9.5	37.78 ± 0.34	3.62 ± 0.06	-0.22 ± 0.07	-1.00	-1.00	0001100	M2FS
LMC	NGC 1841	N1841-1-b091	71.320325	-83.978860	18.73	1.31	5020	4614893396928181504	3.8	208.19 ± 1.40	2.29 ± 0.32	-1.79 ± 0.14	1.00	1.00	0000000	M2FS
LMC	NGC 1841	N1841-1-b092	71.366435	-83.980742	17.58	1.38	4742	4614893401221834752	5.6	211.06 ± 0.60	0.78 ± 0.32	-2.02 ± 0.08	1.00	1.00	0000000	M2FS
LMC	NGC 1841	N1841-1-b093	71.279396	-83.981986	17.18	1.43	4629	4614893401221834496	6.0	209.65 ± 0.65	1.05 ± 0.29	-2.10 ± 0.08	1.00	1.00	0000000	M2FS
LMC	NGC 1841	N1841-1-b094	71.301598	-83.984650	18.43	1.19	4948	4614893401221835136	4.7	210.00 ± 0.82	1.29 ± 0.35	-1.86 ± 0.11	1.00	1.00	0000000	M2FS
LMC	NGC 1841	N1841-1-b095	71.344432	-83.988464	17.82	1.26	4800	4614893396926386048	6.6	207.39 ± 0.78	1.42 ± 0.27	-1.91 ± 0.09	1.00	1.00	0000000	M2FS
LMC	NGC 1841	N1841-1-b096	71.312878	-83.992250	17.83	1.21	4803	4614893366862099840	6.8	211.00 ± 0.70	1.36 ± 0.25	-2.04 ± 0.08	1.00	1.00	0000000	M2FS
LMC	NGC 1841	N1841-1-b098	71.021185	-84.023970	17.50	1.38	4717	4614869933520396800	7.1	211.71 ± 0.51	0.38 ± 0.25	-1.97 ± 0.07	1.00	1.00	0000000	M2FS

Table C.1: (*continued*) Sample of 3095 Targets from 26 Star Clusters

Galaxy	Cluster	ID	RAJ2000 (deg)	DEJ2000 (deg)	G (mag)	$G_{\rm BP} - G_{\rm RP}$ (mag)	$T_{\rm eff}$ (K)	*Gaia* DR2 ID	S/N	$v_{\rm los}$ (km s^{-1})	$\log g$ (dex)	$[{\rm Fe/H}]_{\rm raw}$ (dex)	P_M	P'_M	Flag[a]	Source[b]
(1)	(2)	(3)	(4)	(5)	(6)	(7)	(8)	(9)	(10)	(11)	(12)	(13)	(14)	(15)	(16)	(17)
LMC	NGC 1841	N1841-1-b099	70.297782	-84.022191	17.29	1.38	4657	4614881478392482432	5.9	19.82 ± 0.41	3.98 ± 0.08	0.09 ± 0.08	-1.00	-1.00	0001100	M2FS
LMC	NGC 1841	N1841-1-b101	70.932751	-84.018662	18.33	1.16	4924	4614869929223656192	3.5	2.89 ± 0.94	4.36 ± 0.17	-0.73 ± 0.14	-1.00	-1.00	0001100	M2FS
LMC	NGC 1841	N1841-1-b102	70.722769	-84.009106	18.42	1.14	4948	4614881753268844160	4.3	41.67 ± 0.63	3.94 ± 0.10	-0.20 ± 0.10	-1.00	-1.00	0001100	M2FS
LMC	NGC 1841	N1841-1-b103	71.112253	-83.993776	17.69	1.36	4769	4614870105319223424	5.7	210.06 ± 0.63	1.02 ± 0.34	-2.22 ± 0.08	1.00	1.00	0000000	M2FS
LMC	NGC 1841	N1841-1-b104	70.698087	-83.990494	19.04	1.18	5080	4614881787630129152	4.3	126.07 ± 1.02	4.08 ± 0.15	-0.89 ± 0.12	-1.00	-1.00	0001100	M2FS
LMC	NGC 1841	N1841-1-b105	71.155732	-84.010076	17.69	1.30	4771	4614869864801065216	6.7	42.08 ± 0.59	3.59 ± 0.07	-0.24 ± 0.07	-1.00	-1.00	0001100	M2FS
LMC	NGC 1841	N1841-1-b106	71.178928	-84.007457	18.75	1.17	5024	4614869864799811712	2.7	206.75 ± 1.46	1.06 ± 0.50	-2.02 ± 0.18	1.00	1.00	0000000	M2FS
LMC	NGC 1841	N1841-1-b107	71.177061	-84.003152	18.23	1.23	4898	4614869894864392320	2.8	211.65 ± 1.41	2.25 ± 0.56	-2.07 ± 0.18	1.00	1.00	0000000	M2FS
LMC	NGC 1841	N1841-1-b110	71.150394	-83.996739	17.80	1.33	4796	4614870101022823040	5.1	211.53 ± 0.92	1.20 ± 0.32	-2.00 ± 0.10	1.00	1.00	0000000	M2FS
LMC	NGC 1841	N1841-1-b111	71.180764	-83.994979	17.62	1.30	4752	4614869899160794240	5.5	210.96 ± 0.59	0.73 ± 0.31	-1.87 ± 0.08	1.00	1.00	0000000	M2FS
LMC	NGC 1841	N1841-1-b114	71.219221	-83.925656	17.33	1.32	4667	4614894122776335872	9.0	-16.99 ± 0.28	3.91 ± 0.06	-0.34 ± 0.06	-1.00	-1.00	0001100	M2FS
LMC	NGC 1841	N1841-1-b115	71.178390	-83.940177	18.78	1.25	5029	4614893740522427648	4.8	208.20 ± 0.93	1.19 ± 0.41	-2.07 ± 0.11	0.00	0.00	0000000	M2FS
LMC	NGC 1841	N1841-1-b117	71.188723	-83.972425	17.43	1.41	4696	4614893607380262912	9.8	212.23 ± 0.38	0.89 ± 0.19	-1.94 ± 0.05	1.00	1.00	0000000	M2FS
LMC	NGC 1841	N1841-1-b118	71.171332	-83.978416	18.56	1.30	4981	4614893568723696128	3.3	212.87 ± 2.00	1.57 ± 0.68	-2.41 ± 0.21	-1.00	-1.00	0100000	M2FS
LMC	NGC 1841	N1841-1-b119	71.246944	-83.982914	18.28	1.25	4912	4614893366860787328	4.0	205.72 ± 1.16	2.20 ± 0.34	-2.23 ± 0.13	1.00	1.00	0000000	M2FS
LMC	NGC 1841	N1841-1-b120	71.248872	-83.989405	18.99	1.10	5072	4614893362569109376	2.4	210.27 ± 1.78	1.76 ± 0.86	-1.65 ± 0.21	1.00	1.00	0000000	M2FS
LMC	NGC 1841	N1841-1-b121	70.701537	-83.879746	18.73	1.14	5019	4614906213107507072	2.9	198.14 ± 1.25	3.83 ± 0.15	-0.37 ± 0.12	-1.00	-1.00	0001100	M2FS
LMC	NGC 1841	N1841-1-b123	70.615023	-83.927691	18.28	1.24	4911	4614905663351653760	4.7	-26.08 ± 0.49	4.15 ± 0.09	-0.07 ± 0.08	-1.00	-1.00	0001100	M2FS
LMC	NGC 1841	N1841-1-b124	70.929520	-83.937684	18.24	1.33	4900	4614905525912690048	5.1	-46.97 ± 0.45	4.49 ± 0.09	-0.29 ± 0.08	-1.00	-1.00	0001100	M2FS
LMC	NGC 1841	N1841-1-b125	71.136036	-83.963553	19.07	1.20	5086	4614893603083453056	2.8	212.15 ± 1.80	2.45 ± 0.52	-1.79 ± 0.20	1.00	1.00	0000000	M2FS
LMC	NGC 1841	N1841-1-b126	71.132439	-83.968286	18.61	1.29	4993	4614893603083447552	2.5	206.02 ± 1.38	0.60 ± 0.40	-1.80 ± 0.17	1.00	1.00	0000000	M2FS
LMC	NGC 1841	N1841-1-b127	71.050020	-83.974641	18.98	1.23	5069	4614893637443177344	0.4	1.21 ± 384.36	2.27 ± 1.37	-2.56 ± 1.25	-1.00	-1.00	1000000	M2FS
LMC	NGC 1841	N1841-1-r028	71.318450	-83.998483	17.07	1.31	4602	4614893366862103296	9.4	211.32 ± 0.40	0.87 ± 0.23	-2.30 ± 0.06	-1.00	-1.00	0000001	M2FS
LMC	NGC 1841	N1841-1-r049	71.371408	-84.004153	16.92	1.39	4564	4614893298142632064	5.9	213.22 ± 0.75	0.53 ± 0.25	-2.06 ± 0.08	1.00	1.00	0000000	M2FS
LMC	NGC 1841	N1841-1-r099	71.389316	-83.997979	16.77	1.41	4518	4614893298142627712	15.2	211.45 ± 0.28	0.45 ± 0.15	-1.99 ± 0.04	1.00	1.00	0000000	M2FS
LMC	NGC 1841	N1841-1-r127	71.444873	-83.999280	16.85	1.42	4547	4614893298141374208	9.3	209.02 ± 0.42	0.37 ± 0.20	-2.04 ± 0.05	1.00	1.00	0000000	M2FS
LMC	NGC 1846	N1846-1-b001	76.963303	-67.551070	16.83	1.58	4235	4661811516588698880	15.0	287.98 ± 0.21	0.83 ± 0.05	-0.63 ± 0.03	0.00	0.00	0000000	M2FS
LMC	NGC 1846	N1846-1-b002	76.989781	-67.549459	17.03	1.56	4309	4661811520882995712	16.3	264.56 ± 0.20	1.00 ± 0.04	-0.75 ± 0.03	0.00	0.00	0000000	M2FS
LMC	NGC 1846	N1846-1-b003	76.957930	-67.539223	17.23	1.45	4381	4661811589626839424	14.2	246.96 ± 0.19	0.97 ± 0.05	-0.73 ± 0.03	0.00	0.00	0000000	M2FS
LMC	NGC 1846	N1846-1-b004	76.997971	-67.516428	17.43	1.30	4450	4661813062832549248	12.8	254.71 ± 0.47	0.12 ± 0.09	-0.51 ± 0.06	0.00	0.00	0000000	M2FS
LMC	NGC 1846	N1846-1-b005	76.976339	-67.504899	17.45	1.34	4455	4661813131496525312	12.4	221.33 ± 0.23	0.92 ± 0.06	-0.65 ± 0.03	0.00	0.00	0000000	M2FS
LMC	NGC 1846	N1846-1-b006	76.949481	-67.497958	16.95	1.55	4282	4661813131496544512	14.4	271.31 ± 0.19	1.15 ± 0.05	-0.57 ± 0.03	0.00	0.00	0000000	M2FS
LMC	NGC 1846	N1846-1-b007	76.987201	-67.491377	17.07	1.47	4325	4661813238894290048	14.9	286.79 ± 0.21	1.05 ± 0.05	-0.65 ± 0.03	0.00	0.00	0000000	M2FS
LMC	NGC 1846	N1846-1-b009	77.088657	-67.519734	16.78	1.51	4217	4661812929656669568	15.6	287.39 ± 0.18	0.23 ± 0.08	-1.33 ± 0.03	0.00	0.00	0000000	M2FS
LMC	NGC 1846	N1846-1-b010	77.121747	-67.517620	17.16	1.46	4355	4661809970400559104	13.6	231.93 ± 0.18	0.55 ± 0.06	-1.17 ± 0.03	0.00	0.00	0000000	M2FS
LMC	NGC 1846	N1846-1-b011	77.101437	-67.516156	16.85	1.50	4245	4661812925338063104	15.9	275.80 ± 0.19	0.84 ± 0.05	-0.63 ± 0.03	0.00	0.00	0000000	M2FS
LMC	NGC 1846	N1846-1-b012	77.125855	-67.509543	17.36	1.40	4425	4661810352676302336	12.4	274.74 ± 0.20	0.94 ± 0.06	-0.68 ± 0.03	0.00	0.00	0000000	M2FS
LMC	NGC 1846	N1846-1-b013	77.042561	-67.498696	17.16	1.55	4356	4661812998376136448	12.5	216.81 ± 0.22	0.76 ± 0.06	-0.73 ± 0.03	0.00	0.00	0000000	M2FS
LMC	NGC 1846	N1846-1-b015	77.143968	-67.489989	17.27	1.45	4395	4661810490115260032	13.1	271.03 ± 0.20	0.93 ± 0.06	-0.68 ± 0.03	0.00	0.00	0000000	M2FS
LMC	NGC 1846	N1846-1-b016	77.186731	-67.484896	17.37	1.33	4429	4661810455755531008	13.7	273.19 ± 0.22	1.00 ± 0.05	-0.69 ± 0.03	0.00	0.00	0000000	M2FS
LMC	NGC 1846	N1846-1-b017	77.077979	-67.411702	17.32	1.48	4413	4661819762926316032	8.7	272.44 ± 0.26	1.40 ± 0.07	-0.58 ± 0.04	0.00	0.00	0000000	M2FS
LMC	NGC 1846	N1846-1-b019	77.163784	-67.431501	16.91	1.51	4264	4661819526727291648	19.3	318.50 ± 0.14	0.54 ± 0.04	-0.91 ± 0.03	0.00	0.00	0000000	M2FS
LMC	NGC 1846	N1846-1-b020	77.069342	-67.453737	17.34	1.30	4419	4661813548131956608	16.3	274.41 ± 0.15	0.65 ± 0.06	-1.37 ± 0.03	0.00	0.00	0000000	M2FS
LMC	NGC 1846	N1846-1-b021	77.173279	-67.457186	17.50	1.34	4475	4661816430031549568	13.4	308.68 ± 0.31	1.35 ± 0.08	-1.52 ± 0.04	0.00	0.00	0000000	M2FS
LMC	NGC 1846	N1846-1-b022	77.165005	-67.460902	17.19	1.51	4369	4661816434350985984	13.4	276.57 ± 0.20	0.65 ± 0.05	-0.79 ± 0.03	0.00	0.00	0000000	M2FS
LMC	NGC 1846	N1846-1-b023	77.072825	-67.462473	16.73	1.46	4199	4661813513772219136	19.9	277.80 ± 0.15	0.57 ± 0.04	-0.81 ± 0.03	0.00	0.00	0000000	M2FS
LMC	NGC 1846	N1846-1-b025	77.033603	-67.381265	17.45	1.48	4458	4661820243962756992	12.0	228.48 ± 0.23	1.55 ± 0.06	-0.54 ± 0.04	0.00	0.00	0000000	M2FS
LMC	NGC 1846	N1846-1-b027	77.044036	-67.405834	17.34	1.40	4420	4661819767245391360	15.1	249.67 ± 0.21	1.06 ± 0.05	-0.69 ± 0.03	0.00	0.00	0000000	M2FS
LMC	NGC 1846	N1846-1-b030	76.962050	-67.437165	17.18	1.49	4365	4661814544564249856	13.2	268.99 ± 0.20	0.59 ± 0.06	-1.15 ± 0.03	0.00	0.00	0000000	M2FS
LMC	NGC 1846	N1846-1-b031	77.036007	-67.440131	16.80	1.50	4226	4661813754290272128	20.9	281.87 ± 0.15	0.57 ± 0.04	-1.01 ± 0.03	0.00	0.00	0000000	M2FS
LMC	NGC 1846	N1846-1-b032	77.025958	-67.456740	17.21	1.52	4373	4661813719930638208	13.7	256.59 ± 0.20	0.77 ± 0.06	-0.90 ± 0.03	0.00	0.00	0000000	M2FS
LMC	NGC 1846	N1846-1-b033	76.902555	-67.504560	17.89	1.16	4602	4661813857369543552	9.9	284.63 ± 0.34	1.32 ± 0.08	-0.72 ± 0.04	0.00	0.00	0000000	M2FS
LMC	NGC 1846	N1846-1-b034	76.916082	-67.484642	17.58	1.38	4501	4661813887414759680	8.8	239.78 ± 0.27	1.32 ± 0.07	-0.62 ± 0.04	0.96	0.96	0000000	M2FS
LMC	NGC 1846	N1846-1-b035	76.916687	-67.475350	17.65	1.20	4523	4661813990493975040	10.6	237.57 ± 0.24	1.17 ± 0.07	-0.72 ± 0.04	0.99	0.99	0000000	M2FS

Table C.1: (*continued*) Sample of 3095 Targets from 26 Star Clusters

Galaxy	Cluster	ID	RAJ2000 (deg)	DEJ2000 (deg)	G (mag)	$G_{\rm BP} - G_{\rm RP}$ (mag)	$T_{\rm eff}$ (K)	*Gaia* DR2 ID	S/N	$v_{\rm los}$ ($\rm km\,s^{-1}$)	$\log g$ (dex)	$[{\rm Fe/H}]_{\rm raw}$ (dex)	P_M	P'_M	Flag[a]	Source[b]
(1)	(2)	(3)	(4)	(5)	(6)	(7)	(8)	(9)	(10)	(11)	(12)	(13)	(14)	(15)	(16)	(17)
LMC	NGC 1846	N1846-1-b037	76.900482	-67.468831	17.48	1.21	4467	4661814063527785984	10.3	238.59 ± 0.23	1.25 ± 0.07	-0.67 ± 0.04	1.00	1.00	0000000	M2FS
LMC	NGC 1846	N1846-1-b038	76.908941	-67.466322	16.94	1.31	4276	4661814097887715200	12.7	237.40 ± 0.23	1.06 ± 0.06	-0.59 ± 0.04	1.00	1.00	0000000	M2FS
LMC	NGC 1846	N1846-1-b039	76.914913	-67.460637	16.79	1.34	4221	4661814093573189504	10.9	238.68 ± 0.24	0.99 ± 0.06	-0.56 ± 0.04	1.00	1.00	0000000	M2FS
LMC	NGC 1846	N1846-1-b040	76.904812	-67.458964	16.82	1.18	4231	4661814097887579520	9.6	240.15 ± 0.56	0.08 ± 0.07	-0.45 ± 0.08	-1.00	-1.00	0000001	M2FS
LMC	NGC 1846	N1846-1-b043	76.926418	-67.479485	18.00	1.20	4637	4661813994808513280	5.2	245.81 ± 0.54	1.80 ± 0.13	-0.75 ± 0.07	0.00	0.00	0000000	M2FS
LMC	NGC 1846	N1846-1-b044	76.939629	-67.476185	17.81	1.32	4575	4661814029168257408	10.7	264.24 ± 0.24	1.44 ± 0.07	-0.62 ± 0.04	0.00	0.00	0000000	M2FS
LMC	NGC 1846	N1846-1-b045	76.947411	-67.472186	17.27	1.33	4395	4661814024852092288	8.0	236.41 ± 0.31	1.05 ± 0.07	-0.64 ± 0.04	0.72	0.68	0000000	M2FS
LMC	NGC 1846	N1846-1-b046	76.936439	-67.471822	16.66	1.45	4172	4661814029168356352	14.6	237.52 ± 0.17	0.86 ± 0.04	-0.63 ± 0.03	0.99	0.99	0000000	M2FS
LMC	NGC 1846	N1846-1-b047	76.932149	-67.466246	17.83	1.12	4582	4661814029143864192	7.9	238.01 ± 0.31	1.32 ± 0.09	-0.70 ± 0.04	1.00	1.00	0000000	M2FS
LMC	NGC 1846	N1846-1-b048	76.924057	-67.464261	18.04	1.11	4652	4661814024906688640	8.6	240.26 ± 0.36	1.47 ± 0.10	-0.64 ± 0.04	1.00	1.00	0000000	M2FS
LMC	NGC 1846	N1846-1-b049	76.929123	-67.360007	17.15	1.49	4353	4661820901116687232	12.2	271.28 ± 0.25	0.61 ± 0.07	-1.18 ± 0.04	0.00	0.00	0000000	M2FS
LMC	NGC 1846	N1846-1-b050	76.941323	-67.395180	17.14	1.45	4350	4661820557519313408	12.2	282.04 ± 0.22	1.12 ± 0.05	-0.63 ± 0.03	0.00	0.00	0000000	M2FS
LMC	NGC 1846	N1846-1-b052	76.948719	-67.434918	17.21	1.49	4375	4661814544564247680	12.0	236.71 ± 0.22	0.63 ± 0.06	-0.85 ± 0.03	0.54	0.48	0000000	M2FS
LMC	NGC 1846	N1846-1-b053	76.923522	-67.440959	17.96	1.30	4626	4661814505914158976	9.0	280.20 ± 0.31	1.38 ± 0.09	-0.60 ± 0.04	0.00	0.00	0000000	M2FS
LMC	NGC 1846	N1846-1-b054	76.907320	-67.447758	17.62	1.23	4515	4661814475844761088	10.6	237.86 ± 0.27	1.23 ± 0.07	-0.63 ± 0.04	1.00	1.00	0000000	M2FS
LMC	NGC 1846	N1846-1-b055	76.914434	-67.449986	17.98	1.11	4633	4661814475819730176	9.4	238.91 ± 0.28	1.43 ± 0.08	-0.76 ± 0.04	1.00	1.00	0000000	M2FS
LMC	NGC 1846	N1846-1-b056	76.919739	-67.456192	17.45	1.16	4459	4661814475844847232	11.6	239.42 ± 0.23	0.88 ± 0.07	-0.70 ± 0.03	1.00	1.00	0000000	M2FS
LMC	NGC 1846	N1846-1-b057	76.891786	-67.370059	17.32	1.44	4414	4661820763677716992	10.8	240.14 ± 0.27	1.23 ± 0.06	-0.59 ± 0.04	0.00	0.00	0000000	M2FS
LMC	NGC 1846	N1846-1-b058	76.884633	-67.443153	17.45	1.28	4458	4661814475844641024	13.4	239.83 ± 0.22	1.13 ± 0.06	-0.61 ± 0.03	1.00	1.00	0000000	M2FS
LMC	NGC 1846	N1846-1-b059	76.885204	-67.447123	17.05	1.34	4315	4661814475844641152	10.2	240.29 ± 0.26	0.83 ± 0.06	-0.69 ± 0.04	1.00	1.00	0000000	M2FS
LMC	NGC 1846	N1846-1-b061	76.895048	-67.448224	17.16	1.30	4356	4661814475844757248	12.1	241.40 ± 0.21	0.86 ± 0.06	-0.70 ± 0.03	0.99	0.99	0000000	M2FS
LMC	NGC 1846	N1846-1-b062	76.892772	-67.453800	17.11	1.22	4339	4661814097862554368	12.5	243.24 ± 0.25	0.99 ± 0.06	-0.65 ± 0.04	0.98	0.97	0000000	M2FS
LMC	NGC 1846	N1846-1-b063	76.903609	-67.455354	17.87	0.93	4595	4661814097887594496	8.5	242.10 ± 0.28	1.45 ± 0.09	-0.60 ± 0.04	0.99	0.99	0000010	M2FS
LMC	NGC 1846	N1846-1-b064	76.892598	-67.457515	17.26	1.07	4390	4661814097887596416	8.8	239.47 ± 0.31	0.80 ± 0.09	-0.59 ± 0.04	1.00	1.00	0000010	M2FS
LMC	NGC 1846	N1846-1-b065	76.844199	-67.558750	16.80	1.51	4225	4661811860186061696	15.6	314.17 ± 0.20	0.57 ± 0.05	-0.76 ± 0.03	0.00	0.00	0000000	M2FS
LMC	NGC 1846	N1846-1-b066	76.868735	-67.544663	17.29	1.36	4403	4661812272502959232	9.0	268.11 ± 0.29	1.21 ± 0.06	-0.69 ± 0.04	0.00	0.00	0000000	M2FS
LMC	NGC 1846	N1846-1-b070	76.872907	-67.480188	18.00	1.23	4639	4661813956133069824	8.4	240.26 ± 0.36	1.39 ± 0.10	-0.63 ± 0.04	0.99	0.99	0000000	M2FS
LMC	NGC 1846	N1846-1-b072	76.858761	-67.468950	17.58	1.29	4499	4661814162304777600	11.8	240.53 ± 0.25	1.38 ± 0.06	-0.59 ± 0.03	1.00	0.99	0000000	M2FS
LMC	NGC 1846	N1846-1-b073	76.886079	-67.510340	18.12	1.20	4677	4661812444301739392	8.6	272.51 ± 0.25	1.60 ± 0.09	-0.67 ± 0.04	0.00	0.00	0000000	M2FS
LMC	NGC 1846	N1846-1-b074	76.884714	-67.489438	18.16	1.11	4691	4661813921770550656	8.3	286.05 ± 0.34	1.27 ± 0.10	-0.70 ± 0.04	0.00	0.00	0000000	M2FS
LMC	NGC 1846	N1846-1-b075	76.879501	-67.485032	17.92	1.21	4611	4661813956133059712	9.3	237.78 ± 0.28	1.26 ± 0.08	-0.65 ± 0.04	0.94	0.94	0000000	M2FS
LMC	NGC 1846	N1846-1-b076	76.895691	-67.481911	17.11	1.39	4340	4661813956130315776	14.0	281.20 ± 0.21	0.72 ± 0.05	-0.93 ± 0.03	0.00	0.00	0000000	M2FS
LMC	NGC 1846	N1846-1-b078	76.891643	-67.469640	18.04	0.87	4651	4661814063503523456	6.8	241.27 ± 0.35	1.59 ± 0.11	-0.60 ± 0.05	1.00	0.99	0000010	M2FS
LMC	NGC 1846	N1846-1-b080	76.894089	-67.465473	16.86	1.31	4246	4661814063527824512	11.5	260.14 ± 0.23	1.00 ± 0.06	-0.59 ± 0.04	0.00	0.00	0000000	M2FS
LMC	NGC 1846	N1846-1-b081	76.865362	-67.349782	17.07	1.45	4324	4661820931157644928	11.5	272.37 ± 0.21	0.91 ± 0.06	-0.74 ± 0.04	0.00	0.00	0000000	M2FS
LMC	NGC 1846	N1846-1-b082	76.871925	-67.419313	17.24	1.37	4384	4661814712044751616	11.5	273.62 ± 0.27	0.71 ± 0.07	-0.89 ± 0.03	0.00	0.00	0000000	M2FS
LMC	NGC 1846	N1846-1-b083	76.873375	-67.441039	17.57	1.34	4497	4661814682003065728	12.5	242.83 ± 0.30	0.98 ± 0.07	-0.85 ± 0.03	-1.00	-1.00	0000001	M2FS
LMC	NGC 1846	N1846-1-b085	76.874045	-67.449263	17.97	0.86	4628	4661814304045943552	11.1	238.94 ± 0.32	1.57 ± 0.07	-1.04 ± 0.04	1.00	1.00	0000010	M2FS
LMC	NGC 1846	N1846-1-b086	76.867272	-67.451619	18.10	1.09	4669	4661814299784940672	7.0	264.31 ± 0.81	2.23 ± 0.10	-1.04 ± 0.06	0.00	0.00	0000000	M2FS
LMC	NGC 1846	N1846-1-b087	76.883722	-67.455586	16.86	1.24	4245	4661814093573183488	14.4	239.85 ± 0.23	0.94 ± 0.05	-0.69 ± 0.03	1.00	1.00	0000000	M2FS
LMC	NGC 1846	N1846-1-b088	76.865524	-67.458467	17.01	1.33	4302	4661814269686385920	16.2	238.90 ± 0.21	0.88 ± 0.05	-0.71 ± 0.03	1.00	1.00	0000000	M2FS
LMC	NGC 1846	N1846-1-b089	76.863973	-67.385791	16.84	1.62	4240	4661820793718556288	11.3	209.78 ± 0.21	0.98 ± 0.05	-0.68 ± 0.04	0.00	0.00	0000000	M2FS
LMC	NGC 1846	N1846-1-b090	76.848887	-67.442425	17.53	1.32	4483	4661814299727815168	13.8	271.31 ± 0.24	1.01 ± 0.06	-0.71 ± 0.03	0.00	0.00	0000000	M2FS
LMC	NGC 1846	N1846-1-b095	76.853703	-67.453871	18.14	1.07	4684	4661814269686199168	9.5	235.78 ± 0.30	1.18 ± 0.09	-0.80 ± 0.04	0.97	0.96	0000000	M2FS
LMC	NGC 1846	N1846-1-b097	76.672827	-67.508127	17.16	1.49	4357	4661859139201150464	6.5	264.66 ± 0.37	0.75 ± 0.09	-0.88 ± 0.05	0.00	0.00	0000000	M2FS
LMC	NGC 1846	N1846-1-b098	76.766938	-67.507525	16.99	1.40	4296	4661812586059174144	13.5	315.36 ± 0.23	0.57 ± 0.06	-0.88 ± 0.03	0.00	0.00	0000000	M2FS
LMC	NGC 1846	N1846-1-b099	76.612443	-67.496173	17.33	1.43	4415	4661859418387139584	6.8	250.93 ± 0.39	1.16 ± 0.10	-0.56 ± 0.05	0.00	0.00	0000000	M2FS
LMC	NGC 1846	N1846-1-b100	76.777220	-67.491490	16.83	1.48	4236	4661812689138391040	18.0	316.06 ± 0.20	0.51 ± 0.05	-0.92 ± 0.03	0.00	0.00	0000000	M2FS
LMC	NGC 1846	N1846-1-b103	76.800956	-67.467543	18.11	1.25	4674	4661814200966885120	9.2	277.71 ± 0.27	1.74 ± 0.08	-0.54 ± 0.04	0.00	0.00	0000000	M2FS
LMC	NGC 1846	N1846-1-b105	76.839799	-67.574576	16.89	1.56	4259	4661811761425640832	9.3	275.07 ± 0.29	0.75 ± 0.07	-0.74 ± 0.04	0.00	0.00	0000000	M2FS
LMC	NGC 1846	N1846-1-b106	76.822377	-67.556148	17.38	1.36	4435	4661811864504681856	9.9	274.35 ± 0.25	0.75 ± 0.07	-0.96 ± 0.04	0.00	0.00	0000000	M2FS
LMC	NGC 1846	N1846-1-b111	76.842426	-67.466928	18.25	1.08	4718	4661814166582633472	7.8	240.14 ± 0.39	1.46 ± 0.11	-0.69 ± 0.04	0.99	0.99	0000000	M2FS
LMC	NGC 1846	N1846-1-b112	76.840682	-67.463392	16.90	1.47	4263	4661814166607158144	14.9	240.03 ± 0.23	0.83 ± 0.05	-0.73 ± 0.03	1.00	1.00	0000000	M2FS
LMC	NGC 1846	N1846-1-b114	76.811483	-67.377587	17.39	1.43	4436	4661861853605936896	12.6	288.50 ± 0.24	1.01 ± 0.06	-0.67 ± 0.03	0.00	0.00	0000000	M2FS

Table C.1: (*continued*) Sample of 3095 Targets from 26 Star Clusters

Galaxy	Cluster	ID	RAJ2000 (deg)	DEJ2000 (deg)	G (mag)	$G_{\rm BP} - G_{\rm RP}$ (mag)	$T_{\rm eff}$ (K)	*Gaia* DR2 ID	S/N	$v_{\rm los}$ (km s^{-1})	$\log g$ (dex)	$[{\rm Fe/H}]_{\rm raw}$ (dex)	P_M	P'_M	Flag[a]	Source[b]
(1)	(2)	(3)	(4)	(5)	(6)	(7)	(8)	(9)	(10)	(11)	(12)	(13)	(14)	(15)	(16)	(17)
LMC	NGC 1846	N1846-1-b118	76.837189	-67.428463	17.39	1.42	4435	4661814750722532480	10.6	239.62 ± 0.26	1.20 ± 0.07	-0.66 ± 0.04	0.94	0.94	0000000	M2FS
LMC	NGC 1846	N1846-1-b119	76.833145	-67.442688	17.37	1.39	4429	4661814372765409408	12.6	234.81 ± 0.25	1.27 ± 0.06	-0.58 ± 0.03	0.01	0.00	0000000	M2FS
LMC	NGC 1846	N1846-1-b120	76.824665	-67.453354	17.03	1.57	4309	4661814338405668992	12.3	239.48 ± 0.24	1.03 ± 0.06	-0.64 ± 0.04	0.97	0.97	0000000	M2FS
LMC	NGC 1846	N1846-1-b121	76.746681	-67.385178	16.71	1.51	4189	4661861789209028736	14.7	251.88 ± 0.20	0.60 ± 0.05	-0.72 ± 0.03	0.00	0.00	0000000	M2FS
LMC	NGC 1846	N1846-1-b122	76.635744	-67.405915	17.37	1.38	4428	4661861514313147392	9.0	245.76 ± 0.31	0.15 ± 0.10	-1.08 ± 0.04	0.00	0.00	0000000	M2FS
LMC	NGC 1846	N1846-1-b123	76.745637	-67.407838	17.17	1.40	4361	4661861372569494144	13.5	250.09 ± 0.23	0.87 ± 0.06	-0.79 ± 0.03	0.00	0.00	0000000	M2FS
LMC	NGC 1846	N1846-1-b124	76.621109	-67.411885	17.45	1.42	4456	4661862231562937344	6.8	285.32 ± 0.82	0.43 ± 0.28	-1.87 ± 0.10	0.00	0.00	0000000	M2FS
LMC	NGC 1846	N1846-1-b126	76.632827	-67.437455	17.18	1.43	4362	4661860002502592000	7.9	214.32 ± 0.37	0.47 ± 0.10	-0.94 ± 0.04	0.00	0.00	0000000	M2FS
LMC	NGC 1846	N1846-1-b127	76.702904	-67.453027	17.32	1.49	4412	4661859727624711424	1.1	250.77 ± 1.56	1.48 ± 0.54	0.24 ± 0.35	0.00	0.00	0000000	M2FS
LMC	NGC 1846	N1846-1-b128	76.663265	-67.460030	17.15	1.42	4352	4661859899423490816	5.3	289.30 ± 0.56	0.48 ± 0.18	-1.30 ± 0.07	0.00	0.00	0000000	M2FS
LMC	NGC 1846	N1846-1-r049	76.884175	-67.464323	16.69	1.35	4184	4661814059213445248	11.2	241.96 ± 0.25	0.80 ± 0.05	-0.66 ± 0.04	0.99	0.99	0000000	M2FS
LMC	NGC 1846	N1846-1-r079	76.875467	-67.457687	16.73	1.36	4199	4661814097887699968	18.5	237.80 ± 0.17	0.65 ± 0.05	-0.71 ± 0.03	-1.00	-1.00	0000000	M2FS
LMC	NGC 1846	N1846-1-r099	76.879864	-67.461089	16.59	1.38	4145	4661814063527875968	16.6	239.15 ± 0.19	0.89 ± 0.04	-0.62 ± 0.03	1.00	1.00	0000000	M2FS
LMC	NGC 1846	N1846-1-r127	76.892184	-67.462047	16.61	1.15	4154	4661814093626314496	13.4	239.14 ± 0.20	0.67 ± 0.05	-0.78 ± 0.03	1.00	1.00	0000010	M2FS
LMC	NGC 1846	N1846-1-b036	76.910045	-67.469993	16.64	1.46	4163	4661814063527978496	14.4	237.01 ± 0.18	0.94 ± 0.05	-0.57 ± 0.03	1.00	1.00	0000000	M2FS+Ma13
LMC	NGC 1846	N1846-1-b068	76.876452	-67.493312	17.29	1.43	4404	4661813926089008256	14.2	239.30 ± 0.17	1.09 ± 0.05	-0.64 ± 0.03	0.97	0.97	0000000	M2FS+Ma13
LMC	NGC 1846	N1846-1-b069	76.864168	-67.491053	17.62	1.29	4512	4661813926089000320	14.0	238.80 ± 0.21	1.22 ± 0.06	-0.70 ± 0.03	0.97	0.97	0000000	M2FS+Ma13
LMC	NGC 1846	N1846-1-b071	76.869530	-67.473508	17.21	1.26	4373	4661813956132615168	12.6	238.56 ± 0.20	0.91 ± 0.06	-0.74 ± 0.03	1.00	1.00	0000000	M2FS+Ma13
LMC	NGC 1846	N1846-1-b077	76.893777	-67.473462	17.48	1.15	4466	4661814059213447424	10.0	239.47 ± 0.28	1.25 ± 0.07	-0.66 ± 0.04	1.00	1.00	0000000	M2FS+Ma13
LMC	NGC 1846	N1846-1-b079	76.876663	-67.467907	16.67	1.41	4174	4661814059213444096	14.3	239.54 ± 0.17	0.84 ± 0.04	-0.67 ± 0.03	1.00	1.00	0000000	M2FS+Ma13
LMC	NGC 1846	N1846-1-b084	76.875133	-67.445288	16.78	1.49	4216	4661814304045943808	17.6	239.32 ± 0.18	0.81 ± 0.04	-0.66 ± 0.03	1.00	1.00	0000000	M2FS+Ma13
LMC	NGC 1846	N1846-1-b092	76.848361	-67.447455	16.91	1.45	4266	4661814304045936512	13.6	263.47 ± 0.20	0.98 ± 0.05	-0.71 ± 0.04	0.00	0.00	0000000	M2FS+Ma13
LMC	NGC 1846	N1846-1-b093	76.859490	-67.449180	17.70	1.11	4540	4661814299731611136	10.9	292.18 ± 0.26	0.92 ± 0.07	-0.90 ± 0.04	0.00	0.00	0000000	M2FS+Ma13
LMC	NGC 1846	N1846-1-b094	76.838127	-67.450417	16.74	1.53	4200	4661814269686195456	19.0	249.90 ± 0.18	0.77 ± 0.04	-0.68 ± 0.03	0.00	0.00	0000000	M2FS+Ma13
LMC	NGC 1846	N1846-1-b096	76.840166	-67.457097	17.26	1.28	4393	4661814269686372864	16.8	240.05 ± 0.22	1.09 ± 0.05	-0.62 ± 0.03	1.00	1.00	0000000	M2FS+Ma13
LMC	NGC 1846	N1846-1-b101	76.811033	-67.487760	17.15	1.53	4354	4661812654778660736	16.3	280.33 ± 0.20	1.25 ± 0.05	-0.53 ± 0.03	0.00	0.00	0000000	M2FS+Ma13
LMC	NGC 1846	N1846-1-b102	76.793938	-67.475322	17.79	1.36	4569	4661812719207759232	9.9	280.89 ± 0.26	0.97 ± 0.08	-0.99 ± 0.04	0.00	0.00	0000000	M2FS+Ma13
LMC	NGC 1846	N1846-1-b104	76.809929	-67.463388	17.83	1.35	4583	4661814231008276480	13.9	290.88 ± 0.21	1.07 ± 0.07	-1.03 ± 0.03	0.00	0.00	0000000	M2FS+Ma13
LMC	NGC 1846	N1846-1-b110	76.833048	-67.493631	16.99	1.49	4296	4661812654778667648	18.9	310.77 ± 0.16	0.48 ± 0.05	-1.46 ± 0.03	0.00	0.00	0000000	M2FS+Ma13
LMC	NGC 1846	MCPS-071	76.741170	-67.287080	–	–	–	–	–	261.04 ± 0.54	–	–	0.00	0.00	0000000	Ma13
LMC	NGC 1846	MCPS-066	76.710075	-67.293140	–	–	–	–	–	273.64 ± 0.72	–	–	0.00	0.00	0000000	Ma13
LMC	NGC 1846	MCPS-059	76.669845	-67.273420	–	–	–	–	–	325.02 ± 0.65	–	–	0.00	0.00	0000000	Ma13
LMC	NGC 1846	MCPS-075	76.762935	-67.331450	–	–	–	–	–	237.77 ± 0.52	–	–	0.00	0.00	0000000	Ma13
LMC	NGC 1846	MCPS-050	76.634085	-67.350570	–	–	–	–	–	261.87 ± 0.49	–	–	0.00	0.00	0000000	Ma13
LMC	NGC 1846	MCPS-052	76.644750	-67.352680	–	–	–	–	–	235.66 ± 0.60	–	–	0.00	0.00	0000000	Ma13
LMC	NGC 1846	MCPS-064	76.690785	-67.306630	–	–	–	–	–	272.04 ± 0.54	–	–	0.00	0.00	0000000	Ma13
LMC	NGC 1846	MCPS-042	76.588095	-67.327260	–	–	–	–	–	299.17 ± 0.55	–	–	0.00	0.00	0000000	Ma13
LMC	NGC 1846	MCPS-044	76.609275	-67.356670	–	–	–	–	–	278.65 ± 0.63	–	–	0.00	0.00	0000000	Ma13
LMC	NGC 1846	MCPS-106	76.925205	-67.284870	–	–	–	–	–	243.66 ± 0.55	–	–	0.00	0.00	0000000	Ma13
LMC	NGC 1846	MCPS-096	76.886610	-67.293230	–	–	–	–	–	311.53 ± 0.55	–	–	0.00	0.00	0000000	Ma13
LMC	NGC 1846	MCPS-105	76.916160	-67.293900	–	–	–	–	–	277.79 ± 0.59	–	–	0.00	0.00	0000000	Ma13
LMC	NGC 1846	MCPS-094	76.850175	-67.291410	–	–	–	–	–	247.84 ± 0.54	–	–	0.00	0.00	0000000	Ma13
LMC	NGC 1846	MCPS-082	76.810665	-67.258480	–	–	–	–	–	271.28 ± 0.62	–	–	0.00	0.00	0000000	Ma13
LMC	NGC 1846	MCPS-074	76.757910	-67.322430	–	–	–	–	–	287.43 ± 0.58	–	–	0.00	0.00	0000000	Ma13
LMC	NGC 1846	MCPS-161	77.154660	-67.310160	–	–	–	–	–	237.51 ± 0.58	–	–	0.00	0.00	0000000	Ma13
LMC	NGC 1846	ACS-013-R	76.889943	-67.444777	–	–	–	–	–	238.31 ± 0.46	–	–	1.00	1.00	0000000	Ma13
LMC	NGC 1846	MCPS-139	77.073480	-67.306730	–	–	–	–	–	297.41 ± 0.57	–	–	0.00	0.00	0000000	Ma13
LMC	NGC 1846	MCPS-111	76.949730	-67.386440	–	–	–	–	–	242.89 ± 0.76	–	–	0.00	0.00	0000000	Ma13
LMC	NGC 1846	MCPS-118	76.983855	-67.297630	–	–	–	–	–	299.61 ± 0.49	–	–	0.00	0.00	0000000	Ma13
LMC	NGC 1846	MCPS-137	77.063340	-67.447100	–	–	–	–	–	231.14 ± 0.46	–	–	0.00	0.00	0000000	Ma13
LMC	NGC 1846	MCPS-168	77.173770	-67.337200	–	–	–	–	–	212.83 ± 0.70	–	–	0.00	0.00	0000000	Ma13
LMC	NGC 1846	ACS-090-A	76.875705	-67.462818	–	–	–	–	–	238.23 ± 0.62	–	–	1.00	1.00	0000000	Ma13
LMC	NGC 1846	MCPS-165	77.166855	-67.434940	–	–	–	–	–	312.06 ± 0.42	–	–	0.00	0.00	0000000	Ma13
LMC	NGC 1846	ACS-046-R	76.886005	-67.462650	–	–	–	–	–	237.75 ± 0.62	–	–	1.00	1.00	0000000	Ma13

Table C.1: (*continued*) Sample of 3095 Targets from 26 Star Clusters

Galaxy	Cluster	ID	RAJ2000 (deg)	DEJ2000 (deg)	G (mag)	$G_{\rm BP} - G_{\rm RP}$ (mag)	$T_{\rm eff}$ (K)	*Gaia* DR2 ID	S/N	$v_{\rm los}$ ($\rm km\,s^{-1}$)	$\log g$ (dex)	$[\rm Fe/H]_{\rm raw}$ (dex)	P_M	P'_M	Flag[a]	Source[b]
(1)	(2)	(3)	(4)	(5)	(6)	(7)	(8)	(9)	(10)	(11)	(12)	(13)	(14)	(15)	(16)	(17)
LMC	NGC 1846	ACS-112-A	76.930378	-67.447184	–	–	–	–	–	240.01 ± 0.67	–	–	1.00	1.00	0000000	Ma13
LMC	NGC 1846	ACS-001-R	76.903504	-67.462745	–	–	–	–	–	236.32 ± 0.53	–	–	1.00	1.00	0000000	Ma13
LMC	NGC 1846	ACS-080-A	76.876262	-67.453102	–	–	–	–	–	244.08 ± 0.47	–	–	0.92	-1.00	0000000	Ma13
LMC	NGC 1846	MCPS-142	77.078400	-67.414960	–	–	–	–	–	254.42 ± 0.42	–	–	0.00	0.00	0000000	Ma13
LMC	NGC 1846	MCPS-156	77.129295	-67.463000	–	–	–	–	–	293.09 ± 0.48	–	–	0.00	0.00	0000000	Ma13
LMC	NGC 1846	MCPS-195	77.298990	-67.440750	–	–	–	–	–	241.16 ± 0.54	–	–	0.00	0.00	0000000	Ma13
LMC	NGC 1846	MCPS-184	77.257260	-67.436850	–	–	–	–	–	255.44 ± 0.54	–	–	0.00	0.00	0000000	Ma13
LMC	NGC 1846	MCPS-172	77.198340	-67.434830	–	–	–	–	–	295.41 ± 0.50	–	–	0.00	0.00	0000000	Ma13
LMC	NGC 1846	ACS-066-R	76.956547	-67.483720	–	–	–	–	–	239.64 ± 0.78	–	–	0.96	0.96	0000000	Ma13
LMC	NGC 1846	ACS-051-R	76.902503	-67.459296	–	–	–	–	–	235.81 ± 0.77	–	–	1.00	1.00	0000000	Ma13
LMC	NGC 1846	MCPS-135	77.053230	-67.526940	–	–	–	–	–	289.30 ± 0.43	–	–	0.00	0.00	0000000	Ma13
LMC	NGC 1846	ACS-025-R	76.900772	-67.466334	–	–	–	–	–	238.49 ± 0.49	–	–	1.00	1.00	0000000	Ma13
LMC	NGC 1846	MCPS-162	77.156370	-67.523490	–	–	–	–	–	278.68 ± 0.54	–	–	0.00	0.00	0000000	Ma13
LMC	NGC 1846	MCPS-190	77.275575	-67.521060	–	–	–	–	–	341.16 ± 0.46	–	–	0.00	0.00	0000000	Ma13
LMC	NGC 1846	MCPS-167	77.168805	-67.488850	–	–	–	–	–	285.57 ± 0.55	–	–	0.00	0.00	0000000	Ma13
LMC	NGC 1846	MCPS-200	77.355690	-67.506370	–	–	–	–	–	243.94 ± 0.60	–	–	0.00	0.00	0000000	Ma13
LMC	NGC 1846	ACS-030-R	76.912548	-67.473123	–	–	–	–	–	240.86 ± 0.60	–	–	0.99	0.99	0000000	Ma13
LMC	NGC 1846	MCPS-183	77.256900	-67.591670	–	–	–	–	–	299.81 ± 0.71	–	–	0.00	0.00	0000000	Ma13
LMC	NGC 1846	ACS-059-R	76.869280	-67.479115	–	–	–	–	–	237.96 ± 0.77	–	–	0.99	1.00	0000000	Ma13
LMC	NGC 1846	MCPS-193	77.287635	-67.584790	–	–	–	–	–	268.50 ± 0.72	–	–	0.00	0.00	0000000	Ma13
LMC	NGC 1846	MCPS-166	77.167860	-67.563560	–	–	–	–	–	266.39 ± 0.69	–	–	0.00	0.00	0000000	Ma13
LMC	NGC 1846	MCPS-157	77.137425	-67.595250	–	–	–	–	–	268.99 ± 0.64	–	–	0.00	0.00	0000000	Ma13
LMC	NGC 1846	MCPS-189	77.272755	-67.533840	–	–	–	–	–	284.94 ± 0.65	–	–	0.00	0.00	0000000	Ma13
LMC	NGC 1846	MCPS-176	77.215620	-67.620090	–	–	–	–	–	307.74 ± 0.65	–	–	0.00	0.00	0000000	Ma13
LMC	NGC 1846	MCPS-141	77.077770	-67.602940	–	–	–	–	–	259.77 ± 0.56	–	–	0.00	0.00	0000000	Ma13
LMC	NGC 1846	MCPS-154	77.125035	-67.542530	–	–	–	–	–	231.81 ± 0.74	–	–	0.00	0.00	0000000	Ma13
LMC	NGC 1846	MCPS-103	76.913685	-67.594940	–	–	–	–	–	235.27 ± 0.51	–	–	0.00	0.00	0000000	Ma13
LMC	NGC 1846	MCPS-126	77.028210	-67.624490	–	–	–	–	–	234.65 ± 0.60	–	–	0.00	0.00	0000000	Ma13
LMC	NGC 1846	MCPS-124	77.020230	-67.602780	–	–	–	–	–	262.98 ± 0.43	–	–	0.00	0.00	0000000	Ma13
LMC	NGC 1846	MCPS-136	77.054550	-67.614320	–	–	–	–	–	272.54 ± 0.45	–	–	0.00	0.00	0000000	Ma13
LMC	NGC 1846	MCPS-089	76.840440	-67.610820	–	–	–	–	–	249.61 ± 0.45	–	–	0.00	0.00	0000000	Ma13
LMC	NGC 1846	MCPS-078	76.793460	-67.621420	–	–	–	–	–	311.17 ± 0.70	–	–	0.00	0.00	0000000	Ma13
LMC	NGC 1846	MCPS-079	76.793880	-67.665950	–	–	–	–	–	290.26 ± 0.67	–	–	0.00	0.00	0000000	Ma13
LMC	NGC 1846	MCPS-076	76.780320	-67.597590	–	–	–	–	–	264.04 ± 0.51	–	–	0.00	0.00	0000000	Ma13
LMC	NGC 1846	MCPS-091	76.842735	-67.663820	–	–	–	–	–	240.00 ± 0.55	–	–	0.00	0.00	0000000	Ma13
LMC	NGC 1846	MCPS-070	76.724160	-67.633960	–	–	–	–	–	226.79 ± 0.57	–	–	0.00	0.00	0000000	Ma13
LMC	NGC 1846	MCPS-084	76.816950	-67.625680	–	–	–	–	–	243.64 ± 0.65	–	–	0.00	0.00	0000000	Ma13
LMC	NGC 1846	MCPS-022	76.485375	-67.567500	–	–	–	–	–	279.91 ± 0.48	–	–	0.00	0.00	0000000	Ma13
LMC	NGC 1846	MCPS-029	76.519320	-67.569240	–	–	–	–	–	235.12 ± 0.63	–	–	0.00	0.00	0000000	Ma13
LMC	NGC 1846	MCPS-047	76.622400	-67.547230	–	–	–	–	–	257.59 ± 0.55	–	–	0.00	0.00	0000000	Ma13
LMC	NGC 1846	MCPS-021	76.482690	-67.606700	–	–	–	–	–	258.35 ± 0.95	–	–	0.00	0.00	0000000	Ma13
LMC	NGC 1846	MCPS-060	76.676910	-67.541280	–	–	–	–	–	248.54 ± 1.12	–	–	0.00	0.00	0000000	Ma13
LMC	NGC 1846	MCPS-051	76.641720	-67.620510	–	–	–	–	–	279.81 ± 0.62	–	–	0.00	0.00	0000000	Ma13
LMC	NGC 1846	MCPS-058	76.669650	-67.621310	–	–	–	–	–	298.96 ± 0.48	–	–	0.00	0.00	0000000	Ma13
LMC	NGC 1846	MCPS-067	76.713195	-67.600200	–	–	–	–	–	294.71 ± 0.51	–	–	0.00	0.00	0000000	Ma13
LMC	NGC 1846	MCPS-023	76.486560	-67.517750	–	–	–	–	–	251.00 ± 0.52	–	–	0.00	0.00	0000000	Ma13
LMC	NGC 1846	MCPS-049	76.625640	-67.498450	–	–	–	–	–	252.99 ± 0.54	–	–	0.00	0.00	0000000	Ma13
LMC	NGC 1846	MCPS-040	76.572075	-67.529170	–	–	–	–	–	279.08 ± 0.59	–	–	0.00	0.00	0000000	Ma13
LMC	NGC 1846	MCPS-038	76.567905	-67.503230	–	–	–	–	–	235.31 ± 0.59	–	–	0.00	0.00	0000000	Ma13
LMC	NGC 1846	MCPS-031	76.526220	-67.555500	–	–	–	–	–	285.76 ± 0.65	–	–	0.00	0.00	0000000	Ma13
LMC	NGC 1846	MCPS-017	76.451070	-67.575280	–	–	–	–	–	306.08 ± 0.59	–	–	0.00	0.00	0000000	Ma13
LMC	NGC 1846	MCPS-016	76.451025	-67.445010	–	–	–	–	–	277.61 ± 0.55	–	–	0.00	0.00	0000000	Ma13
LMC	NGC 1846	MCPS-007	76.393185	-67.442830	–	–	–	–	–	253.98 ± 0.85	–	–	0.00	0.00	0000000	Ma13
LMC	NGC 1846	MCPS-043	76.591755	-67.480970	–	–	–	–	–	264.87 ± 0.45	–	–	0.00	0.00	0000000	Ma13

Table C.1: (*continued*) Sample of 3095 Targets from 26 Star Clusters

Galaxy	Cluster	ID	RAJ2000 (deg)	DEJ2000 (deg)	G (mag)	$G_{\rm BP} - G_{\rm RP}$ (mag)	$T_{\rm eff}$ (K)	*Gaia* DR2 ID	S/N	$v_{\rm los}$ (km s^{-1})	$\log g$ (dex)	$[{\rm Fe/H}]_{\rm raw}$ (dex)	P_M	P'_M	Flag[a]	Source[b]
(1)	(2)	(3)	(4)	(5)	(6)	(7)	(8)	(9)	(10)	(11)	(12)	(13)	(14)	(15)	(16)	(17)
LMC	NGC 1846	MCPS-027	76.513245	-67.479530	–	–	–	–	–	279.40 ± 0.55	–	–	0.00	0.00	0000000	Ma13
LMC	NGC 1846	MCPS-035	76.554075	-67.482350	–	–	–	–	–	259.97 ± 0.45	–	–	0.00	0.00	0000000	Ma13
LMC	NGC 1846	MCPS-045	76.611240	-67.493360	–	–	–	–	–	311.75 ± 0.45	–	–	0.00	0.00	0000000	Ma13
LMC	NGC 1846	MCPS-033	76.532460	-67.507370	–	–	–	–	–	270.27 ± 0.52	–	–	0.00	0.00	0000000	Ma13
LMC	NGC 1846	MCPS-048	76.624065	-67.385130	–	–	–	–	–	273.81 ± 0.47	–	–	0.00	0.00	0000000	Ma13
LMC	NGC 1846	ACS-019-R	76.810387	-67.471228	–	–	–	–	–	278.94 ± 0.47	–	–	0.00	0.00	0000000	Ma13
LMC	NGC 1846	MCPS-018	76.454625	-67.405080	–	–	–	–	–	271.92 ± 1.03	–	–	0.00	0.00	0000000	Ma13
LMC	NGC 1846	MCPS-026	76.504770	-67.426350	–	–	–	–	–	298.44 ± 0.57	–	–	0.00	0.00	0000000	Ma13
LMC	NGC 1846	MCPS-010	76.417275	-67.415490	–	–	–	–	–	265.60 ± 0.59	–	–	0.00	0.00	0000000	Ma13
LMC	NGC 1850	N1850-1-b001	77.296346	-68.854431	17.15	0.92	5425	4661263925439703040	12.6	264.08 ± 0.28	1.45 ± 0.14	-0.09 ± 0.04	0.00	0.00	0000000	M2FS
LMC	NGC 1850	N1850-1-b002	77.316379	-68.851376	16.73	1.30	4849	4661263929801891584	12.3	279.68 ± 0.25	1.24 ± 0.10	-0.93 ± 0.04	0.00	0.00	0000000	M2FS
LMC	NGC 1850	N1850-1-b003	77.361522	-68.817987	16.92	1.45	4540	4661269904034296192	16.2	241.82 ± 0.19	1.42 ± 0.05	-0.68 ± 0.03	0.00	0.00	0000000	M2FS
LMC	NGC 1850	N1850-1-b004	77.336870	-68.816350	16.74	1.54	4398	4661269942758214400	16.1	275.34 ± 0.18	1.15 ± 0.06	-0.57 ± 0.03	0.00	0.00	0000000	M2FS
LMC	NGC 1850	N1850-1-b005	77.381822	-68.814339	16.01	2.81	3453	4661269908398510080	14.0	298.81 ± 0.68	0.73 ± 0.10	-1.06 ± 0.08	-1.00	-1.00	0100000	M2FS
LMC	NGC 1850	N1850-1-b007	77.364967	-68.793636	16.68	1.72	4117	4661270080197165312	13.4	226.42 ± 0.20	0.94 ± 0.05	-0.68 ± 0.04	0.00	0.00	0000000	M2FS
LMC	NGC 1850	N1850-1-b008	77.399793	-68.760830	16.78	1.61	4275	4661270561233492992	12.2	294.44 ± 0.24	1.28 ± 0.05	-0.52 ± 0.04	0.00	0.00	0000000	M2FS
LMC	NGC 1850	N1850-1-b009	77.424543	-68.791186	16.95	1.29	4851	4661270217636164736	14.2	257.17 ± 0.26	1.67 ± 0.11	-0.34 ± 0.03	0.00	0.00	0000000	M2FS
LMC	NGC 1850	N1850-1-b010	77.453203	-68.788993	17.06	1.02	5425	4661270251965048832	15.1	272.68 ± 0.40	2.48 ± 0.09	-0.19 ± 0.04	0.00	0.00	0000000	M2FS
LMC	NGC 1850	N1850-1-b011	77.413827	-68.782664	16.95	1.31	4823	4661270423794574464	15.2	276.40 ± 0.22	1.79 ± 0.09	-0.33 ± 0.03	0.00	0.00	0000000	M2FS
LMC	NGC 1850	N1850-1-b012	77.515819	-68.780527	17.07	1.10	5351	4661270316351410048	15.6	267.95 ± 0.26	1.26 ± 0.13	-0.08 ± 0.03	0.00	0.00	0000000	M2FS
LMC	NGC 1850	N1850-1-b013	77.478742	-68.776981	17.08	1.12	5281	4661270350711167360	15.4	268.33 ± 0.28	1.63 ± 0.14	-0.16 ± 0.03	0.00	0.00	0000000	M2FS
LMC	NGC 1850	N1850-1-b014	77.505437	-68.761420	17.13	1.02	5425	4661271798184752896	14.7	272.92 ± 0.37	1.84 ± 0.11	-0.25 ± 0.03	0.00	0.00	0000000	M2FS
LMC	NGC 1850	N1850-1-b015	77.494207	-68.753026	16.93	1.08	5416	4661271862539806976	17.6	273.75 ± 0.29	1.12 ± 0.10	-0.03 ± 0.03	0.00	0.00	0000000	M2FS
LMC	NGC 1850	N1850-1-b017	77.431962	-68.686058	15.99	2.58	3522	4661272687205361024	10.2	247.02 ± 0.50	0.61 ± 0.08	-1.02 ± 0.07	0.00	0.00	0000000	M2FS
LMC	NGC 1850	N1850-1-b018	77.402065	-68.694294	16.91	1.23	5001	4661272313580694912	8.3	248.61 ± 0.51	1.19 ± 0.15	-0.42 ± 0.04	0.00	0.00	0000000	M2FS
LMC	NGC 1850	N1850-1-b019	77.406320	-68.710406	17.15	1.08	5395	4661272176141761792	17.9	275.61 ± 0.24	1.50 ± 0.11	-0.15 ± 0.03	0.00	0.00	0000000	M2FS
LMC	NGC 1850	N1850-1-b020	77.437183	-68.716721	17.04	1.24	4976	4661272206168839552	17.7	257.75 ± 0.24	2.17 ± 0.09	-0.36 ± 0.03	0.00	0.00	0000000	M2FS
LMC	NGC 1850	N1850-1-b022	77.490266	-68.735667	17.06	1.28	4888	4661271896901851264	15.3	329.11 ± 0.23	0.96 ± 0.11	-1.36 ± 0.03	0.00	0.00	0000000	M2FS
LMC	NGC 1850	N1850-1-b023	77.439516	-68.735992	17.05	0.94	5425	4661272073062592896	18.8	285.21 ± 0.23	1.80 ± 0.08	-0.31 ± 0.03	0.00	0.00	0000000	M2FS
LMC	NGC 1850	N1850-1-b024	77.472780	-68.746514	16.90	1.35	4732	4661271862539849600	14.5	258.06 ± 0.20	0.94 ± 0.08	-1.11 ± 0.03	0.00	0.00	0000000	M2FS
LMC	NGC 1850	N1850-1-b025	77.292007	-68.647963	16.85	1.32	4793	4661273722329856768	17.4	274.83 ± 0.19	2.02 ± 0.09	-0.31 ± 0.03	0.00	0.00	0000000	M2FS
LMC	NGC 1850	N1850-1-b026	77.277257	-68.682719	17.08	1.19	5098	4661273206933803008	16.0	277.63 ± 0.28	1.51 ± 0.12	-0.28 ± 0.03	0.00	0.00	0000000	M2FS
LMC	NGC 1850	N1850-1-b027	77.313116	-68.689034	16.94	1.55	4383	4661273000775403520	14.3	290.62 ± 0.23	1.02 ± 0.05	-0.69 ± 0.03	0.00	0.00	0000000	M2FS
LMC	NGC 1850	N1850-1-b028	77.286272	-68.698451	16.98	1.17	5158	4661272966415656960	11.8	287.40 ± 0.30	0.95 ± 0.13	-0.30 ± 0.03	0.00	0.00	0000000	M2FS
LMC	NGC 1850	N1850-1-b029	77.386232	-68.707970	16.81	1.54	4385	4661272171809415424	14.4	246.62 ± 0.22	1.50 ± 0.06	-0.47 ± 0.04	0.00	0.00	0000000	M2FS
LMC	NGC 1850	N1850-1-b030	77.371633	-68.708612	17.10	0.97	5425	4661272932055978368	16.5	241.22 ± 0.27	1.48 ± 0.10	-0.23 ± 0.03	0.00	0.00	0000000	M2FS
LMC	NGC 1850	N1850-1-b031	77.329506	-68.710332	17.25	1.09	5381	4661272893387621888	14.3	248.02 ± 0.31	2.92 ± 0.09	-0.16 ± 0.04	0.00	0.00	0000000	M2FS
LMC	NGC 1850	N1850-1-b033	77.192710	-68.879114	16.82	1.47	4514	4661264200317338368	11.1	255.76 ± 0.35	1.61 ± 0.07	-0.47 ± 0.04	0.00	0.00	0000000	M2FS
LMC	NGC 1850	N1850-1-b034	77.196261	-68.838800	16.93	1.06	5425	4661264926234110592	13.7	245.55 ± 0.33	1.37 ± 0.16	-0.11 ± 0.04	0.00	0.00	0000000	M2FS
LMC	NGC 1850	N1850-1-b035	77.202506	-68.816699	16.86	1.36	4709	4661264960593828864	14.8	241.54 ± 0.21	1.65 ± 0.08	-0.39 ± 0.03	0.00	0.00	0000000	M2FS
LMC	NGC 1850	N1850-1-b036	77.211266	-68.813134	16.90	1.22	5036	4661265059311220224	14.7	268.59 ± 0.25	1.20 ± 0.11	-0.31 ± 0.03	0.00	0.00	0000000	M2FS
LMC	NGC 1850	N1850-1-b037	77.195983	-68.776791	14.71	1.78	4047	4661270973550188800	36.5	249.77 ± 0.22	0.55 ± 0.05	-0.51 ± 0.03	0.97	0.97	0000000	M2FS
LMC	NGC 1850	N1850-1-b038	77.202946	-68.772792	14.24	1.71	4135	4661271007909929728	51.3	248.73 ± 0.24	0.35 ± 0.08	-0.48 ± 0.03	0.97	0.97	0000000	M2FS
LMC	NGC 1850	N1850-1-b040	77.211496	-68.764665	15.66	1.36	4707	4661271007878529664	14.6	251.62 ± 0.32	0.74 ± 0.10	-0.31 ± 0.03	0.95	0.95	0000000	M2FS
LMC	NGC 1850	N1850-1-b041	77.277868	-68.872854	16.95	1.00	5425	4661264273365959424	14.2	66.10 ± 0.28	2.84 ± 0.07	-0.89 ± 0.04	-1.00	-1.00	0000100	M2FS
LMC	NGC 1850	N1850-1-b042	77.247583	-68.856374	16.80	1.51	4451	4661264273399147264	13.9	258.97 ± 0.22	1.77 ± 0.06	-0.45 ± 0.04	0.00	0.00	0000000	M2FS
LMC	NGC 1850	N1850-1-b043	77.231012	-68.854039	16.99	0.97	5425	4661264342118605056	10.0	261.35 ± 0.32	2.12 ± 0.25	-0.04 ± 0.04	0.00	0.00	0000000	M2FS
LMC	NGC 1850	N1850-1-b044	77.221835	-68.835032	16.71	1.64	4224	4661264720075695872	14.2	298.59 ± 0.21	1.33 ± 0.05	-0.54 ± 0.04	0.00	0.00	0000000	M2FS
LMC	NGC 1850	N1850-1-b045	77.213821	-68.771973	15.52	1.55	4373	4661271003548624384	24.3	250.30 ± 0.23	0.73 ± 0.06	-0.52 ± 0.03	0.96	0.96	0000000	M2FS
LMC	NGC 1850	N1850-1-b046	77.226185	-68.771404	14.97	1.23	4992	4661271007909954816	45.5	249.79 ± 0.24	0.03 ± 0.02	-0.32 ± 0.03	0.97	0.97	0000000	M2FS
LMC	NGC 1850	N1850-1-b048	77.249203	-68.762141	14.86	1.66	4207	4661270900517690496	41.6	246.84 ± 0.25	0.01 ± 0.01	-0.60 ± 0.02	0.77	0.72	0000000	M2FS
LMC	NGC 1850	N1850-1-b050	77.244749	-68.681832	17.07	1.27	4902	4661273241293520896	16.0	233.85 ± 0.37	2.72 ± 0.07	-0.59 ± 0.05	0.00	0.00	0000000	M2FS
LMC	NGC 1850	N1850-1-b051	77.242798	-68.692993	16.70	1.52	4429	4661271690741528320	16.4	283.82 ± 0.22	1.49 ± 0.06	-0.45 ± 0.04	0.00	0.00	0000000	M2FS
LMC	NGC 1850	N1850-1-b052	77.238954	-68.746413	16.29	1.36	4719	4661271141035990528	17.0	219.15 ± 0.26	2.57 ± 0.06	-0.27 ± 0.04	0.00	0.00	0000000	M2FS

Table C.1: (*continued*) Sample of 3095 Targets from 26 Star Clusters

Galaxy	Cluster	ID	RAJ2000 (deg)	DEJ2000 (deg)	G (mag)	$G_{\rm BP} - G_{\rm RP}$ (mag)	$T_{\rm eff}$ (K)	*Gaia* DR2 ID	S/N	$v_{\rm los}$ (km s^{-1})	$\log g$ (dex)	$[{\rm Fe/H}]_{\rm raw}$ (dex)	P_M	P'_M	Flag[a]	Source[b]
(1)	(2)	(3)	(4)	(5)	(6)	(7)	(8)	(9)	(10)	(11)	(12)	(13)	(14)	(15)	(16)	(17)
LMC	NGC 1850	N1850-1-b053	77.245242	-68.750995	15.21	1.56	4351	4661271141035855872	35.9	255.79 ± 0.26	0.78 ± 0.06	-0.46 ± 0.03	0.00	0.00	0000000	M2FS
LMC	NGC 1850	N1850-1-b054	77.230415	-68.753527	15.78	1.22	5036	4661271145317511040	31.7	249.46 ± 0.30	2.11 ± 0.29	-0.16 ± 0.03	0.97	0.97	0000000	M2FS
LMC	NGC 1850	N1850-1-b055	77.251983	-68.753847	14.62	1.77	4052	4661270939190478464	42.8	243.29 ± 0.23	0.03 ± 0.03	-0.56 ± 0.02	0.00	0.00	0000000	M2FS
LMC	NGC 1850	N1850-1-b058	77.202409	-68.740461	16.44	1.60	4289	4661271209707049728	-0.3	229.62 ± 73.73	3.29 ± 1.18	0.31 ± 0.87	-1.00	-1.00	1000000	M2FS
LMC	NGC 1850	N1850-1-b059	77.221339	-68.750204	15.64	1.35	4735	4661271145317452544	21.4	248.63 ± 0.26	1.34 ± 0.12	-0.30 ± 0.03	0.97	0.97	0000000	M2FS
LMC	NGC 1850	N1850-1-b061	77.197568	-68.754771	15.21	1.29	4854	4661271179708585472	24.4	250.30 ± 0.27	0.92 ± 0.11	-0.26 ± 0.03	0.97	0.97	0000000	M2FS
LMC	NGC 1850	N1850-1-b062	77.208684	-68.755197	15.60	1.50	4462	4661271110989119488	9.0	305.10 ± 2.63	2.07 ± 0.62	-3.17 ± 0.22	-1.00	-1.00	0110000	M2FS
LMC	NGC 1850	N1850-1-b063	77.201008	-68.758054	15.16	1.12	5279	4661271110989060608	11.0	250.15 ± 0.46	3.96 ± 0.14	0.31 ± 0.06	-1.00	-1.00	0001000	M2FS
LMC	NGC 1850	N1850-1-b064	77.220573	-68.759220	15.30	1.15	5201	4661271106676221824	38.8	248.43 ± 0.34	1.03 ± 0.11	-0.11 ± 0.03	0.97	0.97	0000000	M2FS
LMC	NGC 1850	N1850-1-b065	77.139125	-68.869672	16.83	1.25	4963	4661264376478288000	13.3	207.86 ± 0.25	1.34 ± 0.10	-0.91 ± 0.04	0.00	0.00	0000000	M2FS
LMC	NGC 1850	N1850-1-b066	77.150558	-68.858793	16.68	1.73	4103	4661264410838458368	10.7	228.63 ± 0.25	0.88 ± 0.05	-0.70 ± 0.04	0.00	0.00	0000000	M2FS
LMC	NGC 1850	N1850-1-b069	77.126030	-68.818418	16.56	1.81	4008	4661264990636149504	12.7	214.80 ± 0.23	0.71 ± 0.04	-0.71 ± 0.04	0.00	0.00	0000000	M2FS
LMC	NGC 1850	N1850-1-b070	77.143326	-68.800906	17.16	0.97	5425	4661265029279555968	14.2	271.50 ± 0.26	1.27 ± 0.12	-0.17 ± 0.04	0.00	0.00	0000000	M2FS
LMC	NGC 1850	N1850-1-b071	77.144162	-68.768241	17.08	1.17	5156	4661273997175444224	14.1	247.02 ± 0.26	3.11 ± 0.08	-0.09 ± 0.04	0.84	0.82	0000000	M2FS
LMC	NGC 1850	N1850-1-b072	77.135765	-68.762188	15.38	2.04	3791	4661273997208616832	25.5	277.37 ± 0.25	0.82 ± 0.05	-0.63 ± 0.05	0.00	0.00	0000000	M2FS
LMC	NGC 1850	N1850-1-b074	77.160908	-68.782565	15.15	1.61	4284	4661265162440370560	34.6	246.18 ± 0.25	0.57 ± 0.06	-0.49 ± 0.03	0.16	0.10	0000000	M2FS
LMC	NGC 1850	N1850-1-b075	77.178613	-68.778236	16.24	1.81	4003	4661271042269649408	11.8	220.18 ± 0.38	1.19 ± 0.07	-0.62 ± 0.06	0.00	0.00	0000000	M2FS
LMC	NGC 1850	N1850-1-b076	77.153895	-68.774876	14.98	1.58	4321	4661271042269619840	37.8	246.85 ± 0.23	0.74 ± 0.06	-0.44 ± 0.03	0.80	0.78	0000000	M2FS
LMC	NGC 1850	N1850-1-b077	77.177828	-68.774316	17.27	1.15	5207	4661271037908344576	9.2	203.19 ± 0.34	3.33 ± 0.11	-0.15 ± 0.05	-1.00	-1.00	0001000	M2FS
LMC	NGC 1850	N1850-1-b078	77.160490	-68.766578	17.65	0.75	5425	4661271042269614464	10.6	252.19 ± 0.42	1.94 ± 0.16	-0.24 ± 0.04	0.83	0.82	0000000	M2FS
LMC	NGC 1850	N1850-1-b079	77.174499	-68.764600	14.05	0.89	5425	4661271076629298944	73.7	251.17 ± 0.63	2.16 ± 0.11	-0.76 ± 0.04	-1.00	-1.00	0100000	M2FS
LMC	NGC 1850	N1850-1-b080	77.154844	-68.762738	14.97	1.35	4736	4661271042237956736	42.5	232.80 ± 0.22	2.10 ± 0.09	-0.31 ± 0.03	0.00	0.00	0000000	M2FS
LMC	NGC 1850	N1850-1-b081	77.165866	-68.657890	16.71	1.63	4250	4661276191867484160	11.3	216.73 ± 0.30	1.14 ± 0.06	-0.62 ± 0.04	0.00	0.00	0000000	M2FS
LMC	NGC 1850	N1850-1-b082	77.180548	-68.685470	16.80	1.34	4756	4661274718729702528	17.4	246.68 ± 0.27	1.83 ± 0.07	-0.47 ± 0.03	0.00	0.00	0000000	M2FS
LMC	NGC 1850	N1850-1-b083	77.183377	-68.734147	16.69	1.44	4561	4661271214068133632	18.3	226.19 ± 0.20	1.29 ± 0.06	-0.65 ± 0.03	0.00	0.00	0000000	M2FS
LMC	NGC 1850	N1850-1-b084	77.168890	-68.743490	16.85	1.41	4612	4661271175347293440	13.8	297.49 ± 0.27	2.42 ± 0.06	-0.32 ± 0.04	0.00	0.00	0000000	M2FS
LMC	NGC 1850	N1850-1-b085	77.190768	-68.748152	14.55	1.73	4109	4661271179708571136	46.8	255.49 ± 0.25	0.39 ± 0.06	-0.48 ± 0.03	0.01	0.01	0000000	M2FS
LMC	NGC 1850	N1850-1-b086	77.182636	-68.750027	15.22	1.37	4686	4661271179708564736	38.6	248.39 ± 0.28	1.54 ± 0.09	-0.39 ± 0.03	0.97	0.97	0000000	M2FS
LMC	NGC 1850	N1850-1-b087	77.190871	-68.752220	15.04	1.28	4885	4661271179708419584	31.7	250.06 ± 0.36	2.51 ± 0.09	-0.10 ± 0.04	0.97	0.98	0000000	M2FS
LMC	NGC 1850	N1850-1-b088	77.186780	-68.762571	14.33	0.57	5425	4661271076629254016	34.5	245.48 ± 0.28	0.46 ± 0.08	0.01 ± 0.03	0.97	0.97	0000000	M2FS
LMC	NGC 1850	N1850-1-b089	77.156971	-68.664255	16.92	0.80	5425	4661276264951887488	17.7	275.51 ± 0.37	2.10 ± 0.07	-0.69 ± 0.04	0.00	0.00	0000000	M2FS
LMC	NGC 1850	N1850-1-b091	77.121788	-68.678555	16.85	1.41	4612	4661274753122758400	16.2	247.71 ± 0.21	0.80 ± 0.07	-1.16 ± 0.03	0.00	0.00	0000000	M2FS
LMC	NGC 1850	N1850-1-b092	77.157354	-68.739637	14.83	1.56	4353	4661274130332615936	36.4	245.08 ± 0.21	0.77 ± 0.06	-0.46 ± 0.03	0.01	0.00	0000000	M2FS
LMC	NGC 1850	N1850-1-b093	77.153911	-68.743266	14.64	1.49	4476	4661274134647566592	47.4	249.12 ± 0.26	0.12 ± 0.09	-0.51 ± 0.03	0.89	0.89	0000000	M2FS
LMC	NGC 1850	N1850-1-b094	77.129032	-68.745979	17.04	1.02	5425	4661274027252813824	16.6	247.80 ± 0.33	1.78 ± 0.12	-0.15 ± 0.03	0.76	0.72	0000000	M2FS
LMC	NGC 1850	N1850-1-b095	77.161814	-68.751254	14.67	1.23	5003	4661271072314861056	45.0	254.16 ± 0.28	1.17 ± 0.12	-0.30 ± 0.03	0.10	0.08	0000000	M2FS
LMC	NGC 1850	N1850-1-b096	77.142029	-68.752793	14.64	1.63	4240	4661274027205569664	44.9	254.13 ± 0.25	0.58 ± 0.06	-0.47 ± 0.03	0.00	0.00	0000000	M2FS
LMC	NGC 1850	N1850-1-b097	76.939049	-68.831065	16.89	1.28	4883	4661266261901932160	8.6	321.40 ± 0.33	1.07 ± 0.14	-0.67 ± 0.04	0.00	0.00	0000000	M2FS
LMC	NGC 1850	N1850-1-b099	76.912549	-68.807375	17.02	0.98	5425	4661268495285087616	14.9	234.43 ± 0.30	1.78 ± 0.11	-0.18 ± 0.03	0.00	0.00	0000000	M2FS
LMC	NGC 1850	N1850-1-b100	76.962401	-68.805531	16.95	1.14	5242	4661267778093901696	17.7	230.71 ± 0.30	2.61 ± 0.06	-0.27 ± 0.03	0.00	0.00	0000000	M2FS
LMC	NGC 1850	N1850-1-b101	76.945527	-68.787290	16.67	1.57	4344	4661267881173082112	15.0	316.68 ± 0.19	1.00 ± 0.05	-0.78 ± 0.03	0.00	0.00	0000000	M2FS
LMC	NGC 1850	N1850-1-b102	76.930966	-68.782709	16.98	1.40	4641	4661268637087308416	11.3	241.51 ± 0.23	1.64 ± 0.09	-0.45 ± 0.04	0.00	0.00	0000000	M2FS
LMC	NGC 1850	N1850-1-b103	76.970328	-68.779607	17.13	1.05	5425	4661267911217716352	16.7	274.61 ± 0.28	2.07 ± 0.15	-0.16 ± 0.03	0.00	0.00	0000000	M2FS
LMC	NGC 1850	N1850-1-b104	76.892656	-68.778829	16.99	1.41	4621	4661268701492240640	14.2	242.77 ± 0.28	2.39 ± 0.06	-0.30 ± 0.04	0.00	0.00	0000000	M2FS
LMC	NGC 1850	N1850-1-b105	77.011811	-68.855802	16.90	1.30	4844	4661265991386922624	12.2	278.20 ± 0.38	2.38 ± 0.07	-0.35 ± 0.04	0.00	0.00	0000000	M2FS
LMC	NGC 1850	N1850-1-b106	77.046331	-68.843586	16.94	1.26	4932	4661267468820899584	13.8	264.48 ± 0.29	1.63 ± 0.11	-0.36 ± 0.03	0.00	0.00	0000000	M2FS
LMC	NGC 1850	N1850-1-b107	77.045918	-68.803829	16.99	1.40	4633	4661267640655009792	13.6	262.09 ± 0.26	1.64 ± 0.07	-0.61 ± 0.03	0.00	0.00	0000000	M2FS
LMC	NGC 1850	N1850-1-b109	77.041090	-68.789899	17.02	1.12	5302	4661268018612113280	17.3	252.62 ± 0.24	1.18 ± 0.11	-0.13 ± 0.03	0.00	0.00	0000000	M2FS
LMC	NGC 1850	N1850-1-b110	77.030931	-68.772024	16.74	1.45	4550	4661268259130255232	16.7	306.73 ± 0.26	1.01 ± 0.09	-0.53 ± 0.03	0.00	0.00	0000000	M2FS
LMC	NGC 1850	N1850-1-b111	76.972288	-68.757483	17.15	1.39	4651	4661268327849665792	11.0	232.47 ± 0.26	1.99 ± 0.07	-0.48 ± 0.04	0.00	0.00	0000000	M2FS
LMC	NGC 1850	N1850-1-b112	77.004103	-68.751067	16.66	1.51	4450	4661268430928902528	12.9	266.31 ± 0.26	1.97 ± 0.07	-0.31 ± 0.04	0.00	0.00	0000000	M2FS
LMC	NGC 1850	N1850-1-b115	77.082398	-68.669088	16.81	1.44	4561	4661274959281146240	15.7	277.90 ± 0.25	1.67 ± 0.06	-0.42 ± 0.03	0.00	0.00	0000000	M2FS
LMC	NGC 1850	N1850-1-b117	77.078591	-68.685147	16.92	1.44	4556	4661274851837506816	16.2	225.20 ± 0.22	1.90 ± 0.06	-0.40 ± 0.04	0.00	0.00	0000000	M2FS
LMC	NGC 1850	N1850-1-b118	77.075419	-68.693841	16.93	1.17	5144	4661274817506934528	16.1	249.04 ± 0.26	1.32 ± 0.12	-0.27 ± 0.03	0.00	0.00	0000000	M2FS

Table C.1: (*continued*) Sample of 3095 Targets from 26 Star Clusters

Galaxy	Cluster	ID	RAJ2000 (deg)	DEJ2000 (deg)	G (mag)	$G_{\rm BP} - G_{\rm RP}$ (mag)	$T_{\rm eff}$ (K)	*Gaia* DR2 ID	S/N	$v_{\rm los}$ (km s^{-1})	$\log g$ (dex)	$[{\rm Fe/H}]_{\rm raw}$ (dex)	P_M	P'_M	Flag[a]	Source[b]
(1)	(2)	(3)	(4)	(5)	(6)	(7)	(8)	(9)	(10)	(11)	(12)	(13)	(14)	(15)	(16)	(17)
LMC	NGC 1850	N1850-1-b119	77.098498	-68.710466	17.28	0.85	5425	4661274237693238400	17.2	244.46 ± 0.45	2.73 ± 0.08	-1.02 ± 0.04	0.00	0.00	0000000	M2FS
LMC	NGC 1850	N1850-1-b120	77.040638	-68.746795	16.77	1.50	4456	4661268396569186688	15.6	267.81 ± 0.25	1.62 ± 0.06	-0.45 ± 0.04	0.00	0.00	0000000	M2FS
LMC	NGC 1850	N1850-1-b121	77.016926	-68.664108	16.60	1.51	4440	4661274924921345664	15.8	255.25 ± 0.22	1.80 ± 0.05	-0.55 ± 0.04	0.00	0.00	0000000	M2FS
LMC	NGC 1850	N1850-1-b122	77.009599	-68.701377	16.78	1.44	4567	4661274478244785920	13.8	228.04 ± 0.29	2.28 ± 0.07	-0.38 ± 0.04	0.00	0.00	0000000	M2FS
LMC	NGC 1850	N1850-1-b123	76.976532	-68.706974	16.88	1.08	5416	4661275131079793280	19.3	255.72 ± 0.26	1.96 ± 0.11	-0.09 ± 0.03	0.00	0.00	0000000	M2FS
LMC	NGC 1850	N1850-1-b124	77.014441	-68.709937	16.79	1.42	4602	4661274375165586176	15.7	240.44 ± 0.22	1.82 ± 0.06	-0.46 ± 0.03	0.00	0.00	0000000	M2FS
LMC	NGC 1850	N1850-1-b126	77.034803	-68.716946	16.77	1.33	4782	4661274306446134144	17.5	258.28 ± 0.25	1.97 ± 0.10	-0.29 ± 0.03	0.00	0.00	0000000	M2FS
LMC	NGC 1850	N1850-1-b128	76.971338	-68.742478	17.22	1.16	5195	4661268430928862720	11.9	239.95 ± 0.33	3.24 ± 0.07	-0.12 ± 0.04	-1.00	-1.00	0001000	M2FS
LMC	NGC 1850	N1850-1-r049	77.198620	-68.762603	15.04	0.00	5425	4661271007909722368	14.8	251.60 ± 0.39	2.66 ± 0.13	0.05 ± 0.04	0.98	0.98	0000000	M2FS
LMC	NGC 1850	N1850-1-r079	77.179597	-68.759161	14.53	0.70	5425	4661271076629289856	66.3	237.00 ± 0.17	0.03 ± 0.03	-0.48 ± 0.02	0.00	0.00	0000000	M2FS
LMC	NGC 1850	N1850-1-r099	77.187506	-68.755716	14.43	1.16	5177	4661271179708502272	52.9	248.97 ± 0.36	0.29 ± 0.14	0.04 ± 0.03	0.98	0.98	0000000	M2FS
LMC	NGC 1850	N1850-1-r127	77.202909	-68.767516	14.87	1.37	4693	4661271007909732992	33.4	247.96 ± 0.34	0.93 ± 0.14	-0.32 ± 0.03	0.98	0.98	0000000	M2FS
LMC	NGC 1850	N1850-1-b039	77.183847	-68.767872	15.56	1.20	5077	4661271072315093248	25.2	250.61 ± 0.31	2.64 ± 0.09	-0.05 ± 0.04	0.97	0.97	0000000	M2FS+Fi93
LMC	NGC 1850	N1850-1-b047	77.241624	-68.770220	12.97	1.94	3877	4661270904830752512	53.6	287.97 ± 0.30	0.02 ± 0.02	-0.58 ± 0.03	0.00	0.00	0000000	M2FS+Fi93
LMC	NGC 1850	RV1	77.191750	-68.759556	–	–	–	–	–	250.27 ± 2.10	–	–	1.00	1.00	0000000	Fi93
LMC	NGC 1850	RV2	77.192114	-68.760113	–	–	–	–	–	245.87 ± 1.30	–	–	1.00	1.00	0000000	Fi93
LMC	NGC 1850	RV3	77.189751	-68.760290	–	–	–	–	–	245.97 ± 1.90	–	–	1.00	1.00	0000000	Fi93
LMC	NGC 1850	RV4	77.192654	-68.760654	–	–	–	–	–	249.37 ± 2.60	–	–	1.00	1.00	0000000	Fi93
LMC	NGC 1850	RV5	77.189774	-68.758518	–	–	–	–	–	245.97 ± 4.90	–	–	0.97	0.97	0000000	Fi93
LMC	NGC 1850	RV6	77.190323	-68.760953	–	–	–	–	–	247.37 ± 3.30	–	–	1.00	1.00	0000000	Fi93
LMC	NGC 1850	RV7	77.196239	-68.758999	–	–	–	–	–	249.77 ± 1.90	–	–	0.98	0.98	0000000	Fi93
LMC	NGC 1850	RV8	77.190742	-68.757642	–	–	–	–	–	257.77 ± 4.30	–	–	0.89	0.89	0000000	Fi93
LMC	NGC 1850	RV9	77.197010	-68.759961	–	–	–	–	–	249.87 ± 1.10	–	–	1.00	1.00	0000000	Fi93
LMC	NGC 1850	RV10	77.186983	-68.757415	–	–	–	–	–	254.97 ± 3.00	–	–	0.94	0.93	0000000	Fi93
LMC	NGC 1850	RV11	77.197894	-68.761705	–	–	–	–	–	273.57 ± 2.80	–	–	0.00	0.00	0000000	Fi93
LMC	NGC 1850	RV12	77.200024	-68.760700	–	–	–	–	–	247.67 ± 0.80	–	–	0.99	0.99	0000000	Fi93
LMC	NGC 1850	RV13	77.188852	-68.756524	–	–	–	–	–	252.17 ± 1.30	–	–	0.97	0.97	0000000	Fi93
LMC	NGC 1850	RV14	77.200541	-68.758262	–	–	–	–	–	250.67 ± 2.20	–	–	0.98	0.98	0000000	Fi93
LMC	NGC 1850	RV15	77.183800	-68.761433	–	–	–	–	–	244.27 ± 1.60	–	–	0.96	0.95	0000000	Fi93
LMC	NGC 1850	RV16	77.201284	-68.758726	–	–	–	–	–	246.07 ± 2.20	–	–	0.98	0.98	0000000	Fi93
LMC	NGC 1850	RV17	77.185209	-68.762502	–	–	–	–	–	240.97 ± 3.10	–	–	0.89	0.88	0000000	Fi93
LMC	NGC 1850	RV18	77.183741	-68.756623	–	–	–	–	–	231.97 ± 2.40	–	–	0.00	0.00	0000000	Fi93
LMC	NGC 1850	RV19	77.187857	-68.755436	–	–	–	–	–	258.27 ± 1.00	–	–	0.02	0.01	0000000	Fi93
LMC	NGC 1850	RV20	77.199865	-68.756039	–	–	–	–	–	250.77 ± 0.90	–	–	0.96	0.97	0000000	Fi93
LMC	NGC 1850	RV21	77.204656	-68.759097	–	–	–	–	–	254.27 ± 1.40	–	–	0.91	0.90	0000000	Fi93
LMC	NGC 1850	RV22	77.200778	-68.763087	–	–	–	–	–	245.27 ± 1.70	–	–	0.97	0.97	0000000	Fi93
LMC	NGC 1850	RV23	77.199483	-68.764021	–	–	–	–	–	256.27 ± 3.40	–	–	0.91	0.91	0000000	Fi93
LMC	NGC 1850	RV24	77.177872	-68.761140	–	–	–	–	–	247.67 ± 1.00	–	–	0.97	0.97	0000000	Fi93
LMC	NGC 1850	RV25	77.191776	-68.754170	–	–	–	–	–	239.97 ± 2.90	–	–	0.58	0.58	0000000	Fi93
LMC	NGC 1850	RV26	77.177148	-68.761757	–	–	–	–	–	239.87 ± 2.90	–	–	0.58	-1.00	0000000	Fi93
LMC	NGC 1850	RV27	77.205414	-68.756449	–	–	–	–	–	245.87 ± 1.60	–	–	0.95	0.95	0000000	Fi93
LMC	NGC 1850	RV28	77.177595	-68.756522	–	–	–	–	–	253.27 ± 2.10	–	–	0.91	0.91	0000000	Fi93
LMC	NGC 1850	RV29	77.192725	-68.753607	–	–	–	–	–	247.37 ± 0.70	–	–	0.97	0.97	0000000	Fi93
LMC	NGC 1850	RV30	77.180682	-68.764418	–	–	–	–	–	251.07 ± 1.50	–	–	0.96	0.96	0000000	Fi93
LMC	NGC 1850	RV31	77.188913	-68.752757	–	–	–	–	–	249.77 ± 1.70	–	–	0.97	0.97	0000000	Fi93
LMC	NGC 1850	RV32	77.172877	-68.757240	–	–	–	–	–	248.27 ± 2.00	–	–	0.97	0.97	0000000	Fi93
LMC	NGC 1850	RV33	77.197090	-68.752126	–	–	–	–	–	249.47 ± 1.30	–	–	0.97	0.98	0000000	Fi93
LMC	NGC 1850	RV34	77.195313	-68.751755	–	–	–	–	–	249.47 ± 2.00	–	–	0.96	0.96	0000000	Fi93
LMC	NGC 1850	RV35	77.208670	-68.754034	–	–	–	–	–	247.27 ± 1.50	–	–	0.96	0.96	0000000	Fi93
LMC	NGC 1850	RV37	77.172608	-68.753917	–	–	–	–	–	274.87 ± 3.90	–	–	0.00	0.00	0000000	Fi93
LMC	NGC 1850	RV38	77.217044	-68.759826	–	–	–	–	–	239.27 ± 1.60	–	–	0.02	0.01	0000000	Fi93
LMC	NGC 1850	RV39	77.215621	-68.755882	–	–	–	–	–	230.77 ± 1.00	–	–	0.00	0.00	0000000	Fi93
LMC	NGC 1850	RV40	77.172859	-68.766161	–	–	–	–	–	237.17 ± 3.80	–	–	0.30	0.28	0000000	Fi93
LMC	NGC 1850	RV41	77.197206	-68.750252	–	–	–	–	–	250.07 ± 1.30	–	–	0.96	0.96	0000000	Fi93

Table C.1: (*continued*) Sample of 3095 Targets from 26 Star Clusters

Galaxy	Cluster	ID	RAJ2000 (deg)	DEJ2000 (deg)	G (mag)	$G_{\rm BP} - G_{\rm RP}$ (mag)	$T_{\rm eff}$ (K)	*Gaia* DR2 ID	S/N	$v_{\rm los}$ (km s^{-1})	$\log g$ (dex)	$[{\rm Fe/H}]_{\rm raw}$ (dex)	P_M	P'_M	Flag[a]	Source[b]
(1)	(2)	(3)	(4)	(5)	(6)	(7)	(8)	(9)	(10)	(11)	(12)	(13)	(14)	(15)	(16)	(17)
LMC	NGC 1850	RV42	77.169394	-68.754570	–	–	–	–	–	250.07 ± 2.00	–	–	0.95	0.95	0000000	Fi93
LMC	NGC 1850	RV43	77.212045	-68.766290	–	–	–	–	–	246.67 ± 1.10	–	–	0.95	0.95	0000000	Fi93
LMC	NGC 1850	RV44	77.189762	-68.747775	–	–	–	–	–	247.67 ± 1.70	–	–	0.96	0.96	0000000	Fi93
LMC	NGC 1850	RV45	77.202394	-68.771074	–	–	–	–	–	248.27 ± 1.00	–	–	0.97	0.97	0000000	Fi93
LMC	NGC 1850	RV46	77.198356	-68.746247	–	–	–	–	–	249.97 ± 1.50	–	–	0.96	0.96	0000000	Fi93
LMC	NGC 1850	RV47	77.234446	-68.756878	–	–	–	–	–	247.17 ± 1.50	–	–	0.95	0.95	0000000	Fi93
LMC	NGC 1850	RV48	77.148603	-68.748721	–	–	–	–	–	249.57 ± 1.20	–	–	0.91	0.91	0000000	Fi93
LMC	NGC 1850	RV50	77.246257	-68.751243	–	–	–	–	–	250.87 ± 1.90	–	–	0.73	0.74	0000000	Fi93
LMC	NGC 1850	RV51	77.163536	-68.739816	–	–	–	–	–	237.97 ± 2.00	–	–	0.00	0.00	0000000	Fi93
LMC	NGC 1850	RV52	77.302832	-68.753647	–	–	–	–	–	252.47 ± 1.00	–	–	0.00	0.00	0000000	Fi93
LMC	NGC 1978	N1978-3-b001	82.266121	-66.350023	16.22	1.74	3877	4660337934837282944	17.6	330.92 ± 0.21	0.56 ± 0.04	-0.84 ± 0.03	0.00	0.00	0000000	M2FS
LMC	NGC 1978	N1978-3-b002	82.293785	-66.343548	18.22	1.12	4606	4660339412306034048	7.2	274.82 ± 0.48	1.37 ± 0.12	-1.15 ± 0.06	0.00	0.00	0000000	M2FS
LMC	NGC 1978	N1978-3-b003	82.256409	-66.334467	15.96	1.97	3759	4660339481025527168	19.8	293.23 ± 0.23	0.84 ± 0.05	-0.62 ± 0.04	0.00	0.00	0000000	M2FS
LMC	NGC 1978	N1978-3-b004	82.246910	-66.273140	18.44	1.27	4675	4660340030781456128	4.2	292.83 ± 0.77	1.63 ± 0.17	-0.77 ± 0.08	0.87	0.87	0000000	M2FS
LMC	NGC 1978	N1978-3-b005	82.261727	-66.258300	17.26	1.47	4282	4660340168220446208	9.1	295.38 ± 0.28	1.01 ± 0.06	-0.76 ± 0.04	0.69	0.70	0000000	M2FS
LMC	NGC 1978	N1978-3-b006	82.266885	-66.249847	18.44	1.25	4675	4660340202580228864	3.9	295.04 ± 1.16	1.96 ± 0.18	-0.83 ± 0.10	0.77	0.78	0000000	M2FS
LMC	NGC 1978	N1978-3-b007	82.242391	-66.242196	18.03	1.26	4543	4660340404392397952	6.3	291.69 ± 0.42	0.95 ± 0.12	-0.81 ± 0.05	0.96	0.95	0000000	M2FS
LMC	NGC 1978	N1978-3-b008	82.252484	-66.242127	18.86	0.96	4806	4660340202580228480	3.2	221.43 ± 1.15	1.17 ± 0.62	-1.51 ± 0.13	0.00	0.00	0000000	M2FS
LMC	NGC 1978	N1978-3-b009	82.370402	-66.334036	17.79	1.34	4464	4660327729969738624	7.3	227.30 ± 0.38	0.78 ± 0.11	-0.95 ± 0.05	0.00	0.00	0000000	M2FS
LMC	NGC 1978	N1978-3-b010	82.356002	-66.330468	18.47	1.17	4685	4660327729994060800	4.6	277.29 ± 0.60	1.46 ± 0.16	-0.49 ± 0.06	0.00	0.00	0000000	M2FS
LMC	NGC 1978	N1978-3-b011	82.392993	-66.321880	17.03	1.56	4196	4660327936152503168	11.3	231.90 ± 0.24	0.81 ± 0.05	-0.74 ± 0.04	0.00	0.00	0000000	M2FS
LMC	NGC 1978	N1978-3-b012	82.355062	-66.306608	18.06	0.60	4553	4660328142286680704	8.4	277.27 ± 0.53	0.49 ± 0.20	-1.74 ± 0.05	0.00	0.00	0000010	M2FS
LMC	NGC 1978	N1978-3-b013	82.403821	-66.297161	18.70	1.06	4758	4660328073567245056	5.0	299.04 ± 0.70	1.90 ± 0.16	-1.03 ± 0.09	0.00	0.00	0000000	M2FS
LMC	NGC 1978	N1978-3-b014	82.466281	-66.286898	16.38	1.57	3946	4660351506934696320	15.1	273.33 ± 0.21	0.44 ± 0.04	-0.74 ± 0.03	0.00	0.00	0000000	M2FS
LMC	NGC 1978	N1978-3-b015	82.424338	-66.283969	18.77	0.95	4781	4660351575654171520	4.6	309.15 ± 0.79	2.00 ± 0.19	-1.29 ± 0.09	0.00	0.00	0000000	M2FS
LMC	NGC 1978	N1978-3-b016	82.441163	-66.245371	18.24	1.13	4611	4660351743105299328	6.0	289.51 ± 0.49	1.29 ± 0.12	-0.87 ± 0.06	0.00	0.00	0000000	M2FS
LMC	NGC 1978	N1978-3-b017	82.443412	-66.169332	17.22	1.39	4268	4660353809037369984	7.6	293.74 ± 0.41	0.32 ± 0.13	-1.38 ± 0.05	0.00	0.00	0000000	M2FS
LMC	NGC 1978	N1978-3-b018	82.453081	-66.173974	18.51	1.07	4697	4660353804689696896	3.0	295.82 ± 0.97	1.50 ± 0.27	-1.10 ± 0.12	0.00	0.00	0000000	M2FS
LMC	NGC 1978	N1978-3-b019	82.467417	-66.186034	18.39	1.24	4660	4660353770329939584	4.6	314.66 ± 0.66	1.13 ± 0.19	-1.11 ± 0.08	0.00	0.00	0000000	M2FS
LMC	NGC 1978	N1978-3-b020	82.467319	-66.215984	17.22	1.36	4268	4660352262831041920	10.6	300.72 ± 0.23	0.60 ± 0.06	-0.90 ± 0.04	0.00	0.00	0000000	M2FS
LMC	NGC 1978	N1978-3-b021	82.485231	-66.221616	16.12	1.66	3833	4660352189785625984	17.7	301.89 ± 0.24	0.69 ± 0.04	-0.58 ± 0.03	0.00	0.00	0000000	M2FS
LMC	NGC 1978	N1978-3-b022	82.465482	-66.241616	18.71	1.05	4760	4660352056690594688	3.5	255.51 ± 0.78	1.82 ± 0.22	-0.67 ± 0.09	0.00	0.00	0000000	M2FS
LMC	NGC 1978	N1978-3-b023	82.481151	-66.253684	18.13	1.20	4576	4660351674385809280	6.3	298.85 ± 0.48	1.09 ± 0.13	-0.75 ± 0.05	0.00	0.00	0000000	M2FS
LMC	NGC 1978	N1978-3-b024	82.484293	-66.264782	17.48	1.45	4359	4660351678733441920	7.9	321.88 ± 0.38	1.29 ± 0.07	-0.60 ± 0.04	0.00	0.00	0000000	M2FS
LMC	NGC 1978	N1978-3-b025	82.403467	-66.154694	18.56	1.20	4713	4660354015195812992	3.2	298.57 ± 0.87	1.72 ± 0.20	-0.79 ± 0.09	0.00	0.00	0000000	M2FS
LMC	NGC 1978	N1978-3-b026	82.381892	-66.163569	18.58	1.27	4719	4660354049555535616	3.2	264.86 ± 1.99	2.94 ± 0.23	-1.27 ± 0.16	-1.00	-1.00	0100000	M2FS
LMC	NGC 1978	N1978-3-b027	82.425553	-66.167512	18.64	0.98	4739	4660354015178007296	3.2	300.98 ± 1.12	1.50 ± 0.27	-1.22 ± 0.11	0.00	0.00	0000000	M2FS
LMC	NGC 1978	N1978-3-b028	82.402571	-66.182884	18.69	1.10	4755	4660352503367294720	3.1	303.01 ± 0.96	1.11 ± 0.33	-0.93 ± 0.10	0.00	0.00	0000000	M2FS
LMC	NGC 1978	N1978-3-b029	82.426683	-66.190561	17.89	1.20	4497	4660352499019615232	6.5	279.86 ± 0.45	0.74 ± 0.12	-1.14 ± 0.05	0.00	0.00	0000000	M2FS
LMC	NGC 1978	N1978-3-b030	82.405782	-66.192243	18.57	1.24	4716	4660352464659875584	3.6	265.01 ± 0.63	1.62 ± 0.18	-0.52 ± 0.08	0.00	0.00	0000000	M2FS
LMC	NGC 1978	N1978-3-b031	82.428890	-66.230112	16.79	1.54	4109	4660352125410093696	12.1	252.30 ± 0.22	0.53 ± 0.05	-0.77 ± 0.03	0.00	0.00	0000000	M2FS
LMC	NGC 1978	N1978-3-b032	82.436509	-66.235731	18.37	1.13	4653	4660352125391995776	4.5	281.39 ± 0.44	1.16 ± 0.15	-0.93 ± 0.07	0.00	0.00	0000000	M2FS
LMC	NGC 1978	N1978-3-b033	82.200494	-66.341341	17.52	1.37	4374	4660338175355448960	8.7	276.68 ± 0.32	0.86 ± 0.07	-0.87 ± 0.04	0.00	0.00	0000000	M2FS
LMC	NGC 1978	N1978-3-b035	82.202097	-66.249950	15.71	2.97	3755	4660340266956402944	3.8	296.41 ± 1.77	0.71 ± 0.33	-2.37 ± 0.18	-1.00	-1.00	0110010	M2FS
LMC	NGC 1978	N1978-3-b036	82.194125	-66.246646	16.84	1.37	4126	4660340335675876096	7.9	298.77 ± 0.30	0.79 ± 0.06	-0.67 ± 0.04	1.00	1.00	0000000	M2FS
LMC	NGC 1978	N1978-3-b040	82.206693	-66.237179	18.56	0.72	4713	4660340374381456768	0.6	292.19 ± 4.07	3.41 ± 1.24	0.47 ± 0.54	-1.00	-1.00	0001000	M2FS
LMC	NGC 1978	N1978-3-b041	82.242004	-66.345504	17.13	1.40	4233	4660338003556759296	12.3	280.43 ± 0.25	0.57 ± 0.06	-0.88 ± 0.03	0.00	0.00	0000000	M2FS
LMC	NGC 1978	N1978-3-b043	82.232390	-66.252485	18.81	1.11	4792	4660340374358045184	2.6	294.10 ± 1.00	2.12 ± 0.27	-0.56 ± 0.11	0.96	0.96	0000000	M2FS
LMC	NGC 1978	N1978-3-b044	82.218089	-66.252319	17.78	1.19	4463	4660340266956408576	6.6	294.18 ± 0.42	1.39 ± 0.09	-0.71 ± 0.05	0.99	0.99	0000000	M2FS
LMC	NGC 1978	N1978-3-b045	82.233988	-66.248274	18.78	1.05	4783	4660340374378918784	2.5	294.99 ± 1.21	1.32 ± 0.34	-0.65 ± 0.12	0.99	0.99	0000000	M2FS
LMC	NGC 1978	N1978-3-b046	82.222450	-66.247981	18.82	1.01	4795	4660340374358583808	3.0	297.57 ± 1.17	1.85 ± 0.28	-0.85 ± 0.12	0.97	0.96	0000000	M2FS
LMC	NGC 1978	N1978-3-b047	82.226740	-66.241534	18.74	1.17	4771	4660340374378916992	2.0	296.22 ± 1.23	2.40 ± 0.30	-0.55 ± 0.14	0.98	0.98	0000000	M2FS
LMC	NGC 1978	N1978-3-b048	82.212329	-66.240997	17.70	1.15	4436	4660340374358567296	3.2	294.43 ± 0.70	1.30 ± 0.17	-0.59 ± 0.08	1.00	1.00	0000000	M2FS
LMC	NGC 1978	N1978-3-b049	82.307792	-66.134484	17.73	1.35	4446	4660365903666169344	4.5	294.66 ± 0.57	1.31 ± 0.12	-0.66 ± 0.07	0.00	0.00	0000000	M2FS

Table C.1: (*continued*) Sample of 3095 Targets from 26 Star Clusters

Galaxy	Cluster	ID	RAJ2000 (deg)	DEJ2000 (deg)	G (mag)	$G_{\rm BP} - G_{\rm RP}$ (mag)	$T_{\rm eff}$ (K)	*Gaia* DR2 ID	S/N	$v_{\rm los}$ ($\rm km\,s^{-1}$)	$\log g$ (dex)	$[{\rm Fe/H}]_{\rm raw}$ (dex)	P_M	P'_M	Flag[a]	Source[b]
(1)	(2)	(3)	(4)	(5)	(6)	(7)	(8)	(9)	(10)	(11)	(12)	(13)	(14)	(15)	(16)	(17)
LMC	NGC 1978	N1978-3-b050	82.285551	-66.141933	17.96	1.32	4521	4660365864975241344	5.5	263.69 ± 0.52	0.80 ± 0.14	-0.90 ± 0.06	0.00	0.00	0000000	M2FS
LMC	NGC 1978	N1978-3-b051	82.367678	-66.149355	18.11	1.23	4568	4660354079585690496	5.0	316.38 ± 0.68	1.54 ± 0.13	-0.67 ± 0.07	0.00	0.00	0000000	M2FS
LMC	NGC 1978	N1978-3-b052	82.334892	-66.152118	17.65	1.37	4417	4660365800586919424	5.5	293.06 ± 0.56	0.39 ± 0.17	-1.20 ± 0.06	0.00	0.00	0000000	M2FS
LMC	NGC 1978	N1978-3-b053	82.378595	-66.166820	18.80	1.14	4788	4660354045226052352	2.4	294.16 ± 1.49	1.79 ± 0.30	-0.55 ± 0.12	0.00	0.00	0000000	M2FS
LMC	NGC 1978	N1978-3-b054	82.287576	-66.224875	18.38	1.20	4657	4660363704627800192	3.8	331.29 ± 0.82	1.40 ± 0.23	-1.14 ± 0.10	0.00	0.00	0000000	M2FS
LMC	NGC 1978	N1978-3-b055	82.275356	-66.226149	18.70	1.04	4759	4660363704642811136	3.2	282.05 ± 0.82	1.43 ± 0.25	-0.71 ± 0.10	0.00	0.00	0000000	M2FS
LMC	NGC 1978	N1978-3-b056	82.286728	-66.233409	18.42	1.09	4670	4660363665934536320	3.3	281.93 ± 0.82	1.43 ± 0.20	-0.87 ± 0.10	0.00	0.00	0000000	M2FS
LMC	NGC 1978	N1978-3-b057	82.249399	-66.218009	18.27	0.91	4620	4660363910801247616	4.9	283.53 ± 0.95	1.39 ± 0.20	-1.44 ± 0.09	0.00	0.00	0000010	M2FS
LMC	NGC 1978	N1978-3-b058	82.243902	-66.222159	15.02	1.53	3755	4660363872092981376	36.4	285.42 ± 0.23	0.01 ± 0.01	-0.86 ± 0.03	0.00	0.00	0000010	M2FS
LMC	NGC 1978	N1978-3-b059	82.229026	-66.223288	16.45	1.81	3972	4660363876441508352	8.3	292.89 ± 0.33	0.85 ± 0.06	-0.64 ± 0.04	0.99	0.99	0000000	M2FS
LMC	NGC 1978	N1978-3-b060	82.240341	-66.225817	18.48	1.19	4689	4660363876426379264	2.5	288.90 ± 1.19	1.36 ± 0.30	-0.54 ± 0.11	0.82	0.78	0000000	M2FS
LMC	NGC 1978	N1978-3-b061	82.225558	-66.227635	18.59	1.05	4722	4660340408740194048	2.1	288.18 ± 1.55	1.05 ± 0.39	-0.88 ± 0.13	0.96	0.95	0000000	M2FS
LMC	NGC 1978	N1978-3-b062	82.256832	-66.230291	16.35	1.57	3932	4660363670283071360	2.4	282.05 ± 1.15	0.48 ± 0.21	-1.11 ± 0.11	0.00	0.00	0000000	M2FS
LMC	NGC 1978	N1978-3-b063	82.262086	-66.235106	18.69	0.91	4756	4660363670267954048	2.6	291.76 ± 1.27	1.26 ± 0.36	-0.89 ± 0.12	0.80	0.79	0000000	M2FS
LMC	NGC 1978	N1978-3-b064	82.256113	-66.237838	18.05	1.17	4551	4660340198233226112	5.0	334.32 ± 0.50	1.56 ± 0.12	-0.64 ± 0.06	0.00	0.00	0000000	M2FS
LMC	NGC 1978	N1978-3-b065	82.167433	-66.357807	17.71	1.33	4438	4660338037916476672	9.5	249.10 ± 0.35	0.72 ± 0.09	-1.11 ± 0.04	0.00	0.00	0000000	M2FS
LMC	NGC 1978	N1978-3-b066	82.142808	-66.352463	16.98	1.47	4177	4660338106635969408	11.4	266.66 ± 0.28	0.72 ± 0.05	-0.73 ± 0.03	0.00	0.00	0000000	M2FS
LMC	NGC 1978	N1978-3-b067	82.151127	-66.260498	18.45	0.77	4680	4660339927681416704	5.0	308.96 ± 0.58	1.26 ± 0.17	-1.08 ± 0.07	0.00	0.00	0000010	M2FS
LMC	NGC 1978	N1978-3-b068	82.166955	-66.254006	18.53	1.01	4705	4660340301313173504	3.8	294.33 ± 0.91	1.70 ± 0.19	-0.94 ± 0.09	-1.00	-1.00	0000001	M2FS
LMC	NGC 1978	N1978-3-b069	82.166240	-66.249315	18.06	1.28	4553	4660340305659387008	4.0	292.69 ± 0.69	1.48 ± 0.15	-0.58 ± 0.07	0.99	0.99	0000000	M2FS
LMC	NGC 1978	N1978-3-b070	82.160628	-66.243235	18.75	0.88	4773	4660340339998417280	2.0	291.05 ± 2.34	1.48 ± 0.45	-0.61 ± 0.13	1.00	1.00	0000010	M2FS
LMC	NGC 1978	N1978-3-b071	82.149196	-66.241573	18.38	1.06	4657	4660341095912652928	3.2	289.24 ± 1.00	1.40 ± 0.22	-0.78 ± 0.09	0.97	0.97	0000000	M2FS
LMC	NGC 1978	N1978-3-b072	82.157342	-66.239141	16.99	1.47	4183	4660340339998413056	7.0	291.88 ± 0.37	0.81 ± 0.07	-0.63 ± 0.04	1.00	1.00	0000000	M2FS
LMC	NGC 1978	N1978-3-b073	82.187515	-66.265581	18.20	1.32	4599	4660340305638424704	3.5	22.24 ± 0.85	3.90 ± 0.12	-0.14 ± 0.12	-1.00	-1.00	0001100	M2FS
LMC	NGC 1978	N1978-3-b074	82.193222	-66.256112	17.70	1.31	4436	4660340340019128960	6.3	295.68 ± 0.43	0.86 ± 0.10	-0.83 ± 0.05	0.99	0.99	0000000	M2FS
LMC	NGC 1978	N1978-3-b075	82.183850	-66.254082	17.83	1.25	4477	4660340301316133376	4.9	293.59 ± 0.60	1.32 ± 0.13	-0.66 ± 0.06	0.99	0.99	0000000	M2FS
LMC	NGC 1978	N1978-3-b076	82.191626	-66.251307	18.15	0.94	4584	4660340339999636352	4.2	321.07 ± 0.82	1.54 ± 0.16	-0.97 ± 0.09	0.00	0.00	0000010	M2FS
LMC	NGC 1978	N1978-3-b077	82.179975	-66.246598	16.46	1.22	3976	4660340340021657856	13.4	295.57 ± 0.24	0.41 ± 0.05	-0.84 ± 0.03	1.00	1.00	0000010	M2FS
LMC	NGC 1978	N1978-3-b079	82.177594	-66.243050	16.90	1.37	4148	4660340335675869568	4.9	297.05 ± 0.42	0.65 ± 0.09	-0.60 ± 0.05	1.00	1.00	0000000	M2FS
LMC	NGC 1978	N1978-3-b080	82.179547	-66.239550	16.55	1.37	4016	4660340443100900480	2.8	296.22 ± 0.60	1.32 ± 0.13	-0.42 ± 0.10	1.00	1.00	0000000	M2FS
LMC	NGC 1978	N1978-3-b081	82.202726	-66.213608	16.68	1.62	4063	4660363945160982528	8.1	272.27 ± 0.36	0.45 ± 0.07	-0.91 ± 0.04	0.00	0.00	0000000	M2FS
LMC	NGC 1978	N1978-3-b082	82.210590	-66.217476	17.56	1.41	4389	4660363876441506432	4.8	293.57 ± 0.58	1.23 ± 0.12	-0.65 ± 0.06	0.99	0.99	0000000	M2FS
LMC	NGC 1978	N1978-3-b083	82.202595	-66.224997	17.45	1.36	4348	4660340473114833536	4.8	292.17 ± 0.49	0.80 ± 0.12	-0.68 ± 0.06	1.00	1.00	0000000	M2FS
LMC	NGC 1978	N1978-3-b084	82.217945	-66.225220	17.20	1.44	4258	4660363872096667264	5.1	293.25 ± 0.52	0.82 ± 0.10	-0.76 ± 0.05	0.99	0.99	0000000	M2FS
LMC	NGC 1978	N1978-3-b085	82.203663	-66.228872	17.21	1.29	4263	4660340477458177024	3.6	293.59 ± 0.61	0.97 ± 0.13	-0.53 ± 0.07	1.00	1.00	0000000	M2FS
LMC	NGC 1978	N1978-3-b086	82.217576	-66.229150	18.32	1.13	4638	4660340408718488192	1.3	296.64 ± 1.35	1.44 ± 0.62	-0.46 ± 0.17	0.99	1.00	0000000	M2FS
LMC	NGC 1978	N1978-3-b087	82.211305	-66.233652	18.28	1.07	4623	4660340408718484480	1.2	295.45 ± 1.14	2.67 ± 0.36	-0.14 ± 0.23	-1.00	-1.00	0000001	M2FS
LMC	NGC 1978	N1978-3-b088	82.217995	-66.238388	18.00	1.26	4535	4660340370035623424	2.1	292.42 ± 1.18	2.03 ± 0.27	-0.26 ± 0.13	-1.00	-1.00	0000001	M2FS
LMC	NGC 1978	N1978-3-b089	82.191877	-66.124553	18.42	1.04	4668	4660365422615013248	4.0	259.49 ± 0.81	0.54 ± 0.26	-1.22 ± 0.08	0.00	0.00	0000000	M2FS
LMC	NGC 1978	N1978-3-b090	82.175530	-66.127270	18.67	1.15	4748	4660365388270087936	2.9	287.19 ± 0.97	1.81 ± 0.25	-0.40 ± 0.10	0.00	0.00	0000000	M2FS
LMC	NGC 1978	N1978-3-b091	82.181039	-66.211460	18.75	0.99	4773	4660363945145871104	1.3	290.56 ± 4.28	1.79 ± 0.64	-0.89 ± 0.26	-1.00	-1.00	0100000	M2FS
LMC	NGC 1978	N1978-3-b092	82.189193	-66.218078	17.52	1.32	4375	4660340473114827648	5.9	288.95 ± 0.45	1.04 ± 0.09	-0.66 ± 0.05	0.96	0.95	0000000	M2FS
LMC	NGC 1978	N1978-3-b093	82.178478	-66.218588	17.78	1.26	4461	4660340473114815744	5.2	291.10 ± 0.48	1.09 ± 0.12	-0.69 ± 0.06	0.99	0.99	0000000	M2FS
LMC	NGC 1978	N1978-3-b094	82.192375	-66.222036	18.59	1.10	4724	4660340477458227328	2.0	291.01 ± 2.30	2.06 ± 0.30	-0.48 ± 0.15	1.00	1.00	0000000	M2FS
LMC	NGC 1978	N1978-3-b096	82.193824	-66.230227	18.41	0.81	4666	4660340477460783232	0.5	294.45 ± 1.82	3.43 ± 0.51	0.87 ± 0.25	-1.00	-1.00	1000000	M2FS
LMC	NGC 1978	N1978-3-b097	81.974872	-66.315002	18.61	1.06	4731	4660338828169223680	2.1	241.56 ± 1.67	1.32 ± 0.38	-0.61 ± 0.14	0.00	0.00	0000000	M2FS
LMC	NGC 1978	N1978-3-b098	81.942941	-66.299186	19.13	0.86	4889	4660341783106922880	3.3	313.67 ± 1.48	1.74 ± 0.32	-1.09 ± 0.13	0.00	0.00	0000000	M2FS
LMC	NGC 1978	N1978-3-b099	81.996095	-66.295815	18.75	1.01	4775	4660339240507413248	3.8	310.01 ± 1.01	1.53 ± 0.23	-1.00 ± 0.10	0.00	0.00	0000000	M2FS
LMC	NGC 1978	N1978-3-b100	81.910594	-66.265404	16.98	1.61	4178	4660342264164435968	11.5	263.74 ± 0.27	0.66 ± 0.05	-0.76 ± 0.03	0.00	0.00	0000000	M2FS
LMC	NGC 1978	N1978-3-b101	81.915013	-66.251070	18.31	1.20	4635	4660342401603418368	4.4	286.12 ± 0.79	0.63 ± 0.23	-1.08 ± 0.07	0.00	0.00	0000000	M2FS
LMC	NGC 1978	N1978-3-b102	81.945278	-66.248483	18.18	1.09	4592	4660342332883943296	4.9	292.19 ± 0.72	0.97 ± 0.18	-1.10 ± 0.07	0.00	0.00	0000000	M2FS
LMC	NGC 1978	N1978-3-b103	81.927839	-66.240869	19.04	1.00	4861	4660343879072200448	3.1	289.79 ± 1.40	1.13 ± 0.41	-1.13 ± 0.12	0.00	0.00	0000000	M2FS
LMC	NGC 1978	N1978-3-b104	81.943359	-66.234615	18.72	-0.11	4765	4660343810352723968	1.7	-85.04 ± 110.26	2.30 ± 1.39	-3.83 ± 0.54	-1.00	-1.00	1000010	M2FS
LMC	NGC 1978	N1978-3-b105	82.110951	-66.357054	17.45	1.42	4347	4660338484593072768	10.0	267.31 ± 0.28	1.03 ± 0.06	-0.58 ± 0.04	0.00	0.00	0000000	M2FS

Table C.1: (*continued*) Sample of 3095 Targets from 26 Star Clusters

Galaxy	Cluster	ID	RAJ2000 (deg)	DEJ2000 (deg)	G (mag)	$G_{\rm BP} - G_{\rm RP}$ (mag)	$T_{\rm eff}$ (K)	*Gaia* DR2 ID	S/N	$v_{\rm los}$ (km s^{-1})	log g (dex)	[Fe/H]$_{\rm raw}$ (dex)	P_M	P'_M	Flag[a]	Source[b]
(1)	(2)	(3)	(4)	(5)	(6)	(7)	(8)	(9)	(10)	(11)	(12)	(13)	(14)	(15)	(16)	(17)
LMC	NGC 1978	N1978-3-b106	82.136588	-66.355792	18.65	1.21	4743	4660337724348182400	3.8	262.24 ± 0.97	0.57 ± 0.34	-0.69 ± 0.11	0.00	0.00	0000000	M2FS
LMC	NGC 1978	N1978-3-b107	82.103574	-66.349870	18.75	1.19	4773	4660338484571692160	4.5	247.83 ± 0.72	1.68 ± 0.20	-0.78 ± 0.08	0.00	0.00	0000000	M2FS
LMC	NGC 1978	N1978-3-b108	82.079501	-66.348586	18.81	1.10	4792	4660338480246973184	4.4	253.04 ± 0.75	1.17 ± 0.23	-0.76 ± 0.07	0.00	0.00	0000000	M2FS
LMC	NGC 1978	N1978-3-b109	82.142027	-66.344196	18.65	1.10	4743	4660338106614578688	5.1	297.48 ± 0.74	1.45 ± 0.14	-0.77 ± 0.07	0.00	0.00	0000000	M2FS
LMC	NGC 1978	N1978-3-b110	82.057085	-66.335247	18.16	1.30	4584	4660338553312583936	6.6	243.89 ± 0.53	1.47 ± 0.10	-0.66 ± 0.05	0.00	0.00	0000000	M2FS
LMC	NGC 1978	N1978-3-b111	82.047474	-66.320296	18.42	1.29	4670	4660338931269728128	5.0	247.74 ± 0.72	1.78 ± 0.14	-0.59 ± 0.06	0.00	0.00	0000000	M2FS
LMC	NGC 1978	N1978-3-b112	82.027611	-66.316651	16.18	1.74	3859	4660339137428156928	16.7	271.47 ± 0.23	0.61 ± 0.04	-0.71 ± 0.03	0.00	0.00	0000000	M2FS
LMC	NGC 1978	N1978-3-b113	82.148825	-66.114720	18.71	0.95	4761	4660365487016896512	3.1	353.74 ± 1.71	1.08 ± 0.48	-1.80 ± 0.16	0.00	0.00	0000000	M2FS
LMC	NGC 1978	N1978-3-b114	82.130968	-66.122362	18.38	1.07	4658	4660365456974743552	4.4	272.32 ± 0.72	1.18 ± 0.18	-0.82 ± 0.07	0.00	0.00	0000000	M2FS
LMC	NGC 1978	N1978-3-b115	82.104730	-66.125617	15.69	1.69	3755	4660365560068777344	3.1	364.62 ± 1.06	0.20 ± 0.15	-2.09 ± 0.11	-1.00	-1.00	0000100	M2FS
LMC	NGC 1978	N1978-3-b116	82.177223	-66.225153	18.25	0.85	4614	4660340477458164608	2.3	288.33 ± 1.31	1.61 ± 0.28	-0.59 ± 0.12	1.00	1.00	0000010	M2FS
LMC	NGC 1978	N1978-3-b117	82.164610	-66.226665	16.96	1.36	4171	4660340438755081088	8.2	285.82 ± 0.27	0.79 ± 0.06	-0.67 ± 0.04	0.87	-1.00	0000000	M2FS
LMC	NGC 1978	N1978-3-b118	82.174144	-66.228935	18.47	0.85	4685	4660340443101002368	2.3	288.79 ± 1.90	1.15 ± 0.38	-0.73 ± 0.12	1.00	1.00	0000010	M2FS
LMC	NGC 1978	N1978-3-b119	82.167087	-66.232446	16.67	1.38	4062	4660340443101054592	6.2	294.15 ± 0.42	0.73 ± 0.07	-0.65 ± 0.05	1.00	1.00	0000000	M2FS
LMC	NGC 1978	N1978-3-b120	82.174007	-66.236029	17.07	0.90	4214	4660340443100979200	2.9	293.91 ± 0.77	0.79 ± 0.16	-0.60 ± 0.08	1.00	1.00	0000010	M2FS
LMC	NGC 1978	N1978-3-b121	82.088036	-66.136091	17.68	0.93	4429	4660365143403423872	6.9	40.62 ± 0.79	2.05 ± 0.11	-1.46 ± 0.08	-1.00	-1.00	0000110	M2FS
LMC	NGC 1978	N1978-3-b122	82.074980	-66.147357	18.68	1.24	4751	4660365109043671808	3.7	286.31 ± 0.95	2.05 ± 0.20	-0.57 ± 0.09	0.00	0.00	0000000	M2FS
LMC	NGC 1978	N1978-3-b123	82.028123	-66.148142	18.52	1.09	4700	4660365079017455232	4.9	316.15 ± 0.59	1.69 ± 0.15	-0.86 ± 0.07	0.00	0.00	0000000	M2FS
LMC	NGC 1978	N1978-3-b124	81.991542	-66.157135	17.17	1.43	4247	4660367999610146176	10.8	273.34 ± 0.27	0.74 ± 0.05	-0.83 ± 0.03	0.00	0.00	0000000	M2FS
LMC	NGC 1978	N1978-3-b126	81.982444	-66.162745	18.64	1.04	4738	4660344527560372992	2.7	272.47 ± 1.21	1.39 ± 0.35	-0.88 ± 0.11	0.00	0.00	0000000	M2FS
LMC	NGC 1978	N1978-3-b127	81.947098	-66.169344	17.27	1.59	4286	4660344566267122176	2.8	11.71 ± 0.65	3.41 ± 0.19	-0.48 ± 0.18	-1.00	-1.00	0001100	M2FS
LMC	NGC 1978	N1978-3-b128	81.925591	-66.206838	17.78	1.03	4460	4660344016511241216	6.7	248.58 ± 0.52	0.63 ± 0.18	-1.43 ± 0.06	0.00	0.00	0000010	M2FS
LMC	NGC 1978	N1978-3-r049	82.190452	-66.235682	16.14	1.04	3840	4660340443101129856	4.4	292.97 ± 0.52	0.51 ± 0.10	-0.89 ± 0.07	1.00	1.00	0000010	M2FS
LMC	NGC 1978	N1978-3-b034	82.209310	-66.256802	15.94	1.90	3755	4660340271299657216	13.5	292.38 ± 0.16	0.84 ± 0.04	-0.65 ± 0.04	0.99	0.99	0000000	M2FS+Fi92+Mu08
LMC	NGC 1978	N1978-3-b037	82.211433	-66.245587	15.76	1.95	3755	4660340370035622144	14.7	295.43 ± 0.26	0.84 ± 0.05	-0.66 ± 0.04	1.00	1.00	0000000	M2FS+Fi92
LMC	NGC 1978	N1978-3-b038	82.201988	-66.244076	15.57	1.90	3755	4660340374381613184	13.0	292.54 ± 0.31	0.73 ± 0.05	-0.76 ± 0.05	1.00	1.00	0000000	M2FS+Fi92
LMC	NGC 1978	N1978-3-b039	82.197830	-66.238849	16.78	1.10	4103	4660340443100931840	2.5	295.39 ± 0.59	0.88 ± 0.15	-0.63 ± 0.10	1.00	1.00	0000010	M2FS+Fi92
LMC	NGC 1978	N1978-3-b078	82.170664	-66.246134	16.29	1.67	3908	4660340340019163136	10.8	295.56 ± 0.16	0.82 ± 0.05	-0.63 ± 0.04	1.00	1.00	0000000	M2FS+Mu08
LMC	NGC 1978	N1978-3-b095	82.187577	-66.225603	16.43	1.58	3966	4660340477460768256	10.2	290.70 ± 0.31	0.58 ± 0.05	-0.72 ± 0.04	1.00	1.00	0000000	M2FS+Fi92
LMC	NGC 1978	N1978-3-r079	82.186065	-66.231966	16.19	1.31	3863	4660340443101027584	5.3	290.06 ± 0.40	0.66 ± 0.07	-0.61 ± 0.05	1.00	1.00	0000010	M2FS+Fi92
LMC	NGC 1978	N1978-3-r099	82.201463	-66.233882	15.83	1.53	3755	4660340443100870016	7.6	289.93 ± 0.17	0.64 ± 0.05	-0.68 ± 0.05	1.00	1.00	0000010	M2FS+Fi92+Mu08
LMC	NGC 1978	N1978-3-r127	82.190626	-66.242025	16.08	1.42	3814	4660340443101028224	5.1	298.35 ± 0.17	0.84 ± 0.07	-0.69 ± 0.06	1.00	1.00	0000010	M2FS+Fi92+Mu08
LMC	NGC 1978	01	82.185751	-66.234522	–	–	–	–	–	294.71 ± 1.80	–	–	1.00	1.00	0000000	Fi92
LMC	NGC 1978	02	82.182408	-66.235984	–	–	–	–	–	294.61 ± 1.00	–	–	1.00	1.00	0000000	Fi92
LMC	NGC 1978	03	82.192133	-66.237309	–	–	–	–	–	292.61 ± 1.50	–	–	1.00	1.00	0000000	Fi92
LMC	NGC 1978	04	82.182368	-66.234252	–	–	–	–	–	294.01 ± 1.20	–	–	1.00	1.00	0000000	Fi92
LMC	NGC 1978	05	82.185918	-66.233350	–	–	–	–	–	292.61 ± 1.60	–	–	1.00	1.00	0000000	Fi92
LMC	NGC 1978	06	82.193775	-66.236033	–	–	–	–	–	291.21 ± 1.30	–	–	1.00	1.00	0000000	Fi92
LMC	NGC 1978	07	82.192219	-66.238693	–	–	–	–	–	288.76 ± 0.20	–	–	1.00	1.00	0000000	Fi92+Mu08
LMC	NGC 1978	08	82.193431	-66.233300	–	–	–	–	–	296.11 ± 2.20	–	–	1.00	1.00	0000000	Fi92
LMC	NGC 1978	09	82.177010	-66.235113	–	–	–	–	–	291.51 ± 0.20	–	–	1.00	1.00	0000000	Fi92+Mu08
LMC	NGC 1978	11	82.180660	-66.232327	–	–	–	–	–	296.51 ± 1.00	–	–	1.00	1.00	0000000	Fi92
LMC	NGC 1978	12	82.187500	-66.231512	–	–	–	–	–	292.71 ± 1.40	–	–	1.00	1.00	0000000	Fi92
LMC	NGC 1978	14	82.190057	-66.231349	–	–	–	–	–	290.51 ± 2.10	–	–	1.00	1.00	0000000	Fi92
LMC	NGC 1978	15	82.176686	-66.238930	–	–	–	–	–	295.01 ± 1.50	–	–	1.00	1.00	0000000	Fi92
LMC	NGC 1978	16	82.182505	-66.231450	–	–	–	–	–	291.71 ± 0.90	–	–	1.00	1.00	0000000	Fi92
LMC	NGC 1978	18	82.175510	-66.232532	–	–	–	–	–	292.12 ± 0.20	–	–	1.00	1.00	0000000	Fi92+Mu08
LMC	NGC 1978	19	82.200463	-66.237469	–	–	–	–	–	292.41 ± 1.50	–	–	1.00	1.00	0000000	Fi92
LMC	NGC 1978	20	82.188700	-66.241985	–	–	–	–	–	292.61 ± 0.90	–	–	1.00	1.00	0000000	Fi92
LMC	NGC 1978	21	82.183226	-66.230170	–	–	–	–	–	297.31 ± 2.60	–	–	1.00	1.00	0000000	Fi92
LMC	NGC 1978	23	82.192553	-66.230121	–	–	–	–	–	291.61 ± 1.60	–	–	1.00	1.00	0000000	Fi92
LMC	NGC 1978	25	82.207944	-66.232530	–	–	–	–	–	290.91 ± 1.60	–	–	1.00	1.00	0000000	Fi92
LMC	NGC 1978	26	82.173107	-66.228160	–	–	–	–	–	291.11 ± 2.90	–	–	1.00	1.00	0000000	Fi92
LMC	NGC 1978	29	82.204313	-66.227841	–	–	–	–	–	297.10 ± 0.20	–	–	1.00	1.00	0000000	Fi92+Mu08

Table C.1: (*continued*) Sample of 3095 Targets from 26 Star Clusters

Galaxy	Cluster	ID	RAJ2000 (deg)	DEJ2000 (deg)	G (mag)	$G_{\rm BP} - G_{\rm RP}$ (mag)	$T_{\rm eff}$ (K)	*Gaia* DR2 ID	S/N	$v_{\rm los}$ (km s^{-1})	$\log g$ (dex)	$[{\rm Fe/H}]_{\rm raw}$ (dex)	P_M	P'_M	Flag[a]	Source[b]
(1)	(2)	(3)	(4)	(5)	(6)	(7)	(8)	(9)	(10)	(11)	(12)	(13)	(14)	(15)	(16)	(17)
LMC	NGC 1978	30	82.192849	-66.223610	–	–	–	–	–	297.21 ± 0.70	–	–	1.00	1.00	0000000	Fi92
LMC	NGC 1978	32	82.222149	-66.235230	–	–	–	–	–	296.29 ± 0.20	–	–	1.00	1.00	0000000	Fi92+Mu08
LMC	NGC 1978	33	82.151804	-66.232288	–	–	–	–	–	291.52 ± 0.20	–	–	1.00	1.00	0000000	Fi92+Mu08
LMC	NGC 1978	34	82.219079	-66.242505	–	–	–	–	–	290.11 ± 1.30	–	–	1.00	1.00	0000000	Fi92
LMC	NGC 1978	35	82.164072	-66.222876	–	–	–	–	–	287.31 ± 1.90	–	–	0.94	0.93	0000000	Fi92
LMC	NGC 1978	1978-28	82.177404	-66.207917	–	–	–	–	–	290.51 ± 0.20	–	–	0.66	0.61	0000000	Mu08
LMC	NGC 2121	N2121-1-b001	87.097813	-71.570086	17.15	1.31	4323	4656819257074383872	13.0	274.87 ± 0.23	0.49 ± 0.07	-0.82 ± 0.03	0.00	0.00	0000000	M2FS
LMC	NGC 2121	N2121-1-b002	87.083575	-71.501405	19.03	1.10	4907	4656822070261520640	4.7	220.44 ± 0.56	2.01 ± 0.16	-0.81 ± 0.07	0.00	0.00	0000000	M2FS
LMC	NGC 2121	N2121-1-b003	87.101978	-71.497441	18.31	1.11	4694	4656821348749396096	7.9	294.06 ± 1.14	2.23 ± 0.13	-1.94 ± 0.07	-1.00	-1.00	0100000	M2FS
LMC	NGC 2121	N2121-1-b004	87.087466	-71.497308	18.78	1.18	4837	4656822070265857664	4.8	245.59 ± 0.47	2.35 ± 0.14	-0.60 ± 0.07	0.00	0.00	0000000	M2FS
LMC	NGC 2121	N2121-1-b005	87.093446	-71.490721	17.49	1.32	4435	4656822108932644992	11.0	253.97 ± 0.26	0.88 ± 0.07	-0.82 ± 0.04	0.00	0.00	0000000	M2FS
LMC	NGC 2121	N2121-1-b006	87.108902	-71.487718	18.61	1.01	4786	4656821348735862016	6.5	236.16 ± 0.42	1.35 ± 0.13	-0.78 ± 0.05	0.99	0.99	0000000	M2FS
LMC	NGC 2121	N2121-1-b007	87.098139	-71.486520	18.79	1.07	4838	4656822108932644864	5.5	234.64 ± 0.57	1.56 ± 0.15	-0.77 ± 0.06	0.97	0.97	0000000	M2FS
LMC	NGC 2121	N2121-1-b008	87.092232	-71.479295	17.32	1.37	4380	4656822211997341440	11.1	238.46 ± 0.22	0.87 ± 0.06	-0.72 ± 0.04	1.00	1.00	0000000	M2FS
LMC	NGC 2121	N2121-1-b009	87.159936	-71.574713	17.48	1.30	4434	4656819222714665088	5.9	41.43 ± 0.32	3.78 ± 0.10	-0.54 ± 0.10	-1.00	-1.00	0001100	M2FS
LMC	NGC 2121	N2121-1-b010	87.163663	-71.562800	17.33	1.09	4384	4656819596382046848	12.4	273.44 ± 0.31	0.24 ± 0.11	-1.17 ± 0.03	0.00	0.00	0000010	M2FS
LMC	NGC 2121	N2121-1-b011	87.265114	-71.537259	17.60	1.36	4474	4656820975061340288	7.9	253.84 ± 0.36	1.05 ± 0.08	-0.66 ± 0.04	0.00	0.00	0000000	M2FS
LMC	NGC 2121	N2121-1-b012	87.120953	-71.492437	18.83	0.95	4849	4656821348749428096	5.7	275.50 ± 0.52	1.96 ± 0.15	-1.07 ± 0.07	0.00	0.00	0000000	M2FS
LMC	NGC 2121	N2121-1-b013	87.110388	-71.491196	17.98	1.28	4593	4656821353018404736	7.7	238.39 ± 0.36	1.58 ± 0.09	-0.68 ± 0.05	0.95	0.95	0000000	M2FS
LMC	NGC 2121	N2121-1-b014	87.429848	-71.484167	17.68	1.12	4497	4656833344567735040	7.8	270.93 ± 0.34	0.75 ± 0.11	-0.94 ± 0.05	0.00	0.00	0000000	M2FS
LMC	NGC 2121	N2121-1-b015	87.114270	-71.482596	16.86	1.53	4222	4656821451828803328	14.4	237.87 ± 0.20	0.73 ± 0.05	-0.71 ± 0.03	0.99	0.99	0000000	M2FS
LMC	NGC 2121	N2121-1-b016	87.126016	-71.479953	16.82	1.31	4207	4656821456097620736	14.8	43.86 ± 0.23	3.11 ± 0.08	-0.90 ± 0.09	-1.00	-1.00	0000100	M2FS
LMC	NGC 2121	N2121-1-b017	87.186377	-71.411233	16.90	1.46	4236	4656845473557332224	8.9	236.57 ± 0.23	0.59 ± 0.07	-0.99 ± 0.04	0.00	0.00	0000000	M2FS
LMC	NGC 2121	N2121-1-b018	87.171801	-71.417286	17.37	1.54	4398	4656845439197591424	2.7	262.27 ± 0.78	1.21 ± 0.21	-0.63 ± 0.11	0.00	0.00	0000000	M2FS
LMC	NGC 2121	N2121-1-b019	87.168954	-71.426512	16.89	1.63	4230	4656845439197593472	13.6	268.29 ± 0.20	1.21 ± 0.05	-0.49 ± 0.04	0.00	0.00	0000000	M2FS
LMC	NGC 2121	N2121-1-b020	87.382968	-71.441693	17.33	1.41	4384	4656833550714987136	11.4	280.46 ± 0.22	0.93 ± 0.06	-0.67 ± 0.03	0.00	0.00	0000000	M2FS
LMC	NGC 2121	N2121-1-b021	87.419159	-71.454251	17.60	1.36	4473	4656833482006673024	7.4	300.02 ± 0.29	1.33 ± 0.08	-0.52 ± 0.04	0.00	0.00	0000000	M2FS
LMC	NGC 2121	N2121-1-b024	87.288498	-71.471626	17.43	1.28	4416	4656821662255819520	11.2	282.20 ± 0.25	0.93 ± 0.07	-1.03 ± 0.04	0.00	0.00	0000000	M2FS
LMC	NGC 2121	N2121-1-b025	87.123266	-71.381709	17.73	1.07	4514	4656845679705938944	10.8	252.69 ± 0.35	0.69 ± 0.10	-1.13 ± 0.04	0.00	0.00	0000000	M2FS
LMC	NGC 2121	N2121-1-b026	87.128703	-71.384769	17.03	1.58	4280	4656845641043092864	12.8	259.21 ± 0.22	1.13 ± 0.05	-0.54 ± 0.03	0.00	0.00	0000000	M2FS
LMC	NGC 2121	N2121-1-b027	87.167561	-71.432024	17.15	1.47	4322	4656821967182940416	12.5	219.77 ± 0.23	0.58 ± 0.06	-1.24 ± 0.03	0.00	0.00	0000000	M2FS
LMC	NGC 2121	N2121-1-b028	87.166076	-71.459814	17.53	1.39	4449	4656821834054500864	9.3	275.06 ± 0.29	1.10 ± 0.07	-0.64 ± 0.04	0.00	0.00	0000000	M2FS
LMC	NGC 2121	N2121-1-b029	87.112884	-71.467671	18.64	1.17	4793	4656821486188380800	5.1	242.94 ± 0.47	1.21 ± 0.17	-0.79 ± 0.06	0.00	0.00	0000000	M2FS
LMC	NGC 2121	N2121-1-b030	87.106377	-71.471862	17.67	1.39	4496	4656821486148433152	8.9	238.19 ± 0.27	1.25 ± 0.08	-0.69 ± 0.04	0.98	0.98	0000000	M2FS
LMC	NGC 2121	N2121-1-b031	87.111671	-71.476059	18.84	1.10	4852	4656821451790569856	5.2	240.08 ± 0.46	1.89 ± 0.15	-0.80 ± 0.07	0.87	0.86	0000000	M2FS
LMC	NGC 2121	N2121-1-b032	87.127491	-71.476261	19.01	1.13	4899	4656821486146199424	3.7	252.90 ± 0.64	1.98 ± 0.21	-0.63 ± 0.08	0.00	0.00	0000000	M2FS
LMC	NGC 2121	N2121-1-b033	87.059873	-71.600346	17.33	1.27	4383	4656814000033361024	10.8	282.00 ± 0.26	0.71 ± 0.07	-0.97 ± 0.04	0.00	0.00	0000000	M2FS
LMC	NGC 2121	N2121-1-b035	87.055430	-71.502564	18.23	1.08	4670	4656820597104146432	6.5	278.46 ± 0.36	1.22 ± 0.12	-0.85 ± 0.05	0.00	0.00	0000000	M2FS
LMC	NGC 2121	N2121-1-b036	87.059336	-71.495501	19.27	0.98	4966	4656822074558371968	2.9	235.56 ± 1.24	1.16 ± 0.38	-1.08 ± 0.12	-1.00	-1.00	0000001	M2FS
LMC	NGC 2121	N2121-1-b037	87.057730	-71.490220	18.92	0.85	4876	4656822070282995712	3.5	234.87 ± 0.84	1.85 ± 0.25	-0.81 ± 0.09	1.00	1.00	0000010	M2FS
LMC	NGC 2121	N2121-1-b038	87.064133	-71.487074	18.87	0.00	4861	4656822108918099584	4.2	237.35 ± 0.60	1.76 ± 0.17	-0.71 ± 0.08	1.00	1.00	0000000	M2FS
LMC	NGC 2121	N2121-1-b039	87.053527	-71.474792	17.64	1.27	4486	4656822207708256128	6.7	270.84 ± 0.36	1.57 ± 0.09	-0.46 ± 0.05	0.00	0.00	0000000	M2FS
LMC	NGC 2121	N2121-1-b040	87.053111	-71.468528	16.96	1.27	4257	4656822207742849920	9.7	236.63 ± 0.25	0.29 ± 0.09	-1.08 ± 0.04	-1.00	-1.00	0000001	M2FS
LMC	NGC 2121	N2121-1-b041	87.072404	-71.583928	17.53	1.11	4450	4656819909909410048	10.7	286.73 ± 0.45	0.81 ± 0.09	-1.24 ± 0.04	0.00	0.00	0000000	M2FS
LMC	NGC 2121	N2121-1-b042	87.083631	-71.564625	16.48	1.75	4079	4656820047348360832	16.1	238.52 ± 0.20	1.08 ± 0.05	-0.47 ± 0.04	0.00	0.00	0000000	M2FS
LMC	NGC 2121	N2121-1-b043	87.069963	-71.503661	18.79	1.01	4837	4656820592792750464	2.1	265.65 ± 1.44	1.78 ± 0.30	-0.66 ± 0.15	0.00	0.00	0000000	M2FS
LMC	NGC 2121	N2121-1-b044	87.068307	-71.492779	17.90	1.20	4569	4656822074572896896	9.7	287.26 ± 0.50	1.81 ± 0.10	-1.17 ± 0.06	0.00	0.00	0000000	M2FS
LMC	NGC 2121	N2121-1-b045	87.079004	-71.489135	18.81	0.91	4844	4656822108932638720	4.8	238.72 ± 0.71	1.62 ± 0.15	-0.73 ± 0.07	1.00	0.99	0000000	M2FS
LMC	NGC 2121	N2121-1-b046	87.076818	-71.482425	18.78	0.90	4835	4656822104664112512	5.1	236.96 ± 0.57	1.66 ± 0.15	-0.69 ± 0.06	1.00	1.00	0000000	M2FS
LMC	NGC 2121	N2121-1-b047	87.073785	-71.477421	18.23	1.09	4670	4656822211997318528	5.8	235.22 ± 0.46	1.61 ± 0.12	-0.65 ± 0.05	1.00	1.00	0000000	M2FS
LMC	NGC 2121	N2121-1-b048	87.066368	-71.466105	17.61	1.41	4475	4656822246371348992	10.5	235.55 ± 0.28	1.23 ± 0.07	-0.66 ± 0.04	1.00	1.00	0000000	M2FS
LMC	NGC 2121	N2121-1-b049	87.086491	-71.384493	17.19	1.48	4337	4656846401270213760	12.5	280.41 ± 0.28	1.20 ± 0.06	-1.00 ± 0.04	0.00	0.00	0000000	M2FS
LMC	NGC 2121	N2121-1-b051	87.095219	-71.412157	17.04	1.66	4285	4656846263831278720	11.0	298.64 ± 0.26	1.34 ± 0.06	-0.49 ± 0.04	0.00	0.00	0000000	M2FS
LMC	NGC 2121	N2121-1-b052	87.105343	-71.462345	17.12	1.47	4312	4656821868414232448	11.1	232.81 ± 0.23	0.83 ± 0.06	-0.75 ± 0.04	0.01	0.01	0000000	M2FS

Table C.1: (*continued*) Sample of 3095 Targets from 26 Star Clusters

Galaxy	Cluster	ID	RAJ2000 (deg)	DEJ2000 (deg)	G (mag)	$G_{\rm BP} - G_{\rm RP}$ (mag)	$T_{\rm eff}$ (K)	*Gaia* DR2 ID	S/N	$v_{\rm los}$ ($\rm km\,s^{-1}$)	$\log g$ (dex)	$[{\rm Fe/H}]_{\rm raw}$ (dex)	P_M	P'_M	Flag[a]	Source[b]
(1)	(2)	(3)	(4)	(5)	(6)	(7)	(8)	(9)	(10)	(11)	(12)	(13)	(14)	(15)	(16)	(17)
LMC	NGC 2121	N2121-1-b053	87.093762	-71.466705	18.08	1.24	4623	4656822246356461568	8.2	236.28 ± 0.32	1.51 ± 0.09	-0.80 ± 0.04	0.99	0.99	0000000	M2FS
LMC	NGC 2121	N2121-1-b054	87.086393	-71.471758	18.80	1.12	4842	4656822207700823808	4.6	235.05 ± 0.62	1.43 ± 0.19	-0.74 ± 0.06	1.00	1.00	0000000	M2FS
LMC	NGC 2121	N2121-1-b055	87.098321	-71.475224	18.81	0.99	4843	4656822207742884992	4.5	239.66 ± 0.50	1.85 ± 0.17	-0.92 ± 0.08	0.94	0.94	0000000	M2FS
LMC	NGC 2121	N2121-1-b056	87.084163	-71.476026	17.63	1.27	4482	4656822207743347712	8.1	234.95 ± 0.33	1.29 ± 0.08	-0.69 ± 0.04	1.00	1.00	0000000	M2FS
LMC	NGC 2121	N2121-1-b057	87.073018	-71.363576	17.63	1.38	4484	4656846435630097536	8.9	267.96 ± 0.43	0.19 ± 0.13	-1.41 ± 0.05	0.00	0.00	0000000	M2FS
LMC	NGC 2121	N2121-1-b058	87.084433	-71.365556	17.80	1.07	4537	4656846435630098816	10.2	288.65 ± 0.36	0.88 ± 0.10	-1.21 ± 0.04	0.00	0.00	0000000	M2FS
LMC	NGC 2121	N2121-1-b059	87.068384	-71.453558	17.30	1.19	4374	4656822624328468992	-0.4	-3.58 ± 326.80	2.41 ± 1.39	-3.32 ± 0.97	-1.00	-1.00	1000000	M2FS
LMC	NGC 2121	N2121-1-b061	87.057762	-71.455611	19.13	1.08	4933	4656822242089089408	3.0	304.46 ± 0.94	2.00 ± 0.25	-0.78 ± 0.12	0.00	0.00	0000000	M2FS
LMC	NGC 2121	N2121-1-b062	87.063415	-71.458552	19.02	0.98	4903	4656822242105212160	4.8	261.94 ± 0.75	2.06 ± 0.21	-0.97 ± 0.09	0.00	0.00	0000000	M2FS
LMC	NGC 2121	N2121-1-b063	87.081551	-71.458623	18.20	1.12	4659	4656822246356455424	8.4	282.71 ± 0.41	1.14 ± 0.11	-0.98 ± 0.05	0.00	0.00	0000000	M2FS
LMC	NGC 2121	N2121-1-b064	87.082131	-71.465916	17.95	1.27	4582	4656822242067996672	8.1	237.85 ± 0.34	1.28 ± 0.09	-0.70 ± 0.04	0.99	0.98	0000000	M2FS
LMC	NGC 2121	N2121-1-b065	87.014284	-71.594072	17.34	1.46	4387	4656814068752833792	10.7	269.60 ± 0.24	0.98 ± 0.06	-0.65 ± 0.04	0.00	0.00	0000000	M2FS
LMC	NGC 2121	N2121-1-b066	87.011054	-71.498933	15.31	2.11	3682	4656820661514710528	15.1	251.88 ± 0.30	0.77 ± 0.05	-0.65 ± 0.05	0.00	0.00	0000000	M2FS
LMC	NGC 2121	N2121-1-b068	87.028878	-71.489893	17.50	1.27	4438	4656822143292347392	10.7	237.62 ± 0.26	0.97 ± 0.06	-0.81 ± 0.04	1.00	1.00	0000000	M2FS
LMC	NGC 2121	N2121-1-b069	87.021342	-71.485147	20.48	0.00	5227	4656822143277750784	1.4	241.86 ± 2.23	2.40 ± 0.69	-0.91 ± 0.26	0.98	-1.00	0000000	M2FS
LMC	NGC 2121	N2121-1-b070	87.012095	-71.482142	18.85	1.00	4855	4656822139002388864	3.7	237.01 ± 0.70	1.86 ± 0.22	-0.70 ± 0.08	1.00	1.00	0000000	M2FS
LMC	NGC 2121	N2121-1-b071	87.028278	-71.481838	18.82	1.04	4848	4656822173392416256	2.4	235.71 ± 1.16	1.86 ± 0.31	-0.43 ± 0.10	1.00	1.00	0000000	M2FS
LMC	NGC 2121	N2121-1-b072	87.024834	-71.474040	17.97	1.27	4589	4656822177637477120	7.8	239.64 ± 0.37	1.35 ± 0.09	-0.72 ± 0.05	0.99	0.99	0000000	M2FS
LMC	NGC 2121	N2121-1-b073	87.042227	-71.504459	16.59	1.67	4120	4656820592821627776	13.2	236.73 ± 0.19	0.90 ± 0.05	-0.63 ± 0.04	0.77	0.78	0000000	M2FS
LMC	NGC 2121	N2121-1-b074	87.038296	-71.499908	18.87	0.92	4860	4656820661554633856	3.5	238.19 ± 0.91	1.68 ± 0.25	-0.90 ± 0.10	0.96	0.96	0000000	M2FS
LMC	NGC 2121	N2121-1-b075	87.048280	-71.494717	18.88	1.01	4863	4656822070303911936	3.5	237.84 ± 0.80	2.10 ± 0.20	-0.64 ± 0.10	0.98	0.98	0000000	M2FS
LMC	NGC 2121	N2121-1-b076	87.045315	-71.487125	18.77	1.07	4831	4656822070303910144	4.4	238.80 ± 0.92	1.81 ± 0.21	-1.18 ± 0.09	-1.00	-1.00	0000001	M2FS
LMC	NGC 2121	N2121-1-b077	87.037696	-71.484084	17.83	0.00	4547	4656822143277777024	8.8	236.50 ± 0.28	1.18 ± 0.08	-0.82 ± 0.04	1.00	1.00	0000000	M2FS
LMC	NGC 2121	N2121-1-b078	87.048939	-71.482574	19.40	0.00	4997	4656822108932598528	2.7	237.33 ± 1.09	2.52 ± 0.22	-0.43 ± 0.13	1.00	1.00	0000000	M2FS
LMC	NGC 2121	N2121-1-b079	87.039813	-71.479383	16.54	1.64	4103	4656822177637508352	11.6	238.06 ± 0.22	0.96 ± 0.05	-0.56 ± 0.04	1.00	1.00	0000000	M2FS
LMC	NGC 2121	N2121-1-b080	87.039692	-71.470067	18.23	1.08	4670	4656822280731274240	6.7	236.51 ± 0.39	1.34 ± 0.10	-0.84 ± 0.05	1.00	1.00	0000000	M2FS
LMC	NGC 2121	N2121-1-b081	87.035721	-71.387671	17.21	1.57	4344	4656846366910452224	9.9	267.46 ± 0.27	0.91 ± 0.07	-0.92 ± 0.04	0.00	0.00	0000000	M2FS
LMC	NGC 2121	N2121-1-b082	87.041017	-71.457096	18.36	1.21	4710	4656822310780078080	6.3	271.86 ± 0.35	1.66 ± 0.10	-0.73 ± 0.05	0.00	0.00	0000000	M2FS
LMC	NGC 2121	N2121-1-b083	87.029008	-71.459863	18.74	1.10	4824	4656822276470331904	6.8	237.04 ± 0.49	1.52 ± 0.13	-0.93 ± 0.05	0.97	0.97	0000000	M2FS
LMC	NGC 2121	N2121-1-b084	87.019016	-71.462136	18.87	0.98	4861	4656822280731078272	3.9	237.50 ± 0.72	1.78 ± 0.22	-0.85 ± 0.10	0.99	0.99	0000000	M2FS
LMC	NGC 2121	N2121-1-b085	87.049835	-71.463265	17.84	1.12	4550	4656822207702942976	8.2	235.59 ± 0.39	1.24 ± 0.09	-0.92 ± 0.05	0.98	0.98	0000000	M2FS
LMC	NGC 2121	N2121-1-b086	87.030231	-71.464886	17.32	1.53	4381	4656822276422419456	11.3	236.95 ± 0.25	1.11 ± 0.06	-0.68 ± 0.04	0.99	0.99	0000000	M2FS
LMC	NGC 2121	N2121-1-b087	87.021730	-71.468537	18.91	0.88	4872	4656822276471629696	3.7	237.19 ± 0.67	1.85 ± 0.20	-0.74 ± 0.09	0.99	0.99	0000000	M2FS
LMC	NGC 2121	N2121-1-b088	87.010638	-71.471884	17.66	1.18	4491	4656822173343200768	10.7	254.23 ± 0.34	0.70 ± 0.08	-1.02 ± 0.04	0.00	0.00	0000000	M2FS
LMC	NGC 2121	N2121-1-b089	87.002084	-71.388843	17.67	1.38	4495	4656846538709129728	8.3	276.28 ± 0.40	1.05 ± 0.09	-0.81 ± 0.04	0.00	0.00	0000000	M2FS
LMC	NGC 2121	N2121-1-b091	86.979053	-71.436176	17.12	1.41	4311	4656822521249236480	12.0	225.34 ± 0.26	0.66 ± 0.06	-0.98 ± 0.03	0.00	0.00	0000000	M2FS
LMC	NGC 2121	N2121-1-b092	86.976870	-71.459779	17.55	1.54	4457	4656822379548391936	6.7	235.03 ± 0.53	1.55 ± 0.09	-0.56 ± 0.05	0.47	0.48	0000000	M2FS
LMC	NGC 2121	N2121-1-b093	87.007378	-71.462765	16.97	1.57	4261	4656822280731260544	13.5	236.72 ± 0.21	1.02 ± 0.05	-0.63 ± 0.03	0.98	0.98	0000000	M2FS
LMC	NGC 2121	N2121-1-b094	87.007721	-71.466904	18.77	0.95	4831	4656822177652046848	5.6	228.86 ± 0.94	1.92 ± 0.21	-1.56 ± 0.09	0.00	0.00	0000000	M2FS
LMC	NGC 2121	N2121-1-b096	86.992320	-71.474005	18.83	1.08	4848	4656822138981219584	4.8	237.21 ± 0.56	1.42 ± 0.19	-0.82 ± 0.07	0.99	0.99	0000000	M2FS
LMC	NGC 2121	N2121-1-b097	86.866174	-71.561624	16.62	1.37	4134	4656814343630723584	5.7	47.29 ± 0.42	2.22 ± 0.08	-0.38 ± 0.10	-1.00	-1.00	0000100	M2FS
LMC	NGC 2121	N2121-1-b098	86.762104	-71.539497	17.21	1.55	4343	4656817367287684864	9.1	237.80 ± 0.30	1.07 ± 0.06	-0.65 ± 0.04	0.00	0.00	0000000	M2FS
LMC	NGC 2121	N2121-1-b099	86.772666	-71.533758	17.24	1.31	4353	4656823242803892352	12.6	245.02 ± 0.23	0.57 ± 0.07	-0.79 ± 0.03	0.00	0.00	0000000	M2FS
LMC	NGC 2121	N2121-1-b100	86.772807	-71.528771	17.67	1.39	4494	4656823242803890048	8.1	288.81 ± 0.37	1.41 ± 0.08	-0.71 ± 0.05	0.00	0.00	0000000	M2FS
LMC	NGC 2121	N2121-1-b101	86.766516	-71.521010	18.37	0.95	4711	4656823277163625216	5.7	259.05 ± 0.53	1.25 ± 0.14	-0.95 ± 0.06	0.00	0.00	0000000	M2FS
LMC	NGC 2121	N2121-1-b102	86.974841	-71.499442	17.15	1.54	4324	4656820837622250752	9.7	268.87 ± 0.27	1.19 ± 0.06	-0.78 ± 0.04	0.00	0.00	0000000	M2FS
LMC	NGC 2121	N2121-1-b103	86.974228	-71.494021	19.15	0.87	4938	4656820871967396096	3.5	245.36 ± 1.27	1.99 ± 0.31	-1.21 ± 0.13	0.00	0.00	0000000	M2FS
LMC	NGC 2121	N2121-1-b105	87.000948	-71.497634	17.64	1.32	4485	4656820665823566464	8.0	240.43 ± 0.36	0.88 ± 0.09	-0.81 ± 0.04	0.04	0.04	0000000	M2FS
LMC	NGC 2121	N2121-1-b107	86.999316	-71.488826	17.41	1.47	4409	4656820665823562496	8.6	236.87 ± 0.31	1.00 ± 0.08	-0.74 ± 0.04	0.99	0.99	0000000	M2FS
LMC	NGC 2121	N2121-1-b109	87.003035	-71.485494	18.87	1.24	4861	4656822139032672384	3.9	237.93 ± 0.78	1.58 ± 0.21	-0.75 ± 0.09	0.98	0.98	0000000	M2FS
LMC	NGC 2121	N2121-1-b110	86.979318	-71.482603	19.19	0.99	4948	4656822345142619136	3.6	256.23 ± 0.97	1.47 ± 0.29	-0.96 ± 0.10	0.00	0.00	0000000	M2FS
LMC	NGC 2121	N2121-1-b111	86.988130	-71.479841	18.62	1.23	4787	4656822345139599744	3.4	269.71 ± 0.91	1.81 ± 0.26	-0.71 ± 0.11	0.00	0.00	0000000	M2FS
LMC	NGC 2121	N2121-1-b112	87.009504	-71.478725	18.35	1.30	4707	4656822143277729792	4.0	281.10 ± 0.48	1.91 ± 0.15	-0.59 ± 0.07	0.00	0.00	0000000	M2FS
LMC	NGC 2121	N2121-1-b114	86.953087	-71.381054	17.06	1.29	4289	4656846538709098368	16.0	265.84 ± 0.22	0.32 ± 0.07	-0.88 ± 0.03	0.00	0.00	0000000	M2FS

Table C.1: (*continued*) Sample of 3095 Targets from 26 Star Clusters

Galaxy	Cluster	ID	RAJ2000 (deg)	DEJ2000 (deg)	G (mag)	$G_{\rm BP} - G_{\rm RP}$ (mag)	$T_{\rm eff}$ (K)	*Gaia* DR2 ID	S/N	$v_{\rm los}$ ($\rm km\,s^{-1}$)	$\log g$ (dex)	$[{\rm Fe/H}]_{\rm raw}$ (dex)	P_M	P'_M	Flag[a]	Source[b]
(1)	(2)	(3)	(4)	(5)	(6)	(7)	(8)	(9)	(10)	(11)	(12)	(13)	(14)	(15)	(16)	(17)
LMC	NGC 2121	N2121-1-b115	86.877393	-71.424828	17.58	1.03	4466	4656825544891260800	12.8	278.22 ± 0.32	1.74 ± 0.06	-1.43 ± 0.04	0.00	0.00	0000010	M2FS
LMC	NGC 2121	N2121-1-b118	86.855056	-71.428598	17.71	1.31	4507	4656825510546447488	7.9	288.35 ± 0.44	0.79 ± 0.12	-1.35 ± 0.05	0.00	0.00	0000000	M2FS
LMC	NGC 2121	N2121-1-b119	86.920018	-71.435744	17.19	1.55	4335	4656822551298401920	10.9	236.11 ± 0.23	1.04 ± 0.06	-0.66 ± 0.04	0.00	0.00	0000000	M2FS
LMC	NGC 2121	N2121-1-b121	86.826414	-71.387722	17.30	1.53	4375	4656826025942508544	7.8	197.39 ± 0.35	1.27 ± 0.07	-0.68 ± 0.05	0.00	0.00	0000000	M2FS
LMC	NGC 2121	N2121-1-b122	86.782222	-71.406779	17.46	1.24	4427	4656825574955604736	9.9	271.40 ± 0.28	0.88 ± 0.07	-0.74 ± 0.04	0.00	0.00	0000000	M2FS
LMC	NGC 2121	N2121-1-b123	86.793533	-71.408883	17.03	1.56	4282	4656825579265907584	12.1	250.45 ± 0.25	0.91 ± 0.06	-0.63 ± 0.03	0.00	0.00	0000000	M2FS
LMC	NGC 2121	N2121-1-b124	86.802452	-71.436552	16.96	1.66	4256	4656825441826962560	11.0	272.06 ± 0.28	1.09 ± 0.07	-0.49 ± 0.04	0.00	0.00	0000000	M2FS
LMC	NGC 2121	N2121-1-b125	86.716527	-71.449707	17.08	1.42	4298	4656824136157053568	12.7	246.71 ± 0.26	0.98 ± 0.05	-1.16 ± 0.04	0.00	0.00	0000000	M2FS
LMC	NGC 2121	N2121-1-b126	86.819725	-71.454877	17.21	1.69	4343	4656823964358388224	8.8	296.29 ± 0.33	0.98 ± 0.07	-0.63 ± 0.04	0.00	0.00	0000000	M2FS
LMC	NGC 2121	N2121-1-b127	86.801855	-71.461721	17.18	1.51	4333	4656823929998646400	2.5	280.57 ± 0.95	0.96 ± 0.21	-0.69 ± 0.10	0.00	0.00	0000000	M2FS
LMC	NGC 2121	N2121-1-b128	86.843841	-71.467818	17.31	1.26	4376	4656823861279182848	11.3	269.78 ± 0.27	0.40 ± 0.09	-1.02 ± 0.03	0.00	0.00	0000000	M2FS
LMC	NGC 2121	N2121-1-r028	87.054572	-71.478433	17.25	1.32	4355	4656822108932604800	11.8	238.22 ± 0.21	1.19 ± 0.05	-0.66 ± 0.04	1.00	1.00	0000000	M2FS
LMC	NGC 2121	N2121-1-r049	87.064165	-71.482683	18.28	0.97	4686	4656822104663638144	5.2	236.82 ± 0.54	1.66 ± 0.14	-0.91 ± 0.07	1.00	1.00	0000000	M2FS
LMC	NGC 2121	N2121-1-r079	87.035270	-71.475471	16.81	1.53	4203	4656822173392366080	13.1	234.06 ± 0.22	0.96 ± 0.05	-0.63 ± 0.04	0.99	0.99	0000000	M2FS
LMC	NGC 2121	N2121-1-r099	87.066807	-71.473561	16.91	1.50	4238	4656822212011838336	16.6	232.22 ± 0.19	0.61 ± 0.05	-0.74 ± 0.03	0.93	0.93	0000000	M2FS
LMC	NGC 2155	N2155-1-b001	89.687875	-65.564931	18.80	0.98	4851	4755943558899362816	2.7	319.98 ± 0.92	2.64 ± 0.24	-0.75 ± 0.16	0.00	0.00	0000000	M2FS
LMC	NGC 2155	N2155-1-b003	89.698721	-65.513827	18.91	0.94	4882	4755945586123969664	3.1	289.18 ± 0.80	1.90 ± 0.32	-0.82 ± 0.12	0.00	0.00	0000000	M2FS
LMC	NGC 2155	N2155-1-b004	89.691535	-65.504521	18.96	1.07	4895	4755945624791154688	2.7	287.66 ± 1.00	1.75 ± 0.29	-0.93 ± 0.14	0.00	0.00	0000000	M2FS
LMC	NGC 2155	N2155-1-b005	89.680755	-65.496240	18.39	0.94	4727	4755945624791151488	3.9	331.03 ± 0.73	1.39 ± 0.21	-1.01 ± 0.09	0.00	0.00	0000000	M2FS
LMC	NGC 2155	N2155-1-b006	89.700400	-65.492164	17.26	1.35	4371	4755945727870366848	9.4	328.86 ± 0.26	0.69 ± 0.07	-0.73 ± 0.04	0.00	0.00	0000000	M2FS
LMC	NGC 2155	N2155-1-b007	89.687827	-65.483867	18.77	1.18	4841	4755945723562951296	2.6	302.09 ± 0.70	2.11 ± 0.26	-0.70 ± 0.13	0.00	0.00	0000000	M2FS
LMC	NGC 2155	N2155-1-b008	89.687476	-65.477650	18.76	1.11	4838	4755945757922697216	2.7	312.59 ± 1.32	1.40 ± 0.35	-1.09 ± 0.15	0.63	-1.00	0000000	M2FS
LMC	NGC 2155	N2155-1-b009	89.715350	-65.512568	18.81	1.12	4854	4755945551764232576	2.5	320.77 ± 0.91	1.76 ± 0.30	-0.70 ± 0.16	0.00	0.00	0000000	M2FS
LMC	NGC 2155	N2155-1-b011	89.702540	-65.506107	15.77	1.83	3792	4755945624791156736	14.3	320.36 ± 0.20	0.73 ± 0.04	-0.64 ± 0.04	0.00	0.00	0000000	M2FS
LMC	NGC 2155	N2155-1-b012	89.710424	-65.503165	18.67	1.15	4812	4755945556071679616	3.1	289.60 ± 0.59	1.49 ± 0.24	-0.88 ± 0.10	0.00	0.00	0000000	M2FS
LMC	NGC 2155	N2155-1-b013	89.726660	-65.497521	18.19	0.94	4668	4755945659150894208	4.9	296.06 ± 0.67	1.34 ± 0.16	-0.97 ± 0.08	0.00	0.00	0000000	M2FS
LMC	NGC 2155	N2155-1-b014	89.701487	-65.496687	16.33	1.70	4035	4755945727870368128	9.5	317.32 ± 0.35	0.33 ± 0.11	-0.62 ± 0.06	0.00	0.00	0000000	M2FS
LMC	NGC 2155	N2155-1-b015	89.728199	-65.493750	18.50	1.11	4760	4755945659140557184	3.5	330.27 ± 0.71	1.69 ± 0.22	-0.96 ± 0.10	0.00	0.00	0000000	M2FS
LMC	NGC 2155	N2155-1-b016	89.703604	-65.486745	16.38	1.71	4057	4755945727870365568	11.2	299.67 ± 0.20	0.84 ± 0.05	-0.62 ± 0.04	0.00	0.00	0000000	M2FS
LMC	NGC 2155	N2155-1-b017	89.838225	-65.398645	18.91	1.23	4881	4755951667797793920	2.7	258.23 ± 1.41	2.71 ± 0.23	-0.71 ± 0.16	0.00	0.00	0000000	M2FS
LMC	NGC 2155	N2155-1-b020	89.734086	-65.455378	18.64	1.13	4805	4755946204599321600	4.1	319.52 ± 1.03	1.60 ± 0.23	-1.32 ± 0.10	0.00	0.00	0000000	M2FS
LMC	NGC 2155	N2155-1-b021	89.745002	-65.469614	18.05	1.01	4624	4755946105827484928	5.5	239.64 ± 0.51	1.82 ± 0.12	-1.06 ± 0.08	-1.00	-1.00	0000100	M2FS
LMC	NGC 2155	N2155-1-b022	89.717103	-65.470063	18.65	1.15	4806	4755946067168113152	2.7	302.71 ± 0.81	1.03 ± 0.32	-0.62 ± 0.10	0.00	0.00	0000000	M2FS
LMC	NGC 2155	N2155-1-b023	89.725574	-65.484843	18.97	1.05	4898	4755945689203210624	2.2	319.21 ± 1.32	1.82 ± 0.42	-0.61 ± 0.17	0.00	0.00	0000000	M2FS
LMC	NGC 2155	N2155-1-b024	89.738343	-65.489893	18.89	0.96	4877	4755945689203205504	2.7	320.49 ± 1.30	1.27 ± 0.58	-1.37 ± 0.16	0.00	0.00	0000000	M2FS
LMC	NGC 2155	N2155-1-b025	89.684216	-65.433471	18.75	0.98	4835	4755946273318824576	3.5	308.60 ± 0.92	1.54 ± 0.34	-1.00 ± 0.11	0.00	0.00	0000000	M2FS
LMC	NGC 2155	N2155-1-b026	89.677718	-65.439040	17.88	1.21	4570	4755946276626131456	6.1	296.29 ± 0.40	1.36 ± 0.10	-0.76 ± 0.05	0.00	0.00	0000000	M2FS
LMC	NGC 2155	N2155-1-b027	89.698940	-65.446142	18.47	1.22	4752	4755946273318809472	3.6	338.96 ± 0.41	1.65 ± 0.21	-0.55 ± 0.07	0.00	0.00	0000000	M2FS
LMC	NGC 2155	N2155-1-b028	89.680321	-65.456330	18.88	1.01	4874	4755946135879844224	2.6	305.06 ± 0.70	1.40 ± 0.28	-0.81 ± 0.11	0.00	0.00	0000000	M2FS
LMC	NGC 2155	N2155-1-b029	89.677585	-65.466309	16.59	1.56	4136	4755946140187210368	10.9	315.45 ± 0.21	0.72 ± 0.05	-0.75 ± 0.04	0.94	0.93	0000000	M2FS
LMC	NGC 2155	N2155-1-b030	89.688291	-65.466495	18.59	1.01	4788	4755946135879830016	2.4	301.03 ± 2.01	1.22 ± 0.39	-0.86 ± 0.14	0.00	0.00	0000000	M2FS
LMC	NGC 2155	N2155-1-b031	89.677406	-65.471603	17.73	1.35	4525	4755945762230092800	6.4	302.82 ± 0.32	1.17 ± 0.10	-0.61 ± 0.04	0.00	0.00	0000000	M2FS
LMC	NGC 2155	N2155-1-b032	89.712399	-65.478241	18.96	1.16	4894	4755945689203220224	2.2	296.57 ± 1.33	1.70 ± 0.38	-0.54 ± 0.12	0.00	0.00	0000000	M2FS
LMC	NGC 2155	N2155-1-b035	89.661252	-65.520977	18.81	1.07	4852	4755947067891627904	2.8	316.92 ± 0.89	0.85 ± 0.41	-0.88 ± 0.14	0.00	0.00	0000000	M2FS
LMC	NGC 2155	N2155-1-b036	89.650043	-65.520824	18.75	1.03	4835	4755947033530096000	3.2	295.21 ± 0.90	1.76 ± 0.23	-0.76 ± 0.11	0.00	0.00	0000000	M2FS
LMC	NGC 2155	N2155-1-b037	89.651744	-65.498542	18.76	0.84	4839	4755948545368910336	3.5	314.76 ± 0.80	1.57 ± 0.27	-1.21 ± 0.10	-1.00	-1.00	0000001	M2FS
LMC	NGC 2155	N2155-1-b038	89.652012	-65.494276	17.28	1.44	4377	4755948579728647168	7.0	314.66 ± 0.30	1.18 ± 0.08	-0.56 ± 0.05	0.99	0.99	0000000	M2FS
LMC	NGC 2155	N2155-1-b039	89.657066	-65.490036	18.66	0.88	4810	4755948575421228928	3.1	315.54 ± 0.78	1.70 ± 0.22	-0.87 ± 0.12	0.98	0.98	0000000	M2FS
LMC	NGC 2155	N2155-1-b040	89.643549	-65.481898	18.65	1.01	4806	4755948575438990208	1.9	315.40 ± 1.20	2.02 ± 0.31	-0.51 ± 0.16	1.00	1.00	0000000	M2FS
LMC	NGC 2155	N2155-1-b041	89.676165	-65.518895	18.96	0.90	4896	4755944108672687616	2.7	315.24 ± 2.03	1.89 ± 0.46	-1.76 ± 0.17	0.00	0.00	0000000	M2FS
LMC	NGC 2155	N2155-1-b042	89.665099	-65.514207	15.22	1.64	3673	4755944112962667520	26.7	296.20 ± 0.16	0.04 ± 0.03	-0.67 ± 0.03	0.00	0.00	0000010	M2FS
LMC	NGC 2155	N2155-1-b043	89.675695	-65.510404	18.07	1.26	4629	4755945586141433984	3.4	288.09 ± 0.85	1.56 ± 0.18	-0.77 ± 0.10	0.00	0.00	0000000	M2FS
LMC	NGC 2155	N2155-1-b044	89.676155	-65.491695	18.22	1.06	4676	4755945624780808576	5.8	314.98 ± 0.47	1.36 ± 0.14	-1.15 ± 0.07	-1.00	-1.00	0000001	M2FS
LMC	NGC 2155	N2155-1-b045	89.666116	-65.490010	18.57	1.07	4783	4755945624780803840	2.6	275.76 ± 1.31	1.34 ± 0.38	-0.68 ± 0.11	0.00	0.00	0000000	M2FS

Table C.1: (*continued*) Sample of 3095 Targets from 26 Star Clusters

Galaxy	Cluster	ID	RAJ2000 (deg)	DEJ2000 (deg)	G (mag)	$G_{\rm BP} - G_{\rm RP}$ (mag)	$T_{\rm eff}$ (K)	*Gaia* DR2 ID	S/N	$v_{\rm los}$ ($\rm km\,s^{-1}$)	$\log g$ (dex)	$[{\rm Fe/H}]_{\rm raw}$ (dex)	P_M	P'_M	Flag[a]	Source[b]
(1)	(2)	(3)	(4)	(5)	(6)	(7)	(8)	(9)	(10)	(11)	(12)	(13)	(14)	(15)	(16)	(17)
LMC	NGC 2155	N2155-1-b046	89.669572	-65.482870	18.75	1.03	4836	4755945727860014848	2.5	316.23 ± 0.86	1.96 ± 0.29	-0.65 ± 0.14	0.97	0.97	0000000	M2FS
LMC	NGC 2155	N2155-1-b047	89.664861	-65.477830	18.69	0.98	4818	4755945723562959488	3.1	314.54 ± 1.01	1.82 ± 0.30	-0.92 ± 0.12	0.98	0.98	0000000	M2FS
LMC	NGC 2155	N2155-1-b048	89.680252	-65.475375	18.75	1.07	4835	4755945757930303104	3.1	313.46 ± 0.88	1.51 ± 0.31	-0.65 ± 0.10	0.77	0.74	0000000	M2FS
LMC	NGC 2155	N2155-1-b049	89.658659	-65.430358	18.68	1.17	4815	4755949232553242624	3.1	318.07 ± 1.00	1.43 ± 0.24	-0.72 ± 0.11	0.00	0.00	0000000	M2FS
LMC	NGC 2155	N2155-1-b050	89.667917	-65.440059	18.91	1.05	4882	4755946273318816000	2.7	325.77 ± 1.14	1.94 ± 0.32	-0.75 ± 0.11	0.00	0.00	0000000	M2FS
LMC	NGC 2155	N2155-1-b051	89.646975	-65.443014	18.87	1.24	4872	4755949125177096576	1.8	315.57 ± 1.44	2.56 ± 0.34	-0.68 ± 0.25	0.42	0.43	0000000	M2FS
LMC	NGC 2155	N2155-1-b053	89.663806	-65.465832	18.73	1.08	4830	4755945757922708992	3.2	316.30 ± 0.79	1.67 ± 0.22	-0.73 ± 0.10	0.97	0.97	0000000	M2FS
LMC	NGC 2155	N2155-1-b054	89.654968	-65.466644	18.76	1.06	4837	4755948717157201920	3.4	314.87 ± 0.77	1.87 ± 0.23	-0.86 ± 0.10	0.99	0.99	0000000	M2FS
LMC	NGC 2155	N2155-1-b055	89.646390	-65.468168	18.77	1.04	4841	4755948717167565440	3.1	315.66 ± 0.92	1.17 ± 0.29	-0.62 ± 0.10	0.98	0.98	0000000	M2FS
LMC	NGC 2155	N2155-1-b056	89.648991	-65.474645	18.68	1.11	4816	4755948678518199808	2.9	314.10 ± 0.89	1.96 ± 0.24	-0.48 ± 0.10	1.00	1.00	0000000	M2FS
LMC	NGC 2155	N2155-1-b057	89.638302	-65.429944	18.79	1.00	4849	4755949228256330496	2.9	306.13 ± 1.01	1.09 ± 0.31	-0.73 ± 0.10	0.00	0.00	0000000	M2FS
LMC	NGC 2155	N2155-1-b058	89.632731	-65.433871	18.89	1.00	4877	4755949125177109760	2.9	304.78 ± 0.76	1.85 ± 0.25	-0.64 ± 0.11	0.00	0.00	0000000	M2FS
LMC	NGC 2155	N2155-1-b059	89.644932	-65.436471	18.56	1.26	4778	4755949125177105408	3.6	289.82 ± 0.53	2.16 ± 0.16	-0.40 ± 0.08	0.00	0.00	0000000	M2FS
LMC	NGC 2155	N2155-1-b060	89.629025	-65.446705	17.35	1.36	4400	4755949095124674176	7.5	254.32 ± 0.29	0.83 ± 0.09	-0.86 ± 0.04	-1.00	-1.00	0000100	M2FS
LMC	NGC 2155	N2155-1-b061	89.640564	-65.455158	18.99	1.06	4902	4755949090817345536	2.0	325.39 ± 0.88	1.79 ± 0.39	-0.34 ± 0.12	0.00	0.00	0000000	M2FS
LMC	NGC 2155	N2155-1-b062	89.626641	-65.462995	18.74	1.14	4834	4755948717167559040	3.0	313.56 ± 0.68	1.78 ± 0.24	-0.49 ± 0.10	0.96	0.95	0000000	M2FS
LMC	NGC 2155	N2155-1-b063	89.636814	-65.464137	17.96	1.14	4595	4755948712860214144	6.1	348.98 ± 0.51	0.38 ± 0.24	-1.45 ± 0.06	0.00	0.00	0000000	M2FS
LMC	NGC 2155	N2155-1-b064	89.637435	-65.467772	18.70	1.04	4823	4755948682807825280	3.0	307.00 ± 0.80	1.64 ± 0.25	-0.82 ± 0.10	0.00	0.00	0000000	M2FS
LMC	NGC 2155	N2155-1-b065	89.628679	-65.523817	17.04	1.22	4296	4755946930450878976	9.9	322.46 ± 0.40	0.22 ± 0.15	-2.51 ± 0.05	0.00	0.00	0000000	M2FS
LMC	NGC 2155	N2155-1-b066	89.622749	-65.520768	18.89	1.12	4877	4755947029232974720	2.2	285.78 ± 1.30	2.80 ± 0.28	-0.66 ± 0.15	0.00	0.00	0000000	M2FS
LMC	NGC 2155	N2155-1-b067	89.614362	-65.500826	18.73	1.14	4831	4755947132312207744	3.1	313.38 ± 0.79	1.47 ± 0.27	-0.61 ± 0.11	0.69	0.66	0000000	M2FS
LMC	NGC 2155	N2155-1-b068	89.627691	-65.492167	18.85	1.14	4865	4755948541061488640	2.1	306.41 ± 0.74	2.03 ± 0.29	-0.45 ± 0.12	0.00	0.00	0000000	M2FS
LMC	NGC 2155	N2155-1-b069	89.617288	-65.488519	18.26	0.98	4689	4755948614088376320	4.2	315.43 ± 0.70	1.20 ± 0.19	-0.97 ± 0.09	0.99	0.99	0000000	M2FS
LMC	NGC 2155	N2155-1-b070	89.626876	-65.485170	17.84	1.25	4557	4755948575421259392	2.8	314.70 ± 0.68	0.80 ± 0.25	-0.71 ± 0.10	1.00	1.00	0000000	M2FS
LMC	NGC 2155	N2155-1-b071	89.622292	-65.481435	18.59	0.99	4788	4755948575428590848	3.4	313.36 ± 0.72	1.78 ± 0.23	-0.64 ± 0.10	1.00	1.00	0000000	M2FS
LMC	NGC 2155	N2155-1-b072	89.615019	-65.475806	18.63	1.02	4799	4755948648448088064	2.6	315.09 ± 1.06	1.61 ± 0.28	-0.64 ± 0.13	0.98	0.98	0000000	M2FS
LMC	NGC 2155	N2155-1-b073	89.639252	-65.518526	18.50	1.02	4760	4755947029240445824	3.1	344.86 ± 0.77	1.02 ± 0.37	-1.24 ± 0.12	0.00	0.00	0000000	M2FS
LMC	NGC 2155	N2155-1-b074	89.633932	-65.509366	17.50	1.00	4450	4755947067900162688	6.7	286.72 ± 0.55	0.84 ± 0.17	-1.73 ± 0.06	0.00	0.00	0000010	M2FS
LMC	NGC 2155	N2155-1-b075	89.631547	-65.498959	18.58	1.10	4785	4755948541061482112	2.5	291.26 ± 0.76	1.66 ± 0.24	-0.69 ± 0.11	0.00	0.00	0000000	M2FS
LMC	NGC 2155	N2155-1-b076	89.634831	-65.495022	18.71	0.98	4825	4755948541061485312	2.3	315.12 ± 0.86	1.62 ± 0.35	-0.73 ± 0.13	0.99	0.99	0000000	M2FS
LMC	NGC 2155	N2155-1-b077	89.639698	-65.486243	18.69	0.94	4818	4755948579728642048	2.5	316.01 ± 0.74	1.73 ± 0.29	-0.72 ± 0.13	0.98	0.98	0000000	M2FS
LMC	NGC 2155	N2155-1-b078	89.635087	-65.481855	18.42	0.96	4737	4755948575438982656	2.7	316.24 ± 0.69	1.76 ± 0.23	-0.65 ± 0.10	1.00	1.00	0000000	M2FS
LMC	NGC 2155	N2155-1-b079	89.629103	-65.477579	18.37	1.00	4721	4755948579728630016	2.1	316.67 ± 0.83	2.66 ± 0.22	-0.29 ± 0.14	-1.00	-1.00	0000001	M2FS
LMC	NGC 2155	N2155-1-b080	89.639153	-65.476685	16.32	1.41	4033	4755948682807830528	12.0	315.87 ± 0.23	0.49 ± 0.05	-0.73 ± 0.04	1.00	1.00	0000000	M2FS
LMC	NGC 2155	N2155-1-b081	89.622306	-65.389524	18.66	1.04	4810	4755955176798536832	2.5	347.04 ± 0.95	1.67 ± 0.30	-1.00 ± 0.13	0.00	0.00	0000000	M2FS
LMC	NGC 2155	N2155-1-b082	89.622363	-65.431850	17.86	1.19	4565	4755949129484405760	5.8	323.35 ± 0.41	1.06 ± 0.12	-0.80 ± 0.05	0.00	0.00	0000000	M2FS
LMC	NGC 2155	N2155-1-b083	89.623214	-65.436291	18.92	1.06	4883	4755949129474024576	2.7	332.64 ± 1.06	0.89 ± 0.38	-0.90 ± 0.12	0.00	0.00	0000000	M2FS
LMC	NGC 2155	N2155-1-b084	89.617435	-65.452759	18.95	1.06	4892	4755948781579703552	2.5	304.04 ± 0.91	2.08 ± 0.32	-0.67 ± 0.12	0.00	0.00	0000000	M2FS
LMC	NGC 2155	N2155-1-b085	89.624707	-65.459394	18.07	1.26	4631	4755948717157185536	5.4	266.10 ± 0.45	1.26 ± 0.16	-1.28 ± 0.07	0.00	0.00	0000000	M2FS
LMC	NGC 2155	N2155-1-b086	89.613798	-65.460056	18.38	1.10	4724	4755948785887033216	4.1	315.40 ± 0.71	1.08 ± 0.23	-1.03 ± 0.10	0.92	0.91	0000000	M2FS
LMC	NGC 2155	N2155-1-b087	89.624068	-65.466659	18.67	0.96	4813	4755948678507818880	2.8	314.92 ± 0.63	1.26 ± 0.29	-0.74 ± 0.11	0.99	0.99	0000000	M2FS
LMC	NGC 2155	N2155-1-b088	89.625040	-65.472332	18.76	0.99	4839	4755948678507819520	2.6	315.43 ± 1.17	1.61 ± 0.35	-0.78 ± 0.12	1.00	1.00	0000000	M2FS
LMC	NGC 2155	N2155-1-b090	89.611654	-65.430321	18.66	1.22	4810	4755949193896591616	3.2	289.15 ± 0.67	1.58 ± 0.25	-0.84 ± 0.10	0.00	0.00	0000000	M2FS
LMC	NGC 2155	N2155-1-b091	89.612157	-65.444030	15.46	2.91	3673	4755949163844147712	3.6	287.73 ± 2.26	1.28 ± 0.32	-1.89 ± 0.25	-1.00	-1.00	0110010	M2FS
LMC	NGC 2155	N2155-1-b092	89.606612	-65.452241	17.84	1.36	4560	4755948785887028224	4.1	325.90 ± 0.55	1.34 ± 0.14	-0.69 ± 0.07	0.00	0.00	0000000	M2FS
LMC	NGC 2155	N2155-1-b093	89.594560	-65.457477	18.67	1.08	4813	4755948751527291136	3.3	316.00 ± 0.69	1.50 ± 0.23	-0.80 ± 0.10	0.82	0.83	0000000	M2FS
LMC	NGC 2155	N2155-1-b094	89.589745	-65.473153	18.76	1.16	4839	4755948644140724992	2.6	270.98 ± 0.66	1.83 ± 0.27	-1.16 ± 0.13	0.00	0.00	0000000	M2FS
LMC	NGC 2155	N2155-1-b095	89.606396	-65.475332	16.82	1.51	4219	4755948644140734720	9.1	315.23 ± 0.27	0.92 ± 0.06	-0.72 ± 0.04	0.99	0.99	0000000	M2FS
LMC	NGC 2155	N2155-1-b096	89.582989	-65.484144	17.95	1.27	4594	4755948609780975488	5.5	336.67 ± 0.39	1.49 ± 0.11	-0.67 ± 0.06	0.00	0.00	0000000	M2FS
LMC	NGC 2155	N2155-1-b098	89.564309	-65.515280	17.30	1.01	4383	4755947205339110784	7.9	295.15 ± 0.43	0.43 ± 0.14	-1.20 ± 0.05	0.00	0.00	0000010	M2FS
LMC	NGC 2155	N2155-1-b099	89.536408	-65.503629	18.67	1.04	4812	4755947201031682432	3.1	301.66 ± 0.78	1.44 ± 0.27	-0.95 ± 0.11	0.00	0.00	0000000	M2FS
LMC	NGC 2155	N2155-1-b100	89.553266	-65.497763	18.98	1.08	4900	4755947304110902656	2.5	341.68 ± 1.24	1.89 ± 0.38	-0.91 ± 0.14	0.00	0.00	0000000	M2FS
LMC	NGC 2155	N2155-1-b101	89.533209	-65.495734	16.52	0.94	4109	4755947377137766272	15.6	311.49 ± 0.34	0.07 ± 0.06	-1.80 ± 0.04	0.00	0.00	0000010	M2FS
LMC	NGC 2155	N2155-1-b102	89.555825	-65.494232	16.72	1.50	4185	4755947308418292608	8.1	338.92 ± 0.29	0.50 ± 0.08	-0.94 ± 0.04	0.00	0.00	0000000	M2FS

Table C.1: (*continued*) Sample of 3095 Targets from 26 Star Clusters

Galaxy	Cluster	ID	RAJ2000 (deg)	DEJ2000 (deg)	G (mag)	$G_{\rm BP} - G_{\rm RP}$ (mag)	$T_{\rm eff}$ (K)	*Gaia* DR2 ID	S/N	$v_{\rm los}$ (km s^{-1})	$\log g$ (dex)	$[{\rm Fe/H}]_{\rm raw}$ (dex)	P_M	P'_M	Flag[a]	Source[b]
(1)	(2)	(3)	(4)	(5)	(6)	(7)	(8)	(9)	(10)	(11)	(12)	(13)	(14)	(15)	(16)	(17)
LMC	NGC 2155	N2155-1-b103	89.546993	-65.488306	18.82	1.11	4857	4755947338470650112	2.9	354.26 ± 1.39	1.42 ± 0.45	-1.21 ± 0.13	0.00	0.00	0000000	M2FS
LMC	NGC 2155	N2155-1-b104	89.573016	-65.477567	15.99	1.76	3889	4755948820246773376	15.7	316.21 ± 0.18	0.70 ± 0.04	-0.72 ± 0.03	0.39	0.37	0000000	M2FS
LMC	NGC 2155	N2155-1-b106	89.596269	-65.520947	18.71	1.13	4824	4755946994873236480	2.5	310.73 ± 1.13	1.73 ± 0.27	-0.60 ± 0.12	0.00	0.00	0000000	M2FS
LMC	NGC 2155	N2155-1-b107	89.574176	-65.517205	18.71	1.09	4825	4755947201031670016	2.7	316.29 ± 1.10	1.67 ± 0.27	-0.87 ± 0.14	0.00	0.00	0000000	M2FS
LMC	NGC 2155	N2155-1-b108	89.590849	-65.507985	18.36	1.14	4719	4755947097952462976	1.7	253.65 ± 9.00	1.24 ± 0.88	-3.06 ± 0.36	-1.00	-1.00	1000000	M2FS
LMC	NGC 2155	N2155-1-b109	89.599706	-65.485210	18.34	1.22	4714	4755948609780973824	3.8	315.92 ± 0.61	1.67 ± 0.19	-0.62 ± 0.08	0.98	0.98	0000000	M2FS
LMC	NGC 2155	N2155-1-b110	89.609187	-65.481627	18.77	0.97	4841	4755948648448107648	2.3	286.18 ± 1.02	1.07 ± 0.37	-0.71 ± 0.11	0.00	0.00	0000000	M2FS
LMC	NGC 2155	N2155-1-b111	89.599597	-65.481646	18.69	1.07	4818	4755948609780978816	2.6	315.28 ± 1.13	1.01 ± 0.33	-0.85 ± 0.12	0.98	0.98	0000000	M2FS
LMC	NGC 2155	N2155-1-b112	89.593516	-65.477141	16.39	1.61	4061	4755948644140722304	11.9	314.52 ± 0.21	0.66 ± 0.05	-0.66 ± 0.04	0.99	0.99	0000000	M2FS
LMC	NGC 2155	N2155-1-b115	89.583176	-65.450162	18.01	1.29	4611	4755948781579707008	6.0	308.27 ± 0.48	1.10 ± 0.15	-1.08 ± 0.06	0.00	0.00	0000000	M2FS
LMC	NGC 2155	N2155-1-b116	89.575256	-65.465562	17.41	1.36	4421	4755948854606682240	7.6	319.74 ± 0.29	1.13 ± 0.08	-0.76 ± 0.05	0.00	0.00	0000000	M2FS
LMC	NGC 2155	N2155-1-b117	89.566023	-65.466455	18.81	1.00	4854	4755948854606681472	3.2	316.96 ± 0.78	1.99 ± 0.24	-0.67 ± 0.11	0.09	0.09	0000000	M2FS
LMC	NGC 2155	N2155-1-b118	89.578261	-65.469594	18.52	1.25	4767	4755948648448252416	3.3	316.39 ± 0.68	2.04 ± 0.19	-0.60 ± 0.10	0.76	0.73	0000000	M2FS
LMC	NGC 2155	N2155-1-b119	89.566628	-65.475213	18.05	1.28	4624	4755948815939414784	4.3	314.25 ± 0.58	1.79 ± 0.14	-0.61 ± 0.07	0.81	0.81	0000000	M2FS
LMC	NGC 2155	N2155-1-b120	89.574255	-65.486354	17.72	1.17	4520	4755947338470652160	6.7	298.42 ± 0.34	0.98 ± 0.11	-0.74 ± 0.05	0.00	0.00	0000000	M2FS
LMC	NGC 2155	N2155-1-b122	89.518481	-65.438152	17.89	1.25	4573	4755949022097889408	4.7	267.22 ± 0.50	1.67 ± 0.12	-0.60 ± 0.07	0.00	0.00	0000000	M2FS
LMC	NGC 2155	N2155-1-b123	89.546637	-65.447301	17.78	1.19	4541	4755948953378402560	6.6	349.04 ± 0.48	1.05 ± 0.13	-1.20 ± 0.06	0.00	0.00	0000000	M2FS
LMC	NGC 2155	N2155-1-b124	89.535896	-65.461621	17.33	1.33	4396	4755948854606500608	8.5	346.88 ± 0.23	0.87 ± 0.07	-1.03 ± 0.04	0.00	0.00	0000000	M2FS
LMC	NGC 2155	N2155-1-b125	89.551902	-65.462226	18.22	1.05	4675	4755948854596121344	5.3	297.47 ± 0.47	1.32 ± 0.15	-0.77 ± 0.07	0.00	0.00	0000000	M2FS
LMC	NGC 2155	N2155-1-b126	89.530410	-65.471013	17.95	1.07	4592	4755948888966241920	5.5	302.90 ± 0.59	0.88 ± 0.17	-0.81 ± 0.06	0.00	0.00	0000000	M2FS
LMC	NGC 2155	N2155-1-b127	89.532788	-65.483392	18.80	0.93	4850	4755947411487125760	3.6	372.16 ± 0.81	2.13 ± 0.25	-0.80 ± 0.11	-1.00	-1.00	0000100	M2FS
LMC	NGC 2155	N2155-1-b128	89.552766	-65.485459	18.75	0.77	4837	4755947338470653696	3.0	299.48 ± 1.59	2.13 ± 0.60	-2.65 ± 0.20	-1.00	-1.00	1000010	M2FS
LMC	NGC 2155	N2155-1-r028	89.638683	-65.472997	16.99	1.38	4278	4755948678518195968	10.1	313.50 ± 0.26	0.89 ± 0.06	-0.84 ± 0.04	1.00	1.00	0000000	M2FS
LMC	NGC 2155	N2155-1-r049	89.651140	-65.479663	17.63	1.37	4493	4755948682807854976	8.3	332.88 ± 0.27	1.27 ± 0.08	-0.83 ± 0.04	0.00	0.00	0000000	M2FS
LMC	NGC 2155	N2155-1-r079	89.612105	-65.472133	17.39	1.39	4415	4755948751527299456	8.5	314.86 ± 0.35	1.11 ± 0.08	-0.75 ± 0.04	0.99	0.99	0000000	M2FS
LMC	NGC 2155	N2155-1-r127	89.656820	-65.472076	17.65	1.19	4497	4755948717167587712	7.9	314.53 ± 0.39	1.10 ± 0.09	-0.78 ± 0.05	0.99	0.99	0000000	M2FS
LMC	NGC 2203	N2203-c-b002	91.271774	-75.468020	18.87	1.12	4925	5261691282447293440	2.6	251.19 ± 0.91	1.61 ± 0.32	-0.75 ± 0.14	0.97	0.97	0000000	M2FS
LMC	NGC 2203	N2203-c-b003	91.313464	-75.461492	18.59	1.23	4841	5261691316807043968	3.1	257.21 ± 0.89	1.70 ± 0.25	-0.57 ± 0.12	0.02	0.02	0000000	M2FS
LMC	NGC 2203	N2203-c-b004	91.263582	-75.450221	18.88	1.12	4927	5261692038361584256	3.2	253.56 ± 0.95	1.90 ± 0.25	-0.69 ± 0.13	1.00	1.00	0000000	M2FS
LMC	NGC 2203	N2203-c-b005	91.259147	-75.445557	17.90	1.12	4617	5261692111378495104	6.9	251.69 ± 0.43	0.23 ± 0.16	-1.00 ± 0.06	-1.00	-1.00	0000001	M2FS
LMC	NGC 2203	N2203-c-b006	91.312187	-75.444425	18.12	1.19	4690	5261692141440809344	6.0	254.35 ± 0.49	1.55 ± 0.13	-0.76 ± 0.06	0.98	0.98	0000000	M2FS
LMC	NGC 2203	N2203-c-b007	91.270450	-75.443440	17.98	1.32	4643	5261692107081078016	6.6	252.97 ± 0.38	1.51 ± 0.12	-0.63 ± 0.05	1.00	1.00	0000000	M2FS
LMC	NGC 2203	N2203-c-b008	91.248297	-75.443414	15.29	2.34	3940	5261692111378493440	14.2	253.41 ± 0.35	1.15 ± 0.08	-0.50 ± 0.06	1.00	1.00	0000010	M2FS
LMC	NGC 2203	N2203-c-b009	91.390136	-75.524852	17.65	1.47	4532	5261643801586372864	2.5	250.32 ± 0.79	2.02 ± 0.21	-0.79 ± 0.14	0.00	0.00	0000000	M2FS
LMC	NGC 2203	N2203-c-b010	91.394520	-75.518752	18.91	1.06	4938	5261643797288750080	0.9	183.38 ± 125.95	2.74 ± 1.10	-2.04 ± 0.75	-1.00	-1.00	1000000	M2FS
LMC	NGC 2203	N2203-c-b011	91.520822	-75.510208	18.67	1.12	4867	5261643453691374336	1.2	241.62 ± 10.58	0.95 ± 0.59	-1.54 ± 0.34	-1.00	-1.00	1000000	M2FS
LMC	NGC 2203	N2203-c-b012	91.359706	-75.490406	18.91	1.11	4938	5261644140886196352	1.7	233.37 ± 1.17	1.32 ± 0.43	-0.64 ± 0.18	0.00	0.00	0000000	M2FS
LMC	NGC 2203	N2203-c-b013	91.503240	-75.485925	17.95	1.23	4635	5261644488781147008	4.6	250.35 ± 0.59	1.43 ± 0.16	-0.86 ± 0.07	0.00	0.00	0000000	M2FS
LMC	NGC 2203	N2203-c-b014	91.563843	-75.451776	16.59	1.57	4159	5261691595982451712	10.6	248.30 ± 0.24	0.35 ± 0.08	-1.25 ± 0.04	0.00	0.00	0000000	M2FS
LMC	NGC 2203	N2203-c-b015	91.415483	-75.444041	18.47	1.11	4803	5261691419886295168	5.0	247.86 ± 0.74	1.66 ± 0.20	-1.01 ± 0.09	0.00	0.00	0000000	M2FS
LMC	NGC 2203	N2203-c-b016	91.625293	-75.442403	17.94	1.41	4631	5261691595982456576	4.3	231.69 ± 0.55	1.72 ± 0.16	-0.61 ± 0.08	0.00	0.00	0000000	M2FS
LMC	NGC 2203	N2203-1-b017	91.410623	-75.349435	18.59	0.90	4842	5261696195890163584	2.1	64.19 ± 1.27	2.63 ± 0.44	-1.69 ± 0.23	-1.00	-1.00	0000100	M2FS
LMC	NGC 2203	N2203-1-b018	91.476179	-75.372593	16.84	0.88	4249	5261695856589991424	7.4	-27.05 ± 0.61	1.61 ± 0.09	-1.73 ± 0.07	-1.00	-1.00	0000110	M2FS
LMC	NGC 2203	N2203-c-b019	91.550228	-75.381167	18.99	1.17	4958	5261692867292762240	3.7	257.25 ± 0.93	2.23 ± 0.20	-0.58 ± 0.10	0.00	0.00	0000000	M2FS
LMC	NGC 2203	N2203-c-b020	91.430203	-75.382747	18.90	1.06	4933	5261695852292701824	3.8	255.26 ± 0.80	2.04 ± 0.26	-0.85 ± 0.12	0.00	0.00	0000000	M2FS
LMC	NGC 2203	N2203-c-b021	91.395531	-75.397858	18.22	1.29	4725	5261692519398048000	5.6	254.87 ± 0.48	1.94 ± 0.13	-0.57 ± 0.06	0.00	0.00	0000000	M2FS
LMC	NGC 2203	N2203-c-b022	91.358429	-75.409225	18.37	1.24	4774	5261692454973334144	3.0	252.69 ± 0.85	1.91 ± 0.23	-0.50 ± 0.10	0.99	0.99	0000000	M2FS
LMC	NGC 2203	N2203-c-b023	91.309722	-75.433919	18.76	1.24	4893	5261692210160311168	1.1	259.26 ± 7.76	1.33 ± 0.69	-0.76 ± 0.29	0.94	0.94	0000000	M2FS
LMC	NGC 2203	N2203-c-b024	91.361686	-75.439878	18.84	1.13	4916	5261692180097982208	2.6	253.65 ± 1.11	2.27 ± 0.33	-0.82 ± 0.15	0.98	0.98	0000000	M2FS
LMC	NGC 2203	N2203-c-b026	91.256822	-75.337578	16.71	1.62	4203	5261696715583349632	18.0	248.45 ± 0.17	0.70 ± 0.04	-0.80 ± 0.03	0.00	0.00	0000000	M2FS
LMC	NGC 2203	N2203-c-b027	91.251172	-75.388956	17.85	1.39	4601	5261695611774535552	5.5	253.41 ± 0.39	1.74 ± 0.12	-0.52 ± 0.06	0.98	0.99	0000000	M2FS
LMC	NGC 2203	N2203-c-b028	91.248686	-75.404095	18.65	1.28	4862	5261695341191318016	3.2	253.80 ± 0.75	1.95 ± 0.24	-0.48 ± 0.10	0.98	0.98	0000000	M2FS
LMC	NGC 2203	N2203-c-b029	91.266824	-75.405722	18.99	1.17	4961	5261695336896586752	2.3	256.92 ± 1.37	1.63 ± 0.40	-0.69 ± 0.16	0.67	0.68	0000000	M2FS
LMC	NGC 2203	N2203-c-b030	91.288112	-75.412350	18.07	1.29	4674	5261692485038283008	4.1	253.18 ± 0.60	1.58 ± 0.17	-0.73 ± 0.08	0.99	0.99	0000000	M2FS

Table C.1: (*continued*) Sample of 3095 Targets from 26 Star Clusters

Galaxy	Cluster	ID	RAJ2000 (deg)	DEJ2000 (deg)	G (mag)	$G_{\rm BP} - G_{\rm RP}$ (mag)	$T_{\rm eff}$ (K)	*Gaia* DR2 ID	S/N	$v_{\rm los}$ ($\rm km\,s^{-1}$)	$\log g$ (dex)	$[{\rm Fe/H}]_{\rm raw}$ (dex)	P_M	P'_M	Flag[a]	Source[b]
(1)	(2)	(3)	(4)	(5)	(6)	(7)	(8)	(9)	(10)	(11)	(12)	(13)	(14)	(15)	(16)	(17)
LMC	NGC 2203	N2203-c-b031	91.268891	-75.423924	15.94	1.89	3940	5261692317536923264	11.7	253.08 ± 0.24	1.02 ± 0.05	-0.54 ± 0.04	1.00	1.00	0000000	M2FS
LMC	NGC 2203	N2203-c-b032	91.248505	-75.432285	18.93	0.92	4942	5261692317534362368	2.3	252.64 ± 1.52	2.26 ± 0.34	-0.64 ± 0.15	1.00	1.00	0000000	M2FS
LMC	NGC 2203	N2203-c-b033	91.176434	-75.521527	18.96	1.22	4951	5261643973385042816	0.9	253.25 ± 5.50	2.54 ± 0.68	-0.55 ± 0.31	0.00	0.00	0000000	M2FS
LMC	NGC 2203	N2203-c-b034	91.173633	-75.466753	18.20	1.20	4719	5261692004001812736	3.0	252.44 ± 0.78	1.90 ± 0.22	-0.60 ± 0.10	1.00	1.00	0000000	M2FS
LMC	NGC 2203	N2203-c-b035	91.188668	-75.457825	18.88	0.96	4928	5261692072721312640	1.4	253.65 ± 1.93	1.12 ± 0.65	-0.75 ± 0.21	1.00	1.00	0000000	M2FS
LMC	NGC 2203	N2203-c-b036	91.182369	-75.454599	18.50	1.22	4813	5261692072721418496	3.6	253.53 ± 0.63	2.25 ± 0.17	-0.43 ± 0.09	1.00	1.00	0000000	M2FS
LMC	NGC 2203	N2203-c-b037	91.193545	-75.450498	18.98	0.82	4958	5261692072720628224	2.4	250.57 ± 1.24	2.29 ± 0.29	-0.35 ± 0.14	0.99	0.99	0000000	M2FS
LMC	NGC 2203	N2203-c-b038	91.179919	-75.449306	18.88	0.81	4929	5261692077018742784	3.3	254.83 ± 1.11	2.20 ± 0.24	-0.62 ± 0.11	1.00	1.00	0000010	M2FS
LMC	NGC 2203	N2203-c-b039	91.178339	-75.445792	18.91	1.02	4938	5261692283174571392	4.9	252.99 ± 0.56	2.24 ± 0.15	-0.50 ± 0.07	1.00	1.00	0000000	M2FS
LMC	NGC 2203	N2203-c-b040	91.185808	-75.441907	17.66	1.08	4536	5261692283174483456	3.3	252.66 ± 0.68	1.36 ± 0.20	-0.48 ± 0.08	1.00	1.00	0000000	M2FS
LMC	NGC 2203	N2203-c-b042	91.195148	-75.472130	18.93	1.07	4942	5261691248087551360	2.5	250.56 ± 1.03	2.17 ± 0.25	-0.61 ± 0.13	0.96	0.95	0000000	M2FS
LMC	NGC 2203	N2203-c-b043	91.221787	-75.471844	18.73	1.05	4885	5261691282447289088	1.0	255.72 ± 2.11	2.82 ± 0.52	-0.41 ± 0.33	0.97	0.97	0000000	M2FS
LMC	NGC 2203	N2203-c-b044	91.200568	-75.468382	15.59	2.49	3940	5261691252385031936	3.0	264.16 ± 2.08	0.82 ± 0.30	-1.49 ± 0.22	-1.00	-1.00	0110010	M2FS
LMC	NGC 2203	N2203-c-b045	91.222550	-75.458446	18.38	1.32	4777	5261692038361566720	2.2	253.31 ± 1.20	1.23 ± 0.40	-0.65 ± 0.14	1.00	1.00	0000000	M2FS
LMC	NGC 2203	N2203-c-b046	91.241706	-75.448126	18.87	1.01	4925	5261692107081083648	3.2	253.00 ± 0.93	2.14 ± 0.28	-0.65 ± 0.12	1.00	1.00	0000000	M2FS
LMC	NGC 2203	N2203-c-b047	91.214148	-75.446500	18.86	0.84	4922	5261692107081153920	3.5	249.57 ± 0.81	2.02 ± 0.23	-0.56 ± 0.09	0.99	0.98	0000000	M2FS
LMC	NGC 2203	N2203-c-b048	91.203432	-75.442272	18.86	0.90	4922	5261692283174597760	2.7	254.09 ± 0.93	2.24 ± 0.25	-0.53 ± 0.13	1.00	1.00	0000000	M2FS
LMC	NGC 2203	N2203-c-b049	91.215728	-75.383578	17.69	0.97	4547	5261695684791262848	5.7	57.71 ± 0.59	2.20 ± 0.12	-1.11 ± 0.09	-1.00	-1.00	0000110	M2FS
LMC	NGC 2203	N2203-c-b050	91.214566	-75.394078	18.89	1.09	4933	5261695611774526592	2.4	251.35 ± 1.13	1.86 ± 0.31	-0.59 ± 0.15	0.96	0.96	0000000	M2FS
LMC	NGC 2203	N2203-c-b051	91.244593	-75.412945	18.89	1.09	4933	5261695341193893248	1.3	253.82 ± 3.87	1.44 ± 0.67	-1.03 ± 0.30	0.99	0.99	0000000	M2FS
LMC	NGC 2203	N2203-c-b053	91.227021	-75.432608	17.91	1.25	4620	5261692317534352384	2.8	251.17 ± 0.74	1.97 ± 0.19	-0.39 ± 0.10	1.00	1.00	0000000	M2FS
LMC	NGC 2203	N2203-c-b054	91.244679	-75.436195	16.02	1.85	3940	5261692313246233344	7.7	251.62 ± 0.27	1.01 ± 0.06	-0.52 ± 0.05	1.00	1.00	0000000	M2FS
LMC	NGC 2203	N2203-c-b055	91.226653	-75.438170	18.58	1.07	4839	5261692317536918656	2.3	252.56 ± 1.09	1.94 ± 0.31	-0.50 ± 0.12	1.00	1.00	0000000	M2FS
LMC	NGC 2203	N2203-c-b056	91.218557	-75.441108	18.95	0.87	4947	5261692313239584000	0.6	253.78 ± 32.76	2.44 ± 0.89	-0.45 ± 0.50	-1.00	-1.00	1000000	M2FS
LMC	NGC 2203	N2203-c-b058	91.197514	-75.346983	18.99	1.24	4959	5261696711286265216	2.8	239.93 ± 0.93	1.82 ± 0.33	-0.84 ± 0.13	0.00	0.00	0000000	M2FS
LMC	NGC 2203	N2203-c-b059	91.207328	-75.374599	18.04	1.30	4663	5261695684791458944	5.2	253.17 ± 0.44	1.58 ± 0.13	-0.60 ± 0.06	0.00	0.00	0000000	M2FS
LMC	NGC 2203	N2203-c-b060	91.207408	-75.378604	18.89	0.96	4930	5261695680494041984	3.2	16.95 ± 1.53	3.36 ± 0.21	-1.02 ± 0.16	-1.00	-1.00	0001100	M2FS
LMC	NGC 2203	N2203-c-b061	91.201132	-75.411177	18.75	0.78	4890	5261695341193883648	1.3	272.75 ± 9.18	3.35 ± 0.70	-1.90 ± 0.36	-1.00	-1.00	1000000	M2FS
LMC	NGC 2203	N2203-c-b062	91.210222	-75.423441	17.55	1.37	4501	5261692381963520000	5.2	251.06 ± 0.51	1.20 ± 0.12	-0.61 ± 0.06	1.00	1.00	0000000	M2FS
LMC	NGC 2203	N2203-c-b063	91.212249	-75.430787	15.92	1.78	3940	5261692381959053952	8.4	254.86 ± 0.24	0.92 ± 0.05	-0.50 ± 0.04	1.00	1.00	0000000	M2FS
LMC	NGC 2203	N2203-c-b064	91.201685	-75.433844	18.64	0.97	4858	5261692283174588288	1.2	254.79 ± 1.27	2.74 ± 0.34	-0.03 ± 0.21	-1.00	-1.00	1000000	M2FS
LMC	NGC 2203	N2203-c-b068	91.111261	-75.525556	18.71	1.05	4879	5261685033272381696	1.3	100.19 ± 1.65	2.57 ± 0.41	-0.34 ± 0.26	-1.00	-1.00	0000100	M2FS
LMC	NGC 2203	N2203-c-b069	91.130648	-75.457645	18.99	0.98	4960	5261686197206159616	2.8	251.33 ± 0.84	2.32 ± 0.27	-0.46 ± 0.12	1.00	1.00	0000000	M2FS
LMC	NGC 2203	N2203-c-b070	91.132721	-75.451760	18.99	1.14	4959	5261686407661840128	1.5	254.29 ± 1.81	1.45 ± 0.66	-0.65 ± 0.21	1.00	1.00	0000000	M2FS
LMC	NGC 2203	N2203-c-b071	91.106847	-75.444295	18.65	1.20	4860	5261686472084063104	4.5	250.56 ± 0.59	2.24 ± 0.18	-0.41 ± 0.08	0.99	0.99	0000000	M2FS
LMC	NGC 2203	N2203-c-b072	91.126380	-75.444085	18.56	1.02	4834	5261686472084062720	4.4	253.85 ± 0.45	2.05 ± 0.17	-0.50 ± 0.08	1.00	1.00	0000000	M2FS
LMC	NGC 2203	N2203-c-b073	91.144579	-75.470895	18.77	1.19	4896	5261692004001817472	2.0	252.26 ± 1.21	1.37 ± 0.37	-0.48 ± 0.14	0.99	0.99	0000000	M2FS
LMC	NGC 2203	N2203-c-b074	91.148468	-75.467285	17.87	1.18	4607	5261692008299263616	5.4	203.95 ± 0.69	0.78 ± 0.24	-1.64 ± 0.07	0.00	0.00	0000000	M2FS
LMC	NGC 2203	N2203-c-b075	91.165911	-75.458184	18.97	0.96	4954	5261692077016144896	2.5	254.11 ± 1.28	2.09 ± 0.32	-0.46 ± 0.14	1.00	1.00	0000000	M2FS
LMC	NGC 2203	N2203-c-b076	91.144334	-75.455260	18.51	1.09	4819	5261692077016122368	2.4	251.09 ± 1.17	2.02 ± 0.34	-0.69 ± 0.14	1.00	1.00	0000000	M2FS
LMC	NGC 2203	N2203-c-b077	91.158505	-75.452166	18.32	1.14	4758	5261692077016133120	2.6	256.91 ± 0.80	1.99 ± 0.26	-0.53 ± 0.11	0.96	0.96	0000000	M2FS
LMC	NGC 2203	N2203-c-b078	91.166783	-75.447724	18.74	0.83	4887	5261692278879846272	3.9	255.03 ± 0.79	1.98 ± 0.23	-0.79 ± 0.11	1.00	1.00	0000010	M2FS
LMC	NGC 2203	N2203-c-b079	91.156276	-75.444823	18.12	1.11	4691	5261692283174552704	3.6	250.30 ± 0.57	1.68 ± 0.19	-0.57 ± 0.08	1.00	1.00	0000000	M2FS
LMC	NGC 2203	N2203-c-b080	91.133340	-75.440850	18.93	1.00	4941	5261692351893918080	2.3	254.08 ± 1.20	2.22 ± 0.36	-0.41 ± 0.13	1.00	1.00	0000000	M2FS
LMC	NGC 2203	N2203-c-b081	91.182711	-75.398383	18.12	1.30	4690	5261695577414780928	1.7	252.96 ± 1.28	1.48 ± 0.40	-0.80 ± 0.21	0.98	0.98	0000000	M2FS
LMC	NGC 2203	N2203-c-b082	91.179734	-75.413315	18.15	1.15	4700	5261695371256315648	3.0	253.80 ± 1.02	1.92 ± 0.22	-0.66 ± 0.11	1.00	1.00	0000000	M2FS
LMC	NGC 2203	N2203-c-b083	91.198996	-75.417771	18.96	1.09	4952	5261695302541270912	1.9	253.61 ± 1.65	2.48 ± 0.39	-0.77 ± 0.21	1.00	1.00	0000000	M2FS
LMC	NGC 2203	N2203-c-b084	91.177468	-75.422737	18.13	1.19	4694	5261695306834142592	2.0	249.98 ± 1.28	2.41 ± 0.24	-0.46 ± 0.15	0.99	0.99	0000000	M2FS
LMC	NGC 2203	N2203-c-b085	91.182812	-75.426299	18.91	0.83	4937	5261692351894036352	1.8	251.66 ± 1.48	2.09 ± 0.43	-0.53 ± 0.17	1.00	1.00	0000000	M2FS
LMC	NGC 2203	N2203-c-b086	91.187371	-75.429796	18.89	0.82	4931	5261692351894041600	2.0	256.15 ± 1.33	2.25 ± 0.34	-0.58 ± 0.19	1.00	1.00	0000010	M2FS
LMC	NGC 2203	N2203-c-b087	91.179013	-75.432886	18.70	0.63	4876	5261692351896606464	3.5	252.48 ± 0.87	2.19 ± 0.20	-0.66 ± 0.10	1.00	1.00	0000010	M2FS
LMC	NGC 2203	N2203-c-b088	91.197603	-75.437429	18.31	0.90	4753	5261692278882621952	2.6	252.83 ± 0.94	2.25 ± 0.25	-0.43 ± 0.11	1.00	1.00	0000010	M2FS
LMC	NGC 2203	N2203-c-b090	91.168456	-75.419964	18.98	1.05	4956	5261695302536826496	1.6	253.34 ± 1.60	1.92 ± 0.47	-0.58 ± 0.20	1.00	1.00	0000000	M2FS
LMC	NGC 2203	N2203-c-b091	91.160353	-75.427469	18.25	1.19	4733	5261695302536819456	1.4	253.17 ± 1.46	1.60 ± 0.45	-0.40 ± 0.17	1.00	1.00	0000000	M2FS

Table C.1: (*continued*) Sample of 3095 Targets from 26 Star Clusters

Galaxy	Cluster	ID	RAJ2000 (deg)	DEJ2000 (deg)	G (mag)	$G_{\rm BP} - G_{\rm RP}$ (mag)	$T_{\rm eff}$ (K)	*Gaia* DR2 ID	S/N	$v_{\rm los}$ ($\rm km\,s^{-1}$)	$\log g$ (dex)	$[{\rm Fe/H}]_{\rm raw}$ (dex)	P_M	P'_M	Flag[a]	Source[b]
(1)	(2)	(3)	(4)	(5)	(6)	(7)	(8)	(9)	(10)	(11)	(12)	(13)	(14)	(15)	(16)	(17)
LMC	NGC 2203	N2203-c-b092	91.173712	-75.429125	18.96	0.89	4950	5261692351894028928	1.1	244.67 ± 3.07	2.62 ± 0.62	-0.61 ± 0.45	1.00	-1.00	0000000	M2FS
LMC	NGC 2203	N2203-c-b093	91.154999	-75.431155	18.66	1.01	4864	5261692351893926656	2.4	257.05 ± 1.20	2.59 ± 0.25	-0.50 ± 0.16	1.00	1.00	0000000	M2FS
LMC	NGC 2203	N2203-c-b094	91.163947	-75.435264	18.06	0.91	4670	5261692351896604160	2.5	254.31 ± 1.04	1.97 ± 0.23	-0.48 ± 0.12	1.00	1.00	0000010	M2FS
LMC	NGC 2203	N2203-c-b095	91.148673	-75.438363	18.97	0.78	4954	5261692351893931136	1.0	255.28 ± 1.85	3.12 ± 0.45	0.19 ± 0.25	-1.00	-1.00	1000010	M2FS
LMC	NGC 2203	N2203-c-b096	91.169098	-75.438869	18.77	0.68	4897	5261692283174481792	1.6	253.23 ± 1.19	3.12 ± 0.33	-0.27 ± 0.18	-1.00	-1.00	1000010	M2FS
LMC	NGC 2203	N2203-c-b097	90.782312	-75.482394	18.98	1.21	4957	5261688877269845248	1.4	260.30 ± 38.41	2.26 ± 0.75	-1.03 ± 0.54	-1.00	-1.00	1000000	M2FS
LMC	NGC 2203	N2203-c-b098	90.868945	-75.477864	18.61	0.76	4849	5261686300285243776	2.4	195.74 ± 2.20	2.97 ± 0.87	-2.99 ± 0.25	-1.00	-1.00	0100010	M2FS
LMC	NGC 2203	N2203-c-b099	90.790083	-75.475102	18.36	1.36	4768	5261688945985112192	1.8	-29.86 ± 1.48	4.59 ± 0.23	-0.24 ± 0.24	-1.00	-1.00	0001100	M2FS
LMC	NGC 2203	N2203-c-b100	91.065027	-75.472658	18.14	1.08	4697	5261686197206024320	4.3	254.30 ± 0.58	1.41 ± 0.18	-0.93 ± 0.09	-1.00	-1.00	0000001	M2FS
LMC	NGC 2203	N2203-c-b101	90.817382	-75.465811	18.75	1.21	4892	5261688950282434816	2.1	232.23 ± 1.66	2.36 ± 0.37	-0.69 ± 0.19	0.00	0.00	0000000	M2FS
LMC	NGC 2203	N2203-c-b102	91.081227	-75.465834	18.89	1.27	4931	5261686197206038912	1.6	252.22 ± 1.59	2.67 ± 0.42	-0.60 ± 0.21	0.99	0.99	0000000	M2FS
LMC	NGC 2203	N2203-c-b103	91.046071	-75.443122	17.99	1.39	4647	5261689392661767296	5.9	251.16 ± 0.43	1.75 ± 0.11	-0.55 ± 0.06	0.97	0.97	0000000	M2FS
LMC	NGC 2203	N2203-c-b104	91.023009	-75.442119	18.52	1.31	4821	5261689392661770880	3.4	252.11 ± 0.86	2.05 ± 0.22	-0.52 ± 0.10	0.99	0.99	0000000	M2FS
LMC	NGC 2203	N2203-c-b106	91.099653	-75.513159	18.72	1.08	4883	5261685097694304128	2.2	281.84 ± 1.41	1.23 ± 0.63	-1.61 ± 0.20	0.00	0.00	0000000	M2FS
LMC	NGC 2203	N2203-c-b107	91.097978	-75.476799	18.88	1.07	4927	5261686128486532480	3.4	250.54 ± 0.97	1.87 ± 0.25	-0.60 ± 0.10	0.88	0.86	0000000	M2FS
LMC	NGC 2203	N2203-1-b108	91.106658	-75.456221	18.69	1.19	4874	5261686403364509184	0.7	254.73 ± 2.31	3.90 ± 0.68	0.02 ± 0.45	-1.00	-1.00	1000000	M2FS
LMC	NGC 2203	N2203-c-b109	91.082125	-75.451264	18.83	1.17	4913	5261686472083984512	2.7	253.08 ± 1.00	1.96 ± 0.27	-0.69 ± 0.13	1.00	1.00	0000000	M2FS
LMC	NGC 2203	N2203-c-b110	91.087609	-75.445921	18.88	1.15	4929	5261686472083996160	2.4	252.41 ± 1.01	2.35 ± 0.26	-0.49 ± 0.14	1.00	1.00	0000000	M2FS
LMC	NGC 2203	N2203-c-b111	91.091455	-75.441838	18.98	0.94	4957	5261686476381306880	2.5	251.96 ± 1.02	2.27 ± 0.28	-0.61 ± 0.15	1.00	1.00	0000000	M2FS
LMC	NGC 2203	N2203-c-b112	91.090479	-75.436084	18.56	1.23	4833	5261689431318805376	3.9	252.44 ± 0.71	2.53 ± 0.15	-0.42 ± 0.09	1.00	1.00	0000000	M2FS
LMC	NGC 2203	N2203-c-b114	91.117080	-75.326653	18.61	1.15	4849	5261702689880792960	3.7	256.85 ± 0.92	1.55 ± 0.23	-0.65 ± 0.11	0.00	0.00	0000000	M2FS
LMC	NGC 2203	N2203-c-b116	91.136579	-75.415081	18.94	1.12	4945	5261695371256317696	1.3	214.67 ± 45.96	1.28 ± 0.72	-1.26 ± 0.41	-1.00	-1.00	0100000	M2FS
LMC	NGC 2203	N2203-c-b117	91.122834	-75.417483	18.87	1.07	4925	5261689495747696896	1.7	253.75 ± 1.34	2.85 ± 0.33	-0.60 ± 0.19	1.00	1.00	0000000	M2FS
LMC	NGC 2203	N2203-c-b118	91.134619	-75.426325	18.14	1.23	4697	5261695302536823040	2.3	253.15 ± 1.07	1.75 ± 0.29	-0.51 ± 0.13	1.00	1.00	0000000	M2FS
LMC	NGC 2203	N2203-c-b119	91.127034	-75.431172	18.01	1.18	4654	5261689427020772992	2.2	250.59 ± 0.80	1.86 ± 0.23	-0.43 ± 0.11	0.99	0.99	0000000	M2FS
LMC	NGC 2203	N2203-c-b120	91.135652	-75.435342	18.72	0.83	4880	5261692351893915904	1.9	250.54 ± 1.47	2.43 ± 0.32	-0.23 ± 0.15	1.00	1.00	0000010	M2FS
LMC	NGC 2203	N2203-c-b122	90.975638	-75.373390	18.85	1.03	4920	5261690732691745024	2.4	218.90 ± 1.77	0.80 ± 0.48	-1.57 ± 0.17	0.00	0.00	0000000	M2FS
LMC	NGC 2203	N2203-c-b123	90.922801	-75.375722	17.99	1.36	4648	5261690732691744256	3.9	258.93 ± 0.62	1.02 ± 0.20	-0.84 ± 0.08	0.00	0.00	0000000	M2FS
LMC	NGC 2203	N2203-c-b124	91.037064	-75.400551	18.91	1.14	4937	5261690492173510656	1.7	253.48 ± 2.30	2.43 ± 0.41	-0.62 ± 0.21	0.96	0.96	0000000	M2FS
LMC	NGC 2203	N2203-c-b125	91.052096	-75.416603	18.07	1.23	4673	5261689667539751296	2.8	216.29 ± 1.14	0.64 ± 0.39	-1.86 ± 0.16	0.00	0.00	0000000	M2FS
LMC	NGC 2203	N2203-c-b126	91.022530	-75.426024	17.73	1.17	4562	5261689671836963200	3.2	172.19 ± 0.93	2.42 ± 0.15	-0.48 ± 0.12	0.00	0.00	0000000	M2FS
LMC	NGC 2203	N2203-c-b127	90.834469	-75.426510	18.75	1.30	4890	5261689981074582528	1.8	242.16 ± 1.45	2.46 ± 0.36	-0.64 ± 0.20	0.00	0.00	0000000	M2FS
LMC	NGC 2203	N2203-c-b128	91.115674	-75.433998	19.00	1.10	4961	5261689431318809216	1.2	238.11 ± 1.65	2.80 ± 0.49	-0.08 ± 0.26	-1.00	-1.00	1000000	M2FS
LMC	NGC 2203	N2203-c-r028	91.064006	-75.457376	17.34	0.93	4427	5261686403364493824	9.2	81.29 ± 0.48	1.54 ± 0.09	-1.22 ± 0.06	-1.00	-1.00	0000110	M2FS
LMC	NGC 2203	N2203-2-r049	91.139258	-75.445451	17.65	1.34	4534	5261692283177100928	8.1	286.30 ± 0.47	0.18 ± 0.14	-1.19 ± 0.06	0.00	0.00	0000000	M2FS
LMC	NGC 2203	N2203-c-r099	91.182455	-75.437005	17.57	0.80	4507	5261692283177111168	5.7	254.21 ± 0.99	1.44 ± 0.20	-1.89 ± 0.09	-1.00	-1.00	0100010	M2FS
LMC	NGC 2203	N2203-c-r127	91.196031	-75.446767	17.98	1.14	4644	5261692077018746112	7.5	254.36 ± 0.43	1.55 ± 0.10	-0.69 ± 0.05	1.00	1.00	0000000	M2FS
LMC	NGC 2209	N2209-c-b002	92.219779	-73.874411	19.04	1.22	5043	5265047855230492672	3.5	246.31 ± 0.99	2.08 ± 0.27	-0.61 ± 0.10	0.00	0.00	0000000	M2FS
LMC	NGC 2209	N2209-c-b003	92.211784	-73.871284	19.11	1.22	5060	5265047850929534208	3.1	290.00 ± 0.99	1.09 ± 0.38	-1.12 ± 0.13	0.00	0.00	0000000	M2FS
LMC	NGC 2209	N2209-c-b004	92.208837	-73.845562	17.49	1.33	4525	5265048198827867776	9.3	252.57 ± 0.32	0.53 ± 0.13	-0.80 ± 0.04	0.87	0.84	0000000	M2FS
LMC	NGC 2209	N2209-c-b005	92.237848	-73.844246	19.13	0.88	5067	5265048160167265024	3.7	250.94 ± 0.81	2.09 ± 0.27	-0.84 ± 0.11	0.97	0.97	0000000	M2FS
LMC	NGC 2209	N2209-c-b006	92.213049	-73.841645	18.22	1.26	4774	5265048194527108224	6.9	251.31 ± 0.35	1.59 ± 0.12	-0.61 ± 0.05	0.98	0.98	0000000	M2FS
LMC	NGC 2209	N2209-c-b007	92.218330	-73.837758	15.48	2.13	4481	5265048198828268032	19.5	251.77 ± 0.29	2.60 ± 0.08	-0.13 ± 0.06	0.98	0.98	0000010	M2FS
LMC	NGC 2209	N2209-c-b008	92.217383	-73.832749	18.82	1.13	4980	5265095134223367552	4.2	250.44 ± 0.70	2.10 ± 0.19	-0.72 ± 0.09	0.97	0.96	0000000	M2FS
LMC	NGC 2209	N2209-c-b009	92.252959	-73.878271	17.00	1.63	4481	5265047133675993216	9.6	230.16 ± 0.29	1.19 ± 0.08	-0.60 ± 0.04	0.00	0.00	0000000	M2FS
LMC	NGC 2209	N2209-c-b010	92.272537	-73.874284	19.20	1.33	5086	5265047133668899584	2.6	242.64 ± 1.45	2.79 ± 0.31	-0.26 ± 0.12	0.00	0.00	0000000	M2FS
LMC	NGC 2209	N2209-c-b011	92.241623	-73.872298	19.18	1.34	5081	5265047889583134208	2.3	249.00 ± 1.14	1.87 ± 0.43	-0.66 ± 0.17	0.34	0.30	0000000	M2FS
LMC	NGC 2209	N2209-c-b012	92.252293	-73.862271	18.38	1.35	4831	5265047954008774144	4.5	252.25 ± 0.66	1.92 ± 0.18	-0.47 ± 0.07	0.69	0.70	0000000	M2FS
LMC	NGC 2209	N2209-c-b013	92.270351	-73.858639	18.93	1.05	5011	5265047954008782336	3.9	253.05 ± 1.00	0.86 ± 0.37	-1.30 ± 0.11	0.48	0.49	0000000	M2FS
LMC	NGC 2209	N2209-c-b014	92.252009	-73.857674	18.82	1.23	4980	5265047954008788352	2.8	250.62 ± 1.02	2.37 ± 0.29	-0.64 ± 0.14	0.78	0.76	0000000	M2FS
LMC	NGC 2209	N2209-c-b015	92.253268	-73.853096	18.23	1.28	4778	5265047954008804096	5.4	228.22 ± 0.44	1.80 ± 0.15	-0.56 ± 0.06	0.00	0.00	0000000	M2FS
LMC	NGC 2209	N2209-c-b016	92.240375	-73.849999	18.69	1.08	4938	5265048160167246592	5.1	236.58 ± 0.62	1.65 ± 0.23	-0.91 ± 0.08	0.00	0.00	0000000	M2FS
LMC	NGC 2209	N2209-c-b018	92.274971	-73.826601	19.01	1.16	5033	5265048228886796544	2.8	253.37 ± 0.97	1.73 ± 0.34	-0.61 ± 0.12	0.33	0.33	0000000	M2FS
LMC	NGC 2209	N2209-c-b019	92.313450	-73.827299	19.36	1.29	5142	5265048611137648384	2.5	271.54 ± 0.97	2.49 ± 0.32	-0.24 ± 0.12	0.00	0.00	0000000	M2FS

Table C.1: (*continued*) Sample of 3095 Targets from 26 Star Clusters

Galaxy	Cluster	ID	RAJ2000 (deg)	DEJ2000 (deg)	G (mag)	$G_{\rm BP} - G_{\rm RP}$ (mag)	$T_{\rm eff}$ (K)	*Gaia* DR2 ID	S/N	$v_{\rm los}$ ($\rm km\,s^{-1}$)	$\log g$ (dex)	$[{\rm Fe/H}]_{\rm raw}$ (dex)	P_M	P'_M	Flag[a]	Source[b]
(1)	(2)	(3)	(4)	(5)	(6)	(7)	(8)	(9)	(10)	(11)	(12)	(13)	(14)	(15)	(16)	(17)
LMC	NGC 2209	N2209-c-b020	92.319400	-73.842953	19.27	1.06	5108	5265048331965950208	3.1	226.96 ± 0.92	1.12 ± 0.42	-1.28 ± 0.13	0.00	0.00	0000000	M2FS
LMC	NGC 2209	N2209-c-b021	92.307847	-73.844988	18.34	1.26	4817	5265048336259745024	4.7	243.59 ± 0.44	1.83 ± 0.17	-0.54 ± 0.07	0.00	0.00	0000000	M2FS
LMC	NGC 2209	N2209-c-b022	92.289291	-73.845225	18.85	1.24	4986	5265047954008825088	2.8	233.49 ± 1.15	2.16 ± 0.33	-0.55 ± 0.13	0.00	0.00	0000000	M2FS
LMC	NGC 2209	N2209-c-b023	92.316189	-73.850500	18.22	1.40	4776	5265048331965927168	3.9	236.98 ± 0.53	1.97 ± 0.17	-0.35 ± 0.07	0.00	0.00	0000000	M2FS
LMC	NGC 2209	N2209-c-b024	92.290994	-73.854911	19.18	1.11	5080	5265047958309717248	2.1	244.00 ± 1.29	2.32 ± 0.36	-0.79 ± 0.17	0.00	0.00	0000000	M2FS
LMC	NGC 2209	N2209-c-b026	92.227744	-73.806363	19.03	1.24	5040	5265095409108381696	3.4	239.21 ± 0.76	2.23 ± 0.26	-0.46 ± 0.09	0.00	0.00	0000000	M2FS
LMC	NGC 2209	N2209-c-b027	92.218936	-73.809716	18.79	1.13	4971	5265095198649220864	4.4	231.83 ± 0.71	1.63 ± 0.21	-0.88 ± 0.08	0.00	0.00	0000000	M2FS
LMC	NGC 2209	N2209-c-b028	92.245406	-73.814135	19.20	1.13	5087	5265095233008923136	2.2	233.74 ± 1.03	2.29 ± 0.34	-0.67 ± 0.15	0.00	0.00	0000000	M2FS
LMC	NGC 2209	N2209-c-b029	92.221860	-73.817655	18.90	1.10	5001	5265095202949952256	3.0	249.49 ± 1.03	2.12 ± 0.28	-0.61 ± 0.11	0.91	0.90	0000000	M2FS
LMC	NGC 2209	N2209-c-b030	92.227879	-73.822342	17.71	1.41	4602	5265095134230477312	5.8	270.63 ± 0.50	1.72 ± 0.11	-0.48 ± 0.05	0.00	0.00	0000000	M2FS
LMC	NGC 2209	N2209-c-b031	92.229692	-73.832310	19.42	1.15	5167	5265048194527045760	2.2	250.29 ± 0.85	2.49 ± 0.34	-0.30 ± 0.12	0.96	0.96	0000000	M2FS
LMC	NGC 2209	N2209-c-b032	92.239748	-73.838239	19.19	1.10	5085	5265048228886762240	1.9	252.30 ± 1.04	2.31 ± 0.40	-0.34 ± 0.13	0.95	0.96	0000000	M2FS
LMC	NGC 2209	N2209-c-b033	92.152853	-73.883165	19.00	1.17	5032	5265047752151264256	2.3	226.56 ± 1.10	1.61 ± 0.43	-0.92 ± 0.17	0.00	0.00	0000000	M2FS
LMC	NGC 2209	N2209-c-b034	92.166824	-73.872610	19.43	1.14	5174	5265047816569798400	2.1	251.09 ± 1.28	2.55 ± 0.32	-0.64 ± 0.20	0.77	0.76	0000000	M2FS
LMC	NGC 2209	N2209-c-b035	92.171015	-73.853559	19.35	1.10	5139	5265048091456179840	1.8	252.16 ± 1.71	1.79 ± 0.48	-0.85 ± 0.20	0.95	0.95	0000000	M2FS
LMC	NGC 2209	N2209-c-b036	92.152973	-73.851929	18.45	1.22	4857	5265048095748640896	5.3	251.79 ± 0.50	1.73 ± 0.16	-0.63 ± 0.06	0.97	0.98	0000000	M2FS
LMC	NGC 2209	N2209-c-b037	92.168388	-73.849086	18.89	1.21	4999	5265048095742505344	5.1	241.80 ± 0.81	2.33 ± 0.16	-0.53 ± 0.07	0.00	0.00	0000000	M2FS
LMC	NGC 2209	N2209-c-b038	92.171190	-73.844595	19.14	0.90	5070	5265048198820743424	3.5	251.34 ± 1.32	1.96 ± 0.29	-0.98 ± 0.13	0.98	0.98	0000000	M2FS
LMC	NGC 2209	N2209-c-b039	92.163307	-73.841721	19.01	1.05	5033	5265095031144130048	2.4	251.14 ± 0.83	1.77 ± 0.46	-0.56 ± 0.11	0.98	0.98	0000000	M2FS
LMC	NGC 2209	N2209-c-b040	92.157366	-73.834099	19.01	0.56	5034	5265095031144105856	2.2	260.25 ± 6.10	3.29 ± 0.68	-2.26 ± 0.29	-1.00	-1.00	0100000	M2FS
LMC	NGC 2209	N2209-c-b042	92.198354	-73.878939	19.22	0.98	5094	5265047850929512192	2.7	251.76 ± 1.35	2.17 ± 0.37	-0.89 ± 0.16	0.70	0.70	0000000	M2FS
LMC	NGC 2209	N2209-c-b043	92.176213	-73.869678	19.08	1.31	5053	5265047919649023744	2.0	248.31 ± 1.08	2.34 ± 0.42	-0.63 ± 0.17	0.14	0.10	0000000	M2FS
LMC	NGC 2209	N2209-c-b044	92.180120	-73.860226	19.06	1.03	5047	5265048130108387712	3.8	251.94 ± 0.66	1.91 ± 0.23	-0.61 ± 0.09	0.97	0.97	0000000	M2FS
LMC	NGC 2209	N2209-c-b045	92.194899	-73.858834	16.15	1.04	4481	5265048130108390016	26.0	15.99 ± 0.28	1.69 ± 0.05	-0.79 ± 0.04	-1.00	-1.00	0000110	M2FS
LMC	NGC 2209	N2209-c-b046	92.193199	-73.853569	18.86	1.21	4991	5265048125807501952	3.1	252.79 ± 1.01	2.09 ± 0.29	-0.80 ± 0.11	0.93	0.93	0000000	M2FS
LMC	NGC 2209	N2209-c-b047	92.180191	-73.847963	18.89	1.21	4999	5265048194527006848	2.8	250.54 ± 0.95	2.10 ± 0.29	-0.59 ± 0.11	0.96	0.96	0000000	M2FS
LMC	NGC 2209	N2209-c-b048	92.191576	-73.837273	19.02	0.98	5036	5265095129929719168	4.8	250.33 ± 0.81	2.28 ± 0.21	-0.95 ± 0.10	0.98	0.98	0000000	M2FS
LMC	NGC 2209	N2209-c-b050	92.186847	-73.804688	19.44	1.21	5177	5265095409108370304	2.1	255.42 ± 1.04	2.19 ± 0.42	-0.42 ± 0.14	0.00	0.00	0000000	M2FS
LMC	NGC 2209	N2209-c-b051	92.177147	-73.808895	19.19	1.14	5085	5265095404807657856	2.1	261.03 ± 1.56	2.15 ± 0.53	-0.97 ± 0.19	0.00	0.00	0000000	M2FS
LMC	NGC 2209	N2209-c-b053	92.201055	-73.818879	18.74	1.09	4956	5265095198649179392	4.0	252.73 ± 0.95	2.13 ± 0.23	-0.93 ± 0.11	0.93	0.93	0000000	M2FS
LMC	NGC 2209	N2209-c-b054	92.195777	-73.823600	19.49	1.03	5200	5265095198649164416	2.3	251.57 ± 1.00	2.90 ± 0.29	-0.54 ± 0.14	0.97	0.97	0000000	M2FS
LMC	NGC 2209	N2209-c-b055	92.209576	-73.825185	19.25	1.12	5102	5265095134230474240	3.1	250.68 ± 0.92	1.59 ± 0.37	-0.55 ± 0.10	0.97	0.97	0000000	M2FS
LMC	NGC 2209	N2209-c-b056	92.195910	-73.829628	18.98	1.06	5024	5265095129929719040	2.1	246.17 ± 0.82	2.13 ± 0.57	-0.44 ± 0.14	0.00	0.00	0000000	M2FS
LMC	NGC 2209	N2209-c-b058	92.155000	-73.792269	19.04	1.14	5042	5265096126362219392	3.6	252.09 ± 0.87	1.88 ± 0.29	-0.56 ± 0.10	0.75	0.76	0000000	M2FS
LMC	NGC 2209	N2209-c-b059	92.158759	-73.796259	18.33	1.26	4813	5265096130662864768	6.2	251.02 ± 0.42	1.66 ± 0.13	-0.59 ± 0.05	0.88	0.88	0000000	M2FS
LMC	NGC 2209	N2209-c-b060	92.174345	-73.821301	18.85	1.04	4987	5265095198649197312	2.7	265.84 ± 1.02	1.60 ± 0.34	-0.70 ± 0.12	0.00	0.00	0000000	M2FS
LMC	NGC 2209	N2209-c-b061	92.164338	-73.823567	19.20	0.98	5087	5265095095569982592	2.8	251.14 ± 1.05	2.48 ± 0.27	-0.59 ± 0.13	0.98	0.98	0000000	M2FS
LMC	NGC 2209	N2209-c-b062	92.174236	-73.826089	19.23	0.98	5097	5265095202949942784	2.4	251.31 ± 1.00	2.24 ± 0.36	-0.52 ± 0.13	0.98	0.98	0000000	M2FS
LMC	NGC 2209	N2209-c-b063	92.155841	-73.829601	18.32	0.85	4809	5265095099870722176	5.4	266.94 ± 0.78	1.89 ± 0.16	-1.16 ± 0.08	0.00	0.00	0000010	M2FS
LMC	NGC 2209	N2209-c-b064	92.169987	-73.830094	18.42	1.25	4846	5265095202942818304	3.5	249.81 ± 0.59	2.64 ± 0.14	-0.20 ± 0.08	-1.00	-1.00	0000001	M2FS
LMC	NGC 2209	N2209-c-b066	92.122969	-73.879321	18.79	1.13	4970	5265047820870732928	3.1	254.47 ± 0.88	1.45 ± 0.34	-0.71 ± 0.10	0.01	0.01	0000000	M2FS
LMC	NGC 2209	N2209-c-b067	92.112681	-73.856988	19.36	1.07	5141	5265048091447772672	2.6	250.95 ± 1.14	2.43 ± 0.35	-0.44 ± 0.13	0.97	0.97	0000000	M2FS
LMC	NGC 2209	N2209-c-b068	92.100934	-73.855359	19.34	1.24	5133	5265048057096313344	2.6	245.56 ± 1.02	1.50 ± 0.46	-0.35 ± 0.11	0.00	0.00	0000000	M2FS
LMC	NGC 2209	N2209-c-b069	92.093404	-73.852372	19.36	1.06	5141	5265094996784312832	2.6	287.23 ± 0.91	1.33 ± 0.44	-0.71 ± 0.13	0.00	0.00	0000000	M2FS
LMC	NGC 2209	N2209-c-b070	92.107964	-73.851828	19.01	1.18	5034	5265095026850395264	1.3	228.98 ± 1.96	1.70 ± 0.55	-0.39 ± 0.21	0.00	0.00	0000000	M2FS
LMC	NGC 2209	N2209-c-b071	92.096230	-73.848744	19.10	1.13	5058	5265094992490669824	2.7	249.53 ± 0.76	1.51 ± 0.34	-0.58 ± 0.11	0.89	0.86	0000000	M2FS
LMC	NGC 2209	N2209-c-b072	92.099720	-73.839904	19.07	1.01	5051	5265095065503787648	3.4	253.13 ± 0.98	1.90 ± 0.25	-0.57 ± 0.10	0.89	0.89	0000000	M2FS
LMC	NGC 2209	N2209-c-b073	92.135132	-73.881953	18.26	1.35	4790	5265047816569773952	3.9	243.38 ± 0.64	1.51 ± 0.21	-0.78 ± 0.08	0.00	0.00	0000000	M2FS
LMC	NGC 2209	N2209-c-b074	92.123022	-73.872451	19.25	1.27	5105	5265048022728236672	1.9	263.57 ± 1.07	3.15 ± 0.31	-0.60 ± 0.17	0.00	0.00	0000000	M2FS
LMC	NGC 2209	N2209-c-b075	92.129161	-73.868474	18.93	1.29	5010	5265048022728250496	2.7	262.53 ± 0.84	1.43 ± 0.39	-0.59 ± 0.11	0.00	0.00	0000000	M2FS
LMC	NGC 2209	N2209-c-b076	92.145774	-73.867852	17.71	1.16	4603	5265048027029166720	8.6	257.87 ± 0.36	0.83 ± 0.12	-1.08 ± 0.04	0.00	0.00	0000000	M2FS
LMC	NGC 2209	N2209-c-b077	92.128899	-73.863146	17.99	1.34	4696	5265048022728268672	4.4	227.72 ± 0.49	1.49 ± 0.17	-0.71 ± 0.07	0.00	0.00	0000000	M2FS
LMC	NGC 2209	N2209-c-b078	92.122050	-73.845878	18.10	1.07	4734	5265095026850505216	6.8	295.02 ± 2.15	2.30 ± 0.42	-2.96 ± 0.13	-1.00	-1.00	0100000	M2FS
LMC	NGC 2209	N2209-c-b079	92.133986	-73.839717	18.68	0.87	4934	5265095031151240832	3.8	248.19 ± 1.01	1.78 ± 0.27	-0.89 ± 0.11	0.74	-1.00	0000000	M2FS

Table C.1: (*continued*) Sample of 3095 Targets from 26 Star Clusters

Galaxy	Cluster	ID	RAJ2000 (deg)	DEJ2000 (deg)	G (mag)	$G_{\rm BP} - G_{\rm RP}$ (mag)	$T_{\rm eff}$ (K)	*Gaia* DR2 ID	S/N	$v_{\rm los}$ (km s^{-1})	$\log g$ (dex)	$[{\rm Fe/H}]_{\rm raw}$ (dex)	P_M	P'_M	Flag[a]	Source[b]
(1)	(2)	(3)	(4)	(5)	(6)	(7)	(8)	(9)	(10)	(11)	(12)	(13)	(14)	(15)	(16)	(17)
LMC	NGC 2209	N2209-c-b080	92.148246	-73.838800	19.21	1.28	5090	5265095031144089600	2.5	250.42 ± 1.03	2.58 ± 0.33	-0.33 ± 0.11	1.00	1.00	0000000	M2FS
LMC	NGC 2209	N2209-c-b082	92.124568	-73.794081	17.25	1.54	4481	5265096126362218496	9.4	261.46 ± 0.31	1.18 ± 0.09	-0.58 ± 0.04	0.00	0.00	0000000	M2FS
LMC	NGC 2209	N2209-c-b083	92.138920	-73.804326	18.45	1.13	4858	5265095374748617600	5.5	241.97 ± 0.63	0.92 ± 0.26	-0.68 ± 0.09	0.00	0.00	0000000	M2FS
LMC	NGC 2209	N2209-c-b084	92.116738	-73.817843	18.23	1.24	4778	5265095306029138688	4.6	251.05 ± 0.50	1.58 ± 0.18	-0.65 ± 0.07	0.98	0.98	0000000	M2FS
LMC	NGC 2209	N2209-c-b085	92.154688	-73.818257	19.23	1.05	5096	5265095301728414592	2.8	252.40 ± 0.98	2.13 ± 0.38	-0.54 ± 0.12	0.95	0.95	0000000	M2FS
LMC	NGC 2209	N2209-c-b086	92.132778	-73.819883	19.37	1.02	5146	5265095301728956928	1.9	251.25 ± 1.17	2.67 ± 0.47	-0.68 ± 0.19	0.97	0.97	0000000	M2FS
LMC	NGC 2209	N2209-c-b087	92.141476	-73.825035	18.72	0.65	4949	5265095095569981568	3.7	252.24 ± 2.63	2.37 ± 0.41	-1.82 ± 0.16	-1.00	-1.00	0100010	M2FS
LMC	NGC 2209	N2209-c-b088	92.145361	-73.832673	19.05	0.82	5044	5265095099863558528	3.3	252.53 ± 0.90	2.09 ± 0.29	-0.72 ± 0.11	1.00	1.00	0000000	M2FS
LMC	NGC 2209	N2209-c-b089	92.094513	-73.773551	18.96	1.17	5021	5265096435599928832	3.4	259.87 ± 0.71	1.66 ± 0.34	-0.74 ± 0.11	0.00	0.00	0000000	M2FS
LMC	NGC 2209	N2209-c-b090	92.116427	-73.812324	19.04	1.13	5041	5265095374748614528	3.1	251.49 ± 1.21	1.96 ± 0.30	-0.46 ± 0.11	0.97	0.97	0000000	M2FS
LMC	NGC 2209	N2209-c-b091	92.096248	-73.817032	19.28	1.13	5112	5265095340388871936	2.4	250.21 ± 0.85	2.04 ± 0.31	-0.50 ± 0.13	0.96	0.95	0000000	M2FS
LMC	NGC 2209	N2209-c-b092	92.095714	-73.823274	16.76	1.44	4481	5265095271669396480	11.0	285.45 ± 0.23	0.72 ± 0.07	-0.97 ± 0.04	0.00	0.00	0000000	M2FS
LMC	NGC 2209	N2209-c-b093	92.114616	-73.824942	18.11	1.28	4735	5265095306029139584	6.3	258.70 ± 0.58	0.74 ± 0.22	-1.44 ± 0.06	0.00	0.00	0000000	M2FS
LMC	NGC 2209	N2209-c-b094	92.089396	-73.827262	18.83	1.03	4983	5265095271669395840	4.0	241.51 ± 0.87	1.84 ± 0.25	-0.82 ± 0.10	0.00	0.00	0000000	M2FS
LMC	NGC 2209	N2209-c-b095	92.104677	-73.830512	19.39	1.03	5155	5265095267368634880	2.2	250.62 ± 0.98	2.85 ± 0.34	-0.21 ± 0.14	0.98	0.98	0000000	M2FS
LMC	NGC 2209	N2209-c-b096	92.090241	-73.835487	18.06	1.31	4718	5265095065510967808	6.6	255.54 ± 0.39	1.85 ± 0.11	-0.58 ± 0.05	0.00	0.00	0000000	M2FS
LMC	NGC 2209	N2209-c-b098	92.028776	-73.879123	18.49	1.38	4872	5265024589386660608	4.0	228.71 ± 0.55	1.79 ± 0.21	-0.63 ± 0.09	0.00	0.00	0000000	M2FS
LMC	NGC 2209	N2209-c-b099	91.998513	-73.871272	17.52	1.56	4538	5265071529090176896	7.7	256.33 ± 0.29	1.69 ± 0.08	-0.50 ± 0.04	0.00	0.00	0000000	M2FS
LMC	NGC 2209	N2209-c-b100	91.986064	-73.864578	18.29	1.39	4800	5265071593508803328	5.8	287.92 ± 0.40	2.08 ± 0.14	-0.47 ± 0.06	0.00	0.00	0000000	M2FS
LMC	NGC 2209	N2209-c-b101	92.002813	-73.861509	17.59	1.53	4564	5265071597809652864	7.3	248.22 ± 0.33	1.51 ± 0.09	-0.61 ± 0.05	0.00	0.00	0000000	M2FS
LMC	NGC 2209	N2209-c-b102	92.015705	-73.854362	18.79	1.27	4971	5265071597809654016	2.4	249.74 ± 1.06	1.98 ± 0.34	-0.36 ± 0.12	0.62	0.59	0000000	M2FS
LMC	NGC 2209	N2209-c-b103	91.989805	-73.853201	19.32	1.00	5125	5265071593508841344	1.4	247.01 ± 114.51	1.79 ± 1.07	-2.39 ± 0.72	-1.00	-1.00	1000000	M2FS
LMC	NGC 2209	N2209-c-b104	91.982541	-73.843589	19.46	0.94	5185	5265071799675298304	2.5	272.91 ± 1.09	2.31 ± 0.36	-0.41 ± 0.12	0.00	0.00	0000000	M2FS
LMC	NGC 2209	N2209-c-b106	92.075068	-73.882210	17.75	1.58	4616	5265047988368479616	5.4	251.39 ± 0.39	1.86 ± 0.12	-0.48 ± 0.06	0.72	0.74	0000010	M2FS
LMC	NGC 2209	N2209-c-b107	92.090021	-73.873414	19.21	1.31	5092	5265047988368500608	2.1	243.52 ± 1.40	1.43 ± 0.52	-0.71 ± 0.15	0.00	0.00	0000000	M2FS
LMC	NGC 2209	N2209-1-b108	92.092983	-73.868298	16.80	1.75	4481	5265048061388888320	4.2	249.72 ± 0.45	1.94 ± 0.13	-0.29 ± 0.07	0.23	0.13	0000010	M2FS
LMC	NGC 2209	N2209-c-b109	92.067464	-73.862118	19.46	1.15	5184	5265048061388881152	2.2	225.07 ± 1.82	1.23 ± 0.48	-0.78 ± 0.20	0.00	0.00	0000000	M2FS
LMC	NGC 2209	N2209-c-b110	92.063209	-73.847160	19.35	1.18	5139	5265095061210156288	2.4	250.10 ± 1.18	1.61 ± 0.43	-0.55 ± 0.12	0.95	0.95	0000000	M2FS
LMC	NGC 2209	N2209-c-b111	92.085178	-73.839906	19.10	0.97	5058	5265095061210176768	2.8	250.35 ± 1.12	2.28 ± 0.29	-0.58 ± 0.14	0.96	0.96	0000000	M2FS
LMC	NGC 2209	N2209-c-b112	92.068848	-73.837459	19.08	1.05	5052	5265095267368617728	3.2	253.22 ± 0.99	1.74 ± 0.30	-0.58 ± 0.11	0.87	0.87	0000000	M2FS
LMC	NGC 2209	N2209-c-b113	92.042775	-73.801137	19.04	1.21	5041	5265096160721949056	3.7	279.07 ± 0.94	1.64 ± 0.30	-0.70 ± 0.11	0.00	0.00	0000000	M2FS
LMC	NGC 2209	N2209-c-b114	92.082214	-73.804550	19.48	1.24	5198	5265096096303113728	2.3	249.20 ± 0.95	2.33 ± 0.83	-0.29 ± 0.13	0.38	0.33	0000000	M2FS
LMC	NGC 2209	N2209-c-b115	92.042118	-73.815262	19.12	1.16	5063	5265096092010434944	2.7	260.37 ± 1.39	1.60 ± 0.40	-0.77 ± 0.14	0.00	0.00	0000000	M2FS
LMC	NGC 2209	N2209-c-b116	92.070332	-73.816962	19.48	0.91	5197	5265095340388869504	1.4	251.09 ± 1.32	2.43 ± 0.48	-0.42 ± 0.19	0.81	0.81	0000000	M2FS
LMC	NGC 2209	N2209-c-b117	92.075508	-73.822274	19.31	1.04	5124	5265095336088138368	2.6	250.28 ± 1.09	2.70 ± 0.31	-0.36 ± 0.13	0.96	0.96	0000000	M2FS
LMC	NGC 2209	N2209-c-b118	92.075007	-73.826472	18.96	1.10	5020	5265095267376784384	3.7	250.34 ± 0.85	1.75 ± 0.28	-0.67 ± 0.11	0.96	0.96	0000000	M2FS
LMC	NGC 2209	N2209-c-b119	92.063203	-73.833258	18.19	1.29	4763	5265095267368630144	5.3	251.49 ± 0.53	1.74 ± 0.15	-0.60 ± 0.06	0.98	0.98	0000000	M2FS
LMC	NGC 2209	N2209-c-b120	92.050856	-73.837409	19.20	1.21	5088	5265095267368620544	2.2	283.09 ± 1.43	2.09 ± 0.39	-0.68 ± 0.15	0.00	0.00	0000000	M2FS
LMC	NGC 2209	N2209-c-b123	92.018269	-73.816479	19.19	1.09	5085	5265072628594599040	3.4	274.45 ± 0.98	2.08 ± 0.29	-0.42 ± 0.11	0.00	0.00	0000000	M2FS
LMC	NGC 2209	N2209-c-b124	92.026548	-73.821097	18.94	1.10	5013	5265072628594601600	3.1	235.93 ± 0.92	1.95 ± 0.29	-0.53 ± 0.10	0.00	0.00	0000000	M2FS
LMC	NGC 2209	N2209-c-b125	91.992739	-73.821379	17.55	1.46	4550	5265072628601796224	7.2	236.83 ± 0.35	1.18 ± 0.10	-0.61 ± 0.05	0.00	0.00	0000000	M2FS
LMC	NGC 2209	N2209-c-b126	91.786317	-73.825782	18.96	1.17	5020	5265072796099815040	2.6	252.92 ± 1.09	2.16 ± 0.34	-0.62 ± 0.15	0.00	0.00	0000000	M2FS
LMC	NGC 2209	N2209-c-b127	92.030250	-73.832563	16.33	1.87	4481	5265071872687559936	14.4	252.75 ± 0.28	2.05 ± 0.09	-0.37 ± 0.04	0.06	0.03	0000010	M2FS
LMC	NGC 2209	N2209-c-b128	92.038305	-73.836318	18.82	1.07	4979	5265071799667319552	3.1	250.13 ± 0.93	2.24 ± 0.26	-0.46 ± 0.10	0.77	0.75	0000000	M2FS
LMC	NGC 2209	N2209-2-r028	92.129480	-73.835180	17.84	1.09	4646	5265095099863542144	8.1	246.84 ± 0.27	1.47 ± 0.09	-0.79 ± 0.04	0.00	0.00	0000000	M2FS
LMC	NGC 2209	N2209-2-r049	92.176786	-73.840093	18.13	1.13	4744	5265095134223355008	7.9	250.26 ± 0.38	1.61 ± 0.11	-0.63 ± 0.05	0.98	0.97	0000000	M2FS
LMC	NGC 2209	N2209-2-r079	92.121431	-73.830561	17.86	1.23	4653	5265095099870712192	8.1	250.94 ± 0.36	1.51 ± 0.10	-0.55 ± 0.04	0.99	0.99	0000000	M2FS
LMC	NGC 2209	N2209-2-r099	92.170886	-73.834173	17.88	1.22	4658	5265095129929716224	6.6	252.10 ± 0.50	1.36 ± 0.12	-0.70 ± 0.05	0.98	0.98	0000000	M2FS
LMC	NGC 2257	N2257-1-b001	97.696585	-64.427203	18.79	1.08	5095	5284815592527177216	-0.0	137.57 ± 139.34	3.17 ± 1.42	0.51 ± 0.93	-1.00	-1.00	1000000	M2FS
LMC	NGC 2257	N2257-1-b003	97.691484	-64.386492	18.80	0.98	5096	5284827584075890944	4.1	323.16 ± 0.75	1.80 ± 0.28	-0.61 ± 0.08	0.00	0.00	0000000	M2FS
LMC	NGC 2257	N2257-1-b004	97.708976	-64.368406	18.78	0.96	5093	5284827790234330752	4.2	342.37 ± 0.57	1.80 ± 0.30	-1.00 ± 0.09	-1.00	-1.00	0000100	M2FS
LMC	NGC 2257	N2257-1-b005	97.614869	-64.356718	18.83	1.18	5103	5284828752307011328	2.8	302.23 ± 1.49	2.36 ± 0.42	-1.55 ± 0.17	1.00	0.99	0000000	M2FS
LMC	NGC 2257	N2257-1-b006	97.611976	-64.348103	18.25	1.12	4985	5284828752307020288	6.3	20.92 ± 0.51	3.84 ± 0.08	-0.67 ± 0.08	-1.00	-1.00	0001100	M2FS
LMC	NGC 2257	N2257-1-b007	97.619335	-64.337352	18.16	1.22	4963	5284828825321248640	5.2	305.35 ± 0.79	1.55 ± 0.31	-1.63 ± 0.09	1.00	0.90	0000000	M2FS

Table C.1: (*continued*) Sample of 3095 Targets from 26 Star Clusters

Galaxy	Cluster	ID	RAJ2000 (deg)	DEJ2000 (deg)	G (mag)	$G_{\rm BP} - G_{\rm RP}$ (mag)	$T_{\rm eff}$ (K)	*Gaia* DR2 ID	S/N	$v_{\rm los}$ ($\rm km\,s^{-1}$)	$\log g$ (dex)	$[{\rm Fe/H}]_{\rm raw}$ (dex)	P_M	P'_M	Flag[a]	Source[b]
(1)	(2)	(3)	(4)	(5)	(6)	(7)	(8)	(9)	(10)	(11)	(12)	(13)	(14)	(15)	(16)	(17)
LMC	NGC 2257	N2257-1-b008	97.632158	-64.331375	17.51	1.20	4803	5284828825324758528	9.6	300.65 ± 0.37	1.27 ± 0.17	-1.70 ± 0.05	1.00	1.00	0000000	M2FS
LMC	NGC 2257	N2257-1-b009	97.742448	-64.423744	19.09	1.07	5148	5284815523807702528	2.7	319.90 ± 1.06	2.35 ± 0.49	-1.75 ± 0.14	0.00	0.00	0000000	M2FS
LMC	NGC 2257	N2257-1-b010	97.792722	-64.406189	18.52	1.15	5043	5284909360253030528	4.0	323.59 ± 0.53	1.95 ± 0.26	-0.58 ± 0.08	0.00	0.00	0000000	M2FS
LMC	NGC 2257	N2257-1-b011	97.781558	-64.403373	18.80	1.12	5097	5284909566411517184	3.4	339.79 ± 0.83	2.05 ± 0.33	-0.60 ± 0.10	-1.00	-1.00	0000100	M2FS
LMC	NGC 2257	N2257-1-b012	97.767173	-64.398731	18.56	1.13	5050	5284815798685624960	4.5	325.68 ± 0.73	1.97 ± 0.23	-0.55 ± 0.08	0.00	0.00	0000000	M2FS
LMC	NGC 2257	N2257-1-b013	97.799181	-64.397349	18.60	1.13	5058	5284909566411464064	4.2	295.54 ± 0.66	1.64 ± 0.24	-0.93 ± 0.09	0.00	0.00	0000000	M2FS
LMC	NGC 2257	N2257-1-b014	97.753774	-64.348455	18.78	1.20	5093	5284827893313560320	2.4	328.19 ± 1.59	2.27 ± 0.41	-0.67 ± 0.17	0.00	0.00	0000000	M2FS
LMC	NGC 2257	N2257-1-b016	97.741278	-64.313444	18.47	1.08	5031	5284828924105726464	3.1	28.59 ± 0.92	4.19 ± 0.16	-0.55 ± 0.14	-1.00	-1.00	0001100	M2FS
LMC	NGC 2257	N2257-1-b017	97.769923	-64.222470	18.40	1.13	5016	5284926918079759744	5.1	332.28 ± 0.60	1.74 ± 0.25	-0.51 ± 0.06	0.00	0.00	0000000	M2FS
LMC	NGC 2257	N2257-1-b019	97.738041	-64.254112	18.88	1.06	5111	5284926127805727488	3.0	70.44 ± 0.81	4.20 ± 0.18	-0.55 ± 0.15	-1.00	-1.00	0001100	M2FS
LMC	NGC 2257	N2257-1-b020	97.731838	-64.264196	16.64	1.46	4571	5284832222640628864	12.8	-35.14 ± 2.06	3.46 ± 0.11	-1.08 ± 0.09	-1.00	-1.00	0100000	M2FS
LMC	NGC 2257	N2257-1-b021	97.701831	-64.273649	18.55	1.05	5048	5284832222640626944	3.3	282.51 ± 0.91	1.02 ± 0.38	-0.77 ± 0.11	0.00	0.00	0000000	M2FS
LMC	NGC 2257	N2257-1-b023	97.643128	-64.286730	19.66	1.19	5239	5284832089499884928	3.9	198.51 ± 216.47	2.60 ± 1.32	-4.27 ± 0.33	-1.00	-1.00	0100000	M2FS
LMC	NGC 2257	N2257-1-b024	97.674898	-64.288260	18.63	1.06	5065	5284831982122456064	3.6	356.47 ± 0.93	1.93 ± 0.30	-0.99 ± 0.10	-1.00	-1.00	0000100	M2FS
LMC	NGC 2257	N2257-1-b025	97.607246	-64.236556	18.80	1.10	5098	5284833253432783232	3.6	332.11 ± 0.69	2.13 ± 0.25	-0.51 ± 0.08	0.00	0.00	0000000	M2FS
LMC	NGC 2257	N2257-1-b027	97.597121	-64.295639	17.38	1.25	4770	5284832123859616256	11.4	302.25 ± 0.31	1.27 ± 0.15	-1.86 ± 0.05	1.00	1.00	0000000	M2FS
LMC	NGC 2257	N2257-1-b028	97.613702	-64.301840	17.97	1.13	4917	5284832050841924992	6.4	302.37 ± 0.57	1.28 ± 0.26	-1.80 ± 0.07	1.00	0.99	0000000	M2FS
LMC	NGC 2257	N2257-1-b029	97.577567	-64.307435	18.49	1.16	5037	5284831672884799360	3.8	299.26 ± 0.91	1.83 ± 0.32	-1.56 ± 0.12	1.00	1.00	0000000	M2FS
LMC	NGC 2257	N2257-1-b030	97.592351	-64.308874	18.90	0.98	5114	5284832055136554880	2.7	299.73 ± 1.32	1.79 ± 0.56	-1.50 ± 0.18	1.00	1.00	0000000	M2FS
LMC	NGC 2257	N2257-1-b031	97.592406	-64.312792	17.18	1.26	4718	5284832050843823232	12.3	301.73 ± 0.28	1.03 ± 0.11	-1.55 ± 0.04	1.00	1.00	0000000	M2FS
LMC	NGC 2257	N2257-1-b032	97.586435	-64.327913	17.28	1.17	4746	5284831466726438272	9.8	297.91 ± 0.44	0.56 ± 0.19	-1.74 ± 0.05	1.00	1.00	0000000	M2FS
LMC	NGC 2257	N2257-1-b033	97.571292	-64.350486	17.62	1.22	4829	5284828443069374592	7.5	300.38 ± 0.44	1.36 ± 0.19	-1.53 ± 0.06	1.00	1.00	0000000	M2FS
LMC	NGC 2257	N2257-1-b034	97.581636	-64.346211	18.80	1.01	5097	5284828443069453312	2.9	302.37 ± 1.12	2.49 ± 0.41	-1.69 ± 0.17	1.00	1.00	0000000	M2FS
LMC	NGC 2257	N2257-1-b035	97.587082	-64.340292	17.52	1.19	4804	5284831398006953984	7.9	302.99 ± 0.54	1.10 ± 0.20	-1.67 ± 0.06	1.00	1.00	0000000	M2FS
LMC	NGC 2257	N2257-1-b036	97.573797	-64.337514	18.35	1.07	5006	5284831402301603712	5.3	303.36 ± 0.61	1.78 ± 0.29	-1.65 ± 0.09	1.00	1.00	0000000	M2FS
LMC	NGC 2257	N2257-1-b037	97.580227	-64.335029	17.69	1.16	4846	5284831402305131136	7.2	299.41 ± 0.58	1.27 ± 0.23	-1.57 ± 0.06	1.00	1.00	0000000	M2FS
LMC	NGC 2257	N2257-1-b038	97.572754	-64.333159	17.14	1.21	4704	5284831466726436352	11.1	302.97 ± 0.35	1.09 ± 0.13	-1.64 ± 0.04	1.00	1.00	0000000	M2FS
LMC	NGC 2257	N2257-1-b039	97.589135	-64.331898	19.20	1.00	5166	5284831398009645952	2.3	303.60 ± 1.59	2.37 ± 0.49	-1.17 ± 0.21	1.00	1.00	0000000	M2FS
LMC	NGC 2257	N2257-1-b040	97.572923	-64.326131	18.48	0.97	5034	5284831471024602880	1.9	297.63 ± 2.19	2.22 ± 0.62	-1.20 ± 0.20	1.00	1.00	0000000	M2FS
LMC	NGC 2257	N2257-1-b041	97.608738	-64.419250	18.54	1.08	5047	5284827068679795840	3.9	321.98 ± 0.69	1.68 ± 0.26	-0.59 ± 0.09	0.00	0.00	0000000	M2FS
LMC	NGC 2257	N2257-1-b042	97.592024	-64.351872	18.80	0.98	5097	5284828443069369728	3.8	303.17 ± 0.94	2.36 ± 0.34	-1.62 ± 0.14	1.00	1.00	0000000	M2FS
LMC	NGC 2257	N2257-1-b043	97.608365	-64.343260	17.57	1.22	4817	5284828821026499456	4.2	300.08 ± 0.84	1.43 ± 0.39	-1.66 ± 0.10	1.00	1.00	0000000	M2FS
LMC	NGC 2257	N2257-1-b044	97.599452	-64.338966	18.89	0.99	5114	5284828825321239680	3.6	302.18 ± 1.02	2.18 ± 0.40	-1.35 ± 0.14	1.00	1.00	0000000	M2FS
LMC	NGC 2257	N2257-1-b045	97.598576	-64.326126	17.98	1.15	4920	5284831775964077568	3.6	302.49 ± 0.88	1.76 ± 0.36	-1.61 ± 0.12	1.00	1.00	0000000	M2FS
LMC	NGC 2257	N2257-1-b047	97.610797	-64.320833	17.91	1.15	4901	5284831848981729536	6.6	301.45 ± 0.46	1.44 ± 0.25	-1.59 ± 0.06	1.00	1.00	0000000	M2FS
LMC	NGC 2257	N2257-1-b048	97.598049	-64.305001	17.83	1.17	4882	5284832050841923456	9.1	300.52 ± 0.44	1.43 ± 0.17	-1.64 ± 0.05	1.00	1.00	0000000	M2FS
LMC	NGC 2257	N2257-1-b049	97.557219	-64.253362	18.76	1.15	5089	5284832841115921280	3.5	329.59 ± 0.61	1.88 ± 0.28	-0.52 ± 0.09	0.00	0.00	0000000	M2FS
LMC	NGC 2257	N2257-1-b050	97.566948	-64.298036	18.58	1.10	5055	5284831745902491904	4.4	307.01 ± 0.84	1.88 ± 0.46	-1.60 ± 0.12	0.98	0.30	0000000	M2FS
LMC	NGC 2257	N2257-1-b051	97.552498	-64.309215	18.47	1.12	5031	5284831741604348416	4.6	303.00 ± 0.94	1.27 ± 0.45	-1.68 ± 0.10	1.00	1.00	0000000	M2FS
LMC	NGC 2257	N2257-1-b052	97.570854	-64.312300	18.92	0.92	5119	5284831677179409408	3.3	302.99 ± 0.89	1.56 ± 0.46	-1.59 ± 0.13	1.00	1.00	0000000	M2FS
LMC	NGC 2257	N2257-1-b053	97.555183	-64.312865	18.49	1.06	5035	5284831745898868224	5.5	302.33 ± 0.66	1.98 ± 0.29	-1.68 ± 0.10	1.00	1.00	0000000	M2FS
LMC	NGC 2257	N2257-1-b055	97.572183	-64.316912	17.29	1.19	4746	5284831677179433216	13.6	302.26 ± 0.31	0.85 ± 0.14	-1.75 ± 0.04	1.00	1.00	0000000	M2FS
LMC	NGC 2257	N2257-1-b056	97.550599	-64.318390	18.95	0.93	5123	5284831677179403520	3.0	306.05 ± 1.34	2.69 ± 0.45	-1.78 ± 0.17	1.00	1.00	0000000	M2FS
LMC	NGC 2257	N2257-1-b058	97.546075	-64.295334	18.55	1.13	5049	5284832497518526464	5.0	300.82 ± 0.71	1.24 ± 0.34	-1.50 ± 0.09	1.00	1.00	0000000	M2FS
LMC	NGC 2257	N2257-1-b059	97.545195	-64.312701	17.57	1.19	4818	5284831711542755328	10.1	303.30 ± 0.42	1.24 ± 0.17	-1.67 ± 0.05	1.00	1.00	0000000	M2FS
LMC	NGC 2257	N2257-1-b061	97.540094	-64.315899	18.21	1.07	4975	5284831707246437248	4.5	299.05 ± 0.88	1.93 ± 0.34	-1.55 ± 0.12	1.00	1.00	0000000	M2FS
LMC	NGC 2257	N2257-1-b062	97.537635	-64.320692	17.95	1.09	4911	5284831638525130880	7.4	302.35 ± 0.46	1.74 ± 0.19	-1.47 ± 0.06	1.00	1.00	0000000	M2FS
LMC	NGC 2257	N2257-1-b063	97.550669	-64.323868	18.42	0.74	5022	5284831677179417088	6.2	301.81 ± 1.01	2.21 ± 0.24	-1.69 ± 0.09	-1.00	-1.00	0100000	M2FS
LMC	NGC 2257	N2257-1-b064	97.533772	-64.324676	18.97	0.93	5128	5284831642819660800	3.1	301.16 ± 1.55	3.30 ± 0.39	-1.68 ± 0.19	-1.00	-1.00	0001000	M2FS
LMC	NGC 2257	N2257-1-b065	97.516845	-64.429581	17.75	1.27	4861	5284827137399265536	6.9	36.75 ± 0.41	4.89 ± 0.08	-0.64 ± 0.07	-1.00	-1.00	0001100	M2FS
LMC	NGC 2257	N2257-1-b066	97.514113	-64.344328	18.67	1.14	5072	5284831329287399168	3.1	299.11 ± 1.37	2.11 ± 0.45	-1.70 ± 0.17	1.00	1.00	0000000	M2FS
LMC	NGC 2257	N2257-1-b067	97.537124	-64.342348	18.44	1.07	5025	5284831436661316992	4.7	302.76 ± 0.61	2.21 ± 0.28	-1.76 ± 0.10	1.00	1.00	0000000	M2FS
LMC	NGC 2257	N2257-1-b068	97.522273	-64.334986	17.13	1.26	4702	5284831642823286784	8.7	303.27 ± 0.45	1.27 ± 0.16	-1.69 ± 0.05	1.00	1.00	0000000	M2FS
LMC	NGC 2257	N2257-1-b069	97.532462	-64.332781	17.03	1.26	4674	5284831642820217344	12.6	300.53 ± 0.29	1.04 ± 0.12	-1.60 ± 0.04	1.00	1.00	0000000	M2FS

Table C.1: (*continued*) Sample of 3095 Targets from 26 Star Clusters

Galaxy	Cluster	ID	RAJ2000 (deg)	DEJ2000 (deg)	G (mag)	$G_{\rm BP} - G_{\rm RP}$ (mag)	$T_{\rm eff}$ (K)	*Gaia* DR2 ID	S/N	$v_{\rm los}$ (km s^{-1})	$\log g$ (dex)	$[{\rm Fe/H}]_{\rm raw}$ (dex)	P_M	P'_M	Flag[a]	Source[b]
(1)	(2)	(3)	(4)	(5)	(6)	(7)	(8)	(9)	(10)	(11)	(12)	(13)	(14)	(15)	(16)	(17)
LMC	NGC 2257	N2257-1-b070	97.501454	-64.328447	18.69	1.08	5076	5284831604167981184	1.5	298.53 ± 2.15	1.14 ± 0.67	-1.62 ± 0.29	1.00	1.00	0000000	M2FS
LMC	NGC 2257	N2257-1-b071	97.531751	-64.328338	18.24	1.02	4980	5284831642819674752	4.8	300.65 ± 0.98	1.16 ± 0.41	-1.57 ± 0.10	1.00	1.00	0000000	M2FS
LMC	NGC 2257	N2257-1-b072	97.496461	-64.325194	17.16	1.32	4710	5284831608463538304	10.7	301.77 ± 0.36	0.70 ± 0.15	-1.63 ± 0.04	1.00	1.00	0000000	M2FS
LMC	NGC 2257	N2257-1-b074	97.538661	-64.350533	16.73	1.41	4595	5284831367945392640	10.4	55.61 ± 0.29	4.52 ± 0.10	-0.59 ± 0.07	-1.00	-1.00	0001100	M2FS
LMC	NGC 2257	N2257-1-b076	97.560800	-64.343441	18.49	1.00	5037	5284831402302066304	4.1	303.01 ± 0.82	1.41 ± 0.46	-1.63 ± 0.11	1.00	1.00	0000000	M2FS
LMC	NGC 2257	N2257-1-b077	97.563279	-64.337330	18.35	0.95	5007	5284831402301595136	4.6	297.70 ± 0.88	2.78 ± 0.23	-1.67 ± 0.12	1.00	1.00	0000000	M2FS
LMC	NGC 2257	N2257-1-b078	97.559474	-64.333622	17.73	1.07	4856	5284831471024604032	7.9	306.81 ± 0.61	1.51 ± 0.20	-1.53 ± 0.06	1.00	1.00	0000000	M2FS
LMC	NGC 2257	N2257-1-b079	97.549889	-64.328501	17.60	1.08	4825	5284831436661273088	6.1	307.81 ± 0.71	2.09 ± 0.19	-1.69 ± 0.09	1.00	-1.00	0000000	M2FS
LMC	NGC 2257	N2257-1-b080	97.565338	-64.328179	17.46	1.11	4791	5284831471024602496	7.8	298.19 ± 0.49	1.95 ± 0.15	-1.62 ± 0.06	1.00	1.00	0000000	M2FS
LMC	NGC 2257	N2257-1-b081	97.499731	-64.242934	18.43	1.13	5024	5476986482482796544	4.1	301.40 ± 1.34	2.17 ± 0.44	-1.95 ± 0.14	0.00	0.00	0000000	M2FS
LMC	NGC 2257	N2257-1-b082	97.512312	-64.284478	18.44	1.07	5026	5284832738036700032	4.5	302.21 ± 1.39	1.99 ± 0.32	-1.49 ± 0.11	-1.00	-1.00	0100000	M2FS
LMC	NGC 2257	N2257-1-b084	97.526957	-64.318306	18.38	1.10	5013	5284831711539120256	4.7	301.30 ± 0.86	1.36 ± 0.33	-1.48 ± 0.09	1.00	1.00	0000000	M2FS
LMC	NGC 2257	N2257-1-b085	97.514108	-64.320057	18.21	1.14	4974	5284831707244601728	6.7	299.42 ± 0.70	1.83 ± 0.21	-1.51 ± 0.07	1.00	1.00	0000000	M2FS
LMC	NGC 2257	N2257-1-b086	97.490422	-64.321611	18.49	1.19	5036	5284831608459891712	4.8	298.60 ± 0.82	2.08 ± 0.28	-1.70 ± 0.11	1.00	1.00	0000000	M2FS
LMC	NGC 2257	N2257-1-b087	97.503780	-64.323132	17.31	1.26	4753	5284831608463538560	10.7	302.02 ± 0.33	0.92 ± 0.14	-1.61 ± 0.04	1.00	1.00	0000000	M2FS
LMC	NGC 2257	N2257-1-b088	97.512438	-64.331899	17.52	1.22	4806	5284831642823281408	11.3	302.65 ± 0.45	0.93 ± 0.19	-1.73 ± 0.05	1.00	1.00	0000000	M2FS
LMC	NGC 2257	N2257-1-b089	97.431145	-64.213244	18.67	1.23	5073	5476987444555488768	3.0	329.89 ± 0.60	2.59 ± 0.22	-0.37 ± 0.10	0.00	0.00	0000000	M2FS
LMC	NGC 2257	N2257-1-b090	97.449392	-64.267856	18.47	1.19	5031	5476986345043829632	4.8	302.25 ± 0.87	2.18 ± 0.28	-1.66 ± 0.12	0.00	0.00	0000000	M2FS
LMC	NGC 2257	N2257-1-b091	97.465770	-64.277956	18.67	1.09	5073	5284832703676963328	3.1	336.13 ± 1.06	1.89 ± 0.32	-0.84 ± 0.12	0.00	0.00	0000000	M2FS
LMC	NGC 2257	N2257-1-b093	97.490520	-64.293005	18.38	1.19	5014	5284832634957481088	5.3	321.63 ± 0.77	1.16 ± 0.27	-0.52 ± 0.07	0.00	0.00	0000000	M2FS
LMC	NGC 2257	N2257-1-b094	97.469899	-64.297941	17.08	1.22	4689	5284832639255681920	10.9	36.12 ± 0.24	4.20 ± 0.05	-0.30 ± 0.06	-1.00	-1.00	0001100	M2FS
LMC	NGC 2257	N2257-1-b095	97.458106	-64.329251	18.54	1.19	5046	5284832325719818112	4.5	299.80 ± 0.72	2.07 ± 0.31	-1.67 ± 0.11	1.00	0.99	0000000	M2FS
LMC	NGC 2257	N2257-1-b097	97.307867	-64.429906	18.74	1.10	5086	5284826622003187968	4.0	331.32 ± 0.73	2.46 ± 0.20	-0.39 ± 0.07	0.00	0.00	0000000	M2FS
LMC	NGC 2257	N2257-1-b098	97.410374	-64.411519	17.68	1.08	4844	5284826695020977152	8.2	58.18 ± 0.38	3.90 ± 0.06	-0.28 ± 0.06	-1.00	-1.00	0001100	M2FS
LMC	NGC 2257	N2257-1-b099	97.332746	-64.410343	18.33	1.11	5001	5284829611300438528	5.7	-4.13 ± 0.45	4.24 ± 0.08	-0.35 ± 0.07	-1.00	-1.00	0001100	M2FS
LMC	NGC 2257	N2257-1-b100	97.306948	-64.407662	18.78	1.15	5093	5284829645660178176	4.5	363.07 ± 0.77	1.95 ± 0.24	-0.45 ± 0.08	-1.00	-1.00	0000100	M2FS
LMC	NGC 2257	N2257-1-b101	97.302801	-64.383477	18.56	1.15	5052	5284829920538099456	4.2	302.65 ± 0.58	1.70 ± 0.23	-0.77 ± 0.08	0.00	0.00	0000000	M2FS
LMC	NGC 2257	N2257-1-b102	97.327937	-64.371133	18.68	1.04	5074	5284830710812088704	3.7	326.99 ± 0.75	1.93 ± 0.27	-0.59 ± 0.09	0.00	0.00	0000000	M2FS
LMC	NGC 2257	N2257-1-b103	97.363741	-64.347370	18.43	1.13	5024	5284830886909026432	4.6	72.52 ± 0.66	4.74 ± 0.13	-0.77 ± 0.10	-1.00	-1.00	0001100	M2FS
LMC	NGC 2257	N2257-1-b104	97.414042	-64.335551	17.62	1.15	4829	5284830852549289088	9.2	-8.85 ± 0.33	4.30 ± 0.06	-0.46 ± 0.06	-1.00	-1.00	0001100	M2FS
LMC	NGC 2257	N2257-1-b105	97.482366	-64.431791	17.17	1.27	4713	5284827176057325824	10.6	18.13 ± 0.25	4.32 ± 0.05	-0.31 ± 0.06	-1.00	-1.00	0001100	M2FS
LMC	NGC 2257	N2257-1-b106	97.465002	-64.411389	18.83	1.06	5103	5284828000687540736	4.2	334.68 ± 0.97	2.30 ± 0.19	-0.57 ± 0.09	0.00	0.00	0000000	M2FS
LMC	NGC 2257	N2257-1-b107	97.479750	-64.397314	18.72	1.04	5082	5284828202551174912	4.2	319.48 ± 0.75	2.55 ± 0.18	-0.72 ± 0.09	0.00	0.00	0000000	M2FS
LMC	NGC 2257	N2257-1-b109	97.425401	-64.376762	18.38	1.04	5012	5284829817458888832	5.6	102.56 ± 0.71	4.05 ± 0.08	-0.27 ± 0.07	-1.00	-1.00	0001100	M2FS
LMC	NGC 2257	N2257-1-b110	97.431258	-64.342049	18.84	1.12	5105	5284830092336818816	4.3	301.73 ± 0.69	2.00 ± 0.27	-0.89 ± 0.09	-1.00	-1.00	0000001	M2FS
LMC	NGC 2257	N2257-1-b111	97.490353	-64.340003	18.22	1.15	4976	5284831535445831168	4.9	299.59 ± 0.76	1.85 ± 0.28	-1.71 ± 0.10	1.00	1.00	0000000	M2FS
LMC	NGC 2257	N2257-1-b112	97.486462	-64.328375	18.10	1.22	4949	5284831604165313024	5.4	302.27 ± 0.77	1.40 ± 0.31	-1.58 ± 0.08	1.00	1.00	0000000	M2FS
LMC	NGC 2257	N2257-1-b114	97.386565	-64.256470	19.08	1.02	5146	5476985142452991616	3.2	327.97 ± 1.05	1.52 ± 0.51	-0.94 ± 0.13	0.00	0.00	0000000	M2FS
LMC	NGC 2257	N2257-1-b115	97.395956	-64.262516	18.77	1.08	5091	5476985073733511552	3.8	308.59 ± 0.73	2.23 ± 0.25	-0.67 ± 0.10	0.00	0.00	0000000	M2FS
LMC	NGC 2257	N2257-1-b117	97.385041	-64.296453	18.54	1.14	5046	5476984798858096000	5.1	300.48 ± 0.64	1.95 ± 0.24	-1.34 ± 0.09	0.00	0.00	0000000	M2FS
LMC	NGC 2257	N2257-1-b118	97.365100	-64.317825	18.19	1.19	4970	5284831157488718208	5.1	75.99 ± 0.55	4.51 ± 0.09	0.01 ± 0.08	-1.00	-1.00	0001100	M2FS
LMC	NGC 2257	N2257-1-b119	97.375583	-64.325038	18.60	1.08	5058	5284831088769239168	4.7	333.52 ± 0.72	2.08 ± 0.22	-1.05 ± 0.09	0.00	0.00	0000000	M2FS
LMC	NGC 2257	N2257-1-b120	97.411160	-64.327028	17.05	1.24	4681	5284830921268764544	11.1	96.97 ± 0.27	3.96 ± 0.05	0.06 ± 0.06	-1.00	-1.00	0001100	M2FS
LMC	NGC 2257	N2257-1-b121	97.314135	-64.227129	18.62	1.17	5062	5476986104525682944	2.3	101.46 ± 1.34	4.42 ± 0.18	0.07 ± 0.17	-1.00	-1.00	0001100	M2FS
LMC	NGC 2257	N2257-1-b122	97.334504	-64.272855	18.52	1.17	5043	5476985108093246208	3.2	321.47 ± 0.99	1.87 ± 0.34	-0.67 ± 0.11	0.00	0.00	0000000	M2FS
LMC	NGC 2257	N2257-1-b123	97.322452	-64.295423	18.16	1.15	4962	5476984936294544128	4.9	319.97 ± 0.66	2.10 ± 0.22	-1.33 ± 0.09	0.00	0.00	0000000	M2FS
LMC	NGC 2257	N2257-1-b124	97.277341	-64.303622	18.77	1.09	5092	5476984901934802944	3.2	320.90 ± 0.91	1.89 ± 0.32	-0.88 ± 0.12	0.00	0.00	0000000	M2FS
LMC	NGC 2257	N2257-1-b125	97.288970	-64.308260	18.76	1.17	5090	5476984695776370944	3.7	326.99 ± 0.85	2.59 ± 0.21	-0.49 ± 0.09	0.00	0.00	0000000	M2FS
LMC	NGC 2257	N2257-1-b126	97.348005	-64.326744	18.71	1.09	5081	5284831054409498752	2.5	323.77 ± 1.29	1.46 ± 0.53	-0.62 ± 0.13	0.00	0.00	0000000	M2FS
LMC	NGC 2257	N2257-1-b127	97.360127	-64.326958	18.08	1.15	4942	5284831093063777280	7.0	-13.33 ± 0.56	4.06 ± 0.07	-0.29 ± 0.06	-1.00	-1.00	0001100	M2FS
LMC	NGC 2257	N2257-1-b128	97.289118	-64.335748	18.54	1.18	5047	5284831020049757056	3.5	327.45 ± 1.35	1.49 ± 0.46	-1.26 ± 0.12	0.00	0.00	0000000	M2FS
LMC	NGC 2257	N2257-1-r028	97.547719	-64.332279	16.85	0.00	4627	5284831436661287168	18.3	301.22 ± 0.28	0.73 ± 0.18	-1.82 ± 0.04	1.00	1.00	0000000	M2FS
LMC	NGC 2257	N2257-1-r049	97.557680	-64.325656	16.83	1.24	4621	5284831471024597376	15.5	300.76 ± 0.22	1.00 ± 0.10	-1.69 ± 0.03	1.00	1.00	0000000	M2FS
LMC	NGC 2257	N2257-1-r079	97.543403	-64.325822	17.41	1.12	4779	5284831642823285632	9.6	305.78 ± 0.49	1.45 ± 0.17	-1.80 ± 0.06	1.00	1.00	0000000	M2FS

Table C.1: (*continued*) Sample of 3095 Targets from 26 Star Clusters

Galaxy	Cluster	ID	RAJ2000 (deg)	DEJ2000 (deg)	G (mag)	$G_{\rm BP} - G_{\rm RP}$ (mag)	$T_{\rm eff}$ (K)	*Gaia* DR2 ID	S/N	$v_{\rm los}$ (km s^{-1})	$\log g$ (dex)	$[{\rm Fe/H}]_{\rm raw}$ (dex)	P_M	P'_M	Flag[a]	Source[b]
(1)	(2)	(3)	(4)	(5)	(6)	(7)	(8)	(9)	(10)	(11)	(12)	(13)	(14)	(15)	(16)	(17)
LMC	NGC 2257	N2257-1-r127	97.571653	-64.321614	16.98	1.24	4660	5284831471021021952	14.3	300.44 ± 0.27	0.75 ± 0.12	-1.76 ± 0.04	1.00	1.00	0000000	M2FS
LMC	NGC 2257	N2257-1-b054	97.561597	-64.315990	16.83	1.30	4621	5284831677183022464	14.4	304.22 ± 0.15	0.60 ± 0.11	-1.65 ± 0.03	1.00	1.00	0000000	M2FS+Mu10
LMC	NGC 2257	2257-136	97.582381	-64.326296	–	–	–	–	–	300.52 ± 0.20	–	–	1.00	1.00	0000000	Mu10
LMC	NGC 2257	2257-189	97.574160	-64.329938	–	–	–	–	–	302.02 ± 0.20	–	–	1.00	1.00	0000000	Mu10
LMC	NGC 2257	2257-586	97.532718	-64.312934	–	–	–	–	–	303.02 ± 0.20	–	–	1.00	1.00	0000000	Mu10
LMC	NGC 2257	2257-842	97.559121	-64.339490	–	–	–	–	–	299.82 ± 0.20	–	–	1.00	1.00	0000000	Mu10
LMC	NGC 2257	2257-993	97.485588	-64.317426	–	–	–	–	–	301.32 ± 0.20	–	–	1.00	1.00	0000000	Mu10
LMC	SL 663	SL663-1-b001	85.710975	-65.393556	15.76	1.98	3708	4660075048446994688	20.2	324.44 ± 0.22	0.63 ± 0.04	-0.81 ± 0.04	0.00	0.00	0000000	M2FS
LMC	SL 663	SL663-1-b002	85.714530	-65.383253	18.01	1.30	4559	4660075048446994432	8.9	302.68 ± 0.30	1.19 ± 0.08	-0.75 ± 0.04	0.00	0.00	0000000	M2FS
LMC	SL 663	SL663-1-b003	85.705469	-65.374995	18.78	1.11	4794	4660075288965165184	5.8	327.79 ± 0.50	1.19 ± 0.17	-0.94 ± 0.06	0.00	0.00	0000000	M2FS
LMC	SL 663	SL663-1-b004	85.712643	-65.371049	18.03	1.08	4564	4660075082806733568	9.4	297.07 ± 0.36	1.08 ± 0.09	-1.06 ± 0.04	0.00	0.00	0000000	M2FS
LMC	SL 663	SL663-1-b005	85.714190	-65.362942	18.99	1.10	4857	4660075185879904896	4.4	293.38 ± 0.57	1.65 ± 0.16	-0.70 ± 0.08	0.00	0.00	0000000	M2FS
LMC	SL 663	SL663-1-b006	85.701475	-65.341832	18.94	1.24	4842	4660076903866843264	5.5	262.21 ± 0.53	2.01 ± 0.14	-0.49 ± 0.06	0.00	0.00	0000000	M2FS
LMC	SL 663	SL663-1-b007	85.704262	-65.336870	16.39	1.70	3994	4660076903872869632	18.4	284.33 ± 0.18	0.57 ± 0.04	-0.83 ± 0.03	0.00	0.00	0000000	M2FS
LMC	SL 663	SL663-1-b008	85.699752	-65.329880	17.24	1.18	4309	4660076903872870784	14.7	282.24 ± 0.26	0.14 ± 0.08	-1.06 ± 0.03	0.00	0.00	0000000	M2FS
LMC	SL 663	SL663-1-b009	85.715255	-65.390303	17.69	1.30	4458	4660075044132368256	9.3	298.48 ± 0.36	0.96 ± 0.09	-0.97 ± 0.05	0.00	0.00	0000000	M2FS
LMC	SL 663	SL663-1-b010	85.716221	-65.378067	18.21	1.31	4619	4660075078492141312	6.5	286.60 ± 0.42	1.45 ± 0.11	-0.67 ± 0.06	0.00	0.00	0000000	M2FS
LMC	SL 663	SL663-1-b011	85.730911	-65.371694	18.46	1.20	4695	4660075185885945216	6.1	327.52 ± 0.43	1.49 ± 0.13	-0.70 ± 0.06	0.00	0.00	0000000	M2FS
LMC	SL 663	SL663-1-b012	85.718506	-65.368055	18.82	1.09	4805	4660075185879897088	5.2	341.15 ± 0.49	1.10 ± 0.21	-0.89 ± 0.07	0.00	0.00	0000000	M2FS
LMC	SL 663	SL663-1-b013	85.740320	-65.365743	18.72	1.09	4776	4660075185879867776	5.4	294.10 ± 0.55	1.38 ± 0.17	-0.99 ± 0.06	0.00	0.00	0000000	M2FS
LMC	SL 663	SL663-1-b014	85.721330	-65.359382	18.12	1.13	4592	4660075220245685760	6.7	308.16 ± 0.35	1.45 ± 0.10	-0.78 ± 0.05	0.00	0.00	0000000	M2FS
LMC	SL 663	SL663-1-b015	85.729988	-65.352313	18.80	1.19	4801	4660075220239622144	4.6	311.68 ± 0.51	1.01 ± 0.21	-0.98 ± 0.07	0.00	0.00	0000000	M2FS
LMC	SL 663	SL663-1-b016	85.730121	-65.344335	18.81	1.09	4803	4660076693414242048	5.0	301.75 ± 0.63	1.42 ± 0.20	-0.89 ± 0.08	0.00	0.00	0000000	M2FS
LMC	SL 663	SL663-1-b017	85.668533	-65.319021	18.76	0.93	4788	4660077006946118016	6.2	320.43 ± 0.46	2.18 ± 0.11	-0.72 ± 0.07	0.00	0.00	0000000	M2FS
LMC	SL 663	SL663-1-b018	85.680196	-65.325793	18.26	1.04	4635	4660076903872875776	8.9	334.33 ± 0.31	1.00 ± 0.11	-1.00 ± 0.04	0.00	0.00	0000000	M2FS
LMC	SL 663	SL663-1-b019	85.675760	-65.336645	17.39	1.35	4360	4660075422089634432	14.8	300.16 ± 0.19	0.75 ± 0.05	-0.75 ± 0.03	0.24	0.08	0000000	M2FS
LMC	SL 663	SL663-1-b020	85.675603	-65.340760	18.90	1.03	4830	4660075422089623552	6.1	282.13 ± 0.46	1.26 ± 0.16	-0.98 ± 0.06	0.00	0.00	0000000	M2FS
LMC	SL 663	SL663-1-b021	85.661063	-65.355114	17.74	1.30	4472	4660075353370108928	10.1	301.45 ± 0.24	0.95 ± 0.07	-0.81 ± 0.04	0.87	0.94	0000000	M2FS
LMC	SL 663	SL663-1-b022	85.680892	-65.362740	18.39	0.94	4675	4660075288959167104	7.5	299.64 ± 0.47	1.55 ± 0.12	-1.15 ± 0.06	0.70	0.61	0000010	M2FS
LMC	SL 663	SL663-1-b023	85.690064	-65.364036	18.78	1.04	4794	4660075288959153792	5.1	297.75 ± 0.47	1.96 ± 0.12	-0.69 ± 0.07	0.34	0.00	0000000	M2FS
LMC	SL 663	SL663-1-b024	85.663008	-65.365007	18.88	1.07	4825	4660075357678675072	4.5	293.75 ± 0.65	1.52 ± 0.19	-0.76 ± 0.08	0.28	0.00	0000000	M2FS
LMC	SL 663	SL663-1-b025	85.646876	-65.315639	18.91	1.04	4833	4660076968294845056	5.4	324.35 ± 0.46	1.66 ± 0.16	-0.85 ± 0.06	0.00	0.00	0000000	M2FS
LMC	SL 663	SL663-1-b026	85.656155	-65.318107	18.79	1.01	4797	4660076972586401664	5.8	260.71 ± 0.51	1.20 ± 0.17	-0.70 ± 0.06	0.00	0.00	0000000	M2FS
LMC	SL 663	SL663-1-b027	85.645813	-65.330753	18.05	1.39	4569	4660075495123609600	8.7	309.18 ± 0.32	1.15 ± 0.09	-0.77 ± 0.04	0.00	0.00	0000000	M2FS
LMC	SL 663	SL663-1-b028	85.649192	-65.334012	17.56	1.26	4416	4660075495123608960	10.9	293.98 ± 0.19	1.08 ± 0.06	-0.71 ± 0.04	0.01	0.00	0000000	M2FS
LMC	SL 663	SL663-1-b029	85.643270	-65.339432	18.90	1.06	4829	4660075460757932288	4.7	294.73 ± 0.52	1.03 ± 0.21	-0.86 ± 0.07	0.20	0.00	0000000	M2FS
LMC	SL 663	SL663-1-b030	85.642860	-65.344495	18.93	0.95	4838	4660075456463334784	4.1	309.37 ± 0.56	2.05 ± 0.18	-0.79 ± 0.09	0.06	0.00	0000000	M2FS
LMC	SL 663	SL663-1-b031	85.655979	-65.346114	18.88	0.96	4824	4660075460757907712	5.7	313.03 ± 0.62	1.53 ± 0.20	-1.33 ± 0.08	0.00	0.00	0000000	M2FS
LMC	SL 663	SL663-1-b032	85.657177	-65.368311	17.48	1.27	4388	4660075323324914176	11.3	301.74 ± 0.23	0.74 ± 0.07	-0.79 ± 0.04	0.86	0.93	0000000	M2FS
LMC	SL 663	SL663-1-b033	85.633939	-65.410166	18.83	1.01	4810	4660074769254400640	4.4	272.66 ± 0.62	1.69 ± 0.17	-0.68 ± 0.08	0.00	0.00	0000000	M2FS
LMC	SL 663	SL663-1-b034	85.662028	-65.409434	18.86	1.05	4819	4660074739203375104	4.1	308.94 ± 0.66	2.02 ± 0.19	-0.73 ± 0.08	0.00	0.00	0000000	M2FS
LMC	SL 663	SL663-1-b035	85.637789	-65.403433	18.70	1.04	4770	4660074803614158080	3.3	284.16 ± 0.78	1.45 ± 0.23	-0.84 ± 0.10	0.00	0.00	0000000	M2FS
LMC	SL 663	SL663-1-b036	85.647697	-65.400805	17.73	1.12	4471	4660074803614166656	11.7	310.33 ± 0.30	0.83 ± 0.07	-1.09 ± 0.04	0.00	0.00	0000000	M2FS
LMC	SL 663	SL663-1-b037	85.628258	-65.400517	17.75	1.13	4475	4660074803614166784	11.2	306.76 ± 0.25	0.84 ± 0.07	-0.89 ± 0.04	0.03	0.00	0000000	M2FS
LMC	SL 663	SL663-1-b038	85.654253	-65.398295	18.66	1.08	4758	4660074906693388288	5.4	324.46 ± 0.33	1.99 ± 0.11	-0.46 ± 0.05	0.00	0.00	0000000	M2FS
LMC	SL 663	SL663-1-b039	85.653306	-65.381042	18.76	1.06	4787	4660074945367911040	5.5	301.73 ± 0.44	1.90 ± 0.12	-0.71 ± 0.06	0.71	0.78	0000000	M2FS
LMC	SL 663	SL663-1-b040	85.638844	-65.379397	18.88	1.23	4823	4660074945362660736	2.7	300.60 ± 0.82	1.59 ± 0.36	-0.79 ± 0.12	0.86	0.93	0000000	M2FS
LMC	SL 663	SL663-1-b041	85.676869	-65.403139	18.77	1.10	4792	4660074842282566400	5.0	305.59 ± 0.42	1.56 ± 0.15	-0.75 ± 0.06	0.00	0.00	0000000	M2FS
LMC	SL 663	SL663-1-b042	85.665474	-65.403053	18.86	1.07	4818	4660074842288574336	5.9	294.01 ± 0.45	1.20 ± 0.16	-1.04 ± 0.06	0.00	0.00	0000000	M2FS
LMC	SL 663	SL663-1-b043	85.683975	-65.400962	18.89	0.87	4828	4660074842282557312	3.7	292.41 ± 0.62	2.18 ± 0.19	-0.93 ± 0.09	0.00	0.00	0000010	M2FS
LMC	SL 663	SL663-1-b044	85.677392	-65.395731	18.99	0.91	4855	4660074872333658496	5.7	349.71 ± 0.47	0.65 ± 0.26	-1.41 ± 0.06	0.00	0.00	0000000	M2FS
LMC	SL 663	SL663-1-b045	85.687719	-65.394104	17.28	1.32	4323	4660074872333671808	10.2	310.45 ± 0.23	0.81 ± 0.06	-0.71 ± 0.04	0.00	0.00	0000000	M2FS
LMC	SL 663	SL663-1-b046	85.689253	-65.388670	18.65	0.99	4754	4660074876642289536	5.6	271.19 ± 0.72	1.47 ± 0.18	-1.23 ± 0.07	0.00	0.00	0000000	M2FS
LMC	SL 663	SL663-1-b047	85.688399	-65.379765	17.28	1.35	4323	4660075254605556224	13.6	293.99 ± 0.19	0.66 ± 0.05	-0.86 ± 0.03	0.01	0.00	0000000	M2FS

Table C.1: (*continued*) Sample of 3095 Targets from 26 Star Clusters

Galaxy	Cluster	ID	RAJ2000 (deg)	DEJ2000 (deg)	G (mag)	$G_{\rm BP} - G_{\rm RP}$ (mag)	$T_{\rm eff}$ (K)	*Gaia* DR2 ID	S/N	$v_{\rm los}$ ($\rm km\,s^{-1}$)	$\log g$ (dex)	$[{\rm Fe/H}]_{\rm raw}$ (dex)	P_M	P'_M	Flag[a]	Source[b]
(1)	(2)	(3)	(4)	(5)	(6)	(7)	(8)	(9)	(10)	(11)	(12)	(13)	(14)	(15)	(16)	(17)
LMC	SL 663	SL663-1-b048	85.677578	-65.376534	18.53	1.08	4719	4660075250290836224	6.8	272.28 ± 0.50	1.15 ± 0.26	-1.99 ± 0.07	0.00	0.00	0000000	M2FS
LMC	SL 663	SL663-1-b050	85.628740	-65.324303	18.87	1.01	4822	4660078445746637568	5.0	287.05 ± 0.52	1.63 ± 0.16	-0.81 ± 0.07	0.00	0.00	0000000	M2FS
LMC	SL 663	SL663-1-b051	85.639438	-65.334965	18.34	1.04	4659	4660075490809111680	6.0	307.63 ± 0.42	1.26 ± 0.14	-1.00 ± 0.06	0.02	0.00	0000000	M2FS
LMC	SL 663	SL663-1-b053	85.620533	-65.357578	18.60	1.16	4738	4660078278256528128	5.5	301.06 ± 0.48	1.73 ± 0.13	-0.58 ± 0.06	1.00	1.00	0000000	M2FS
LMC	SL 663	SL663-1-b054	85.617427	-65.362242	18.55	1.08	4725	4660078278256533632	6.8	301.38 ± 0.36	1.42 ± 0.11	-0.78 ± 0.05	1.00	1.00	0000000	M2FS
LMC	SL 663	SL663-1-b055	85.620337	-65.367294	18.56	1.01	4726	4660078278256525696	6.2	301.22 ± 0.32	1.91 ± 0.10	-0.60 ± 0.05	1.00	1.00	0000000	M2FS
LMC	SL 663	SL663-1-b056	85.630545	-65.390274	18.99	1.13	4856	4660074906693410304	4.1	305.49 ± 0.43	1.94 ± 0.18	-0.99 ± 0.09	0.46	0.00	0000000	M2FS
LMC	SL 663	SL663-1-b059	85.613532	-65.336881	18.78	1.03	4795	4660078415695502976	6.4	300.39 ± 0.66	1.49 ± 0.14	-0.87 ± 0.06	0.71	0.78	0000000	M2FS
LMC	SL 663	SL663-1-b060	85.615696	-65.346818	18.21	1.30	4620	4660078308307628288	7.5	301.96 ± 0.34	1.46 ± 0.09	-0.56 ± 0.05	0.86	0.92	0000000	M2FS
LMC	SL 663	SL663-1-b061	85.605709	-65.353460	18.74	0.97	4781	4660078278256560512	3.7	348.96 ± 0.66	0.85 ± 0.32	-0.91 ± 0.08	0.00	0.00	0000000	M2FS
LMC	SL 663	SL663-1-b062	85.612643	-65.355440	18.95	1.07	4843	4660078278256547072	4.4	301.56 ± 0.62	1.97 ± 0.18	-0.52 ± 0.10	1.00	1.00	0000000	M2FS
LMC	SL 663	SL663-1-b063	85.609381	-65.360562	18.69	1.00	4767	4660078278256550400	5.3	301.76 ± 0.41	1.51 ± 0.14	-0.63 ± 0.06	1.00	1.00	0000000	M2FS
LMC	SL 663	SL663-1-b064	85.605162	-65.369813	18.85	1.06	4815	4660077900299434752	4.8	299.97 ± 0.68	1.84 ± 0.15	-0.77 ± 0.07	1.00	1.00	0000000	M2FS
LMC	SL 663	SL663-1-b067	85.589203	-65.407302	18.20	1.36	4616	4660077724191905664	7.1	277.98 ± 0.66	0.34 ± 0.25	-0.94 ± 0.10	0.00	0.00	0000000	M2FS
LMC	SL 663	SL663-1-b068	85.611177	-65.395656	18.36	1.16	4665	4660077758551678976	6.9	321.47 ± 0.42	1.30 ± 0.11	-0.80 ± 0.05	0.00	0.00	0000000	M2FS
LMC	SL 663	SL663-1-b069	85.598843	-65.393294	18.85	1.09	4814	4660077762860487040	5.2	299.78 ± 0.59	1.83 ± 0.15	-0.72 ± 0.07	0.47	0.13	0000000	M2FS
LMC	SL 663	SL663-1-b070	85.587106	-65.384627	18.02	1.13	4560	4660077762866357248	4.7	287.05 ± 0.45	1.30 ± 0.14	-1.02 ± 0.07	0.00	0.00	0000000	M2FS
LMC	SL 663	SL663-1-b071	85.598761	-65.383589	18.45	1.22	4694	4660077861630926848	5.8	320.52 ± 0.44	1.63 ± 0.11	-0.70 ± 0.06	0.00	0.00	0000000	M2FS
LMC	SL 663	SL663-1-b072	85.601373	-65.376147	17.84	1.17	4503	4660077865945673088	9.9	295.11 ± 0.30	1.22 ± 0.07	-0.72 ± 0.04	0.51	0.00	0000000	M2FS
LMC	SL 663	SL663-1-b073	85.616175	-65.408106	18.75	1.21	4785	4660077724191904640	4.7	270.16 ± 0.52	1.82 ± 0.15	-0.78 ± 0.07	0.00	0.00	0000000	M2FS
LMC	SL 663	SL663-1-b074	85.612502	-65.403931	18.35	1.17	4663	4660077724191917056	6.0	231.15 ± 0.37	1.46 ± 0.12	-1.05 ± 0.06	-1.00	-1.00	0000100	M2FS
LMC	SL 663	SL663-1-b075	85.622421	-65.394111	17.86	0.87	4510	4660074807922934784	10.4	283.66 ± 0.42	0.88 ± 0.11	-1.56 ± 0.04	0.00	0.00	0000010	M2FS
LMC	SL 663	SL663-1-b076	85.620478	-65.390513	18.74	0.96	4784	4660077865945563136	4.8	319.67 ± 0.59	1.66 ± 0.16	-0.70 ± 0.07	0.00	0.00	0000000	M2FS
LMC	SL 663	SL663-1-b077	85.614044	-65.384725	18.15	1.25	4602	4660077861630925568	3.1	293.87 ± 0.81	1.49 ± 0.19	-0.81 ± 0.09	0.14	0.00	0000000	M2FS
LMC	SL 663	SL663-1-b078	85.627014	-65.383803	18.74	0.97	4783	4660074906693428736	5.4	314.39 ± 0.68	0.43 ± 0.29	-0.91 ± 0.08	0.00	0.00	0000000	M2FS
LMC	SL 663	SL663-1-b079	85.621427	-65.376515	16.66	1.61	4105	4660077895990692480	14.5	301.53 ± 0.19	0.71 ± 0.04	-0.69 ± 0.03	0.86	0.94	0000000	M2FS
LMC	SL 663	SL663-1-b080	85.613732	-65.374700	18.82	1.00	4806	4660077900305305600	5.0	300.50 ± 0.66	1.80 ± 0.16	-1.03 ± 0.08	-1.00	-1.00	0000001	M2FS
LMC	SL 663	SL663-1-b082	85.602578	-65.314498	17.28	1.36	4321	4660078445746657920	14.8	268.55 ± 0.22	0.24 ± 0.09	-1.39 ± 0.03	0.00	0.00	0000000	M2FS
LMC	SL 663	SL663-1-b083	85.598474	-65.325479	18.98	1.14	4852	4660078415695533696	4.8	354.24 ± 0.52	1.09 ± 0.22	-0.87 ± 0.07	-1.00	-1.00	0000100	M2FS
LMC	SL 663	SL663-1-b084	85.596814	-65.335434	18.70	1.13	4771	4660078415695532672	5.5	293.50 ± 0.51	2.01 ± 0.12	-0.69 ± 0.06	0.03	0.00	0000000	M2FS
LMC	SL 663	SL663-1-b085	85.601023	-65.338567	18.52	0.89	4715	4660078308307649024	7.5	307.84 ± 0.51	1.61 ± 0.12	-1.24 ± 0.06	0.16	0.00	0000010	M2FS
LMC	SL 663	SL663-1-b086	85.599118	-65.359881	18.05	0.91	4569	4660078278262431360	8.5	310.33 ± 0.47	1.09 ± 0.11	-1.35 ± 0.05	0.99	-1.00	0000010	M2FS
LMC	SL 663	SL663-1-b087	85.600723	-65.365017	18.75	1.05	4786	4660077900299444352	5.9	297.49 ± 0.57	1.72 ± 0.13	-0.80 ± 0.06	1.00	1.00	0000000	M2FS
LMC	SL 663	SL663-1-b088	85.596211	-65.371215	17.60	1.33	4426	4660077900305309696	10.8	300.77 ± 0.24	0.95 ± 0.06	-0.74 ± 0.04	1.00	1.00	0000000	M2FS
LMC	SL 663	SL663-1-b089	85.583854	-65.329211	18.98	0.99	4854	4660078480106362624	4.2	325.88 ± 0.69	1.12 ± 0.23	-0.95 ± 0.08	0.00	0.00	0000000	M2FS
LMC	SL 663	SL663-1-b090	85.572579	-65.343221	18.85	1.12	4815	4660078342681092736	5.8	300.94 ± 0.54	1.70 ± 0.14	-0.86 ± 0.07	0.72	0.82	0000000	M2FS
LMC	SL 663	SL663-1-b091	85.584655	-65.346758	18.68	1.03	4764	4660078346976072832	5.6	322.21 ± 0.51	1.58 ± 0.12	-0.80 ± 0.06	0.00	0.00	0000000	M2FS
LMC	SL 663	SL663-1-b092	85.583781	-65.350794	18.79	1.04	4797	4660078346976073728	4.2	300.62 ± 0.73	1.70 ± 0.18	-0.84 ± 0.08	0.86	0.93	0000000	M2FS
LMC	SL 663	SL663-1-b093	85.570236	-65.350899	18.13	1.27	4594	4660078346981915904	8.1	296.58 ± 0.30	1.40 ± 0.09	-0.66 ± 0.05	0.44	0.00	0000000	M2FS
LMC	SL 663	SL663-1-b094	85.593203	-65.351097	18.85	0.95	4816	4660078278256582144	4.6	280.53 ± 0.72	1.70 ± 0.18	-0.82 ± 0.08	0.00	0.00	0000000	M2FS
LMC	SL 663	SL663-1-b095	85.577687	-65.353214	18.84	1.09	4812	4660078346976082432	4.7	301.53 ± 0.48	1.69 ± 0.15	-0.83 ± 0.08	0.86	0.94	0000000	M2FS
LMC	SL 663	SL663-1-b096	85.586648	-65.362718	18.75	1.06	4786	4660077900299466624	5.9	291.97 ± 0.49	1.62 ± 0.15	-0.70 ± 0.06	0.09	0.00	0000000	M2FS
LMC	SL 663	SL663-1-b099	85.542719	-65.397322	17.49	1.31	4390	4660071917409905280	13.1	265.19 ± 0.25	0.49 ± 0.09	-1.48 ± 0.04	0.00	0.00	0000000	M2FS
LMC	SL 663	SL663-1-b100	85.516106	-65.385921	18.68	1.22	4765	4660078003378775808	5.4	283.58 ± 0.48	1.77 ± 0.15	-0.73 ± 0.07	0.00	0.00	0000000	M2FS
LMC	SL 663	SL663-1-b101	85.517989	-65.382488	18.76	1.13	4789	4660078003378772096	5.0	289.20 ± 0.61	1.51 ± 0.21	-1.37 ± 0.08	0.00	0.00	0000000	M2FS
LMC	SL 663	SL663-1-b102	85.544531	-65.380192	17.74	1.22	4472	4660077831585846784	8.6	310.99 ± 0.25	1.25 ± 0.07	-0.62 ± 0.04	0.00	0.00	0000000	M2FS
LMC	SL 663	SL663-1-b103	85.507736	-65.378236	18.86	0.94	4820	4660077999069891456	5.0	281.99 ± 0.73	0.86 ± 0.29	-1.45 ± 0.08	0.00	0.00	0000000	M2FS
LMC	SL 663	SL663-1-b104	85.527746	-65.376223	17.39	1.41	4357	4660078033429637376	13.8	314.15 ± 0.37	0.16 ± 0.11	-0.71 ± 0.05	0.00	0.00	0000000	M2FS
LMC	SL 663	SL663-1-b109	85.563269	-65.388897	18.67	1.18	4761	4660077792911433728	5.3	292.79 ± 0.39	1.85 ± 0.11	-0.52 ± 0.05	0.00	0.00	0000000	M2FS
LMC	SL 663	SL663-1-b110	85.569294	-65.374512	18.83	1.03	4809	4660077934659230208	4.9	266.95 ± 0.68	1.13 ± 0.27	-1.51 ± 0.08	0.00	0.00	0000000	M2FS
LMC	SL 663	SL663-1-b111	85.580061	-65.373845	17.38	1.42	4355	4660077934665051520	10.6	312.43 ± 0.24	1.16 ± 0.06	-0.64 ± 0.04	0.01	0.00	0000000	M2FS
LMC	SL 663	SL663-1-b112	85.552563	-65.373314	18.58	1.10	4734	4660077827271214976	6.9	301.47 ± 0.43	1.17 ± 0.13	-0.74 ± 0.05	0.72	0.81	0000000	M2FS
LMC	SL 663	SL663-1-b114	85.546158	-65.332794	18.56	1.17	4726	4660078583185565696	7.3	321.56 ± 0.36	1.62 ± 0.11	-0.74 ± 0.05	0.00	0.00	0000000	M2FS
LMC	SL 663	SL663-1-b115	85.556632	-65.336918	17.69	1.29	4458	4660078346981920768	11.1	293.30 ± 0.22	1.01 ± 0.06	-0.77 ± 0.04	0.00	0.00	0000000	M2FS

Table C.1: (*continued*) Sample of 3095 Targets from 26 Star Clusters

Galaxy	Cluster	ID	RAJ2000 (deg)	DEJ2000 (deg)	G (mag)	$G_{\rm BP} - G_{\rm RP}$ (mag)	$T_{\rm eff}$ (K)	*Gaia* DR2 ID	S/N	$v_{\rm los}$ (km s^{-1})	$\log g$ (dex)	$[{\rm Fe/H}]_{\rm raw}$ (dex)	P_M	P'_M	Flag[a]	Source[b]
(1)	(2)	(3)	(4)	(5)	(6)	(7)	(8)	(9)	(10)	(11)	(12)	(13)	(14)	(15)	(16)	(17)
LMC	SL 663	SL663-1-b116	85.566946	-65.339874	18.82	1.00	4805	4660078346976099968	3.8	295.08 ± 0.88	1.54 ± 0.20	-0.60 ± 0.10	0.04	0.00	0000000	M2FS
LMC	SL 663	SL663-1-b117	85.563787	-65.344411	17.70	1.33	4459	4660078346976103168	11.6	306.46 ± 0.24	1.35 ± 0.06	-0.64 ± 0.04	0.14	0.00	0000000	M2FS
LMC	SL 663	SL663-1-b118	85.558810	-65.347774	18.29	1.28	4645	4660078342667362176	7.2	312.64 ± 0.40	1.31 ± 0.11	-0.81 ± 0.05	0.00	0.00	0000000	M2FS
LMC	SL 663	SL663-1-b119	85.563414	-65.364247	15.98	1.79	3811	4660077934665057280	21.0	303.32 ± 0.20	0.69 ± 0.04	-0.67 ± 0.03	0.66	0.12	0000000	M2FS
LMC	SL 663	SL663-1-b120	85.567566	-65.367769	18.93	1.03	4838	4660077930350448000	5.1	292.90 ± 0.57	1.61 ± 0.15	-0.75 ± 0.07	0.06	0.00	0000000	M2FS
LMC	SL 663	SL663-1-b121	85.530159	-65.342704	18.80	0.91	4801	4660078170868680064	6.0	293.77 ± 0.81	0.74 ± 0.35	-1.99 ± 0.08	0.00	0.00	0000000	M2FS
LMC	SL 663	SL663-1-b122	85.525527	-65.345952	18.74	1.08	4782	4660078175177462272	6.2	320.37 ± 0.47	1.49 ± 0.15	-0.78 ± 0.06	0.00	0.00	0000000	M2FS
LMC	SL 663	SL663-1-b123	85.509943	-65.354732	18.63	1.05	4750	4660078136508909568	6.8	263.34 ± 0.53	1.44 ± 0.16	-1.34 ± 0.06	0.00	0.00	0000000	M2FS
LMC	SL 663	SL663-1-b124	85.534663	-65.359038	17.26	1.32	4315	4660078140823495040	14.7	302.97 ± 0.21	0.69 ± 0.05	-0.78 ± 0.03	0.20	0.01	0000000	M2FS
LMC	SL 663	SL663-1-b125	85.522939	-65.362336	18.58	1.10	4732	4660078140817723008	7.2	359.89 ± 0.49	1.29 ± 0.13	-1.03 ± 0.06	-1.00	-1.00	0000100	M2FS
LMC	SL 663	SL663-1-b126	85.534708	-65.364258	18.92	1.14	4835	4660078140817711488	4.7	307.20 ± 0.48	2.03 ± 0.15	-0.85 ± 0.08	0.03	0.00	0000000	M2FS
LMC	SL 663	SL663-1-b127	85.545283	-65.365760	18.63	1.09	4749	4660077934659265664	7.5	287.62 ± 0.38	1.29 ± 0.11	-0.84 ± 0.05	0.00	0.00	0000000	M2FS
LMC	SL 663	SL663-1-b128	85.534866	-65.370127	18.37	1.17	4670	4660078033429653120	6.2	321.14 ± 0.45	1.29 ± 0.13	-0.81 ± 0.06	0.00	0.00	0000000	M2FS
LMC	SL 663	SL663-1-r028	85.589422	-65.358557	16.77	1.51	4143	4660077900305311232	13.6	301.28 ± 0.73	0.12 ± 0.10	-0.99 ± 0.11	-1.00	-1.00	0110000	M2FS
LMC	SL 663	SL663-1-r049	85.644510	-65.376752	16.87	1.58	4181	4660074941053194368	21.7	263.29 ± 0.24	0.66 ± 0.04	-1.10 ± 0.03	0.00	0.00	0000000	M2FS
LMC	SL 663	SL663-1-r079	85.548127	-65.355332	16.88	1.38	4185	4660077969024800128	19.9	288.68 ± 0.19	0.04 ± 0.03	-1.64 ± 0.03	0.00	0.00	0000000	M2FS
LMC	SL 663	SL663-1-r127	85.664515	-65.388540	17.08	1.46	4252	4660074945367789824	18.4	319.93 ± 0.20	0.56 ± 0.05	-1.04 ± 0.03	0.00	0.00	0000000	M2FS

[a] Median S/N per pixel of M2FS spectrum.

[b] These seven-digit flags denote with a '1' the following: Rejection due to poor skew/kurtosis values in the Bayesian spectra fits (Digit 1); Excessive velocity error (Digit 2); Carbon star (Digit 3); Foreground dwarf (Digit 4); Member of a non-cluster/non-MC population (Digit 5); Has a large color offset for $T_{\rm eff}$ determination (Digit 6); Likely metallicity non-member (Digit 7). Details about how these flags are set can be found in Section 3.3.4.1, Section 3.3.4.2, Section 3.3.4.3, Section 4.1.1 and Section 4.1.2.

[c] Sources for the LOS velocities. M2FS denotes this work. Other codes are listed in column 4 of Table 3.4.

BIBLIOGRAPHY

BIBLIOGRAPHY

Alcaino, G. (1978), UBV photometry for star clusters in the Small Magellanic Cloud., *A&AS*, *34*, 431–437.

Alcaino, G., F. Alvarado, J. Borissova, and R. Kurtev (2003), The Small Magellanic Cloud star cluster NGC 458. A new UBVI photometric study, *A&A*, *400*, 917–921, doi:10.1051/0004-6361:20030069.

Anders, F., et al. (2019), Photo-astrometric distances, extinctions, and astrophysical parameters for Gaia DR2 stars brighter than G = 18, *A&A*, *628*, A94, doi:10.1051/0004-6361/201935765.

Anders, P., H. J. G. L. M. Lamers, and H. Baumgardt (2009), The photometric evolution of dissolving star clusters. II. Realistic models. Colours and M/L ratios, *A&A*, *502*(3), 817–832, doi:10.1051/0004-6361/200810615.

Bastian, N., and C. Lardo (2018), Multiple Stellar Populations in Globular Clusters, *ARA&A*, *56*, 83–136, doi:10.1146/annurev-astro-081817-051839.

Baumgardt, H. (2017), N -body modelling of globular clusters: masses, mass-to-light ratios and intermediate-mass black holes, *MNRAS*, *464*(2), 2174–2202, doi:10.1093/mnras/stw2488.

Baumgardt, H., and M. Hilker (2018), A catalogue of masses, structural parameters, and velocity dispersion profiles of 112 Milky Way globular clusters, *MNRAS*, *478*(2), 1520–1557, doi:10.1093/mnras/sty1057.

Baumgardt, H., and J. Makino (2003), Dynamical evolution of star clusters in tidal fields, *MNRAS*, *340*(1), 227–246, doi:10.1046/j.1365-8711.2003.06286.x.

Baumgardt, H., G. Parmentier, P. Anders, and E. K. Grebel (2013), The star cluster formation history of the LMC, *MNRAS*, *430*(1), 676–685, doi:10.1093/mnras/sts667.

Baumgardt, H., M. Hilker, A. Sollima, and A. Bellini (2019), Mean proper motions, space orbits, and velocity dispersion profiles of Galactic globular clusters derived from Gaia DR2 data, *MNRAS*, *482*(4), 5138–5155, doi:10.1093/mnras/sty2997.

Beers, T. C., K. Flynn, and K. Gebhardt (1990), Measures of Location and Scale for Velocities in Clusters of Galaxies—A Robust Approach, *AJ*, *100*, 32, doi:10.1086/115487.

Bell, E. F., and R. S. de Jong (2001), Stellar Mass-to-Light Ratios and the Tully-Fisher Relation, *ApJ*, *550*(1), 212–229, doi:10.1086/319728.

Bell, E. F., D. H. McIntosh, N. Katz, and M. D. Weinberg (2003), The Optical and Near-Infrared Properties of Galaxies. I. Luminosity and Stellar Mass Functions, *ApJS*, *149*(2), 289–312, doi:10.1086/378847.

Bell, E. F., C. Wolf, K. Meisenheimer, H.-W. Rix, A. Borch, S. Dye, M. Kleinheinrich, L. Wisotzki, and D. H. McIntosh (2004), Nearly 5000 Distant Early-Type Galaxies in COMBO-17: A Red Sequence and Its Evolution since z˜1, *ApJ*, *608*(2), 752–767, doi:10.1086/420778.

Bellazzini, M., A. Bragaglia, E. Carretta, R. G. Gratton, S. Lucatello, G. Catanzaro, and F. Leone (2012), Na-O anticorrelation and HB. IX. Kinematics of the program clusters A link between systemic rotation and HB morphology?, *A&A*, *538*, A18, doi:10.1051/0004-6361/201118056.

Bernard, A. (1975), UBV and uvby photometry of globular clusters in the Large Magellanic Cloud., *A&A*, *40*(1-2), 199–202.

Bertelli, G., M. Mateo, C. Chiosi, and A. Bressan (1992), The Star Formation History of the Large Magellanic Cloud, *ApJ*, *388*, 400, doi:10.1086/171163.

Bianchini, P., G. van de Ven, M. A. Norris, E. Schinnerer, and A. L. Varri (2016), A novel look at energy equipartition in globular clusters, *MNRAS*, *458*(4), 3644–3654, doi:10.1093/mnras/stw552.

Bianchini, P., R. P. van der Marel, A. del Pino, L. L. Watkins, A. Bellini, M. A. Fardal, M. Libralato, and A. Sills (2018), The internal rotation of globular clusters revealed by Gaia DR2, *MNRAS*, *481*(2), 2125–2139, doi:10.1093/mnras/sty2365.

Bica, E., J. J. Claria, H. Dottori, J. Santos, J. F. C., and A. E. Piatti (1996), Integrated UBV Photometry of 624 Star Clusters and Associations in the Large Magellanic Cloud, *ApJS*, *102*, 57, doi:10.1086/192251.

Blanton, M. R., and S. Roweis (2007), K-Corrections and Filter Transformations in the Ultraviolet, Optical, and Near-Infrared, *AJ*, *133*(2), 734–754, doi:10.1086/510127.

Boutloukos, S. G., and H. J. G. L. M. Lamers (2003), Star cluster formation and disruption time-scales - I. An empirical determination of the disruption time of star clusters in four galaxies, *MNRAS*, *338*(3), 717–732, doi:10.1046/j.1365-8711.2003.06083.x.

Bressan, A., P. Marigo, L. Girardi, B. Salasnich, C. Dal Cero, S. Rubele, and A. Nanni (2012), PARSEC: stellar tracks and isochrones with the PAdova and TRieste Stellar Evolution Code, *MNRAS*, *427*(1), 127–145, doi:10.1111/j.1365-2966.2012.21948.x.

Bruzual, G., and S. Charlot (2003), Stellar population synthesis at the resolution of 2003, *MNRAS*, *344*(4), 1000–1028, doi:10.1046/j.1365-8711.2003.06897.x.

Cappellari, M., et al. (2013), The ATLAS^{3D} project - XV. Benchmark for early-type galaxies scaling relations from 260 dynamical models: mass-to-light ratio, dark matter, Fundamental Plane and Mass Plane, *MNRAS*, *432*(3), 1709–1741, doi:10.1093/mnras/stt562.

Cardelli, J. A., G. C. Clayton, and J. S. Mathis (1989), The Relationship between Infrared, Optical, and Ultraviolet Extinction, *ApJ*, *345*, 245, doi:10.1086/167900.

Carrera, R., C. Gallart, A. Aparicio, and E. Hardy (2011), Metallicities, Age-Metallicity Relationships, and Kinematics of Red Giant Branch Stars in the Outer Disk of the Large Magellanic Cloud, *AJ*, *142*(2), 61, doi:10.1088/0004-6256/142/2/61.

Carretta, E., and R. G. Gratton (1997), Abundances for globular cluster giants. I. Homogeneous metallicities for 24 clusters, *A&AS*, *121*, 95–112, doi:10.1051/aas:1997116.

Carretta, E., J. G. Cohen, R. G. Gratton, and B. B. Behr (2001), An Abundance Analysis for Four Red Horizontal-Branch Stars in the Extremely Metal-Rich Globular Cluster NGC 6528, *AJ*, *122*(3), 1469–1485, doi:10.1086/322116.

Carvalho, L., T. A. Saurin, E. Bica, C. Bonatto, and A. A. Schmidt (2008), Structures in surface-brightness profiles of LMC and SMC star clusters: evidence of mergers?, *A&A*, *485*(1), 71–80, doi:10.1051/0004-6361:20079298.

Chen, Y.-M., et al. (2012), Evolution of the most massive galaxies to z= 0.6 - I. A new method for physical parameter estimation, *MNRAS*, *421*(1), 314–332, doi:10.1111/j.1365-2966.2011.20306.x.

Choi, J., A. Dotter, C. Conroy, M. Cantiello, B. Paxton, and B. D. Johnson (2016), Mesa Isochrones and Stellar Tracks (MIST). I. Solar-scaled Models, *ApJ*, *823*(2), 102, doi:10.3847/0004-637X/823/2/102.

Cole, A. A., E. Tolstoy, I. Gallagher, John S., and T. A. Smecker-Hane (2005), Spectroscopy of Red Giants in the Large Magellanic Cloud Bar: Abundances, Kinematics, and the Age-Metallicity Relation, *AJ*, *129*(3), 1465–1482, doi:10.1086/428007.

Conroy, C. (2013), Modeling the Panchromatic Spectral Energy Distributions of Galaxies, *ARA&A*, *51*(1), 393–455, doi:10.1146/annurev-astro-082812-141017.

Conroy, C., and J. E. Gunn (2010), The Propagation of Uncertainties in Stellar Population Synthesis Modeling. III. Model Calibration, Comparison, and Evaluation, *ApJ*, *712*(2), 833–857, doi:10.1088/0004-637X/712/2/833.

Conroy, C., and P. G. van Dokkum (2012), The Stellar Initial Mass Function in Early-type Galaxies From Absorption Line Spectroscopy. II. Results, *ApJ*, *760*(1), 71, doi:10.1088/0004-637X/760/1/71.

Conroy, C., J. E. Gunn, and M. White (2009), The Propagation of Uncertainties in Stellar Population Synthesis Modeling. I. The Relevance of Uncertain Aspects of Stellar Evolution and the Initial Mass Function to the Derived Physical Properties of Galaxies, *ApJ*, *699*(1), 486–506, doi:10.1088/0004-637X/699/1/486.

Correnti, M., P. Goudfrooij, J. S. Kalirai, L. Girardi, T. H. Puzia, and L. Kerber (2014), New Clues to the Cause of Extended Main-Sequence Turnoffs in Intermediate-age Star Clusters in the Magellanic Clouds, *ApJ*, *793*(2), 121, doi:10.1088/0004-637X/793/2/121.

Correnti, M., P. Goudfrooij, A. Bellini, J. S. Kalirai, and T. H. Puzia (2017), Dissecting the extended main-sequence turn-off of the young star cluster NGC 1850, *MNRAS*, *467*(3), 3628–3641, doi:10.1093/mnras/stx010.

Cote, P., D. L. Welch, P. Fischer, and K. Gebhardt (1995), Dynamics of the Galactic Globular Cluster NGC 3201, *ApJ*, *454*, 788, doi:10.1086/176532.

Crowl, H. H., A. Sarajedini, A. E. Piatti, D. Geisler, E. Bica, J. J. Clariá, and J. Santos, João F. C. (2001), The Line-of-Sight Depth of Populous Clusters in the Small Magellanic Cloud, *AJ*, *122*(1), 220–231, doi:10.1086/321128.

Da Costa, G. S., and D. Hatzidimitriou (1998), Ca II Triplet Spectroscopy of Giants in Small Magellanic Cloud Star Clusters: Abundances, Velocities, and the Age-Metallicity Relation, *AJ*, *115*(5), 1934–1945, doi:10.1086/300340.

Dalgleish, H., et al. (2020), The WAGGS project-III. Discrepant mass-to-light ratios of Galactic globular clusters at high metallicity, *MNRAS*, *492*(3), 3859–3871, doi:10.1093/mnras/staa091.

de Freitas Pacheco, J. A., B. Barbuy, and T. Idiart (1998), Age and metallicity of star clusters in the Magellanic Clouds, *A&A*, *332*, 19–24.

de Vaucouleurs, G., and K. C. Freeman (1972), Structure and dynamics of barred spiral galaxies, in particular of the Magellanic type, *Vistas in Astronomy*, *14*(1), 163–294, doi:10.1016/0083-6656(72)90026-8.

de Vaucouleurs, G., A. de Vaucouleurs, J. Corwin, Herold G., R. J. Buta, G. Paturel, and P. Fouque (1991), *Third Reference Catalogue of Bright Galaxies*.

Dias, W. S., B. S. Alessi, A. Moitinho, and J. R. D. Lépine (2002), New catalogue of optically visible open clusters and candidates, *A&A*, *389*, 871–873, doi:10.1051/0004-6361:20020668.

Djorgovski, S. (1993), Physical Parameters of Galactic Globular Clusters, in *Structure and Dynamics of Globular Clusters*, *Astronomical Society of the Pacific Conference Series*, vol. 50, edited by S. G. Djorgovski and G. Meylan, p. 373.

Dobbie, P. D., A. A. Cole, A. Subramaniam, and S. Keller (2014a), Red giants in the Small Magellanic Cloud - I. Disc and tidal stream kinematics, *MNRAS*, *442*(2), 1663–1679, doi:10.1093/mnras/stu910.

Dobbie, P. D., A. A. Cole, A. Subramaniam, and S. Keller (2014b), Red giants in the Small Magellanic Cloud - II. Metallicity gradient and age-metallicity relation, *MNRAS*, *442*(2), 1680–1692, doi:10.1093/mnras/stu926.

Dolphin, A. E. (2000), WFPC2 Stellar Photometry with HSTPHOT, *PASP*, *112*(776), 1383–1396, doi:10.1086/316630.

Dotter, A. (2016), MESA Isochrones and Stellar Tracks (MIST) 0: Methods for the Construction of Stellar Isochrones, *ApJS*, *222*(1), 8, doi:10.3847/0067-0049/222/1/8.

Dubath, P., G. Meylan, and M. Mayor (1997), Core velocity dispersions for 25 Galactic and 10 old Magellanic globular clusters., *A&A*, *324*, 505–522.

Evans, D. W., et al. (2018), Gaia Data Release 2. Photometric content and validation, *A&A*, *616*, A4, doi:10.1051/0004-6361/201832756.

Feast, M. W., and C. Black (1980), The cluster NGC 330 in the SMC: radial velocities of individual stars., *MNRAS*, *191*, 285–292, doi:10.1093/mnras/191.2.285.

Feast, M. W., and A. R. Walker (1987), Cepheids as distance indicators., *ARA&A*, *25*, 345–375, doi:10.1146/annurev.aa.25.090187.002021.

Ferraro, F. R., A. Mucciarelli, E. Carretta, and L. Origlia (2006), On the Iron Content of NGC 1978 in the LMC: A Metal-rich, Chemically Homogeneous Cluster, *ApJ*, *645*(1), L33–L36, doi:10.1086/506178.

Feuillet, D. K., N. E. Q. Paust, and B. Chaboyer (2014), BVI Photometry and the Red Giant Branch Luminosity Function of M15, *PASP*, *126*(942), 733, doi:10.1086/677845.

Fischer, P., D. L. Welch, P. Cote, M. Mateo, and B. F. Madore (1992a), Dynamics of the Young LMC Clusters NGC 1866, *AJ*, *103*, 857, doi:10.1086/116107.

Fischer, P., D. L. Welch, and M. Mateo (1992b), Dyanamics of the Intermediate-Age Elliptical LMC Cluster NGC 1978, *AJ*, *104*, 1086, doi:10.1086/116299.

Fischer, P., D. L. Welch, and M. Mateo (1993), Dynamics of the Young Binary LMC Cluster NGC 1850, *AJ*, *105*, 938, doi:10.1086/116483.

Fukugita, M., C. J. Hogan, and P. J. E. Peebles (1998), The Cosmic Baryon Budget, *ApJ*, *503*(2), 518–530, doi:10.1086/306025.

Gaia Collaboration, et al. (2016), The Gaia mission, *A&A*, *595*, A1, doi:10.1051/0004-6361/201629272.

Gaia Collaboration, et al. (2018a), Gaia Data Release 2. Summary of the contents and survey properties, *A&A*, *616*, A1, doi:10.1051/0004-6361/201833051.

Gaia Collaboration, et al. (2018b), Gaia Data Release 2. Kinematics of globular clusters and dwarf galaxies around the Milky Way, *A&A*, *616*, A12, doi:10.1051/0004-6361/201832698.

Geha, M., et al. (2013), The Stellar Initial Mass Function of Ultra-faint Dwarf Galaxies: Evidence for IMF Variations with Galactic Environment, *ApJ*, *771*(1), 29, doi:10.1088/0004-637X/771/1/29.

Gieles, M., and A. Zocchi (2015), A family of lowered isothermal models, *MNRAS*, *454*(1), 576–592, doi:10.1093/mnras/stv1848.

Girardi, L., C. Chiosi, G. Bertelli, and A. Bressan (1995), Age distribution of LMC clusters from their integrated UBV colors: history of star formation., *A&A*, *298*, 87.

Girardi, L., A. Bressan, G. Bertelli, and C. Chiosi (2000), Evolutionary tracks and isochrones for low- and intermediate-mass stars: From 0.15 to 7 M_{sun}, and from Z=0.0004 to 0.03, *A&AS*, *141*, 371–383, doi:10.1051/aas:2000126.

Girardi, L., G. Bertelli, A. Bressan, C. Chiosi, M. A. T. Groenewegen, P. Marigo, B. Salasnich, and A. Weiss (2002), Theoretical isochrones in several photometric systems. I. Johnson-Cousins-Glass, HST/WFPC2, HST/NICMOS, Washington, and ESO Imaging Survey filter sets, *A&A*, *391*, 195–212, doi:10.1051/0004-6361:20020612.

Glatt, K., et al. (2008), Age Determination of Six Intermediate-Age Small Magellanic Cloud Star Clusters with HST/ACS, *AJ*, *136*(4), 1703–1727, doi:10.1088/0004-6256/136/4/1703.

Glatt, K., et al. (2009), Structural Parameters of Seven Small Magellanic Cloud Intermediate-Age and Old Star Clusters, *AJ*, *138*(5), 1403–1416, doi:10.1088/0004-6256/138/5/1403.

Gonzalez, G., and G. Wallerstein (1999), Elemental Abundances in Evolved Supergiants. I. NGC 330, a Young SMC Cluster, *AJ*, *117*(5), 2286–2295, doi:10.1086/300853.

Goudfrooij, P., D. Gilmore, M. Kissler-Patig, and C. Maraston (2006), Integrated-light VRI imaging photometry of globular clusters in the Magellanic Clouds, *MNRAS*, *369*(2), 697–704, doi:10.1111/j.1365-2966.2006.10314.x.

Goudfrooij, P., T. H. Puzia, V. Kozhurina-Platais, and R. Chandar (2009), Population Parameters of Intermediate-Age Star Clusters in the Large Magellanic Cloud. I. NGC 1846 and its Wide Main-Sequence Turnoff, *AJ*, *137*(6), 4988–5002, doi:10.1088/0004-6256/137/6/4988.

Goudfrooij, P., T. H. Puzia, V. Kozhurina-Platais, and R. Chandar (2011), Population Parameters of Intermediate-age Star Clusters in the Large Magellanic Cloud. II. New Insights from Extended Main-sequence Turnoffs in Seven Star Clusters, *ApJ*, *737*(1), 3, doi:10.1088/0004-637X/737/1/3.

Goudfrooij, P., et al. (2014), Extended Main Sequence Turnoffs in Intermediate-age Star Clusters: A Correlation between Turnoff Width and Early Escape Velocity, *ApJ*, *797*(1), 35, doi:10.1088/0004-637X/797/1/35.

Gratton, R. G., E. Carretta, and A. Bragaglia (2012), Multiple populations in globular clusters. Lessons learned from the Milky Way globular clusters, *A&A Rev.*, *20*, 50, doi:10.1007/s00159-012-0050-3.

Grocholski, A. J., A. A. Cole, A. Sarajedini, D. Geisler, and V. V. Smith (2006), Ca II Triplet Spectroscopy of Large Magellanic Cloud Red Giants. I. Abundances and Velocities for a Sample of Populous Clusters, *AJ*, *132*(4), 1630–1644, doi:10.1086/507303.

Grocholski, A. J., A. Sarajedini, K. A. G. Olsen, G. P. Tiede, and C. L. Mancone (2007), Distances to Populous Clusters in the Large Magellanic Cloud via the K-band Luminosity of the Red Clump, *AJ*, *134*(2), 680–693, doi:10.1086/519735.

Gunn, J. E., and R. F. Griffin (1979), Dynamical studies of globular clusters based on photoelectric radial velocities of individual stars. I. M3., *AJ*, *84*, 752–773, doi:10.1086/112477.

Harris, J., and D. Zaritsky (2009), The Star Formation History of the Large Magellanic Cloud, *AJ*, *138*(5), 1243–1260, doi:10.1088/0004-6256/138/5/1243.

Hénault-Brunet, V., M. Gieles, A. Sollima, L. L. Watkins, A. Zocchi, I. Claydon, E. Pancino, and H. Baumgardt (2019), Mass modelling globular clusters in the Gaiaera: a method comparison using mock data from an N-body simulation of M 4, *MNRAS*, *483*(1), 1400–1425, doi:10.1093/mnras/sty3187.

Hill, V., P. François, M. Spite, F. Primas, and F. Spite (2000), Age-metallicity relation and chemical evolution of the LMC from UVES spectra of Globular Cluster giants, *A&A*, *364*, L19–L25.

Hollyhead, K., N. Kacharov, C. Lardo, N. Bastian, M. Hilker, M. Rejkuba, A. Koch, E. K. Grebel, and I. Georgiev (2017), Evidence for multiple populations in the intermediate-age cluster Lindsay 1 in the SMC, *MNRAS*, *465*(1), L39–L43, doi:10.1093/mnrasl/slw179.

Hollyhead, K., C. Lardo, N. Kacharov, N. Bastian, M. Hilker, M. Rejkuba, A. Koch, E. K. Grebel, and I. Georgiev (2018), Kron 3: a fourth intermediate age cluster in the SMC with evidence of multiple populations, *MNRAS*, *476*(1), 114–121, doi:10.1093/mnras/sty230.

Iben, J., I., and A. Renzini (1983), Asymptotic giant branch evolution and beyond., *ARA&A*, *21*, 271–342, doi:10.1146/annurev.aa.21.090183.001415.

Illingworth, G. (1976), The masses of globular clusters. II. Velocity dispersions and mass-to-light ratios., *ApJ*, *204*, 73–93, doi:10.1086/154152.

Jeon, Y.-B., J. M. Nemec, A. R. Walker, and A. M. Kunder (2014), B, V Photometry for ~19,000 Stars in and around the Magellanic Cloud Globular Clusters NGC 1466, NGC 1841, NGC 2210, NGC 2257, and Reticulum, *AJ*, *147*(6), 155, doi:10.1088/0004-6256/147/6/155.

Johnson, J. A., I. I. Ivans, and P. B. Stetson (2006), Chemical Compositions of Red Giant Stars in Old Large Magellanic Cloud Globular Clusters, *ApJ*, *640*(2), 801–822, doi:10.1086/498882.

Johnson, R. C. (1927), The Structure and Origin of the Swan Band Spectrum of Carbon, *Philosophical Transactions of the Royal Society of London Series A*, *226*, 157–230, doi:10.1098/rsta.1927.0005.

Kalirai, J. S., et al. (2013), Ultra-Deep Hubble Space Telescope Imaging of the Small Magellanic Cloud: The Initial Mass Function of Stars with M ¡~1 M , *ApJ*, *763*(2), 110, doi:10.1088/0004-637X/763/2/110.

Kamann, S., et al. (2016), MUSE crowded field 3D spectroscopy of over 12 000 stars in the globular cluster NGC 6397. II. Probing the internal dynamics and the presence of a central black hole, *A&A*, *588*, A149, doi:10.1051/0004-6361/201527065.

Kamann, S., et al. (2018), Cluster kinematics and stellar rotation in NGC 419 with MUSE and adaptive optics, *MNRAS*, *480*(2), 1689–1695, doi:10.1093/mnras/sty1958.

Kassin, S. A., R. S. de Jong, and B. J. Weiner (2006), Dark and Baryonic Matter in Bright Spiral Galaxies. II. Radial Distributions for 34 Galaxies, *ApJ*, *643*(2), 804–824, doi:10.1086/502959.

Kauffmann, G., et al. (2003), Stellar masses and star formation histories for 10^5 galaxies from the Sloan Digital Sky Survey, *MNRAS*, *341*(1), 33–53, doi:10.1046/j.1365-8711.2003.06291.x.

Kerber, L. O., B. X. Santiago, and E. Brocato (2007), Physical parameters of 15 intermediate-age LMC clusters from modelling of HST colour-magnitude diagrams, *A&A*, *462*(1), 139–156, doi:10.1051/0004-6361:20066128.

Kimmig, B., A. Seth, I. I. Ivans, J. Strader, N. Caldwell, T. Anderton, and D. Gregersen (2015), Measuring Consistent Masses for 25 Milky Way Globular Clusters, *AJ*, *149*(2), 53, doi:10.1088/0004-6256/149/2/53.

King, I. (1962), The structure of star clusters. I. an empirical density law, *AJ*, *67*, 471, doi:10.1086/108756.

King, I. R. (1966), The structure of star clusters. III. Some simple dynamical models, *AJ*, *71*, 64, doi:10.1086/109857.

King, R. B. (1948), Relative Transition Probabilities of the Swan Bands of Carbon., *ApJ*, *108*, 429, doi:10.1086/145078.

Kontizas, E., A. Dapergolas, D. H. Morgan, and M. Kontizas (2001), A Catalogue of carbon stars in the LMC, *A&A*, *369*, 932–938, doi:10.1051/0004-6361:20010152.

Kotulla, R., U. Fritze, P. Weilbacher, and P. Anders (2009), GALEV evolutionary synthesis models - I. Code, input physics and web interface, *MNRAS*, *396*(1), 462–484, doi:10.1111/j.1365-2966.2009.14717.x.

Kranz, T., A. Slyz, and H.-W. Rix (2003), Dark Matter within High Surface Brightness Spiral Galaxies, *ApJ*, *586*(1), 143–151, doi:10.1086/367551.

Kroupa, P. (2001), On the variation of the initial mass function, *MNRAS*, *322*(2), 231–246, doi:10.1046/j.1365-8711.2001.04022.x.

Kroupa, P., C. Weidner, J. Pflamm-Altenburg, I. Thies, J. Dabringhausen, M. Marks, and T. Maschberger (2013), *The Stellar and Sub-Stellar Initial Mass Function of Simple and Composite Populations*, vol. 5, p. 115, doi:10.1007/978-94-007-5612-0_4.

Kruijssen, J. M. D. (2008), Explaining the mass-to-light ratios of globular clusters, *A&A*, *486*(3), L21–L24, doi:10.1051/0004-6361:200810237.

Krumholz, M. R., C. F. McKee, and J. Bland -Hawthorn (2019), Star Clusters Across Cosmic Time, *ARA&A*, *57*, 227–303, doi:10.1146/annurev-astro-091918-104430.

Lada, C. J., and E. A. Lada (2003), Embedded Clusters in Molecular Clouds, *ARA&A*, *41*, 57–115, doi:10.1146/annurev.astro.41.011802.094844.

Lamers, H. J. G. L. M., M. Gieles, N. Bastian, H. Baumgardt, N. V. Kharchenko, and S. Portegies Zwart (2005a), An analytical description of the disruption of star clusters in tidal fields with an application to Galactic open clusters, *A&A*, *441*(1), 117–129, doi:10.1051/0004-6361:20042241.

Lamers, H. J. G. L. M., M. Gieles, and S. F. Portegies Zwart (2005b), Disruption time scales of star clusters in different galaxies, *A&A*, *429*, 173–179, doi:10.1051/0004-6361:20041476.

Lane, R. R., L. L. Kiss, G. F. Lewis, R. A. Ibata, A. Siebert, T. R. Bedding, and P. Székely (2009), Testing Newtonian gravity with AAOmega: mass-to-light profiles of four globular clusters, *MNRAS*, *400*(2), 917–923, doi:10.1111/j.1365-2966.2009.15505.x.

Lane, R. R., L. L. Kiss, G. F. Lewis, R. A. Ibata, A. Siebert, T. R. Bedding, and P. Székely (2010a), Testing Newtonian gravity with AAOmega: mass-to-light profiles and metallicity calibrations from 47 Tuc and M55, *MNRAS*, *401*(4), 2521–2530, doi:10.1111/j.1365-2966.2009.15827.x.

Lane, R. R., L. L. Kiss, G. F. Lewis, R. A. Ibata, A. Siebert, T. R. Bedding, P. Székely, Z. Balog, and G. M. Szabó (2010b), Halo globular clusters observed with AAOmega: dark matter content, metallicity and tidal heating, *MNRAS*, *406*(4), 2732–2742, doi:10.1111/j.1365-2966.2010.16874.x.

Larsen, S. S., J. P. Brodie, A. Sarajedini, and J. P. Huchra (2002), Structural Parameters and Dynamical Masses for Globular Clusters in M33, *AJ*, *124*(5), 2615–2624, doi:10.1086/344110.

Lee, Y. S., et al. (2008a), The SEGUE Stellar Parameter Pipeline. I. Description and Comparison of Individual Methods, *AJ*, *136*(5), 2022–2049, doi:10.1088/0004-6256/136/5/2022.

Lee, Y. S., et al. (2008b), The SEGUE Stellar Parameter Pipeline. II. Validation with Galactic Globular and Open Clusters, *AJ*, *136*(5), 2050–2069, doi:10.1088/0004-6256/136/5/2050.

Lejeune, T., F. Cuisinier, and R. Buser (1997), Standard stellar library for evolutionary synthesis. I. Calibration of theoretical spectra, *A&AS*, *125*, 229–246, doi:10.1051/aas:1997373.

Lejeune, T., F. Cuisinier, and R. Buser (1998), A standard stellar library for evolutionary synthesis. II. The M dwarf extension, *A&AS*, *130*, 65–75, doi:10.1051/aas:1998405.

Lupton, R. H., S. M. Fall, K. C. Freeman, and R. A. W. Elson (1989), The Internal Velocity Dispersions of Three Young Star Clusters in the Large Magellanic Cloud, *ApJ*, *347*, 201, doi:10.1086/168110.

Mackey, A. D., and P. Broby Nielsen (2007), A double main-sequence turn-off in the rich star cluster NGC 1846 in the Large Magellanic Cloud, *MNRAS*, *379*(1), 151–158, doi:10.1111/j.1365-2966.2007.11915.x.

Mackey, A. D., and G. F. Gilmore (2003a), Surface brightness profiles and structural parameters for 53 rich stellar clusters in the Large Magellanic Cloud, *MNRAS*, *338*(1), 85–119, doi:10.1046/j.1365-8711.2003.06021.x.

Mackey, A. D., and G. F. Gilmore (2003b), Surface brightness profiles and structural parameters for 10 rich stellar clusters in the Small Magellanic Cloud, *MNRAS*, *338*(1), 120–130, doi:10.1046/j.1365-8711.2003.06022.x.

Mackey, A. D., P. Broby Nielsen, A. M. N. Ferguson, and J. C. Richardson (2008), Multiple Stellar Populations in Three Rich Large Magellanic Cloud Star Clusters, *ApJ*, *681*(1), L17, doi:10.1086/590343.

Mackey, A. D., G. S. Da Costa, A. M. N. Ferguson, and D. Yong (2013), A VLT/FLAMES Study of the Peculiar Intermediate-age Large Magellanic Cloud Star Cluster NGC 1846. I. Kinematics, *ApJ*, *762*(1), 65, doi:10.1088/0004-637X/762/1/65.

Maíz Apellániz, J., and M. Weiler (2018), Reanalysis of the Gaia Data Release 2 photometric sensitivity curves using HST/STIS spectrophotometry, *A&A*, *619*, A180, doi:10.1051/0004-6361/201834051.

Mandushev, G., A. Staneva, and N. Spasova (1991), Dynamical masses for galactic globular clusters., *A&A*, *252*, 94.

Maraston, C. (2005), Evolutionary population synthesis: models, analysis of the ingredients and application to high-z galaxies, *MNRAS*, *362*(3), 799–825, doi:10.1111/j.1365-2966.2005.09270.x.

Maraston, C., et al. (2013), Stellar masses of SDSS-III/BOSS galaxies at z 0.5 and constraints to galaxy formation models, *MNRAS*, *435*(4), 2764–2792, doi:10.1093/mnras/stt1424.

Marigo, P., L. Girardi, A. Bressan, M. A. T. Groenewegen, L. Silva, and G. L. Granato (2008), Evolution of asymptotic giant branch stars. II. Optical to far-infrared isochrones with improved TP-AGB models, *A&A*, *482*(3), 883–905, doi:10.1051/0004-6361:20078467.

Martini, P., and L. C. Ho (2004), A Population of Massive Globular Clusters in NGC 5128, *ApJ*, *610*(1), 233–246, doi:10.1086/421458.

Martocchia, S., et al. (2017), The search for multiple populations in Magellanic Cloud Clusters - III. No evidence for multiple populations in the SMC cluster NGC 419, *MNRAS*, *468*(3), 3150–3158, doi:10.1093/mnras/stx660.

Martocchia, S., et al. (2018), The search for multiple populations in Magellanic Cloud clusters - IV. Coeval multiple stellar populations in the young star cluster NGC 1978, *MNRAS*, *477*(4), 4696–4705, doi:10.1093/mnras/sty916.

Mateo, M., D. Welch, and P. Fischer (1991), Mass-To Ratios of Large Magellanic Cloud Clusters, in *The Magellanic Clouds*, *IAU Symposium*, vol. 148, edited by R. Haynes and D. Milne, p. 191.

Mateo, M., J. I. Bailey, J. Crane, S. Shectman, I. Thompson, I. Roederer, B. Bigelow, and S. Gunnels (2012), M2FS: the Michigan/Magellan Fiber System, in *Proc. SPIE, Society of Photo-Optical Instrumentation Engineers (SPIE) Conference Series*, vol. 8446, p. 84464Y, doi:10.1117/12.926448.

McGaugh, S. S., and J. M. Schombert (2014), Color-Mass-to-light-ratio Relations for Disk Galaxies, *AJ*, *148*(5), 77, doi:10.1088/0004-6256/148/5/77.

McGaugh, S. S., J. M. Schombert, W. J. G. de Blok, and M. J. Zagursky (2010), The Baryon Content of Cosmic Structures, *ApJ*, *708*(1), L14–L17, doi:10.1088/2041-8205/708/1/L14.

McLaughlin, D. E., and R. P. van der Marel (2005), Resolved Massive Star Clusters in the Milky Way and Its Satellites: Brightness Profiles and a Catalog of Fundamental Parameters, *ApJS*, *161*(2), 304–360, doi:10.1086/497429.

Mermilliod, J. C. (1981), Comparative studies of young open clusters., *A&A*, *97*, 235–244.

Michie, R. W. (1963), On the distribution of high energy stars in spherical stellar systems, *MNRAS*, *125*, 127, doi:10.1093/mnras/125.2.127.

Milone, A. P., L. R. Bedin, G. Piotto, and J. Anderson (2009), Multiple stellar populations in Magellanic Cloud clusters. I. An ordinary feature for intermediate age globulars in the LMC?, *A&A*, *497*(3), 755–771, doi:10.1051/0004-6361/200810870.

Milone, A. P., et al. (2018), Multiple stellar populations in Magellanic Cloud clusters - VI. A survey of multiple sequences and Be stars in young clusters, *MNRAS*, *477*(2), 2640–2663, doi:10.1093/mnras/sty661.

Mucciarelli, A., E. Carretta, L. Origlia, and F. R. Ferraro (2008), The Chemical Composition of Red Giant Stars in Four Intermediate-Age Clusters of the Large Magellanic Cloud, *AJ*, *136*(1), 375–388, doi:10.1088/0004-6256/136/1/375.

Mucciarelli, A., L. Origlia, F. R. Ferraro, and E. Pancino (2009), Looking Outside the Galaxy: The Discovery of Chemical Anomalies in Three Old Large Magellanic Cloud Clusters, *ApJ*, *695*(2), L134–L139, doi:10.1088/0004-637X/695/2/L134.

Mucciarelli, A., L. Origlia, and F. R. Ferraro (2010), Chemical Composition of the Old Globular Clusters NGC 1786, NGC 2210, and NGC 2257 in the Large Magellanic Cloud, *ApJ*, *717*(1), 277–288, doi:10.1088/0004-637X/717/1/277.

Mucciarelli, A., E. Dalessandro, F. R. Ferraro, L. Origlia, and B. Lanzoni (2014), No Evidence of Chemical Anomalies in the Bimodal Turnoff Cluster NGC 1806 in the Large Magellanic Cloud, *ApJ*, *793*(1), L6, doi:10.1088/2041-8205/793/1/L6.

O'Donnell, J. E. (1994), R v-dependent Optical and Near-Ultraviolet Extinction, *ApJ*, *422*, 158, doi:10.1086/173713.

Olszewski, E. W., R. A. Schommer, N. B. Suntzeff, and H. C. Harris (1991), Spectroscopy of Giants in LMC Clusters. I. Velocities, Abundances, and the Age-Metallicity Relation, *AJ*, *101*, 515, doi:10.1086/115701.

Olszewski, E. W., N. B. Suntzeff, and M. Mateo (1996), Old and Intermediate-Age Stellar Populations in the Magellanic Clouds, *ARA&A*, *34*, 511–550, doi:10.1146/annurev.astro.34.1.511.

Parisi, M. C., D. Geisler, J. J. Clariá, S. Villanova, N. Marcionni, A. Sarajedini, and A. J. Grocholski (2015), Ca II Triplet Spectroscopy of Small Magellanic Cloud Red Giants. III. Abundances and Velocities for a Sample of 14 Clusters, *AJ*, *149*(5), 154, doi:10.1088/0004-6256/149/5/154.

Parmentier, G., and R. de Grijs (2008), The poorly constrained cluster disruption time-scale in the Large Magellanic Cloud, *MNRAS*, *383*(3), 1103–1120, doi:10.1111/j.1365-2966.2007.12602.x.

Patrick, L. R., et al. (2020), Multiplicity of the red supergiant population in the young massive cluster NGC 330, *A&A*, *635*, A29, doi:10.1051/0004-6361/201936741.

Paust, N. E. Q., B. Chaboyer, and A. Sarajedini (2007), BVI Photometry and the Luminosity Functions of the Globular Cluster M92, *AJ*, *133*(6), 2787–2798, doi:10.1086/513511.

Paxton, B., L. Bildsten, A. Dotter, F. Herwig, P. Lesaffre, and F. Timmes (2011), Modules for Experiments in Stellar Astrophysics (MESA), *ApJS*, *192*(1), 3, doi:10.1088/0067-0049/192/1/3.

Paxton, B., et al. (2013), Modules for Experiments in Stellar Astrophysics (MESA): Planets, Oscillations, Rotation, and Massive Stars, *ApJS*, *208*(1), 4, doi:10.1088/0067-0049/208/1/4.

Paxton, B., et al. (2015), Modules for Experiments in Stellar Astrophysics (MESA): Binaries, Pulsations, and Explosions, *ApJS*, *220*(1), 15, doi:10.1088/0067-0049/220/1/15.

Pessev, P. M., P. Goudfrooij, T. H. Puzia, and R. Chand ar (2006), A Database of 2MASS Near-Infrared Colors of Magellanic Cloud Star Clusters, *AJ*, *132*(2), 781–800, doi:10.1086/505625.

Pessev, P. M., P. Goudfrooij, T. H. Puzia, and R. Chand ar (2008), A comparison of optical and near-infrared colours of Magellanic Cloud star clusters with predictions of simple stellar population models, *MNRAS*, *385*(3), 1535–1560, doi:10.1111/j.1365-2966.2008.12935.x.

Pietrinferni, A., S. Cassisi, M. Salaris, and F. Castelli (2004), A Large Stellar Evolution Database for Population Synthesis Studies. I. Scaled Solar Models and Isochrones, *ApJ*, *612*(1), 168–190, doi:10.1086/422498.

Portegies Zwart, S. F., S. L. W. McMillan, and M. Gieles (2010), Young Massive Star Clusters, *ARA&A*, *48*, 431–493, doi:10.1146/annurev-astro-081309-130834.

Pryor, C., and G. Meylan (1993), Velocity Dispersions for Galactic Globular Clusters, in *Structure and Dynamics of Globular Clusters*, *Astronomical Society of the Pacific Conference Series*, vol. 50, edited by S. G. Djorgovski and G. Meylan, p. 357.

Rebeirot, E., M. Azzopardi, and B. E. Westerlund (1993), Carbon stars in the Small Magellanic Cloud. II. Catalogue of 1707 objects with identifications and spectrophotometry., *A&AS*, *97*, 603–728.

Renaud, F. (2018), Star clusters in evolving galaxies, *New Astron. Rev.*, *81*, 1–38, doi:10.1016/j.newar.2018.03.001.

Roederer, I. U., et al. (2016), Detailed Chemical Abundances in the r-process-rich Ultra-faint Dwarf Galaxy Reticulum 2, *AJ*, *151*(3), 82, doi:10.3847/0004-6256/151/3/82.

Salim, S., J. C. Lee, S. Janowiecki, E. da Cunha, M. Dickinson, M. Boquien, D. Burgarella, J. J. Salzer, and S. Charlot (2016), GALEX-SDSS-WISE Legacy Catalog (GSWLC): Star Formation Rates, Stellar Masses, and Dust Attenuations of 700,000 Low-redshift Galaxies, *ApJS*, *227*(1), 2, doi:10.3847/0067-0049/227/1/2.

Sánchez-Blázquez, P., R. F. Peletier, J. Jiménez-Vicente, N. Cardiel, A. J. Cenarro, J. Falcón-Barroso, J. Gorgas, S. Selam, and A. Vazdekis (2006), Medium-resolution Isaac Newton Telescope library of empirical spectra, *MNRAS*, *371*(2), 703–718, doi:10.1111/j.1365-2966.2006.10699.x.

Shanahan, R. L., and M. Gieles (2015), Biases in the inferred mass-to-light ratio of globular clusters: no need for variations in the stellar mass function., *MNRAS*, *448*, L94–L98, doi:10.1093/mnrasl/slu205.

Sollima, A., H. Baumgardt, A. Zocchi, E. Balbinot, M. Gieles, V. Hénault-Brunet, and A. L. Varri (2015), Biases in the determination of dynamical parameters of star clusters: today and in the Gaia era, *MNRAS*, *451*(2), 2185–2197, doi:10.1093/mnras/stv1079.

Sollima, A., H. Baumgardt, and M. Hilker (2019), The eye of Gaia on globular clusters kinematics: internal rotation, *MNRAS*, *485*(1), 1460–1476, doi:10.1093/mnras/stz505.

Song, Y.-Y., M. Mateo, M. G. Walker, and I. U. Roederer (2017), An Expanded Chemo-dynamical Sample of Red Giants in the Bar of the Large Magellanic Cloud, *AJ*, *153*(6), 261, doi:10.3847/1538-3881/aa6eaa.

Song, Y.-Y., M. Mateo, A. D. Mackey, E. W. Olszewski, I. U. Roederer, M. G. Walker, and J. I. Bailey (2019), Dynamical masses and mass-to-light ratios of resolved massive star clusters - I. NGC 419 and NGC 1846, *MNRAS*, *490*(1), 385–407, doi:10.1093/mnras/stz2502.

Spitzer, L. (1987), *Dynamical evolution of globular clusters.*

Strader, J., G. H. Smith, S. Larsen, J. P. Brodie, and J. P. Huchra (2009), Mass-to-Light Ratios for M31 Globular Clusters: Age Dating and a Surprising Metallicity Trend, *AJ*, *138*(2), 547–557, doi:10.1088/0004-6256/138/2/547.

Strader, J., N. Caldwell, and A. C. Seth (2011), Star Clusters in M31. V. Internal Dynamical Trends: Some Troublesome, Some Reassuring, *AJ*, *142*(1), 8, doi:10.1088/0004-6256/142/1/8.

Suntzeff, N. B., R. A. Schommer, E. W. Olszewski, and A. R. Walker (1992), Spectroscopy of Giants in LMC Clusters. III. Velocities and Abundances for NGC 1841 and Reticulum and the Properties of the Metal-Poor Clusters, *AJ*, *104*, 1743, doi:10.1086/116356.

Tojeiro, R., S. Wilkins, A. F. Heavens, B. Panter, and R. Jimenez (2009), A Public Catalog of Stellar Masses, Star Formation and Metallicity Histories, and Dust Content from the Sloan Digital Sky Survey using VESPA, *ApJS*, *185*(1), 1–19, doi:10.1088/0067-0049/185/1/1.

Torres-Flores, S., B. Epinat, P. Amram, H. Plana, and C. Mendes de Oliveira (2011), GHASP: an Hα kinematic survey of spiral and irregular galaxies - IX. The near-infrared, stellar and baryonic Tully-Fisher relations, *MNRAS*, *416*(3), 1936–1948, doi:10.1111/j.1365-2966.2011.19169.x.

van den Bergh, S. (1981), UBV observations of globular clusters in the Magellanic Clouds., *A&AS*, *46*, 79–87.

van der Marel, R. P., and N. Kallivayalil (2014), Third-epoch Magellanic Cloud Proper Motions. II. The Large Magellanic Cloud Rotation Field in Three Dimensions, *ApJ*, *781*(2), 121, doi:10.1088/0004-637X/781/2/121.

van der Marel, R. P., and J. Sahlmann (2016), First Gaia Local Group Dynamics: Magellanic Clouds Proper Motion and Rotation, *ApJ*, *832*(2), L23, doi:10.3847/2041-8205/832/2/L23.

van Dokkum, P. G. (2001), Cosmic-Ray Rejection by Laplacian Edge Detection, *PASP*, *113*(789), 1420–1427, doi:10.1086/323894.

Van Eck, S., A. Jorissen, S. Udry, M. Mayor, and B. Pernier (1998), The HIPPARCOS Hertzsprung-Russell diagram of S stars: probing nucleosynthesis and dredge-up, *A&A*, *329*, 971–985.

VandenBerg, D. A., K. Brogaard, R. Leaman, and L. Casagrand e (2013), The Ages of 55 Globular Clusters as Determined Using an Improved $\Delta V_{\rm TO}^{\rm HB}$ Method along with Color-Magnitude Diagram Constraints, and Their Implications for Broader Issues, *ApJ*, *775*(2), 134, doi:10.1088/0004-637X/775/2/134.

Varri, A. L., and G. Bertin (2012), Self-consistent models of quasi-relaxed rotating stellar systems, *A&A*, *540*, A94, doi:10.1051/0004-6361/201118300.

Vasiliev, E. (2019), Proper motions and dynamics of the Milky Way globular cluster system from Gaia DR2, *MNRAS*, *484*(2), 2832–2850, doi:10.1093/mnras/stz171.

Vazdekis, A., P. Sánchez-Blázquez, J. Falcón-Barroso, A. J. Cenarro, M. A. Beasley, N. Cardiel, J. Gorgas, and R. F. Peletier (2010), Evolutionary stellar population synthesis with MILES - I. The base models and a new line index system, *MNRAS*, *404*(4), 1639–1671, doi:10.1111/j.1365-2966.2010.16407.x.

Wagner-Kaiser, R., D. Mackey, A. Sarajedini, B. Chaboyer, R. E. Cohen, S.-C. Yang, J. D. Cummings, D. Geisler, and A. J. Grocholski (2017), Exploring the nature and synchronicity of early cluster formation in the Large Magellanic Cloud - II. Relative ages and distances for six ancient globular clusters, *MNRAS*, *471*(3), 3347–3358, doi:10.1093/mnras/stx1702.

Walker, M. G., M. Mateo, E. W. Olszewski, J. Peñarrubia, N. W. Evans, and G. Gilmore (2009), A Universal Mass Profile for Dwarf Spheroidal Galaxies?, *ApJ*, *704*(2), 1274–1287, doi:10.1088/0004-637X/704/2/1274.

Walker, M. G., M. Mateo, E. W. Olszewski, I. Bailey, John I., S. E. Koposov, V. Belokurov, and N. W. Evans (2015a), Magellan/M2FS Spectroscopy of the Reticulum 2 Dwarf Spheroidal Galaxy, *ApJ*, *808*(2), 108, doi:10.1088/0004-637X/808/2/108.

Walker, M. G., E. W. Olszewski, and M. Mateo (2015b), Bayesian analysis of resolved stellar spectra: application to MMT/Hectochelle observations of the Draco dwarf spheroidal, *MNRAS*, *448*(3), 2717–2732, doi:10.1093/mnras/stv099.

Wallerstein, G., and G. R. Knapp (1998), Carbon Stars, *ARA&A*, *36*, 369–434, doi:10.1146/annurev.astro.36.1.369.

Watkins, L. L., R. P. van der Marel, S. T. Sohn, and N. W. Evans (2019), Evidence for an Intermediate-mass Milky Way from Gaia DR2 Halo Globular Cluster Motions, *ApJ*, *873*(2), 118, doi:10.3847/1538-4357/ab089f.

Weiler, M. (2018), Revised Gaia Data Release 2 passbands, *A&A*, *617*, A138, doi:10.1051/0004-6361/201833462.

Wenger, M., et al. (2000), The SIMBAD astronomical database. The CDS reference database for astronomical objects, *A&AS*, *143*, 9–22, doi:10.1051/aas:2000332.

Westera, P., T. Lejeune, R. Buser, F. Cuisinier, and G. Bruzual (2002), A standard stellar library for evolutionary synthesis. III. Metallicity calibration, *A&A*, *381*, 524–538, doi:10.1051/0004-6361:20011493.

Westerlund, B. E. (1997), *The Magellanic Clouds*.

Westerlund, B. E., M. Azzopardi, J. Breysacher, and E. Rebeirot (1991), The evolution of carbon stars in the Magellanic Clouds., *A&AS*, *91*, 425–451.

Whitmore, B. C. (2004), Survival Rates and Consequences, in *The Formation and Evolution of Massive Young Star Clusters*, *Astronomical Society of the Pacific Conference Series*, vol. 322, edited by H. J. G. L. M. Lamers, L. J. Smith, and A. Nota, p. 419.

Zacharias, N., D. G. Monet, S. E. Levine, S. E. Urban, R. Gaume, and G. L. Wycoff (2004), The Naval Observatory Merged Astrometric Dataset (NOMAD), in *American Astronomical Society Meeting Abstracts*, vol. 205, p. 48.15.

Zaritsky, D., J. Harris, I. B. Thompson, E. K. Grebel, and P. Massey (2002), The Magellanic Clouds Photometric Survey: The Small Magellanic Cloud Stellar Catalog and Extinction Map, *AJ*, *123*(2), 855–872, doi:10.1086/338437.

Zaritsky, D., J. Harris, I. B. Thompson, and E. K. Grebel (2004), The Magellanic Clouds Photometric Survey: The Large Magellanic Cloud Stellar Catalog and Extinction Map, *AJ*, *128*(4), 1606–1614, doi:10.1086/423910.

Zaritsky, D., J. E. Colucci, P. M. Pessev, R. A. Bernstein, and R. Chandar (2012), Evidence for Two Distinct Stellar Initial Mass Functions, *ApJ*, *761*(2), 93, doi:10.1088/0004-637X/761/2/93.

Zaritsky, D., J. E. Colucci, P. M. Pessev, R. A. Bernstein, and R. Chandar (2013), Evidence for Two Distinct Stellar Initial Mass Functions: Revisiting the Effects of Cluster Dynamical Evolution, *ApJ*, *770*(2), 121, doi:10.1088/0004-637X/770/2/121.

Zaritsky, D., J. E. Colucci, P. M. Pessev, R. A. Bernstein, and R. Chandar (2014), Evidence for Two Distinct Stellar Initial Mass Functions: Probing for Clues to the Dichotomy, *ApJ*, *796*(2), 71, doi:10.1088/0004-637X/796/2/71.

Zinn, R., and M. J. West (1984), The globular cluster system of the Galaxy. III. Measurements of radial velocity and metallicity for 60 clusters and a compilation of metallicities for 121 clusters., *ApJS*, *55*, 45–66, doi:10.1086/190947.

Zonoozi, A. H., H. Haghi, and P. Kroupa (2016), A Possible Solution for the M/L-[Fe/H] Relation of Globular Clusters in M3. I. A Metallicity- and Density-dependent Top-heavy IMF, *ApJ*, *826*(1), 89, doi:10.3847/0004-637X/826/1/89.